Palaeontology

VOLUME 41 · PART 4 · AUGUST 1998

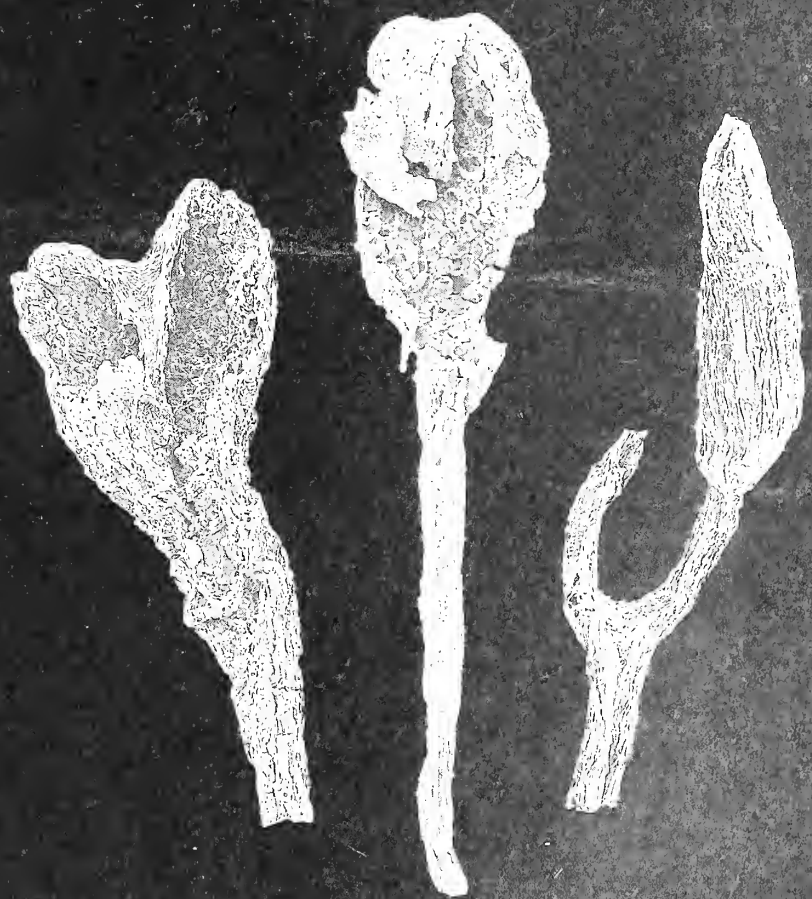

Published by

The Palaeontological Association · London

Price £38·00

THE PALAEONTOLOGICAL ASSOCIATION

(Registered Charity No. 276369)

The Association was founded in 1957 to promote research in palaeontology and its allied sciences.

COUNCIL 1997–1998

MEMBERSHIP

Membership is open to individuals and institutions on payment of the appropriate annual subscription. Rates for 1998 are:

Institutional membership . . .	£90·00 (U.S. $175)	Student membership	£10·00 (U.S. $20)
Ordinary membership . . .	£28·00 (U.S. $50)	Retired membership	£14·00 (U.S. $25)

There is no admission fee. Correspondence concerned with Institutional Membership should be addressed to **Dr J. E. Francis, Department of Earth Sciences, The University, Leeds LS2 9JJ.** Student members are persons receiving full-time instruction at educational institutions recognized by the Council. On first applying for membership, an application form should be obtained from the Membership Treasurer: **Dr M. J. Barker, Department of Geology, University of Portsmouth, Burnaby Road, Portsmouth PO1 3QL.** Subscriptions cover one calendar year and are due each January; they should be sent to the Membership Treasurer. All members who join for 1998 will receive *Palaeontology,* Volume 41, Parts 1–6. Enquiries concerning back numbers should be directed to the Marketing Manager.

Non-members may subscribe, and also obtain back issues up to five years old, at cover price through Blackwell Publishers Journals, P.O. Box 805, 108 Cowley Road, Oxford OX4 1FH, UK. For older issues contact the Marketing Manager.

US Mailing: Periodicals postage paid at Rahway, New Jersey. Postmaster: send address corrections to *Palaeontology*, c/o Mercury Airfreight International Ltd, 2323 E–F Randolph Avenue, Avenel, NJ 07001, USA (US mailing agent).

Cover: coalified terminal sporangia from the Lower Devonian of the Welsh Borderland containing permanent tetrads (far left) and dyads. Similar spores found dispersed in Ordovician rocks are considered the earliest evidence for embryophytic life on land (from left to right, NMW94.76G.1; NMW96.11G.6; NMW97.42G.4. All × 45).

A NEW SPECIES OF THE SAUROPTERYGIAN *CYMATOSAURUS* FROM THE LOWER MUSCHELKALK OF THURINGIA, GERMANY

by OLIVIER RIEPPEL *and* RALF WERNEBURG

ABSTRACT. The sauropterygian *Cymatosaurus*, *C. minor* sp. nov., from the Lower Muschelkalk of Hetschburg near Bad Berka, Thuringia, Germany, is described. It differs from other species of its genus by its relatively small overall size, the development of a parietal sagittal crest, a comparatively long and narrow upper temporal fossa, the anterior extent of the parietals reaches to a level well in front of the posterior margins of the orbits, and the vomers are fused. The acid-prepared skull preserves some interesting anatomical detail, and documents for *Cymatosaurus* the same derived course of the internal carotid through the basicranium that has previously been described for *Nothosaurus* and *Simosaurus*. A detailed geographical and stratigraphical analysis of the occurrence of the genera *Nothosaurus* and *Cymatosaurus* in the Muschelkalk suggests competitive exclusion between the two genera.

CYMATOSAURUS first appears in the fossil record in the uppermost Buntsandstein of Rüdersdorf near Berlin (E. von Huene 1944). Additional material has come from the Lower Muschelkalk of eastern Germany (Halle/Saale: von Fritsch 1894) and Upper Silesia (now Poland: Gürich 1884, 1891; Koken 1893; Schrammen 1899). Early westward expansion through the Muschelkalk Basin may be documented by a humerus, possibly referable to the genus *Cymatosaurus*, from the Lower Muschelkalk of Winterswijk, Netherlands (Oosterink 1986; Rieppel 1994*a*; but see the discussion of the genus *Anarosaurus* in Rieppel and Lin 1995). The early invasion of the Alpine Triassic is documented by the appearance of the genus in the Lower Anisian of the Lechtaler Alps, Austria (F. von Huene 1958; Rieppel 1995*a*; Rieppel and Hagdorn 1996). The occurrence of the genus in the Lower Muschelkalk of Wadi Ramon, Israel, remains controversial at this time (Haas 1963; Sues 1987). The genus is not known from deposits younger than the Lower Muschelkalk.

Cymatosaurus has not previously been recorded from Thuringia. Jaekel (1911, p. 148, fig. 161; this specimen has not been located) figured a skull from the Lower Muschelkalk of Mühlhausen, which he referred to '*Nothosaurus* (*Cymatosaurus*) cf. *fridericianus*'. *Cymatosaurus fridericianus* von Fritsch, 1894, is the type species of the genus, but the skull figured by Jaekel (1911) represents *Nothosaurus marchicus* (Rieppel and Wild 1996), as is indicated by its proportions. All other sauropterygians from Thuringia (*Placodus*: Rieppel 1995*b*; Cyamodontoidea indet: Rieppel 1995*c*; *Nothosaurus*: Rieppel and Wild 1996) are from the Upper Muschelkalk of Bad Sulza. In this paper, we describe a recently located (by RW) incomplete skull from the Lower Muschelkalk of Hetschburg near Bad Berka, Thuringia. This skull lacks the rostrum, but can be referred to the genus *Cymatosaurus* on the basis of shared diagnostic characters (see description below).

A recent review of the genus *Cymatosaurus* (Rieppel 1997) showed that of all the species previously described, only three can be considered valid, viz. *Cymatosaurus fridericianus* von Fritsch, 1894, *Cymatosaurus latifrons* Gürich, 1884, and *Cymatosaurus nultidentatus* (F. von Huene, 1958). All other previously described species of *Cymatosaurus* are considered to be junior synonyms of *Cymatosaurus latifrons* (*C. gracilis* Schrammen, 1899; *C. silesiacus* Schrammen, 1899), or a *nomen dubium* (*C. erythreus* E. von Huene, 1944). Although incomplete, the skull described here can be assigned to a separate species.

[Palaeontology, Vol. 41, Part 4, 1998, pp. 575–589]

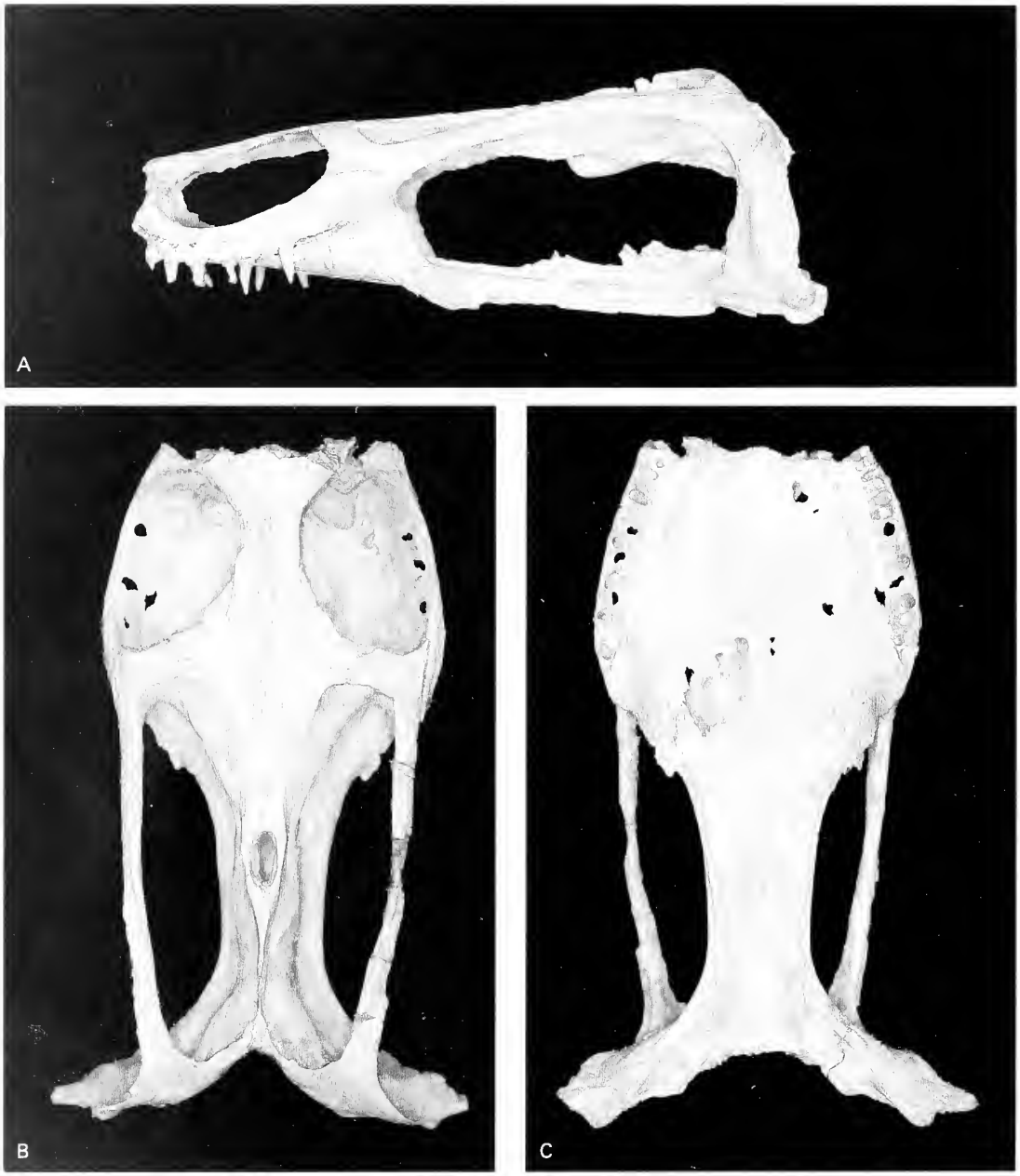

TEXT-FIG. 1. *Cymatosaurus minor* sp. nov.; holotype, NHMS-GT 21; skull in A, left lateral view; B, dorsal view; C, ventral view. All × 1·125.

Institutional abbreviations. BGR, Bundesanstalt für Geowissenschaften und Rohstoffe, Berlin; MB, Museum für Naturkunde, Humboldt University, Berlin; MHI, Muschelkalkmuseum Hagdorn, Ingelfingen; NHMS, Naturhistorisches Museum Schloss Bertholdsburg, Schleusingen; SMNS, Staatliches Museum für Naturkunde, Stuttgart.

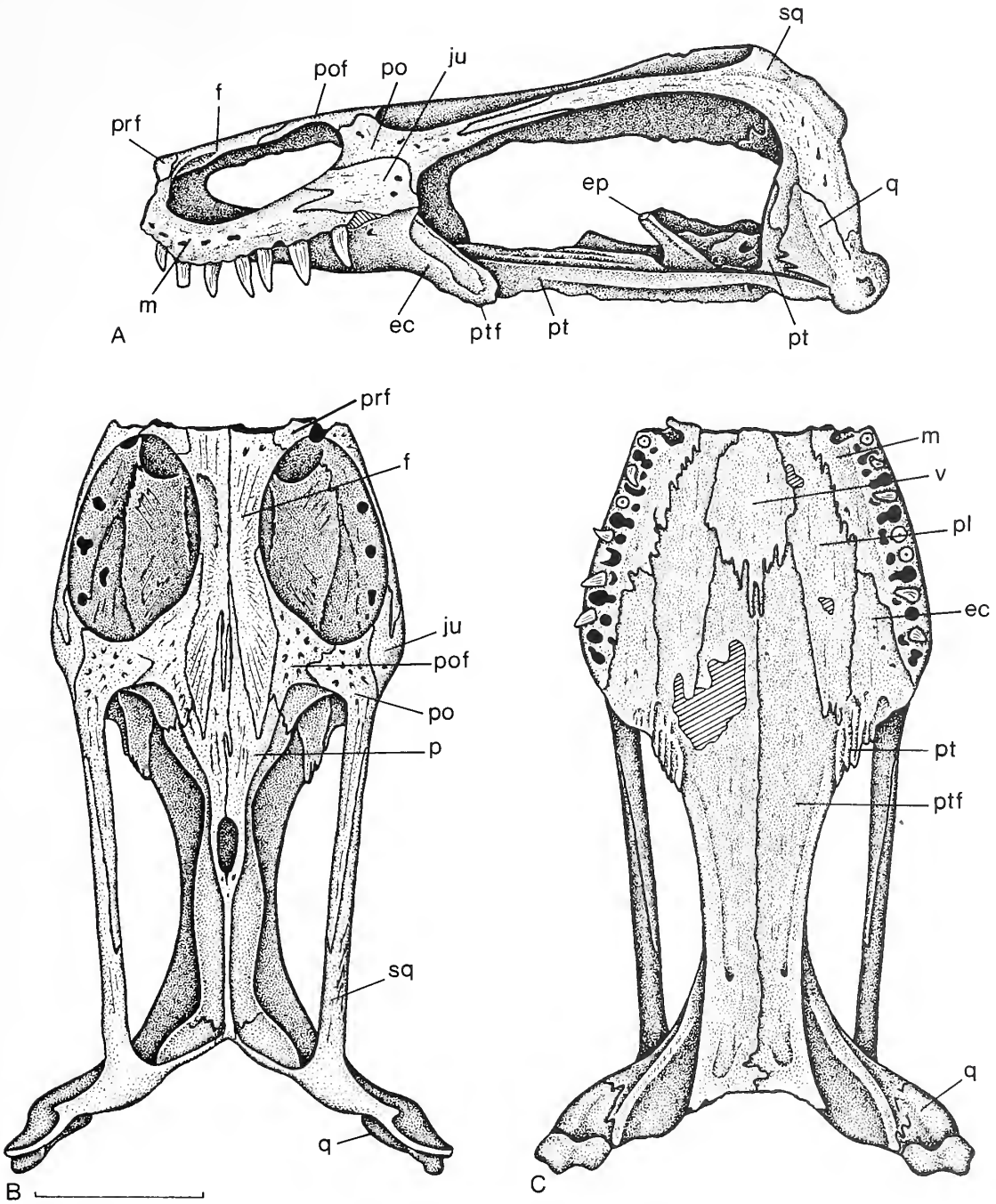

TEXT-FIG. 2. The skull of *Cymatosaurus minor* sp. nov. A, left lateral view; B, dorsal view; C, ventral view. Scale bar represents 20 mm. Abbreviations: ec, ectopterygoid; ep, epipterygoid; f, frontal; ju, jugal; m, maxilla; p, parietal; pl, palatine; po, postorbital; pof, postfrontal; prf, prefrontal; pt, pterygoid; ptf, pterygoid flange; q, quadrate; sq, squamosal; v, vomer.

MATERIAL AND METHODS

The new species of *Cymatosaurus* described here is based on an incomplete skull kept at the Naturhistorisches Museum Schloss Bertholdsburg in Schleusingen, Thuringia, Germany (NHMS-GT 21). The specimen was located by one of us (RW) in the private collection of Paul Georgi, a teacher at the Schleusingen school, and was probably collected in the period between the years 1930 and 1950. The skull was enclosed in a block of limestone, with the rostrum already broken off. The back end of the skull was still covered by approximately 20 mm of matrix, but no part of the cervical vertebral column was attached to the skull. The skull must therefore have been disarticulated before being buried in sediment.

The skull was collected near Hetschburg, *c.* 2 km north-east of Bad Berka and 7 km south-south-west of Weimar in Thuringia. The limestone block containing the skull was most probably collected in the Ilm-valley near Hetschburg, where almost the entire *Wellenkalk* sequence (Lower Muschelkalk, Lower Anisian) crops out. The specimen derives from a bed of limestone about 50 mm thick, which cannot be attributed to any marker horizon of the Lower Muschelkalk. The limestone bed is densely packed with allochthonous bivalves (*Myophoria* cf. *vulgaris*) and gastropods (*Loxenema*), and probably represents a thin-bedded tempestite of the *Wellenkalk* facies.

The skull was completely removed from the surrounding matrix through chemical preparation, by exposing the specimen to 5 per cent. formic acid over a period of 4 weeks. Every time the exposure of bone had progressed by 2 mm, the specimen was thoroughly washed, dried, and the newly exposed bone stabilized by application of a thin film of resin. The only organic remains in the residue were teeth and scales of actinopterygians; it did not contain any bony elements that might have belonged to the endocranium or the postcranial skeleton of the *Cymatosaurus* specimen.

SYSTEMATIC PALAEONTOLOGY

Order SAUROPTERYGIA Owen, 1860
Suborder EOSAUROPTERYGIA Rieppel, 1994*a*
Family CYMATOSAURIDAE F. von Huene, 1948

Cymatosaurus von Fritsch, 1894

Type species. Cymatosaurus fridericianus von Fritsch, 1894, from the Lower Muschelkalk (lower Middle Triassic) of Halle/Saale, Germany.

Diagnosis. Eosauropterygians with a moderately depressed skull; snout constricted; postorbital skull distinctly elongated; occiput deeply concave; supraoccipital vertically oriented and in loose connection with the dermatocranium; distinctly reduced nasals that may or may not enter the external naris; frontals paired; posterolateral processes of frontals closely approach the upper temporal fossa and may enter its anteromedial margin; parietals incompletely or completely fused; jugal enters posterior margin of the orbit and remains excluded from upper temporal arch; quadratojugal absent.

Distribution. Uppermost Buntsandstein and Lower Muschelkalk, Lower Anisian, Middle Triassic, Europe.

Cymatosaurus minor sp. nov.

Text-figures 1–3

Holotype. NHMS-GT 21: incomplete skull (Text-fig. 1). The skull is the only material known for this taxon.

Locality and Horizon. Ilm-valley near Hetschburg, Thuringia, Germany. *Wellenkalk*, Lower Muschelkalk (Lower Anisian, Middle Triassic).

Diagnosis. A relatively small species of *Cymatosaurus* distinguished from all other species by a comparatively long and/or a relatively narrow upper temporal fossa, by the presence of a parietal

sagittal crest, by the anterior extent of the parietals, which reach to a level well in front of the posterior margins of the orbits, and by the fused vomers.

DESCRIPTION

General remarks and measurements. The new species is represented by an incomplete skull with the preorbital region missing due to transverse breakage just in front of the orbits. The basicranium (basisphenoid) is well preserved, but the remainder of the braincase is missing. For reasons discussed below, the skull is interpreted as that of a mature animal, and hence is indicative of a relatively small size for the new species as compared with the other species of *Cymatosaurus* from the Germanic Triassic (the neotype of *Cymatosaurus latifrons* (Gürich, 1884), is considered a juvenile for reasons discussed in Rieppel 1997, and below). Measurements of the specimen are given in Table 1.

Lateral view of skull (Text-fig. 2A). The skull appears moderately depressed, as is characteristic for *Cymatosaurus*. The orbits face dorsolaterally, the upper temporal arch is a delicate structure, and the cheek region is widely open. A fragment of the prefrontal can be located at the anterodorsal margin of the orbit. Its anterior edge is broken, indicating a relatively large dorsal exposure of the prefrontal as is characteristic of *Cymatosaurus*, but unlike *Nothosaurus* where the dorsal exposure of the prefrontal is distinctly reduced. The maxilla forms a relatively high ascending process at the anterior margin of the orbit, again with a broken anterior edge. As in *Nothosaurus*, the lacrimal foramen is located entirely within the maxilla. The maxilla defines most of the ventral edge of the orbit, and meets the jugal at the posteroventral corner of the orbit in a deeply interdigitating suture. The posterior tip of the maxilla is broken, but does not seem to have extended beyond the level of the anterior margin of the upper temporal fossa. The maxillary tooth row does not extend beyond the level of the posterior margin of the orbit, as is characteristic of *Cymatosaurus* (Rieppel 1997). The jugal is a rather broad element with a forked anterior end, one prong narrowly entering the posteroventral margin of the orbit, the second (ventral) prong interdigitating with the maxilla. Dorsally, the jugal contacts the postorbital. Posteroventrally, the jugal contacts the ectopterygoid on the lateral aspect of the prominent pterygoid-ectopterygoid flange. A similar contact of jugal and ectopterygoid is observed in the three dimensionally preserved skull of *Cymatosaurus latifrons* (SMNS 10977; Rieppel 1994*b*, fig. 11), but not in *Nothosaurus* (Rieppel 1993*a*, text-fig. 4), due to the backward extension of the maxilla and the reduction of the jugal.

Below the posterior end of the maxilla and of the jugal, the ectopterygoid gains prominent exposure due to the well developed ectopterygoid-pterygoid flange serving as the origin of the superficial pterygoideus muscle. The insertion of the pterygoid aponeurosis is marked by a distinct ridge on the lateral aspect of the ectopterygoid flange. This ridge creates the impression of a separate element sutured to the lateral aspect of the ectopterygoid-pterygoid flange.

The postorbital defines the posterior margin of the orbit and meets the squamosal in a broadly overlapping suture in the upper temporal arch. The anterior tip of the squamosal remains broadly separated from the jugal, as is characteristic of *Cymatosaurus* (*C. latifrons*, SMNS 10977), but unlike *Nothosaurus*, in which the squamosal closely approaches the jugal (*N. marchicus*: Rieppel and Wild 1996). The posterior end of the squamosal forms a broad flange which descends far down towards the ventral margin of the skull, embracing the tapering dorsal margin of the laterally exposed quadrate. The posterior end of the pterygoid forms an interdigitating suture with the anterior margin of the quadrate, and reaches up to contact the descending flange of the squamosal in front of the quadrate. Behind the laterally exposed quadrate, and below the descending flange of the squamosal, the bone surface is rugose, suggesting the possible presence of a quadratojugal. However, there is no positive evidence for the presence of a quadratojugal in *Cymatosaurus minor*, and the quadratojugal appears absent in the other skulls of *Cymatosaurus* well enough preserved to show structural details (BGR S44/3: Rieppel 1994*a*, fig. 39B).

Dorsal view of the skull (Text-fig. 2B). The prefrontal remains widely separated from the postfrontal along the dorsal margin of the orbit, which is formed by the concave lateral margin of the frontal. The presence or absence of a contact of prefrontal and postfrontal along the dorsal margin of the orbit is highly variable within the species of the genus *Cymatosaurus*, and cannot be used in the diagnosis of separate species (Rieppel 1997). The frontals remain separated (unfused). Their anterior edge is broken, such that the relation of the frontal to the premaxilla, the nasal, and the maxilla cannot be established. A distinct posterolateral lappet of the frontal

TABLE 1. Measurements for *Cymatosaurus minor* sp. nov.; holotype, NHMS-GT21; values in brackets are those of the right side of the skull; all measurements are in mm.

Length of the skull (as preserved)	85·5
Width across the mandibular condyles of the quadrate	52
Width across the posterior ends of the squamosals	27·5
Width across postorbital arches	41
Width at level of anterior margins of orbits	27·5
Width of postorbital arch	4·7 (4·7)
Width of frontal bridge between orbits	7
Longitudinal diameter of orbits	22 (—)
Transverse diameter of orbits	16·5 (17)
Longitudinal diameter of upper temporal fossa	43·9 (44·3)
Transverse diameter of upper temporal fossa	12·5 (11·5)
Longitudinal diameter of pineal foramen	6·3
Transverse diameter of pineal foramen	2·5

extends backwards to a level well beyond the anterior margin of the upper temporal fossa. It does not enter the anteromedial margin of the upper temporal fossa, however, as is the case in *Cymatosaurus fridericianus*, but remains narrowly separated from it by a contact of the postfrontal with the parietal.

The anteromedial margin of the upper temporal fossa is formed by the postfrontal, which also defines the posterodorsal margin of the orbit. Laterally, the postfrontal meets the postorbital in the middle of the postorbital arch, and with an elongate posterior process the postorbital meets the anterior process of the squamosal within the upper temporal arch. The squamosal defines the posterolateral and posterior margin of the upper temporal fossa, and meets the parietal in a slightly interdigitating suture at the posteromedial corner of the fossa.

The parietals remain paired (unfused) in front of the relatively large pineal foramen. A trace of a median suture is retained at the posterior margin of the pineal foramen, beyond which, however, the parietals are fused. The relatively large pineal foramen is located close to the midpoint of the parietal as is typical for *Cymatosaurus*, but not for *Nothosaurus*, where the pineal foramen is displaced backwards. The anterior end of the parietals is forked: a short anterolateral process meets the postfrontal in a narrow suture along the anteromedial margin of the upper temporal fossa, whereas narrow and elongated anteromedial processes of the parietals enter deeply between the posterior lappets of the frontals, reaching to a level in front of the posterior margin of the orbits. This degree of anterior extent of the parietal(s) is not known in other species of *Cymatosaurus*, and hence is a diagnostic feature of *Cymatosaurus minor*. The posterior part of the parietal skull table is elaborated into a narrow sagittal crest, unknown in any other species of *Cymatosaurus*, and hence is another diagnostic character of *Cymatosaurus minor*. The posterior corner of the upper temporal fossa is rounded, and the occiput is deeply excavated in dorsal view, as is characteristic for *Cymatosaurus*.

Ventral view of the skull (Text-fig. 2c). The palate is of typical eusauropterygian structure, with the exception of the fused vomers. The anterior end of the skull is broken just behind the internal nares, whose posterior margins can no longer be identified. However, the broad posterior part of the vomer can be seen to enter deeply between the palatines, meeting the pterygoids in a deeply interdigitating, more-or-less transversely oriented suture which lies level with the anterior end of the ectopterygoid. In other species of *Cymatosaurus*, the vomers remain separate. The palatine is located between the maxilla and vomer anteriorly, and between the ectopterygoid and pterygoid posteriorly. As in other sauropterygians, it appears to form a broad portion of the posterior margin of the internal nares, but it does not participate in the formation of the anterolaterally trending flange which serves as the origin of the superficial pterygoideus muscle. This flange is formed by the posterior end of the ectopterygoid, and the distinct transverse process of the pterygoid.

The pterygoids are paired (unfused) elements which extend backwards to the level of the basioccipital condyle (not preserved), thus covering the entire endocranial skull base in ventral view. The slightly concave lateral margin of the pterygoid defines the medial margin of the subtemporal fossa. Posterolaterally, the pterygoid extends into a distinct quadrate ramus with well-developed ventrolateral and ventromedial flanges

serving as the origin of the deep pterygoideus muscle. A small foramen on the ventral surface of the posterior part of the pterygoid may have served as the exit for a branch of the palatine artery that continued anteriorly in a shallow groove running along the lateral edge of the pterygoid.

Posterolaterally, the pterygoid meets the quadrate in an interdigitating suture. The prominent mandibular condyle of the quadrate, located somewhat behind the level of the occipital condyle (not preserved), shows a bipartite articular surface that would have fitted a saddle-shaped articular surface on the mandible.

Posterior view of the skull (Text-fig. 3A). The squamosal has a broad occipital exposure which meets the broad occipital exposure of the quadrate in a ventrolaterally trending suture. The braincase is missing, and must have dropped out from the dermatocranial framework before the skull was buried by sediment. Due to the reduction of the posterior skull table to a sagittal crest, the occipital exposure of the parietal is restricted to a narrow strip of bone located between the broad squamosals. The parietal broadens ventrally, but the ventral margin of the occipital exposure of the parietal is deeply concave, forming a notch which must have received the supraoccipital. The smooth edge of the parietal along this notch suggests that the supraoccipital was not fused to the parietal, but that the two bones met in a rather loose connection, much as in a metakinetic skull. Lateral to the parietal, the ventral margin of the occipital exposure of the squamosal shows a shallow yet distinct embayment (on both sides of the skull) with a smooth finished margin, representing the dorsal margin of a distinct notch which is also observed in other, adequately preserved *Cymatosaurus* skulls (BGR S44/3: Rieppel 1994*a*, fig. 39B). Further preparation of the holotype of *Corosaurus alcovensis*, from the Mid Triassic Alcova Limestone of Casper, Wyoming (Storrs 1991), revealed a similar notch in the squamosal, which receives the distal tip of the (articulated) paroccipital process in a loose articulation. A similar arrangement may be assumed to have been present in *Cymatosaurus*. The loose connection of the braincase with the dermatocranium explains why the otico-occipital segment is missing in all known *Cymatosaurus* skulls. This contrasts with pachypleurosaurs, *Simosaurus* and the *Nothosaurus–Lariosaurus* clade, in which the occiput is closed and plate-like, and the braincase is fused with the dermatocranium.

The basicranium (Text-fig. 3B). The skull described here is remarkable for its preservation of the basicranium which indicates that in spite of a loose suspension of the otico-occipital segment (supraoccipital, paroccipital process) from the parietal unit (parietal, squamosal), the palatobasal articulation was fused in *Cymatosaurus*, as in all other Sauropterygia, and the skull thus was akinetic. A rugose surface of unfinished bone on the posteromedial part of the pterygoid indicates the sutural facet for the basioccipital which, although not preserved here, forms the occipital condyle in other *Cymatosaurus* skulls (BGR S44/3: Rieppel 1994*a*, fig. 39B). In front of the sutural facet for the basioccipital, the sella turcica rises as a shallow yet prominent feature, separated in two halves by a distinct longitudinal furrow. Each half assumes the shape of an elevated oval platform. In front of the sella turcica lies the deeply recessed, narrow and elongated fossa hypophyseos with paired foramina in its posteriormost part, serving as the exit for the cerebral carotids. The cerebral carotids continued anteriorly in deep grooves within the fossa hypophyseos, separated from one another by a distinct ridge or septum, longitudinally subdividing the fossa hypophyseos. In front of the fossa hypophyseos, the bone surface is slightly damaged, but more anteriorly a distinct yet narrow longitudinal ridge is observed, running anteriorly on the dorsal surface of the pterygoids. This ridge must have supported the trabecula communis (the fused trabeculae cranii), which indicates a tropibasic skull.

Anterolateral to the sella turcica, rudiments of the epipterygoid are preserved on both sides of the skull. The epipterygoid has a broad base sutured to the dorsal surface of the pterygoid, but seems to have extended dorsally into a narrow strut, as both its anterior and posterior margins are strongly concave. A canal running between the sella turcica and the epipterygoid represents the cavum epiptericum, and must have accommodated the lateral head vein. This vein must have entered the cavum epiptericum through a deep recess or foramen located between the lateral margin of the pterygoid and the overhanging margin of the raised sutural facet on the pterygoid which received the basioccipital.

Of special interest are the grooves exposed on the posterodorsal surface of the quadrate ramus of the pterygoids, and bridging the transition from the smooth bone surface to the unfinished surface of the basioccipital facet. In the complete skull, these grooves served as the entry of the internal carotid into the basicranium, and must have opened on the posterodorsal surface of the quadrate ramus of the pterygoid half way between the basioccipital anteromedially and the quadrate posterolaterally. From there, the canal continued anteriorly to enter the sutural interface between the pterygoid and basioccipital, now exposed as a groove on the sutural surface of the pterygoid which received the basioccipital. More anteriorly, the canal pierces the basisphenoid to pass below the sella turcica, where it subdivides. The medial branch opens into the posterior part of the fossa hypophyseos, and served as the passage for the cerebral carotid into the brain cavity.

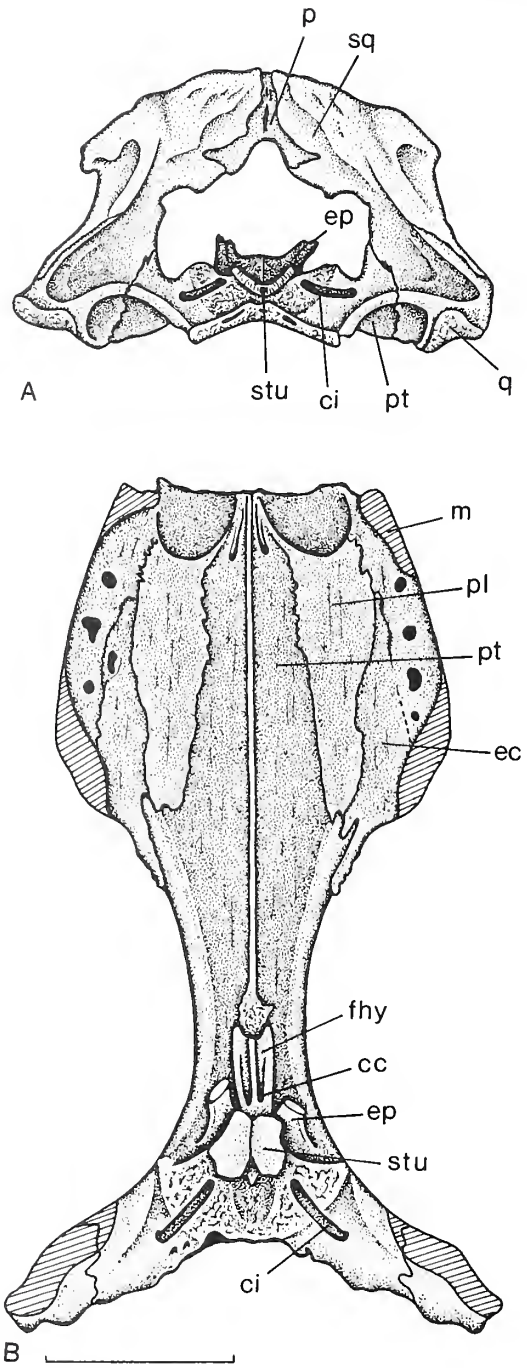

TEXT-FIG. 3. The skull of *Cymatosaurus minor* sp. nov. A, occipital view; B, dorsal view of basicranium. Scale bar represents 20 mm. Abbreviations: cc, foramen for cerebral carotid; ci, canal for internal carotid; ec, ectopterygoid; ep, epipterygoid; fhy, fossa hypophyseos; m, maxilla; p, parietal; pl, palatine; pt, pterygoid; q, quadrate; stu, sella turcica; sq, squamosal.

The lateral branch carried the palatine artery. The same unusual course of the internal carotid artery, piercing the quadrate ramus of the pterygoid and passing between pterygoid and basisphenoid on its way to the fossa hypophyseos, was previously reported for the eosauropterygian genera *Simosaurus* and *Nothosaurus* (Rieppel 1994*b*).

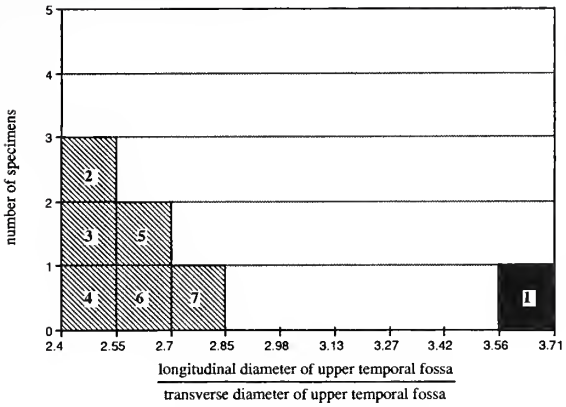

TEXT-FIG. 4. The relation of the longitudinal diameter to the transverse diameter of the upper temporal fossa in *Cymatosaurus*. The numbers refer to the following specimens: 1, *Cymatosaurus minor*, 2, 'specimen I' of *Cymatosaurus gracilis* described by Schrammen (1899; data taken from the literature); 3, 'specimen I' of *Cymatosaurus silesiacus* described by Schrammen (1899; data taken from the literature); 4, holotype of *Cymatosaurus fridericianus* von Fritsch, 1894; 5, neotype for *Cymatosaurus latifrons* (SMNS 10109; 'specimen II' of *Cymatosaurus gracilis* described by Schrammen 1899); 6, incomplete skull; BGR S44/3; 7, skull; SMNS 109877.

Skull proportions. The incomplete nature of the skull renders the assessment of a number of skull proportions impossible. In particular, *Cymatosaurus* (and *Germanosaurus*) have been shown to differ from *Nothosaurus* by a relatively more anterior position of the internal nares (Rieppel 1996), a character which cannot be ascertained for *Cymatosaurus minor*. Dividing the longitudinal diameter of the temporal fossa by the longitudinal diameter of the orbit yields a quotient of 1·3–2·0 for *Cymatosaurus* (including all skulls described in the literature, as well as the skull of *Cymatosaurus minor*), 1·87 for the only known skull of *Germanosaurus*, and 2·1–3·9 for *Nothosaurus* (all skulls deposited in public repositories). As this quotient is correlated with the relative size of the orbit and, therefore, with allometric growth of the orbit, further comments on its utility in taxonomic studies are in order.

The neotype for *Cymatosaurus latifrons* (Gürich, 1844) is the 'second specimen' referred to by Schrammen (1899) in his description of *Cymatosaurus gracilis* (SMNS 10109; see Rieppel 1997 for further discussion). In view of its relatively small size (skull length: 98 mm) relative to other skulls referred to the same species, the specimen may be considered to represent a juvenile. Indeed, the ratio of the longitudinal diameter of the upper temporal fossa to the longitudinal diameter of the orbit is 1·3, indicating relatively large orbits. In the holotype of *Cymatosaurus fridericianus* von Fritsch, 1894 (a large specimen with a skull length of 195 mm), the corresponding ratio is 1·9. The skull of *Cymatosaurus minor* is incomplete, but the specimen can be estimated to be somewhat larger than the neotype of *Cymatosaurus latifrons*, yet it is distinctly smaller than the holotype of *Cymatosaurus fridericianus*, and the corresponding ratio is 2·0. This indicates a relatively smaller orbit, or a relatively longer upper temporal fossa, but the high quotient (2·0, as compared to 1·3 for the juvenile neotype of *Cymatosaurus latifrons*) does not indicate a juvenile status.

The most significant relationship is the longitudinal diameter of the upper temporal fossa divided by its transverse diameter. The ratio for all the skulls of *Cymatosaurus* described in the literature ranges from 2·4 to 2·8, but it is 3·68 for *Cymatosaurus minor*. This indicates that *Cymatosaurus minor* has a comparatively long and narrow upper temporal fossa (Text-fig. 4), another diagnostic character of this new species.

DISCUSSION

Cymatosaurus minor is the smallest species of the genus in which the skull is known; the only species smaller than *Cymatosaurus minor*, if represented by an adult individual, is *Cymatosaurus multidentatus* (see Rieppel 1995*a* for a complete description). This raises the question of whether *Cymatosaurus minor* is represented by an adult individual. Whereas the orbit usually exhibits negative allometry with respect to skull length in sauropterygians, the relative size of the orbit is not indicative of a juvenile status of the holotype of *Cymatosaurus minor*. The adult status of the holotype of *Cymatosaurus minor* is further supported by the fusion of the vomers, and by the fusion of the parietals in their posterior part. Moreover, extant reptiles, which in the adult feature a sagittal crest, show a flat and broad parietal skull table in early developmental stages (*Sphenodon*: Rieppel 1992; *Chamaeleon*: Rieppel 1993*b*).

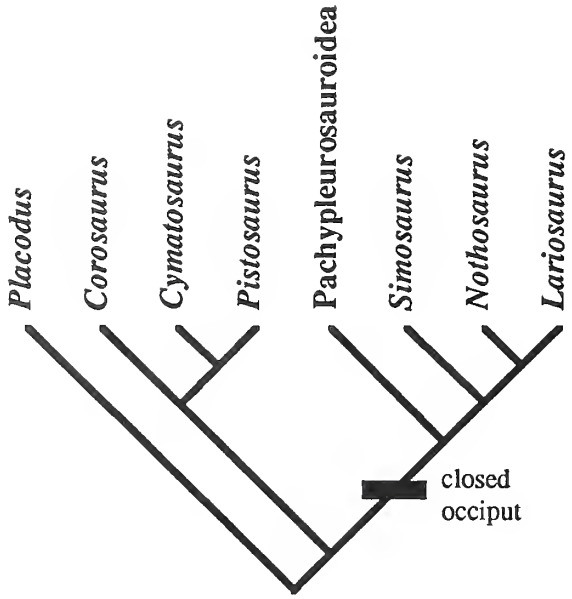

TEXT-FIG. 5. The phylogeny of stem-group Sauropterygia based on cladistic analysis (see Rieppel 1997 for further discussion).

All of the skulls of *Cymatosaurus* currently accessible in public repositories (see Rieppel 1997) lack the posterior neurocranial elements, in particular the supraoccipital, the otic capsules, and the exoccipitals (the otico-occipital segment). In view of the exceptional preservation and preparation of the holotype of *Cymatosaurus minor*, and of the fact that it is represented by an adult individual, the loss of the otico-occipital segment in this specimen cannot be attributed to incomplete ossification in an immature specimen. In generalized reptiles, the skull is metakinetic, with the supraoccipital loosely connected to the parietal (as in *Cymatosaurus*), and the paroccipital process, composed of the opisthotic and exoccipital, loosely abutting against the quadrate suspension (against the squamosal in *Cymatosaurus*). This is not to say that *Cymatosaurus* retained a functionally metakinetic skull; only that it is less derived from the more generalized reptile skull than the skulls of pachypleurosaurs and nothosaurs in that it retains paroccipital processes in loose articulation with the dermatocranium, a loose connection of the supraoccipital with the parietal, and in all likelihood, a small but well-defined posttemporal fossa. Preservation of the endocranial basicranium, solidly fused to the underlying pterygoids, indicates complete fusion of the palatobasal articulation in *Cymatosaurus*, a prerequisite for metakinesis in a more generalized reptile skull. Closure of the dermal palate and fusion of the palatobasal articulation would therefore seem to have preceded fusion of the otico-occipital segment to the dermatocranium in the loss of metakinesis during the evolution of Sauropterygia. Alternatively, and depending on the phylogenetic interrelationships of *Cymatosaurus* and its fossil relatives, the open occiput might have to be considered a secondary development due to character reversal.

A distinct paroccipital process defining the ventral margin of a well defined posttemporal fossa (of variable size) is present in *Placodus* (Rieppel 1995*b*), *Corosaurus* (Storrs 1991; pers. obs.), and *Pistosaurus* (Edinger 1935) among Triassic stem-group Sauropterygia, and is also the pattern observed in plesiosaurs and pliosaurs (Brown 1981; Taylor 1992; Taylor and Cruickshank 1993). The previous revision of the genus (Rieppel 1997) showed *Cymatosaurus* to be the sister-taxon of *Pistosaurus*, supporting the concept of the Pistosauria proposed by Sanz (1983; see also Sues 1987; Storrs 1991, 1993; Alafont and Sanz 1996). *Pistosaurus*, on the other hand, has traditionally been interpreted as a sister-group or 'structural ancestor' of the Plesiosauroidea (Carroll and Gaskill 1985; Sues 1987; Storrs 1991). Indeed, both *Pistosaurus* (Edinger 1935) and plesiosaurs share the following characters: an open occiput with a well defined paroccipital process and a large

TEXT-FIG. 6. The stratigraphical distribution of the genus *Cymatosaurus* in the German Triassic.

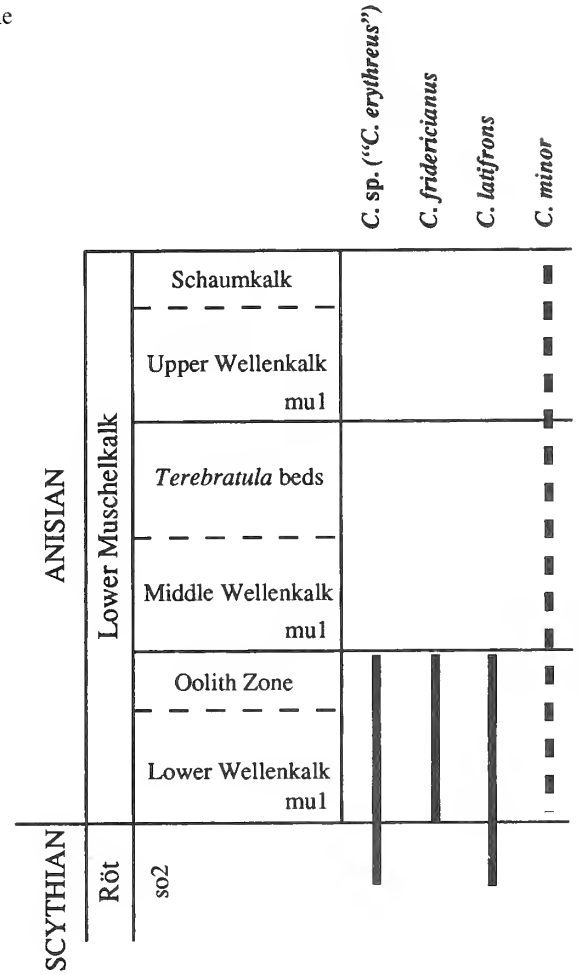

posttemporal fenestra, and a fused palatobasal articulation. The most recent cladistic analysis of the phylogenetic relationships of Sauropterygia (Rieppel 1997, based on 23 taxa and 119 characters) indicates a basal dichotomy within the Eosauropterygia, of which *Placodus* is the sister-group (Text-fig. 5). The one eosauropterygian lineage comprises *Corosaurus*, *Cymatosaurus*, *Pistosaurus* and, by extension, the plesiosaurs and pliosaurs. The second lineage comprises pachypleurosaurs, *Simosaurus* and the nothosaurs (*Germanosaurus*, *Nothosaurus* and *Lariosaurus*) (Text-fig. 5). Based on this pattern of relationships, closure of the occiput and fusion of the otico-occipital segment with the dermatocranium appears to be a synapomorphy of the second lineage, whereas the open occiput represents the generalized condition where it occurs among the Eosauropterygia. However, Testudines also show the fusion of the otico-occipital segment with the dermatocranial unit, and, as long as they continue to be found as the sister-group of the Sauropterygia, the interpretation of the status of the open occiput in the Eosauropterygia (generalized condition or secondarily derived) must remain equivocal.

Assuming that the otico-occipital segment fused with the dermatocranium independently in turtles, closure of the dermal palate and fusion of the palatobasal articulation would be the first step in the evolution of the akinetic skull of Sauropterygia. This development resulted in the derived condition, wherein the internal carotid passed through the basicranium. The entry of the internal

carotid into the quadrate ramus of the pterygoid, and its passage through the pterygoid-basioccipital suture on its way to the fossa hypophyseos, has previously been reported for the eosauropterygian genera *Simosaurus* and *Nothosaurus* (Rieppel 1994*b*), and is here documented for *Cymatosaurus*. Unfortunately, the pathway of the internal carotid is unknown in *Corosaurus*, pachypleurosaurs and lariosaurs (lack of adequate preservation), whereas the internal carotid follows the more generalized path through the cranioquadrate passage in *Placodus*, where the relationship of the basicranium to the dermal palate is drastically different (Rieppel 1995*b*). Unfortunately, lack of knowledge precludes any conclusion, at the present time, at which level of generality the derived course of the internal carotid would be synapomorphic within the Eosauropterygia.

Our current understanding of sauropterygian phylogeny and palaeobiology indicates that the clade entered the Germanic Basin during the period of deposition of the uppermost Buntsandstein and lowermost Muschelkalk (Lower Anisian) through an eastern gateway (Rieppel and Hagdorn 1986; Rieppel 1997). The genus *Cymatosaurus* diversified within the Germanic Basin, giving rise to three species (*C. fridericianus*, *C. latifrons*, and *C. minor*), but at the top of the Lower Muschelkalk, the genus disappears from the fossil record. Looking in more detail at the stratigraphical distribution of *Cymatosaurus* as documented by diagnostic cranial material (Text-fig. 6), its first occurrence is in the uppermost Buntsandstein of Rüdersdorf near Berlin ('*C. erythreus*': E. von Huene 1944) and Jenzig near Jena (SMNS 19077, referred to *C. latifrons*: Rieppel 1997). Most of the skull material comes from the Gogolin beds of Upper Silesia. Unfortunately, the exact stratigraphical correlation within the Lower Muschelkalk remains unknown for the skull of *Cymatosaurus minor*. Probable younger occurrences of the genus in the Germanic basin are documented by an isolated neural arch (MHI 1293/1), associated (but not articulated) with a centrum (MHI 1293/2), from the upper Lower Muschelkalk (*Spiriferina*-Bank, *decurtata* biozone) of Hettingen near Buchen, Badenia (Rieppel and Hagdorn 1996), and by a humerus from the *Schaumkalk* (uppermost Lower Muschelkalk) of Freyburg/Unstrut (Rieppel 1994*a*, fig. 57B). All the diagnostic *Cymatosaurus* material comes from the eastern part of the Germanic Basin, with the exception of the isolated vertebra from Badenia mentioned above (southern part of the Germanic Basin), and an isolated humerus from the Lower Muschelkalk of Winterswijk, Netherlands (western part of the Germanic basin), again probably referable to *Cymatosaurus* (Rieppel 1994*b*, fig. 57A).

The stratigraphical and geographical distribution of *Cymatosaurus* compares in an interesting way with the stratigraphical and geographical distribution of the genus *Nothosaurus*, which first appears in the Upper Buntsandstein ('*N. schimperi*' from Soultz-les-Bains, Alsace (France): von Meyer 1847–55; the specimen is now lost), and which is represented by rare and fragmentary material in the lower Gogolin beds (Kunisch 1888) of Upper Silesia (eastern part of the Germanic basin). Well preserved material of *Nothosaurus* comes from the Lower Muschelkalk of Winterswijk, Netherlands (Oosterink 1986), i.e. from strata of the western part of the Germanic basin which are geologically somewhat younger than Lower Muschelkalk deposits in the eastern part of the Germanic Basin (Rieppel and Hagdorn 1996). But, whereas the Lower Muschelkalk of Winterswijk yielded a fair abundance of *Nothosaurus* material (undescribed specimens in private collections), the possible occurrence of *Cymatosaurus* in that locality is documented only by an isolated humerus (Rieppel 1994*a*, text-fig. 57A; Rieppel and Lin 1995). In the eastern part of the Germanic basin, the fossil record of the genus *Nothosaurus* starts to improve in the uppermost Lower Muschelkalk (*Schaumkalk*) and lowermost Middle Muschelkalk (*orbicularis*-beds, now attributed to the Middle Muschelkalk) with a fair abundance of *Nothosaurus marchicus* (Rieppel and Wild 1996). Relatively large remains (undescribed) of *Nothosaurus* in the Schaumkalk deposits of Freyburg/Unstrut, as well as a specimen (MB.I.007.16, possibly referable to *N. mirabilis*) from the lower Middle Muschelkalk of Oberdorla, document the existence, at that time, of a second species of *Nothosaurus*, again in the eastern part of the Germanic Basin (Rieppel and Wild 1996). The frequency of occurrence of *Nothosaurus* in the eastern part of the Muschelkalk Basin, therefore, increased significantly at a time only (transition from the Lower to the Middle Muschelkalk) when the occurrence of *Cymatosaurus* had already declined. Also, the taxonomic diversification of the genus

Nothosaurus, most notable in the Upper Muschelkalk and beyond, occurred at a time when *Cymatosaurus* had become rare or extinct.

Given the provision that fragmentary sauropterygian remains from the Lower Muschelkalk are sometimes difficult or even impossible to identify, it appears on the basis of abundant material from well sampled localities (lower Lower Muschelkalk: Gogolin (Upper Silesia), Halle/Saale; Lower Muschelkalk: Winterswijk (Netherlands); upper Lower Muschelkalk: Freyburg/Unstrut, Rüdersdorf; lower Middle Muschelkalk: Rüdersdorf, Esperstädt, Jena, Querfurt), that the coexistence of *Cymatosaurus* and *Nothosaurus* was limited, and that the abundance and taxonomic diversity of *Nothosaurus* increased only in the absence of *Cymatosaurus*. This correlation possibly reflects the similar ecological requirements of the two genera. Indeed, the skull morphology of *Cymatosaurus* and early *Nothosaurus* (Winterswijk material, as well as *N. marchicus*) is very similar: both genera share an elongated and constricted rostrum bearing a procumbent dentition, the presence of maxillary fangs, and an elongated postorbital region of the skull characteristic of a dual jaw adductor system (Rieppel 1989, 1994*a*). Apart from the anatomical details pointed out in the descriptive section above, the main morphological changes distinguishing the genus *Nothosaurus* from *Cymatosaurus* are an increase in absolute size (in two species, *N. mirabilis* and *N. giganteus*), a further depression of the postorbital region of the skull, further relative elongation of the postorbital skull (dividing the distance from the tip of the snout to the posterior end of the parietal skull table by the distance from the tip of the snout to the posterior margin of the orbit yields a ratio of 1·4 for *Cymatosaurus*, and 1·7–2·1 for *Nothosaurus*), and the posterior extension of the maxillary tooth row beyond the level of the anterior margin of the upper temporal fossa. Further depression of the increasingly elongated postorbital skull required further differentiation of the dual jaw adductor system (Rieppel 1989), which, together with an elongated tooth row, may indicate increased efficiency of feeding mechanics in *Nothosaurus*.

Acknowledgements. A number of colleagues granted generous access to the collections in their care, and allowed us to make the necessary comparisons for our study: H. U. Schlüter, Bundesanstalt für Geowissenschaften und Rohstoffe, Berlin; H. Haubold, Institut für Geowissenschaften, Martin-Luther-Universität, Halle/Saale; H. Hagdorn, Ingelfingen; G. Kaufmann, Fachbereich Geowissenschaften, Philipps Universität, Marburg/ Lahn; G. Höck, Naturhistorisches Museum, Vienna; and R. Wild, Staatliches Museum für Naturkunde, Stuttgart. The comparative material is listed in Rieppel (1997). This study was supported by NSF-grants DEB-9220540 and DEB-9419675 (to OR).

REFERENCES

ALAFONT, L. S. and SANZ, J. J. 1996. Un nuevo Sauropterigio (Reptilia) en el Triasico de la Sierra de Prades (Tarragona). *Cuadernos de Geologia Iberica*, **20**, 313–329.

BROWN, D. S. 1981. The English Upper Jurassic Plesiosauroidea (Reptilia) and a review of the phylogeny and classification of the Plesiosauria. *Bulletin of the British Museum (Natural History), Geology Series*, **35**, 253–347.

CARROLL, R. L. and GASKILL, P. 1985. The nothosaur *Pachypleurosaurus* and the origin of plesiosaurs. *Philosophical Transactions of the Royal Society of London, Series B*, **309**, 343–393.

EDINGER, T. 1935. *Pistosaurus. Neues Jahrbuch für Mineralogie, Geologie, und Paläontologie, Abhandlungen*, **74**, *Beilageband*, 321–359.

FRITSCH, K. von 1894. Beitrag zur Kenntnis der Saurier des Halle'schen unteren Muschelkalkes. *Abhandlungen der Naturforschenden Gesellschaft zu Halle*, **20**, 273–302.

GÜRICH, G. J. E. 1884. Über einige Saurier des Oberschlesischen Muschelkalkes. *Zeitschrift der Deutschen Geologischen Gesellschaft*, **36**, 125–144.

—— 1891. Über einen neuen *Nothosaurus* von Gogolin, Oberschlesien. *Zeitschrift der Deutschen Geologischen Gesellschaft*, **43**, 967–970.

HAAS, G. 1963. *Micronothosaurus stensiöi*, ein neuer Nothosauride aus dem Oberen Muschelkalk des Wadi Ramon, Israel. *Paläontologische Zeitschrift*, **37**, 161–178.

HUENE, E. von 1944. *Cymatosaurus* und seine Beziehungen zu anderen Sauropterygiern. *Neues Jahrbuch für Mineralogie, Geologie und Paläontologie, Monatshefte, Abteilung B*, **1944**, 192–222.

HUENE, F. von 1948. Short review of the lower tetrapods, 65–106. *In* DUTOIT, A. L. (ed.). *Robert Broom Commemorative Volume. Special Publication of the Royal Society of South Africa*. Royal Society of South Africa, Cape Town. v + 257 pp.

—— 1958. Aus den Lechtaler Alpen ein neuer *Anarosaurus*. *Neues Jahrbuch für Geologie und Paläontologie, Monatshefte*, **1958**, 382–384.

JAEKEL, O. 1911. *Die Wirbeltiere*. Gebrüder Bornträger, Berlin, viii + 252 pp.

KOKEN, E. 1893. Beiträge zur Kenntnis der Gattung *Nothosaurus*. *Zeitschrift der Deutschen Geologischen Gesellschaft*, **45**, 337–377.

KUNISCH, H. 1888. Ueber eine Saurierplatte aus dem oberschlesischen Muschelkalke. *Zeitschrift der Deutschen Geologischen Gesellschaft*, **40**, 671–693.

MEYER, H. von 1847–1855. *Zur Fauna der Vorwelt. Die Saurier des Muschelkalkes mit Rücksicht auf die Saurier aus buntem Sandstein und Keuper*. Heinrich Keller, Frankfurt a.M., viii + 167 pp.

OOSTERINK, H. W. 1986. Winterswijk, geologie deel II. De Trias-periode (geologie, mineralen en fossielen). *Wetenschappelijke Mededelingen van de Koninklijke Nederlandse Natuurhistorische Vereniging*, **178**, 1–120.

OWEN, R. 1860. *Palaeontology; or, a systematic summary of extinct animals and their geologic remains*. Adam and Charles Black, Edinburgh, xv + 420 pp.

RIEPPEL, O. 1989. A new pachypleurosaur (Reptilia: Sauropterygia) from the Middle Triassic of Monte San Giorgio, Switzerland. *Philosophical Transactions of the Royal Society of London, Series B*, **323**, 1–73.

—— 1992. The skull in a hatchling of *Sphenodon punctatus*. *Journal of Herpetology*, **26**, 80–84.

—— 1993*a*. The status of the nothosaurian reptile *Ehmosaurus lehmensis*, with comments on *Nothosaurus mirabilis* Münster, 1834 (Reptilia, Sauropterygia). *Palaeontology*, **36**, 967–974.

—— 1993*b*. Studies on skeleton formation in reptiles. II. The postembryonic development of the skeleton in *Chamaeleo hoehnelii* (Reptilia: Chamaeoleoninae). *Herpetologica*, **49**, 66–78.

—— 1994*a*. Osteology of *Simosaurus* and the interrelationships of stem-group Sauropterygia (Reptilia, Diapsida). *Fieldiana (Geology), New Series*, **28**, 1–85.

—— 1994*b*. The braincases of *Simosaurus* and *Nothosaurus*: monophyly of the Nothosauridae (Reptilia: Sauropterygia). *Journal of Vertebrate Paleontology*, **14**, 9–23.

—— 1995*a*. The status of *Anarosaurus multidentatus* Huene (Reptilia, Sauropterygia), from the Lower Anisian of the Lechtaler Alps (Arlberg, Austria). *Paläontologische Zeitschrift*, **69**, 287–297.

—— 1995*b*. The genus *Placodus*: systematics, morphology, paleobiogeography, and paleobiology. *Fieldiana (Geology), New Series*, **31**, 1–44.

—— 1995*c*. Fragmenta Sauropterygiana. *Neues Jahrbuch für Geologie und Paläontologie, Abhandlungen*, **197**, 383–397.

—— 1997. Revision of the sauropterygian reptile genus *Cymatosaurus* von Fritsch, 1894, from the Middle Triassic of Europe, and the relationships of *Germanosaurus* Nopcsa, 1928, from the Middle Triassic of Europe. *Fieldiana (Geology), New Series*, **36**, 1–38.

—— and HAGDORN, H. 1996. Paleobiogeography of Middle Triassic Sauropterygia in Central and Western Europe, with comments on the status of *Proneusticosaurus* Volz 1902. 121–144. *In* NICHOLLS, E. L. and CALLAWAY, J. M. (eds). *Sea reptiles of the past*. Academic Press, San Diego. xlvi + 501 pp.

—— and LIN, K. 1995. Pachypleurosaurs (Reptilia: Sauropterygia) from the Lower Muschelkalk, and a review of the Pachypleurosauroidea. *Fieldiana (Geology), New Series*, **32**, 1–44.

—— and WILD, R. 1996. A revision of the genus *Nothosaurus* (Reptilia, Sauropterygia) from the Germanic Triassic, with comments on the status of *Conchiosaurus clavatus*. *Fieldiana (Geology), New Series*, **34**, 1–82.

SANZ, J. L. 1983. Consideraciones sobre el genero *Pistosaurus*. El suborden Pistosauria (Reptilia, Sauropterygia). *Estudios geologicos*, **39**, 451–458.

SCHRAMMEN, A. 1899. 3. Beitrag zur Kenntnis der Nothosauriden des unteren Muschelkalkes in Oberschlesien. *Zeitschrift der Deutschen Geologischen Gesellschaft*, **51**, 388–408.

STORRS, G. W. 1991. Anatomy and relationships of *Corosaurus alcovensis* (Diapsida: Sauropterygia) from the Triassic Alcova Limestone of Wyoming. *Bulletin of the Peabody Museum of Natural History*, **44**, 1–151.

—— 1993. The systematic position of *Silvestrosaurus* and a classification of Triassic sauropterygians (Neodiapsida). *Paläontologische Zeitschrift*, **67**, 177–191.

SUES, H.-D. 1987. Postcranial skeleton of *Pistosaurus* and interrelationships of the Sauropterygia (Diapsida). *Zoological Journal of the Linnean Society*, **90**, 109–131.

TAYLOR, M. A. 1992. Functional anatomy of the head of the large aquatic predator *Rhomaleosaurus zetlandicus* (Plesiosauria, Reptilia) from the Toarcian (Lower Jurassic) of Yorkshire, England. *Philosophical Transactions of the Royal Society of London, Series B*, **335**, 247–280.

—— and CRUICKSHANK, A. R. I. 1993. Cranial anatomy and functional morphology of *Pliosaurus brachyspondylus* (Reptilia: Plesiosauria) from the Upper Jurassic of Westbury, Wiltshire. *Philosophical Transactions of the Royal Society of London, Series B*, **341**, 399–418.

OLIVIER RIEPPEL
Department of Geology
The Field Museum
Roosevelt Road at Lake Shore Drive
Chicago, IL 60605-2496, USA

RALF WERNEBURG
Naturhistorisches Museum
Schloss Bertholdsburg
Postfach 44
D98553 Schleusingen
Germany

Typescript received 13 August 1996
Revised typescript received 31 May 1997

FIRST COMPLETE FOREFIN OF THE ICHTHYOSAUR *GRIPPIA LONGIROSTRIS* FROM THE TRIASSIC OF SPITSBERGEN

by RYOSUKE MOTANI

ABSTRACT. A new and nearly complete forefin has been discovered on a slab containing a specimen of the ichthyosaur *Grippia longirostris*. It is the only well-articulated forefin of this poorly known species, and is one of the most complete forefins known for the earliest ichthyosaurs from the Lower Triassic (Spathian). Contrary to the proposals of previous authors, the terminal phalanges did not support 'hooves'. The forefin resembles that of *Utatsusaurus hataii*, another Spathian ichthyosaur, but is more derived, sharing four synapomorphies with *Mixosaurus cornalianus*, a slightly younger ichthyosaur from the Middle Triassic. Ichthyosaurian forefins, described from British Columbia and assigned to *Grippia*, lack at least two of these synapomorphies, and thus do not belong to this genus. A 'partial hindfin' of *Grippia*, also from British Columbia, is similar to the new forefin, casting doubt on its identification as a hindfin.

THE earliest ichthyosaur species are found in the Lower Triassic (Spathian; Callaway and Massare 1989), with *Grippia longirostris* from Spitsbergen (Wiman 1929, 1933) the first to have been described. Although additional Spathian genera, including *Chaohusaurus* Young and Dong, 1972, *Utatsusaurus* Shikama, Kamei and Murata, 1978 and *Chensaurus* Mazin, Suteethorn, Buffetaut, Jaeger, and Helmcke-Ingavat, 1991 (= *Anhuisaurus* Chen, 1985, which was preoccupied), have subsequently been described, studies of early ichthyosaurs have been biased towards *G. longirostris* (Mazin 1981, 1982, 1986; Callaway 1989; Massare and Callaway 1990). However, this species is known only from fragmentary materials (Wiman 1933; Mazin 1981; Motani 1997*a*), which restricted previous authors to speculative reconstructions of the skull and the forefin. Because the understanding of basal forms is important to phylogenetic systematics, the incompleteness of *G. longirostris* has been a major impediment to the study of ichthyosaurian evolution.

Forefins are among the most informative structures for ichthyosaurian systematics (McGowan 1991), but are poorly known for *Grippia longirostris*. Wiman's (1929) first description of the species was based upon one specimen, a skull with mandibles, but lacking the snout. Preserved between the mandibular rami was an isolated, key-hole-shaped fin element, which Wiman (1929) believed was an ungual phalanx. A later expedition to Spitsbergen brought back additional specimens (Wiman 1933), but none was complete. The best preserved forefin material comprised the proximal part of a fin, complete as far as the level of the distal carpals (Wiman 1933, nodule 8); the other specimens were mainly composed of isolated elements. In the absence of a complete forelimb, Wiman (1933) maintained his earlier claim for ungual phalanges, arguing that *G. longirostris* retained a limb that was not as well adapted to the aquatic environment as the fins of later ichthyosaurs. Almost half a century later and without any additional material, Mazin (1981) published a reconstruction of the forelimb of *G. longirostris*, in which, following Wiman's (1929) supposition, he depicted a limb with a 'hoof' at the tip of each digit. Mazin (1986) further argued that *G. longirostris* was more primitive than *Utatsusaurus hataii*, another Spathian ichthyosaur, based on the supposed possession of fewer adaptations in the forelimbs for an aquatic lifestyle.

A close examination of Wiman's (1933) nodule 8 revealed an undescribed humerus, lying beside the described one. The subject of the present paper is to report a new, well-articulated forefin discovered distal to this humerus.

[Palaeontology, Vol. 41, Part 4, 1998, pp. 591–599]

MATERIALS AND METHODS

Abbreviations used for the institutions are: BMNH, Natural History Museum, London; PMU, Paleontologiska Museet, Uppsala Universitet, Uppsala, Sweden; and RTMP, Royal Tyrrell Museum of Paleontology, Drumheller, Alberta. The principal specimen described in this study, which Wiman (1933) called nodule 8, is now registered as PMU R472. Reference is also made to specimens of *Grippia longirostris*, including PMU R447, R449, R453, R456, and R474 (nodules 11, 5, 7, 15, and 9 respectively, of Wiman 1933). Localities for the specimens are summarized in Wiman (1933). Canadian specimens referred to *Grippia* (Brinkman *et al.* 1992) include RTMP 89.127.3, 89.127.12, and 89.128.5, and were also examined. Hindfins of *Mixosaurus cornalianus* (BMNH R5702) and *M. nordenskioeldii* (PMU R158) were used for comparison.

Only the middle part of PMU R472, where the new fin is located, was prepared, to preserve as much of this historically important specimen as possible. Preparation was performed under a binocular microscope, using an airscriber and mounted needles. Acid preparation, using 10 per cent. acetic acid, proved unsuccessful. A CT-scanner (General Electric Advantage Hispeed) was used to locate the hidden forefin before preparation. Scans with a thickness of 1 mm were made at 1 mm intervals, and used to reconstruct the two-dimensional image of the hidden forefin on a computer. This image was utilized during the preparation process, in order to reduce the risk of damaging the bones.

DESCRIPTION

A partial forefin, originally exposed along the circular edge of PMU R472 (Text-fig. 1), was figured by Wiman (1933, pl. 2, fig. 2). The bones are weathered, some badly, and the distal part of the fin is not preserved. The newly discovered forefin is located on the right side of this fin (Text-fig. 1). The humerus, radius, ulna, pisiform, and fifth metacarpal were also partially exposed, and suffered from the same weathering that damaged the other fin. The pisiform and the fifth metacarpal have been further damaged by a crack which runs through the middle of the slab (Text-fig. 1); this has been filled with plaster, probably during Wiman's study. The two forefins are nearly equal in size, and are associated with an articulated vertebral column and gastralia: thus they most probably belong to the same individual. The new forefin underlies the original one, with the gastralia lying in between them. Because the leading edges of both forefins are towards the left-hand side, the newly exposed one is interpreted as the right forefin, visible in the ventral view, whilst the other is the left forefin, exposed dorsally.

The description in the following paragraphs is based on the right forefin of PMU R472, unless otherwise stated. The forefin is pentadactyl, with a preserved phalangeal formula of 2-4-5-5-2. Distal elements may be missing from digits one, two and five, but, judging from the small size of the preserved bones, this probably does not amount to more than one element per digit. The fifth phalanges of digits three and four are so small that they are likely to be the terminal elements. If this is correct, then there were no more than five phalangeal ossifications in any of the digits. This does not preclude the possibility, however, of further unossified phalanges distal to the ossified elements. All manual elements are well spaced from each other, in contrast to the forefin of *Utatsusaurus* where elements are more closely packed (Motani 1997*b*).

Both humeri of PMU R472 are badly eroded, and only their outlines can be observed. The humerus is as wide as it is long (Text-fig. 1), largely due to a well-developed articular facet for the radius, and a bony flange anterior to the shaft. Wiman (1933) figured two variations for the anterior flange on the humerus of *Grippia longirostris*: one is well developed (PMU R474), and the other is narrow (PMU R447 and R453). However, in PMU R447 and R453, bones are preserved as natural moulds, and the moulds of the humeri are incomplete anteriorly, suggesting that only the posterior parts of the anterior flanges are preserved. It is likely therefore that the narrow variation is an artefact of preservation, and that the well-developed flange represents the true morphology. Mazin's (1981) reconstruction seems to be based on PMU R447, without considering the incompleteness of the specimen, and is too slender.

The proximal part of the radius was exposed, and has been weathered away. However, its impression is preserved as a natural mould, enabling a reasonably accurate reconstruction of the outline. The radius is similar to that depicted by Wiman (1933) for PMU R449, although Wiman's figure is upside down (i.e. the distal end is at the top). There is a prominence proximally, anterior to the articular facet for the humerus (indicated by the 'bracket' symbol in Text-fig. 1), as in *Utatsusaurus* (Motani 1997*b*), but this prominence is entirely absent from Mazin's (1981) reconstruction. The ulna is also similar to that of *Utatsusaurus*, in that it

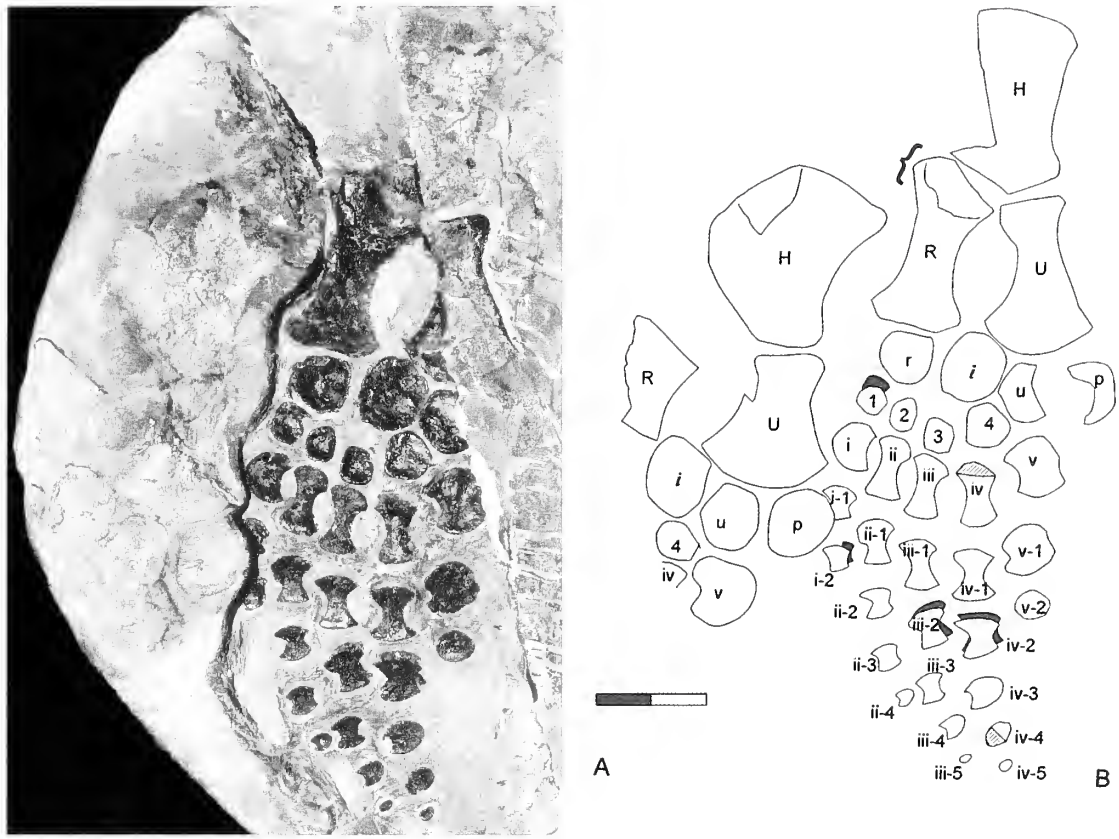

TEXT-FIG. 1. *Grippia longirostris* Wiman, 1929; PMU R472. A, a photograph of the area containing fin elements. B, identification of each element. The partial left forefin (white) was originally exposed, and was described by Wiman (1933). The newly discovered right forefin (light grey) is nearly complete. The left ulna seems to be broken, and is therefore shorter than the right one. Some elements have been split into dorsal and ventral plates, which have slipped with respect to each other (black). Hatched areas represent the indentation described in the text, and dashed lines are reconstructions of the missing parts. The bracket symbol indicates the antero-proximal prominence of the radius. Abbreviations: H, humerus; R, radius; U, ulna; *i*, intermedium; p, pisiform; r, radiale; u, ulnare; 1–4, distal carpals; i–v, metacarpals; i1–v2, phalanges. Scale bar represents 20 mm.

expands distally into a fan-shape (Text-fig. 2). The articular facet for the humerus is wider than that of the humerus for the ulna, again resembling *Utatsusaurus*. The only ulna depicted by Wiman (1933) was the left one of PMU R472, which is 23 per cent. shorter than the newly exposed right one. The left ulna appears to be broken in the middle, and it seems likely that this accounts for the observed shortness. Both radius and ulna are more robust than those of *Utatsusaurus* (Text-fig. 2).

There are four proximal carpals, all of similar size, although the intermedium is slightly larger than the others (Text-fig. 1). The outline of each element resembles the corresponding carpal of *Utatsusaurus*; thus the pisiform is oval, the ulnare is somewhat pentagonal, but with a rounded distal margin, the intermedium is elongated, and the radiale has a straight proximal margin (Text-fig. 2B–C). Four distal carpals are present, and support the first four digits. The fourth one is the largest, but its diameter is only about half that of the proximal carpals (Text-fig. 1). Mazin (1986) claimed that the distal carpals were equal in size to the proximal carpals, but this is not evident in any of the specimens. All carpals are well separated from each other, indicating the osteological immaturity of the individual.

Two forms of metacarpals are recognizable: normal (second to fourth) and lunate (the first and fifth). The normal form resembles the cylindrical phalanges of other amniotes, but is flattened. The extremities of these

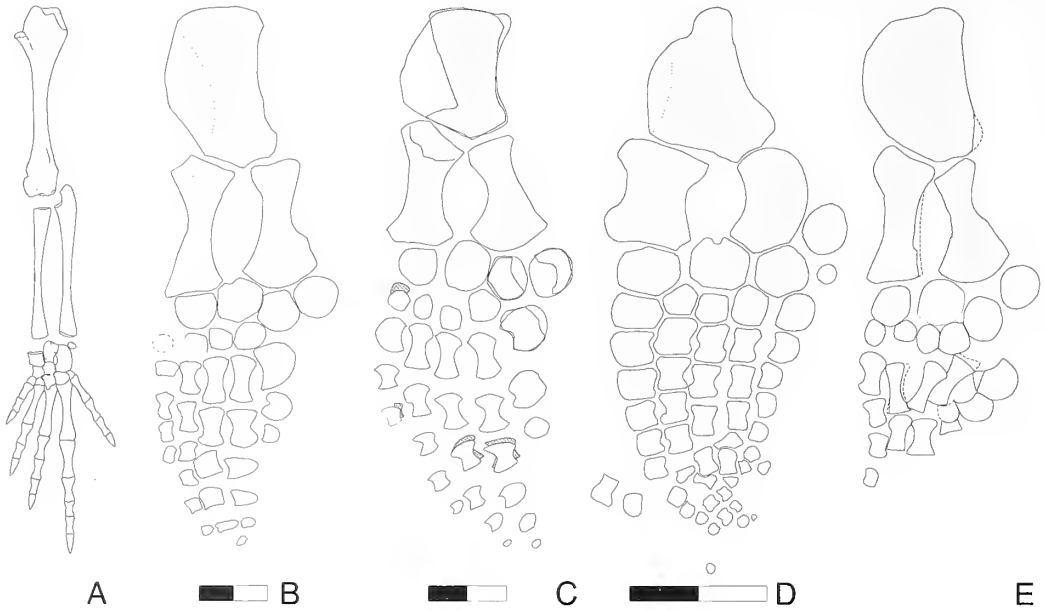

TEXT-FIG. 2. Comparison of anterior appendages of early ichthyosaurs and a primitive diapsid. A, *Petrolacosaurus kansensis*, modified from Reisz (1981); the elbow and wrist joints are disarticulated. B, *Utatsusaurus hataii*, modified from Motani (1997*b*). C, *Grippia longirostris*, a composite of the right and left forefin of PMU R472; dark grey indicates split elements. D, *Mixosaurus cornalianus*, drawn from BMNH R5702. E, '*Grippia*' from British Columbia, described by Brinkman *et al.* (1992); a composite of RTMP 89.127.12 (humerus) and 89.127.3 (the rest), as retrodeformed according to the method of Motani (in press). Scale bars represent 20 mm, but do not apply to A and E (composite figures).

metacarpals are markedly expanded, indicating a degree of osteological maturity for this individual, although this is contrary to the immaturity indicated by the well-spaced carpals and phalanges. The lunate metacarpals occur along the anterior and posterior margins of the fin, with their concave sides facing inwards, towards the longitudinal axis. This type of metacarpal may derive from the normal type through the lack of perichondral ossification along the side of the bone facing the fin margin (Caldwell in press), resulting in the convexity of the bone on that side. The fifth metacarpal is located more proximally than in *U. hataii*, and, with further growth, it would have contacted the ulnare.

The phalanges are similar to the metacarpals in that there are normal and lunate forms, and the latter occur near the margins of the fin. However, in addition to these two forms, there is a third form that is entirely oval, and occurs toward the distal end of the fin (e.g. the fourth and fifth phalanges of the fourth digit; see Text-fig. 1B). This oval form, which entirely lacks perichondral ossification, is not known in *Utatsusaurus* (Motani 1997*b*), but is commonly observed towards the tip of the fins in later ichthyosaurs (McGowan 1991, fig. 4). There are no traces of ungual phalanges, contrary to Wiman's (1929, 1933) supposition which was followed by Mazin (1981, 1986). Wiman's supposed ungual phalanx is probably a proximal phalanx, because some of these elements are also key-hole shaped (e.g. the second phalanx of the third digit; see Text-fig. 1B). The fourth phalanx of the fourth digit is deeply grooved antero-ventrally, and although this may appear to be mechanical damage caused during preparation, it is natural (Text-fig. 1B, hatched). The fourth metacarpal is also naturally indented at the proximal end (Text-fig. 1B, hatched).

The second phalanges of digits one, three and four show an unusual feature: they have been split into dorsal and ventral plates, and the two plates have slipped with respect to each other (Text-fig. 1B, elements in black). The dorsal plates are located proximal to their ventral counterparts, and exhibit a spongy inner structure. These elements are constricted in the middle, but the margins along the constrictions are sharply edged, instead of being smooth and round as in the shafts of metacarpals. It is possible that the constricted parts of these phalanges were associated with little perichondral bone, leading to a weak bond between the dorsal and ventral

plates. A similar slippage occurs in the first distal carpal, suggesting that the ossification patterns may have been similar in this element. The dorsal and ventral plates are almost identically shaped in all displaced elements, and the spongy structure is not covered by a secondary ossification; therefore, the slippage was probably a post-mortem phenomenon. All four elements were probably dislocated by the same force, because the direction and magnitude of the slippage is nearly uniform among the elements. One possible explanation is that the deposition of the dead animal rotated the horizontal forefin in a parasagittal direction, pulling the dorsal connective tissues proximally while pushing the ventral ones distally, creating shearing stress inside the fin and splitting some elements along mechanically weak planes.

DISCUSSION

An important question concerns the osteological maturity of PMU R472. Johnson (1977) pointed out four forefin features that indicate osteological immaturity in the Upper Liassic ichthyosaur *Stenopterygius*: (1) humeral head incompletely ossified; (2) rough surface of the humeral shaft; (3) proximal elements not well packed; and (4) absence of notched elements on the leading-edge (only applicable to those species whose adults have notched elements). Features 1 and 2 are probably useful for *Grippia longirostris*, but not applicable to PMU R472 due to the poor preservation of the humeri. Feature 4 is not applicable to *G. longirostris*, because notched elements are absent from the leading edge. This only leaves feature 3, and since proximal elements are well spaced from each other in PMU R472, the specimen probably represents an immature individual. Immaturity of PMU R472 is further supported by the fact that the specimen has the smallest humerus of all the referred specimens of *G. longirostris*. Although size is not always a good indicator of osteological maturity, the humerus of PMU R472 is much shorter than the largest known humerus (PMU R474), being about 63 per cent. of the latter. Also, the vertebrae of PMU 472 are only half the size of those in the largest vertebral series (PMU R456). Moreover, the well spaced phalanges suggest that the ossification of the epiphyses was incomplete, thus the expanded extremities of the metacarpals and phalanges reflect the shape of the diaphyses rather than that of the epiphyses. I therefore conclude that PMU R472 is osteologically immature, and that the well-expanded extremities of the metacarpals and phalanges do not necessarily indicate maturity.

A second question is whether the forefin of *Grippia* is more plesiomorphic than that of *Utatsusaurus*, as suggested by previous authors although based on incomplete information. To address this question, the pectoral limbs of these two genera were compared with those of *Petrolacosaurus kansensis* (the earliest known diapsid, from the Upper Carboniferous; Text-fig. 2A) and *Mixosaurus cornalianus*, a Middle Triassic ichthyosaur (Text-fig. 2D). *P. kansensis* was used as the outgroup because ichthyosaurs are probably diapsids (Massare and Callaway 1990). The monophyly of *U. hataii*, *G. longirostris*, and *M. cornalianus* is established by at least five forelimb features that are absent in *P. kansensis*: (1) anterior flange on the humerus; (2) lunate fifth metacarpal; (3) flattened limb elements; (4) hyperphalangy in the second and third digits; and (5) antero-proximal prominence of the radius. *G. longirostris* and *M. cornalianus* share the following features that are absent in *U. hataii* and *P. kansensis*: (1) round distal elements (i.e. the occurrence of phalanges without perichondral ossification); (2) lunate first metacarpal (i.e. loss of perichondral ossification on the leading edge of the first metacarpal); (3) humerus with a large articular facet for the radius, resulting in the prominent distal expansion of the bone; and (4) manus clearly longer than the combined length of the propodial and epipodials. Although no complete first metacarpal is known for *U. hataii*, it is obviously not lunate, judging from the preserved remains in the holotype. On the other hand, there are no obvious derived character states shared by *U. hataii* and *M. cornalianus* that are not present in *P. kansensis* or *G. longirostris*. In addition, *U. hataii* and *G. longirostris* do not share any derived character state that is absent in *M. cornalianus* and *P. kansensis*. Therefore, by a simple three-taxon comparison, *G. longirostris* forms a clade with *M. cornalianus*, and *U. hataii* is the sister group of this clade (Text-fig. 3). This was confirmed by analysing the data matrix in Table 1 (last four characters only, since the first five are cladistically uninformative), using the exhaustive search option of PAUP 3.1.1 (Swofford 1993) which resulted in a single most parsimonious tree (tree length = 4, retention index = 1·0). Clearly a larger scale

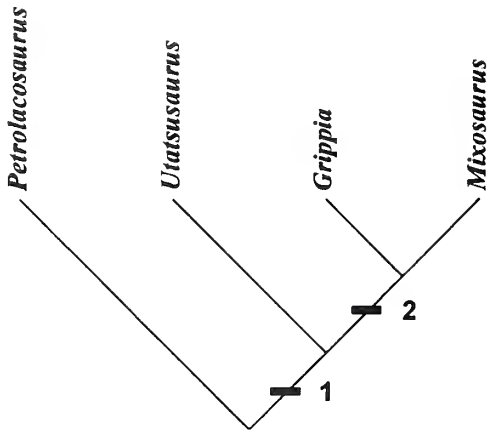

TEXT-FIG. 3. Preliminary phylogenetic hypotheses for early ichthyosaurs, based on forefin features. The cladogram contains *Utatsusaurus hataii*, *Grippia longirostris*, and *Mixosaurus cornalianus* as early ichthyosaurs, with *Petrolacosaurus kansensis* as the outgroup. The numbered internodes are characterized by the following synapomorphies: 1, anterior flange on the humerus; lunate fifth metacarpal; flattened fin elements; hyperphalangy in the second and third digits; antero-proximal prominence on the radius; 2, lunate first metacarpal; rounded distal forefin elements; humerus with an expanded articular facet for the radius; manus longer than the humerus and epipodials combined. See text for discussion.

TABLE 1. The character matrix used in the discussion.

The character states were coded in the following manner.

1. Anterior flange of the humerus: (0) absent; (1) present.
2. Antero-proximal prominence of the radius: (0) absent; (1) present.
3. Fifth metacarpal: (0) cylindrical, with complete perichondral bone sheath; (1) lunate, with posterior perichondral bone absent.
4. Limb elements: (0) not flattened; (1) flattened.
5. Hyperphalangy: (0) absent; (1) present.
6. Distal end of the humerus: (0) similar size to the proximal end; (1) well expanded, with a large articular facet for the radius.
7. First metacarpal: (0) cylindrical, with complete perichondral bone sheath; (1) lunate, with anterior perichondral bone absent.
8. Combined length of propodial and epipodial: (0) longer than manual length; (1) shorter than manual length.
9. Distal manual elements: (0) with perichondral bone; (1) round, without perichondral bone.

Taxon	123456789
Petrolacosaurus	000000000
Utatsusaurus	111110000
Grippia	111111111
Mixosaurus	111111111

cladistic analysis that involves other characters from the rest of the skeleton, as well as other ichthyosaur species, is required. Little is known about these early ichthyosaurs, however, hence such an analysis will necessitate extensive studies of these forms, and is beyond the scope of the present paper.

Now that details of the forefin osteology have been established for *Grippia*, it is possible to assess some problematical fin specimens from the Lower Triassic. Thus a third question concerns the identity of incomplete forefins (RTMP 89.127.3 and 89.127.12) from the Lower Triassic of British Columbia, described by Brinkman *et al.* (1992) as belonging to the monotypic genus *Grippia*. Brinkman *et al.* (1992) referred these specimens to *Grippia* on the basis of six features, five of which were first used by Mazin (1986). I show elsewhere (Motani in press) that these specimens were tectonically deformed, and linear retrodeformation of images of the forefins, calibrated against measurements of the vertebral centra, revealed somewhat wider shapes than originally described. I also argue that none of the six features was useful for the taxonomic identification of the British

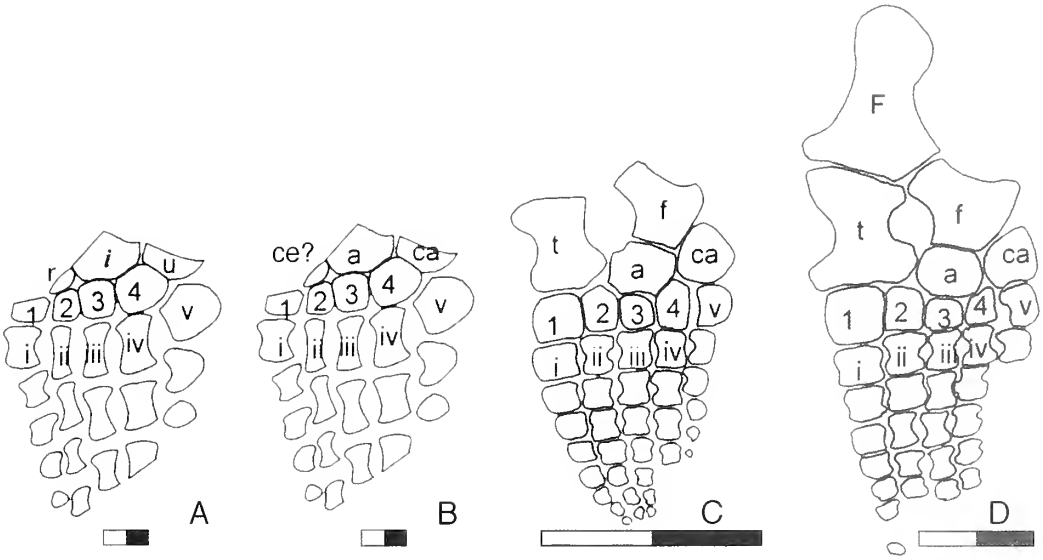

TEXT-FIG. 4. Fins of Triassic ichthyosaurs. Because of its similarity to the newly reported forefin of *Grippia* (Text-fig. 1), RTMP 89.128.5 can be reasonably identified as a forefin (A), although it was originally described as the hindfin, assuming the presence of the centrale (B). The hindfins of *Mixosaurus cornalianus* (C, based on BMNH R5702) and *M. nordenskioeldii* (D, based on PMU R185), which are the oldest known articulated hindfins of ichthyosaurs, lack the centrale. See text for discussion. Scale bars represent 20 mm.

Columbia fins (Motani in press). Now that the new forefin of *G. longirostris* is available, it is possible to extend this taxonomic discussion. The ichthyosaur represented by RTMP 89.127.3 and 89.127.12 has a first metacarpal that is not lunate, and a humerus that is not distally expanded (Text-fig. 2E). Therefore, this species lacks synapomorphies that unite *G. longirostris* and *M. cornalianus* (Text-fig. 3A). Whether this species had oval phalanges, or whether the manus was large, is unknown, due to poor preservation. In addition, there seem to be no derived character states shared uniquely by *Grippia* and this species. I therefore conclude that these specimens cannot be referred to *Grippia*. The forefin of the British Columbian ichthyosaur resembles that of *U. hataii* in many respects, but is much smaller than the latter. Small ichthyosaurs of similar size to the British Columbian specimens have been reported from the Lower Triassic of China (Young and Dong 1972; Chen 1985; Motani *et al.* 1996), and examination of these taxa may help to resolve the taxonomic identification of the specimens from British Columbia.

Brinkman *et al.* (1992) described another incomplete fin of an ichthyosaur from the Lower Triassic of British Columbia (RTMP 89.128.5), referring to it as a hindfin. The propodial and epipodial elements are not preserved in this supposed hindfin, and the proximal mesopodials are incomplete (Text-fig. 4A–B), causing much difficulty in determining whether it is a pectoral or pelvic fin. Brinkman *et al.* (1992) identified the fin as a hindfin because they found the arrangement of the proximal mesopodials to be similar to that in the hindlimbs of primitive diapsids. However, the new forefin of *Grippia* casts doubt on this identification: the mesopodial arrangements in this forefin and the BC fin are so similar to each other that the BC fin can be reasonably interpreted as a pectoral fin (Text-fig. 4A). On the other hand, the interpretation of the BC fin as a pelvic fin (Text-fig. 4B) postulates the presence of a centrale in this limb, which has yet to be confirmed for any ichthyosaur. For example, in the oldest known articulated hindfins of ichthyosaurs, represented by *Mixosaurus* from the Middle Triassic (Text-fig. 4C–D), the centrale is clearly absent. Many derived ichthyosaurs from the Jurassic have three elements distal to the epipodials, one of which may be identified as the centrale (Caldwell in press). However, some *Stenopterygius* even have three elements in the

epipodial row of the hindfin, suggesting a breakdown of the usual limb-developmental pattern, and the presence of a mechanism to increase the number of proximal elements. Hence, further study is necessary before the homology of the hindfin elements of derived ichthyosaurs from the Jurassic can be established. For these reasons, I conclude that there is insufficient justification for identifying the BC fin as the hindfin.

Acknowledgements. I am grateful to S. Stuenes of the Paleontologiska Museet, Uppsala Universitet, for permission to prepare PMU R472 and I. Morrison, T. Ecclestone, and B. Iwama of the Royal Ontario Museum for their technical advice during the preparation. I also thank S. Stuenes, S. Jensen, and V. Berg-Madsen for their help during my two visits to Uppsala. A. Milner, of The Natural History Museum, London, allowed me to examine BMNH R5702. C. McGowan provided generous intellectual and financial support. M. Caldwell made available his manuscript in press. This study was supported by a Natural Sciences and Engineering Research Council grant to C. McGowan (A9550) and a grant from the Fujiwara Natural History Foundation, Tokyo, to the author.

REFERENCES

BRINKMAN, D. B., ZHAO XIJIN, and NICHOLLS, E. L. 1992. A primitive ichthyosaur from the Lower Triassic of British Columbia, Canada. *Palaeontology*, **35**, 465–474.

CALDWELL, M. W. in press. Limb ossification patterns in the ichthyosaur *Stenopterygius*, with a discussion of the proximal tarsal row of ichthyosaurs and other neodiapsid reptiles. *Zoological Journal of the Linnean Society*.

CALLAWAY, J. M. 1989. Systematics, phylogeny, and ancestry of Triassic ichthyosaurs. Unpublished Ph.D. thesis, University of Rochester, USA.

—— and MASSARE, J. A. 1989. Geographic and stratigraphic distribution of the Triassic Ichthyosauria (Reptilia; Diapsida). *Neues Jahrbuch für Geologie und Paläontologie, Abhandlungen*, **178**, 37–58.

CHENLIE-ZU 1985. [Ichthyosaurs from the Lower Triassic of Chao County, Anhui.] *Regional Geology of China*, **15**, 139–146. [In Chinese].

JOHNSON, R. 1977. Size independent criteria for estimating relative age and the relationship among growth parameters in a group of fossil reptiles (Reptilia: Ichthyosauria). *Canadian Journal of Earth Sciences*, **14**, 1916–1924.

MASSARE, J. A. and CALLAWAY, J. M. 1990. The affinities and ecology of Triassic ichthyosaurs. *Bulletin of the Geological Society of America*, **102**, 409–416.

MAZIN, J.-M. 1981. *Grippia longirostris* Wiman, 1929, un Ichthyopterygia primitif du Trias inférieur du Spitsberg. *Bulletin du Muséum National d'Histoire Naturelle*, **4**, 317–340.

—— 1982. Affinités et phylogénie des Ichthyopterygia. *Geobios, Mémoire Spécial*, **6**, 85–98.

—— 1986. A new interpretation of the fore-fin of *Utatsusaurus hataii* (Reptilia, Ichthyopterygia). *Paläontologische Zeitschrift*, **60**, 313–318.

—— SUTEETHORN, V., BUFFETAUT, E., JAEGER, J.-J. and HELMCKE-INGAVAT, R. 1991. Preliminary description of *Thaisaurus chonglakmanii* n. g., n. sp., a new ichthyopterygian (Reptilia) from the Early Triassic of Thailand. *Comptes Rendus de l'Académie des Sciences, Série 2*, **313**, 1207–1212.

MCGOWAN, C. 1991. An ichthyosaur forefin from the Triassic of British Columbia exemplifying Jurassic features. *Canadian Journal of Earth Sciences*, **28**, 1553–1560.

MOTANI, R. 1997*a*. Redescription of the dentition of *Grippia longirostris* (Ichthyosauria) with a comparison with *Utatsusaurus hataii*. *Journal of Vertebrate Paleontology*, **17**, 39–44.

—— 1997*b*. New information on the forefin of *Utatsusaurus hataii* (Ichthyosauria). *Journal of Paleontology*, **71**, 475–479.

—— in press. New technique for retrodeforming tectonically deformed fossils, with an example for ichthyosaurian specimens. *Lethaia*.

—— YOU HAILU and MCGOWAN, C. 1996. Eel-like swimming in the earliest ichthyosaurs. *Nature*, **382**, 347–348.

REISZ, R. R. 1981. A diapsid reptile from the Pennsylvanian of Kansas. *Special Publication of the Museum of Natural History, University of Kansas*, **7**, 1–74.

SHIKAMA, T., KAMEI, T. and MURATA, M. 1978. Early Triassic Ichthyosaurus, *Utatsusaurus hataii* Gen. *et* Sp. Nov., from the Kitakami Massif, Northeast Japan. *Science Reports of the Tohoku University, Sendai, Second Series (Geology)*, **48**, 77–97.

SWOFFORD, D. L. 1993. *PAUP-Phylogenetic Analysis Using Parsimony, Version 3.1.1.* Laboratory of Molecular Systematics, Smithsonian Institution, Washington DC.

WIMAN, C. 1929. Eine neue Reptilien-Ordnung aus der Trias Spitzbergens. *Bulletin of the Geological Institutions of the University of Upsala*, **22**, 183–196.

—— 1933. Über *Grippia longirostris*. *Nova Acta Regiae Societatis Scientiarum Upsaliensis*, **9**, 1–19.

YOUNG CHUNG-CHIEN and DONG ZHI-MING 1972. [*Chaohusaurus geishanensis* from Anhui Province.] *In* YOUNG CHUNG-CHIEN and DONG ZHI-MING (eds). [Aquatic reptiles from the Triassic of China.] *Memoir of the Institute of Vertebrate Palaeontology and Palaeoanthropology, Academia Sinica*, **9**, 11–14. [In Chinese].

RYOSUKE MOTANI
University of California
Museum of Paleontology
1101 Valley Life Sciences Building
Berkeley CA 94720, USA

Typescript received 9 September 1996
Revised typescript received 20 July 1997

MANTLE-BODY ARRANGEMENT ALONG THE HINGE OF EARLY PROTREMATOUS BRACHIOPODS: EVIDENCE FROM *CROZONORTHIS*

by ANTHONY D. WRIGHT *and* MICHEL MELOU

ABSTRACT. The earlier discovery of mantle canals lining the interareas of protrematous brachiopods and the implication that these areas were lined with mantle and not simply outer epithelium is supported by evidence from *Crozonorthis*. In this genus the ventral interareas show a clear external differentiation, reflecting a lining of mantle laterally and of outer epithelium medianly. Moreover, this morphology provides clear evidence, contrary to popular opinion, that setae could develop along the growing margin of a protrematous interarea. A well-defined junction, between parts adjacent to the delthyrium which are smooth and lateral parts with perforations that housed successive generations of setae during life, marks the position where, on the interior, the inner epithelium separated from the outer epithelium to form the body wall.

THE discovery of mantle canals preserved on the interareas of some protrematous brachiopods (Wright 1994) implies that in life these areas were lined with mantle, and not simply outer epithelium as was previously thought (Williams and Rowell 1965, fig. 8). The mantle edge of brachiopods typically houses sensory setae, although this is not invariable. They are absent, for example, from the adults of modern *Neocrania* and *Lacazella*; and would appear to be absent from fossil *Acanthambonia*, where the sensory function was seemingly taken over by the spines (Wright and Nõlvak 1997). The fossil evidence for differing setal densities, non-retractile setae relating to strongly differentiated and deep follicular embayments, setal incorporation into the shell via aditicules and a setal function for the perforations along the posterior margin of *Eochonetes* was considered recently (Wright 1996). The canals in *Eochonetes* as noted by Reed (1917), and in *Chonetoidea* and *Sentolunia* as noted by Havlíček (1967) as opening to the exterior along the posterior edge of the interareas were interpreted as being incorporated into this position sequentially as each contained seta was developed at the cardinal angle (Wright 1996, p. 301).

Dr R. B. Neuman subsequently commented (pers. comm. to ADW) that perforations were present also in *Heterorthina macfarlani* Neuman, 1967, along the intersection of the interarea and the shell surface on the dorsal valves, a feature which had been drawn to his attention after seeing the illustrations of *Heterorthina* by Melou (1975). The perforations, termed cardinal canals by Melou (1975, p. 195), are like those of *Eochonetes* in that they pass through to the valve interior, but are much more densely distributed and have an orientation which grades from being perpendicular to the margin around the cardinal angles, through being perpendicular to the hinge and then, as their size reduces medianly, convergent towards the umbo. Melou (1975, p. 176) noted that these canals were present on several genera of Heterorthidae and that Williams (1974, p. 108) had observed that members of this family have reflexed costellae which open along the posterior edges of the shells with corresponding follicular embayments, indicating the presence of backwardly projecting setae, although Williams expressed doubt as to whether functional setae persisted much within the cardinal angles.

Wright (1996, p. 301) commented that there 'seems to be no case of setae developing along the growing margin of the interareas of protrematous brachiopods'. This was taken as indicating that although the interareas were lined with mantle, this mantle was modified so that it did not possess setal follicles, an arrangement which would not be exceptional in view of the lack of setae in some

[Palaeontology, Vol. 41, Part 4, 1998, pp. 601–603]

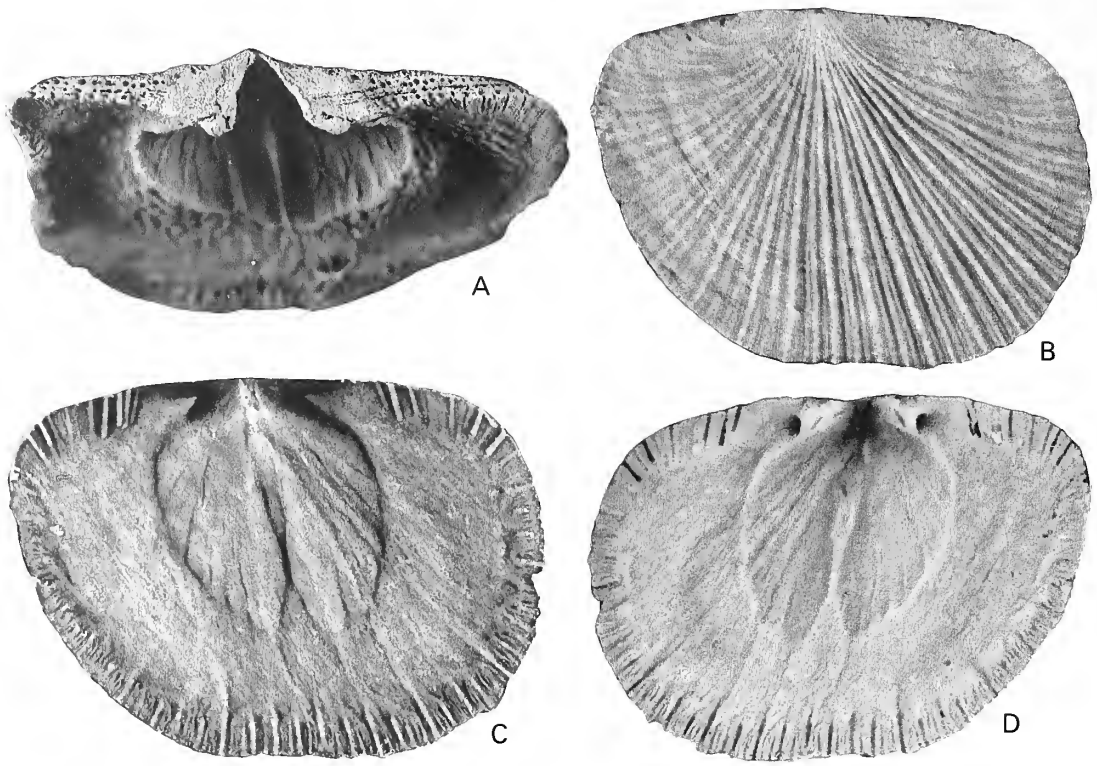

TEXT-FIG. 1. *Crozonorthis musculosa* Melou, 1976. A, LPB 3784a; Schistes Botella, La Almeda, Jaen, Spain; posterior view of latex cast of ventral valve. B–D, LPB3780a; Schistes de Postolonnec, Postolonnec beach, Crozon, France; Ordovician (Llandeilo); latex cast of external mould, internal mould, and latex cast of internal mould of ventral valve. Repository: Laboratoire de Paléontologie, Brest (LPB). All × 6.

extant stocks. This may be the general situation, but, nevertheless, successive rows of perforations are in fact well displayed on the ventral interareas of the heterorthid species described as *Crozonorthis musculosa* by Melou (1976). (Although this species has been ascribed to *Eorhipidomella* Hints, there are morphological differences and both genera will be recognized (D. A. T. Harper, pers. comm.) in the forthcoming revision of the brachiopod *Treatise*). The function of these perforations could only have been to accommodate setae, but it is their distribution (Melou 1976, p. 702 and pl. 8, partly re-figured here as Text-fig. 1) which provides significant additional evidence regarding mantle-body distribution in the hinge region.

As indicated by Melou (1976, p. 702), the interarea of the ventral valve of *C. musculosa* (Text-fig. 1A) is unusual in being divisible into two parts. The parts adjacent to the delthyrium are slightly raised and show striations parallel to the hinge; whilst laterally the lower area additionally shows at least three rows of perforations parallel to the hinge. The sporadic earliest canals together with the three rows of non-functional canals are followed by a row of functional canals seen as indented grooves on either side of the posterior margin of the hinge (Melou 1976, p. 704).

With the knowledge that the lateral parts of the interareas in protrematous brachiopods are underlain by mantle, the interpretation of the unusual area of *Crozonorthis musculosa* becomes clear. The outer parts would have been lined by normal mantle with functional setae, with successive rows becoming incorporated in the area with growth, whilst the median parts were lined simply by the shell secreting outer epithelium within the body cavity of the animal. The position of the separation of the inner from the outer epithelium to form the body wall is clearly indicated by the

change in texture of the surface of the interarea lateral to the position of the teeth. Whilst the canals along the posterior edge of the area are related to the openings of the recurved costellae along this edge (Text-fig. 1B), the subsequent rows of canals are not so constrained, and simply reflect the distribution of setal follicles more-or-less perpendicular to the posterior growing edge (Text-fig. 1C–D). As commented by Melou (1976, p. 704), canals occur also on the dorsal valve; but it is on the ventral valve, with its relatively long interarea, where the distribution of the setal apertures is so well displayed.

REFERENCES

HAVLÍČEK, V. 1967. Brachiopoda of the suborder Strophomenidina in Czechoslovakia. *Rozpravy Ústředního Ústavu Geologického*, **33**, 1–235.

MELOU, M. 1975. Le genre *Heterorthina* (*Brachiopoda*, *Orthida*) dans la Formation des Schistes de Postolonnec (Ordovicien) Finistère, France. *Géobios*, **8**, 191–208.

—— 1976. Orthida (Brachiopoda) de la Formation de Postolonnec (Ordovicien) Finistère, France. *Géobios*, **9**, 693–717.

NEUMAN, R. B. 1967. Some silicified Middle Ordovician brachiopods from Kentucky. *Professional Paper of the United States Geological Survey*, **583A**, A1–A14.

REED, F. R. C. 1917. The Ordovician and Silurian Brachiopoda of the Girvan District. *Transactions of the Royal Society of Edinburgh*, **51**, 795–998.

WILLIAMS, A. 1974. Ordovician Brachiopoda from the Shelve District, Shropshire. *Bulletin of the British Museum* (*Natural History*), *Geology*, Supplement **11**, 1–163.

—— and ROWELL, A. J. 1965. Morphology. H57–H155. *In* MOORE, R. C. (ed.). *Treatise on invertebrate paleontology. Part H. Brachiopoda 1*. Geological Society of America and University of Kansas Press, Lawrence, Kansas, 521 pp.

WRIGHT, A. D. 1994. Mantle canals on brachiopod interareas and their significance in brachiopod classification. *Lethaia*, **27**, 223–226.

—— 1996. Taxonomic importance of body-mantle relationships in the Brachiopoda. 299–304. *In* COPPER, P. and JISUO JIN (eds). *Brachiopods. Proceedings of the Third International Brachiopod Congress Sudbury/Ontario/Canada/2–5 September 1995*. Balkema, Rotterdam and Brookfield, 373 pp.

—— and NÕLVAK, J. 1997. The spines of the Ordovician lingulate brachiopod *Acanthambonia*. *Palaeontology*, **40**, 113–119.

ANTHONY D. WRIGHT
School of Geosciences
Queen's University of Belfast
Belfast BT7 1NN
Northern Ireland

MICHEL MELOU
Laboratoire de Paléontologie
Université de Bretagne Occidentale
29283 Brest Cedex, France

Typescript received 16 September 1997
Revised typescript received 5 November 1997

A NEW TREMATOPID AMPHIBIAN FROM THE LOWER PERMIAN OF CENTRAL GERMANY

by STUART S. SUMIDA, DAVID S BERMAN *and* THOMAS MARTENS

ABSTRACT. A new genus and species of trematopid amphibian, *Tambachia trogallas*, is described on the basis of the greater portion of a skeleton, including the skull. The holotype was collected from the Early Permian Tambach Formation, the lowermost unit of the Upper Rotliegend, of the Bromacker locality in the midregion of the Thuringian Forest near Gotha, central Germany. Not only is this the first trematopid to be reported outside the United States, but it is the first specimen to include the greater portion of the postcranial skeleton. Analysis of the interrelationships of the trematopids agrees with the results of other recent studies: (1) *Tambachia* and the Late Pennsylvanian *Anconastes*, on the one hand, and the Early Permian *Acheloma* and *Phonerpeton* on the other, form sister clades of the monophyletic Trematopidae; and (2) *Actiobates*, although almost certainly a trematopid, is too poorly known to determine its intrafamilial relationships.

The Bromacker locality is the only Early Permian site in Europe to produce a diverse assemblage of terrestrial or semi-terrestrial tetrapods, several of which are known otherwise only from the Upper Pennsylvanian and Lower Permian of the United States. The Bromacker assemblage is, therefore, of great interest in indicating: (1) an earliest Permian Wolfcampian age for the Tambach Formation, the basal unit of the Upper Rotliegend of the Thuringian Forest. This in turn suggests a Late Pennsylvanian age for all or most of the underlying Lower Rotliegend, rather than the widely accepted Early Permian; (2) a cosmopolitan, Euramerican distribution of Early Permian terrestrial or semi-terrestrial tetrapods previously reported only from the United States. This suggests an absence of any strong physical barriers to tetrapod dispersal across Euramerica during the Early Permian.

MOST terrestrial members of the widely diverse late Palaeozoic amphibian order Temnospondyli belong to the families Dissorophidae and Trematopidae, united by Bolt (1969) under the superfamily Dissorophoidea. The close relationship between these two families was originally recognized by Olson (1941). Later descriptions (DeMar 1966; Vaughn 1969; Eaton 1973; Berman *et al.* 1985) of forms exhibiting a combination of 'dissorophid' and 'trematopid' features has since justified their unification into a superfamily. Dissorophidae contains a larger number of taxa (16 or more genera) and has a greater temporal and spatial range, occurring in the Upper Pennsylvanian and Lower Permian of the United States (Carroll 1964; Berman and Berman 1975; Berman *et al.* 1985) to the lower Upper Permian of the cis-Uralian forelands of Russia (Gubin 1980). However, the family is difficult to define, and its ingroup relationships are not well understood (Berman *et al.* 1985, 1987; Dilkes 1990; Daly 1994). Conversely, the more conservative Trematopidae is composed of only four genera, not including the new genus described here, and, except for a single specimen from the Lower Permian of Ohio (Olson 1970), all known are from the Upper Pennsylvanian and Lower Permian of the midcontinental and south-western regions of the United States (Berman *et al.* 1987; Dilkes 1990). Recent analyses of the family have yielded very consistent conclusions (Dilkes 1990; Daly 1994), that recognized only three genera: the Late Pennsylvanian *Anconastes* and the Early Permian *Acheloma* and *Phonerpeton*. On the basis of a restudy of the holotypes of the type species of the well-known *Acheloma* and *Trematops*, Dilkes and Reisz (1987) identified the latter as a subjective junior synonym of the former, but retained the family name Trematopidae. Although Berman *et al.* (1987) considered the Late Pennsylvanian *Actiobates* as a trematopid (originally described as a dissorophid by Eaton 1973), Dilkes (1990) and Daly (1994) assigned it only tentatively to the Trematopidae.

[Palaeontology, Vol. 41, Part 4, 1998, pp. 605–629]

A new genus and species of trematopid, *Tambachia trogalles*, based on a skull and the greater portion of the postcranium of a single individual is described here. The specimen is from the Early Permian Tambach Formation, lowermost unit of the Upper Rotliegend, of the well-known Bromacker locality (Pabst 1896; Martens 1980, 1988; Berman and Martens 1993) in the midregion of the Thuringian Forest of central Germany.

Abbreviations used in figures are as follows: a, angular; ac, acetabulum; clt pr, cultriform process; cr, caudal rib; cv, caudal vertebra; d, dentary; ec, ectopterygoid; f, frontal; fe, femur; fi, fibula; h, humerus; ic, interclavicle; il, ilium; imf, inframeckelian foramen; j, jugal; l, lacrimal; m, maxilla; n, nasal; na, neural arch; p, parietal; pa, palatine; paf, para-articular foramen; pf, postfrontal; pm, premaxilla; po, postorbital; pp, postparietal; pra, prearticular; prf, prefrontal; ps, parasphenoid; psp, postsplenial; pt, pterygoid; q, quadrate; qj, quadratojugal; r, radius; s1, s2, sacral vertebrae; sa, surangular; sf, supratympanic flange; sm, septomaxilla; sp, splenial; sq, squamosal; sr, sacral rib; st, supratemporal; t, tabular; tk, tusk; u, ulna; v, vomer; I–IV, metapodials and digits.

BROMACKER QUARRY VERTEBRATE ASSEMBLAGE

Principally a commercial quarry for the sandstones of the Early Permian Tambach Formation, which is the lowermost formational unit of the Upper Rotliegend near Tambach–Dietharz, central Germany, the Bromacker locality has been an important source of excellent tetrapod trackways for a century (Pabst 1896, 1908; Mueller 1954, 1969; Haubold 1971, 1973). More recently, however, the Bromacker locality has yielded a diverse assemblage of articulated skeletal remains of terrestrial or semi-terrestrial amphibians and reptiles (Martens 1980, 1988; Boy and Martens 1991; Berman and Martens 1993; Sumida *et al.* 1996), as well as some invertebrates (conchostracans, insects and myriapods). Among the vertebrate taxa already described from the Bromacker locality are the seymouriamorph amphibian *Seymouria* cf. *sanjuanensis* (Berman and Martens 1993) and the protorothyridid reptile *Thuringothyris mahlendorffae* (Boy and Martens 1991). Bromacker specimens currently being described or prepared include: a complete skeleton (more than 1 m long), an isolated skull, and the greater portion of the postcranium of a new species of the diadectomorph *Diadectes*; a complete skeleton (nearly 1 m long) of a new, primitive diadectomorph that is closely related to *Diadectes*; and a complete skeleton (about 0·3 m long) of a small, possible neodiapsid.

Apart from the Bromacker locality, the Early Permian trematopids *Seymouria*, and *Diadectes* are known only from the United States, where they are frequently encountered. The Bromacker locality is also unique as the only European site to have yielded a large assemblage of Early Permian terrestrial or semi-terrestrial tetrapods. Vertebrates of this type and age from central and western Europe are very rare, are typically found as isolated specimens varying in completeness from fragments to partial skeletons, and occur at widely distant locales and various stratigraphical levels (Berman and Martens 1993; Sumida *et al.* 1996). An explanation of why Early Permian terrestrially adapted vertebrates are so rare in Europe, despite a long history of intensive prospecting of the highly productive Rotliegend and equivalent-aged deposits, has been offered by Martens (1988, 1989) and Berman and Martens (1993). They suggested that this is due to a bias in exploration which has traditionally ignored the fluvial, red-bed deposits where such discoveries are most likely to be made. Poor exposures of sedimentary rocks of this type in the Lower Permian of Europe and the long-standing, widely accepted misconception that they represent an inhospitable, dry climate in which preservation of vertebrate skeletal remains would have been unlikely, discouraged interest in their exploration. The result has been a paucity of vertebrates collected from the terrestrial red-beds and an overwhelming concentration by palaeontologists on the lacustrine grey sediments and black shales in which have been found highly productive sites characteristically yielding obligatory aquatic amphibians.

Two obvious conclusions can be drawn from the above observations: (1) the similarity between the widely separated Early Permian assemblages of the Bromacker locality and those of the United

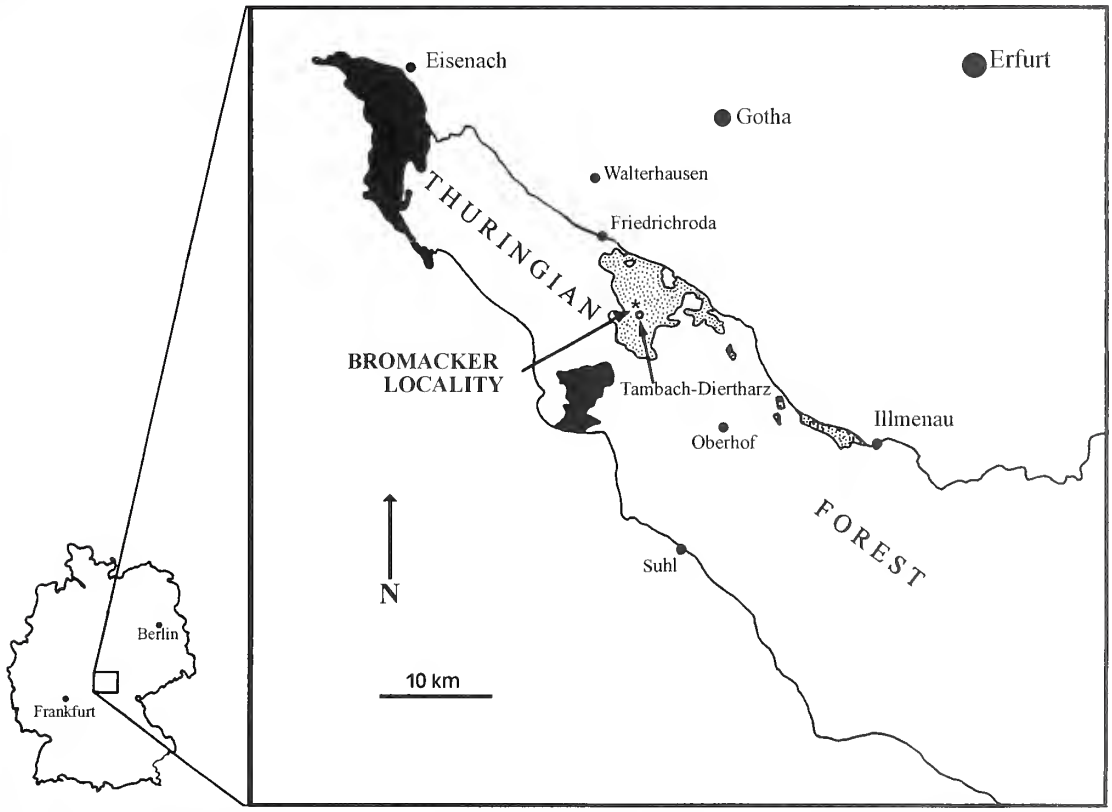

TEXT-FIG. 1. Map of Germany with inset showing Thuringian Forest area and Bromacker locality. Stippled areas indicate the extent of the Tambach Formation and solid areas the extent of other Early Permian strata (primarily Eisenach Formation) in the Thuringian Forest.

States can be attributed to a sampling of similar environments of deposition (Sumida *et al.* 1996); and (2) fluvial red-bed deposits, such as those at the Bromacker locality, are the most likely source of Early Permian terrestrial tetrapods in Europe. The broader aspect of these conclusions is that, with the expansion of the taxonomic similarities between the Early Permian tetrapod assemblages of North America and Europe, it can be assumed that barriers to faunal dispersal across Euramerica could not have been great, although regional differences are apparent and to be expected. Similar interpretations were offered by Milner (1993) based on similar taxa; however, the Bromacker assemblage offers the first example of a European assemblage that includes both similar genera as well as taxa congeneric with those found in North America.

GEOLOGY AND AGE OF THE BROMACKER LOCALITY

The Bromacker sandstone quarry is located near the village of Tambach–Dietharz, approximately 20 km south of the town of Gotha in the midregion of the Thuringian Forest (Text-fig. 1). The quarry is in the Tambach Formation, which in the Thuringian Forest is the lowermost unit of the Early Permian Upper Rotliegend, and is part of a sequence of terrestrial formations dated as Late Carboniferous (Stephanian) and Early Permian (Lower and Upper Rotliegend). The Stephanian–Rotliegend sediments of the Thuringian Forest were deposited in the south-western portion of the north-east-trending, intramontane Saale Basin which extends about 200 km to the north-east to include also the Halle Basin. The Saale Basin is one of many intramontane basins in central and

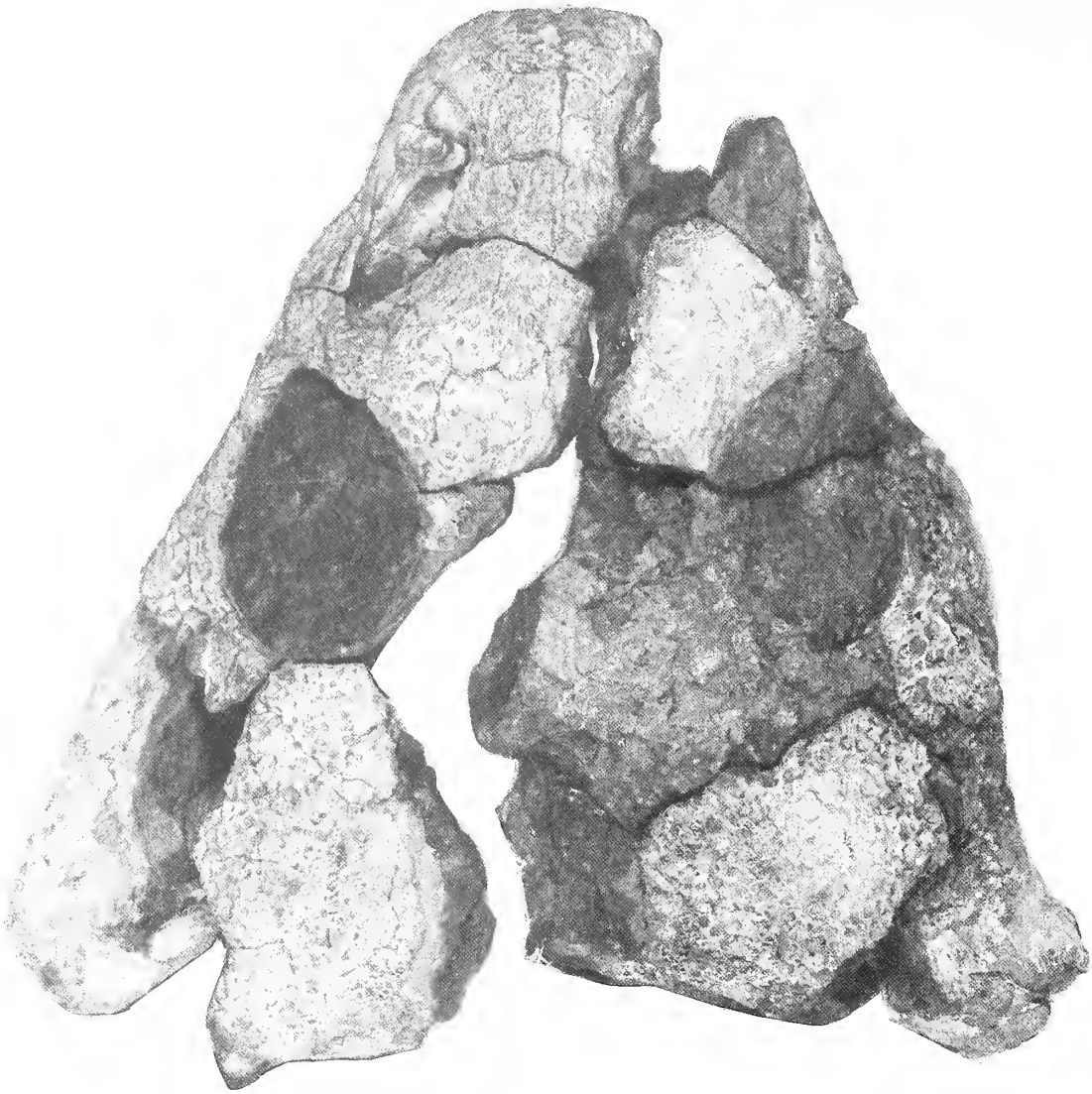

TEXT-FIG. 2. *Tambachia trogallas* gen. et sp. nov.; holotype, MNG 7722; skull in dorsal view; ×2.

western continental Europe that formed in close association with the Hercynian Orogeny. The basin sediments, originating mainly from the erosion of areas uplifted during the Hercynian Orogeny and filling associated with subsiding basins and fault blocks, lie disconformably on crystalline basement rocks of the uplift. They are overlain in places by the Late Permian marine Zechstein.

Exposures at the Bromacker locality are limited to the Tambach Formation, which consists of typical red-bed fluvial deposits that can be divided into three units: a basal streamflood-dominated conglomerate unit; a 60 m thick sandstone unit; and an overlying sheetflood-dominated fanglomerate unit (Berman and Martens 1993). An 8 m section of the upper level of the middle sandstone unit is exposed at the Bromacker locality. Within this section three distinct fluvial facies can be recognized, each containing particular types of fossils. The lower half of the section consists

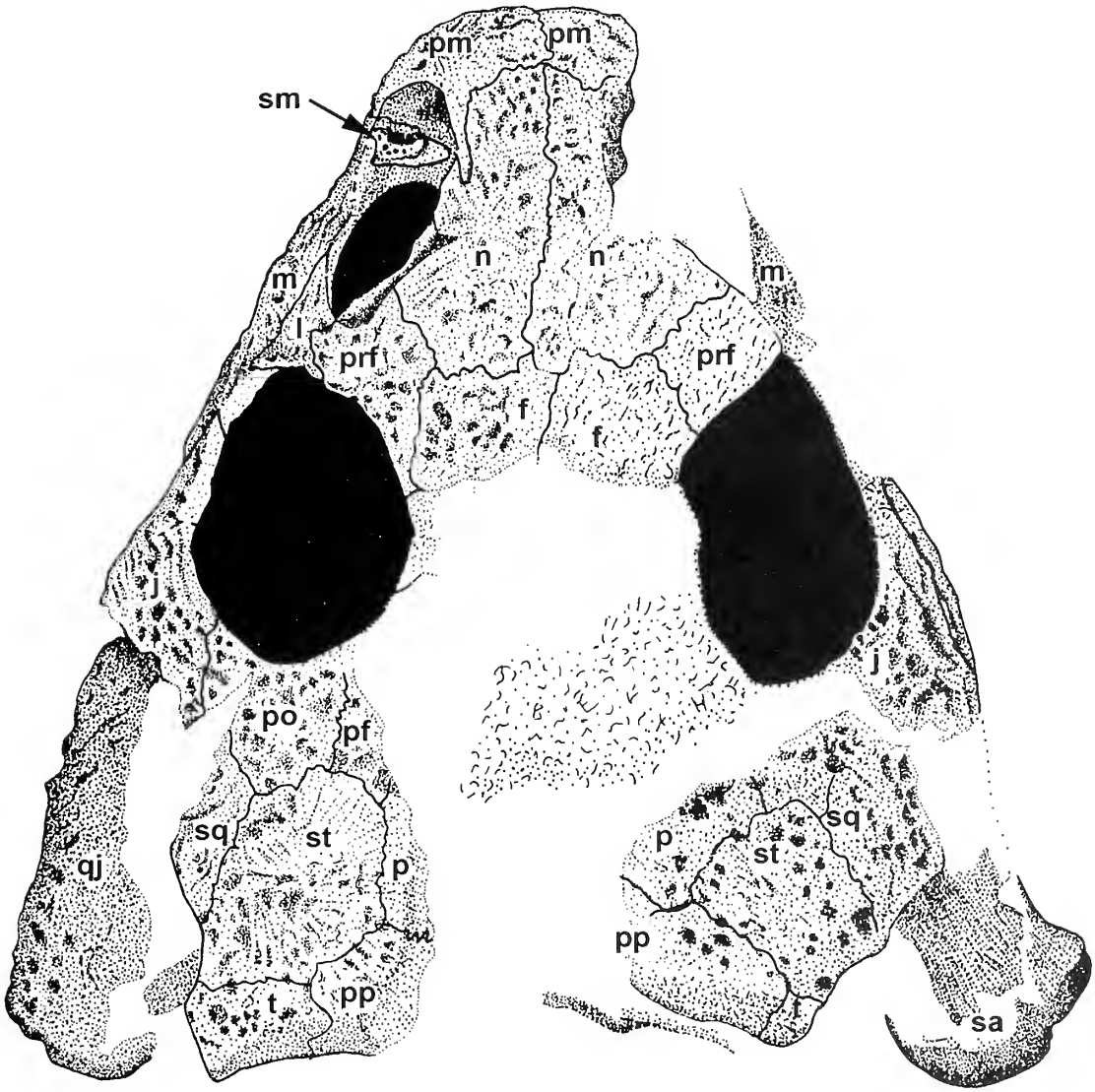

TEXT-FIG. 3. *Tambachia trogallas* gen. et sp. nov.; holotype, MNG 7722; illustration of skull in dorsal view as seen in Text-figure 2. Scale bar represents 10 mm.

of thick-bedded sandstones containing thin intercalations of silty mudstones originating from (possibly seasonal) floods, with mudcracks and numerous vertebrate trackways (Haubold 1971, 1973). In the middle portion of the section are flat-bedded channel fills composed primarily of mudstones and thin layers of unconsolidated clay pebbles. The channels are generally well consolidated and have yielded isolated insect and tetrapod remains the latter ranging from isolated bones to partially or completely articulated skeletons, including the new trematopid described here, and previously described tetrapods (Martens 1980, 1988, 1989; Boy and Martens 1991; Berman and Martens 1993).

Rock samples associated with the Bromacker trematopid were subjected to thin sectioning and

microscopic examination. They agree with the gross, sedimentological features of this level, revealing a brown to red-brown, silty claystone that is well cemented and contains small micaceous flakes. Cementation of the grains is indicative of a depositional environment of relatively low energy, possibly a flood plain or flood basin.

Determining the precise age of the Bromacker locality, as well as the stratigraphical levels of any of the Permian basinal sections of central or western Europe, is difficult for several reasons. The Rotliegend is strictly a lithostratigraphical term which refers to sediments that are underlain by the uppermost part of the Carboniferous (i.e. Stephanian C) and overlain by marine beds of the Zechstein (i.e. Upper Permian); the Rotliegend, therefore, cannot be considered to be either a biostratigraphical or chronostratigraphical unit. The same applies to the two divisions of the Rotliegend, the Lower, also called the Autunian (derived from the Permian basin in Autun, France) and the Upper, also called the Saxonian (derived from the Sachsen region in central Germany). The Carboniferous–Permian (C–P) boundary has traditionally been established on the basis of the lowest stratigraphical occurrence of a macroflora, the most important elements of which are *Callipteris conferta* and *C. naumanni*. However, the irregular occurrence of this in different basins or even within the same basin has made recognition of the C–P boundary difficult. In such instances the C–P boundary, as well as that between the Lower and Upper Rotliegend, has been identified by lithostratigraphical marker beds, in most cases conglomerates, which indicate the beginning of a rejuvenation of the Hercynian Orogeny. The absence of interbedded, easily dated marine sediments also makes it difficult to recognize a precise C–P boundary in the terrestrial sections of Europe. In several reviews of these problems, Kozur (1984, 1988, 1989) has rejected the widely accepted notion that the Rotliegend marks the base of the Lower Permian and can be recognized by the first appearance of certain plant fossils. Alternatively, Kozur redefined the C–P boundary in central Germany to agree with published accounts of abrupt changes in the flora and fauna that occur at a high level in the Lower Rotliegend (i.e. within the Lower Oberhof Formation in the Saale Basin of the Thuringian Forest). Furthermore, Kozur's reassignment of the C–P boundary agrees with the Early Permian Wolfcampian age assessment of the Bromacker locality based on the recently discovered tetrapod assemblage that includes the protorothyridid *Thuringothyris*, the seymouriamorph *Seymouria sanjuanensis*, and the diadectomorph *Diadectes* (Berman and Martens 1993; Sumida *et al.* 1996). The new trematopid described here also supports this age estimate for the Bromacker locality, as all known trematopids are from deposits ranging from the Late Pennsylvanian to Early Permian (Wolfcampian).

SYSTEMATIC PALAEONTOLOGY

Class AMPHIBIA Linnaeus, 1758
Order TEMNOSPONDYLI Zittel, 1888
Superfamily DISSOROPHOIDEA Bolt, 1969
Family TREMATOPIDAE Williston, 1910

Genus TAMBACHIA gen. nov.

Derivation of name. Refers to the formational unit in which the holotype was found.

Type species. *Tambachia trogalles* sp. nov.

Diagnosis. Trematopid temnospondyl amphibian that can be distinguished from all other members of the family by the following unique features: (1) subnarial process of lacrimal very short; (2) dorsal margin of otic notch extended posteriorly by a sculptured, downturned lateral expansion of the tabular; (3) the midline, occipital margin of the skull roof lies at a level nearly equal to the posteroventral corner of the skull roof; (4) a deep channel on the ventral surface of the parasphenoid separates the basipterygoid process from the body of the braincase; (5) the width of

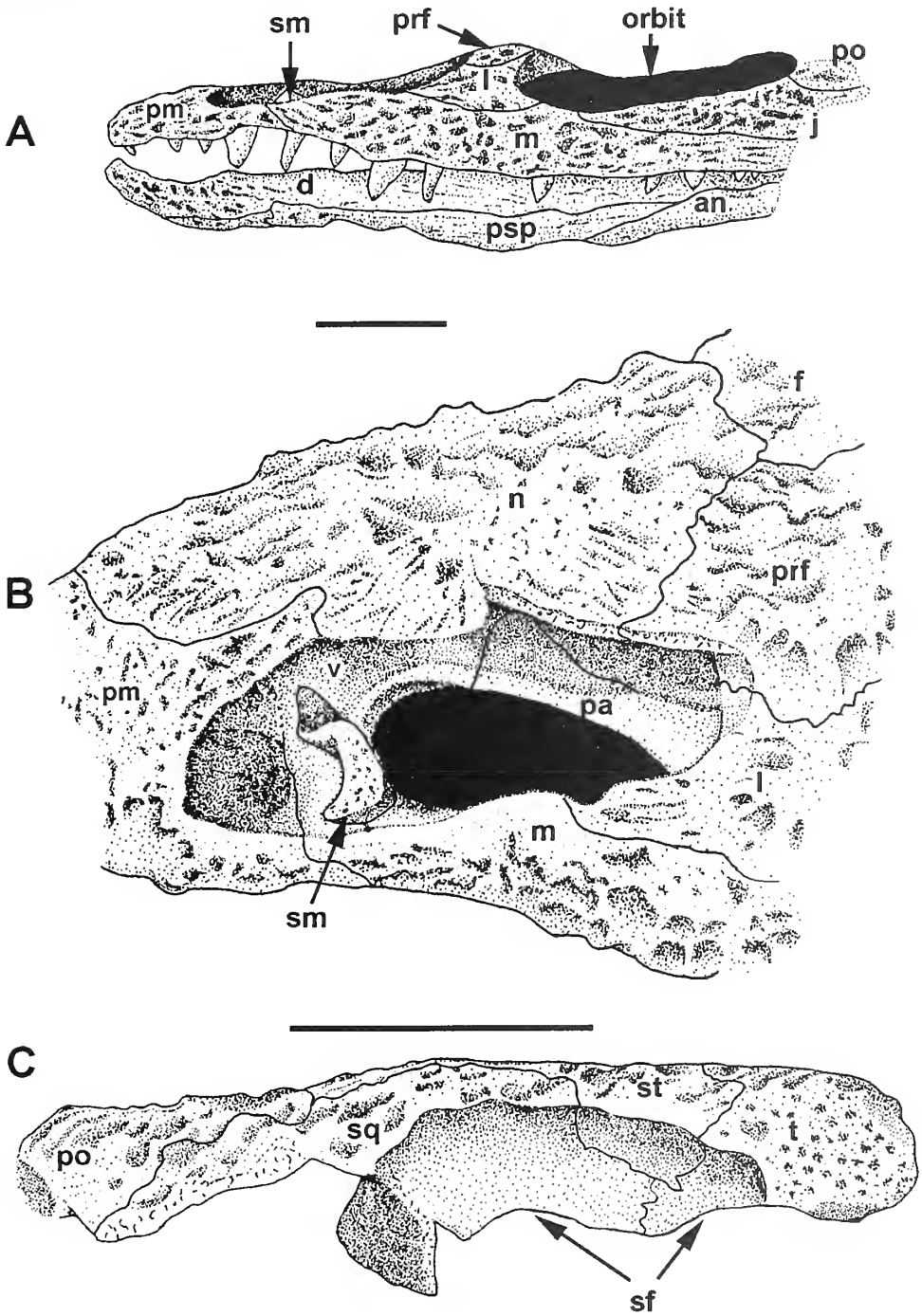

TEXT-FIG. 4. *Tambachia trogallas* gen. et sp. nov.; holotype, MNG 7722. A, snout region of skull and lower jaw in lateral view; B, left narial region of skull in dorsolateral view (lower jaw omitted); C, partial left otic region in lateral view. Scale bars represent 10 mm.

the basipterygoid process is extremely broad, extending along almost the entire lateral margin of the parasphenoid, and slightly exceeds the width of the internal process of the pterygoid.

Tambachia trogallas sp. nov.

Text-figures 2–9

Derivation of name. From the Greek *trogo*, munch or nibble, and *allas*, sausage, referring to the Thuringian bratwurst eaten frequently by the authors at Bromacker quarry.

Holotype. Museum der Natur Gotha, MNG 772; consists of isolated or displaced articulated portions of a skeleton, representing all major regions except the presacral column.

Horizon and locality. Uppermost level of the 60 m thick middle sandstone unit of the Early Permian Tambach Formation, Upper Rotliegend. The locality is a reactivated sandstone quarry known as the Bromacker locality near the village of Tambach–Dietharz, approximately 20 km south of the town of Gotha, in the Thuringian Forest of central Germany.

Diagnosis. As for genus.

DESCRIPTION

General. The only major portion of the skeleton of *Tambachia trogallas* MNG 772 not represented is the presacral column. The rest of the skeleton is preserved as isolated or displaced articulated portions that were distributed over an area of *c.* 0·02 m² and includes: the skull with the right interclavicle (Text-figs 2–3, 6–7), the greater portion of the tail (not figured), portions of the right and left forelimbs and manus without the carpals (Text-fig. 8), the right femur and portions of the sacral region (Text-fig. 9A), and the right hindlimb and pes, without femur and tarsals (Text-fig. 9B). It is difficult to assess the maturity of MNG 7722. On the one hand, the non-ossification of the carpals, tarsals, and endochondral portion of the braincase, and the absence of most of the detailed structures of the limb elements suggest an early stage of development. However, the pronounced sculpturing and the tightly closed sutures of the skull roofing bones suggests a mature specimen. This combination of developmental features probably indicates an early adult stage of development.

Skull roof. Most of the bones of the skull roof of *Tambachia trogallas* MNG 7722 are well represented, with the primary exception being a wide midline area that extends from between the orbits to the occipital margin and includes much of the frontals, parietals, postfrontals, and postparietals (Text-figs 2–3). During the course of preparation, the skull was separated grossly from the matrix covering its dorsal roof. The area of the bone-matrix contact was preserved in a shallow, natural, mould-like depression that contained the skull as a very light-green, reduced area which clearly defines most of the skull-roof margins against an otherwise red-brown matrix (Text-fig. 6). Whereas the orbit and external naris are preserved accurately, the skull width and curvature, particularly in the posterior region have been distorted severely by post-mortem, dorsoventral crushing. In dorsal view the restored skull (Text-fig. 5) appears sub-triangular in outline, with the ventrolateral margins of the postorbital cheek region being nearly parallel and the straight or slightly concave ventrolateral margins of the preorbital region converging strongly on a broad, blunt snout whose tip is truncated. It is impossible to determine the exact angle between the skull roof table and postorbital cheek region, but it must have approached at least 120°, giving the posterior half of the skull a box-like morphology. The occipital margin of the skull table is slightly concave and lies at a level nearly equal to the posteroventral corner of the cheek region. The left external naris and orbit are well preserved. Of the otic notches, only the horizontal dorsal border of the left is well preserved, and determination of the posteroventral slope of the ventral border cannot be determined due to crushing and loss of bone. Much of the dermal sculpturing of the skull roof is badly eroded, but enough remains to indicate that it was strongly developed. Preserved portions typically exhibit a pattern of shallow pits that are occasionally elongated into short furrows. On some of the larger dorsal roofing bones the sculpturing radiates from what were presumably centres of ossification.

The stoutly constructed premaxilla forms the anterior margin of the external naris, as well as the anterior and lateral walls of the rostral end of the nasal chamber. Its posterodorsal process is a narrow splint of bone

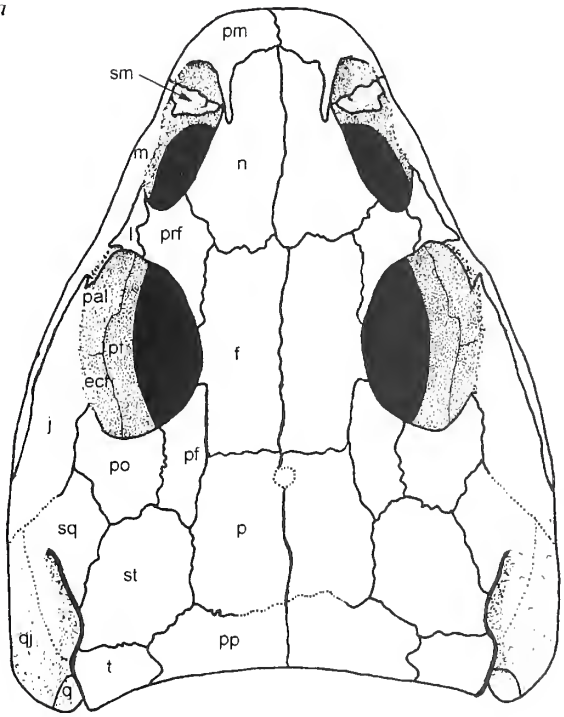

TEXT-FIG. 5. Reconstruction of the skull of *Tambachia trogallas* in dorsal view.

whose distal end penetrates the anterolateral margin of the nasal. There is no evidence of an internarial foramen at the junction of the premaxillae and nasals, as reported in some trematopids (Bolt 1974*a*; Dilkes 1990). Determination of the exact number of premaxillary teeth is difficult, due to incomplete preservation. Partial remains of four teeth and spaces for four more are evident in the left premaxilla, giving a minimum count of eight. The preserved series of teeth increase in size posteriorly, with the posteriormost being significantly larger and having a 'caniniform' appearance. They are blunt cones, but were undoubtedly sharply pointed and possibly recurved slightly in life. The long, slender maxilla can be observed clearly only on the left side of the skull. Anteriorly, it overlaps dorsally the maxillary process of the premaxilla as it forms the central-lateral border of the external naris and a narrow portion of the lateral floor of the narial chamber. As such, it also forms most of the lateral margin of the internal naris. A short distance posterior to its contact with the premaxilla and at the posterior end of its contribution to the ventral rim of the external naris the maxilla attains its greatest dorsal height producing a partial subdivision of the external naris. Immediately posterior to this point there is an abrupt, but slight reduction in the height of the maxilla, which is essentially maintained until just behind the antorbital bar. Here, the maxilla makes a very small entrance into the ventral margin of the orbit before steadily narrowing posteriorly; although not complete posteriorly, it undoubtedly tapered to a very thin splint that ended at a level well behind the orbit. The left maxilla possesses nine teeth identical in shape to those of the premaxilla, with spaces for approximately 12 or more teeth; an exact count is impossible due to poor preservation and the extremely small size of the posteriormost teeth, but is estimated as well over 20. The third preserved tooth, probably representing the fifth tooth position, is clearly the largest of the series, and thus, as in the similarly sized posteriormost premaxillary tooth, has a 'caniniform' appearance.

As in other trematopids, the external naris (Text-fig. 4A–B) is elongated and subdivided into two portions by the low, broad, dorsal expansion of the maxilla a short distance posterior to the septomaxilla. Bolt (1974*a*) described the division in trematopids as being formed by the dorsal expansion of the maxilla and a ventrolateral process of the nasal. That the anterior, sub-circular division of the external naris was the true or functional narial opening has been generally accepted (Bolt 1974*a*; Berman *et al.* 1987; Dilkes 1993). Bolt (1974*a*) interpreted the longer posterior division of the external naris as probably having accommodated a specialized gland, possibly a salt gland that developed lateral to the nasal capsule and homologous to the external nasal gland found in most living reptiles. On the other hand, Dilkes (1993) argued convincingly that, if the trematopids possessed a salt gland like that found in modern reptiles, it would not account for the posterior

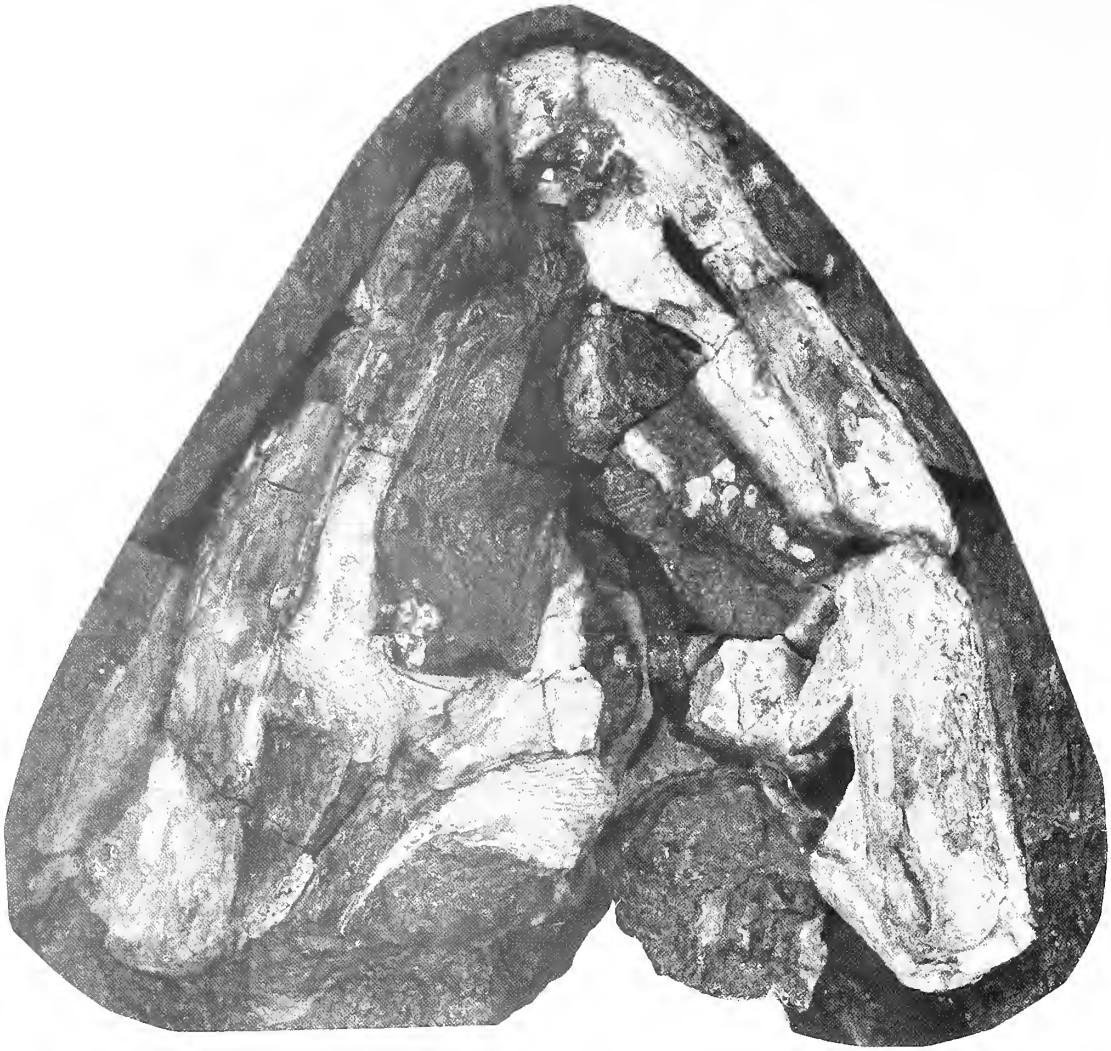

TEXT-FIG. 6. *Tambachia trogallas* gen. et sp. nov.; holotype, MNG 7722; skull in ventral view with right clavicle covering posterior margin of braincase; skull has been replaced in a natural, mould-like depression from which it was removed during preparation; × 1·74.

expansion of the external naris. The existence of the salt gland is equivocal, and although Dilkes (1993) suggested that the posterior expansion is possibly related to alterations of cranial stresses during feeding, the function remains unclear. The anterior portion of the external narial opening, the true external naris, is floored by the vomer, whereas the posterior portion directly overlies the internal naris.

Only the left septomaxilla is preserved and appears to occupy nearly its correct position. It is supported by the anterior end of the maxilla along the ventral margin of the external naris, but has apparently tilted inward on its base at *c.* 45° from a nearly vertical orientation which would have brought it into close proximity and, possibly even contact with, the lateral margin of the nasal. A helical twisting of the septomaxilla divides it into two components: a ventral portion consisting of an externally sculptured, laterally directed, lunate flange and a smaller dorsal portion that has the form of a triangular process.

Of the medial roofing bones, only the nasals are well represented. Although their margins bordering the external nares are incomplete, enough remains to suggest the absence of the triangular, ventrolateral projection

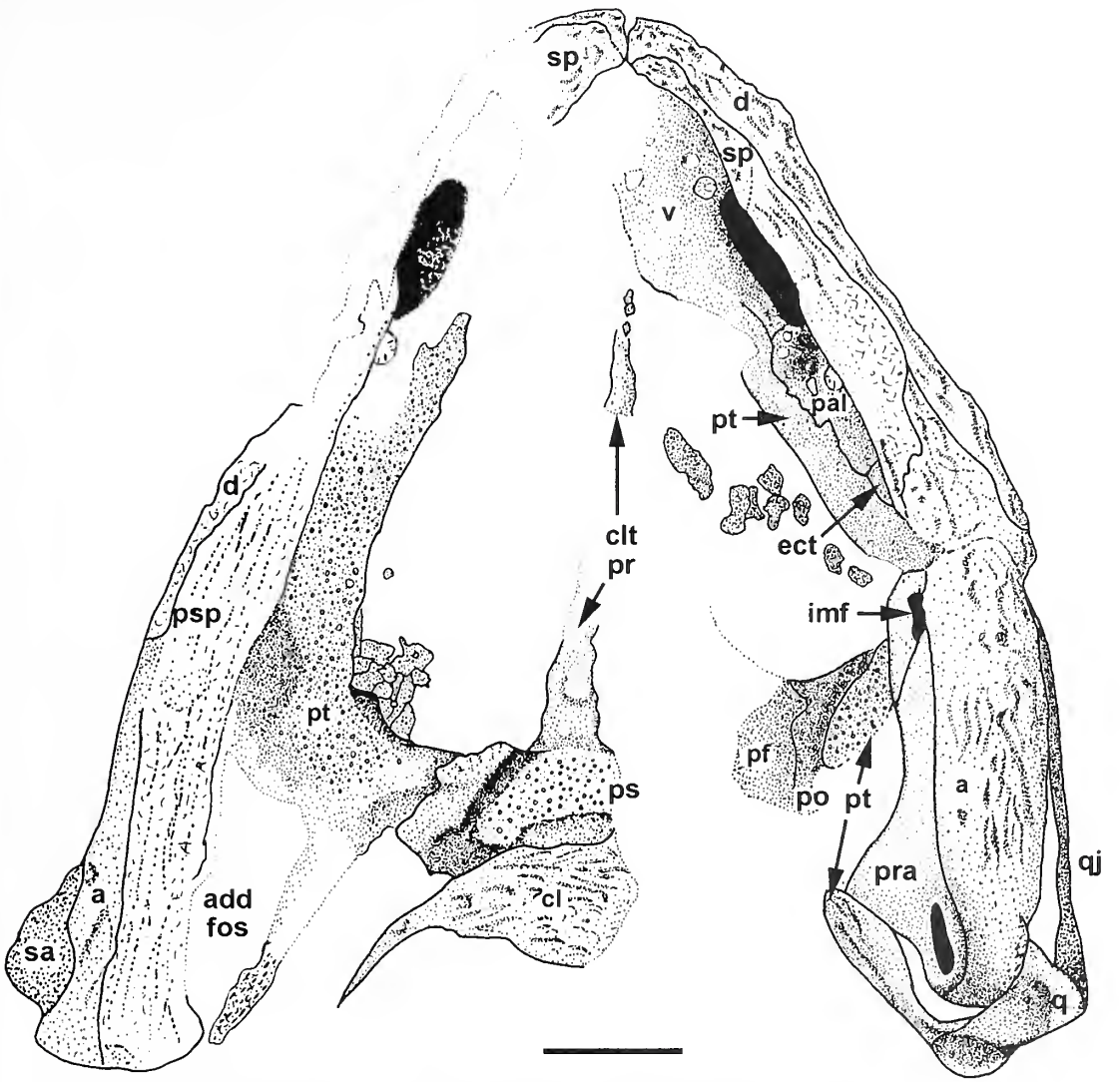

TEXT-FIG. 7. *Tambachia trogallas* gen. et sp. nov.; holotype, MNG 7722; illustration of skull and right clavicle in ventral view as seen in Text-figure 6. Scale bar represents 10 mm.

that partially divides this opening in some trematopids (Bolt 1974*a*; Dilkes and Reisz 1987; Dilkes 1990). A pronounced lateral expansion of the nasals as they extend posteriorly along the margin of the external naris gives them a pentagonal outline and a combined transverse width that is slightly greater than their midline length. The left frontal indicates that this bone had a moderate entrance into the orbit. What remains of the parietals indicates no deviation from the expected trematopid pattern. The sub-rectangular postparietals have a combined transverse width that is approximately four times their midline length. Although their occipital margins are poorly preserved and the posteroventral projecting occipital flanges are absent, the postparietals clearly define a very shallow, concave occipital margin of the skull roof.

The left and only preserved lacrimal is complete and forms the lower half of the very narrow antorbital bar. From its base it sends forward a very short, stout subnarial process along the ventral margin of the posterior portion of the external naris. The subnarial process ends at the posterior margin of the low, anterior dorsal expansion of the maxilla. There is almost no posterior extension of the base of the lacrimal in the form of a suborbital process. The left prefontal is essentially complete and exhibits the general pattern for dissorophoids,

whereas the right is missing the posterior extension along the orbital margin. A ventral process of the prefontal, extending along the anterior wall of the orbit medial to the lacrimal in various dissorophoids (Bolt 1974*b*; Dilkes 1990), is not evident in MNG 7722. Projecting from the ventral surfaces of the nasal, prefrontal and lacrimal just medial to the dorsal rim of the external naris is a vertical flange (not visible in the Text-figures given here) designated as the nasal flange by Bolt (1974*a*) and the narial flange by Dilkes (1990, 1993). For most of its anterior length the narial flange is oriented in a parasagittal plane. Posteriorly, the flange gradually deepens ventrally, then curves abruptly laterally to merge with the medial surface of the antorbital bar.

Only small portions of the postfrontals remain, and their relationships to neighbouring elements remain mostly undeterminable. The nearly complete left postorbital is like that in all dissorophoids.

Only the left supratemporal and tabular bones of the temporal series are well preserved, including their contributions to the otic notch, but the posteroventrally projecting occipital flange of the tabular is missing. The supratemporal is large, with a greatest width-to-length ratio of approximately 0·72. The sculptured, dorsal-roof portion of the tabular is rectangular; its lateral margin curves abruptly downward to form a large, rectangular sculptured area at the posterior end of the dorsal margin of the otic notch; clearly the postero-lateral corner of the tabular was not drawn out into a horn-like extension as in some trematopids (Olson 1941; Dilkes and Reisz 1987). The otic notch is represented only by the complete dorsal margin of the left otic region (Text-fig. 4c). The ventral margin of the notch, which was presumably formed by the squamosal and quadratojugal and sloped posteroventrally, is not preserved on either side of the skull. The greater anterior portion of the vertical shelf of bone forming the dorsal margin of the otic notch consists of a broad, well-defined smooth or unsculptured area, the supratympanic flange, which compares closely to that of other trematopids (Bolt 1974*b*; Berman *et al.* 1987; Dilkes 1990). As the supratympanic flange extends posteriorly it gradually narrows, with its slightly dorsally convex margin curving downward to the otic notch to form the anterior border of the laterally downturned, sculptured portion of the tabular. The squamosal, supratemporal, and tabular portions of the supratemporal flange are clearly visible. There is a substantial contact between the squamosal and tabular that excludes a subrounded supratemporal portion, the 'semilunar flange of the supratemporal' of Bolt (1974*b*), from the ventral margin of the supratympanic shelf. At the level of this contact the squamosal and tabular contribute to a short, broadly convex process of the ventral margin of the supratympanic flange which projects into the otic notch. This flange, designated the 'semilunar curvature' by Bolt (1974*b*), is present in dissorophids (Carroll 1964; DeMar 1968; Bolt 1974*c*; Berman *et al.* 1985) and the trematopid *Phonerpeton* (Dilkes, 1990).

Palatal complex. Not only are large portions of the palate missing or poorly preserved, but its description is also limited by the tightly attached lower jaws (Text-figs 6–7). However, enough of the palate remains to give a reasonable account, with the added advantage that a small portion of it can be seen in dorsal view through the left external naris and orbit (Text-fig. 4b). Almost the entire left vomer is visible, and the portion bounding the anterior end of the internal naris is visible through the external naris. The area of the medial union of the vomers is too poorly preserved to indicate whether they formed a deep, wide internarial pit on their ventral surface, as is typical in trematopids (Olson 1941; Dilkes 1990). A palatine process of the vomer appears to form almost the entire narrow, lateral border of the internal naris before contacting the anterior end of the pterygoid to exclude the palatine from the widely expanded interpterygoid vacuity. A moderately sized tusk and matching socket is located on the vomer near the anterior margin of the internal naris. Viewed through the left external naris (Text-fig. 4b) the vomer can be seen to form much of the floor and medial wall of the nasal chamber. Anteriorly, at the level of the anterior portion of the true external naris, the medial wall curves laterally and appears to extend dorsally to the ventral surface of the nasal. Posteriorly, at the level of the internal naris, the medial wall lies medial to the narial flange, is oriented anteroposteriorly, and slopes dorsomedially to an undetermined height. The vomerine medial wall of the nasal chamber was described by Dilkes (1990, p. 230) in the trematopid *Phonerpeton* as the 'median bony lamina' of the vomer. In addition, he referred to the paired medial laminae of the vomers as a single structure, the median vomerine septum. Bolt (1974*a*) and Olson (1941) described the same structure in trematopids, but used different terminologies.

All but the lateral margin of the left palatine is exposed in palatal view. Anteriorly it forms the posterior margin of the internal naris, and its posterior extent and level of contact with the ectopterygoid is also comparable to that of other trematopids. A short distance posterior to the internal naris the palatine bears a large tooth; it probably was associated with a socket of equal size. Only a very small portion of the anterolateral margin of the left ectopterygoid is visible. Neither the ectopterygoid nor the palatine has an exposure on the dorsal or lateral surface of the ventral orbital rim, as is common in dissorophoids (DeMar 1968; Bolt 1974*b*; Dilkes 1990).

Although neither pterygoid is complete, the combined features of both exhibit the standard temnospondyl

form that can be divided into palatal (anterior) and quadrate rami, and a basipterygoid region. The palatal ramus and basipterygoid region form most of the lateral and posterior margins of the heart-shaped interpterygoid vacuity. The ventral surface of the right pterygoid is well enough preserved to indicate a dense shagreen covering of tiny denticles on the palatal ramus and the base of the basipterygoid region. The medially directed, process-like basipterygoid region, referred to here by Daly's (1994) designation as the internal process, is a very stoutly built, broad, flat structure that is directed medially and slightly dorsally to its distal articulation with the basipterygoid process of the braincase. An articular facet extends as a broad band across the entire ventral width of the distal end of the internal process, faces ventromedially, and appears to have a very shallow, concave surface. The basicranial joint was clearly open and mobile. The narrow quadrate ramus bordered the sub-triangular subtemporal fossa medially.

The only preserved and visible portion of the quadrates is the ventral surface of the left condyle. Although its posterior margin is incompletely preserved, what remains indicates a typical bicondylar structure. It is not possible to determine whether a posterodorsal process of the quadrate was present, as in other dissorophoids (Bolt 1977*a*).

Within the interpterygoid vacuity and occupying the same level as the palate are numerous, small, widely distributed, irregularly shaped plates. Most are scattered, but along the posterolateral margin of the right pterygoid they are arranged in a tightly fitting mosaic, with some appearing to possess minute denticles. The plates are interpreted as remnants of a mosaic of tight-fitting, denticulated ossifications which lay within the skin covering the palate, but were restricted to the area of the interpterygoid vacuity. Similar structures have been reported in other dissorophoids. Carroll (1964) described an ossified 'skin' membrane covering the entire palate of *Amphibamus lyelli*, whereas Berman and Berman (1975) noted the presence of an ossified, denticulated 'skin' covering the interpterygoid vacuity region of the palate in *Broiliellus hektotopos*.

Braincase. The only visible and presumably preserved portion of the braincase is the parasphenoid, which is visible in the ventral view of the skull (Text-figs 6–7). A large, central portion of the narrow, anteriorly tapering cultriform process is missing. The process obviously extended to at least the posterior, midline union of the vomers. Near the base of the process is a small, hemispherical protuberance. Its function is unknown, but Clack and Holmes (1988) have noted paired depressions in the same location in anthracosaurian amphibians which they suggest may have provided for attachment of extraoccular muscles. Although the left side of the body of the parasphenoid is missing and its posterior margin is concealed by the right clavicle, it obviously had the outline of a laterally expanded quadrangle whose lateral margins angled anteromedially. In the anteromedial region is a slightly raised, triangular field of denticles of the same size as those of the pterygoid. A conspicuously deep furrow separates the right margin of the field and the smoothly surfaced, basipterygoid process. The basipterygoid process is unusual in being extraordinarily broad, having a width that extends across the entire lateral margin of the body of the parasphenoid and slightly exceeds the width of the distal portion of the internal process of the pterygoid. The basipterygoid process of the braincase is directed slightly ventrally, and its dorsal articular surface faces dorsolaterally and has a slightly convex surface that fits snugly into the concave articular surface on the internal process of the pterygoid.

Lower jar. The mandible is firmly attached to the skull, with only the left rami being preserved well enough to allow substantial description of the ventral portions of the lateral and medial surfaces (Text-figs 4A, 6–7). The jaw shows no strong deviation from the general trematopid pattern (Berman *et al.* 1987; Dilkes 1990), and only a few comments are necessary. Much of the sculpturing, which is mainly limited to the lateral surface of the jaw, has been severely damaged due to weathering. What remains indicates a coarse texture of irregular, longitudinal grooves which are replaced by small oval to circular pits near the symphysis. Although both the dentary and splenial enter the symphysis, the former element is the dominant contributor. An inframeckelian foramen is located on the ventromedial margin of the jaw at the posterior end of the postsplenial and adjacent to the angular-prearticular suture. At the posterior end of the medial rim of the adductor fossa there is a pronounced, medially directed, flange-like inflection of the prearticular. A large, oblong para-articular foramen penetrates the prearticular near its posteriormost margin.

Axial skeleton. Very little remains of the axial skeleton. Remnants of a string of three poorly preserved vertebrae are exposed in dorsal view between the dorsal blades of the associated ilia (Text-fig. 9A). The anterior two vertebrae are too fragmentary to comment upon, except to note that the configuration of the second suggests that it is a true sacral vertebra. The much better preserved third vertebra of the series, represented by the neural arch in dorsal view, is therefore believed to be the first caudal. Its short, stout neural spine appears circular in horizontal section. The buttresses of the prezygapophyses slope ventrally as they diverge anteriorly

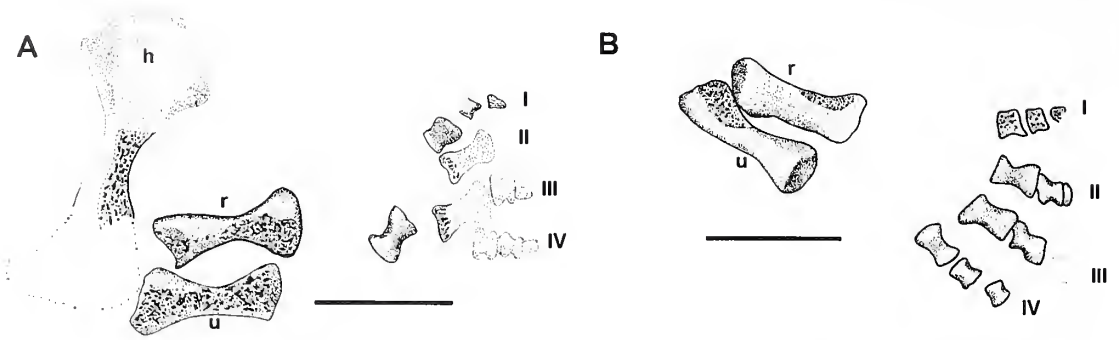

TEXT-FIG. 8. *Tambachia trogallas* gen. et sp. nov.; holotype MNG 7722; partial right, A, and left, B, forelimbs and manus. Scale bars represent 10 mm.

from the base of the spine, producing a shallow V-shaped depression between them. Short, broad transverse processes are directed laterally and slightly posteriorly. What is undoubtedly the right sacral rib exposed in posterior view is closely associated with the vertebrae. The broadly expanded head tapers quickly to the thin, arcuate posterior edge of the shaft. A confusion of remnants of several unidentified bones is also preserved in close association with the sacral elements.

A large portion of the tail (not shown) is represented by an impression of an articulated series of vertebrae that has been displaced several tens of millimetres from the first caudal vertebra described above. The impression is 85 mm long and very faint, and the only structures that can be discerned clearly are short neural spines and haemal arches of the anterior 6 mm of the series. They attain a maximum length of approximately 4 mm at the anterior end of the series.

What may be an isolated neural arch and rib are closely associated with the right hindlimb (Text-fig. 9B).

Appendicular skeleton. All that remains of the pectoral girdle is the right clavicle preserved in a position covering the posterior ventral margin of the braincase (Text-figs 6–7). The clavicle consists of a relatively broad, triangular ventral plate that is approximately as long as it is wide. It is continued with a narrow, dorsal stem that tapers distally, but, due to dorsoventral crushing, the two components occupy the same plane with their external surfaces exposed. The medial margin of the ventral plate is incomplete, and the remainder of its external surface exhibits a sculpturing pattern of transversely oriented, irregular ridges and grooves. The non-sculptured stem joins the ventral plate in a smooth arc.

A partial right humerus is preserved (Text-fig. 8A), but, unfortunately, most of the information about this element is derived from an impression, leaving little or no account of its detailed structure. The length of the humerus can be estimated to be at least 26 mm. The proximal head is broadly flared, and the presence of a well-developed deltopectoral tuberosity is indicated by a deep depression adjacent to the anterior margin of the head. The shaft is distinctly differentiated from the proximal head and is oval in cross section, with the long axis lying in the same plane as the head; the oval cross section may have been exaggerated by post-mortem crushing. The proximal and distal heads are not twisted about the shaft and thus lie in the same plane. However, this probably does not reflect the life position and is possibly also due to crushing. Although most trematopids exhibit a well developed supinator process, *Tambachia* is not preserved well enough to allow confident determination of its presence or absence.

The radius, ulna, and manus of both forelimbs are preserved (Text-fig. 8). The radius is 13 mm long, with the right one more accurately portraying the outline shape of the element. The proximal and distal ends taper, more strongly so on the lateral margin, to a short, narrow shaft that is sub-circular in cross section. There is no evidence of a laterally directed shelf of the shaft as in *Phonerpeton* (Dilkes 1990). The ulna is approximately 16 mm long. Its shaft is strongly waisted, more so on the medial margin, and mediolaterally is oval in cross section. Although there is no obvious development of an ossified olecranon process or semilunar notch, there is a pronounced extension of the lateral margin of the proximal head; the olecranon process is apparently one of the last appendicular skeletal structures to ossify fully (Berman *et al.* 1985).

No carpal elements are preserved. Each manus (Text-fig. 8) consists of four metacarpals and the digits that they support. The metacarpals and phalanges are short and stout; those of the left manus, however, are represented primarily as impressions. As a complete manus is unknown in trematopids, it cannot be assumed

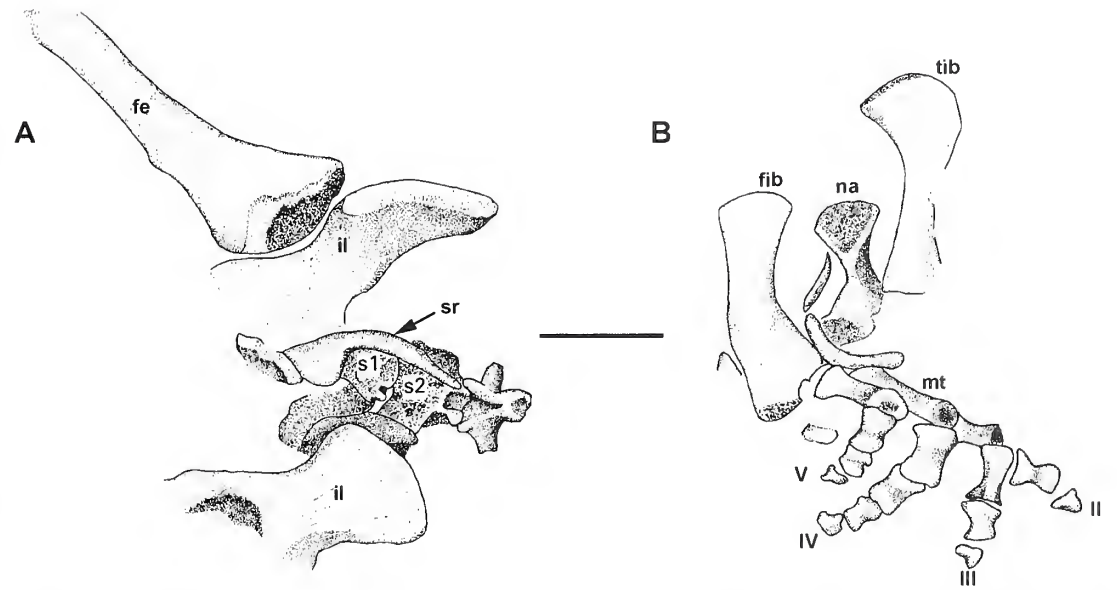

TEXT-FIG. 9. *Tambachia trogallas* gen. et sp. nov.; MNG 7722. A, portion of pelvic-sacral region and right femur in mainly dorsal view. B, partial right hindlimb and pes. Second metatarsal is not visible in this view. Scale bar represents 10 mm.

that a fifth metacarpal and digit were not present. A manus consisting only of the carpus was described (Williston 1909; Olson 1941) in *Acheloma* (as *Trematops*) as having five distal carpals. If true, then it might be expected that five digits were also present. On the other hand, the primitive, Late Pennsylvanian dissorophoids *Amphibamus* and *Eoscopus* both possess four metacarpals with digits (Carroll 1964; Daly 1994). The metacarpals in *Tambachia* increase in size through to the third, whereas the fourth is intermediate in size between the first and second. On the basis of both left and right manus, the preserved phalangeal formula is 2,2,2,3; the second and third digits obviously each lack at least the distal phalanx.

All that is visible of the pelvic girdles are the dorsal blades of the ilia (Text-fig. 9A), the right in medial and the left in lateral view. The blades are low and slightly waisted, lack indications of a posterior extension or process, and thicken slightly toward the crest. Their smoothly finished surfaces exhibit no scars for muscular or ligamentous attachments.

Of the hindlimb and pes only elements from the right side are represented. The femur (Text-fig. 9A) is preserved in association with the pelvis and separated by a short distance from the rest of the limb and pes (Text-fig. 9B), which include the tibia, fibula, and four metatarsals and digits preserved in articulation, or in nearly their correct association. The absence of the tarsals is almost certainly due to non-ossification and reflects immaturity. All that remains of the femur is the proximal head, exposed in dorsal or anterodorsal view, and most of the shaft preserved as an impression. As preserved, the femur measures 26 mm long, but the total length was probably about 30 mm. Its expanded head bears no distinct processes and quickly tapers to a long, narrow shaft. The partially exposed articular surface is of unfinished bone. The strongly compressed tibia and fibula are essentially complete and measure *c.* 18 mm long. The articular margin of the greatly expanded proximal head of the tibia is strongly convex in dorsal view, but much less so along its more expanded lateral portion. The medial and lateral margins of the bone are deeply concave; more so along the lateral margin because of the greater lateral expansion of the proximal head. The shaft is narrowest at the midlength of the bone, where it is sub-circular in cross section. The distal head is modestly expanded and symmetrical, and, although not complete, appears to end in a transverse articular margin that is oval in end view. Neither the proximal nor the distal articular surface of the fibula is completely preserved or visible. The proximal head is only modestly expanded, with the articular margin being slightly convex in dorsal view. In end view the articular surface is weakly crescentic in outline, with the convex margin being dorsad. The distal head is more expanded than the proximal head, and its articular margin is very slightly convex in dorsal view. A dorsal thickening of the lateral half of the distal head produces a low, broad ridge that becomes slightly more

pronounced as it extends to the articular margin. Only the lateral half of the distal articular surface is visible and is clearly sub-elliptical in outline, with the medial end gradually tapering to a much thinner surface. The shaft, which is narrowest at the midlength of the bone, has a straight or very slightly convex lateral margin and a strongly convex medial margin, giving the bone a bowed appearance.

It is assumed that the pes originally possessed five metatarsals and digits. Of the four preserved metatarsals, the two central ones are the longest and are subequal in length. Four digits are associated with the metatarsals and are complete, as indicated by their terminal phalanges ending in a narrow, pointed core support for a claw. Because the third preserved digit possesses the greatest number of phalanges and is the longest, it undoubtedly represents the fourth digit. Therefore, it is assumed that the preserved metatarsals and associated digits represent two through to five and that the first metatarsal and digit are absent. On this basis the phalangeal formula for the pes would be ?–2–3–4–3. There is evidence to accept this partial formula, and the first digit probably possessed two phalanges. Daly (1994) described the phalangeal formula of the pes in the Late Pennsylvanian amphibamid dissorophoid *Eoscopus* as 2–2–3–4–3. Further, she reinterpreted the 2–3–4–4–2 pes formula given by DeMar (1968) for *Dissorophus* as more probably 2–2–3–4–3, concluding that this is a more common formula among temnospondyls.

ASSIGNMENT AND RELATIONSHIPS OF *TAMBACHIA*

Tambachia *as a trematopid*

Significant work has been done on the structure and relationships of dissorophoids by Boy (1972); however, the two most recent phylogenetic schemes of intrarelationships of this group, both based on cladistic methodology, have been presented by Dilkes (1990) and Daly (1994). These can be utilized to determine the phylogenetic position of *Tambachia* within the superfamily. In Daly's (1994) analysis, the more comprehensive of the two, three major families of the Dissorophoidea are recognized: Amphibamidae, consisting of the aquatic genera *Amphibamus*, *Eoscopus*, *Doleserpeton* and *Tersomius*, was determined to be an early derivative of the Dissorophoidea, whereas the terrestrial families Trematopidae and Dissorophidae were considered more closely related to one another than either is to Amphibamidae. Boy (1972) has also argued for the removal of *Amphibamus* from Dissorophidae and placement in its own family. In considering the aberrant dissorophoids *Platyhystrix*, *Astreptorhachis*, and *Ecolsonia*, viewed as dissorophids by most authors (Vaughn 1971; Berman *et al.* 1981; Berman *et al.* 1985), Daly united the first two in a new family, the Platyhystricidae, whereas the familial assignment of *Ecolsonia* was judged as unresolved and best left as *incertae sedis*. In Dilkes' (1990) analysis, Dissorophoidea was treated as if consisting only of the families Trematopidae and Dissorophidae. However, the problematical genera *Amphibamus* and *Tersomius*, traditionally considered as unarmoured members of the Dissorophidae (Carroll 1964; DeMar 1968; Bolt 1974*a*), were suspected by Dilkes to have probably shared a more distant relationship with the trematopids and other dissorophids. On the basis of this relationship, Dilkes used *Amphibamus* as the outgroup, although still considering it a dissorophoid, in his analysis of the intrarelationships of the Trematopidae. The validity of his choice of *Amphibamus* as an outgroup was, therefore, reaffirmed by the results of Daly's (1994) study. Here we utilize both *Amphibamus* and the more recently described *Eoscopus* for outgroup information.

In addition to *Tambachia*, only four other genera can be assigned to the Trematopidae: *Acheloma* Cope, 1882, *Actiobates* Eaton, 1973, *Anconastes* Berman, Reisz and Eberth, 1987 and *Phonerpeton* Dilkes, 1990. Familial assignment of two of these genera, however, has been questioned. Dilkes (1990) only tentatively assigned *Anconastes* to the Trematopidae, as available material permits recognition of only two of the five synapomorphies recognized by him as uniting it with other members of the family. On the other hand, three of the five characters used by Daly (1994) to define Trematopidae can be confirmed in *Anconastes*, and, as it exhibits no dissorophid features (Berman *et al.* 1987), there is little doubt that its original assignment was correct. In addition, *Anconastes* shares three derived characters with *Tambachia* (discussed below) that not only further support a trematopid assignment of the former, but indicates that the two genera are more closely related to one another than either is to any other trematopid. *Actiobates* was excluded by Dilkes (1990) from his analysis of the interrelationships of the trematopids on the assertion that it possessed a

combination of trematopid and dissorophid characters. This view was also expressed in the original description of *Actiobates* by Eaton (1973), who believed it to be a dissorophid with a trematopid-like external naris. However, Berman *et al.* (1985) effectively argued that *Actiobates* is a trematopid and that the few dissorophid-like features it appears to exhibit most probably represent a juvenile, probably early postmetamorphic, stage of development. Daly (1994) apparently also viewed *Actiobates* as a trematopid, but excluded it from her cladistic analysis of the dissorophoids. Of the five characters she used to diagnose Trematopidae, the holotype and only known specimen of *Actiobates* allows examination of three, all of which confirm her assignment. This was further confirmed by Milner (1985), who, on reconsidering the familial status of *Actiobates*, provisionally placed it in Trematopidae. Finally, after re-examining the holotypes of *Acheloma cumminsi* Cope, 1882, and *Trematops milleri* Williston, 1909, Dilkes and Reisz (1987) declared the latter to be a subjective junior synonym of the former. Thus, as they asserted, the commonly applied name *Trematops* is invalid and must be replaced by *Acheloma*.

In view of the similarity of the assessments by Dilkes (1990) and Daly (1994) of the relationship of the Amphibamidae as the sister outgroup to the Trematopidae and Dissorophidae, it is not surprising that they presented nearly identical lists of characters to define Trematopidae. In the following list of synapomorphies uniting the trematopids, characters 1 through to 4 were used by both authors, whereas characters 5 (with modifications) and 6 were used only by Dilkes and Daly, respectively.

1. *Presence of an elongate external naris.* This character was expanded by Dilkes (1990, p. 238) to include the presence of 'a concave narial flange composed of separate sheets from the nasal, prefrontal, and lacrimal that meets the antorbital bar'. The use of the shorter, traditional version of this character was argued for by Daly (1994), because she noted the presence of a narial flange in the amphibamids *Eoscopus* and *Tersomius*. On the basis of this distribution, the presence of a narial flange was instead used by Daly to define Dissorophoidea. The presence of an elongated external naris in the dissorophid *Ecolsonia* must, therefore, be considered a homoplastic feature (Berman *et al.* 1985). An elongated external naris and a nasal flange are present in *Tambachia*, and both structures conform in detail to those in all other trematopids.

2. *Presence of a premaxillary caniniform tooth beneath the functional external naris and a pair of maxillary caniniform teeth below the posterior expansion of the external naris.* This character, originally noted by Olson (1941) as distinguishing the trematopids from dissorophids, was later used by Berman *et al.* (1987), as well as by Dilkes (1990) and Daly (1994); it is present in *Tambachia* and all other trematopids.

3. *Presence of a median vomerine septum.* This character was originally described as unique to the trematopids by Dilkes and Reisz (1990) and Dilkes (1990), and was accepted by Daly (1994) as defining the family. This structure appears to be present in *Tambachia*, and additional preparation has also revealed its presence in *Anconastes*. The area of the median vomerine septum was not described in the original description of *Actiobates* by Eaton (1973), and its presence or absence probably could not be demonstrated without partial destruction of the holotype.

4. *Inflection of the prearticular along the medial rim of the adductor fossa.* The use of this character to define Trematopidae was proposed by Dilkes (1990) and was subsequently accepted by Daly (1994). Dilkes (1990) was able to identify this character with certainty only in *Acheloma* and *Phonerpeton*; the area of the adductor fossa is unknown in *Actiobates* and *Anconastes*. According to Dilkes, the medial inflection of the prearticular in *Phonerpeton* doubles the width of the jaw at that level; although the inflection appears to be less developed in *Tambachia*, it is pronounced.

5. *Unsculptured supratympanic flange of the otic notch includes the squamosal, semilunar flange of the supratemporal, and a small area of the tabular which has a broad contact between the tabular and the*

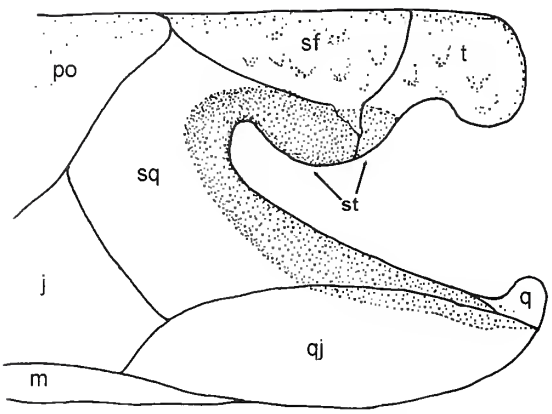

TEXT-FIG. 10. Diagrammatic reconstruction of the otic notch and associated supratympanic flange of a trematopid amphibian in left lateral view.

squamosal beneath the semilunar flange of the supratemporal. This character was originally proposed by Dilkes (1990, p. 239) as the 'Absence of dermal sculpturing along the entire dorsal rim of the otic notch.' As presented by Dilkes, this character was rejected by Daly (1994), because she considered it to be present also in *Eoscopus*. Alternatively, she used this character to unite the Dissorophoidea, and considered (p. 50) the 'replacement of the supratympanic shelf with sculpturing that covers the lateral area above the otic notch and most of the tabular' as a character uniting the Dissorophidae, including platyhystricids and *Ecolsonia*. According to Daly (1994), *Eoscopus* possesses an unsculptured supratympanic flange that is accompanied by a supratympanic shelf, semilunar flange of the supratemporal, and semilunar flange of the squamosal (Bolt 1974*c*). However, there is still some reason to doubt whether the supratympanic flange in amphibamids is entirely like that in trematopids. In *Eoscopus* the tabular contribution to the supratympanic flange is relatively much smaller and does not extend anteriorly beneath the semilunar flange of the supratemporal. As a result, Daly (1994) was unable to determine whether the squamosal and tabular contact one another along the ventral margin of the supratympanic flange. The contribution of the tabular to the flange is also reduced posteriorly, as Daly notes, by a ventral curvature of its lateral margin, which also exhibits a light pitting. Bolt (1974*c*) described the supratympanic flange in the *Tersomius* specimens studied by him as representing an intermediate state between the primitive state of being absent and the advanced state exhibited by the trematopids as follows: 'the smooth supratympanic flange is weakly developed with a straight ventral margin that does not end posteriorly by rising up to the ventral surface of the tabular, and the squamosal-tabular contact is indeterminate.' A supratympanic flange does not appear to have been present in *Amphibamus* (Carroll 1964; Daly 1994) and is absent in *Doleserpeton* (Bolt 1974*c*). The structure of the supratympanic flange in the amphibamids is obviously quite variable and apparently expressed in its most derived state in *Eoscopus*. For this reason character 5 has been expanded to include the presence of a broad, squamosal-tabular contact beneath the semilunar flange of the supratemporal (Text-fig. 10). In addition, the definition of the supratympanic flange is restricted here to include only the unsculptured portion of the vertical, laterally facing shelf of bone that forms the dorsal margin of the otic notch. This definition of the supratympanic flange seems more appropriate than one which includes the entire vertical, dorsal margin of the otic notch, inasmuch as the probable dorsal limit of the attachment of the tympanum was the boundary between the smooth-surfaced and sculptured bone (Bolt and Lombard 1985).

The structure of the supratympanic flange is, unfortunately, not known in all trematopids. Although this area of the skull appears to be preserved in *Actiobates*, it was neither described nor illustrated sufficiently by Eaton (1973) to enable the detailed comparisons necessary here. In *Anconastes* (Berman *et al.* 1987) only enough of the supratympanic flange remains to demonstrate its presence. On the other hand, the otic notch regions in *Acheloma* and *Phonerpeton* are exceptionally well preserved and not only exhibit an unsculptured supratympanic flange that

includes the squamosal, semilunar flange of the supratemporal, and the tabular, but a broad squamosal-tabular contact beneath the semilunar flange of the supratemporal.

Casual inspection of the otic notch of *Tambachia* would seem to suggest that its supratympanic flange does not conform to the trematopid pattern in one important feature: the smooth portion of the supratympanic flange extends along only the anterior two-thirds of the dorsal margin of the otic notch, with the posterior third being completed by a strongly sculptured contribution from the tabular. However, the supratympanic flange in *Tambachia* conforms exactly to that in other trematopids in its relative size and structure, and the relationships and proportions of the squamosal, tabular and supratemporal. Therefore, the posterior, sculptured portion of the dorsal margin of the otic notch is not a part of the original or true supratympanic flange. Rather, the supratympanic flange in *Tambachia* is considered unique among trematopids in having a sculptured, posterior extension formed by the tabular (discussed below). With the exception of *Ecolsonia*, in those instances where the dorsal margin of the otic notch in dissorophids is well documented (DeMar 1968; Bolt 1974*b*) it consists of the same three elements and exhibits the identical sutural pattern as in trematopids. Noticeably different, however, is that the smooth portion of the supratympanic flange in dissorophids does not include the semilunar flange of the supratemporal, and the tabular is limited to a relatively much smaller area adjacent to its contact with the squamosal. As a consequence, the dorsal border of the smooth supratympanic flange angles sharply downward and posteriorly in dissorophids, rather than being horizontal or slightly convex dorsally as in trematopids (Text-figs 4C, 10). Character 5, therefore, has been altered here to exclude the dissorophid features of the supratympanic flange described above. Among the nontrematopid dissorophoids, only in the aberrant *Ecolsonia* is the supratympanic flange like that in trematopids (Berman *et al.* 1985).

6. *Internal process of the pterygoid is hemicylindrical with the articular facet facing dorsally.* This character was proposed by Daly (1994). Its usefulness, however, is equivocal, because the structure of the internal process of the pterygoid and the nature of its union with the basipterygoid process of the braincase in dissorophoids are quite variable and often poorly known or vaguely described. The primitive state of this character, as described by Daly (1994) in the amphibamids *Eoscopus*, *Tersomius* and *Amphibamus*, is a cylindrical internal process that is slotted posteriorly for the reception of the basipterygoid process of the braincase. However, judging from Bolt's (1969) illustrations, in *Doleserpeton*, which was not accounted for by Daly, the internal process is also cylindrical, but has a transverse contact with the basipterygoid process.

Although the structure of the internal process of the pterygoid in *Tambachia* and *Anconastes* conforms largely to the derived state ascribed to trematopids by Daly (1994), those of other trematopids do not strictly agree. Eaton's (1973) illustration of *Actiobates* suggests that its internal process is cylindrical, but has a dorsally facing contact with the basipterygoid process. In *Phonerpeton*, judging from Dilkes' (1990) illustrations, the internal process is hemicylindrical, but has a transverse contact with the basipterygoid process. The palate and braincase are indistinguishably fused and appear to be joined by a rod-like structure in *Acheloma* (Olson 1941; Dilkes and Reisz 1987).

Daly's (1994) use of character 6 to unite the trematopids is also greatly weakened, as Daly admits, by fusion which obliterates the nature of the basicranial joint in most dissorophids. To this must be added that in some dissorophids, such as *Dissoroplus* (DeMar 1964) and *Kamacops* (Gubin 1980), the pterygoid and braincase appear to be joined by a continuous, nearly cylindrical, thick, rod-like structure. In addition, although Daly (1994) views *Ecolsonia* as an aberrant dissorophoid whose family status is unresolved, she describes its internal process and basicranial articulation as duplicating exactly the primitive amphibamid condition.

Shared derived characters uniting Tambachia *and* Anconastes

7. *Absence of an internarial fenestra.* Believing that an internarial fenestra is absent in *Amphibamus* and *Anconastes*, Dilkes (1990) interpreted the presence of this structure as a synapomorphy of

Phonerpeton and *Acheloma*. An internarial fenestra, however, is present in all amphibamids, as well as in the trematopids *Actiobates*, *Phonerpeton* and *Acheloma*. Among the dissorophids, including *Ecolsonia*, only the poorly known *Conjunctio* appears to possess this structure (Carroll 1964). Therefore, we judge that the absence of an internarial fenestra is a shared derived character uniting *Tambachia* and *Anconastes* and which evolved in parallel in dissorophids.

8. *Suborbital process of the lacrimal is greatly reduced or absent and not accompanied by an exposure of the palatine on the lateral and/or dorsal surface of the ventral rim of the orbit.* Two primitive states of this character are randomly distributed in all other dissorophoids: (1) suborbital process of the lacrimal is very short or absent and is accompanied by an exposure of the palatine on the lateral and/or the dorsal surface of the ventral rim of the orbit; or (2) suborbital process of the lacrimal is long, but not accompanied by a lateral and/or dorsal exposure of the palatine along the ventral rim of the orbit.

In the amphibamids *Tersomius* and *Doleserpeton* the suborbital process of the lacrimal is greatly abbreviated and the palatine is not only exposed along the dorsal margin of the ventral rim of the orbit, but also has a sculptured exposure on the lateral margin (Bolt 1969, 1974*c*). Although the palatine is restricted to the dorsal surface of the ventral rim of the orbit in *Eoscopus* (Daly 1994), the suborbital bar of the lacrimal is greatly shortened. A lateral and/or dorsal exposure of the palatine accompanying the long suborbital process of the lacrimal has not been documented in *Amphibamus*, yet Daly (1994) has reported that a laterally exposed palatine may be present.

Among the trematopids, only *Phonerpeton* exhibits a short suborbital process of the lacrimal that is accompanied by a lateral exposure of the palatine (Dilkes 1990). *Actiobates* provides the only example of an alternative character-state. In Eaton's (1973) description and illustration of *Actiobates* there is no indication of an exposure of the palatine on either the dorsal or lateral surface of the ventral rim of the orbit. Instead, long suborbital processes of the lacrimal and jugal are narrowly separated by the maxilla. *Acheloma* is unique among the dissorophoids in the absence of the palatine, ectopterygoid, and maxilla from the ventral rim of the orbit. Here, the suborbital bar has become extraordinarily deep, and the great displacement of these bones from the ventral rim of the orbit is seemingly replaced by a very broad lacrimal-jugal contact. The long suborbital process of the lacrimal in *Acheloma* is interpreted as a character reversal. As far as can be determined, in those dissorophids in which the ventral margin of the orbit is well preserved and has been carefully examined, a laterally exposed palatine is present and the suborbital process of the lacrimal is either greatly reduced or absent (DeMar 1968; Bolt 1974*c*). When the first primitive state of this character is present, it is assumed that the suborbital process of the lacrimal has been reduced or lost by the encroachment of the palatine on the lateral and/or dorsal surface of the orbital rim.

9. *Maxilla contributes to both the dorsal and lateral surfaces of the ventral orbital rim in the absence of a contribution to either surface by the palatine.* Three primitive states of this character are randomly distributed in all other dissorophoids except the trematopid *Acheloma*: (1) the maxilla is excluded from both the dorsal and lateral surfaces of the orbital rim with the palatine contributing to both surfaces; (2) the maxilla contributes to the lateral surface, but is excluded from the dorsal surface of the orbital rim by the palatine; or (3) the maxilla and palatine contribute to the dorsal and lateral surfaces of the orbital rim.

Among the amphibamids, *Doleserpeton* (Bolt 1969, 1974*c*) exhibits primitive state 1, *Tersomius* (Carroll 1964; Bolt 1974*c*; Daly 1994) exhibits primitive states 1 and 2, and *Eoscopus* (Daly 1994) exhibits primitive state 2. The structure of the ventral orbital rim in *Amphibamus* is apparently not determinable in existing specimens (Bolt 1974*c*; Daly 1994).

In the trematopids, *Phonerpeton* exhibits primitive state 1, but there is also an exposure of the ectopterygoid on the dorsal and lateral surfaces of the ventral rim of the orbit (Dilkes 1990). *Acheloma*, on the other hand, is unique among all dissorophoids in the exclusion of the palatine, ectopterygoid, and maxilla from the orbital rim. Its extraordinarily deep suborbital bar has seemingly resulted in the wide displacement of these three elements from the orbital rim by a very

broad contact between the lacrimal and jugal. It cannot be determined, however, from what ancestral state the unique structure of the suborbital bar in *Acheloma* was derived. Unfortunately, the structure of the suborbital bar in *Actiobates* is not clear from Eaton's (1973) description, which shows the lacrimal and jugal narrowly separated by the maxilla along the ventral rim of the orbit; the entrance of the maxilla into the very large orbit in *Actiobates* may reflect an early postlarval stage of development (Berman *et al.* 1985).

Unfortunately, the ventral rim of the orbit has been re-examined in only a few genera of dissorophids (DeMar 1968; Bolt 1974*c*; Berman *et al.* 1985) in light of the recent discoveries of the participation of the palatine in the formation of this structure in other dissorophoids. Most recent studies, however, suggest that the dissorophids, including *Ecolsonia* (Berman *et al.* 1985), exhibit primitive state 3.

This survey strongly suggests that the participation of the palatine in the structure of the ventral rim of the orbit is a primitive feature of dissorophoids and that, as far as is known, only *Tambachia* and *Anconastes* on the one hand, and *Acheloma* on the other, exhibit different derived states of this character.

Unique characters of Tambachia

10. *Subnarial process of the lacrimal is short.* With the possible exception of *Actiobates*, the lacrimal in *Tambachia* is unique among trematopids in having a very short subnarial process that does not appear to reach the midlength level of the posterior portion of the external naris. On the other hand, in all other trematopids the subnarial process of the lacrimal extends anteriorly to nearly the level of the subdivision of the external naris and, therefore, equals or slightly exceeds half the total length of the opening. This is interpreted as the primitive state, because in the amphibamids and typically in temnospondyls the lacrimal extends forward to the unexpanded external naris. A short subnarial process in *Actiobates* is unexpected considering its early occurrence (Upper Pennsylvanian) and the otherwise primitive anatomy of this genus (Eaton 1973). The short subnarial process of the lacrimal in this taxon may represent an early ontogenetic stage of development, as do many other features of its skull (Berman *et al.* 1985).

11. *Dorsal margin of the otic notch is extended posteriorly by a sculptured, downturned lateral expansion of the tabular.* In all dissorophids, including *Platyhystrix* (Berman *et al.* 1981) and *Ecolsonia* (Berman *et al.* 1985), the dorsal margin of the otic notch is also extended posteriorly by a sculptured, downturned lateral expansion of the tabular. However, since this feature does not appear to be present in either the amphibamids or any trematopid except *Tambachia*, it is judged to be a unique character of this genus that developed in parallel in the dissorophids. As a consequence of this character, in *Tambachia* and dissorophids the dorsal margin of the otic notch extends posteriorly to a level equal to the posteroventral corner of the skull roof.

It is difficult to confirm the absence of this feature in *Actiobates*, because of the inadequate description and illustrations given by Eaton (1973). However, the small, triangular exposure of the tabular on the skull table lies a short distance anterior to the level of the posteroventral corner of the skull roof. It is also possible that the moderately long posterior extent of the dorsal margin of the otic notch may reflect an early postlarval feature (Berman *et al.* 1985) or an illusion created by severe dorsoventral crushing of the holotype. In *Phonerpeton* (Dilkes 1990) the posterior extent of the dorsal margin of the otic notch lies far anterior to the level of the posteroventral corner of the skull roof. Although the dorsal margin of the otic notch is incomplete in *Anconastes* (Berman *et al.* 1987), enough of the tabular portions of the skull table remain to indicate that the posterior margin of the tabulars failed to reach the level of the posteroventral corners of the skull roof by a considerable degree. In *Acheloma*, the dorsal margin of the otic notch is of typical trematopid structure except for the presence of a greatly elongated tabular horn (Dilkes and Reis 1987). However, the tabular horn is basically a posterior extension of the skull table, rather than a downturned lateral expansion of the tabular.

12. *Occipital margin of the skull table lies at a level nearly equal to the posteroventral corner of the skull roof.* In all amphibamids and trematopids except *Tambachia* the midline occipital margin of the skull roof lies far anterior to the level of the posteroventral corner of the skull cheek. On the other hand, in *Tambachia* and all dissorophids (Carroll 1964; DeMar 1968), including *Platyhystrix* and *Ecolsonia* (Berman *et al.* 1981, 1985), the midline occipital margin of the skull roof lies at or just anterior to the level of the posteroventral corner of the skull roof. The distribution of these two character states suggests that the relatively farther posterior level of the midline occipital margin of the skull roof in *Tambachia* and dissorophids represents the derived state. The occurrence of the derived state only in *Tambachia* among the trematopids is judged here as a unique character of the genus that evolved in parallel with the condition in dissorophids.

13. *Deep channel on the ventral surface of the parasphenoid separates the basipterygoid process from the body of the braincase.* Among the dissorophoids, only in *Tambachia* is there a deep, well-defined channel on the ventral surface of the parasphenoid that separates the basipterygoid process from the body of the braincase. The only possible exception to this distribution is seen in *Actiobates*, where Eaton (1973, p. 5) reported that 'The basisphenoid is exposed on either side of the converging, ventralmost part of the parasphenoid; the bone bears grooves for the internal carotids. The medial edges of these grooves are bounded by the parasphenoid except in their anterior parts, where the basipterygoid processes project laterally.'

14. *Width of the basipterygoid process extremely broad and extends along almost the entire lateral margin of the parasphenoid and slightly exceeds the width of the internal process of the pterygoid.* This character is not duplicated in any dissorophoid in which this area of the braincase is known.

Shared derived characters uniting Phonerpeton *and* Acheloma

15. *Absence of parasphenoidal denticle field.* This synapomorphy of *Phonerpeton* and *Acheloma* was first recognized by Dilkes (1990). Among the amphibamids and trematopids, a parasphenoidal denticle field is absent only in *Phonerpeton* and *Acheloma*. With one exception, in the few specimens of dissorophids (*Broiliellus*, *Dissorophus*) in which this feature would probably be preserved if present, it is apparently absent; re-examination of the aberrant *Ecolsonia*, however, has indicated the presence of a small parasphenoidal denticle field.

16. *The length and width of the parasphenoidal plate of the braincase are subequal.* In *Phonerpeton* and *Acheloma* the body of the parasphenoidal plate of the braincase is approximately square, with the maximum width posterior to the basipterygoid processes being equal to or slightly less than the length of the parasphenoid, excluding the rostrum. In the amphibamids and the other trematopids the width of the parasphenoidal plate exceeds the length by as little as 30 to over 200 per cent., whereas in those dissorophids in which this measurement is available, the width exceeds the length from *c.* 10 to 60 per cent.

These hypotheses of interrelationships of the trematopids reaffirm those presented by Dilkes (1990), with the exception of the addition of *Tambachia*, and are shown here diagrammatically in Text-figure 11. The analysis presented supports the following conclusions.

1. Trematopidae is a monophyletic group (characters 1–6).
2. *Tambachia* is definitely a trematopid (characters 1–6). Assignment of *Anconastes* to the Trematopidae is considered very likely and is based on two sets of characters: first, although characters 3–5 are not observable in the holotype, and character 6 is too derived to determine its ancestral state, it exhibits trematopid characters 1 and 2; and second, three shared derived characters (7–9) unite it with *Tambachia*.
3. *Tambachia* and *Anconastes* share a more recent common ancestor than either does with any other

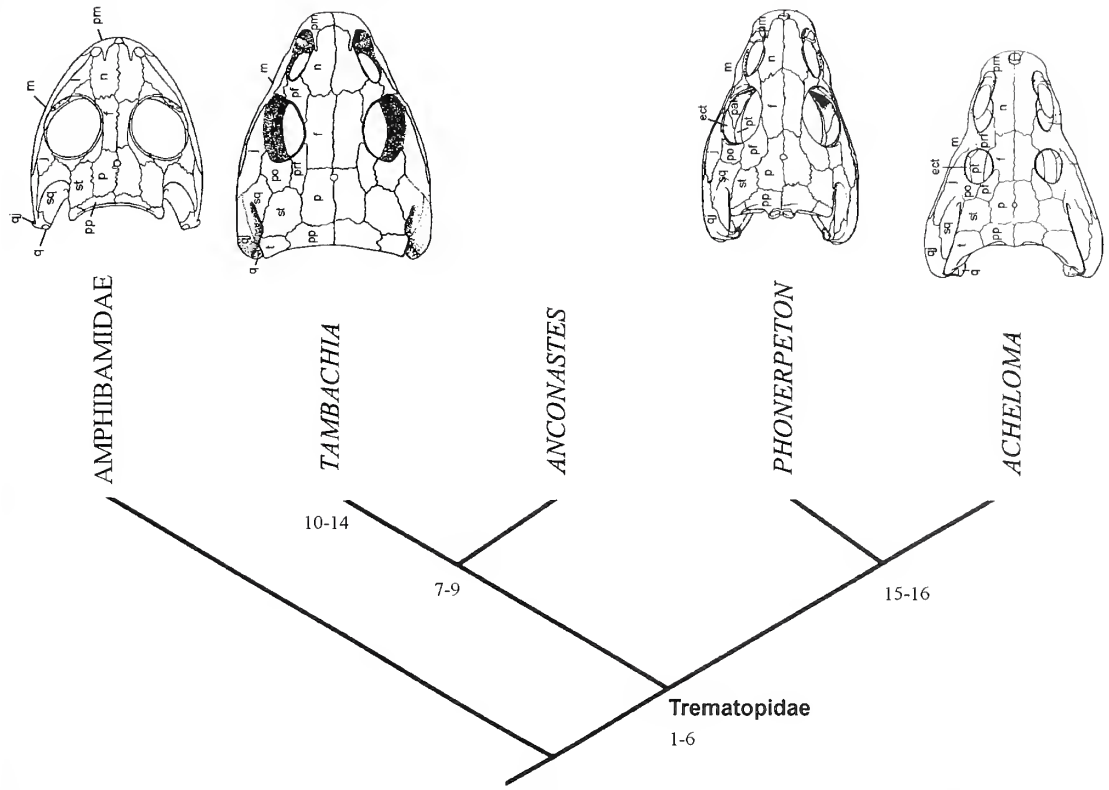

TEXT-FIG. 11. Cladogram indicating hypothesis of intrarelationships of Trematopidae (*Actiobates* excluded). Amphibamidae is represented by *Eoscopus* (Daley 1994). *Phonerepeton* and *Acheloma* are after Dilkes (1990) and Dilkes and Reisz (1987) respectively.

trematopid (characters 7–9), and *Phonerpeton* and *Acheloma* share a more recent common ancestor than either does with any other trematopid (characters 16 and 17).

4. *Tambachia* and *Anconastes*, on the one hand, and *Phonerpeton* and *Acheloma* on the other, form sister group clades.
5. *Actiobates* is probably a trematopid, as it exhibits characters 1, 2, and possibly 6. However, the absence of well-documented synapomorphies prevents confident determination of its relationships with other members of the family.

Acknowledgements. We thank Dr David Dilkes (Redpath Museum, Montreal) for valuable information on and discussion of trematopid structure and intrarelationships. Dr Andrew Milner reviewed the manuscript, made suggestions that improved the substance of the study significantly, and provided access to unpublished information that clarified significantly certain portions of the discussion. The authors thank Ms Sadie Ann Howell (California State University, San Bernardino) for providing microsedimentological analysis of rock samples, Dr Elizabeth Rega (Claremont Colleges) for translating critical German literature and reviewing the translation of our typescript into the form of English appropriate to a British journal, and Ms Amy Henrici for careful preparation of the holotype. Ms Heike Sheffel of the Comtel Hotel Wandersleben is due particular thanks for her hospitality to SSS and DSB during our fieldwork in Germany. This research was supported by a National Geographic Society grant 5182-94 (to SSS and DSB), a NATO grant CRG.940779 and California State University San Bernardino Minigrant (to SSS), and Edward O'Neil Endowment Fund and M. Graham Netting Research Fund, of the Carnegie Museum of Natural History (to DSB).

REFERENCES

BERMAN, D. S and BERMAN, S. L. 1975. *Broiliellus hektotopos* sp. nov. (Temnospondyli: Amphibia), Washington Formation, Dunkard Group, Ohio. 69–78. *In* BARLOW, J. A. (ed.). *Proceedings of the First I.C. White Memorial Symposium, The Age of the Dunkard, West Virginia Geologic and Economic Survey*, 352 pp.

—— REISZ, R. R. and FRACASSO, M. A. 1981. Skull of the Lower Permian dissorophid amphibian *Platyhystrix rugosus*. *Annals of Carnegie Museum*, **50**, 391–416.

—— —— and EBERTH, D. A. 1985. *Ecolsonia cutlerensis*, an Early Permian dissorophid amphibian from the Cutler Formation of north-central New Mexico. *Circular of the New Mexico Bureau of Mines and Mineral Resources*, **191**, 1–31.

—— —— —— 1987. A new genus and species of trematopid amphibian from the Late Pennsylvanian of north-central New Mexico. *Journal of Vertebrate Paleontology*, **7**, 252–269.

—— and MARTENS, T. 1993. First occurrence of *Seymouria* (Amphibia: Batrachosauria) in the Lower Permian Rotliegend of central Germany. *Annals of the Carnegie Museum*, **62**, 63–79.

BOLT, J. R. 1969. Lissamphibian origins: possible protolissamphibian from the Lower Permian of Oklahoma. *Science*, **166**, 888–891.

—— 1974*a*. Osteology, function, and evolution of the trematopid (Amphibia: Labyrinthodontia) nasal region. *Fieldiana, Geology*, **33**, 11–30.

—— 1974*b*. A trematopsid skull from the Lower Permian, and an analysis of some characters of the dissorophoid (Amphibia: Labyrinthodontia) otic notch. *Fieldiana, Geology*, **37**, 61–73.

—— 1974*c*. Evolution and functional interpretation of some suture patterns in Paleozoic labyrinthodont amphibians and other lower tetrapods. *Journal of Paleontology*, **48**, 434–458.

—— 1977. *Cacops* (Amphibia: Labyrinthodonia) from the Fort Sill Locality, Lower Permian of Oklahoma. *Fieldiana, Geology*, **37**, 61–73.

—— and LOMBARD, R. E. 1985. Evolution of the amphibian tympanic ear and the origin of frogs. *Biological Journal of the Linnean Society*, **24**, 83–99.

BOY, J. A. 1972. Die Branchiosaurier (Amphibia) des saarpfalzischen Rotliegenden (Perm, SW-Deutschland). *Hessisches Landesamt für Bodenforschung, Abhandlungen*, **65**, 5–137.

—— and MARTENS, T. 1991. A new captorhinomorph reptile from the Rotliegend of Thuringia (Lower Permian; eastern Germany). *Paläontologische Zeitschrift*, **65**, 363–389.

CARROLL, R. L. 1964. Early evolution of the dissorophid amphibians. *Bulletin of the Museum of Comparative Zoology*, **131**, 161–250.

CLACK, J. A. and HOLMES, R. 1988. The braincase of the anthracosaur *Archeria crassidisca* with comments on the interrelationships of primitive tetrapods. *Palaeontology*, **31**, 85–107.

COPE, E. D. 1882. Third contribution to the history of the Vertebrata of the Permian formation of Texas. *Proceedings of the American Philosophical Society*, **20**, 447–461.

DALY, E. 1994. The Amphibamidae (Amphibia: Temnospondyli), with a description of a new genus from the Upper Pennsylvanian of Kansas. *Miscellaneous Publications of the University of Kansas Museum of Natural History*, **85**, 1–59.

De MAR, R. E. 1966. *Longiscitula houghae*, a new genus of dissorophid amphibian from the Permian of Texas. *Fieldiana, Geology*, **16**, 45–53.

—— 1968. The Permian labyrinthodont amphibian *Dissorophus multicinctus*, and adaptations and phylogeny of the family Dissorophidae. *Journal of Paleontology*, **42**, 1210–1242.

DILKES, D. W. 1990. A new trematopid amphibian (Temnospondyli: Dissorophoidea) from the Lower Permian of Texas. *Journal of Vertebrate Paleontology*, **10**, 22–43.

—— 1993. Biology and evolution of the nasal region in trematopid amphibians. *Palaeontology*, **36**, 839–853.

—— and REISZ, R. R. 1987. *Trematops milleri* Williston, 1909 identified as a junior synonym of *Acheloma cumminisi* Cope, 1882, with a revision of the genus. *American Museum Novitates*, **2902**, 1–12.

EATON, T. H. 1973. A Pennsylvanian dissorophid amphibian from Kansas. *Occasional Papers of the University of Kansas Museum of Natural History*, **14**, 1–8.

GUBIN, Yu. M. 1980. New Permian dissorophids of the Ural forelands. *Paleontologichesky Zhurnal*, **3**, 82–90.

HAUBOLD, H. 1971. Die Tetrapodenfahrten aus dem Permosiles des Thueringer Waldes. *Abhandlungen und Berichte des Museums der Natur Gotha*, **6**, 15–41.

—— 1973. Lebewelt and Oekologie des Tambacher Sandsteins (Unteres Perm, Saxon) im Rotliegenden des Thueringer Waldes. *Zeitschrift für Geologische Wissenschaften*, **1**, 247–268.

KOZUR, H. 1984. Carboniferous-Permian boundary in marine and continental sediments. *Comptes Rendues 9^e Congres International Stratigraphie et Geologie Carbonifere, Washington and Champain-Urbana 1979*, **2**, 577–586.

KOZUR, H. 1988. The age of the Central European Rotliegendes. *Zeitschrift für Geologische Wissenschaften*, **16**, 907–915.

—— 1989. Biostratigraphic zonations in the Rotliegends and their correlations. *Acta Musei Reginaehradecensis, Serie A*, **22**, 15–30.

LINNAEUS, C. 1758. *Systema Naturae*. 10th Edition. Volume 1. Salvi, Stockholm, 824 pp.

MARTENS, T. 1980. Zur Fauna des Oberrotliegenden (Unteres Perm) im Thueringer Wald-Vorlaeufige Mitteilung. *Abhandlungen und Berichte des Museum der Natur Gotha*, **10**, 19–20.

—— 1988. Die Bedeutung der Rotsedimente für die Analyse der Lebewelt des Rotliegenden. *Zeitschrift für Geologische Wissenschaften*, **16**, 933–938.

MILNER, A. R. 1985. On the identity of *Trematopsis seltini* (Amphibia: Temnospondyli) from the Lower Permian of Texas. *Neues Jahrbuch für Geologie und Palaeontologie, Monatshefte*, **1985**, 357–367.

—— 1993. Biogeography of Palaeozoic tetrapods. 324–353. *In* LONG, J. A. (ed.). *Palaeozoic vertebrate biostratigraphy and biogeography*. Bellhaven Press, London, 369 pp.

MUELLER, A. H. 1954. Zur Ichnologie and Stratonomie des Oberrotliegenden von Tambach (Thueringen). *Paläontologische Zeitschrift*, **28**, 189–203.

—— 1969. Ueber ein neues Ichnogenus (*Tambia* n.g) und andere Problematica aus dem Rotliegended (Unterperm) von Thueringen. *Monatsberichte der Deutschen Akademie der Wissenschaften*, **11**, 922–931.

OLSON, E. C. 1941. The family Trematopsidae. *Journal of Geology*, **49**, 149–176.

—— 1970. *Trematops stonei* sp. nov. (Temnospondyli: Amphibia) from the Washington Formation, Dunkard Group, Ohio. *Kirtlandia*, **8**, 1–12.

PABST, W. 1896. Tierfahrten aus dem Oberrotliegenden von Tambach in Thueringen. *Zeitschrift der Deutsche Geologischen Gesellschaft*, **47**, 570–576.

—— 1908. Die Thierfahrten in dem Rotliegended 'Deutschlands'. *Nova Acta Leopoldina*, **89**, 1–166.

SUMIDA, S. S., BERMAN, D. S and MARTENS, T. 1996. Biostratigraphic correlations between the Lower Permian of North America and central Europe using the first record of an assemblage of terrestrial tetrapods. *PaleoBios*, **17**, 1–12.

VAUGHN, P. P. 1969. Further evidence of close relationship of the trematopsid and dissorophid labyrinthodont amphibians with a description of a new genus and species. *Bulletin of the Southern California Academy of Sciences*, **68**, 121–130.

—— 1971. A *Platyhystrix*-like amphibian with fused vertebrae, from the Upper Pennsylvanian of Ohio. *Journal of Paleontology*, **45**, 121–130.

WILLISTON, S. W. 1909. New or little-known Permian vertebrates: *Trematops*, new genus. *Journal of Geology*, **17**, 636–658.

—— 1910. *Cacops*, *Desmospondylus*; new genera of Permian vertebrates. *Bulletin of the Geological Society of America*, **21**, 249–284.

ZITTEL, K. A. von 1888. *Handbuch der Paläontologie, Abteilung 1. Paläzoologie Band III: (Vertebrata)*. Oldenbourg, Munich and Leipzig, 1699 pp.

STUART S. SUMIDA

Department of Biology
California State University San Bernardino
5500 University Parkway
San Bernardino, California 92407, USA

DAVID S BERMAN

Section of Vertebrate Paleontology
Carnegie Museum of Natural History
4400 Forbes Avenue
Pittsburgh, Pennsylvania 15213, USA

THOMAS MARTENS

Abteilung Palaeontologie
Museum der Natur Gotha
Parkallee 15, Postfach 217
99853 Gotha, Germany

Typescript received 15 August 1996
Revised typescript received 26 June 1997

TAPHONOMY OF THE ORDOVICIAN SOOM SHALE *LAGERSTÄTTE*: AN EXAMPLE OF SOFT TISSUE PRESERVATION IN CLAY MINERALS

by SARAH E. GABBOTT

ABSTRACT. The late Ordovician Soom Shale of South Africa contains exceptionally preserved fossils of several taxa, the soft tissues of which are uniquely composed of clay and alunite group minerals. In addition, originally phosphatic brachiopod shells and conodont elements have been replaced by clays. Sub-cellular structural details of conodont muscle tissues are faithfully replicated by the clay minerals. Geochemical analyses have constrained interpretation of the conditions in the sediment and bottom waters of the Soom Shale basin during deposition and early diagenesis. Anoxic-euxinic conditions prevailed with low carbonate and iron concentrations in the sediment; hence there was no mechanism to buffer or fix H_2S produced by organic matter decomposition. Under low pH conditions and in the presence of cations, organic substrates would have had an affinity for colloidal clay minerals and may have acted as templates, controlling the absorption of clay minerals which eventually completely replaced them. An initial phase of mineralization involving phosphate, followed by its replacement by clay minerals, is unlikely because the low pH conditions in the sediment would have been inimical to phosphate concentration, and the high fidelity of some soft tissue replication militates against two phases of replacement.

THE preservational history of fossils from the Soom Shale is complex. A variety of minerals was involved in replacing and/or replicating fossil material and there was more than one phase of demineralization of the original biominerals. The transformation of normally labile tissues to mineralized replacements was controlled not only by decay of the organisms themselves, but also by the geochemistry of the sedimentary environment. Some soft tissues, notably the myotomes of a conodont animal, preserve structures on a sub-cellular scale of resolution (Gabbott *et al.* 1995). In other parts of the fossil record, comparable replacement of organic structures involves phosphate mineralization, but the Soom Shale specimens are uniquely preserved through replacement by clay minerals (Gabbott *et al.* 1995). The main aim of this paper is to describe the taphonomy and early diagenesis of the Soom Shale biota with special emphasis on the mechanism of preservation of soft tissues. The mode of preservation of the various fossil components in a deposit can provide valuable evidence of the conditions which contributed to their preservation. In particular, authigenic mineral species are indicative of specific depositional conditions such as levels of Eh, pH, organic content, rate of burial, salinity and degree of oxygenation (Allison 1988*a*). A subsidiary aim, therefore, is to use the taphonomic information to help determine the environment of deposition in the basin, the Eh/pH of the bottom and pore waters, and the level of oxygenation at and above the sea floor. In addition, the relative timing of diagenetic processes resulting in mineral transformations has been determined. The effects of Neogene weathering on the preserved assemblage are also noted.

STRATIGRAPHY, LOCALITIES AND SEDIMENTOLOGY

The Soom Shale is the basal member of the Cedarberg Formation which is part of the Lower Palaeozoic Table Mountain Group (Theron and Thamm 1990). The stratigraphy of the Lower Palaeozoic of South Africa has been reviewed by Rust (1981) and aspects of the Cedarberg Formation were described by Cocks *et al.* (1970) and Theron *et al.* (1990). Good fossiliferous

[Palaeontology, Vol. 41, Part 4, 1998, pp. 631–667]

exposures of the Soom Shale occur at Keurbos (18°58′ E, 32°16′ S) near Clanwilliam, and at Sandfontein (19°14′ E, 32°40′ S) 52 km from Clanwilliam. Two cores have been drilled by the Geological Survey of South Africa close to the Keurbos locality, one 5 m behind the Keurbos quarry face, and the other in a stream section approximately 1 km south-west of the quarry.

The Soom Shale comprises a fine siltstone and mudstone laminated on a millimetric scale. It has been subject to Neogene weathering which in most areas has changed it from an original black, as at Sandfontein, to yellow-brown; at Keurbos, it is grey. The most obvious primary sedimentary structure is the fine-grained lamination which is occasionally interrupted by thicker homogenous siltstones up to 10 mm thick. The laminae comprise alternations of silt and mud with darker layers which may be degraded organic matter. The lamination may have been formed by intercalation of distal turbidites with hemipelagites (Jan Zalasiewicz, pers. comm. 1996). However, as shown by the lack of bedding structures, the turbidite flows must have lost most of their energy. Penetrative and surface bioturbation structures are absent. The sediment is composed mostly of clay minerals, especially illites and mixed-layer clays, and detrital quartz. Diagenetic minerals include pyrite, chlorites and clay minerals.

The setting of the basin at the time of deposition of the Soom Shale has been described as glaciolacustrine to shallow marine (Theron *et al.* 1990). Water depth is unknown but cannot have been very great as the Soom Shale overlies the Pakhuis Formation tillites with glacial pavements, and is overlain by the Disa Siltstone Member which is dominantly shallow marine (Rust 1967, 1981). However, there are no indications of storm-wave induced sedimentary structures which may ripple the sediment under water depths of up to 100 m during moderate storms (Elliot 1991). It is therefore likely that a depth of 100 m must have existed over the majority of the depobasin unless the sediment was bound by microbial mats or the sea surface was ice covered. Evidence for periodic ice-coverage comes from the presence of dropstones in the shale particularly towards the base (Rust 1967). However, the climate at the time was generally one of amelioration, resulting in retreat of the ice sheet responsible for the underlying tillites and diamictites.

BIOTA

The palaeontology of the Soom Shale has been examined by a number of authors (Cramer *et al.* 1974; Gray *et al.* 1986; Moore and Marchant 1981; Kovács-Endrödy 1986; Theron *et al.* 1990; Chesselet 1992; Aldridge and Theron 1993; Aldridge *et al.* 1994; Braddy *et al.* 1995; Gabbott *et al.* 1995; Fortey and Theron 1995). Trace fossils are rare but include a variety of faecal pellets. The microbiota includes chitinozoans (Cramer *et al.* 1974), acritarchs and spores (Gray *et al.* 1986). Metaphyte algae cover most of the lamination surfaces and probably constituted the greatest biomass of the biota. It is not yet clear whether the algae were benthonic, and thus stabilized the sediment, or planktonic. At present, the evidence of dominantly inhospitable bottom water conditions favours the latter.

MATERIAL AND METHODS

The repository of most specimens (prefixed C) used in this study is the Geological Survey of South Africa. Specimen numbers prefixed IT are at The Natural History Museum, London.

Fossil analyses

The fossils (Table 1) were studied in two ways; firstly by observation, noting the mode of preservation, degree of compaction and fracturing, presence or absence of biominerals, presence or absence of hard part or soft tissue structures and fidelity of soft part replication, and secondly by determination of the mineralogy of hard parts and soft tissues where present. Biomineralized tissues were investigated on the following material: orthocone shell, lingulate brachiopod shell, trilobite exoskeleton, ostracode carapace and conodont elements. More refractory organic biomolecules

TABLE 1. Fossils from the Soom Shale with their original composition, fossil composition and mode of preservation indicated. ill. = illite and alun. = alunite group minerals.

Fossils	Original composition	Fossil composition	Mode of preservation
Orthocone	Calcium carbonate $CaCO_3$ (aragonite)	—	Mouldic
Trilobite	Outer calcite, inner calcite in organic base $CaCO_3$ (calcite)	—	Mouldic + possible replacement
Lingulate brachiopods	Chitinophosphatic; apatite with 11–42 per cent. organic (chitin and protein)	ill./alun.	Mouldic + replacement
Conodont elements	Calcium phosphate (apatite)	basal bodies, ill./alun. denticle cores, quartz	Mouldic + replacement
Naraoiid	Chitinous	—	Mouldic
Eurypterid exoskeleton	Chitinous	ill./alun.	Replacement
Chitinozoan	Pseudochitin	illite and coalified organic	Replacement and coalified original
Acritarchs + spores	Sporopollenin	coalified organics	Coalified original
Conodont muscle tissue	Labile organic	illite	Replacement
Siphonacis parva	Unknown	organic and alun.	Original and replacement

investigated were from naraoiid carapace, chitinozoan vesicles, conodont sclerotic eye capsules, eurypterid cuticle and *Siphonacis parva* (Kovács-Endrödy), a small enigmatic needle-shaped fossil (Chesselet 1992). Labile soft tissues examined were from the trunk musculature of the conodont *Promissum pulchrum* (Kovács-Endrödy) and eurypterid podomere musculature.

The fossil material was studied by combinations of optical microscopy, SEM EDX (scanning electron microscope energy dispersive X-rays) and electron microprobe (JEOL JXA-8600 microprobe). All specimens used in compositional analyses are shown in Table 2.

There were some difficulties in gaining analyses from some fossil material. Great care was taken to ensure that only fossil material was mounted and that it was analysed without contamination from surrounding sediment. All the fossils from the Soom Shale are soft and contained within friable rock, making it very difficult to remove coherent pieces of fossil material. Extraction of conodont muscle tissue was particularly problematical due to its extreme friability. A small amount of EPOTEK resin dropped directly on to the fossil and allowed to dry for 24 hours proved an effective consolidant. However, some fossil material is so soft that it would not take a sufficient polish for accurate electron microprobe analysis, even after induration; other compacted fossils (e.g. myodocopid ostracodes, chitinozoan vesicles, conodont sclerotic eye capsules, *Lingula*, *Siphonacis parva* and algal strands) are too thin for a polished section to be prepared. SEM EDX analysis of such thin specimens in the matrix is risky because the beam penetrates up to depths of 5 μm giving spurious analyses incorporating the underlying sediment, although it can be used to test for the presence of minerals in the fossils that are not represented in the matrix.

Although only very small quantities of fossil material are required for these analyses, some Soom Shale fossils are extremely rare, with only one or two specimens known (e.g. scolecodont apparatuses and enigmatic taxa). Until other specimens of these rare fossils are found, destructive analysis has been deferred.

TABLE 2. A, summary of SEM EDX data. Eurypterid material is from: C373I and C874II = prosoma; C427a, C809dI and C874Ib = preabdomen; C373ll, eurypterid muscle tissue from podomere on appendage VI and C809dll, muscle tissue between podomeres 2 and 3 on appendage VI. B, summary of electron microprobe data. Eurypterid material is from: C809a = prosoma; C373 and C731b = preabdomen; C427b = margin of the postabdomen just above the telson. K = Keurbos, S = Sandfontein, B = Buffel's Dome, mt. = muscle tissue.

Fossil	Locality	Total number of analyses	Illite only	Alunite only	Illite and alunite
A					
Orbiculoid					
unlabelled 1	K	7	0	3	4
unlabelled 2	K	3	0	3	0
Eurypterids					
C373l	K	4	1	0	3
C373ll mt.	K	3	0	0	3
C427a	K	2	2	0	0
C809dl	K	2	1	0	1
C809dll mt.	K	2	0	2	0
C874bl	K	2	0	0	2
C874bll	K	2	2	0	0
Conodont muscle tissue					
C721b	S	20	20	0	0
Trilobite					
IT18902	B	7	2	0	5
Ostracods					
C945a	K	5	5	0	0
Chitinozoans					
C732a	K	4	3	0	1
896a	S	11	11	0	0
B					
Orbiculoids					
Unlabelled × 2	K	12	0	2	10
C855	K	9	0	8	1
Trematids					
C412a	K	6	2	3	1
C764a	K	3	2	1	0
C903b	S	3	0	3	0
Eurypterids					
C373	K	9	9	1	0
C427b	K	8	3	5	0
C731b	K	6	3	0	3
C809a	K	7	5	1	1
Conodont muscle tissue					
C721b	S	16	16	0	0

SEM, energy dispersive X-rays (EDX). For SEM EDX analysis, a small piece of fossil material was mounted on to an SEM stub and silver- or gold-coated in a Polaron automatic sputter coater. Uncoated conodont muscle tissue was analysed using a SEM EDX at Medical Sciences, Leicester University, and within an environmental chamber at The Natural History Museum, London. EDX analysis is qualitative and some clay mineral species cannot be determined using these data.

Electron microprobe analysis. Microprobe analyses were performed on fossil sections with a focused beam at 15 Kv. Electron microprobe analyses are quantitative, so cation proportions can be

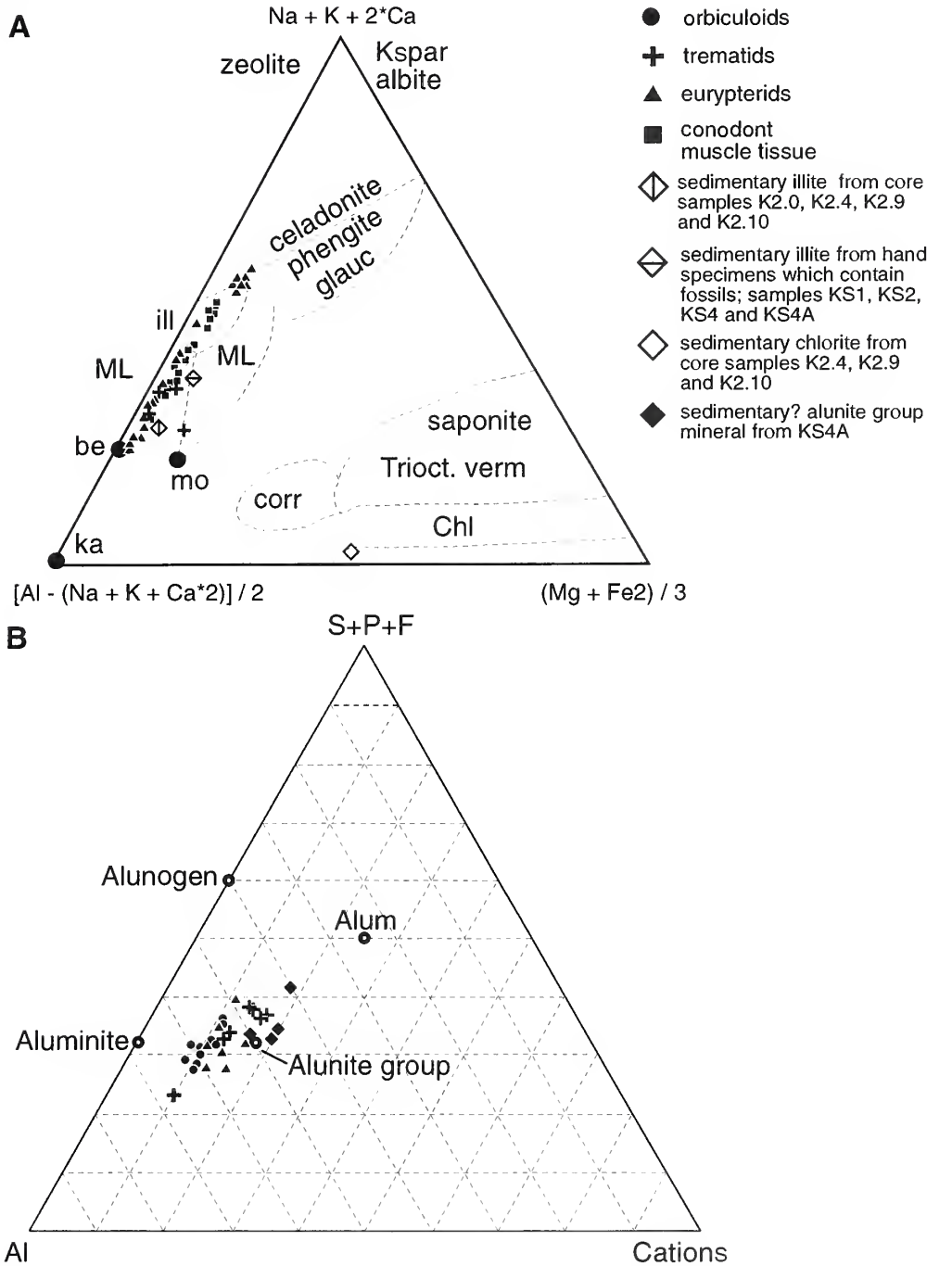

TEXT-FIG. 1. A, Velde and Meunier (1987) diagram for clay minerals showing where the fossil compositions in the illitic solid solution series plot. be = beidellite, Chl = chlorite, corr = corrensite, glauc = glauconite, ill = illite, ka = kaolinite, ML = mixed layer clay, mo = montmorillonite, Trioct. = tricotahedral, and verm = vermiculite. B, triangular plot with anions, cations and aluminium at the apices showing the position of alunitic fossil compositions and the alunite group minerals. Cations: $Fe_2 + Mg + Ca + Na + K + La + Ce + Y + Sr$.

TABLE 3. Mean electron microprobe analyses, standard deviations and cation proportions for fossils with an illitic component (A) and an alunitic group component (B). Ttet = tetrahedral layer total, Toct = octahedral layer total, Tint = interlayer site total.

A	Illitic fossil analyses						B	Alunitic fossil analyses					
	Eurypterid		Trematid		Conodont muscle tissue			Eurypterid		Trematid		Orbiculoid	
Oxides	Mean	SD	Mean	SD	Mean	SD	Oxides	Mean	SD	Mean	SD	Mean	SD
SiO_2	53·47	1·88	49·6	2·3	49·4	1·48	SiO_2	0·37	0·57	0·24	0·62	0·18	0·17
Al_2O_3	34·71	1·06	32	2·62	31·8	2·07	Al_2O_3	47·09	4·26	39·64	7·12	47·87	4·91
FeO	0·72	0·17	2·06	1·7	0·89	0·13	FeO	1·28	0·26	3·17	2·86	1·22	0·62
MgO	1·05	0·06	1·18	0·59	1·38	0·09	MgO	0·09	0·03	0·02	0·03	0·03	0·01
CaO	0·12	0·15	0·31	0·38	0·01	0·03	CaO	5·09	1·21	5·06	2·90	5·53	0·28
Na_2O	0·15	0·03	0·13	0·04	0·14	0·03	Na_2O	0·90	0·55	0·45	0·69	0·20	0·17
K_2O	5·39	1·14	4·96	0·65	7·27	1·3	K_2O	3·25	1·66	1·82	2·09	1·21	0·39
P_2O_5	0·19	0·6	0·41	0·78	0	0	La_2O_3	0·05	0·09	0·40	0·37	0·06	0·09
Calc total	95·8	2·08	90·7	0·72	90·8	3·02	Ce_2O_3	0·41	0·11	1·47	1·10	0·58	0·11
O equivalents	22		22		22		Y_2O_3	0·09	0·07	0·20	0·17	0·01	0·03
	Cations		Cations		Cations		SrO	0·77	0·29	1·69	1·20	0·85	0·10
Si	6·74		6·66		6·68		P_2O_5	13·38	4·52	19·36	7·87	12·94	0·66
Al1v	1·26		1·34		1·32		F	1·22	0·58	1·05	0·44	0·84	0·09
Ttet	8·00		8·00		8·00		SO_3	22·33	3·06	15·89	6·42	22·14	3·69
Alv1	3·9		3·73		3·75		Calc total	96·32	2·87	90·44	3·84	93·66	7·19
Fe^{2+}	0·08		0·23		0·1		O equivalents	22		22		22	
Mg	0·2		0·24		0·28			Cations		Cations		Cations	
Toct	4·18		4·2		4·13		Si	0·05		0·03		0·02	
Ca	0·02		0·04		0		Al	6·91		6·33		7·17	
Na	0·04		0·03		0·04		Fe^{2+}	0·13		0·36		0·13	
K	0·87		0·85		1·26		Mg	0·02		0·00		0·01	
Tint	0·93		0·92		1·3		Ca	0·68		0·73		0·75	
P_2O_5	0·02		0·05		0		Na	0·22		0·12		0·05	
							K	0·52		0·31		0·03	
							La	0·00		0·02		0·00	
							Ce	0·02		0·07		0·03	
							Y	0·01		0·01		0·00	
							Sr	0·06		0·13		0·06	
							P_2O_5	1·41		2·22		1·39	
							SO_3	2·08		1·61		2·11	
							F	0·48		0·45		0·34	

TABLE 4. Mean electron microprobe analyses, standard deviations and cation proportions for sedimentary samples from the Soom Shale Member. Samples analysed: illites from core specimens K2.0, K2.4, K2.9 and K2.10; chlorites from core specimens K2.4, K2.9 and K2.10; illites from hand specimens with fossils KS1 (C275b), KS2 (C937a), KS4 and KS4A (C907a); alunite group minerals from KS4A (C907a). KS1–KS3 are from Keurbos and KS4 and KS4A from Sandfontein. The negative total charges are probably due to the absence of a Ti analysis. Ttet = tetrahedral layer total; Toct = octahedral layer total; Tint = interlayer site total.

	Illites from core sections		Illites from KS1, KS2, KS4, KS4A		Chlorites from core sections		Alunites from KS4A	
Oxides	Mean	SD	Mean	SD	Mean	SD	Mean	SD
SiO_2	54·02	2·58	52·86	2·33	29·38	1·81	0·11	0·23
Al_2O_3	35·17	2·77	29·96	4·02	21·42	1·17	25·03	4·23
FeO	1·66	0·71	1·87	0·7	23·58	1·19	5·12	0·87
MnO	0·00	0·02	0·01	0·01	0·14	0·13	0·00	0·00
MgO	1·4	0·74	1·53	0·42	13·26	2·08	0·00	0·00
CaO	0·02	0·02	0·08	0·1	0·07	0·04	3·35	0·13
Na_2O	0·24	0·23	0·2	0·18	0·02	0·02	0·18	0·03
K_2O	4·29	1·22	5·1	1·57	0·41	0·26	3·19	0·13
La_2O_3	0·03	0·07	0·00	0·00	0·00	0·00	1·17	0·06
Ce_2O_3	0·00	0·00	0·01	0·03	0·00	0·00	2·62	0·17
SrO	0·00	0·00	0·00	0·00	0·00	0·00	1·43	0·31
P_2O_5	0·01	0·02	0·0	0·11	0·00	0·00	15·42	1·61
SO_3	0·00	0·00	0·06	0·12	0·00	0·00	12·35	1·03
F	0·13	0·12	0·19	0·12	0·00	0·00	0·37	0·21
Calc total	97·22	2·62	91·91	3·48	89·31	0·79	70·34	4·64
O equivalents	22		22		28			22
	Cations		Cations			Cations		Cations
Si	6·71		6·97			6·01	Si	0·02
Allv	1·29		1·03			1·99	Al	5·45
Ttet	8		8		Ttet	8		
Alvl	3·86		3·63			3·18		
Fe^{2+}	0·17		0·21			4·03	Fe^{2+}	0·79
Mg	0·26		0·30			4·03	Mg	0
Toct	4·29		4·14				Ca	0·66
							Na	0·06
Ca	0		0·01			0·02	K	0·75
Na	0·06		0·05			0	La	0·08
K	0·68		0·86			0·12	Ce	0·18
Tint	0·74		0·92		Toct	11·38	Sr	0·15
P_2O_5	0		0			0·05	P_2O_5	2·41
OH	—		—			—	SO_3	1·71
Total charge	−0·11		−0·19			−0·19	F	0·22

calculated allowing determination of clay mineral species (Text-fig. 1). When using the electron microprobe to investigate mineral chemistries quantitatively, total counts of lower than 85 per cent. are not usually valid and are discarded. However, alunite group minerals, which are important components of some of the Soom Shale fossils, contain structural and free water and would therefore give very low total counts. For this study, therefore, all counts for alunite group minerals have been considered (Table 3).

TABLE 5. Mineralogy of the Soom Shale Member from core sections (K1.1A–K2.14) and hand specimens (K3.0–K3.4) as determined by XRD clay and whole rock analyses.

		Sample	K1.1A	K1.1B	K1.2	K1.3	K1.4	K1.5	K1.6	K1.7	K1.8	K2.0	K2.1	K2.2	K2.3	K2.4	K2.5	K2.6	K2.6A	K2.7	K2.8	K2.9A	K2.9B	K2.10	K2.11	K2.12	K2.13	K2.14A	K2.14B	K2.15A	K2.15B	K3.0	K3.1	K3.2	K3.3	K3.4
XRD WHOLE ROCK ANALYSIS	Alunite				●																														
	Pyrite				●	●	●		●			●	●	●	●	●	●	●	●	●				●			●								
	Kotschubeite											●												●											
	Chlorite					●			●				●	●	●	●	●	●	●	●	●		●	●	●	●	●								
	Illite	●		●	●	●		●	●	●	●	●	●	●	●	●	●	●	●	●			●	●	●	●	●					●	●	●	●
	Quartz	●	●	●	●	●		●	●	●	●	●	●	●	●	●	●	●	●	●			●	●	●	●	●					●	●	●	●
XRD CLAY ANALYSIS	Chlorite		●	●	●	●	●		●		●	●	●	●	●	●	●	●	●	●	●	●	●	●	●	●	●	●			●	●			●
	Kaolinite		●	●	●	●	●	●	●	●	●	●	●	●	●	●	●	●	●	●	●	●	●	●	●	●	●	●			●	●			●
	Illite	●	●	●	●	●	●	●	●	●	●	●	●	●	●	●	●	●	●	●	●	●	●	●	●	●	●	●			●	●	●	●	●
	Quartz	●	●	●	●	●	●	●	●	●	●	●	●	●	●	●	●	●	●	●	●	●	●	●	●	●	●	●			●	●	●	●	●

Treatment of possible organics from Siphonacis. The needle-like specimens of *Siphonacis parva* appear to have an organic composition. This was tested on a small piece of shale taken from C829 on which the *Siphonacis* are black and unmineralized. The sample was split into two where the preservation of the *Siphonacis* was identical on each piece. One piece was placed into 10% HF overnight to dissolve the matrix and any mineral matter (excepting sulphides). The residue consisted of very small black pieces (1–2 mm long) of indeterminable shape. These were probably broken up pieces of *Siphonacis* and their survival after HF maceration indicates them to be of either organic or sulphide mineral composition. The remaining half specimen was placed into a 10% solution of HNO_3 for three days and showed no sign of alteration in the black *Siphonacis* material. The black material did not oxidize in the nitric acid (a strong oxidizing agent) and is therefore probably organic in composition.

Sediment analyses

Bulk sediment from core sections, hand specimens and fossil-bearing hand specimens was analysed using a variety of techniques (see Tables 4–6).

Sediments analysed show a variation in the degree of weathering. Least weathered are the core samples, but even these sometimes show pervasive shear zones and split easily into discs; therefore, they may have been altered to some degree from an original early diagenetic mineralogy by contact with meteoric waters. Sediment samples from Sandfontein have been similarly affected and, in addition, have been subjected to surface weathering processes, including those induced by percolating meteoric waters. The least pristine sediment samples are from Keurbos, which, in addition to exhumation, have been subjected to deep Neogene weathering and alteration by extensive shear zone fluids. Attempts to constrain the early diagenetic conditions prevalent at the time of dissolution of biominerals and mineralization of soft tissues in the Soom Shale biota can only be conducted on the freshest material. However, mineralogical changes produced by more recent processes must be distinguished because they have an important effect on the final mode of preservation. The identification of minerals produced by weathering also allows more accurate determination of the original early diagenetic mineralogy. Backscatter imaging can be a powerful

TABLE 6. TOC (total organic carbon wt %), % S (sulphur wt %) and DOP (degree of pyritization) for core and hand specimen samples (see Table 5) from the Soom Shale Member.

Sample	Carbon wt %	Sulphur wt %	C/S	DOP	Sample	Carbon wt %	Sulphur wt %	C/S	DOP
K1.1A	2·01	0·77	2·61		K2.7	0·4	2·49	0·16	
K1.1B	0·79	3·68	0·21		K2.8	0·4	0·85	0·47	0·27
K1.2	1·03	3·79	0·27	0·68	K2.9A	0·49	2·31	0·21	
K1.3	0·71	3·87	0·18		K2.9B	0·11	0·18	0·61	
K1.4	0·42	1·53	0·27	0·72	K2.10	0·37	0·96	0·39	0·21
K1.5	0·93	3·39	0·27		K2.11	0·39	0·2	1·95	
K1.6	0·84	3·22	0·26		K2.12	0·33	0·29	1·14	
K1.8	0·23	0·03	7·67		K2.13	0·34	0·36	0·94	
K2.0	1·19	2·51	0·47		K2.14A	0·35	1·07	0·33	
K2.1	0·57	2·48	0·23		K2.14B	0·2	0·16	1·25	
K2.2	1·4	3·27	0·43	0·66	K3·0	0·13	0·26	0·50	
K2.3	0·73	3·91	0·19		K3.1	0·19	0·06	3·17	
K2.4	1·2	4·38	0·27		K3.2	0·09	0·03	3·00	
K2.5	0·76	3·56	0·21		K3.3	0·96	0·04	24·00	
K2.6	0·59	2·73	0·22		K3.4	0·12	0·14	0·86	
K2.6A	0·6	2·83	0·21						

TABLE 7. Summary of the mineralogy of the Soom Shale sediment from core samples, Sandfontein and Keurbos as determined by EM and XRD analyses.

Core samples	Sandfontein	Keurbos
Quartz	Quartz	Quartz
Illite	Illite	Illite
Kaolinite	—	Kaolinite
Chlorite	Chlorite	Chlorite
—	Anatase	Anatase
Apatite	—	—
Pyrite	—	—
Alunite	Alunite	—

tool in determining whether a mineral is detrital or diagenetic (see Macquaker 1994) and will be used in future research. Preliminary backscatter imaging on Soom Shale sediment, however, was not rewarding because the grain size is too fine to be resolved on the available equipment.

Electron microprobe analysis. Polished thin sections were prepared, carbon coated and probed with a focused beam. Samples were chosen to represent a range of lithologies and to investigate the difference in mineralogy between fresh (core samples) and weathered rock from Keurbos and Sandfontein. Owing to the importance of the presence or absence of alunite group minerals, analyses were considered even if total counts were less than 85 per cent. (see Table 4).

X-ray diffraction. X-ray diffraction was carried out on both whole rock and < 2 μm fractions using a Philips PW1729 X-ray generator and PW1710 diffractometer with multiple sample changer. The diffractometer was Ni-filtered with Cu K at 35 Kv, 55 mA. The < 2 μm fractions were run: (1) air dried, (2) following glycolation at 75 °C for 12 hours, and (3) after heating at 550 °C for 1·5 hours.

Total organic carbon and sulphur. Total organic carbon and % sulphur were determined using a LECO CS-125 analyser, using steel standards, after 10% HCl treatment. Samples were identical with those used in XRD analysis (see Table 5).

Degree of pyritization. Degree of pyritization (DOP) is defined as:

$$\mathrm{DOP} = \frac{\%\ \mathrm{Fe\ as\ pyrite}}{\%\ \mathrm{Fe\ as\ pyrite} + \%\ \mathrm{Fe\ HCl}}$$

where the % Fe HCl is the amount of iron liberated on treatment with hot concentrated HCl, and is a measure of the Fe still available that would be reactive to H_2S (see Berner 1970; Raiswell *et al.* 1987). Acid soluble iron was determined by the technique of Berner (1970). This method, using an ICP (inductively coupled plasma-Philips PV8060) has an average precision of 5 per cent. (Raiswell *et al.* 1994). Berner (1970) found the solubilities of iron minerals in HCl (by the method used here) to be similar to their reactivity with H_2S. It should be noted, however, that the concentration of HCl used may lead to solution of greater quantities of iron than would have been available to react with normally low concentrations of H_2S. Thus the DOP values given have a maximum value for % acid soluble iron and consequently provide a minimum value for DOP.

Conventional methods determine the amount of pyrite sulphur and hence pyrite iron (Westgate and Anderson 1982; Canfield *et al.* 1986). These methods are prone to some ambiguity and overlap in the separation of pyrite, elemental sulphur and organic sulphur species (Lord 1982). These ambiguities are eliminated by using an iron based technique as in this study. This procedure not only yields a higher selectivity but allows lower detection limits (Lord 1982). Samples analysed for DOP were from core material only (Table 6) and were chosen as they are all relatively fresh, and represent a wide spread through the Soom Shale sequence. In addition all samples, except K2.8, were known to contain pyrite from XRD analysis (Table 5).

X-ray fluorescence (XRF) whole rock analysis. Major oxide analyses were determined using the method described by Pickering *et al.* (1993).

Trace element analysis. Trace element analyses were performed on powdered pellets using the methods described by Tarney and Marsh (1991).

RESULTS

Fossil analyses

Eurypterids. Analyses of the exoskeleton by EDX (Text-fig. 2A–C) and electron microprobe have shown it to be composed of illite, alunite or a mix of illite and alunite (Tables 2–3). There is no correlation between the colour of the material (pink, yellow, buff brown or silver) and the presence of illite and mixed-layer clay and/or alunite.

Most eurypterids in the fossil record are exuviae but the preservation of internal muscle tissues in specimen C373 (holotype of *Onychopterella augusti* Braddy, Aldridge and Theron, 1995) shows this specimen, at least, to be the remains of an actual carcass (Braddy *et al.* 1995). Eurypterids from the Soom Shale comprise external and internal moulds but with considerable exoskeletal material present. In all cases, the original complex of chitin and proteinaceous material of the exoskeleton has been replaced by clays and alunite group minerals. Chitin is a polysaccharide carbohydrate and has been shown in decay experiments on the shrimp *Crangon* to be a relatively decay resistant biomolecule, especially when tanned or sclerotized (Briggs and Kear 1994). It is an important component of many non-mineralized marine arthropods which have an extensive fossil record (e.g. Briggs and Clarkson 1989; Butterfield 1990, 1994). However, there is a lack of evidence for the presence of chitin in fossils, suggesting that the preservation of chitinous tissues involves a gradual substitution of chitin by more resistant organic matter (Baas *et al.* 1995).

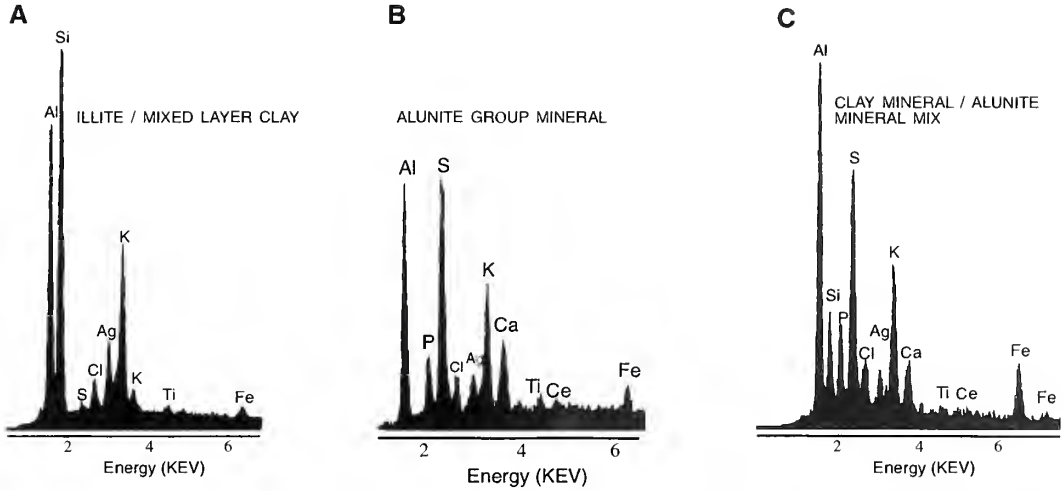

TEXT-FIG. 2. EDX traces of eurypterid specimens from Keurbos. A, cuticle from the prosoma of specimen C809d; B, eurypterid muscle tissue between podomeres on appendage VI from specimen C809d; C, cuticle from the prosoma of specimen C874b.

Trilobites. Specimens of *Mucronaspis olini* Moore and Marchant from the Soom Shale occur as external moulds with no trace of original exoskeleton. The absence of $CaCO_3$ was corroborated by seven EDX analysis which showed pure illitic and mixed illitic and alunitic compositions (Table 2A). Cl was recorded in one analysis and Ce was recorded in one analysis. It is not clear in which mineral phase Cl occurs; Ti probably occurs in the illites and Ce is probably within an alunitic mineral. Trilobite exoskeletons are composed of two layers: an inner layer composed of microcrystalline calcite set in an organic base and an outer thinner layer composed of prismatically arranged calcite crystals (Teigler and Towe 1975). It is unclear whether the illite and alunite grew on the exoskeleton or represent background sediment.

Specimens of the naraoiid *Soomaspis splendida* Fortey and Theron, 1995 preserve little of their original relief. The entire exoskeleton in all specimens shows signs of crushing, especially on the pygidium (Fortey and Theron 1995). Cracks are present on the pygidium and cephalic shield of the holotype (Fortey and Theron 1995). Only the holotype (C453) shows any cuticle preservation, lying anterior to the cephalic margin (Fortey and Theron 1995); other specimens are preserved as internal and external moulds. *Soomaspis splendida* had a non-mineralized cuticle which may have been chitinous (Fortey and Theron 1995).

Orthoconic nautiloids. In the Soom Shale, orthocones are preserved as internal or external moulds, or as composite moulds. Despite the absence of original aragonitic shell material, details of the conchs, such as growth lines and ornament, are evident. All show some degree of flattening. Many of the orthocones are colonized by discinisid brachiopods. There are three broad styles of conch preservation: (1) retention of some relief and lacking fracture patterns: these conchs were probably filled with sediment prior to compaction; (2) with little of the original relief and with longitudinal fracture patterns in the body-chamber, but chaotic fracture patterns in the phragmocone, produced by crushing; and (3) with body-chambers nearly completely flat with longitudinal wrinkles and the phragmocones severely flattened.

Four orthocone specimens contain radulae in their body-chambers, preserved as external moulds. Radulae were originally composed of chitin (Hunt and Nixon 1981).

Lingulate brachiopods. SEM EDX and electron microprobe analyses of orbiculoid shells from Keurbos show alunite and mixed alunite and illite compositions (Tables 2–3). The orbiculoid shell

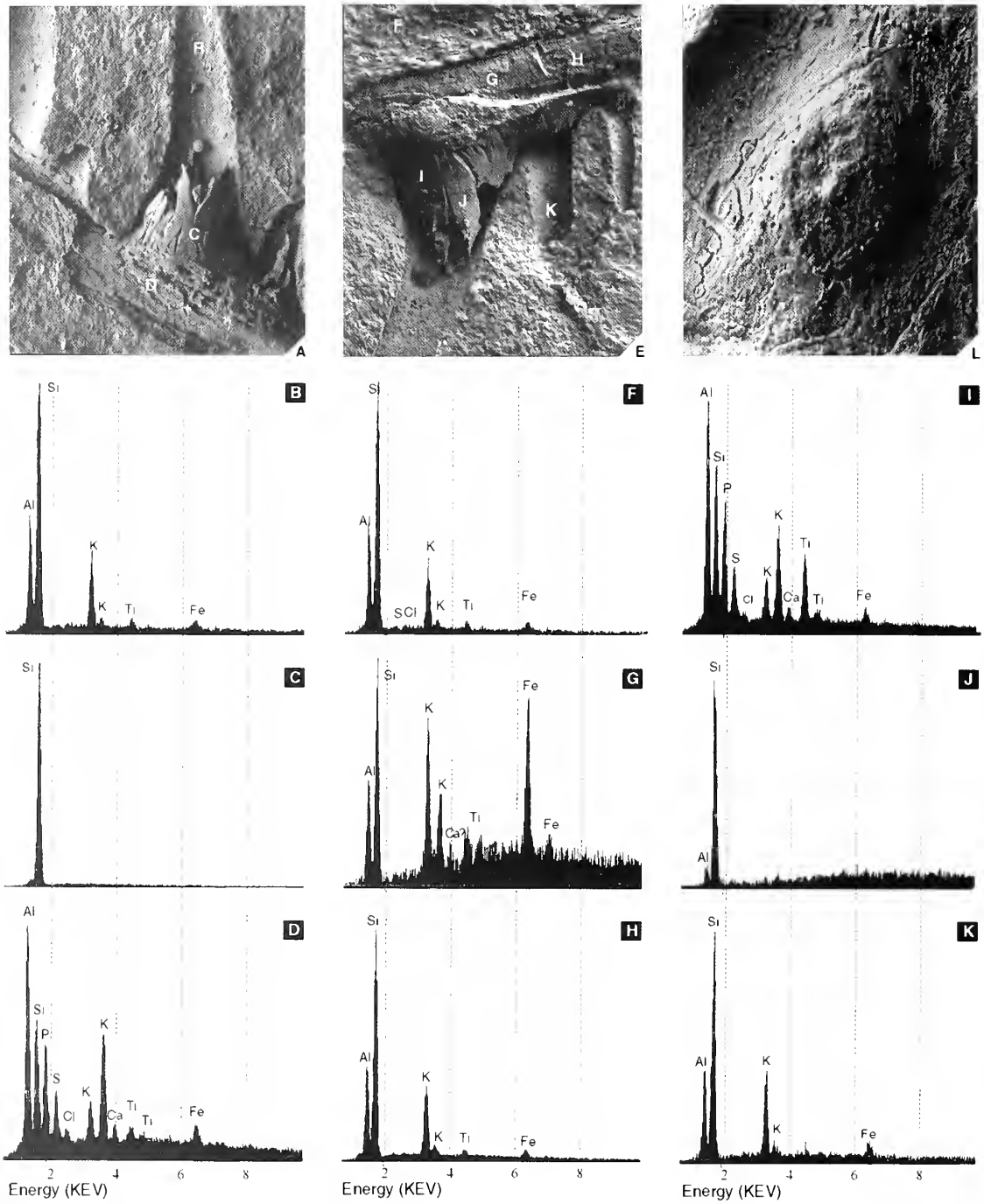

TEXT-FIG. 3. Photographs and EDX traces of conodont S elements and surrounding sediment from Keurbos (C424a). A, basal body/process (bottom), prismatic enamel and mouldic denticle crown; letters B–D denote positions where EDX analyses B–D were taken. E, basal body/process (top), prismatic enamel and mouldic denticle crown; letters F–K denote positions where EDX analyses F–K were taken. L, shows severe dissolution of the denticle and cracking of the basal body/process. A, × 55; E, × 80; L, × 200.

from Sandfontein was composed of alunite only (Tables 2B and 3B). Electron microprobe analyses of trematid shells from Keurbos showed either illite only, alunite only or both minerals (Tables 2B and 3).

Orbiculoids are the most abundant brachiopods in the Soom Shale; they have a complex mode of preservation where internal and external moulds co-occur. Most still retain a high proportion of shell material, particularly on the external surface. Growth lines are clearly distinguishable on the internal surfaces of the valves and fila are apparent on some of the external surfaces. A few shells have solid material in the position of the muscle scars, possibly representing the remains of soft tissues.

Trematids are not nearly so common in the Soom Shale as orbiculoids but show excellent preservation of their radially arranged ornament when found isolated in the sediment, unassociated with orthocones. Isolated trematids are dominantly mouldic and display details of growth lines, but some shell material is preserved. However, where they are found on or in close proximity to orthocones they are flat and very poorly preserved.

Orbiculoids and trematids are discinisicids, having chitinophosphatic shells with an organic content accounting for 25 per cent. of the exoskeletal dry weight (Jope 1965, p. H158). The inorganic phase is dominantly calcium phosphate (75·2% $CaPO_4$) with subordinate amounts of calcium carbonate (8·6% $CaCO_3$) (Williams *et al.* 1992). The shell structure of living and fossil discinisicids has been thoroughly studied by Williams *et al.* (1992). Beneath the periostracum of the discinisicid shells (e.g. *Discinia striata* Schumacher) lies the primary shell consisting of bands representing apatitic and organic concentrations which have many different configurations. Four types of biomineral laminae are distinguishable in the secondary shell, all composed, in varying proportions, of apatite granules (4–8 nm in diameter) with a chitino-proteinaceous coat. The biomineral component of the shells from the Soom Shale has been largely dissolved, but some clay and alunite mineral replacement has occurred.

Conodonts elements. Several elements contain mineralized material in their denticle cores and along the basal bodies and/or processes (Text-fig. 3A, E). Elements from Keurbos only rarely retain such material which is often yellow or pink due to weathering, but may appear black. Survival of mineral material in the elements is more common at Sandfontein. Here, black, shiny mineralized material is most commonly situated in the denticle cores. The distinct preservational mineralogies of the basal bodies, prismatic and aprismatic enamel within the conodont elements (see below), probably reflects differences in the original compositions of these tissues.

The basal bodies/processes of S elements from both Keurbos and Sandfontein show mineral replacements which are commonly fractured and cracked (Text-fig. 3L, from Keurbos). The mineralogy of the basal body in specimen C424a from Keurbos was found to be a mixture of illite and alunite group minerals; EDX analyses are shown in Text-figure 3D (illite and alunite) and 3G–H (illite). A single analysis of the basal body of specimen C679a from Sandfontein gave a dominantly illitic EDX trace.

In all the conodont elements observed, the aprismatic enamel from the denticle crown is absent, resulting in mouldic preservation (Text-fig. 3A, E). The mouldic trace of the aprismatic enamel may be used to delineate its former position in the elements; in some examples, mouldic preservation is seen to occur in the denticle crown and along the edge of the basal body linking separate denticles (Text-fig. 3A, E). The prismatic enamel, when present, shows three styles of preservation. In many of the denticles from Keurbos, the original prismatic structure is present (Text-fig. 3A, E). In three of the four EDX analyses of the prismatic enamel from specimen C424a (Keurbos), excitation peaks corresponding to quartz ($\pm$ small amounts of Al in two of the three analyses, see Text-fig. 3C, J for two of the EDX traces) were obtained. In a single analysis of the prismatic material from the same specimen (Text-fig. 3I), the composition was of illite and alunite. The prismatic enamel is most commonly preserved by quartz with no trace of apatite. Specimen C679a from Sandfontein shows another mode of preservation of prismatic enamel, in which denticle cores have an outer smooth surface and the prismatic structure is not apparent. Of eight EDX analyses of the denticle core

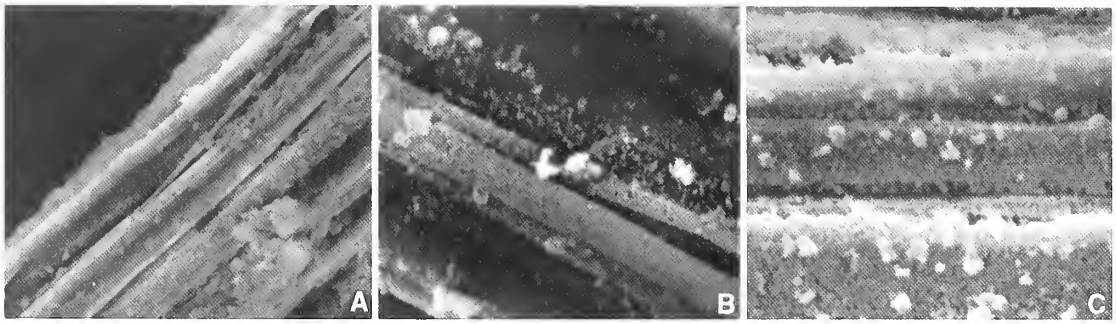

TEXT-FIG. 4. Conodont specimen C721a, Soom Shale, Sandfontein, South Africa; Ordovician (Ashgill). A, smooth muscle fibres *c.* 5 μm in diameter showing longitudinal lineation reflecting myofibrillar structure; × 1200. B, myofibrils showing microgranular texture; × 6300. C, myofibrils showing microgranular texture; × 7500.

material in C679a, seven gave a quartz composition and one gave excitation peaks in Al, Si, S, Cl and Fe, which is problematical, but may represent illite and alunite. The third, and most common mode of preservation of the denticle core prismatic enamel is mouldic (see Text-fig. 3L). The severe apatite dissolution suffered by conodont elements from the Soom Shale can be seen clearly in Text-figure 3L where the denticle should point out of the plane of the photograph. Instead, only a stub representing its former position is seen.

Conodont elements are composed of calcium phosphate in which fluorine substitutes for hydroxides, producing francolite (Pietzner *et al.* 1968). There are three vertebrate hard tissue types that are pertinent to the taphonomy of the conodont elements from the Soom Shale. These are dentine of the basal body, and prismatic and aprismatic enamel of the denticle crowns (Phil Donoghue, pers. comm. 1996). Dentine is an organic-mineral composite in which the apatite crystallites are considerably smaller (average 200–1000 angstroms long, 30 angstroms wide) than those in enamel (1600–10000 angstroms long, 400 angstroms wide) (Carlson 1990). The inorganic component of dentine constitutes approximately 70–75 wt % and the organic component constitutes 18–21 wt % (Carlson 1990). The organic material is largely collagen (Scott and Symons 1977) within which the hydroxyapatite crystallites are more or less randomly orientated (Carlson 1990). In the Soom Shale conodont elements, dentine tissue has been replaced by illite and alunite. Conversely, enamel has non-collagenous organic matter which comprises typically less than 1 wt % of the tissue, and is a highly mineralized tissue with an inorganic component constituting up to 97 wt %. The enamel crystallites may be orientated in different ways. In aprismatic enamel, all crystallites are more-or-less mutually parallel and are perpendicular to the enamel dentine junction. Prismatic enamel shows a repetitive pattern of variation in crystallite orientation producing 'prisms' (Carlson 1990). This tissue type has been most commonly replaced by quartz (and rarely by illite and alunite) in the Soom Shale. In light acid preparations of conodonts, dentine is more sensitive to acid dissolution than aprismatic enamel which is more sensitive than prismatic enamel (Phil Donoghue, pers. comm. 1996).

Theron *et al.* (1990) noted the poor preservation of the original apatite in the elements from the Soom Shale, with several represented by internal or external moulds. On analysis of greenish material by EDX, peaks in silicon, aluminium and potassium were obtained, presumably representing illite from the matrix. Peaks in calcium and phosphorus were obtained from some relatively unaltered amber-coloured areas of one of the ramiform elements (Theron *et al.* 1990, text-fig. 4); this may represent an alunite group mineral. The mode and mineralogy of conodont element preservation in the Soom Shale is unique and its elucidation will require detailed chemical mapping.

Conodont soft tissues. The preserved soft tissues of the trunk myomeres were shown by both EDX

(Table 2A) and electron microprobe analysis (Tables 2B and 3A) to be composed only of illite/mixed layer clay. The muscle blocks, or myomeres, preserve ultrastructural details of the muscle fibres including fibrils and sarcomeres (Gabbott *et al.* 1995). The muscle fibres in the myomeres are *c.* 3–5 μm in diameter and have a circular cross section (Text-fig. 4A). Their preservational textures vary; most fibres are very smooth (Text-fig. 4A) whereas others have a distinct granularity (Text-fig. 4B–C). The smooth fibres are unlike any other fossilized muscle fibres figured from fish or other taxa. The granular texture, where present, usually composes the whole fibre, but it may appear on smooth fibres as a patchy coating. The texture comprises spherical–sub-spherical granules with a diameter of *c.* 90–150 nm. The nature of these microspheres is not yet known because the resolution of the image at the levels of magnification required to view them is very poor. They may be mineralized microbes; fossil nannobacteria have been found as small as 0·1 μm in diameter (Folk 1993). Alternatively, they may be inorganic in origin and analogous to the microspheres/microgranules composed of calcium phosphate recorded in other mineralized muscle tissue (Wilby 1993*a*, 1993*b*).

The sclerotic eye capsules from Keurbos show a similar style of preservation to the chitinozoans from this locality. Some comprise the flattened, black remains of the sclerotized tissues (e.g. C288, C351, C358; see Aldridge and Theron 1993, pl. 1, figs 2–4), whilst others are partially or completely mineralized by a silvery white mineral (C279; see Aldridge and Theron 1993, pl. 1, fig. 1), presumably illite. Often, the part of a specimen preserves the eyes dominantly in black coalified organic material whereas the counterpart is dominantly mineralized. The conodont eye capsules from Sandfontein are composed of a silvery-white mineral which appears the same as the illite/mixed layer clay preserving the somites of specimen C721. These silvery-white patches may be amorphous or have a fibrous texture. The mineralized extrinsic eye musculature has not yet been analysed because specimens are too rare for destructive analysis, and the slabs of shale are too large for the eyes to be positioned under the beam in an SEM chamber. However, the texture, colour and form of the mineral suggest that it is illite/mixed layer clay.

The eye capsules (Aldridge and Theron 1993) of *Promissum pulchrum* are thought to have been composed originally of scleratin, a decay-resistant structural polymer. Decay experiments (Briggs and Kear 1993*a*) on polychaetes have demonstrated the resistance of sclerotized tissue; it was the only tissue type to survive beyond 30 days in the absence of early diagenetic mineralization. Thirty-eight pairs of sclerotic eye capsules have been found from the Soom Shale associated with bedding plane assemblages (eyes occurring with 20–25 per cent. of the conodont apparatuses), whereas only specimen C721 preserves both trunk somites and evidence of eyes, in the form of extrinsic eye musculature. Two additional specimens (C699 and C712) from Sandfontein display very poorly preserved eye musculature but no trunk trace is evident.

Spores and acritarchs. Spores and acritarchs have walls composed of sporopollenin and were recovered following dissolution of the matrix in hydrofluoric acid (Gray *et al.* 1986). These organic-walled microfossils were highly resistant to microbial decay and inorganic degradation. Spores and acritarchs from the Soom Shale are dark brown to black due to considerable thermal alteration and are probably composed of altered sporopollenin. It is possible that some may now be composed of illite but owing to their method of extraction and their small size rendering them invisible on bedding surfaces, this is not testable.

Chitinozoans. EDX analysis on a silver-white chitinozoan from Keurbos gave compositions of illite and illite and alunite, with an iron oxide phase and accessory Cl and Ti (Table 2A). It is not known in which mineral phase(s) the Cl occurs, but Ti probably occurs in illite. Chitinozoans on weathered bedding surfaces from Keurbos are often dark grey/black in colour with a reticulate surface pattern consistent with fractures produced by heating (see Burmann 1969). Other vesicles are preserved in a silvery-white material. Some chitinozoans appear flat whereas others are more three-dimensional; in the latter case, some sediment infill is evident.

EDX analyses on chitinozoans from Sandfontein all gave illitic compositions ± an iron oxide. Ti was recorded in two analyses and Cl in three analyses but these elements did not occur together. At Sandfontein, the chitinozoans are completely mineralized by illite, but again it is unclear whether the mineralization represents an overgrowth or a replacement of the organic wall. The illite crystals on the margin of the vesicle are aligned parallel to it (perpendicular to the bulk of the crystals), whereas the crystals replacing the bulk of the vesicle are aligned approximately parallel to each other and to the long axis of the chitinozoan. These crystals show typical illite habit but are relatively large, being up to 30 μm long, indicating the onset of conversion to muscovite. It is possible that at Sandfontein these are vesicles composed of organic material but they may have been overlooked as the matrix is black.

The original pseudochitinous composition (Traverse 1988) of chitinozoans has been replaced by illitic clay minerals which appear to have formed as a film-like sheet on to the organic surfaces of the vesicles. However, it is not clear whether the organic vesicle survives beneath the clay mineral sheet or has been replaced by it. Soom Shale chitinozoans have been found after HF digestion of the matrix and occur as highly coalified individual vesicles (Cramer *et al.* 1974) or as individuals, chains and clusters on bedding surfaces from Keurbos and Sandfontein. Thus two preservational styles for chitinozoans are distinguishable: organic walled coalified forms found after HF digestion, and those found preserved in clay minerals on bedding surfaces (Table 2A).

Summary of fossil analyses

Table 1 shows the original and fossil compositions of various taxa in the Soom Shale. A summary of the results of EDX analysis is shown in Table 2A and a summary of electron microprobe results in Table 2B. The data clearly split into three compositional groups. One group shows a range of illite mineral group compositions, another group shows a range of compositions in the alunite mineral group, and a third group shows a mixture of illitic and alunitic signatures. This third group is the result of the electron beam overlapping and analysing both minerals. An iron oxide phase was also recorded in a small number of analyses.

No alunite component was recorded from the conodont muscle tissue. The eurypterids, orbiculoids and trematids analysed had both illitic and alunitic mineral signatures. Light microscope, SEM and secondary electron images failed to reveal any distinct pattern to the partitioning of these two minerals. They appear to be intimately mixed.

Illite. Table 3A shows the mean electron microprobe analysis and cation proportions (calculated to 22 oxygens) for the illitic component of the eurypterids, trematids and conodont muscle tissue. It can be seen from the triangular plot (Velde and Meunier 1987; Text-fig. 1A) of the full gamut of analyses that there is some variation in composition, although nearly all samples plot within the illite and mixed-layer clay solid solution series. For simplicity, the fossil compositions which lie in the illite to mixed-layer clay compositional fields will be referred to as illites hereafter because the quantitative electron microprobe analyses demonstrate a continuum of Fe and Mg values from low weight per cent. in purer illites up to 4·08 (Fe) and 2·06 (Mg) in mixed-layer clays.

Alunite. Table 3B shows the mean electron microprobe analyses and cation proportions (calculated to 22 oxygens) for the alunitic component of the eurypterids, trematids and orbiculoids. The compositional field of the alunitic Soom Shale fossils relative to related mineral species is shown on the triangular plot in Text-figure 1B. Note that if more cations, such as Pb, had been analysed for and were present, then fossil compositions would cluster more towards the cation apex. Quantitative electron microprobe analyses show that crandallite ($CaAl_3(PO_4)_2(OH)_5.H_2O$) is the most common alunite group mineral present especially in the orbiculoids; alunite ($KAl_3(SO_4)_2(OH))_6$ also occurs commonly. Calcium constitutes the cation with the greatest weight per cent. in most analyses (19 out of 24), followed by potassium and then iron. A bivariant plot of CaO against P_2O_5 (Text-fig. 5B) for the alunitic fossil compositions shows a positive correlation coefficient (0·41). A

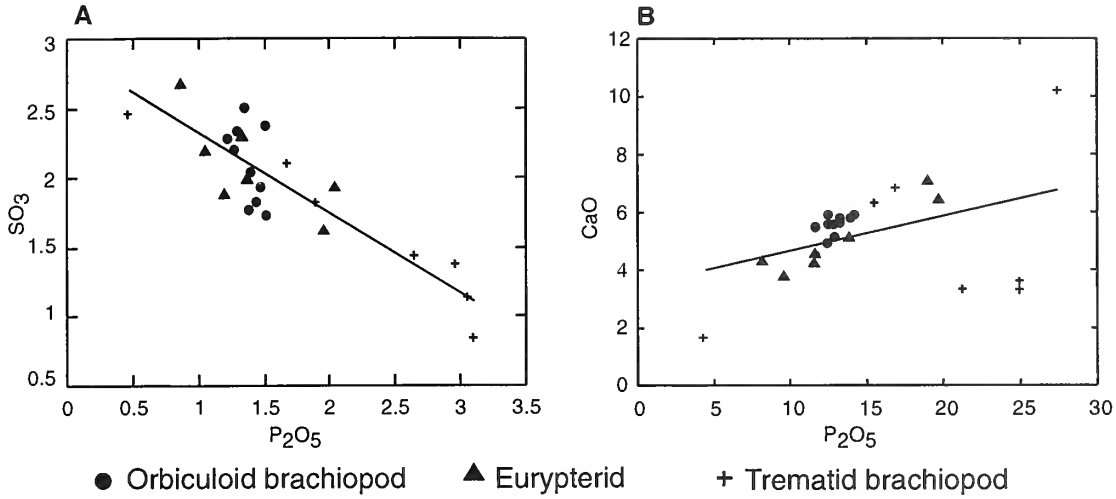

TEXT-FIG. 5. Bivariant plots of fossil material with alunitic compositions analysed by the electron microprobe. A, SO_3 against P_2O_5; there is a strong negative correlation coefficient (R = 0·88) demonstrating extensive anion substitution. B, CaO against P_2O_5 showing a slight positive correlation (R = 0·41) suggesting that both occur, at least quite often, in the same mineral: crandallite.

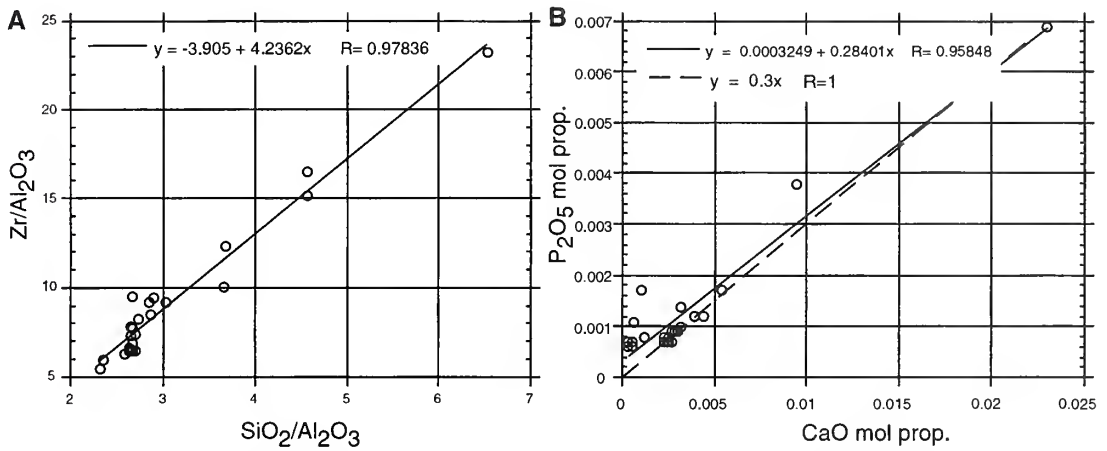

TEXT-FIG. 6. A, alumina normalized bivariant plot of Zr against SiO_2. Zr (ppm.) and SiO_2 (wt %), values from XRF analyses. B, bivariant plot of calculated P_2O_5 (molecular proportion) against CaO (molecular proportion). Stochiometric apatite is represented by the dashed line and has a slope of 0·3; oxide analyses from XRF data.

student *t*-test (n = 24) shows that there is only a one in 20 chance of this correlation coefficient occurring by chance between CaO and P_2O_5. Substitution between the anions P_2O_5 and SO_3 is indicated by their high negative correlation coefficient (Text-fig. 5A).

Discussion of sediment analyses

Mineralogy. The most pristine sediment is from the core material and comprises dominant quartz and illite, together with chlorite, kaolinite, pyrite, and less commonly apatite and alunite. The quartz is probably detrital in origin, as shown by its high correlation coefficient with Zr on an Al_2O_3

normalized plot (Text-fig. 6A, R = 0·98) (see Norry *et al.* 1994). The origin of the illite is more equivocal. It may be detrital or authigenic, formed by the breakdown of K-feldspar (producing mica and/or illite), or both:

$$\underset{\text{K-feldspar}}{3KalSi_3O_8} + 2H^+12H_2O \rightarrow \underset{\text{illite and/or mica}}{KAl_3Si_3O_{10}(OH)_2} + 6H_4SiO_4 + 2K^+ \quad (1)$$

The breakdown of K-feldspar to form illite and/or mica yields excess potassium (equation 1) which may be used to form additional illite. K-feldspar becomes unstable as pore water acidity increases [as$(K^+)/(H^+)$ decreases], so that breakdown is most likely to have occurred during early diagenesis when organic decomposition by sulphate reducing bacteria produced H_2S ions (equation 2).

$$18CH_2O + 9SO_4^{2-} \rightarrow 18HCO^{3-} + 9H_2S \quad (2)$$

No K-feldspars have been observed in the Soom Shale, either by XRD or SEM, indicating that if illite was formed from their breakdown, this process was very active and complete. The X-ray data indicate that the illite is the $2M_1$ polytype. After changing to mica (equation 1), the K-feldspars may alter to kaolinite (equation 3) (Krauskopf 1982) as porewater acidity increased as a result of organic matter decomposition.

$$\underset{\text{mica}}{KAl_3Si_3O_{10}(OH)_2} + H^+ + 3H_2O \rightarrow \underset{\text{kaolinite}}{3Al_2Si_2O_5(OH)_4} + K^+ \quad (3)$$

The presence of kaolinite in the core samples is shown by fairly sharp peaks in diffractometer traces but was not detected by electron microprobe analyses. This is probably due to beam overlap, with illite swamping the kaolinite signature. Small amounts of kaolinite may also have formed during the deep arid weathering.

The composition of chlorites in core samples (Table 4 and Text-fig. 1) is consistent with them being clinochlore-chamosite chlorites with approximately equal amounts of Fe and Mg on an atomic basis (Bayliss 1975; Bailey 1988). There is no excess Al, so that the analyses fall into the normal range for chlorites formed by metamorphism rather than in the diagenetic range (Velde and Meunier 1987). This is a slightly higher temperature than that estimated for the Soom Shale (200 °C) from the colour of palynomorphs (Cramer *et al.* 1974; Gray *et al.* 1986). In addition, some chlorites of clinochore-chamosite composition may have been derived and therefore introduced detritally into the Soom Shale sediment.

Apatite was detected, by electron microprobe analysis, in one of the more silty core samples. XRD analysis failed to find any further apatite in any core samples so it is either rare or amorphous. A bivariant plot of the calculated molecular proportions for CaO against P_2O_5 demonstrates an excellent positive correlation coefficient (R = 0·96), a near zero intercept and a slope of 0·284, which is very close to the slope value of 0·3 that would apply if all the calcium and phosphorus were situated in apatite (Text-fig. 6B). This indicates that the sediment is extremely calcium carbonate deficient.

Finely disseminated pyrite occurs in most of the core samples; it is of diagenetic and syngenetic origin and will be discussed later under the heading DOP (degree of pyritization).

A single XRD trace (out of the 35 samples) from core sample K1.2 indicated the presence of alunite, the formation of which is discussed later.

Sediment from Keurbos consists of quartz, illite ($2M_1$ polytype), chlorite, kaolinite and anatase (detected by XRD analyses). With the exception of the presence of kaolinite and the absence of alunite, this is the same mineralogy as at Sandfontein. The absence of sedimentary alunite from Keurbos again indicates that it is an extremely rare component of the matrix, although fossil material from Keurbos always contains some alunite (Table 2A–B).

Samples from Sandfontein contain quartz, illite, anatase, possible chlorite and, in one sample only (KS4A), alunite (detected by electron microprobe and XRD analyses). Again, the illite is of the $2M_1$ polytype and constitutes the largest component of the sediment. The absence of kaolinite in samples from Sandfontein remains to be explained, as it is present in the core samples and heavily

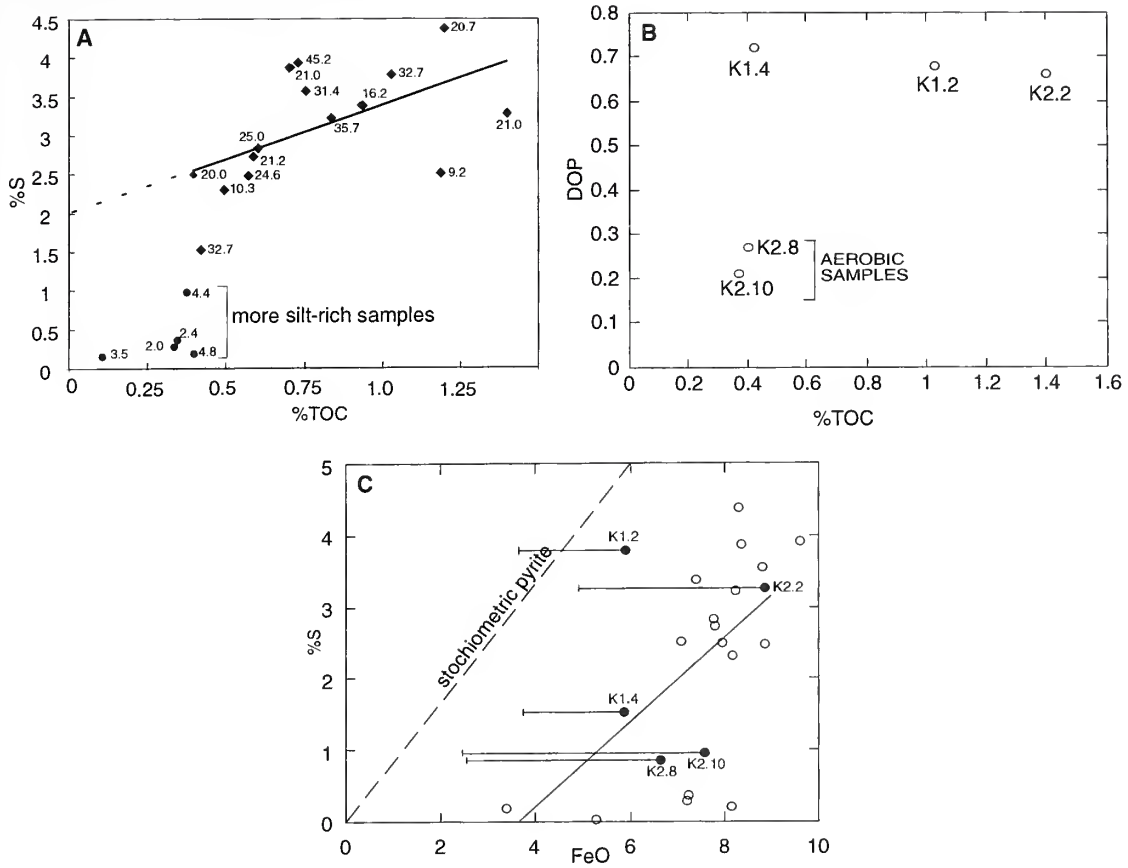

TEXT-FIG. 7. A, bivariant plot of % S against TOC (total organic carbon wt %) for unweathered core samples. Diamonds represent samples with high Mo contents (indicated in ppm.); circles represent samples with low Mo contents (indicated in ppm.). For samples with high Mo, % TOC and % S, R = 0·31. B, bivariant plot of DOP (degree of pyritization) against TOC for five core samples. C, bivariant plot of % S against FeO wt % for unweathered samples. Solid circles denote samples on which DOP has been analysed and the solid lines to the left of each sample represent the amount of acid soluble iron extracted from each sample in wt %. The dashed line represents calculated stochiometric pyrite. Note that for sample K1.2 pyrite becomes soluble during iron extraction. $y + -2{\cdot}1379 + 0{\cdot}58507x$; R = 0·56982.

weathered samples from Keurbos. Although only two samples from Sandfontein (K3.1 and K3.2) have been analysed by X-ray diffraction, kaolinite was also not detected by electron microprobe analysis. Chlorite was absent in the two XRD analyses, but electron microprobe analyses show a probable mix of illite and chlorite in KS4A from Sandfontein. The sources of the illite and chlorite are probably the same as discussed for the core sample sediments, but the origin of the anatase is unclear. It is commonly a detrital mineral in sedimentary rocks, but may be authigenic or produced by low temperature hydrothermal fluids. Its absence from fresh core material, however, indicates that the anatase in the Soom Shale is probably the result of a near surface, weathering process.

The electron microprobe analyses of alunite grains show that FeO is the most abundant cation, with roughly equal amounts of CaO and K_2O and smaller, but significant amounts of Ce_2O_3, La_2O_3 and SrO. Of the anions, P_2O_5 is only slightly higher in abundance than SO_3 (Table 4; Text-fig. 1B) and any single end-member alunite group mineral is not distinguishable; this is unlike the fossil

alunites where end member minerals are clearly distinguished. Viewed optically and under secondary electrons, the alunitic grains (three analysed in total) are rounded with a discontinuous halo and all are very poorly preserved. The grains of alunite found within the sediment may have been associated with a fossil fragment. Alternatively, alunite may form a rare but authigenic component of the sediment. In any case, alunite group minerals are an extremely uncommon component of the matrix with only three grains being found in polished thin sections. Unlike the sedimentary alunite analyses, those from fossil material commonly show SO_3 and P_2O_5 substitution as demonstrated by their good negative correlation coefficient ($R = 0{\cdot}88$, Text-fig. 5A). Their possible genesis is discussed later.

Molybdenum. The molybdenum concentration in unweathered core samples, with no significant silty component, is 9·20–45·20 ppm. (average = 24·46 ppm.), considerably higher than in PAAS (Post Archean Average Shale; 1·0–2·0 ppm., Taylor and McLennan 1985). Molybdenum enrichment in black shales has been documented by several workers (e.g. see Brumsack 1989). Helz *et al.* (1996) have shown using EXAFS (extended X-ray absorption fine structure) spectra that molybdenum, a conservative element in normal marine waters, becomes particle reactive when the action point of HS^- reaches $10^{-3{\cdot}6}$–$10^{-4{\cdot}3}$; hence HS^- acts as a geochemical switch. When aHS^- approaches this value Mo may form covalent bonds, via S bridges, with sedimenting particles containing transition metals (e.g. Fe) and organic molecules; in this way, Mo is scavenged from the water column and incorporated into the sediment (Helz *et al.* 1996). Since HS^- concentrations in natural anaerobic waters range to values above 10^{-3} M, the aHS^- switch will be activated in many such environments (Helz *et al.* 1996). The elevated Mo content in the Soom Shale sediment, therefore, strongly suggests that anoxic conditions prevailed. Where low Mo concentrations are recorded in unweathered samples, these are invariably from more silt-rich rock (see Text-fig. 7A).

Total organic carbon, total sulphur and degree of pyritization (*DOP*). Table 6 shows the results of total organic carbon, % sulphur and DOP analyses. In unweathered samples and samples with no silty laminations, the TOC ranges from 0·11–1·4 wt % and S ranges from 0·2–4·38 wt %. A plot of % S/TOC (Text-fig. 7A) for unweathered Soom Shale shows two distinct data groupings which are well defined by their Mo contents. Samples with high Mo contents (9·20–45·20 ppm.) show a positive correlation with a positive intercept on the y axis (y = 2·0). Samples with low Mo, % S and TOC values occur towards the top of the Soom Shale, where coarser silty laminations are common. C/S ratios are listed in Table 6, and all the unweathered samples plotted (Text-fig. 7A) range between 0·16–1·95. In euxinic conditions, C/S ratios are consistently less than 3 and regression lines with positive intercepts on the S axis have been demonstrated (Berner and Raiswell 1983; Levental 1983), but it is important to note that some of the organic C may have been lost during anchimetamorphism.

During the deposition of the Soom Shale, bottom and pore waters became rapidly aggressive towards aragonite and calcite resulting in their complete dissolution. Apatite was also dissolved, but at greater burial depths than the carbonate phases. Corrosive fluids could have been produced by the build-up of H_2S and H^+ in solution as a result of active sulphate reduction, where there was a paucity of reactive iron. Thermal maturation probably accounts for the relatively low TOC content and may have remobilized sulphur and iron phases so that caution is necessary when interpreting the results of these analyses.

In normal marine environments, with oxygenated bottom waters containing adequate reactive iron, the principal factor limiting pyrite formation is the amount of buried organic matter. However, in euxinic environments, H_2S is present above the sediment-water interface as well as within the sediments. Consequently, pyrite can form before burial in the presence of sedimenting minerals containing reactive iron. In this situation, it is not organic carbon that limits the production of pyrite, owing to the omnipresence of H_2S, but the amount of reactive iron in the sediment (Raiswell 1982; Berner 1984; Fisher and Hudson 1985). Reactive iron may be defined as the fraction of iron in marine sediments which readily reacts with sulphide (a product of sulphate reduction) to form

iron sulphide minerals and eventually pyrite (e.g. Berner 1970; Raiswell and Berner 1985; Canfield 1989). The two most important sources of reactive iron in fine-grained sediments are probably iron oxides (Canfield 1989) and colloidal ferric oxides adsorbed on to clay minerals (Berner and Rao 1994). Canfield (1989) has shown that there was a complete consumption of iron oxides at the FOAM (Friends Of Anoxic Muds) site at Long Island Sound, USA, by 70–100 mm depth. The FOAM site sediment is anoxic and Fe-poor and early pyrite appears to form at the expense of iron oxides (e.g. ferrihydrite, lepidocrocite, goethite and hematite) with no evidence for substantial involvement of iron silicates (Canfield 1989). At this locality, reoxidation of pyrite due to bioturbation and other processes (e.g. wave action) constantly replenishes iron oxides, without which the sediment would have become considerably more 'sulphidic' (Canfield 1989). The reactivity of iron adsorbed on to clay minerals towards H_2S has not been studied in any detail.

In sediments of Devonian to Cretaceous ages, the DOP may give a fair indication of the degree of bottom water oxygenation (Raiswell *et al.* 1987). However, pre-Devonian sediments would have had relatively more reactive organic carbon material (due to the absence of terrestrial plant-derived organic matter) and would therefore produce more sulphur fixation (as pyrite) per unit of buried carbon (Raiswell and Berner 1986). To date, then, the use of DOP as an indicator of bottom water oxygenation in pre-Devonian sediments is not secure, but it can be used to gauge the amount of iron reactive towards H_2S. The amount of reactive iron would have been important in controlling the pH of the pore waters in the Soom Shale sediment. For example, sufficient quantities of reactive iron oxides (and ferric oxides sorbed onto clay minerals) could have effectively buffered the concentration of pore water sulphide to very low levels, even in the presence of active sulphate reduction.

The five samples analysed for DOP from the Soom Shale fall into two groups (Table 6), one with moderately high DOP values (0·72, 0·68 and 0·66) and another with low DOP values (0·21 and 0·27). The samples with low DOP values also have low Mo, % S and TOC (Text-fig. 7A), are more silt-rich and occur towards the top of the Soom Shale. A plot of DOP against TOC (Text-fig. 7B) shows that there is no correlation between the amount of organic carbon and the DOP in the three samples with high DOP values. In this situation, the amount of detrital iron minerals reactive towards H_2S is the limiting factor in pyrite formation rather than the amount of organic carbon. In this case, the plot of % S against % TOC (Text-fig. 7A), demonstrating a positive correlation, indicates that there was more Fe available for increased levels of syngenetic pyrite formation at higher C values (Raiswell and Berner 1985). Thus, at least at times when the bottom waters were O_2-depleted, it would appear that pyrite formation was syngenetic and limited by the amount of reactive iron. However, this is in contradiction with the DOP values, which are not excessively high, and with the amount of acid soluble iron (Table 6 and Text-fig. 7C) which would have been available for pyrite formation. There are two possible and related explanations to account for the discrepancy between demineralized carbonate phases and moderate DOP values; one involves experimental error in the determination of acid-soluble iron which should have been reactive towards H_2S.

The plot of % S against FeO (Text-fig. 7C) shows the amount of acid soluble iron determined after boiling in HCl for the five samples on which DOP was analysed (represented as solid horizontal lines). In sample K1.2 (DOP = 0·68), some of the pyrite iron became soluble through boiling in HCl. This obviously places some doubt on the accuracy of the amount of acid soluble Fe determined in the other samples. Furthermore, the amount of acid soluble iron determined may have been further enhanced by Fe from chlorite and illite. In an examination of iron extraction techniques for the determination of DOP, Raiswell *et al.* (1994) found that during boiling in HCl (the technique used here) some iron was released from silicate phases, particularly nontronite ($7{\cdot}13 \pm 0{\cdot}36$ wt %) and chlorite ($2{\cdot}19 \pm 0{\cdot}11$ wt %) that would not have been reactive towards H_2S. In the Soom Shale, Fe contained within silicate phases may have come from chlorite (mean Fe wt % = 23·58; see Table 4 for electron microprobe analysis) and illite (mean Fe wt % = 1·66, see Table 4). Therefore, experimentally determined values of acid soluble Fe may be higher than the amount of Fe that would have actually been available to react with H_2S during early diagenesis. Thus syngenetic pyrite formation may have exhausted all or most of the detrital iron so that diagenetic pyrite formation did not occur or at least was very slow.

Another explanation may be that there was a paucity of iron oxides available for reaction with the H_2S produced by sulphate reduction. It may be that pyrite formation was initially inhibited, by a lack of reactive iron oxides, allowing increased bottom/pore water acidity, and could only commence when pore waters became aggressive towards iron-containing silicate minerals and released iron from them. In addition, there would have been no recycling of iron by bioturbation or wave activity. A paucity of iron oxide minerals in the Soom Shale is corroborated by XRD and EM analyses of the sediment and may be explained by an iron oxide-poor sedimentary source to the basin. Furthermore, sediments at this time would not have supported a soil horizon in the absence of land plants and the land surface had presumably been scraped clean by ice.

SOFT TISSUE PRESERVATION

Soft tissues, such as muscle, are subject to rapid autolysis and metabolization by bacteria. They are lost very rapidly unless preserved by early authigenic mineralization (Allison 1988*a*, 1988*b*, 1988*c*; Briggs and Kear 1993*b*, 1994). In the fossil record, examples of authigenic minerals which replace soft tissues are phosphate (e.g. Müller and Walossek 1985; Martill, 1988, 1990), and more rarely and with less fidelity, pyrite (e.g. Stürmer 1970; Cisne 1973; Conway Morris 1986; Briggs *et al.* 1991*a*; Briggs *et al.* 1996; Wilby *et al.* 1996) and carbonate (Wuttke 1983). Silicification of soft tissues is known only from one example, the Eocene lignite of Geiseltal (Voigt 1988).

In the Soom Shale, soft tissues are replicated by clay minerals (conodont muscle tissue) and by clay minerals and alunite group minerals (eurypterid cuticle and muscle tissue); these minerals have hitherto not been recorded preserving soft tissues in the fossil record. The fidelity of replication is at a sub-cellular scale, a level of detail which has only previously been reported in soft tissues replaced by phosphate (e.g. Martill 1990; Wilby 1993*a*, 1993*b*). Any model proposed to explain the preservation of extremely labile tissues by clay minerals must also account for the mode of preservation of more recalcitrant organic molecules such as chitin (eurypterid and naraoiid exoskeleton), pseudochitin (chitinozoan vesicles) and scleratin (conodont eye capsules). All of these organics have been partly or wholly replaced, or surface coated, by clay minerals. Only the inert organic compound sporopollenin, which makes up the walls of acritarch and spore palynomorphs seems unaffected by the mineralization event(s) that affected most other biomolecules. It is possible that bacterial mediation is a requirement, and some bacterial decay is necessary before mineralization of organic substrates can occur (Wilby 1993*a*, 1993*b*). In addition, replication of biomolecules by any mineral may require some prior decay of the substrate so that charged broken bonds become available as potential nucleation sites. The fidelity of replication of scleratin, pseudochitin and chitin is not as high as in the labile muscle tissue. Indeed, only the gross morphology of structures composed of scleratin and pseudochitin is preserved. Thus, the variation in biomolecule preservation (presence or absence as altered coalified organics, mineralized films or mineralized replacements) is probably most strongly influenced by their relative resistance to decay and thermal degradation. In addition, the fluctuation of ambient bottom and pore water conditions would have affected the mode of preservation. For example, the variation in the preservation of chitinozoan vesicles demonstrates that the conditions necessary for the mineral replacement and/or overgrowth were not always prevalent during early diagenesis. The mode of preservation of phosphatic fossils with an integral organic component, such as the conodont elements and lingulate brachiopods, must also be considered.

The evidence strongly suggests that the soft tissues of organisms in the Soom Shale were replaced directly by clay minerals. The sub-cellular fidelity of replication is difficult to reconcile with more than one stage of mineralization. In addition, the geochemical environment at the time of deposition would have aided clay mineral/organic interactions whilst militating against phosphate, pyrite or carbonate interactions with the organic material. However, the involvement of a phosphate precursor phase has been demonstrated in a number of cases (e.g. Allison 1988*b*; Martill 1988; Wilby 1993*b*) and should not be dismissed without further consideration here.

Two stage replacement model

The possibility of a carbonate or pyrite precursor to the replacive clay minerals is not considered tenable, given the acidic nature of the bottom waters and the demonstrated paucity of reactive iron oxide minerals. Authigenic mineralization of soft tissues by calcium phosphate has, however, been shown to occur commonly and extremely rapidly (Martill and Harper 1990; Briggs and Kear 1993*b*, 1994). Chitin is known to be phosphatized in arthropods from the Orsten and the Alum Shale (Upper Cambrian, Sweden), where preservation of soft integument and cuticular structures may have occurred as either a coating or complete replacement (Müller 1985). However, there are no examples yet known of phosphatized chitinozoans, and tissues originally composed of scleratin have not been reported as phosphatized replacements.

One example of soft tissues having been phosphatized and subsequently replaced by other minerals comes from the marine Jurassic biota of La Voulte (Wilby *et al.* 1996). Here, three-dimensional soft-bodied animals and their internal organs are preserved in an unusual suite of minerals with a consistent diagenetic sequence (apatite → calcite ± gypsum → pyrite ± chalcopyrite → galena) (Wilby *et al.* 1996). This is believed to show the importance of apatite as a 'template' for calcification and pyritization in soft tissue preservation (Wilby *et al.* 1996). With each mineral transformation, a loss in the fidelity of soft tissue replication occurred, so that the apatite shows details of muscle fibres, whereas replacement calcite preserves gross morphology only. The calcite phase not only replaced apatite but also filled voids between and within soft tissues, while the pyrite coated previously phosphatized, thick (white) muscle fibres of crustaceans and replaced their calcified thin (red) muscle fibres (Wilby *et al.* 1996). Although the La Voulte deposit appears to be singular in its preserving mineral suite, it does demonstrate that replacement of phosphate by other minerals is possible.

However, a number of lines of evidence militates against precursive phosphatization of either labile or recalcitrant biomolecules in the Soom Shale: (1) the geochemical environment in the Soom Shale was not conducive to phosphate concentration and precipitation; (2) no traces of calcium or phosphorus have been detected in the conodont or eurypertid muscle tissue from EDX or electron microprobe analyses, signifying that clay minerals have entirely replaced phosphatized muscle tissue and have not simply coated an earlier phosphate phase; (3) no clay minerals have been found replacing the crown tissue in conodont elements, so crystalline apatite was not replaced by clays; and (4) the clay minerals preserve sub-cellular details indicating that they were not a later void fill.

The myomeres of the conodont animal are extensively mineralized but there is no evidence to suggest that conodonts contained large quantities of phosphate. Hence, concentration of phosphate within the sediment, either on to mineral surfaces or into bacteria, would have been a prerequisite for such extensive phosphatization. However, the anoxic condition of the sediment, even on the sea floor, would have prohibited any concentration of phosphorus by adsorbtion on to ferric oxides/hydroxides and clay minerals (see Ingall *et al.* 1993). In addition, the storage and release of phosphorus by bacteria is redox-dependent, and uptake and storage of phosphorus is favoured under aerobic conditions where excess phosphorus is available (Gächter and Meyer 1993). Therefore, it is unlikely that any phosphorus liberated from organic matter decomposition would have been extensively incorporated into bacteria in the anaerobic Soom Shale sediment. It seems arguable that the anoxic sediment and bottom waters could not have concentrated sufficient phosphorus to phosphatize soft tissues.

For replacement of an initial phosphate phase by clay minerals, geochemical conditions would have been required in which the pore waters entering the carcass were aggressive towards apatite and simultaneously precipitated clay minerals, or contained clays as a colloidal component capable of replacing the phosphate crystallite by crystallite. That dissolution of calcium phosphate has occurred in the Soom Shale is demonstrated by the mouldic preservation of lingulate brachiopods and conodont elements; this would have required the presence of large quantities of acidic waters. Kaolinite can precipitate authigenically from acidic waters so acidic conditions suitable for the dissolution of calcium phosphate do not prohibit authigenesis of kaolinite nor, indeed, the presence

of colloidal clay minerals. Thus, during calcium phosphate dissolution, clay minerals may have been able to replace apatite almost instantaneously.

The relative timing of any clay mineral replacement of phosphate is hard to constrain. The dissolution of apatite from the conodont elements probably could not have occurred post-lithification as fluid would not have flowed easily through the rock. Dissolution by Recent weathering is also unlikely because it affects the conodont elements from both Keurbos and the less-weathered Sandfontein. A further test of the effects of weathering would be examination of phosphatic fossils from fresh core material to see if they are also mouldic. However, the presence of silica replacements of apatitic conodont material from Sandfontein provides strong evidence: it is difficult to envisage corrosive meteoric fluids capable of dissolving phosphate and of concomitant silica precipitation to be present during weathering. Furthermore, if apatite dissolution occurred during weathering it would be more likely for the replacement clays and silica to be void-filling rather than being high fidelity replacements of the apatite.

The muscle tissue in the conodont animal from the Soom Shale shows good sub-cellular detail (Gabbott *et al.* 1995). By comparison with the La Voulte fossils, this is difficult to reconcile with there having been two stages of replacement. However, colloidal clay minerals are extremely small (1 μm–1 nm in diameter) and it is possible that they could coat on to and replace an apatite precursor without as much information loss as in the calcite and pyrite in the La Voulte deposit. Unfortunately, the morphology of the clay minerals cannot be seen under the SEM because the crystallites are too small. As yet no TEM sections have been made of the conodont muscle tissue but this technique may enable the crystallites to be resolved.

If one mineral phase completely replaces another, it may be extremely difficult to determine whether the initial mineral was ever present unless its crystal habit is pseudomorphed. Lucas and Prévôt (1981, 1984) have reported the transformation of biomineralized carbonate materials into apatite where the original crystal form of the carbonate is conserved. If clay minerals have replaced an initial phosphate phase, then the habit of the apatite crystallites in microspherulitic and microgranular textures may be pseudomorphed. Ideally, microtomed sections of the Soom Shale soft tissues suitable for TEM studies should be made in order to check the crystal habit of the clay minerals for the presence of pseudomorphs. However, the presence of microspherulitic or microgranular textures would not indicate unequivocally the former presence of apatite as other minerals precipitate with this habit. For example, framboidal pyrite consists of discrete equi-granular pyrite microcrysts (usually 5 μm in diameter) which can be packed with varying degrees of ordering into nearly spherical aggregates (usually 500 μm) (Canfield and Raiswell 1991, p. 342). Although pyritic framboids are approximately five times the size of apatite microspheres, they demonstrate that microspherulitic aggregates are not exclusive to apatite crystallites.

There is, overall, little evidence to sustain a two-stage phosphate precursor–clay mineral replacement model. The sea floor conditions at the time of deposition of the Soom Shale seem to have been inimical for phosphate concentration, and the high fidelity of muscle replication militates against two phases of replacement.

Direct clay mineral replacement model

Illite and kaolinite may both have been involved in the original replication of soft tissues in the Soom Shale biota, and may also have precipitated on to templates provided by the more recalcitrant chitin, pseudochitin and scleratin. Subsequently, complete replacement of chitin and some pseudochitin occurred but most scleratin was just coated with a thin veneer of clay minerals. Clay minerals at the periphery of the chitinozoan vesicle walls have a mutually parallel orientation different from the random orientation of matrix clay minerals. This supports the hypothesis that the organic matrix acted as a template for the clays. It is possible that scleratin did not promote complete replacement by clays because it did not decay sufficiently for clays to penetrate and nucleate beyond the surface. Alternatively, the chitin and pseudochitin may also have been coated with the organics lost during later diagenesis. This is not supported by the existence of organic

chitinozoans in standard palynological preparations, attesting to the ability of pseudochitin to survive the burial temperatures reached in the Soom Shale (Cramer *et al.* 1974).

In the model developed here, kaolinite is considered as the principal clay mineral initially responsible for mineralizing the biomolecules. There is no evidence as yet to suggest that illite could not have formed in the same way, but more is known about the interactions of kaolinite with microorganisms and organic substrates (e.g. Skujins *et al.* 1974; Burns 1979; Theng 1979; Stotzky 1980; Avnimelech *et al.* 1982; Barker and Hurst 1985), and the acidic conditions in the sediment bottom/pore waters would have favoured kaolinite authigenesis.

Colloidal clay particles are well known for their affinity for organic substrates in the presence of cations (Avnimelech *et al.* 1982). A practical use of this has been the clarification of algal blooms in polluted lakes by kaolinite (Avnimelech *et al.* 1982; Ferris *et al.* 1987). This affinity coupled with the small particle size (1 nm–1 μm) of colloidal clays offers the potential for high fidelity soft tissue replication. A model to account for the preservation of soft tissues by clay minerals in the Soom Shale must explain (1) the speed of the reaction, (2) the exclusion of other mineral phases, and (3) why clay mineral preservation appears to be so rare elsewhere.

Kaolinite and/or illite may have been detrital components of the Soom Shale and some probably existed as colloids. Kaolinite could also have grown authigenically in the slightly acidic bottom waters of the basin. MacKenzie and Garrels (1966) proposed that authigenic clay minerals could form rapidly, on a time scale of hours to days, upon contact of detrital clay minerals with seawater. This has been corroborated by Mackin and Aller (1984) based upon dissolved Al distributions from nearshore, low pH sediments of the East China Sea. It has been suggested that Al-Si-H^+ relations are affected by pH, and most authigenesis of mineral phases involving these species occurs under low pH conditions (Mackin and Aller 1984). Moreover, in a low pH environment, a more H^+-rich or cation depleted phase may have been favoured, and would compose the majority of the authigenic material (Mackin and Aller 1984). In their study, Mackin and Aller (1984) showed that dioctahedral chlorites formed authigenically. It is tentatively suggested, therefore, that if clay authigenesis occurred in the Soom Shale under low pH conditions, it was kaolinite, which is extremely depleted in cations, that may have been formed.

The preservation of soft tissues by clay minerals would have been dependent on the properties of the muscle tissue and cuticular cells, especially the charge on the cell membranes. In the aqueous environment, the cell membrane, if similar to that of Recent cells, would have existed as a continuum of lipid and protein organized as a molecular double layer, with the hydrophobic portions of the lipid molecules being opposed and the hydrophilic groups projecting outwards into the aqueous phase (Fletcher *et al.* 1980). The charge of Recent organic cells is dependent upon ionic changes determined by the isoelectric point (pI) or dissociation constant (pK) of exposed functional groups and the pH of the environment (Burns 1979; Theng 1979); it is not known, however, what, if any, effect the death of the cell would have upon the charge. At physiological pH in aqueous environments, most organic substances will have a negative charge with compensatory DDL (diffuse double layer) (Theng 1979; Stotzky 1980); this is presumed to have been the case for the organic substrates of the preserved soft tissues from the Soom Shale.

Detrital kaolinite or illite, or authigenic, colloidal kaolinite and the organic substrate would probably have had net negative charges under the low pH conditions, i.e. a pH that was above the isoelectric point (pI) or the dissociation constant (pK) for both the participants. A prelude to any interaction between the kaolinite/illite and the organic substrate must have been a sufficient reduction in the electrokinetic potentials (EKP) of the participants so that they were able to get close enough to each other for attractive forces, either chemical or physical, to overcome electrostatic repulsion (Stotzky 1980, p. 231). Kaolinite/illite may have become sorbed on to organic surfaces in the presence of an electrolyte; in the marine Soom Shale basin, cations such as Na^+ and Ca^{2+} would have been in abundance. In addition, upon death, cell membranes would have become highly permeable to Ca^{2+} which would have been released and available as an electrolyte (Rob Hirst, pers. comm. 1996). Some investigators have suggested that polyvalent cations are necessary to reduce the electrostatic repulsion through forming complex bridges between the two negatively charged

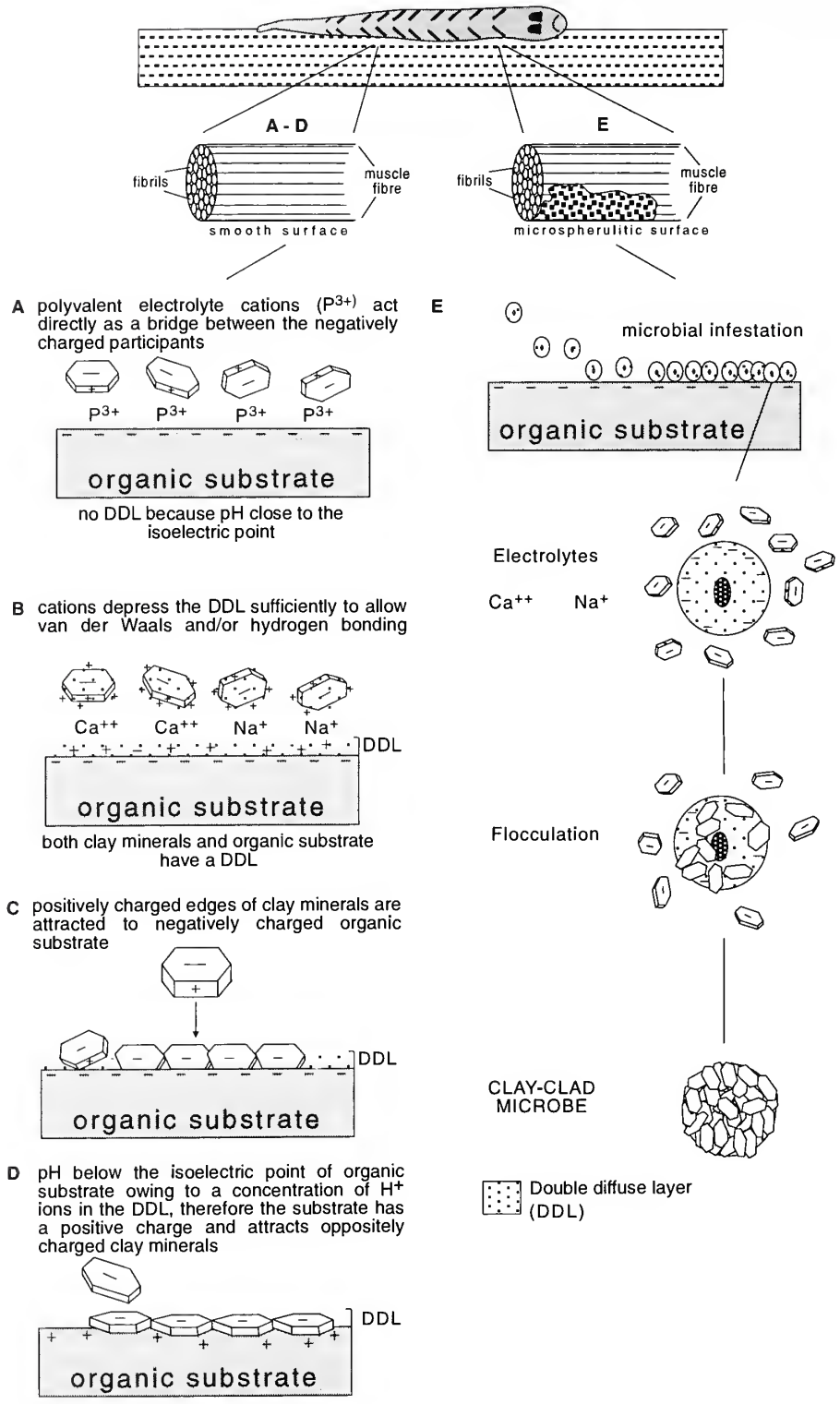

TEXT-FIG. 8. Idealized cartoons to show the possible interaction between clay minerals and organic substrates (A–D), and clay minerals, microbes and organic substrates (E) to replicate soft tissues directly by clay minerals. DDL = diffuse double layer.

participants (Santoro and Stotzky 1967) (Text-fig. 8A). Theng (1979) and Burns (1980) have shown that monovalent cations, by depression of the DDL, may have enabled clay minerals to approach the organic substrate closely enough to bond, by van der Waals and/or hydrogen bonding (Text-fig. 8B). Alternatively, the two participants may have been effectively oppositely charged. For example, the positively charged edges of the clay mineral may have been attracted to the negatively charged organic substrate (Text-fig. 8C). Another possibility is that a localized acidic environment may have been produced by the inclusion of H^+ ions (prevalent in the bottom/pore waters) into the DDL of one of the participants (McLaren and Skujins 1968; Stotzky 1980). As a result, the participants may not have been like-charged (i.e. the pH could have been below the isoelectric point of one of the participants thereby imparting a net positive charge) (Burns 1980). This is shown in Text-figure 8D where H^+ ions have become concentrated in the DDL of the organic substrate thus lowering the pH sufficiently to induce a net positive charge on the substrate because the pH is less than its isoelectric point. The net negatively charged clay minerals would have subsequently been attracted to and adsorbed on to the organic substrate. Thus, it is possible for colloidal clays to be attracted to and adsorbed on to organic substrates either through the presence of electrolytes neutralizing the electrostatic repulsion or by the participants having had opposite charges.

Recently, labile organic matter in marine sediments has been shown to be stabilized by sorption on to mineral surfaces (Mayer 1993; Keil *et al.* 1994); essentially the same process may have occurred in the Soom Shale, but in an opposite direction to that proposed by Mayer (1993) and Keil *et al.* (1994). There is no reason to believe that adsorption can operate only in one direction, i.e. that clays (or mineral surfaces) are always the adsorbates and organics the adsorbents (Stotzky 1980).

Colloidal clay minerals could have nucleated by flocculation and subsequent adsorption on to specific organic substrate templates so that the structural proteins of the conodont muscle tissue were replicated at sub-cellular levels. This specificity is presumed to be related to the abundance and nature of nucleating sites on the template molecule, and indeed, such template specificity has been noted for phosphatized soft tissues (Wilby 1993*b*); quite what control such molecules exert over clay mineral authigenesis is unclear.

Flocculation and adsorption of colloidal clay minerals would have continued until all available nucleating sites were occupied. However, kaolinite authigenesis may have continued, resulting in further mineralization of the soft tissue by accretion of additional crystallites on to the pre-mineralized substrate. Flocculation and adsorption of clay minerals may have terminated when all available organic matter had been bacterially reworked and/or when Eh-pH conditions exceeded those of the stability field for the minerals involved. The latter was possibly initiated by the breakdown of proteins to produce ammonia and consequently a local alkaline environment (Berner 1981). It is not yet understood how surface coating of organic tissues by clay minerals produced three-dimensionally preserved muscle tissues. This is, however, also a problem when phosphatizing soft tissues.

Direct and co-ordinated precipitation of colloidal clay mineral platelets on to organic substrates is consistent with the very smooth appearance of the mineralized muscle tissue in the conodont animal and the eurypterid cuticle. However, in some places on the conodont muscle tissue the surface is composed of small spheres of clay (90–150 nm in diameter) reminiscent of the microspherulitic and microgranular texture reported in phosphatized soft tissues (Wilby 1993*a*, 1993*b*). This does not necessarily mean that there was a precursive phosphate phase of replication; such microspheres may represent bacterial bodies/cells which were subsequently preserved in clay minerals. Prokaryotes actively involved in the breakdown of dead organisms can become autolithified as the tissues they are invading become authigenically mineralized (Wuttke 1983). Fossil bacteria in association with soft tissues have been reported as being preserved in a number of inorganic mineral phases including calcium phosphate (Martill 1988; Willems and Wuttke 1987), silica (Voigt 1988), siderite (Wuttke 1983) and clay minerals (Barker and Hurst 1985). In the Soom Shale, infesting microorganisms may have adsorbed colloidal clay minerals in the same way as organic substrates (see Text-fig. 8A–E). In addition, bacteria have been shown to have a greater flocculating tendency in declining growth or death phases (Harris and Mitchell 1973). In this way,

certain portions of the conodont muscle tissue would have become covered with microspheres (see Text-fig. 8E); it would not be expected that autolithified microorganisms could preserve the detail of the soft tissues with the degree of fidelity produced by direct nucleation of clay minerals on to the organic substrate. This, however, will remain untested until more conodont specimens with muscle tissue are recovered so that destructive analysis can be undertaken. No evidence for a microspherical texture has been seen in eurypterid cuticle.

Although the initial clay mineral responsible for preserving the soft tissues may have been kaolinite, the composition is now illitic. Therefore, at some time between early diagenesis and discovery, the kaolinite must have gained K^+ and converted to illite. The K^+ may have come from the breakdown of any K-feldspars in the sediment at elevated temperatures and/or pressures. Illitization of kaolinite may take place at temperatures as low as 50 °C (Bjørkum and Gjelsvik 1988), but more usually occurs at intermediate burial depths (3–4 km) or elevated temperatures (130–150 °C) (Bjorkum and Gjelsvik 1988), both of which occurred in the Soom Shale. The reaction can be represented as:

$$\underset{\text{illite}}{KAl_3Si_3O_{10}(OH)_2} + 2SiO_{2(aq)} + H_2O \rightarrow \underset{\text{K-feldspar}}{KAlSi_3O_8} + \underset{\text{kaolinite}}{Al_2Si_2O_5(OH)_4} \quad (4)$$

where the direction of the reaction at low temperatures is determined by the degree of supersaturation of silica in the formation water with respect to quartz (Bjørkum and Gjelsvik 1988). However, for 100 °C and 300 bars, K-feldspar and kaolinite would have become unstable independent of silica activity, and K-feldspar and kaolinite would have reacted to form illite (muscovite) and quartz (Bjorkum and Gjelsvik 1988).

Organophosphatic fossils

The variable style in preservation of phosphatic fossils is problematical and at present only broad constraints can be placed upon the possible diagenetic pathways responsible. Lingulate brachiopods and conodont elements would have originally been composed of biomineralized calcium phosphate and organic components. Clays replaced at least some of the brachiopod shell but only the basal body of the conodont elements. How, then, are the different modes of preservation of these fossils with originally phosphatic-organic compositions accounted for?

The over-riding controls on the style of preservation in these fossils were the nature and configuration of the apatite crystallites and the abundance and position of the organics. Two diagenetic zones within the sediment may have existed: Zone 1, where the acidity was sufficient to begin to dissolve apatite, where clays existed as colloids and conditions may have been favourable for clay authigenesis, and below this, Zone 2, where the sediment began to lithify, colloidal clays were not present but pore waters were still corrosive to apatite. Note that these zones were transitional and occurred below the zone of calcium carbonate dissolution. In addition, colloidal clays would probably have been present in low abundances in the bottom waters and would have increased in abundance in the sediment pore waters.

Brachiopods. The shells are preserved in three dimensions, so replacement could not have taken place after complete dissolution of the calcium phosphate. The brachiopod apatite may have been partially dissolved in zone 1, allowing colloidal clays to coat and subsequently replace the organic portion within the shell. Williams and Cusack (1996) have shown that the living organophosphatic shells of Carboniferous lingulid contained an acidic, hydrophilic gel, glycosaminoglycan (GAG) as one of their organic components. These GAGs mediated clay mineral (kaolinite) formation in the shell as they were degrading (Williams and Cusack 1996). It is very likely that Ordovician discinoids would have had a lot of GAGs in their shells (Alwyn Williams, pers. comm. 1997) and this may have encouraged not only clay mineral formation but also replacement of the organic material by clays. In addition, the periostracum may have acted as an organic substrate on which clays nucleated. The

clay replacements would have been unaffected by the more acidic conditions in the second zone, but any remaining apatite would have been dissolved, accounting for the mouldic clay mineral preservation seen in the majority of shells.

Conodont elements. The phosphate of the dentine in the basal body tissue was more susceptible to dissolution than the enamel, owing to its greater porosity, and so may have been largely dissolved early in zone 1. The organic portion of the dentine was then available to be replaced by clay minerals. However, the enamel only possesses a small proportion of organic material (1 wt %) and its crystalline nature protected this from colloidal clays. At greater burial depths (zone 2), the acidity increased to a level where the aprismatic enamel crown tissue could be dissolved to leave a mould. Finally, the prismatic enamel of the crown was replaced by silica; pseudomorphing of original prismatic crystallites (Text-fig. 3A, E) indicates that the silica is not a mould fill, but the result of a metasomatic replacement of apatite by quartz. The prismatic quartz crystallites do not show any signs of dissolution such as ragged or etched surfaces. This strongly suggests that the quartz did not originally replace the whole denticle, with subsequent dissolution leaving only the denticle base mineralized, but that quartz replaced the remaining apatite after and/or during its removal. The retention of void space in the elements indicates that the dissolution of apatite and replacement by quartz must have taken place not long before the sediment became lithified so that the void was not compacted. Alternatively, dissolution of apatite and replacement by quartz may have taken place relatively recently when the shale was exhumed. In any case, large scale dissolution of apatite from conodont elements has occurred. Very low pH conditions would have been necessary for this. A possible source of silica may come from the transformation of kaolinite to illite which yields silica into solution (Bjørkum and Gjelsvik 1988; see equation (4) above).

Alunite genesis

Alunite is one end member of this large group of isomorphous basic sulphates with the general formula $AB_3(SO_4)_2(OH)_6$ (Scott 1987). There is essentially complete solid solution between alunite ($KAl^{3+}{}_3$) and some other members of the group, the most common of which are jarosite (KFe^{3+}) and natroalunite ($NaAl^{3+}$). There is also a wide range of less common substitutions by other anions and cations in all available sites in the structure (Brophy *et al.* 1962; Dutrizac and Kaiman 1976; Scott 1987). End members are: alunite- $KAl_3(SO_4)_2(OH)_6$; jarosite- $KFe_3(SO_4)_2(OH)_6$; natroalunite- $NaAl_3(SO_4)_2(OH)_6$; natrojarosite- $NaFe_3(SO_4)_2(OH)_6$; gorceixite- $BaAl_3(PO_4)_2(OH)_5 . H_2O$; crandallite- $CaAl_3(PO_4)_2(OH)_5 . H_2O$; goyazite- $SrAl_3(PO_4)_2(OH)_5 . H_2O$; and florencite- $CeAl_3(PO_4)_2(OH)_6 . H_2O$.

Three hypotheses are available for the genesis of the alunite/crandallite associated with the fossils in the Soom Shale. It may have been derived from: (1) oxidation of pyrite during early diagenesis or weathering; (2) drying out of the regolith after intense weathering; or (3) intense weathering of apatite.

Although there is currently little evidence to determine the mechanisms for the genesis of the alunite/crandallite, the timing of the event may be constrained. If the alunite minerals were formed during a weathering process, they would be expected to be common throughout the sediment, but this is not the case. Four core samples and four fossil-bearing hand specimens from both Keurbos and Sandfontein were analysed using the electron microprobe and only three grains of alunite were found in a sample from Sandfontein. In addition, all core samples and hand specimens from both Keurbos and Sandfontein were analysed using XRD and only one sample showed alunite peaks (sample K1.2). Fossil material containing alunite comes from lingulate brachiopods, conodont elements, eurypterids and trilobites; compared with its occurrence in the sediment, it is relatively commonly associated with fossils. Indeed, the alunite in the sediment may also be associated with scattered fossil fragments. Evidence strongly suggests that the fossils have all been replaced by clay minerals at some time during early diagenesis. Therefore, if the fossil material and sediment were largely composed of clay minerals upon lithification, there would seem to be no reason for weathering to cause the alunite minerals to be preferentially associated with the fossils. It seems

more likely that alunite minerals grew prior to or concurrently with the clay replacement of the fossils when the fossil composition was distinct from that of the matrix. One tentative suggestion for the genesis of the alunite may be through the oxidation of pyrite associated with the fossils at times of bottom water oxygenation. The DOP values indicate that at some periods the bottom waters of the basin were oxygenated. Fossils decaying on the sea floor or when shallowly buried may have been in close proximity to active pyrite formation, or may have acted as loci for pyrite genesis by producing an anoxic decay halo. An oxygenation event would have resulted in pyrite oxidation, with the sulphate necessary for alunite genesis becoming available. There is no evidence for this scenario and it is only introduced as one of several possibilities.

It remains possible that the crandallite may have been formed by the intense weathering of apatite (Flicoteaux and Lucas 1984). However, in the Soom Shale only the lingulate brachiopods and conodont elements, both of which have crandallite associated with them, were originally composed of apatite. In addition, the arthropods may have had concentrations of phosphate in their cuticle. Briggs and Kear (1993*b*, 1994) demonstrated that sufficient phosphate was concentrated in the cuticle of decapod shrimps for soft tissue phosphatization to occur, when the source of phosphorus was entirely from the shrimp itself. Crandallite is present in the eurypterid and trilobite exoskeletons although it is unlikely that they contained enough phosphate in their cuticles to produce the amount of crandallite present upon weathering. Therefore, the near ubiquity of crandallite in fossil material suggests that weathering of apatite is not responsible for crandallite genesis. Alternatively, the crandallite may have formed by the alteration during weathering of previously formed alunite by substitution of potassium by calcium and sulphate by phosphate; anion substitution is in evidence in Text-figure 5A where SO_3 against P_2O_5 has a high negative correlation coefficient ($R = 0{\cdot}88$). However, the genesis of alunite and crandallite (and related minerals) allied to some of the fossils in the Soom Shale remains enigmatic.

Is preservation in clay minerals unique to the Soom Shale?

Flocculation of clay minerals on to bacteria occurs naturally in lakes (Avnimelech *et al.* 1982; Ferris *et al.* 1987), and clay mineral-microbial interactions are well recorded in soil horizons (e.g. Burns 1979; Stotzky 1980). Clay minerals are ubiquitous in marine black shale deposits. So why should the known preservation of soft tissues by clay minerals be restricted to the Soom Shale?

It may well be that comparable preservation does occur, but has not been recognized. One of the problems with clay minerals is that they form an almost ubiquitous component of sediments, so clay analyses obtained on fossil material may have been discarded as being due to sediment contamination. They should now be treated more seriously. One other case in which clay minerals have been implicated in soft tissue preservation is the Burgess Shale.

The Burgess Shale. The mode of preservation of the often shiny fossils from the Burgess Shale has a history of debate. Whittington (1971) presented evidence that the fossils were at least partly carbonaceous; however, preservation was thought to involve clay minerals by Conway Morris (1986). Butterfield (1990) employed acid maceration techniques and obtained organic fossil films which are coated by aluminosilicate films, principally potassium and chlorite micas (Conway Morris 1990*a*). The term Burgess-Shale-type preservation was introduced by Butterfield (1990, 1994) to describe the taphonomic pathway responsible for exceptional organic preservation of non-mineralizing organisms in fully marine siliciclastic sediments. The preservation of organics without mineralization requires some process to act to terminate decay, in particular the autolytic degradation by the organism's own enzymes (Butterfield 1990, 1995). There is good evidence that adsorption of degradative enzymes on to and within clay minerals achieves this (Butterfield 1990, 1995; Keil *et al.* 1994). Although the principal taphonomic mode of the Burgess Shale biota is organic, there is some degree of early diagenetic mineralization (e.g. Bruton and Whittington 1983; Butterfield 1990, 1995; Budd 1993). The role of clay minerals in the preservation of Burgess Shale biota is still being debated (Butterfield 1996; Towe 1996).

A result of the determination of organic preservation may be that the rôle of the aluminosilicate films covering the organics has not been adequately researched. Clay minerals probably became aligned on the surface of the tissue before it decayed completely and, in this way, the outlines of organisms are preserved (Briggs *et al.* 1994). Other minerals, such as barium sulphate and cerium phosphate, have been reported in association with the aluminosilicate films (Conway Morris 1990*b*); analyses of these minerals have not been published but it is possible that they are alunite group minerals (gorceixite and florencite). In addition, the remains of some hard parts are unusual, being composed of clay minerals; the exoskeleton of *Olenoides* is preserved in chlorite, illite and mica, and other shelly remains which were also originally calcareous appear to have a broadly similar composition (Conway Morris 1986). This alteration is currently presumed to have taken place relatively late in the diagenetic history because cracking and fracturing of the fossils has occurred, probably due to overburden pressure (Conway Morris 1986).

It is possible that a similar adsorption and coating of clay minerals on to organics occurred in the Burgess Shale as has been described in this study for the Soom Shale. However, in the Soom Shale, adsorption and coating have, in most instances, progressed further so that the organic tissues are completely replaced by clay minerals. An exception is the sclerotized material of the conodont eye capsules which remains as organic films coated by clay minerals. This may suggest that scleratin is one of the most recalcitrant structural biopolymers and/or that it was not sufficiently reactive to encourage complete replacement. It is possible that the structural biopolymers constituting some of the Burgess Shale fossils were relatively inert and inhibited complete replacement. Nearly all of the Burgess Shale fossils preserve the outlines of the organisms and not their more labile and reactive organic biomolecules, such as the muscle tissue. Alternatively, the sediment, pore water, bottom water and Eh/pH conditions may have been different in the Burgess Shale and affected the degree of clay mineralization. The role of clay mineral-organic interactions in the preservation of the Burgess Shale fossils requires more study. Clay minerals may have performed more than one rôle, that of inhibiting degradative enzymes (Butterfield 1990, 1995), but may also have been involved in mineralizing and perhaps stabilizing the organic components.

CONCLUSIONS

Upon death, carcasses from the Soom Shale biota would have sunk at varying rates to the sea floor unless they were buoyed up either by air already within them (e.g. in the chambers of orthoconic nautiloids) or by decay gases. There is no evidence to suggest that any significant lateral transport of carcasses took place before they reached the sea floor. Sedimentological evidence for this comes from the fine-grained, millimetric laminations consisting of extremely distal turbidites and hemipelagites. Palaeontological evidence indicating an autochthonous biota that underwent negligible lateral transport includes (1) fully articulated fossils especially conodont bedding plane assemblages, although disarticulation does not always result from transport if the organism is freshly dead (see Allison 1986); (2) randomly oriented *Siphonacis*, which would have become aligned even in weak currents; (3) attachment to orthoconic nautiloids of brachiopods which might have become detached in a turbidity current; and (4) the preservation of soft tissues in the orthoconic nautiloids, which would have decayed during prolonged floating.

The substrate may have been soupy but this is unlikely because no fossils lie at an angle to bedding as, for example, in the Posidonia Shales (Martill 1993). However, it is possible that fossils were rotated to become bedding parallel upon compaction of the shale. At times when the bottom waters were oxygenated, carcasses lying on the sea floor would have been susceptible to scavenging as well as decay. However, bottom waters in the basin were probably anoxic for most of the time, when carcasses on the sediment surface would not have been scavenged and would have undergone decomposition mainly via sulphate reducing bacteria. The carcasses would therefore have had a greater preservation potential during times of anoxia. It should also be pointed out that the bottom-waters in the Soom Shale basin may have been quite cool given the reasonably high latitude (60° S), and this would have retarded the decay rate. It has been shown that a twofold increase in decay rate

can be expected for a temperature rise of 10° C (Swift *et al.* 1979), and experiments (Briggs and Kear 1993*a*) have shown that decay decreases with lowered temperature.

Aragonite underwent very early dissolution, sometimes whilst still on the sea floor, and calcite probably dissolved at the same time or very soon after. Apatite dissolution occurred later, at approximately the same time as clay minerals were growing on to and replacing organic material. The labile soft tissues, such as muscle tissue, would have been mineralized rapidly post-mortem by clay minerals. More recalcitrant organics such as chitin, pseudochitin and scleratin were also mineralized to varying degrees; this possibly began at the same time as mineralization of muscle tissue or may have occurred later. The organic components of organophosphatic fossils such as conodont dentine and brachiopod shells, were replaced by clay minerals. After the process of clay mineral replacement had ceased, apatite dissolution continued and conodont crown tissue was removed. Finally, the most crystalline apatite with a low organic content from the denticle cores was replaced by silica, probably at the same time as illitization of kaolinite.

This unusual sequence of early diagenetic events was nearly entirely controlled by the composition of the organic and sediment matter supplied to the sea floor, which in turn controlled the Eh-pH conditions of the ambient waters. In addition, the basin did not have a strong circulation system, so mixing of the water was negligible. With a thickness of approximately 3500 m, 90 per cent. of the Table Mountain sediments are composed of supermature quartz (Visser 1974). The possible source-areas of the sands, deduced from compositional and textural analyses, is believed by Visser (1974) to have consisted largely (*c.* 60 per cent. of the area) of granite gneisses (Precambrian basement of the Namaqualand area), with subordinate input from sediments and lavas from the northern Cape Province. These gneisses and sediments would have undergone considerable mechanical and chemical erosion before deposition as the silts and muds of the Cedarberg Formation. The geochemistry of the sediment has been shown to have had an influence on the bottom and pore water Eh/pH conditions and hence on the mode of preservation of both hard and soft parts of the organisms. Perhaps one attribute, the very low pH, was of fundamental importance in producing the unusual taphonomy of much of the biota and, in particular, the preservation of soft tissues in clay minerals. A consequence of the source area consisting largely of granite gneisses, with subordinate sediment input, and in particular few carbonate rocks, may have been the low pH conditions attained in the Soom Shale sediment; there was insufficient carbonate to act as a pH buffer, and too few reactive iron oxides to fix the H_2S produced by the sulphate reduction of organic matter. The paucity of calcium carbonate may also reflect its increased solubility in colder waters. In addition, iron oxides may not have been extensively developed in the Ordovician due to the lack of terrestrial plants producing soil profiles. It is possible that other diagenetic minerals which may stabilize soft tissues, such as phosphate, pyrite and siderite, may have to be inhibited by low pH before clay minerals can mineralize the tissues. Whether the Soom Shale provided a unique environment in which fossilization occurred or represents an end member in a continuum of geochemical environments where soft tissues are preserved is still to be tested.

Acknowledgements. I am indebted to Prof. R. J. Aldridge and to Dr J. N. Theron for many helpful discussions, advice and reading manuscript proofs; RJA was particularly patient and helpful with the manuscript drafting. Professors J. D. Hudson and A. C. Dunham helped me enormously with the problems encountered with pyrite and clay minerals, respectively. Drs D. M. Martill, R. G. Clements, M. J. Norry, N. J. Butterfield and P. R. Wilby helped with reading sections of the manuscript and discussion of ideas. Professor D. E. G. Briggs is especially thanked for rigorously refereeing the manuscript and making it much more readable. R. Branson (SEM and photography), R. N. Wilson (electron microprobe), A. Smith (XRD), N. G. Marsh and R. Kelly (XRF) gave excellent technical support. Mr and Mrs J. N. Nieuwoudt, Keurbos Farm, and Mr and Mrs J. D. Kotze, Sandfontein, kindly allowed access to fossil localities. Financial support for this work was partly from NERC Research Grant GR9/957 to Professor Aldridge; SEG held a NERC research studentship (GT4/92/190/G), and is currently a PDRA on NERC Research grant GR3/10177 to Prof. Aldridge. I also acknowledge with thanks the facilities provided by the Geological Survey of South Africa, Cape Town.

REFERENCES

ALDRIDGE, R. J. and THERON, J. N. 1993. Conodonts with preserved soft tissue from a new Ordovician Konservat-Lagerstätte. *Journal of Micropalaeontology*, **12**, 113–117.

—— —— and GABBOTT, S. E. 1994. The Soom Shale: a unique Ordovician fossil horizon in South Africa. *Geology Today*, **10**, 218–221.

ALLISON, P. A. 1986. Soft-bodied animals in the fossil record; the role of decay in fragmentation during transport. *Geology*, **14**, 979–981.

—— 1988*a*. Konservat-Lagerstätten: cause and classification. *Paleobiology*, **14**, 331–344.

—— 1988*b*. Soft-bodied squids from the Jurassic Oxford Clay. *Lethaia*, **21**, 403–410.

—— 1988*c*. The role of anoxia in the decay and mineralization of proteinaceous macro-fossils. *Paleobiology*, **14**, 139–154.

AVNIMELECH, Y., TROEGER, B. W. and REED, L. W. 1982. Mutual flocculation of algae and clay. *Science*, **216**, 63–65.

BAAS, M., BRIGGS, D. E. G., VAN HEEMST, J. D. H., KEAR, A. J. and DE LEEUW, J. W. 1995. Selective preservation of chitin during the decay of shrimp. *Geochemica et Cosmochimica Acta*, **59**, 945–951.

BAILEY, S. W. 1988. Chlorites: structures and crystal chemistry. 347–404. *In* BAILEY, S. W. (ed.). *Reviews in mineralogy, hydrous phyllosilicates (exclusive of micas)*. Mineralogical Society of America, Washington, 725 pp.

BARKER, C. C and HURST, U. J. 1985. Authigenic kaolinite with fossil bacteria in Eocene kaolin. *Geological Society of America, Abstracts with Programme, Southeastern Section*, **17**, 79.

BAYLISS, P. 1975. Nomenclature of trioctahedral chlorites. *Canadian Mineralogist*, **13**, 178–180.

BERNER, R. A. 1970. Sedimentary pyrite formation. *American Journal of Science*, **268**, 19–42.

—— 1981. Authigenic mineral formation resulting from organic matter decomposition in modern sediments. *Fortschur Mineral*, **59**, 117–135.

—— 1984. Sedimentary pyrite formation: an update. *Geochimica et Cosmochimica Acta*, **48**, 605–615.

—— and RAISWELL, R. 1983. Burial of organic carbon and pyrite sulphur in sediments over Phanerozoic time: a new theory. *Geochemica et Cosmochimica Acta*, **47**, 855–862.

—— and RAO, J. L. 1994. Phosphorous in sediments of the Amazon River and estuary: implications for the global flux of phosphorous to the sea. *Geochemica et Cosmochimica Acta*, **58**, 2333–2339.

BJØRKUM, P. A. and GJELSVIK, N. 1988. An isochemical model for formation of authigenic kaolinite, k-feldspar and illite in sediments. *Journal of Sedimentary Petrology*, **58**, 506–511.

BRADDY, S. J., ALDRIDGE, R. J. and THERON, J. N. 1995. A new eurypterid from the late Ordovician Table Mountain Group, South Africa. *Palaeontology*, **38**, 563–581.

BRIGGS, D. E. G. and CLARKSON, E. N. K. 1989. Environmental controls on the taphonomy and distribution of Carboniferous malacostracan crustaceans. *Transactions of the Royal Society of Edinburgh: Earth Sciences*, **80**, 293–301.

—— and KEAR, A. J. 1993*a*. Decay and preservation of polychaetes: taphonomic thresholds in soft-bodied organisms. *Paleobiology*, **19**, 107–135.

—— —— 1993*b*. Fossilization of soft tissue in the laboratory. *Science*, **259**, 1439–1442.

—— —— 1994. Decay and mineralization of shrimps. *Palaios*, **9**, 431–456.

—— BOTTRELL, S. H. and RAISWELL, R. 1991*a*. Pyritization of soft-bodied fossils: Beecher's Trilobite Bed, Upper Ordovician, New York State. *Geology*, **19**, 1221–1224.

—— ERWIN, D. H. and COLLIER, F. J. 1994. *Fossils of the Burgess Shale*. Smithsonian Institution Press, Washington and London, 238 pp.

—— RAISWELL, R., BOTTRELL, S. H., HATFIELD, D. and BARTELS, C. 1996. Controls on the pyritization of exceptionally preserved fossils: an analysis of the Lower Devonian Hunsruck Slate of Germany. *American Journal of Science*, **296**, 633–663.

BROPHY, G. P., SCOTT, E. S. and SNELLGROVE, R. A. 1962. Sulphate studies 2: solid solution between alunite and jarosite. *American Mineralogist*, **47**, 112–136.

BRUMSACK, H. J. 1989. Geochemistry of recent TOC-rich sediments from the Gulf of California and the Black Sea. *Geologische Rundschau*, **78**, 851–882.

BRUTON, D. L. and WHITTINGTON, H. B. 1983. *Emeraldella* and *Leanchoilia*, two arthropods from the Burgess Shale, British Columbia. *Philosophical Transactions of the Royal Society of London, Series B*, **300**, 553–585.

BUDD, G. 1993. A Cambrian gilled lobopod from Greenland. *Nature*, **364**, 709–711.

BURMANN, G. 1969. Inkohlung und Mechanische Deformation. Abgehandelt am Erhaltungsz Organischer Mikrofossilien. *Zeitschrift fur Angewandte Geologie*, **15**, 355–364.

BURNS, R. G. 1979. Interactions of microorganisms, their substrates and their products with soil surfaces. 109–138. *In* ELLWOOD, D. C., MELLING, J. and RUTTER, P. (eds). *Adhesion of microorganisms to surfaces*. Academic Press, London, 216 pp.

BURNS, R. G. 1980. Microbial adhesion to soil surfaces: consequences for growth and enzyme activity. 249–262. *In* BERKELEY, R. C. W., LYNCH, J. M., MELLING, J., RUTTER, P. R. and VINCENT, B. (eds). *Microbial adhesion to surfaces*. Ellis Harwood Ltd, Chichester, 559 pp.

BUTTERFIELD, N. J. 1990. Organic preservation of non-mineralizing organisms and the taphonomy of the Burgess Shale. *Paleobiology*, **16**, 272–286.

—— 1994. Burgess Shale-type fossils from a Lower Cambrian shallow-shelf sequence in northwestern Canada. *Nature*, **369**, 477–479.

—— 1995. Secular distribution of Burgess-Shale-type preservation. *Lethaia*, **28**, 1–13.

—— 1996. Fossil preservation in the Burgess Shale – reply. *Lethaia*, **29**, 109–112.

CANFIELD, D. E. 1989. Reactive iron in marine sediments. *Geochemica et Cosmochimica Acta*, **53**, 619–632.

—— and RAISWELL, R. 1991. Pyrite formation and fossil preservation. 338–388. *In* ALLISON, P. A. and BRIGGS, D. E. G. (eds). *Topics in geobiology: taphonomy; releasing the data locked in the fossil record*. Plenum Press, New York and London, 560 pp.

—— RAISWELL, R., WESTRICH, J. T., REAVES, C. M. and BERNER, R. A. 1986. The use of chromium reduction in the analysis of reduced inorganic sulfur in sediments and shales. *Quarterly Journal of the Geological Society, London*, **124**, 149–155.

CARLSON, S. 1990. Vertebrate dental structures. 531–554. *In* CARTER, J. G. (ed.). *Skeletal biomineralization: patterns, processes and evolutionary trends*. Van Nostrand Reinhold, New York, 797 pp.

CHESSELET, P. 1992. Disarticulated remains of an Ordovician Metazoan from the Cedarberg Formation, South Africa: a re-interpretation of *Eohostimella parva* Kovács. *Palaeontology of South Africa*, **29**, 11–20.

CISNE, J. L. 1973. Anatomy of *Triarthrus* and the relationships of the Trilobita. *Fossils and Strata*, **4**, 45–64.

COCKS, L. R. M., BRUNTON, C. H. C., ROWELL, A. J. and RUST, I. C. 1970. The first Lower Palaeozoic fauna proved from South Africa. *Quarterly Journal of the Geological Society, London*, **125**, 583–603.

CONWAY-MORRIS, S. 1986. The community structure of the Middle Cambrian Phyllopod bed (Burgess Shale). *Palaeontology*, **29**, 423–467.

—— 1990*a*. Late Precambrian and Cambrian soft-bodied faunas. *Annual Review of Earth and Planetary Sciences*, **18**, 101–122.

—— 1990*b*. Burgess Shale. *In* BRIGGS, D. E. G. and CROWTHER, P. R. (eds). *Palaeobiology: a synthesis*. Blackwell Scientific Publications, Oxford, 583 pp.

CRAMER, F. H., RUST, I. C. and DIEZ DE CRAMER, M. D. C. R. 1974. Upper Ordovician chitinozoans from the Cedarberg Formation of South Africa. Preliminary note. *Geologische Rundschau*, **63**, 340–345.

DUTRIZAC, J. E. and KAIMAN, S. 1976. Synthesis and properties of jarosite-type compounds. *Canadian Mineralogist*, **14**, 151–158.

ELLIOT, T. 1991. Siliciclastic shorelines. 155–188. *In* READING, H. G. (ed.). *Sedimentary environments and facies*. Blackwell Scientific Publications, Oxford, 615 pp.

FERRIS, F. G., FYFE, W. S. and BEVERIDGE, T. J. 1987. Bacteria as nucleation sites for authigenic minerals in a metal-contaminated lake sediment. *Chemical Geology*, **63**, 225–232.

FISHER, I. S. J. and HUDSON, J. D. 1985. Pyrite geochemistry and fossil preservation in shales. *Philosophical Transactions of the Royal Society of London, Series B*, **311**, 167–169.

FLETCHER, M., LATHAM, M. J., LYNCH, J. M. and RUTTER, P. R. 1980. The characteristics of interfaces and their role in microbial attachment. 67–78. *In* BERKELEY, R. C. W., LYNCH, J. M., MELLING, J., RUTTER, P. R. and VINCENT, B. (eds). *Microbial adhesion to surfaces*. Ellis Harwood Ltd, Chichester, 559 pp.

FLICOTEAUX, R. and LUCAS, J. 1984. Weathering of phosphate minerals. 292–317. *In* NRIAGU, J. O. and MOORE, P. B. (eds). *Phosphate minerals*. Springer Verlag, Berlin, 442 pp.

FOLK, R. L. 1993. SEM imaging of bacteria and nannobacteria in carbonate sediments and rocks. *Journal of Sedimentary Petrology*, **63**, 990–999.

FORTEY, R. A. and THERON, J. N. 1995. A new Ordovician arthropod, *Soomaspis*, and the agnostid problem. *Palaeontology*, **37**, 841–861.

GABBOTT, S. E., ALDRIDGE, R. J. and THERON, J. N. 1995. A giant conodont with preserved muscle tissue from the Upper Ordovician of South Africa. *Nature*, **374**, 800–803.

GÄCHTER, R. and MEYER, J. S. 1993. The role of microorganisms in sediment phosphorous dynamics in relation to mobilization and fixation of phosphorus. *Hydrobiologia*, **53**, 112–131.

GRAY, J., THERON, J. N. and BOUCOT, A. J. 1986. Age of the Cedarberg Formation, South Africa and early plant evolution. *Geological Magazine*, **123**, 445–454.

HARRIS, R. H. and MITCHELL, R. 1973. The role of polymers in microbial aggregation. *Annual Review of Microbiology*, **27**, 27–50.

HELZ, G. R., MILLER, C. V., CHARNOCK, J. M., MOSSELMANS, J. F. W., PATTRICK, R. A. D., GARNER, C. D. and VAUGHAN, D. J. 1996. Mechanism of molybdenum removal from the sea and its concentration in black shales: EXAFS evidence. *Geochimica et Cosmochimica Acta*, **60**, 3631–3642.

HUNT, S. and NIXON, M. 1981. A comparative study of protein composition in the chitin-protein complexes of the beak, pen, sucker disc, radula and oesophageal cuticle of cephalopods. *Comparative Biochemistry and Physiology*, **68B**, 535–546.

INGALL, E. D., BUSTIN, R. M. and CAPPELLEN, P. V. 1993. Influence of water column anoxia on the burial and preservation of carbon and phosphorus in marine shales. *Geochimica et Comsochimica Acta*, **57**, 303–316.

JOPE, H. M. 1965. Composition of brachiopod shell. H156–H164. *In* MOORE, R. C. (ed.). *Treatise on invertebrate paleontology. Part H. Brachiopoda.* Geological Society of America and University of Kansas Press, Boulder, Colorado and Lawrence, Kansas, 521 pp.

KEIL, R. G., MONTLUCON, D. B., PRAHL, F. G. and HEDGES, J. I. 1994. Sorptive preservation of labile organic-matter in marine-sediments. *Nature*, **370**, 549–552.

KOVÁCS-ENDRÖDY, E. 1986. The earliest known vascular plant, or a possible ancestor of vascular plants in the flora of the Lower Silurian Cedarberg Formation, Table Mountain Group, South Africa. *Annals of the Geological Survey of South Africa*, **20**, 93–118.

KRAUSKOPF, K. B. 1982. *Introduction to geochemistry*. McGraw-Hill International Series in Earth and Planetary Sciences, Singapore, 617 pp.

LEVENTHAL, J. S. 1983. An interpretation of carbon and sulfur relationships in Black Sea sediments as indicators of environments of deposition. *Geochemica et Cosmochimica Acta*, **47**, 133–138.

LORD, C. J. 1982. A selective and precise method for pyrite determination in sedimentary materials. *Journal of Sedimentary Petrology*, **52**, 664–666.

LUCAS, J. and PRÉVÔT, L. 1981. Synthèse d'apatite á partir de matière organique phosphorée (ARN) et de calcite par voie bactérienne. *Compte Rendu Academie des Sciences de Paris, Série 2*, **292**, 1203–1208.

—— —— 1984. Apatite synthesis by bacterial activity from phosphatic organic matter and several calcium carbonates in natural freshwater and seawater. *Chemical Geology*, **42**, 101–118.

MACKENZIE, F. T. and GARRELS, R. M. 1966. Chemical mass balance between rivers and oceans. *American Journal of Science*, **264**, 507–525.

MACKIN, J. E. and ALLER, R. C. 1984. Dissolved aluminium in sediments and water of the East China Sea: implications for authigenic mineral formation. *Geochemica et Cosmochimica Acta*, **48**, 281–297.

MACQUAKER, J. H. S. 1994. A lithofacies study of the Peterborough Member, Oxford Clay Formation (Jurassic), UK: an example of sediment bypass in a mudstone succession. *Journal of the Geological Society, London*, **151**, 161–172.

MARTILL, D. M. 1988. Preservation of fish in the Cretaceous Santana Formation of Brazil. *Palaeontology*, **31**, 1–18.

—— 1990. Macromolecular resolution of fossilized muscle tissue from an elopomorph fish. *Nature*, **346**, 171–172.

—— 1993. Soupy substrates: a medium for the exceptional preservation of ichthyosaurs of the Posidonia Shale (Lower Jurassic) of Germany. *Kaupia: Darmstäder Beiträge zur Naturgeschichte*, **2**, 77–97.

—— and HARPER, L. 1990. An application of critical point drying to the comparison of modern and fossilized soft tissue of fishes. *Palaeontology*, **33**, 423–428.

MAYER, L. M. 1993. Surface-area control of organic-carbon accumulation in continental-shelf sediments. *Geochemica et Cosmochimica Acta*, **58**, 1271–1284.

MCLAREN, A. D. and SKUJINS, J. 1968. The physical environment of microorganisms in soil. 3–25. *In* GRAY, T. R. G. and PARKINSON, D. (eds). *The ecology of soil bacteria*. Liverpool University Press, Liverpool, 681 pp.

MOORE, A. E. and MARCHANT, J. W. 1981. A preliminary note on two trilobites from the Soom Member, Table Mountain Group. *Transactions of the Geological Society of South Africa*, **86**, 51–54.

MÜLLER, K. J. 1985. Exceptional preservation in calcareous nodules. *Philosophical Transactions of the Royal Society of London, Series B*, **311**, 67–73.

—— and WALOSSEK, D. 1985. A remarkable arthropod fauna from the Upper Cambrian 'Orsten' of Sweden. *Transactions of the Royal Society of Edinburgh: Earth Sciences*, **76**, 161–172.

NORRY, M. J., DUNHAM, A. C. and HUDSON, J. D. 1994. Mineralogy and element fractionation during mudrock sedimentation. *Journal of the Geological Society, London*, **151**, 195–207.

PICKERING, K. T., MARSH, N. G. and DICKIE, B. 1993. Data report: inorganic major, trace and rare earth element

analyses of the muds and mudstones from Site 808. 427–451. *In* HILL, I. *et al. Proceedings of the Ocean drilling Program, Scientific Results*, **131.**

PIETZNER, H., VAHL, J., WERNER, H. and ZIEGLER, W. 1968. Zur chemischen Zusammensetzung und Mikromorphologie der Conodonten. *Palãeontographica, Abteilung A*, **128**, 115–152.

RAISWELL, R. 1982. Pyrite texture, isotopic composition and the availability of iron. *American Journal of Science*, **282**, 1244–1263.

—— and BERNER, R. A. 1985. Pyrite formation in euxinic and semi-euxinic sediments. *American Journal of Science*, **285**, 710–724.

—— —— 1986. Pyrite and organic matter in Phanerozoic normal marine shales. *Geochemica et Cosmochimica Acta*, **50**, 1967–1976.

—— BUCKLEY, F., BERNER, R. A. and ANDERSON, T. F. 1987. Degree of pyritization of iron as a palaeoenvironmental indicator of bottom-water oxygenation. *Journal of Sedimentary Petrology*, **58**, 812–819.

—— CANFIELD, D. E. and BERNER, R. A. 1994. A comparison of iron extraction methods for the determination of degree of pyritization and the recognition of iron-limited pyrite formation. *Chemical Geology*, **111**, 101–110.

RUST, I. C. 1967. On the sedimentation of the Table Mountain Group in the Western Cape Province. Unpublished D.Sc. thesis, University of Stellenbosch.

—— 1981. Lower Palaeozoic rocks of southern Africa. 165–187. *In* HOLLAND, C. H. (ed.). *Lower Palaeozoic of the Middle East, eastern and southern Africa, and Antarctica*. John Wiley & Sons Ltd, Chichester, 331 pp.

SANTORO, T. and STOTZKY, G. 1967. Influence of cations on the flocculation of clay minerals as determined by the electrical sensitizing zone particle analyser. *Proceedings of the Soil Science Society of America*, **31**, 761–765.

SCOTT, J. H. and SYMONS, N. B. B. 1977. Dental mineralization mechanisms, enamel, dentine, cementum. *In Introduction to dental anatomy*. Churchill Livingstone, Edinburgh, 464 pp.

SCOTT, K. M. 1987. Solid solution in, and classification of, gossan derived members of the alunite-jarosite family, northwest Queensland, Australia. *American Mineralogist*, **72**, 178–187.

SKUJINS, J., PUKITE, A. and MCLAREN, A. D. 1974. Adsorption and activity of chitinase on kaolinite. *Soil Biology and Biochemistry*, **6**, 179–182.

STOTZKY, G. 1980. Surface interactions between clay minerals and microbes, viruses and soluble organics, and the probable importance of these interactions to the ecology of microbes in soil. 231–248. *In* BERKELEY, R. C. W., LYNCH, J. M., MELLING, J., RUTTER, P. R. and VINCENT, B. (eds). *Microbial adhesion to surfaces*. Ellis Horwood Ltd, Chichester, 559 pp.

STÜRMER, W. 1970. Soft parts of cephalopods and trilobites: some surprising results of X-ray examination of Devonian Slates. *Science*, **170**, 1300–1302.

SWIFT, M. J., HEAL, O. W. and ANDERSON, J. M. 1979. *Decomposition in terrestrial ecosystems*. Blackwell, Oxford, 372 pp.

TARNEY, J. T. and MARSH, N. G. 1991. Major and trace element geochemistry of holes CY-1 and CY-4: implications for petrogenetic models. *In* GIBSON, I. J., MALPAS, J., ROBINSON, P. T. and XENOPHONTOS, C. (eds). Cyprus crustal study project: initial Report, Holes CY-1 and 1a. *Paper of the Geological Survey of Canada*, **90–20**, 133–176.

TAYLOR, S. R. and MCLENNAN, S. M. 1985. *The continental crust: its composition and evolution. An examination of the geochemical record preserved in sedimentary rocks*. Geoscience texts. Blackwell Scientific Publications, Oxford, 312 pp.

TEIGLER, D. J. and TOWE, K. M. 1975. Microstructure and composition of the trilobite exoskeleton. *Fossils and Strata*, **4**, 137–149.

THENG, B. K. G. 1979. Developments in soil science. *Formation and properties of clay-polymer complexes*. Elsevier, Amsterdam and New York, 362 pp.

THERON, J. N., RICKARDS, R. B. and ALDRIDGE, R. J. 1990. Bedding plane assemblages of *Promissum pulchrum*, a new giant Ashgill conodont from the Table Mountain Group, South Africa. *Palaeontology*, **33**, 577–594.

—— and THAMM, A. G. 1990. *Stratigraphy and sedimentology of the Cape Supergroup in the Western Cape. Guidebook Geocongress 1990*. Geological Society of South Africa, 64 pp.

TOWE, K. M., 1996. Fossil preservation in the Burgess Shale. *Lethaia*, **29**, 107–108.

TRAVERSE, A. 1988. *Paleopalynology*. Unwin Hyman, Boston, 600 pp.

VELDE, B. and MEUNIER, A. 1987. Petrologic phase equilibria in natural clay systems. 423–458. *In* NEWMAN, A. C. D. (ed.). *Chemistry of clays and clay minerals*. Mineralogical Society Monograph, Longman Scientific and Technical and the Mineralogical Society, Harlow, 480 pp.

VISSER, J. N. J. 1974. The Table Mountain Group: a study in the deposition of quartz arenites on a stable shelf. *Transactions of the Geological Society of South Africa*, **77**, 229–237.

VOIGT, E. 1988. Preservation of soft tissues in the Eocene lignite of the Geiseltal near Halle/S. *Courier Forschungsinstitut Senckenberg*, **107**, 325–343.

WESTGATE, L. M. and ANDERSON, T. F. 1982. Extraction of various forms of sulphur from coal and shale for stable isotope analysis. *Analytical Chemistry*, **54**, 2136–2139.

WHITTINGTON, H. B. 1971. Redescription of *Marella splendens* (Trilobitoidea) from the Burgess Shale, Middle Cambrian, British Columbia. *Bulletin of the Geological Survey of Canada*, **231**, 1–21.

WILBY, P. R. 1993*a*. The mechanisms and timing of mineralization of fossil phosphatized soft tissues. Unpublished Ph.D. thesis, Open University.

—— 1993*b*. The role of organic matrices in post-mortem phosphatization of soft-tissue. *Kaupia: Darmstädter Beiträge zur Naturgeschichte*, **2**, 99–113.

—— BRIGGS, D. E. G. and RIOU, B. 1996. Mineralization of soft-bodied invertebrates in a Jurassic metalliferous deposit. *Geology*, **24**, 847–850.

WILLEMS, H. and WUTTKE, M. 1987. Lithogenese lakustriner Dolomite und mikrobiell induzierte Weichyeil-Erhartung bei Tetrapoden des Unter-Rotliegenden (Perm, Saar-Nahe-Becken, SW-Deutschlund). *Neues Jahrbuch für Geologie und Paläontologie, Abhandlungen*, **174**, 213–238.

WILLIAMS, A. and CUSACK, M. 1996. Lingulid shell mediation in clay formation. *Lethaia*, **29**, 349–360.

MACKAY, S. and CUSACK, M. 1992. Structure of the organo-phosphatic shell of the brachiopod *Discina*. *Philosophical Transactions of the Royal Society of London, Series B*, **337**, 83–104.

WUTTKE, M. 1983. Weichteil-Erhaltung durch lithifizierte Microorganismen bei mittelozänen Vertebraten aus den Ölschiefern der Grube Messel bei Darmstadt. *Senckenberg Lethaea*, **64**, 509–527.

SARAH E. GABBOTT
Department of Geology
University of Leicester
University Road
Leicester LE1 7RH, UK
e-mail SG21@le.ac.uk

Typescript received 4 February 1997
Revised typescript received 11 August 1997

PIPID FROGS FROM THE UPPER CRETACEOUS OF IN BECETEN, NIGER

by ANA MARÍA BÁEZ *and* JEAN-CLAUDE RAGE

ABSTRACT. A vertebrate assemblage from the Coniacian–Santonian Ibeceten Formation of southern Niger includes pipid frogs, which are described herein. The fossils occur within fluviatile-lacustrine strata and consist of disarticulated elements. Two pipid taxa are present: the hyperossified *Pachybatrachus taqueti* gen. et sp. nov., and another unidentified taxon. The phylogenetic relationships of both are discussed in the context of recent hypotheses of pipid evolution. *Pachybatrachus* exhibits some derived features unknown in other pipids. These include supplementary accretion of bone on the atlantal centrum, which is involved in an additional articulation with the skull, as well as on the ventral surface of other vertebral centra. Following cladistic analysis, it is proposed that *Pachybatrachus* is a pipine closely related to the living African forms *Hymenochirus* and *Pseudhymenochirus*. The presence of the primitive state for some hymenochirine synapomorphies suggests that *Pachybatrachus* is their sister taxon. The relationships of the unidentified taxon remain equivocal owing to the fragmentary condition of available remains.

THE aquatic freshwater pipids have one of the most extensive fossil record of all frogs, with the oldest remains attributed to this group being early Cretaceous (Nevo 1968; Estes *et al.* 1978). Apart from their putative occurrence in the Lower Cretaceous of Israel, all known fossil pipids are from Africa and South America (Báez 1996). To date, the earliest known pipids from South America are from the middle Cretaceous of Patagonia (Báez and Calvo 1990), whereas recent finds in Africa extend their record back to the Albian–Cenomanian in this continent (Evans *et al.* 1996). Living representatives of this family are restricted to the latter two continents: they inhabit sub-Saharan Africa and tropical South America east of the Andes, extending as far north as Panama. However, the fossil record shows that pipids had a wider geographical range on those continents in the past, reaching further north and south than they do today (Báez 1981, 1996, and references cited therein). It should be noted here that the name Pipidae is used in the traditional broad sense, i.e. applied to those pipoid taxa that are closer to the living *Xenopus*, *Silurana*, *Pipa*, *Hymenochirus* and *Pseudhymenochirus* than to Rhinophrynidae and the extinct Palaeobatrachidae. Pipidae was defined by Ford and Cannatella (1993) as the node-based name for the most recent common ancestor of living pipids and all of its descendants. However, the uncertain position of several fossil taxa still needs to be clarified; hence we use Pipidae in the traditional sense.

The material described here is from the Upper Cretaceous (Coniacian–Santonian) of In Beceten, Niger. This site (about 15° 3′ N, 6° 2′ E) is located in the Iullemmeden Basin (or Iullmeden Basin; Hartley and Allen 1994), a vast interior tectonic depression that extends south-west of the Air Massif (Text-fig. 1). The fossils occur in the Ibeceten Formation, a sequence of shales and sandstones deposited in a fluvial-lacustrine environment (Moody and Sutcliffe 1991). This formation overlies marine limestones, containing ammonites, including vascoceratids of the genus *Nigericeras* Schneegans and is thus early Turonian. A succession of siltstones and shales overlies the sequence that includes the In Beceten frog-bearing beds. These overlying strata have been dated as Campanian–Maastrichtian on the basis of the presence of the ammonite genus *Lybicoceras* and by correlation with the *Mosasaurus* shales of Nigeria. All these data suggest an early 'Senonian' (Broin *et al.* 1974; Taquet 1976), or, more precisely, a late Coniacian–Santonian (Mateer *et al.* 1992), age for the frog-bearing beds.

The fossil material was collected during several field trips led by Drs D. E. Russell and P. Taquet.

[Palaeontology, Vol. 41, Part 4, 1998, pp. 669–691, 1 pl.]

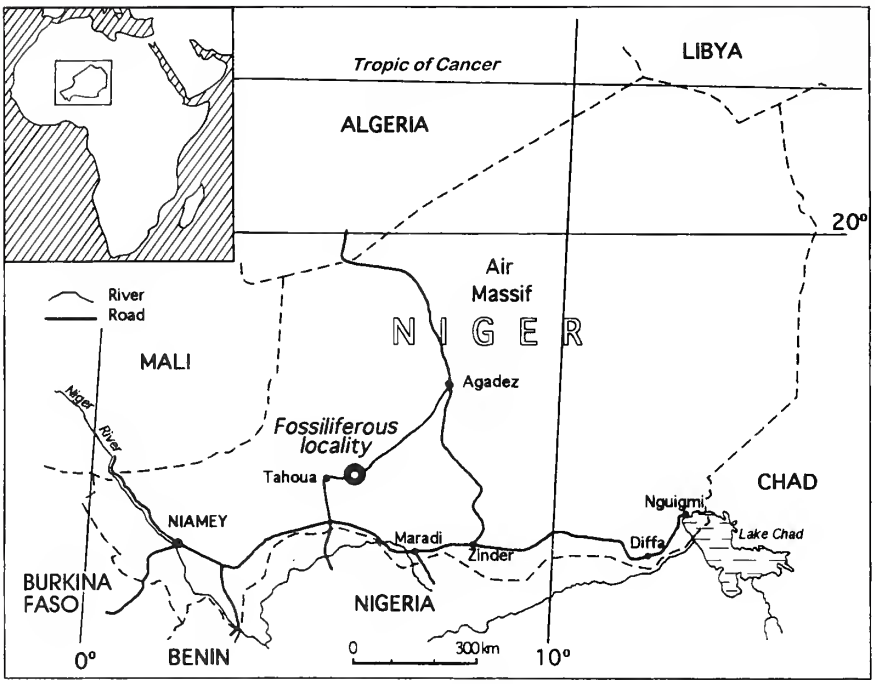

TEXT-FIG. 1. Map of Niger showing the location of the fossil site.

Most fossils lie exposed on the ground surface, the matrix having been removed during the rainy seasons. This may explain traces of erosion visible on several bones, although post-mortem transportation might also have caused some of this erosion. A large number of the specimens collected came from screen-washing operations.

The In Beceten fauna includes dipnoan and actinopterygian fishes, anuran and caudate amphibians, lizards, snakes, turtles, crocodilians, and sauropod and theropod dinosaurs (de Broin *et al.* 1974; Buffetaut 1976; Rage 1984; Rage *et al.* 1993). The material is housed in the Institut de Paléontologie, Muséum National d'Histoire Naturelle, Paris (MNHN), France.

In an earlier and preliminary paper on the In Beceten fauna (Broin *et al.* 1974), Vergnaud-Grazzini mentioned the presence of pipid and ranid frogs. Subsequently, assignment of some of the remains to Ranidae was questioned by Rage (1984). In this contribution we present the results of the study of the material representing a species 'très proche des *Xenopus*', and a new form, of which some skeletal elements 'évoqueraient *Hymenochirus* ou *Pipa*', according to Vergnaud-Grazzini (Broin *et al.* 1974, p. 470). The non-pipid remains are not discussed herein.

Recently, Cannatella and Trueb (1988*a*, 1988*b*) presented a hypothesis of relationships based on shared derived character states for extant pipid genera including *Xenopus*, *Silurana*, *Hymenochirus* and *Pseudhymenochirus* from Africa, and *Pipa* from South America. These authors proposed *Xenopus* as the sister taxon to all other extant pipids, and *Silurana* (a generic name resurrected for *X. tropicalis* and *X. epitropicalis* by Cannatella and Trueb 1988*a*) as the sister taxon of the pipines, that is [*Pipa*+[*Hymenochirus*+*Pseudhymenochirus*]]. This placement of *Silurana*, however, was discussed in a subsequent paper by Cannatella and de Sá (1993). Data from DNA sequences and reappraisal of morphology suggest, instead, that *Silurana* and *Xenopus* are sister groups (de Sá and Hillis 1990), which comprise the clade Xenopodinae (Cannatella and de Sá 1993). The evolutionary relationships of the taxa represented by the remains from In Beceten are discussed in the context

of such hypotheses, although the non-congruence of character states in several fossil taxa suggests that a reanalysis including extant and extinct pipids is necessary (see Báez 1996).

Institutional abbreviations. CPBA-V, Paleontología Vertebrados, Facultad de Ciencias Exactas, Universidad de Buenos Aires; DGM: Divisão de Geologia e Mineralogia, Departamento Nacional da Producão Mineral, Rio de Janeiro; KU, Natural History Museum, The University of Kansas; MCZ, Museum of Comparative Zoology, Harvard University; MNHN, Muséum National d'Histoire Naturelle, Paris; UMMZ, Museum of Zoology, University of Michigan.

SYSTEMATIC PALAEONTOLOGY

Class AMPHIBIA Linnaeus, 1758
Order ANURA Rafinesque, 1815
Family PIPIDAE Gray, 1825

Genus PACHYBATRACHUS gen. nov.

Derivation of name. From the Greek *pachus*, meaning thick, and *batrachos*, meaning frog.

Type and only known species. Pachybatrachus taqueti sp. nov.

Diagnosis. As for the only known species.

Pachybatrachus taqueti sp. nov.

Plate 1, figures 1–6; Text-figures 2A–K, 3A–G

Derivation of specific name. After Dr Philippe Taquet, palaeontologist of the Muséum National d'Histoire Naturelle, Paris, France, who conducted several expeditions to In Beceten.

Holotype. MNHN-IBC 1404 (braincase and otic capsules); Ibeceten Formation (Coniacian–Santonian) (Moody and Sutcliffe 1991); In Beceten (or Ibeceten), approximately 90 km east-north-east of Tahoua, Republic of Niger (Text-fig. 1).

Referred material. MNHN-IBC 1605 (braincase and otic capsules); 1606 (right otoccipital); 1607 (incomplete right otoccipital); 1608 (left otoccipital); 1609 (braincase and otic capsules); 1610 (anterior portion of braincase); 1611–1612 (atlantal complexes); 1613–1615 (presacral vertebrae, III); 1614 (presacral vertebra, V?); 1616–1618 (presacral vertebrae); 1619–1623 (sacrococcyx).

Diagnosis. Hyperossified pipine (*sensu* Cannatella and Trueb 1988*a*); frontoparietal heavily exostosed with vermicular ornamentation; deep and narrow Eustachian canals cross otic capsules obliquely; sphenethmoid fused to frontoparietal and parasphenoid; nerve foramina between fused vertebra I and II small, but not minute; bony accretion on atlantal centrum forming an odontoid process that articulates with an excavation on ventral surface of the braincase, articular surface of prezygapophyses of presacral vertebrae simple; articular surface of postzygapophyses curved ventromedially to form a groove; accretions of bone present on ventral surface of presacral vertebral centra and sacrococcyx.

Description. The skull as well as the postcranial skeletal elements are hyperossified. The dorsal surface of the cranium bears a peculiar, and presumably dermal, vermicular sculpturing that is coarse and compact. Maxillae, premaxillae, nasals, squamosals and mandibles are not preserved. Despite the absence of the anterior parts of

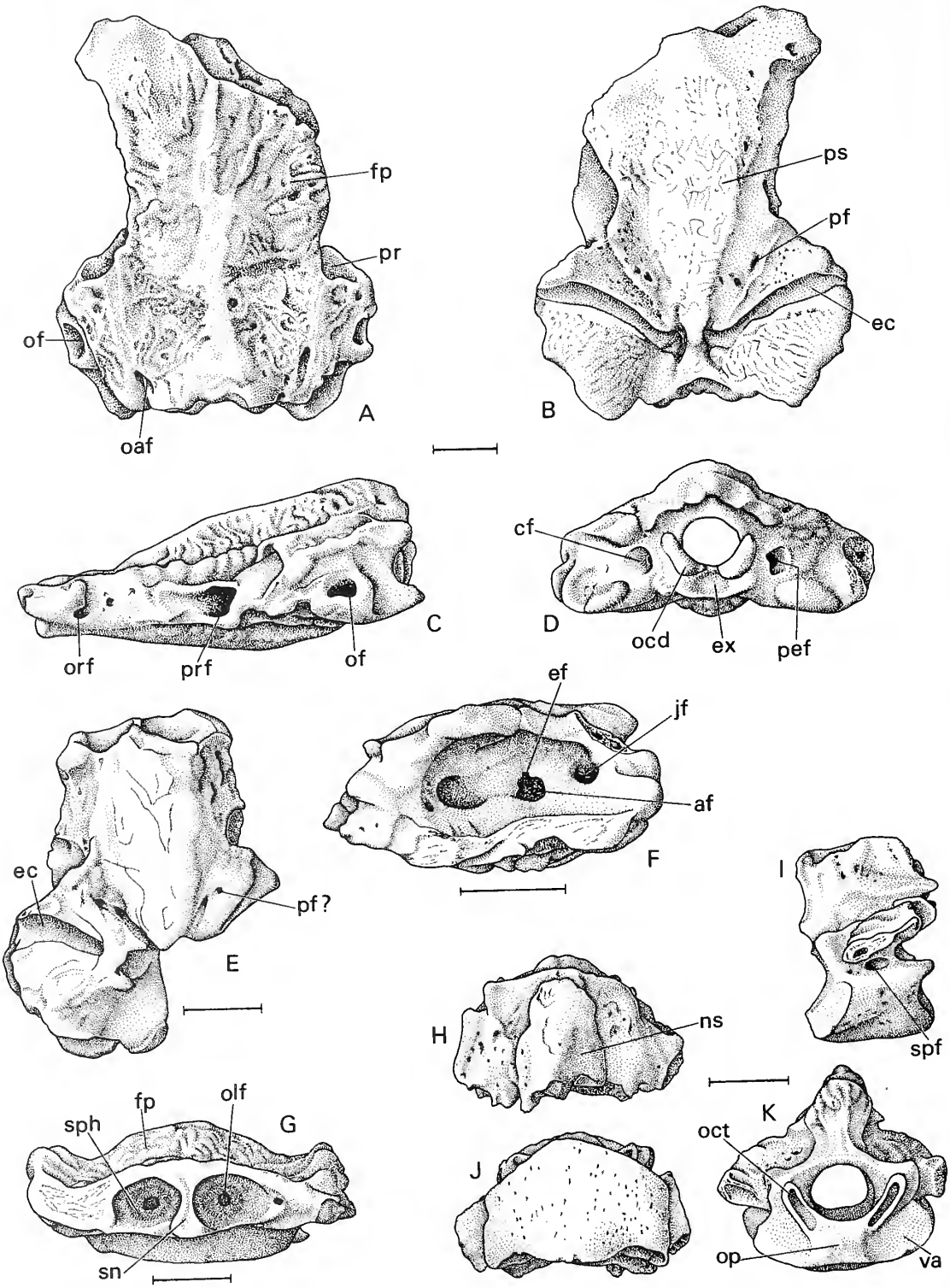

TEXT-FIG. 2. For caption see opposite.

the skull, it is evident from the parts that do exist that the cranium was distinctly wedge-shaped in lateral profile (Text-fig. 2C). The postcranial remains consist of presacral vertebrae, along with the sacrococcyx, all of which bear accretions of bone on their ventral surfaces.

Cranial skeleton. The frontoparietal is azygous, extraordinarily robust and heavily exostosed, and lacks any indication of a medial suture or parietal foramen (Text-fig. 2A). Anteriorly, this element is fused completely with the sphenethmoid. Owing to this fact and the breakage in most specimens, it is difficult to reconstruct precisely the shape of the anterior margin of the frontoparietal. However, in one specimen (MNHN-IBC 1610), the configuration of the anterior border seems to be biconcave, consisting of an anteromedial, rostral projection and, on each side, an anterolateral process associated with the well-ossified post-nasal wall (planum antorbitale *sensu* Paterson 1945). In the largest specimens (e.g. MNHN-IBC 1604), the dorsal surface of the frontoparietal is not flat: there is a dorsolaterally oriented supraorbital flange on each side and a medial frontoparietal dome that extends from the midorbital region to the posterior margin of the bone. In another much smaller, but nonetheless well-ossified specimen (MNHN-IBC 1609), the frontoparietal is flat. The ventral margin of the lamina perpendicularis cannot be discerned owing to fusion between the frontoparietal and the side wall of the neurocranium. Although the dermal ornamentation of the frontoparietal is united synostotically to that of the prootics and exoccipitals, it is possible to discern the rounded posterolateral and posterior margin of the frontoparietal by the orientation of the sculpturing.

The prootics and the exoccipital are indistinguishably fused to form a single bone – the otoccipital of some authors. Furthermore, the paired exoccipitals are fused dorsomedially and dorsoventrally; the nature of the medial association of the prootics is unknown. The roof of the otic capsule bears the same kind of vermicular sculpturing as the frontoparietal; presumably, this exostosis is dermal in origin despite the endochondral origin of the bone beneath. By contrast, the dorsal surface of the pars cranialis of the prootic is smooth. The posterolateral margin of the frontoparietal is united to the dermal sculpturing of the otic capsule, and forms the roof of a bony canal that probably housed the occipital artery. Anteriorly, this canal ends at the level of the anterior limit of the dermal sculpturing on the otic capsule. Near the anteromedial margin of the prootic, where it articulates with the frontoparietal, there is a foramen from which the ramus ophthalmicus superficialis of the facial nerve probably exited the cranium. The small prootic foramen lies between the side wall of the neurocranium, medially, and the anterior portion of the prootic, laterally. Owing to this position, the foramen is not visible in the lateral view of the skull (Text-fig. 2C). In MNHN-IBC 1605, there is a second foramen of uncertain identity lateral to the prootic foramen. On the lateral wall of the neurocranium, in all specimens examined, there is at least one foramen, possibly the optic foramen, immediately anterior to the prootic foramen. The ventral surface of the otic capsule bears a deep excavation for the Eustachian tube. The Eustachian canal is narrow, deep and almost straight, crossing the capsule in an anterolateral-posteromedial direction (Text-fig. 2B, D). By contrast to the irregular surface of most of the otic capsule, the walls of the Eustachian canal are smooth. A distinct mark, running along the posterolateral margin of the canal, probably corresponds to the posterior limit of the otic plate of the pterygoid. A shallow, curved channel that may have accommodated the carotid artery lies at the medial terminus of each Eustachian canal. Posterolateral to the Eustachian canal, the otic capsule is flat in the larger specimens, but inflated slightly in the smaller one (Text-fig. 2F). Ventrolateral to the condyloid fossa there is a distinct posterior projection of the otic capsule.

A large fenestra ovalis and an anterodorsal opening for the ramus hyomandibularis of cranial nerve VII are evident when the otic capsule is seen in lateral aspect. The ramus hyomandibularis passes from the prootic ganglion and exits the skull via a wide passage that represents the cranioquadrate passage (Paterson 1945). Because of breakage in NMHN-IBC 1606, it is possible to observe a large acoustic foramen and, above it, a small endolymphatic opening on the medial wall of the otic capsule (Text-fig. 2F). In one specimen (MNHN-IBC 1609), two acoustic foramina are present, separated from one another by a thin bridge of bone. The jugular foramen lies posterior to the acoustic foramen. Posterior to the former lie one or two perilymphatic foramina, but these do not open into the cranial cavity. It seems likely that two foramina were actually present, but in some specimens (e.g. MNHN-IBC 1605), the delicate bony partition separating the foramina has been destroyed.

TEXT-FIG. 2. *Pachybatrachus taqueti* gen. et sp. nov. A–D, MNHN-IBC 1604, holotype; braincase and otic capsules in A, dorsal; B, ventral; C, left lateral; and D, posterior views. E, MNHN-IBC 1609; braincase and otic capsules, ventral view. F, MNHN-IBC 1606; right otic capsule, medial view. G, MNHN-IBC 1610; braincase, anterior view. H–K, MNHN-IBC 1611; atlantal complex in H, dorsal; I, left lateral; J, ventral; and K, anterior views. Scale bars represent 2 mm.

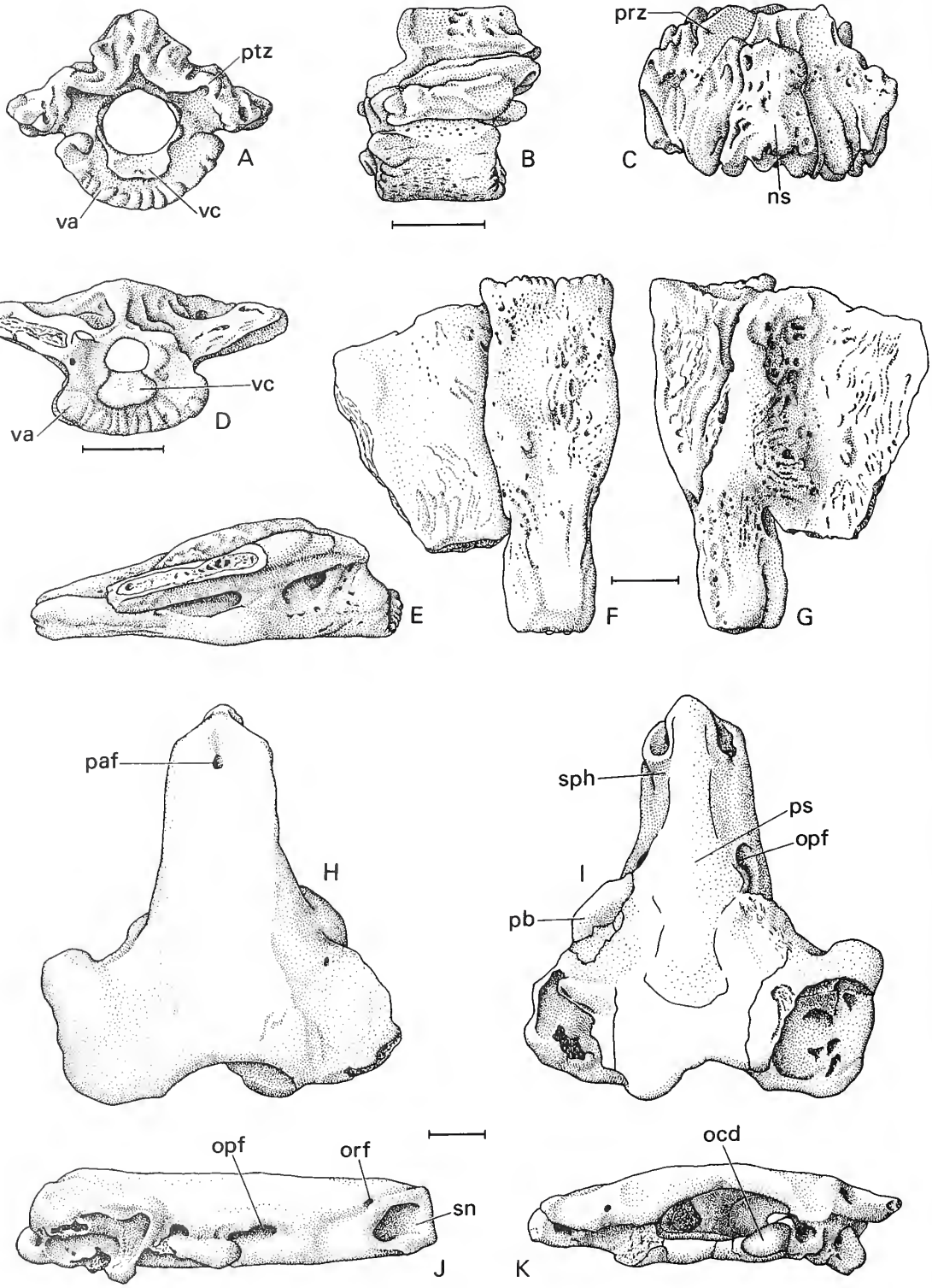

TEXT-FIG. 3. For caption see opposite.

The margin of the foramen magnum is completely ossified. Slightly anterior to the foramen magnum, the ventral surface of the fused prootics and exoccipitals is excavated to accommodate the hypertrophied 'odontoid' process of the atlas (Text-fig. 2D). The occipital condyles are reniform and posteromedially oriented; the articular facets are well separated. Large condyloid fossae housing the perilymphatic and jugular foramina flank the condyles, bounded medially and posteriorly by heavy deposits of bone adjacent to the condyles themselves. A sheet of bone bridging the medial end of the right Eustachian canal, which might correspond to a poorly preserved pterygoid, is evident in only one specimen (MNHN-IBC 1609). Examination of this specimen suggests that each pterygoid formed an extensive otic plate that invested the otic capsule ventrally. The exoccipitals lack ventral ridges associated with the posteromedial margins of the Eustachian canals; thus, it seems unlikely that the pterygoids were expanded medially to form a single, medial opening for the canals. Therefore, it is assumed that paired, bony openings were present. The boundaries of the pterygoid otic plates may be inferred from the relief on the ventral surface of the otic capsules. Thus, they could have extended from the posterolateral margin of the parasphenoid, anteriorly, to a point just to the rear of the Eustachian canal, posteriorly. No significant synostotic fusion of the pterygoid to the otic capsule is evident.

The sphenethmoid is united synostotically to adjacent elements. Thus, it is fused to the overlying frontoparietal and to the parasphenoid ventrally. Anterolaterally, the sphenethmoid is united synostotically to the planum antorbitale; thus, the orbitonasal foramen is enclosed in bone. Sphenethmoidal ossification also forms the boundaries of the large foramina for the olfactory nerves. Lateral to each olfactory foramen, there is a small foramen (MNHN-IBC 1609–1610) which may have housed the medial branch of the ramus ophthalmicus profundus of the trigeminal nerve. Although the most frontal portion of the sphenethmoid (i.e. the anterior part of the septum nasi) is not preserved, the anterior neurocranium can be observed. In transverse section, the latter is thick-walled and composed of two adjacent compartments probably corresponding to the paired olfactory canals. Each compartment extends posteriorly from the region of the anterior margin of the orbit to a point level with the anterior margin of the frontoparietal dome, which is located approximately in the midorbital region. The wide, bony medial septum that separates the compartments becomes narrower toward the anterior end and projects beyond the level of the planum antorbitale, but it is not possible to assess its total length owing to breakage. In a small specimen (MNHN-IBC 1609), the bony septum terminates posteriorly at the level of the orbitonasal foramina, and does not reach the orbital region. Two small foramina (probably for the optic and trochlear nerves), completely enclosed in bone, are located in the side walls of the braincase in the posterior region of the orbit.

The parasphenoid is wide and fused completely to the neurocranial bones; thus, its anterior and posterior ends are difficult to determine. However, it does not seem to extend much beyond the level of the planum antorbitale, nor does it extend in an anterolateral direction ventral to the planum antorbitale. The posterior terminus of the parasphenoid lies between the otic capsules and seemingly lacks a well-developed posteromedial process. The ventral surface of the parasphenoid is slightly convex. Two foramina are present on each side, near the union of the parasphenoid with the otic capsules. The anterior, and more lateral, opening may represent the palatine foramen, whereas the posterior one probably corresponds to a foramen for the carotid artery.

Postcranial skeleton. The postcranium is represented by several incomplete vertebrae and portions of the fused sacrum and coccyx. The vertebral centra are opisthocoelous. The atlas and the second vertebra are fused to form an atlantal complex (MNHN-IBC 1611–1612) and the bilateral spinal nerve foramina between these vertebrae although small, are not minute. In one specimen (MNHN-IBC 1612), traces of the fusion of the neural arches of the first two vertebrae are evident, whereas the fusion of the centra is complete. The anterior margin of the lamina of the atlas (*sensu* Cannatella and Trueb 1988*a*) is slightly convex (Text-fig. 2H); hence, the spinal cord was not exposed dorsally between this vertebra and the occiput. The atlantal complex (vertebrae I+II) bears a thick and rather high neural spine (Text-fig. 2I). On each side, slightly below the level of the postzygapophyses, a thick horizontal lamina runs from the posterior border of the second vertebral neural arch to an area located between the spinal nerve foramen and the corresponding articular cotyle. These laminae do not project strongly laterally, but, as they are partly broken off, their true lateral extension remains unknown. On the anterior face, the articular cotyles appear as narrow furrows on MNHN-IBC 1611, whereas they are slightly wider on 1612. The centrum of the atlantal complex is thickened by accretion of bone on the ventral

TEXT-FIG. 3. A–G, *Pachybatrachus taqueti* gen. et sp. nov. A–C, MNHN-IBC 1614; presacral vertebra (5° ?) in A, posterior; B, left lateral; and C, dorsal views. D, MNHN-IBC 1619; sacrococcyx, anterior view. E–G, MNHN-IBC 1620; sacrococcyx in E, right lateral; F, ventral; and G, dorsal views. H–K, pipid, unidentified genus and species, MNHN-IBC 1602; braincase and otic capsules in H, dorsal; I, ventral; J, right lateral; and K, posterior views. Scale bars represent 2 mm.

surface (see below). This accretion extends anteriorly where it forms a short sagittal projection that mimics an 'odontoid' process. On either side of this process, the bone growth forms a surface that resembles the articular cotyles of the atlas of most anurans. The latter surfaces could be considered as the articular cotyles; however, from their shape and orientation the rather narrow furrows cited above appear to be the true cotyles. The additional surfaces apparently articulated with the swellings that are located ventral to the occipital condyles of the skull.

The vertebrae are imbricate with thick neural arches, each of which bears a well-developed spinous process that terminates posteriorly in short parasagittal processes. Anterior to the neural spine, between the prezygapophyses, the neural arch is elevated and bears a delicate medial ridge that articulates with a groove located on the ventral surface of the spinous process of the neural arch of the preceding vertebra. There is some variation in the anterior–posterior length of the neural arches of the vertebrae, possibly reflecting regional variation in the vertebral lengths, with the more anterior vertebrae having relatively shorter neural arches. The articular surface of each prezygapophysis is simple, whereas the articular surface of each postzygapophysis is curved ventromedially to form a distinct tongue-and-groove articulation with the prezygapophysis of the preceding vertebra; this is especially evident in specimens MNHN-IBC 1614 and 1616 (Text-fig. 3A). Transverse processes are not preserved on any of the available vertebrae, but, as in the atlantal complex, a horizontal expansion of variable thickness runs along each side of the vertebrae. This expansion may be either a modified transverse process or the base of a broken transverse process.

All vertebrae referred to this species, including the atlantal complex, are characterized by a thick accretion of bone on the ventral surface of each centrum. The anterior and posterior margins of this bony accumulation bear several furrows and ridges that may have articulated with similar structures on adjacent vertebrae. The articular condyle, anteriorly, and the articular cotyle, posteriorly, occupy only a reduced part of the anterior and posterior faces of the centrum.

The sacrum is fused to the coccyx (Text-fig. 3E–G). Dorsally, the sacral portion of the bone bears a thick spinous process, only the anterior part of which is distinguishable; posteriorly, the process widens markedly then vanishes, merging with the dorsal surface of the sacral diapophyses. As in the presacral vertebrae, a thin medial ridge anterior to the neural spine is present on the neural arch of the sacrum, but in general it is more reduced than in the other vertebrae. The sacral diapophyses are broadly expanded. Two large spinal nerve foramina and, occasionally, a third small foramen, are present on each side of the sacrococcyx, indicating that more than one vertebra participates in the formation of the sacral portion of the sacrococcyx. There is a ventral accretion of bone on the sacrococcyx similar to that on the presacral vertebrae (Text-fig. 3D). Posterior to the level at which the posterior margin of the sacral diapophyses unites with the coccygeal part (= urostyle), the bony deposition decreases in width and is fused indistinguishably to the wide, well-ossified hypochord. Dorsally, the coccygeal part of the sacrococcyx lacks a distinct ridge.

Remarks. In this hyperossified species, the fused prootics and exoccipitals bear a groove to accommodate the Eustachian tube, the optic foramina are enclosed in bone, the sacrum is fused with the coccyx, the vertebral centra are opisthocoelous and dorsoventrally flattened, and thus presumably epichordal, and it seems likely that the otic plate, formed by the medial and posterior branches of the pterygoid, at least partially floored the Eustachian canal. These character states are some of the diagnostic characters of extant pipids (Cannatella and Trueb 1988*a*), although consideration of some fossil pipoid taxa, such as palaeobatrachids, indicates that some of these synapomorphies diagnose more inclusive groups of pipoids (Cannatella and de Sá 1993; Báez 1996).

The monophyly of Pipinae [*Pipa* + [*Hymenochirus* + *Pseudhymenochirus*]] was supported by 18 osteological derived character states in the analysis performed by Cannatella and Trueb (1988*a*), but only a few of those characters could be assessed in *Pachybatrachus* because of the lack of preservation of appropriate structures. *Pachybatrachus* shares with pipines the wedge-shape of the skull in lateral profile, a posteriorly acuminate parasphenoid, and presacral vertebrae bearing parasagittal spinous processes. 'Anterior margin of the atlas not indented and concealing the spinal cord' was listed as a synapomorphy of Pipinae by Cannatella and Trueb (1988*b*), but this condition occurs in some fossil pipid taxa lacking several derived character states shared by pipines and thus either diagnoses a more inclusive group or is homoplastic. The presence of a crest on the dorsal surface of the otic capsule for the insertion of the external portion of the depressor mandibulae muscle, another pipine synapomorphy (Cannatella and Trueb 1988*a*, 1988*b*), might not be evident

in *Pachybatrachus* owing to intense accumulation of dermal bone in this region. In *Pachybatrachus*, the dermal sculpturing extends anteriorly up to the level of the passage for the ramus hyomandibularis of the facial nerve, whereas the anterior portion of the prootic lacks this secondary deposition of bone, thus forming a 'ridge' that might have provided an attachment site for that muscle. There is some variation, however, in the development of that crest among pipines: for example, it is not well developed in *Pseudhymenochirus* (Cannatella and Trueb 1988*b*). As in pipines, the spinal nerve foramina between the atlas and the second vertebra are small in *Pachybatrachus*, but they are not minute; thus, in this feature, *Pachybatrachus* appears less derived than extant pipines. In addition, the frontoparietal bears supraorbital flanges and the neural arches are completely imbricated, as in pipines, but not as in *Xenopus* and *Silurana*.

A few, presumably derived, character states are shared by *Pachybatrachus*, pipines and *Silurana*. These characters are: the presence of anterolateral alae on the frontoparietal; fusion of the first and second vertebrae; and, apparently, absence of discrete vomers. However, the hypothesis that *Silurana* is the sister taxon of *Xenopus*, as discussed by Cannatalla and de Sá (1993), implies that these characters might be homoplastic in *Silurana* and the pipines.

The evidence discussed above indicates that *Pachybatrachus* is either a stem pipine (i.e. a sister group of the clade that includes the most recent common ancestor of *Pipa*, *Pseudhymenochirus* and *Hymenochirus* and all of its descendants), or should be placed within the node-based Pipinae (*sensu* Cannatella and de Sá 1993). In general, this is in agreement with the opinion of Vergnaud-Grazzini (*in* Broin *et al.* 1974), who cited the presence of a new species resembling *Hymenochirus* or *Pipa* in the Cretaceous of In Beceten.

Within Pipinae, the species of *Pipa* form a well-corroborated clade (Trueb and Cannatella 1986), whereas the Hymenochirini, including *Pseudhymenochirus* and *Hymenochirus*, constitute another monophyletic subgroup (Cannatella and Trueb 1988*b*; Cannatella and de Sá 1993). The remarkable degree of ossification and coalescence of dermal and endochondral elements in the species from Niger, as well as its incomplete preservation, limit comparison and assessment of the osteological synapomorphies diagnostic of these two groups in *Pachybatrachus*.

Cannatella and Trueb (1988*b*) listed several characters that are present in their derived state in Hymenochirini, but none of these characters can be examined in the available material, except for the fusion of the cultriform process of the parasphenoid to the sphenethmoid and prootics, and of the medial and lateral rami of the pterygoid to the otic capsules. The cultriform process of the parasphenoid is not evident owing to its fusion to the sphenethmoid and prootics, a derived condition, whereas in the probable absence of fusion of both rami of pterygoid to the otic capsules, *Pachybatrachus* exhibits the plesiomorphic conditions.

The nearly straight and narrow, but deep, Eustachian canals, which cross the ventral surface of the otic capsules obliquely, presumably represent a derived character state that supports closer relationships with the Hymenochirini, because canals with these characteristics occur in members of this group among the pipids examined. By contrast, in *Xenopus* and *Pipa* (except for the highly derived *P. pipa* and *P. snethlageae*), the Eustachian canal curves anteromedially, circumscribing the inner ear region. Although the quadrate complex of *Pachybatrachus* seems to occupy a more posterior position than in living hymenochirines, the morphology of this region resembles that found in this group. As in the Hymenochirini, however, the detailed configuration and relationships of the individual elements of this region are difficult to determine, owing to the extensive ossification. If the ridge posterior to the margin of the Eustachian canal marks the posterior terminus of the otic plate of the pterygoid, the broad and approximately triangular shape of this plate resembles the condition seen in *Hymenochirus* and *Pseudhymenochirus*.

Only one large acoustic foramen is present on the medial wall of the otic capsule in the larger specimens of *Pachybatrachus*. Possibly this is a consequence of post-mortem breakage, because in one of the specimens (MNHN-IBC 1605) it is evident that a delicate bony partition lying slightly lateral to the medial wall of the otic capsule was present. Anterior and posterior acoustic foramina occur in extant *Xenopus*, *Silurana* and *Hymenochirus*, as well as in many pipoids (Trueb and Cannatella 1982; Henrici 1991). Thus, the presence of a single wide acoustic foramen in *Pipa* (*P.*

carvalhoi, *P. pipa*, Paterson 1955, 1960; *P. snethlageae*, *P. parva*, pers. obs.) seems to be a derived character state.

Pachybatrachus has two perilymphatic foramina, as in *Hymenochirus* and *Pseudhymenochirus*, but unlike *Xenopus*, *Silurana* and *Pipa*, in which only one foramen is present. However, in *Xenopus* and *Silurana* this single opening occurs on the posterior wall of the otic capsule and corresponds to the inferior perilymphatic foramen, whereas in *Pipa* it is located on the medial wall of the otic capsule and corresponds to the superior perilymphatic foramen (Paterson 1960; AMB, pers. obs.). In *Hymenochirus*, the superior perilymphatic foramen opens into the cranial cavity, whereas a second foramen, the foramen accessorius, occurs near the jugular foramen (Paterson 1960). In *Pseudhymenochirus* (KU 206875) two perilymphatic foramina appear at the level of the jugular foramen, but their identity remains unknown. In *Pachybatrachus*, the two closely spaced foramina are located slightly posterior to the jugular foramen, and thus lead into an extracranial space. A similar superficial arrangement occurs in rhinophrynids, in which superior and inferior foramina are present; thus this might represent the plesiomorphic condition for pipoids.

Cannatella and Trueb (1988*a*) listed six uniquely derived osteological character states that support the clade *Pipa*, but only two of those synapomorphies could be assessed in *Pachybatrachus* owing to incomplete preservation or the high degree of ossification. *Pachybatrachus* is more plesiomorphic than *Pipa* in having, as in other pipids, occipital condyles with elongated articular facets, and condyles oriented posteromedially in ventral view. Cannatella and Trueb (1988*a*) interpreted the orbitonasal foramen enclosed in bone in *Pipa* as a reversal to the plesiomorphic state found in the outgroups, but this condition occurs in other fossil and living pipid taxa lacking other autopomorphies of *Pipa* or many pipine synapomorphies (e.g. *Silurana epitropicalis*, KU 195661; '*Xenopus*' *romeri* Estes, 1975*b*; see also below); thus the phylogenetic meaning of this trait is unclear. *Pachybatrachus* resembles the most derived of the living species of *Pipa*, *P. pipa*, in having an extremely flat neurocranium, a dorsal dome on the frontoparietal which is coupled with a midorbital transverse depression, and dorsally oriented supraorbital flanges. This last feature also occurs in *Hymenochirus*.

Several features of the vertebrae warrant comment. The marked anterior protrusion of the neural arches between the prezygapophyses occurs in Hymenochirini, as well as in the more derived species of *Pipa*, *P. pipa* and *P. snethlageae*. In all these taxa, this part of the neural arch has an elaborate surface that may provide additional areas of articulation between successive vertebrae, as it does in *Pachybatrachus*. However, in both *Pipa pipa* and *P. snethlageae*, the anterior part of the arch forms a structure separated from the prezygapophyses by a notch. Each side of this structure bears slanting articular surfaces, and resembles the zygosphene of many squamates. In these two species, as in other members of the genus *Pipa*, the articular surfaces of the pre- and postzygapophyses of the presacral vertebrae are relatively flat. By contrast, the Hymenochirini lack the zygosphene-like structure and the ventrally curved lateral part of the postzygapophyses wraps around the lateral margin of the prezygapophyses, as in *Pachybatrachus*. It is noteworthy that in extant *Xenopus* and *Silurana*, the zygapophyses develop a system of interlocking ridges and grooves (Vergnaud-Grazzini 1966), but this character state has not been reported in any Cretaceous–Miocene pipid taxon hitherto described. The presence of 'normal' zygapophyses lacking complex articular surfaces is clearly evident in disarticulated vertebrae referred to *Xenopus* (including *S. tropicalis*) from the Paleocene of Brazil (Estes 1975*a*, 1975*b*) and the Miocene of Morocco (Vergnaud-Grazzini 1966), and in the Eocene *Shelania* from Patagonia (AMB, pers. obs.). The vertebrae of *Pachybatrachus* resemble those of some species of *Hymenochirus* (e.g. *H. boettgeri*, *H. curtipes*) in having extremely thick neural spines.

The relationship of *Pachybatrachus* to the pipines was explored using PAUP 3.1 for Macintosh (Swofford 1993). Only the 13 characters that could be assessed in the fossil taxon were included in the analysis (Appendix 2). *Palaeobatrachus* and Rhynophrynidae were employed as outgroups, according to the hypothesis of pipoid relationships proposed by Cannatella and de Sá (1993). Data on *Palaeobatrachus* and Rhynophrynidae were obtained from the literature (Špinar 1978; Trueb and Cannatella 1982; Henrici 1991). Character states used in the analysis for *Silurana* were identical

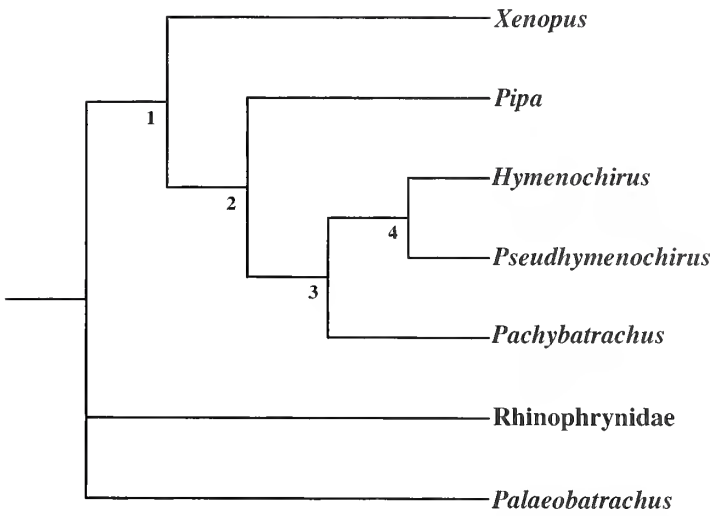

TEXT-FIG. 4. Cladogram depicting the hypothetized relationships of *Pachybatrachus* and selected pipids. Node 1. (Pipidae): sphenethmoid enclosing optic foramina; parasphenoid fused to the braincase; sacrum and coccyx fused. Node 2 (Pipinae): skull wedge-shaped in lateral profile; frontoparietal bearing supraorbital flanges; posterior terminus of parasphenoid acuminate; presacral vertebrae with parasagittal spinous processes. Node 3 (unnamed): Eustachian canals straight and cross the otic capsules diagonally; extensive contact between pterygoid and parasphenoid; articular surface of postzygapophyses of presacral vertebrae curved ventrally. Node 4 (Hymenochirini): medial and lateral rami of pterygoid synostotically fused to prootic.

to those for *Xenopus*; hence the former was not included as a separate taxon. All character transformations were unordered and the character-state optimization used the ACCTRAN setting. An exhaustive search yielded one minimal tree of 15 steps, and a CI, excluding uninformative characters, of 0·92 (Text-fig. 4). *Pachybatrachus* appears to be a pipine and is more closely related to the Hymenochirini than to *Pipa*. This is supported by a few, presumably derived, character states, including the straight Eustachian canal crossing the otic capsules diagonally, a (probable) broad contact between the parasphenoid and the otic plate formed by the pterygoid, and the elaborate articular surfaces of the postzygapophyses (node 3, Text-fig. 4). This relationship implies that the spinal foramen between vertebrae I and II may have been minute in the ancestor of pipines, but that reversal to an intermediate condition occurred in *Pachybatrachus*, or that reduction of the foramen occurred convergently in the two pipine lineages. The lack of fusion of the otic plate of the pterygoid to the otic capsules and of the squamosal to the prootic in adults are primitive traits of *Pachybatrachus*, unlike the derived condition of these characters in extant hymenochirines. No derived character states supporting a closer relationship to either *Hymenochirus* or *Pseuhymenochirus* was found. This suggests that *Pachybatrachus* might be the sister group of the Hymenochirini; however, it differs from them in having a broader braincase and a relatively more posterior position of the quadrate. Judging by the size of some of the bones referred to *Pachybatrachus*, we estimate that the largest individuals could have reached snout–vent lengths of up to 70 mm, thus falling outside the size range of living hymenochirine species (24–46 mm). In addition, this taxon possesses some uniquely derived character states, such as the coarse vermicular sculpturing of the skull, the additional accumulation of bone on the vertebral centra and sacrococcyx, and the supplementary areas of articulation between atlas and skull.

Whereas no autapomorphies of *Pipa* were found in *Pachybatrachus*, the plesiomorphic state of two unambiguous derived features of this extant genus are present. Thus, the overall resemblance of the skull of *Pachybatrachus* to that of *Pipa pipa* is parsimoniously interpreted as the result of convergent evolution. In this regard, it is interesting to note that a flattened snout and shovel-like

skull are some of the cranial modifications for burrowing among vertebrates (Wake 1993). However, comparison is difficult because little is known of the mode of life of this bizarre living pipid species.

Family PIPIDAE Gray, 1825

Unidentified genus and species

Plate 1, figures 7–11; Text-figure 3H–K

Referred material. MNHN-IBC 1602 (braincase and otic capsules).

Horizon and locality. Ibeceten Formation (Coniacian–Santonian) (Moody and Sutcliffe 1991); In Beceten (or Ibeceten), approximately 90 km east-north-east of Tahoua, Niger (Text-fig. 1).

Description. This species is represented by a well-ossified braincase (Text-figs. 3H–K; Pl. 1, figs 8–11). Nasals, pterygoids, squamosals, palatoquadrates, maxillary arches and mandibles are not preserved.

The frontoparietal is azygous, and fused anteriorly to the underlying sphenethmoid and posteriorly to the fused prootics and exoccipitals. The bone has a flat, relatively wide dorsal table bounded by weak parasagittal crests. A narrow depression located at about the level of the orbitonasal foramina possibly corresponds to the pineal opening. The frontoparietal lacks both anterolateral processes and a conspicuous rostral projection and the anterior margin of the bone is smoothly convex. Although the limits of the frontoparietal are not obvious, owing to its fusion with neighbouring elements, its posterior margin seems to lie near the dorsal margin of the foramen magnum.

The prootic and exoccipital are completely fused. Similarly, the exoccipitals are fused to one another dorsally and ventromedially. The nature of the medial association of the prootics is unknown. The dorsal surface of each prootic is smooth and lacks crests. Anteriorly, weak sutures mark the border of the overlying frontoparietal. A ventrally deflected flange lies along the posterior margin of the dorsal surface of the prootic. One unidentified foramen occurs on this margin, and pierces the prootic flange, dorsally and laterally to the foramen magnum (Text-fig. 3K). Anteroventrally, a prominent process abuts the neurocranium slightly posterior and ventral to the wide optic foramen; thus, the prootic foramen is not visible in the ventral view of the skull. Although most of the floor of each otic capsule is not preserved, the medial portion of the wide furrow that, in life, accommodated the Eustachian tube is visible on the right side of the skull, anterior to the inner ear region. The margins of the wide foramen magnum are completely ossified, and the occipital condyles are located on its ventral margin. A condyloid fossa is visible lateral to the right condyle (Text-fig. 3K), but as a result of breakage and poor preservation no foramen is evident.

The sphenethmoid is well ossified and extends from the nasal region, anteriorly, to the prootic foramen region, posteriorly. Its anterior portion forms the thick-walled housing for the posterior end of the nasal organs. A bony septum, presumably derived from the sphenethmoid cartilage and representing the septum nasi, separates the nasal capsules medially (Text-fig. 3J). The anterior terminus of the septum is broken whereas the posterior end lies at the level of the orbitonasal foramina; the latter are completely enclosed in bone. In the orbital region, the sphenethmoid continues the floor and sides of the braincase; ventrally, it is encrusted by the cultriform process of the parasphenoid (Text-fig. 3I). The sides of the sphenethmoid diverge dorsolaterally to meet the overlying frontoparietal. The dorsal extent of the sphenethmoid in the orbital region is difficult to assess owing to fusion of this bone with the frontoparietal. The large optic foramina are enclosed by the sphenethmoid (Text-fig. 3J). Posterior to these foramina, a wide, ventrally directed pillar of bone meets

---

EXPLANATION OF PLATE 1

Figs 1–6. *Pachybatrachus taqueti* gen. et sp. nov. 1–4, MNHN-IBC 1604, holotype; braincase and otic capsules in 1, dorsal; 2, ventral; 3, left lateral; and 4, posterior views; all × 4. 5, MNHN-IBC 1611; atlantal complex, dorsal view; × 6. 6, MNHN-IBC 1614; presacral vertebra, posterior view; × 5.

Figs 7–11, unidentified pipids. 7, MNHN-IBC 1650; posterior presacral vertebra, ventral view; × 5. 8–11, MNHN-IBC 1602; braincase and otic capsules in 8, dorsal; 9, ventral; 10, right lateral; and 11, posterior views; all × 4.

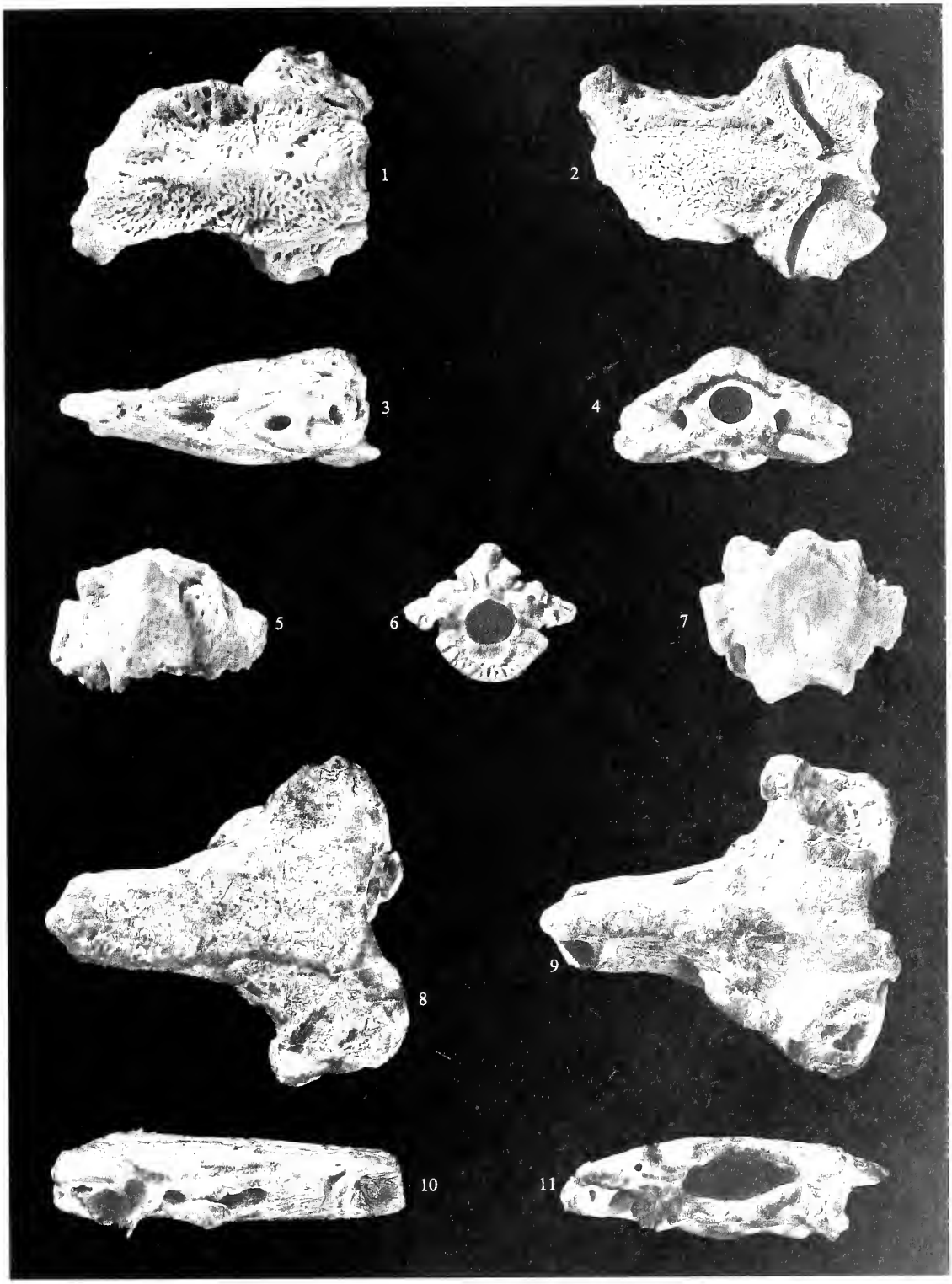

BÁEZ and RAGE, *Pachybatrachus*, unidentified pipids

the anteroventral portion of the otic capsule, separating two foramina. The anterior foramen lies between the side wall of the neurocranium, medially, and the prootic, laterally. The posterior foramen is relatively more lateral than the anterior foramen, and its posterior margin is formed by the prootic at the anteromedial corner of the otic capsule. One of these two openings corresponds to the prootic foramen.

The parasphenoid is partially fused to the sphenethmoid and only the margins of the posteromedial portion lying between the otic capsules are clearly visible (Text-fig. 31). The anteriormost end of the bone is not preserved. The cultriform process is relatively narrow anteriorly, but widens slightly at a point immediately anterior to the level of the orbitonasal foramina. There is no evidence that discrete vomers were attached to the ventral surface of the parasphenoid. The lateral margins of the parasphenoid are difficult to trace posterior to the level of the orbitonasal foramina owing to its fusion to the overlying sphenethmoid. Each side of the parasphenoid bears a laterally directed expansion at the level of the posterior margin of the optic foramen and adjacent to the union of the pseudobasal process and the sphenethmoid (Text-fig. 31). The posterior portion of the parasphenoid terminates between the otic capsules, reaching a point corresponding only to the midlength of the latter.

Remarks. The azygous frontoparietal and the lanceolate shape of the parasphenoid, which lacks alae and has a long cultriform process extending forwards beyond the level of the orbitonasal foramina, leave no doubts as to the pipoid affinities of this specimen. Moreover, the presence on the ventral surface of the otic capsules of excavations for the Eustachian tubes and the enclosure of the optic foramina in bone suggest that it represents a pipid taxon. The skull is not wedge-shaped in lateral aspect, and the dorsal surface of the otic capsules lacks crests, thus indicating that the depressor mandibulae muscle originated from connective tissue fascia overlying the crista parotica, as in *Xenopus* and *Silurana*, but unlike the derived condition in most pipines (Cannatella and Trueb 1988*a*, 1988*b*).

Overall, there is a superficial resemblance to *Xenopus*, but species of this taxon have departed little from the most recent common ancestor of the pipid lineages alive today. Only a few diagnostic synapomorphies have been recognized in the osteology of *Xenopus*: fused and shallow nasals, azygous vomers, and strongly posteriorly curved transverse processes of the fourth vertebra (Cannatella and Trueb 1988*a*). A single median vomer has been considered a synapomorphy of *Xenopus sensu stricto* (i.e. not including *X. tropicalis* and *X. epitropicalis*) by Cannatella and Trueb (1988*a*). This condition was also commented on by Paterson (1939), who mentioned that no indications of a paired origin of the vomer is found in *X. laevis*, even during metamorphosis. However, this evidence is contradicted by the recent work of Trueb and Hanken (1992) on this species. It is of interest to point out, therefore, that paired vomers occur in several postmetamorphic specimens of *Xenopus* including *X. fraseri* (MNHN 4402), *X. borealis* (UMMZ 152330) and *X. largeni* (KU 206863).

Nasals and the fourth presacral vertebra are not preserved in the fossil species from Niger; thus, it is not possible to assess the presence of the proposed diagnostic synapomorphies of *Xenopus* that involve these elements.

The two living species of *Silurana* are united by two unambiguous derived characters (Cannatella and Trueb 1988*a*), but neither of these can be assessed in the species from Niger because the appropriate soft structures are not preserved. Diagnostic derived character states of *Silurana* also include three osteological features (absence of discrete vomers, frontoparietals with anterolateral processes and fusion of the first and second vertebrae), which have been used to support the monophyly of a clade including *Silurana* + the pipines (Cannatella and Trueb 1988*a*). However, the morphological evidence for this hypothesis of relationships remains equivocal (Cannatella and de Sá 1993) and thus these characters may be homoplastic within Pipidae, as commented on above. In this regard, it is interesting to consider the evidence provided by fossil species. In the specimen from Niger there is no evidence that a discrete vomer (or vomers) was present: a slight expansion of the parasphenoid at the level of the orbitonasal foramina might be an indication that the vomers were fused to this bone, but no conclusive statement can be made based on the available evidence. The possible absence of discrete vomers is important because the absence of vomers characterizes *Silurana* and the pipines. In '*Xenopus*' *romeri* (cited as *Silurana romeri* by Rage, *in* Buffetaut and

Rage 1993, but still of uncertain phylogenetic position) from the middle Paleocene of Brazil (Estes 1975*a*, 1975*b*), a large azygous vomer is present and is attached or fused to the overlying bones in the anterior region of the braincase. In this taxon, this condition is associated with the presence of anterolateral processes on the frontoparietal and fusion of the atlas and second presacral vertebra.

The fossil species from Niger has a more heavily and extensively ossified braincase than in any living species of *Xenopus* and *Silurana* examined, especially in the ethmoidal region. The anterior end of the nasal capsules was probably roofed by the nasals, whereas the posterior part was completely surrounded by the ethmoidal ossifications. Moreover, ventrally, these ossifications support (or are continuous with) the septum nasi, at least throughout the preserved portion. No distinct anterolateral processes on the sphenethmoid are evident, unlike the condition in *Silurana* and the pipines. Enclosure of the orbitonasal foramen in bone is interpreted as a consequence of this intense ossification, a condition which occurs convergently in the genus *Pipa*.

The parasphenoid resembles that of *Xenopus* and *Silurana* in being of lanceolate shape, with a well-developed posteromedial process between the otic capsules which is lacking in the pipines. This shape is probably primitive for pipids, because it also occurs in other pipoids (e.g. palaeobatrachids; Špinar 1972). However, in the species from Niger, the posterior terminus of this bone lies far anterior to the ventral margin of the foramen magnum, unlike the condition in *Xenopus* and *Silurana*. Even in metamorphosing larvae of *Xenopus laevis*, the parasphenoid extends well posteriorly (Trueb and Hanken 1992), although data for other species of this genus are not available. Conversely, in the pipines it does not extend so far posteriorly, a condition that appears to occur not only in adults, but also in larvae and juveniles (e.g. in *Pipa carvalhoi*; Sokol 1977, pl. 7; and *Hymenochirus curtipes*, KU 204134, snout–vent length 16·5 mm, AMB pers. obs). In *Pipa*, remnants of cartilage, probably representing the solum synoticum, are visible between the otic capsules and posterior to this bone, but this does not occur in the species from Niger, this region being completely ossified and lacking any evidence of a suture.

The otic capsules extend far forward, which, despite the intense ossification of the skull, is a juvenile feature. Another potentially juvenile feature is the presence of a narrow pila metoptica separating the large optic foramen from the prootic foramen, on each side of the braincase. The absence of a dorsal table defined by well-developed parasagittal crests might also be the consequence of immaturity. This evidence suggests that the fossil specimen represents a young individual.

To summarize, this taxon exhibits the plesiomorphic condition for three pipine synapomorphies (skull wedge-shaped, parasphenoid posteriorly acuminate, otic capsule bearing hypertrophied crests): this suggests that it is not a member of that clade. In addition, it lacks one of the two apomorphic features of the cranium (presence of anterolateral alae on the frontoparietal) present in *Silurana* and Pipinae. If discrete vomers are truly absent, this is a resemblance to the condition in Pipinae and *Silurana*. However, we note that information on the osteogenesis of the skull is critical for evaluation of this character. These bones appear at a late stage in the development of *Xenopus laevis* (Trueb and Hanken 1992); thus, it is possible that loss of the centre of ossification may have occurred as a result of heterochronic changes. Discrete vomers are absent in developmental material of *Hymenochirus curtipes*, but data on other pipids are not available. Synostotic fusion of the vomers to overlying bones might also result in their apparent absence in adults, as occurs in '*Xenopus*' *romeri*.

The available material is fragmentary and non-diagnostic; until additional material is found we prefer not to establish a formal name on the basis of these remains. Some similarity between the Paleocene '*Xenopus*' *romeri* and the species from Niger was noted by Vergnaud-Grazzini (*in* Broin *et al.* 1974). These species resemble each other in the extent to which the skull bones are fused, the high degree of ossification in the ethmoidal region, and, consequently, the enclosure of orbitonasal foramina in bone, and the rather extensive bony septum nasi, which in '*X.*' *romeri* extends forward or almost the entire length of the nasals (AMB, pers. obs). It is noteworthy that this latter feature was considered a pipine synapomorphy by Cannatella and Trueb (1988*a*). The two fossil taxa differ significantly in the proportions of the braincase (broader in '*X.*' *romeri*), the shape of the

frontoparietal which bears anterolateral processes in '*X.*' *romeri*, and the shape of the parasphenoid which in '*X.*' *romeri* has a narrower anterior region of the cultriform process, and a posterior terminus that almost reaches the ventral margin of the foramen magnum.

OTHER DISARTICULATED BONES OF PIPID FROGS

Other isolated skeletal elements of anurans recovered from the Ibeceten Formation may also represent pipid taxa. However, it is difficult to determine the proper association of bones with each other or with the material described above; thus, they are described and discussed separately below.

Angulosplenial

The posterior portion of a lower jaw (MNHN-IBC 1631), which bears a well-developed coronoid process expanded into a flange (a pipid synapomorphy; Cannatella and Trueb 1988*a*), undoubtedly represents a member of the Pipidae. Moreover, as in pipids, the Meckelian canal is closed. The coronoid flange is secondarily reduced in *Pipa pipa* and *P. snethlageae*; furthermore, in these living taxa the posterior end of the angulosplenial has a distinct medially directed curve (Trueb and Cannatella 1986) that is not evident in the fossil specimen. The preserved portion is 12 mm long, indicating an individual of large size.

Presacral vertebra

One opisthocoelous vertebra (MNHN-IBC 1650; Text-fig. 5A–C; Pl. 1, fig. 7), lacking the thick accretion of bone present in the vertebrae referred to *Pachybatrachus*, is tentatively assigned to the Pipidae. It is larger and in general more elongate than the vertebrae referred to *Pschybatrachus*. The anterior third of the neural arch is smooth and extends laterally into the rectangular and flat-surfaced prezygapophyses. This part of the vertebra lies in a more ventral plane than the posterior two-thirds, which bears irregular longitudinal wrinkles on both sides of the fine and rib-like neural spine. This morphology indicates that the neural arch of the preceding vertebra overlapped the anterior portion of the succeeding vertebra (i.e. the neural arches were completely imbricated). The posterior part of the neural arch is somewhat damaged and the postzygapophyses are not preserved, but it is clear that a posteriorly projecting spinous process was not present. The anterior condyle and posterior cotyle are large and depressed. Although the distal portions of the transverse processes are broken off, the pronounced anterior orientation of the dorso-ventrally flattened basal parts of these processes indicates that this vertebra is a posterior presacral. A large spinal foramen opens at the base of the neural arch on each side of the central cotyle. The presence of an intravertebral spinal foramen is uncommon in anurans: for example, it is present in Tertiary pelobatid material, as yet undescribed, from Europe. The opisthocoelous condition and the anterior orientation of the transverse processes are consistent with referral to the Pipidae, despite the presence of bilateral intravertebral spinal foramina. This vertebra differs from those of extant *Xenopus* and *Silurana* and resembles those of pipines in having fully imbricated neural arches and prezygapophyses lacking complex articular surfaces.

Ilia

Sixteen incomplete basal portions of ilia (MNHN-IBC 1630, 1635–1649), all with the same general morphology, can be referred to the Pipidae. This is based on the presence of a conspicuous dorsal prominence, an elongate or dumbbell-shaped (Trueb 1996) acetabulum and the absence of a preacetabular expansion in the lateral plane. The dorsal prominence is relatively wide-based and low, unlike the high and knobbed prominence of *Hymenochirus* which represents the derived condition. The shaft has an oval cross section and a fine ridge runs diagonally from the acetabulum on to the ventral margin of the preserved portion of the shaft. No ridge is present in specimens of extant *Xenopus* and *Silurana* examined for this feature, but does occur in some specimens of '*Xenopus*' *romeri* (DGM 577 and 578), and the pipines. The presence or absence of a prominent

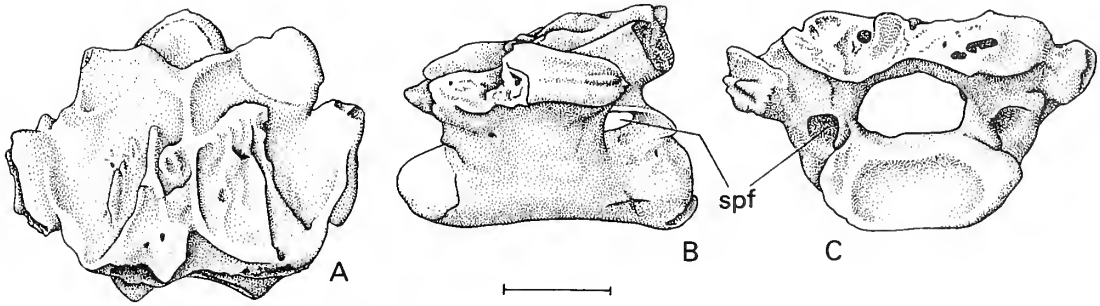

TEXT-FIG. 5. Unidentified pipid, MNHN-IBC 1650; posterior presacral vertebra in A, dorsal; B, left lateral; and C, posterior views. Scale bar represents 2 mm.

crest on the dorsolateral aspect of the iliac shaft could not be assessed because only the most posterior part of the shaft is preserved.

Scapula

One scapula (MNHN-IBC 1632) is clearly referable to the Pipidae because of its relative shortness and configuration. It bears a small articular surface for the clavicle on the anterior margin, thus indicating that scapula and clavicle were separate elements and that the former was slightly overlain anteriorly by the latter. The scapula has a straight anterior margin and its posterolateral angle has a distinct projection. Although the pars acromialis is broken off in this specimen, it is evident that a small notch separated it from the pars glenoidalis. The anterior margin of the preserved portion is 5 mm wide and its lateral margin is 4·5 mm long.

A fused scapula and clavicle is a derived condition, present in *Xenopus*, *Silurana* and *Hymenochirus*, and, although reversed in *Pipa*, has been considered a synapomorphy of extant pipids (Cannatella and Trueb 1988*a*). The presence of a medial notch is a primitive character state for pipids; this notch is lacking in the living species of *Pipa*. The scapula MNHN-IBC 1632 has a well-developed body, thus contrasting with the extreme reduction of the portion lateral to the glenoid region in extant *Xenopus* and *Silurana*, as well as in some fossil taxa (e.g. '*Xenopus*' *romeri*; Estes 1975*b*). In all these taxa, and unlike the Hymenochirini, the area of fusion between the clavicle and scapula is marked by a distinct bump on the anterior edge of the combined element. The articular surface of the pars glenoidalis has a transverse orientation in the fossil scapula, whereas in extant pipines it is usually posteriorly directed.

Humeri

Five fragments representing the distal end of humeri (MNHN-IBC 1651–1655) are referred to the Pipidae. In all cases the eminentia capitata is spherical, well-ossified, and relatively small with respect to the well-developed epicondyles. The medial epicondyle is particularly large, producing an asymmetrical shape to the distal end of the bone. In ventral view, a fine longitudinal crest extending almost to the humeral ball is visible. There is some variation in the definition of fine crests on the medial and lateral sides of the bone, and of the ventral fossa in the sample, but the taxonomic significance of this variation is unknown as there have been no studies of these features. In specimens MNHN-IBC 1651–1654, the olecranon scar is relatively short and the fossa cubitalis is triangular, deep and clearly demarcated anterior to the eminentia capitata. By contrast, in MNHN-IBC 1655, the ventral fossa is not well demarcated and forms a long triangular depressed area between the epicondyles. Furthermore, in this specimen, the crests along the sides are barely discernible. The small size of the humeral ball relative to the distal width of all these bones resembles the general condition in pipines. In *Xenopus* and *Silurana*, the epicondyles are relatively narrower, and equally developed. The distal end of the humerus has a symmetrical appearance. The wide medial epicondyle and crests on the epicondyles (particularly in specimens 1651–1654), resembles hymenochirine humeri (at least in *H. boettgeri*, the only species available for comparison), although in the latter, the crests are more strongly developed. Referral to *Pachybatrachus* would be in agreement with the proposed hymenochirine affinities of this taxon.

Discussion

The ilia and the humeri may belong to *Pachybatrachus* because these elements show some resemblance to pipines and this agrees with the pipine relationships of this taxon. The portion of the lower jaw might represent either of the two taxa described above, but because of its large size, we suppose that it does not represent *Pachybatrachus*. It seems possible that individuals of the unidentified taxon, represented by a braincase exhibiting juvenile features, might have attained a large body size. The presacral vertebra that is distinct from those referred to *Pachybatrachus*, and the scapula MNHN-IBC 1632 might belong to this same taxon.

DISCUSSION

At least two pipid taxa are present in the Coniacian–Santonian Ibeceten Formation: the hyperossified hymenochirini *Pachybatrachus* and an unidentified taxon the relationships of which remain equivocal. The suggested phylogenetic relationships of *Pachybatrachus*, coupled with the relationships of the living pipid genera as currently understood, indicate that the divergence of the lineages represented today by *Pipa* and Hymenochirini had already occurred by the late Coniacian, and, consequently, that of xenopodines (*Xenopus* + *Silurana*) from pipines.

The main phase of Mesozoic sedimentation in the Iullemmeden Basin, as in other basins in the western and central part of Africa, developed in relation to the opening of the South Atlantic (Moody and Sutcliffe 1991; Janssen *et al.* 1995). Throughout the Aptian (121–113 Ma; Gradstein *et al.* 1994), Africa and South America were still connected north of the Niger Delta, but became completely separated from each other in the Albian–Cenomanian (Szatmari *et al.* 1987), *c.* 99 Ma (Gradstein *et al.* 1994). The divergence of pipines from their common ancestor may have been coincident with the final break-up of Western Gondwanaland. Furthermore, at this time, marine incursions and subsidence periodically isolated the north-western part of Africa from the rest of the continent (Reyment and Dingle 1987; Genik 1993) and this might have acted as an important vicariant factor, resulting in the isolation of pipid populations and enabling divergence.

The area in which the pipids, described herein, lived in the late Cretaceous was probably well within the wet-tropical belt, because the locality was close to the position of the equator, which ran diagonally through the Saharan region at that time (Scotese and Golonka 1993). A diverse fauna, including fish, salamanders, anurans, pelomedusid turtles, crocodiles, squamates and sauropod and theropod dinosaurs, was established in a fluvial-lacustrine environmental setting. The presence of lungfishes, particularly *Protopterus* (de Broin *et al.* 1974; Werner 1993), suggests seasonal climatic conditions. In general, anurans that live in arid or seasonally arid environments tend to have hyperossified skulls (Trueb 1993). Perhaps, the intense ossification of *Pachybatrachus* was related to the acquisition of a degree of burrowing ability to avoid periods of desiccation. Some features of pipids, such as the expanded sacral diapophyses and sliding ilia, have been interpreted as advantageous for burrowing either in bottom muds or on land (Whiting 1961); moreover, it has been reported that extant pipids occasionally burrow underwater in mud, and are considered to be facultative burrowers (Emerson 1976). Several features of *Pachybatrachus*, including the strongly ossified ethmoidal region, the additional articulation between the skull and the fused first and second presacral vertebrae, and the ventrally reinforced vertebral centra, might be specializations in this respect.

Acknowledgements. We express our sincere thanks to Philippe Taquet for permission to study this interesting material. For access to specimens of extant pipids we thank Linda Trueb (University of Kansas), Arnold Kluge (University of Michigan) and Alain Dubois (Museum National d'Histoire Naturelle, Paris). Raymond Laurent (Instituto Miguel Lillo, Tucumán) and Richard Tinsley (University of Bristol) kindly provided specimens of living African pipids for comparisons. We also acknowledge L. Trueb's generosity in sharing specimens with the senior author that she had on loan for her own studies, and thank her for reading an early draft of this

paper. We are grateful to David Cannatella (University of Texas), Andrew Milner (Birkbeck College, London), Hernán Dopazo (University of Buenos Aires) and two anonymous reviewers for their critical comments on the manuscript. David Unwin (University of Bristol) offered appreciated comments and improved the English.

REFERENCES

BÁEZ, A. M. 1981. Redescription and relationships of *Saltenia ibanezi*, a late Cretaceous pipid frog from northwestern Argentina. *Ameghiniana*, **18**, 127–154.

—— 1996. The fossil record of the Pipidae. 329–347. *In* TINSLEY, R. C. and KOBEL, H. R. (eds). *The biology of* Xenopus. Symposia of the Zoological Society of London, 68. Clarendon Press, Oxford, 440 pp.

—— and CALVO, J. 1990. Nuevo anuro pipoideo del Cretácico medio del noroeste de Patagonia. *Ameghiniana*, **26**, 238.

BOULENGER, G. A. 1905. On a collection of batrachians and reptiles made in South Africa and presented to the British Museum. *Proceeding of the Zoological Society of London*, **2**, 248–255.

BROIN, F. de, BUFFETAUT, E., KOENIGER, J.-C., RAGE, J.-C., RUSSELL, D., TAQUET, P., VERGNAUD-GRAZZINI, C. and WENZ, S. 1974. La faune de Vertébrés continentaux du gisement d'In Beceten (Sénonien du Niger). *Comtes Rendus de l'Académie des Sciences de Paris, Série D*, **262**, 2326–2329.

BUFFETAUT, E. 1976. Ostéologie et affinités de *Trematochampsa taqueti* (Crocodylia, Mesosuchia) du Sénonien inférieur d'In Beceten (République du Niger). *Géobios*, **9**, 143–198.

—— and RAGE, J.-C. 1993. Fossil amphibians and reptiles and the Africa–South-America connection. 87–99. *In* GEORGE, W. and LAVOCAT, R. (eds). *The Africa–South America connection*. Clarendon Press, Oxford, 166 pp.

CANNATELLA, D. and DE SÁ, R. O. 1993. *Xenopus laevis* as a model organism. *Systematic Biology*, **42**, 476–507.

—— and TRUEB, L. 1988*a*. Evolution of pipoid frogs: intergeneric relationships of the aquatic frog family Pipidae (Anura). *Zoological Journal of the Linnean Society*, **94**, 1–38.

—— 1988*b*. Evolution of pipoid frogs: morphology and phylogenetic relationships of *Pseudhymenochirus*. *Journal of Herpetology*, **22**, 439–456.

CHABANAUD, P. 1920. Contribution à l'étude de la faune herpétologique de l'Afrique occidentale. *Bulletin Comité d'études Historiques et scientifiques de l'Afrique occidentale française*, **1920**, 489–497.

DAUDIN, F. M. 1802. *Histoire naturelle des rainettes, des grenouilles et des crapauds*. Levrault, Paris, 71 pp.

DE SÁ, R. O. and HILLIS, D. M. 1990. Phylogenetic relationships of the pipid frogs *Xenopus* and *Silurana*: an integration of ribosomal DNA and morphology. *Molecular Biology and Evolution*, **7**, 365–376.

DUMÉRIL, A. M. C. and BIBRON, G. 1841. *Erpétologie générale ou histoire naturelle complète des reptiles*. 8. Roret, Paris, 784 pp.

EMERSON, S. B. 1976. Burrowing in frogs. *Journal of Morphology*, **149**, 437–458.

ESTES, R. 1975*a*. Fossil *Xenopus* from the Paleocene of South America and the zoogeography of pipid frogs. *Herpetologica*, **31**, 263–278.

—— 1975*b*. *Xenopus* from the Palaeocene of Brazil and its zoogeographic importance. *Nature*, **254**, 46–50.

—— ŠPINAR, Z. and NEVO, E. 1978. Early Cretaceous tadpoles from Israel (Amphibia: Anura). *Herpetologica*, **34**, 374–393.

EVANS, S., MILNER, A. and WERNER, C. 1996. Sirenid salamanders and a gymnophionan from the Cretaceous. *Palaeontology*, **39**, 77–95.

FISCHBERG, M., COLOMBELLI, B. and PICARD, J.-L. 1982. Diagnose préliminaire d'une espèce nouvelle de *Xenopus* du Zaïre. *Alytes*, **1**, 53–55.

FORD, L. and CANNATELLA, D. C. 1993. The major clades of frogs. *Herpetological Monographs*, **7**, 94–117.

GENIK, G. J. 1993. Petroleum geology of Cretaceous–Tertiary rift basins in Niger, Chad and Central African Republic. *Bulletin of the American Association of Petroleum Geologists*, **77**, 1405–1434.

GRADSTEIN, F. M., ARGTERBERG, F. P., OGG, J. G., HARDENBOL, J., VAN VEEN, P., THIERRY, J. and HUANG, Z. 1994. A Mesozoic time scale. *Journal of Geophysical Research*, **99**, 24051–24074.

GRAY, J. E. 1825. A synopsis of the genera of Reptiles and Amphibians, with a description of some new species. *Annals of Philosophy*, **10**, 193–217.

GRAY, J. E. 1864. Notice on a new genus (*Silurana*) of frog from West Africa. *Annals and Magazine of Natural History*, **1864**, 315.

HARTLEY, R. W. and ALLEN, P. A. 1994. Interior cratonic basins of Africa: relation to continental break-up and role of mantle convection. *Basin Research*, **6**, 95–113.

HENRICI, A. 1991. *Chelomophrynus bayi* (Amphibia, Anura, Rhinophrynidae), a new genus and species from the middle Eocene of Wyoming: ontogeny and relationships. *Annals of the Carnegie Museum*, **60**, 97–144.

JANSSEN, M. E., STEPHENSON, R. A. and CLOETHINGH, S. 1995. Temporal and spatial correlations between changes in plate motions and the evolution of rifted basins in Africa. *Bulletin of the Geological Society of America*, **107**, 1317–1332.

LINNAEUS, C. 1758. *Systema Naturae*. 10th edition. L. Salvii, Stockholm, 824 pp.

MATEER, N. J., WYCISK, P., JACOBS, L. P., BRUNET, M., LUGER, P., ARUSH, M., HENDRIKS, F., WEISSBROD, T., GVIRTZMAN, G., MBEDE, E., DINA, A., MOODY, R., WEIGELT, G., EL-NAKHAL, H., HELL, J. and STETS, J. 1992. Correlation of nonmarine Cretaceous strata of Africa and the Middle East. *Cretaceous Research*, **13**, 273–318.

MIRANDA-RIBEIRO, A. de 1937. Sobre uma colleccao de vertebrados do nordeste brasileiro. Primeria parte: Peixes e batrachios. *O Campo*, **8**, 54–56.

MOODY, R. T. J. and SUTCLIFFE, P. J. C. 1991. The Cretaceous deposits of the Iullemmeden Basin of Niger, central West Africa. *Cretaceous Research*, **12**, 137–157.

MÜLLER, L. 1914. On a new species of the genus *Pipa* from northern Brazil. *Annals and Magazine of Natural History*, **8**, 102.

NEVO, E. 1968. Pipid frogs from the Early Cretaceous of Israel and pipid evolution. *Bulletin of the Museum of Comparative Zoology, Harvard University*, **136**, 256–316.

NOBLE, G. K. 1924. Contribution to the herpetology of the Belgian Congo based on the collection of the American Museum Congo expedition 1909–1915. *Bulletin of the American Museum of Natural History*, **49**, 147–347.

PATERSON, N. F. 1939. The head of *Xenopus laevis*. *Quarterly Journal of Microscopical Science*, **81**, 161–234.

—— 1945. The skull of *Hymenochirus curtipes*. *Proceedings of the Zoological Society of London*, **115**, 327–354.

—— 1955. The skull of the toad, *Hemipipa carvalhoi* Mir.-Rib. with remarks on other Pipidae. *Proceedings of the Zoological Society of London*, **125**, 223–252.

—— 1960. The inner ear of some members of the Pipidae. *Proceedings of the Zoological Society of London*, **134**, 509–546.

PETERS, W. C. H. 1844. Diagnosen neuer Batrachier, welche zusammen mit der früher (24 July und 17 August) gegebenen Übersicht der Schlangen und Eidechsen mit getheilt werden. *Monatsberichte der Preussischen Akademie der Wissenschaften zu Berlin*, **19**, 614–628.

RAFINESQUE, C. S. 1815. *Analyse de la nature ou tableau de l'univers et des corps organisés*. J. Barravecchia, Palermo, 224 pp.

RAGE, J.-C. 1984. Are the Ranidae (Anura, Amphibia) known prior to the Oligocene? *Amphibia-Reptilia*, **5**, 281–288.

—— MARSHALL, L. G. and GAYET, M. 1993. Enigmatic Caudata (Amphibia) from the upper Cretaceous of Gondwana. *Geobios*, **26**, 515–519.

REYMENT, R. A. and DINGLE, R. V. 1987. Palaeogeography of Africa during the Cretaceous period. *Palaeogeography, Palaeoclimatology, Palaeoecology*, **59**, 93–116.

ROSE, W. and HEWITT, J. 1927. Description of a new species of *Xenopus* from the Cape Peninsula. *Transactions of the Royal Society of South Africa*, **14**, 343–346.

RUTHVEN, A. G. and GAIGE, H. T. 1923. Description of a new species of *Pipa* from Venezuela. *Occasional Papers of the Museum of Zoology, University of Michigan*, **136**, 1–2.

SCOTESE, C. R. and GOLONKA, J. 1993. *PALEOMAP Paleogeographic atlas. PALEOMAP Progress Report No. 20*. Department of Geology, University of Texas at Arlington, 74 pp.

SOKOL, O. 1977. The free swimming *Pipa* larvae, with a review of pipid larvae and pipid phylogeny (Anura: Pipidae). *Journal of Morphology*, **154**, 357–426.

ŠPINAR, Z. 1972. *Tertiary frogs from central Europe*. W. Junk, The Hague, 286 pp.

SWOFFORD, D. O. 1993. *Phylogenetic analysis using parsimony; version 3.1*. Illinois Natural History Museum, Champaign.

SZATMARI, P., FRANCOLIN, J. B. L., ZANOTTO, O. and WOLFF, S. 1987. Evolução tectônica da margem equatorial brasileira. *Revista Brasileira de Geôciencias*, **17**, 180–188.

TAQUET, P. 1976. *Géologie et paléontologie du gisement de Gadoufaoua (Aptien du Niger)*. Cahiers de Paléontologie, Centre National de la Recherche Scientifique, Paris, 191 pp.

TINSLEY, R. C. 1995. A new species of *Xenopus* (Anura: Pipidae) from the highlands of Ethiopia. *Amphibia-Reptilia*, **16**, 375–388.

TINSLEY, R. C., KOBEL, H. R. and FISCHBERG, M. 1979. The biology and systematics of a new species of *Xenopus* (Anura: Pipidae) from the highlands of Central Africa. *Journal of Zoology*, **188**, 69–102.

TORNIER, G. 1896. *Die Thierwelt Ost-Afrikas und der Nachbargebiete. Die Kriechthiere Deutsch-Ost-Afrikas. Beiträge zur Systematik und Descendenzlehere*. Reimer, Berlin, 163 pp.

TRUEB, L. 1993. Patterns of cranial diversity among the Lissamphibia. 255–343. *In* HANKEN, J. and HALL, B. K. (eds). *The skull. 2. Patterns of structural and systematic diversity*. The University of Chicago Press, 566 pp.
—— 1996. Historical constraints and morphological novelties in the evolution of the skeletal system of pipid frogs (Anura: Pipidae). 349–377. *In* TINSLEY, R. C. and KOBEL, H. R. (eds). *The biology of* Xenopus. Symposia of the Zoological Society of London, 68. Clarendon Press, Oxford, 440 pp.
—— and CANNATELLA, D. 1982. The cranial osteology and hyolaryngeal apparatus of *Rhinophrynus dorsalis* (Anura: Rhinophrynidae) with comparisons to recent pipoid frogs. *Journal of Morphology*, **171**, 11–40.
———— 1986. Systematics, morphology, and phylogeny of genus *Pipa* (Anura: Pipidae). *Herpetologica*, **42**, 412–449.
—— and HANKEN, J. 1992. Skeletal developmental in *Xenopus laevis* (Anura: Pipidae). *Journal of Morphology*, **214**, 1–41.
VERGNAUD-GRAZZINI, C. 1966. Les amphibiens du Miocène de Beni-Mellal. *Notes du Service Géologique du Maroc*, **27**, 43–69.
WAKE, M. H. 1993. The skull as a locomotor organ. 197–240. *In* HANKEN, J. and HALL, B. K. (eds). *The skull. 3. Functional and evolutionary mechanisms*. The University of Chicago Press, 460 pp.
WERNER, C. 1993. Late Cretaceous continental vertebrate faunas of Niger and Northern Sudan. 401–405. *In* THORWEIHE, U. and SCHANDELMEIER, H. (eds). *Geoscientific research in northeast Africa*. A. A. Balkema, Rotterdam, 776 pp.
WHITING, H. P. 1961. Pelvic girdle in amphibian locomotion. 43–57. In *Vertebrate locomotion*. Symposium of the Zoological Society of London 5. Oxford University Press, 132 pp.
WITTE, G. F. de 1930. Liste des batraciens du Congo belge à Tervuren. *Revue de Zoologie et Botanique africaine*, **19**, 232–274.

ANA MARÍA BÁEZ
Department of Geology
Facultad de Ciencias Exactas,
Universidad de Buenos Aires,
Pabellón 2, Ciudad Universitaria,
1428 Buenos Aires, Argentina

JEAN-CLAUDE RAGE
URA12 du CNRS
Laboratoire de Paléontologie
Muséum National d'Histoire
Naturelle,
8, rue Buffon,
75005, Paris, France

Typescript received 18 July 1996
Revised typescript received 26 May 1997

APPENDIX 1

Abbreviations used in figures

af	acoustic foramen	orf	orbitonasal foramen
cf	condyloid fossa	paf	parietal foramen
ec	Eustachian canal	pb	pseudobasal articulation
ef	endolymphatic foramen	pef	perilymphatic foramen
ex	excavation for the odontoid process	pf	palatine foramen
fp	frontoparietal	pr	prootic
jf	jugular foramen	prf	prootic foramen
ns	neural spine	prz	prezygapophysis
oaf	occipital artery foramen	ps	parasphenoid
ocd	occipital condyle	ptz	postzygapophysis
oct	occipital cotyle	sn	nasal septum
of	oval fenestra	spf	spinal nerve foramen
olf	olfactory foramen	sph	sphcnethmoid
op	odontoid process	va	ventral accretion of bone
opf	optic foramen	vc	vertebral centrum

APPENDIX 2

List of specimens of extant species examined (cleared-and-stained, and dry skeletons)

Rhinophrynus dorsalis Duméril and Bibron, 1841, Tehuantepec, Oaxaca, Mexico. KU 69084–085
Xenopus fraseri Boulenger, 1905, no locality data. MNHN 4402
Xenopus gilli Rose and Hewitt, 1927, South Africa. UMMZ 152290
Xenopus laevis Daudin, 1802, no locality data. KU 129701
Xanopus laevis Daudin, 1802, no locality data. MCZ 26585
Xenopus largeni Tinsley, 1995, Ethiopia. KU 206863
Xenopus muelleri (Peters, 1844), Kenya. KU 129699
Xenopus muelleri (Peters, 1844), Dodoma, Tanzania. MCZ 14799
Xenopus muelleri (Peters, 1844), near Ft Johnston. MCZ 85213
Xenopus muelleri (Peters, 1844), Morogoro, Tanzania. MCZ 51689
Xenopus wittei Tinsley, Kobel and Fischberg, 1979, Kigezi, Uganda. CPBA-V-42
Silurana epitropicalis (Fischberg, Colombelli and Picard, 1982), Kinshasa F.D., Zaire. KU 195661
Silurana tropicalis Gray, 1864, Paiata, Liberia. MCZ 11866
Silurana tropicalis Gray, 1864, no locality data. MNHN GR 30–32
Silurana tropicalis Gray, 1864, Sierra Leone. KU 195667
Silurana tropicalis Gray, 1864, no locality data. CPBA-V-36
Pseudhymenochirus merlini Chabanaud, 1920, Sierra Leone. KU 206875
Hymenochirus boettgeri (Tornier, 1896), Ngiti, Kivu, East Congo. MCZ 46080
Hymenochirus boettgeri (Tornier, 1896), Zaire. UMMZ 132927
Hymenochirus boettgeri (Tornier, 1896), Zaire. CPBA-V-51
Hymenochirus boulengeri Witte, 1930, Kpteli, near Buta, Zaire. MCZ21615
Hymenochirus sp., no locality data. UMMZ 154773
Hymenochirus curtipes Noble, 1924, Kinshasha, Zaire. KU 204130, 31, 34, 37
Hymenochirus curtipes Noble, 1924, no locality data. KU 204126
Pipa carvalhoi (Miranda-Ribeiro, 1937), Espirito Santo, Brazil. CPBA-V-9
Pipa carvalhoi (Miranda-Ribeiro, 1937), Santa Tereza, Espirito Santo, Brazil. CPBA-V-30
Pipa parva Ruthven and Gaige, 1923, El Vigia, Mérida, Venezuela. CPBA-V-24
Pipa pipa (Linnaeus, 1758), Leticia, Colombia. UMMZ 152284
Pipa pipa (Linnaeus, 1758), Santa Cecilia, Ecuador. UMMZ 168408
Pipa pipa (Linnaeus, 1758), Belem, Para, Brazil. CPBA-V-7
Pipa snethlageae Müller, 1914, Belem, Para, Brazil. CPBA-V-20
Pipa snethlageae Müller, 1914, River Ampyacu, Estirén, Peru. MCZ 85571

APPENDIX 3

Characters and character states used in the analysis of *Pachybatrachus* relationships. For each character (0) denotes the primitive condition.

1. skull shape in lateral profile: rounded and domed (0); wedge-shaped (1).
2. frontoparietal: supraorbital flanges present (0); supraorbital flanges absent (1).
3. sphenethmoid: not enclosing the optic foramina (0); enclosing the optic foramina (1).
4. parasphenoid: not fused to the braincase (0); at least partially synostotically fused to the braincase (1).
5. parasphenoid posterior terminus: expanded between the otic capsules (0); acuminate (1).
6. pterygoid medial ramus–parasphenoid contact: limited or no contact (0); extensive contact (1).
7. medial and lateral rami of pterygoid: not fused to the otic capsule (0); fused to the otic capsule (1).
8. Eustachian canal: curved, circumventing the inner ear region, or horizontal (0); crosses the otic capsule diagonally (1).
9. shape of articular surface of the occipital condyles: elongate, reniform (0); circular (1).
10. orientation of the articular surface of the occipital condyles: posteromedial in ventral view (0); posterolateral in ventral view (1).
11. postzygapophyses of presacral vertebrae: articular surface simple (0); articular surface ventrally curved forming a groove (1); articular surface bears grooves and ridges (2).
12. spinous processes of presacral vertebrae: single (0); paired, parasagittal (1).
13. sacrum–coccyx relationship: articulated (0); fused (1).

APPENDIX 4

Distribution of character states among the seven taxa examined in the analysis. Numbers in the top row refer to characters described in Appendix 3. ?: the character does not apply owing to a logical conflict.

	Characters												
Taxon	1	2	3	4	5	6	7	8	9	10	11	12	13
Rhinophrynidae	0	1	0	0	0	?	0	?	0	0	0	0	0
Palaeobatrachus	0	0	0	0	0	0	0	?	0	0	0	0	0
Xenopus	0	0	0	1	0	0	0	0	0	0	2	0	1
Pipa	1	1	1	1	1	0	0	0	1	1	0	1	1
Hymenochirus	1	1	1	1	1	1	1	1	0	0	1	1	1
Pseudhymenochirus	1	1	1	1	1	1	1	1	0	0	1	1	1
Pachybatrachus	1	1	1	1	1	1	0	1	0	0	1	1	1

ORDOVICIAN TRILOBITES FROM THE DAWANGOU FORMATION, KALPIN, XINJIANG, NORTH-WEST CHINA

by ZHOU ZHIYI, W. T. DEAN, YUAN WENWEI *and* ZHOU TIANRONG

ABSTRACT. Sixteen trilobite taxa are described from the type section of the Dawangou Formation (late Arenig–early Llanvirn) at Dawangou, Kalpin, north-western Tarim, Xinjiang, north-west China. They include two new genera: the asaphine *Mioptychopyge* and the pterygometopine *Yanhaoia*. Evidence from the lithofacies and from the composition and taphonomy of the assemblages suggests that the fauna lived in a generally calm, upper slope environment. More than 80 per cent. of the species are common, or closely allied, to coeval forms in the Yangtze region, indicating a close palaeogeographical relationship between the Tarim and South China blocks during the late early Ordovician. Some genera, such as *Birmanites*, *Eccoptochile*, *Ovalocephalus* and *Pseudocalymene*, are typical of Gondwanan faunas, and it is likely that the Tarim Block formed part of peri-Gondwana in the Ordovician.

EIGHT trilobite species were previously recorded from the Upper Qiulitag Group in the Kalpin area (Zhang 1981), all from the uppermost part of the group (Zhou, *in* Zhou and Chen 1990, 1992), recently referred by Zhou *et al.* (1991) to a new rock unit, the Dawangou Formation. The specimens described herein were mostly collected in 1987 from the measured section at the stratotype of the formation at Dawangou, about 9 km north-west of Yingan village, Kalpin County (Text-fig. 1). The work formed part of an extensive field investigation of the periphery of the Tarim Basin by geologists of the Nanjing Institute of Geology and Palaeontology, Academia Sinica, and the 05 Project Administration, Bureau of Petroleum Geology of Southwest China. The large, new collection includes representatives of 16 genera and provides evidence for the range of variation in species previously known from limited material, as well as a more complete knowledge of faunal composition and species diversity in the type Dawangou Formation.

AGE AND STRATIGRAPHICAL SUMMARY

The Dawangou Formation is exposed extensively along the north-western margin of the Tarim Basin and is composed of grey, medium- to thinly-bedded biocalcilutites, biocalcarenites and nodular biocalcilutites, some of which contain glauconite and masses and bands of chert (Text-fig. 2). The formation is conformably underlain by the Upper Qiulitag Group and overlain by the Saergan Formation.

Three conodont zones have been recognized in the Dawangou Formation (Zhou *et al.*, *in* Zhou and Chen 1990, 1992) at Dawangou; they are, in ascending order, *Baltoniodus* aff. *navis*, *Amorphognathus variabilis* and *Eoplacognathus suecicus*. The *Baltoniodus* aff. *navis* Zone was established in the upper part of the Dawan Formation in the Nanjing Hills, Jiangsu, and in the upper part of the Meitan Formation at Qijiang and Huayingshan, Sichuan, in the Yangtze area (An 1987), where its horizon lies between the *Amorphognathus variabilis* and *Paroistodus originalis* zones. As An (1987, p. 75) pointed out, the *B.* aff. *navis* Zone may correspond to the *Microzarkodina parva* Zone of Baltoscandia. The *A. variabilis* and *E. suecicus* zones were founded in the North Atlantic Ordovician conodont province. In the Yangtze area both have been recognized in, respectively, the uppermost Dawan Formation to lowermost Kuniutan Formation, and the lower part of the Kuniutan Formation (An 1987). Graptolites from the overlying lower part of the Saergan

[Palaeontology, Vol. 41, Part 4, 1998, pp. 693–735, 8 pls]

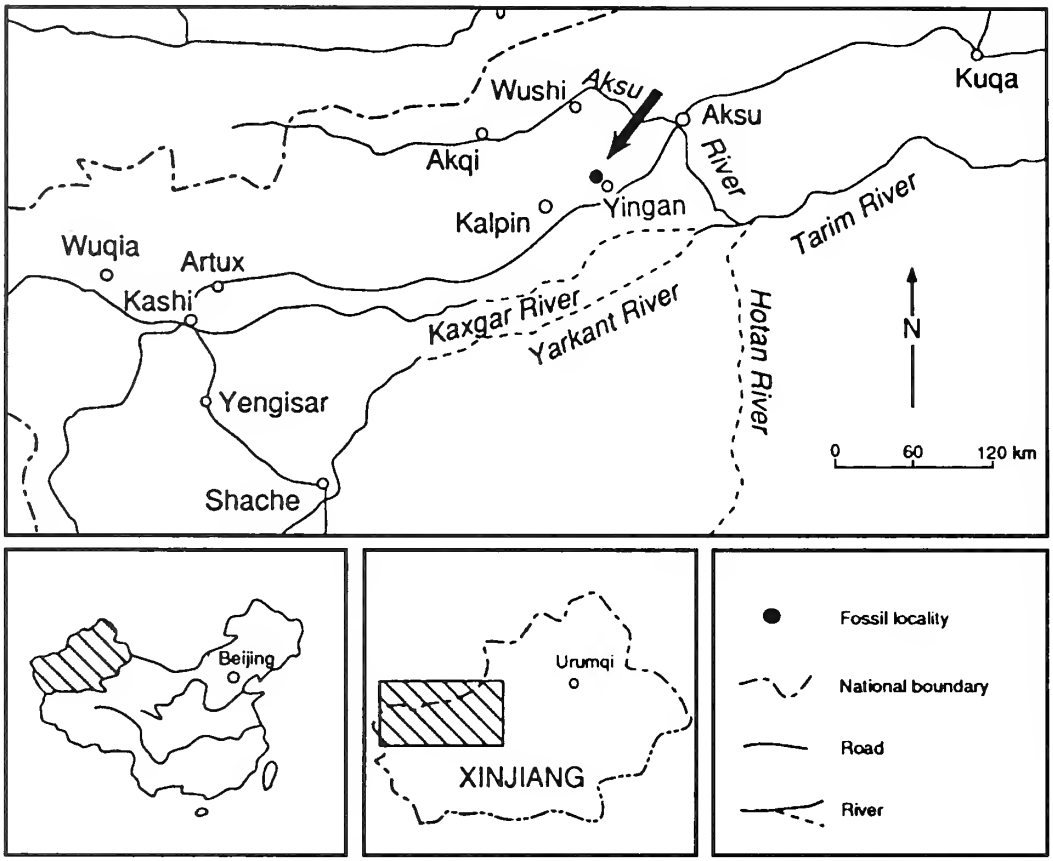

TEXT-FIG. 1. Outline maps showing location of the measured section through the Dawangou Formation.

Formation include, amongst others, *Pterograptus elegans* Holm, *Amplexograptus confertus* (Lapworth) and *Isograptus lyra* Ruedemann, which belong to the *Pterograptus elegans* Subzone of the *Didymograptus nurchisoni* Zone (Zhou *et al.* 1990, 1992).

Evidence from conodonts and graptolites indicates that the Dawangou Formation is of late Arenig–early Llanvirn age in terms of the British chronostratigraphical standard advocated by Fortey *et al.* (1995). It is correlated with the upper part of the Dawan Formation and the lower part of the Kuniutan Formation, or coeval beds, in the Yangtze area, south China. Chen and Bergström (1995) suggested that the *Undulograptus austrodentatus* Zone may well be the basal unit of the Darriwilian or 'Llanvirn' in terms of the international Ordovician chronostratigraphical scheme. The *U. austrodentatus* interval has been referred approximately to the *M. parva* conodont zone and the lower part of the *A. variabilis* Zone (Bergström and Wang, *in* Chen and Bergström 1995). It is likely that the base of the *U. austrodentatus* Zone corresponds approximately with that of the Dawangou Formation.

BIOFACIES AND ENVIRONMENTAL IMPLICATIONS

Trilobites occur mostly in the upper part of the Dawangou Formation. The fauna includes six species of Asaphidae, two of Illaenidae, two of Cheiruridae, one of Nileidae, one of Leiostegiidae,

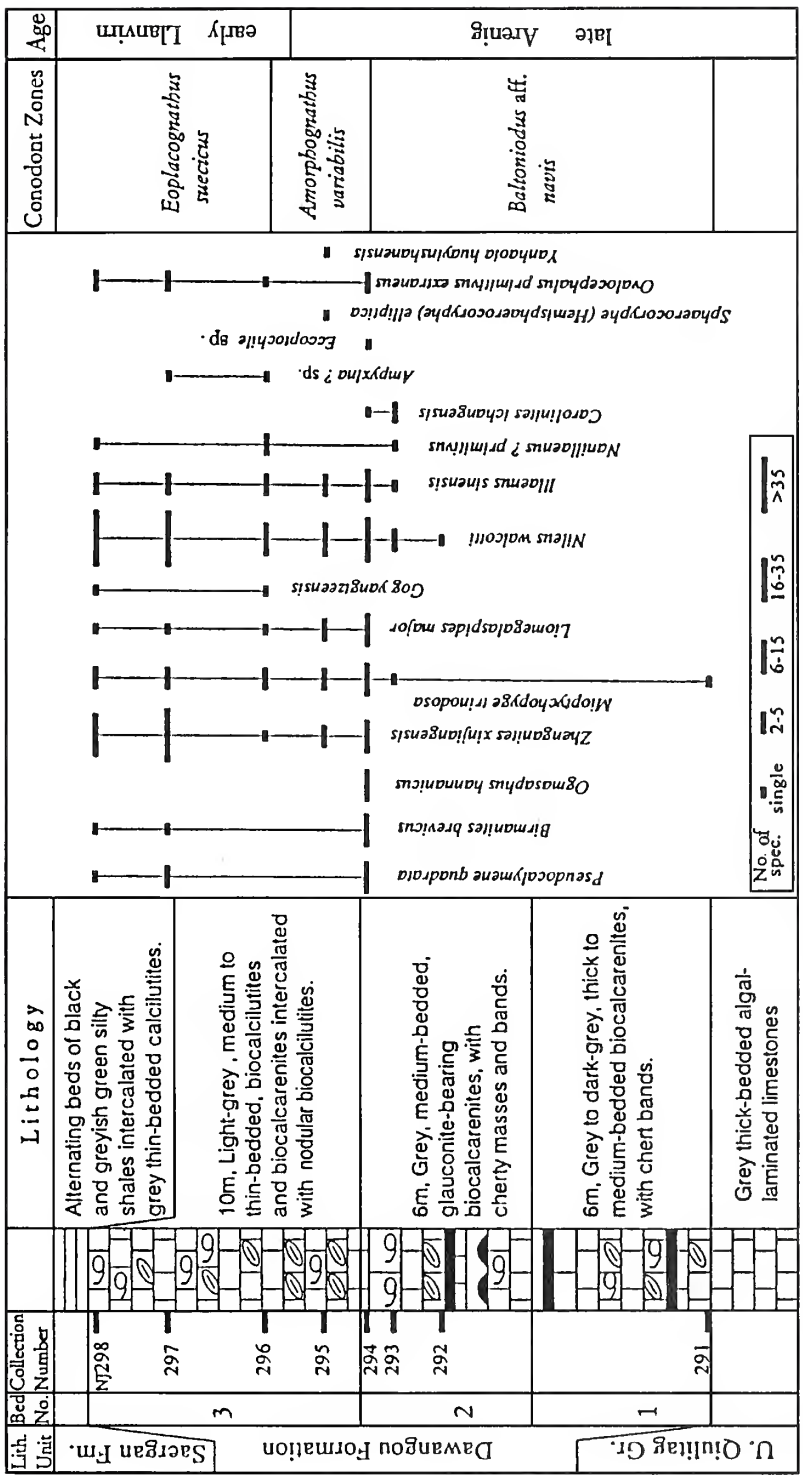

TEXT-FIG. 2. Columnar section of the Dawangou Formation at Dawangou, near Yingan, Kalpin, Xinjiang, showing vertical ranges of identified trilobite species. Fm = Formation; Gr. = Group; No. of spec. = Number of specimens.

one of Hammatocnemidae, one of Raphiophoridae, one of Pterygometopidae and one of Telephinidae. Species diversity is 16. Of the 350 trilobite specimens collected, *Nileus walcotti* makes up 47 per cent., asaphids (*Zhenganites xinjiangensis* 22 per cent., *Mioptychopyge trinodosa* 8 per cent., *Liomegalaspides major* 4·7 per cent., *Birmanites brevicus* 3 per cent., *Ogmasaphus hannanicus* 1·7 per cent., *Gog yangtzeensis* 0·6 per cent.) 40 per cent., and illaenids (*Illaenus sinensis* 7 per cent., *Nanillaenus*? *primitivus* 1 per cent.) 8 per cent.; other forms are rare. The association of species indicates the Nileid Biofacies (cf. Nileid Community of Fortey 1975*a*). On the basis of analyses of Arenig–Llanvirn lithofacies and faunal composition in Spitsbergen, Fortey (1975*a*) suggested that the lower depth limit of the nileid fauna might be some 100 m (corresponding roughly to the oxidizing-reducing boundary) but it may extend shorewards to overlap with the illaenid-cheirurid assemblage, which was typically distributed along the platform margin, in carbonate build-ups deposited in a shallow-water environment at or near wave-base (Fortey 1980*a*). The mingling of a considerable number of illaenids and a few cheirurids with the present nileid assemblage indicates that the fauna inhabited an area not far from the platform.

More than 30 per cent. of specimens in our collection, especially the nileids, illaenids and asaphids, are articulated exoskeletons. Most are randomly distributed and poorly sorted on the bedding surface. The evidence suggests that the association is mainly an autochthonous benthonic fauna which lived in a generally calm environment, normally below storm-wave base (> 70 m). Biodebris-bearing flags occur only occasionally in the Dawangou Formation and contain fragments of trilobites, nautiloids and cystids, all poorly sorted and probably transported by storm-induced debris flows from the adjacent platform edge.

The occurrence of benthic trilobites in relation to a shallow- to deeper-water environment gradient in north-western Tarim has been discussed by Zhou *et al.* (*in* Zhou and Chen 1990, 1992). Based on the late Arenig–early Llanvirn palaeogeographical map (Zhou *et al.*, *in* Zhou and Chen 1990, 1992, text-fig. 3-13), the fossiliferous section at Dawangou lies only about 30 km north of the platform-marginal reef-facies belt. A few algal-bound bioclastic limestones recently found in the Dawangou Formation (Zhou *et al.* 1991) indicate the presence of sparse, small, lenticular carbonate mounds in the Kalpin area in the late Arenig–early Llanvirn. They may have formed exceptional ecological niches on the sea-floor, and a few specimens of *Illaenus sinensis* and *Nanillaenus*? *primitivus* from the bioherm 'pockets' show much coarser terrace ridges on the dorsal surface than specimens from surrounding beds.

According to Zhou *et al.* (1990, 1992), the sea on the Tarim Block deepened gradually during the early Ordovician and, following the late Arenig transgression, the platform edge shifted shorewards so that the previous platform in the Kalpin area deepened to a shallow shelf slope. The above evidence suggests that the slope was fairly gentle with a depth generally little more than 70 m during the interval represented by the Dawangou Formation.

FAUNAL AFFINITIES AND PALAEOGEOGRAPHICAL RELATIONSHIPS

Of the 16 species described here, half are new to the Kalpin area, and the fauna exhibits strong affinities with that of the Yangtze region, the shallower part of the South China Block. On the basis of the new material, nine species are common to both areas: *Pseudocalymene quadrata*, *Birmanites brevicus*, *Ogmasaphus hannanicus*, *Gog yangtzeensis*, *Nileus walcotti*, *Illaenus sinensis*, *Carolinites ichangensis*, *Sphaerocoryphe* (*Hemisphaerocoryphe*) *elliptica* and *Yanhaoia huayinshanensis*. Four forms (*Zhenganites xinjiangensis*, *Mioptychopyge trinodosa*, *Liomegalaspides major* and *Ovalocephalus primitivus extraneus*) are closely allied to coeval taxa from the Yangtze region (*Zhenganites guizhouensis* Yin, *in* Yin and Lee, 1978, *Mioptychopyge sumi* (Endo, 1935), *Liomegalaspides blackwelderi* (Weller, 1907), *Ovalocephalus primitivus primitivus* (Lu, 1975)). It is concluded that the Tarim and South China blocks formed a single palaeogeographical unit during the late early Ordovician. Biotic evidence from the rest of the Palaeozoic shows that Tarim, an independent block, was situated very close to the South China Block, and the two were not

separated by large oceanic basins (Zhou and Chen 1990, p. iv; 1992, p. ii; Zhou *et al.* 1996, pp. 11, 20).

Of the 15 trilobite genera and one subgenus in the Dawangou Formation, four are endemic to the Tarim and Yangtze regions, namely *Zhenganites*, *Mioptychopyge* gen. nov., *Liomegalaspides* and *Yanhaoia* gen. nov. A small number of trilobites such as *Pseudocalymene*, *Birmanites* and *Ovalocephalus* are found only in Ordovician Gondwanaland (Zhou and Dean 1989); *Eccoptochile*, typically known elsewhere from the upper Llanvirn–Ashgill of Spain, Portugal, France, Bohemia and, probably, Morocco and Turkey (Rabano 1990), is also referred to this group.

Carolinites is an epipelagic genus which occurs in North America, Greenland, Spitsbergen, Siberia, Tasmania, Australia, South China and, uncommonly, northern Baltica, Turkey and Argentina, a distribution suggesting Ordovician lower latitudinal zones (Fortey 1985). *Nileus* is also widespread but is mainly restricted to the Nileid Biofacies belts or slope areas adjacent to carbonate platforms in the Ordovician tropical to temperate zones (Fortey 1975*a*; Zhou *et al.* 1989). The occurrence of *Gog* is linked to the Nileid Biofacies, although it has been found elsewhere only in Spitsbergen, Sweden, the north Arctic Urals (Fortey 1975*b*) and the western marginal area of the North China platform (Zhou *et al.* 1982).

Illaenus has a world-wide distribution, and is especially predominant in carbonate build-ups (Fortey 1975*a*; Mikulic 1980; Zhou *et al.* 1989). *Nanillaenus*, recorded from North America, Scotland and Argentina, and *Sphaerocoryphe* (*Hemisphaerocoryphe*), known from Baltoscandia, Australia and the Yangtze region, are both members of the Illaenid-Cheirurid Association. However, judging from their occurrences in China, all three genera may have tolerated a wide range of environments, from platform to upper slope.

Excluding those genera that are endemic, pelagic and facies-restricted, the trilobite fauna shows strong Gondwanan affinities, and the Tarim Block may have formed part of Ordovician Gondwanaland. This landmass, extending from the South Pole to north of the equator during the Ordovician, was large enough to account for the considerable faunal differences between the cold and warm areas, and there appears to be no evidence for the presence of oceanic barriers that might have prevented migration and dispersal of trilobites between different areas (Zhou and Dean 1989; Cocks and Fortey 1990). Palaeomagnetic data show that the Kalpin area was located at 19·6° S (Zhou and Zheng 1990).

The trilobites from the Dawangou Formation include largely warm-water elements, with some, such as *Eccoptochile* (see Přibyl *et al.* 1985), that were once considered as cold-water forms. Asaphids have a strong Baltoscandian aspect: *Ogmasaphus*, previously thought to be endemic to Scandinavia; *Gog*, recently recorded from Sweden; *Liomegalaspides*, considered by Lu (1975) to be derived from *Megalaspides*; and others, such as *Zhenganites* and *Mioptychopyge*, which are closely related to *Ptychopyge* (*s.l.*) and *Pseudobasilicus* (*s.l.*). Baltoscandia is widely considered to have been located in the temperate zones, at least during the early Ordovician. The mixture of trilobites from different temperature zones in the Dawangou fauna may suggest ecological conditions appropriate to an upper slope environmental gradient.

Interestingly, the oldest recorded species of *Nanillaenus*, *Eccoptochile* and *Sphaerocoryphe* (*Hemisphaerocoryphe*) occur in the Dawangou fauna, and a probably new raphiophorid is referred questionably to *Ampyxina*, a principally North American form. If the latter determination is correct, it may lend support to the view (Fortey 1984; Dean 1985) that faunal exchange between Laurentia and Gondwanaland may have started in the early Ordovician.

SYSTEMATIC PALAEONTOLOGY

The terminology used here is essentially that of the first edition of the *Treatise on invertebrate paleontology* (Harrington *et al.*, *in* Moore 1959), with the modifications proposed in the second edition (Whittington and Kelly 1997). Repositories of described and cited specimens are: NI, Nanjing Institute of Geology and Palaeontology, Academia Sinica; USNM, National Museum of

Natural History, Washington, D.C.; XTR, Regional Geological Survey Team of Xinjiang; YI, Yichang Institute of Geology and Mineral Resources, Academy of Geological Sciences of China.

Family LEIOSTEGIIDAE Bradley, 1925

Remarks. We follow Fortey and Shergold (1984) in considering Eucalymenidae Lu, 1975 to be a junior synonym of Leiostegiidae.

Genus PSEUDOCALYMENE Pillet, 1973
(= *Eucalymene* Lu, 1975, p. 245)

Type species. Pseudocalymene superba Pillet, 1973.

Remarks. Eucalymene was established by Lu (1975) mainly on the basis of the type species *E. quadrata*, and the diagnostic features, including small eyes, lack of cephalic border, and the presence of interpleural furrows on the pygidium agree well with the definition of *Pseudocalymene*. Pillet's (1976) suggestion that the two genera are synonymous is followed here. Except for the type species, *P. superba* Pillet (1973, p. 36, pl. 6, figs 6–8; pl. 7, figs 1–6; pl. 8, fig. 9) from the Ordovician of eastern Iran, other forms of the genus have been recorded from the upper Arenig–Llanvirn of the Yangtze region (Li *et al.* 1975; Lu 1975; Zhou *et al.* 1977; Lee 1978; Xia 1978; Yin and Lee 1978; Zhou *et al.* 1982; Sun 1984) and of Tarim (Zhang 1981), China.

Pseudocalymene quadrata (Lu, 1975)

Plate 1, figures 1–3

1975 *Eucalymene quadrata* Lu, p. 460, pl. 48, fig. 15; pl. 49, figs 1–10; pl. 50, figs 1–5.
1975 *Eucalymene quadrata* Lu; Li *et al.*, p. 148, pl. 13, fig. 13.
1977 *Eucalymene quadrata* Lu; Zhou *et al.*, p. 264, pl. 80, fig. 1a–d.
1978 *Eucalymene quadrata* Lu; Xia, p. 183, pl. 36, fig. 18.
1981 *Pseudocalymene quadrata* (Lu); Zhang, p. 212, pl. 79, figs 1–3.
1982 *Pseudocalymene quadrata* (Lu); Zhou *et al.*, p. 289, pl. 71, figs 5–6.
1984 *Pseudocalymene quadrata* (Lu); Sun, p. 419, pl. 54, figs 7–8.

Holotype. Enrolled exoskeleton (NI 16987), figured Lu (1975, pl. 59, figs 1–5), Zhou *et al.* (1977, pl. 80, fig. 1a–d) and Sun (1984, pl. 154, figs 7–8), from the uppermost Dawan Formation (latest Arenig) at Fenxiang, Yichang, western Hubei.

Figured specimens. Two pygidia (NI 80715–80716) and a juvenile librigena (NI 80714), from Bed 2.

EXPLANATION OF PLATE 1

Figs 1–3. *Pseudocalymene quadrata* (Lu, 1975); Bed 2. 1, NI 80714; small right librigena; ×6. 2, NI 80715; pygidium; ×1·5. 3, NI 80716; pygidium; ×1·5.

Figs 4–11. *Birmanites brevicus* Xiang and Zhou, 1987; Bed 2. 4, NI 80717; cephalon with thorax. 5, NI 80718; cephalon with thorax. 6–7, NI 80719; enrolled exoskeleton, dorsal views. 8, 11, NI 80720; incomplete exoskeleton, lateral views. 9, NI 80721; incomplete cephalon with thorax. 10, NI 80722; thorax and pygidium of complete exoskeleton. All ×1·5.


1


2

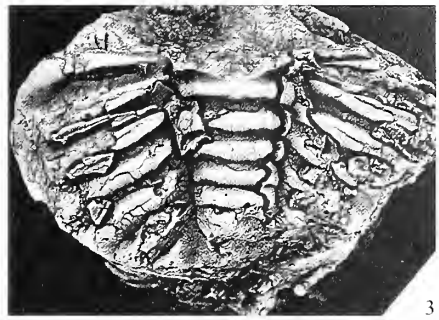
3


4


5

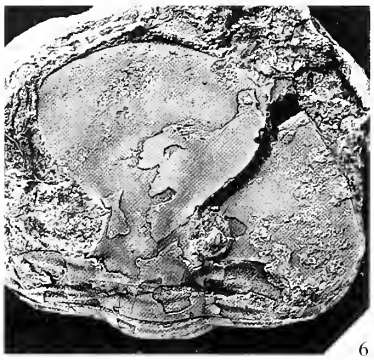
6

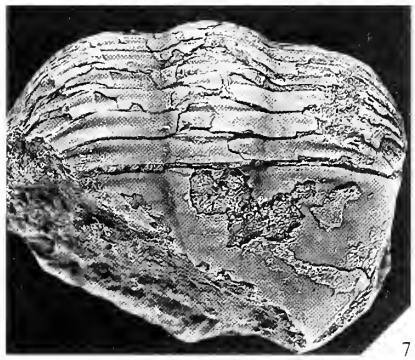
7


8


9

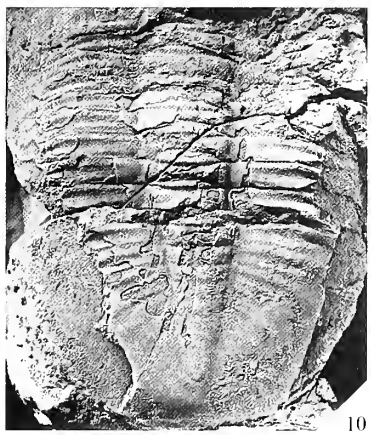
10


11

ZHOU *et al.*, *Pseudocalymene*, *Birmanites*

Remarks. The species was described fully by Lu (1975, p. 460) and the present pygidia, although poorly preserved, agree with his account. Two enrolled exoskeletons and a pygidium from the same horizon and locality were referred to the species by Zhang (1981, p. 212, pl. 79, figs 1–3). An associated juvenile librigena shows five widely spaced terrace ridges on the strongly convex border; surface is covered with distinct scattered tubercles in adaxial part of genal field, coarsely granular in anterior part of border, and otherwise smooth, but in the holotype, the whole surface of the librigena is densely granular. These differences are considered as intraspecific and may represent morphological changes during ontogeny.

Family ASAPHIDAE Burmeister, 1843
Subfamily ASAPHINAE Burmeister, 1843

Genus BIRMANITES Sheng, 1934

Type species. *Ogygites birmanicus* Reed, 1915.

Remarks. As noted by Zhou *et al*. (1984), Zhou and Dean (1986) and Tripp *et al*. (1989), *Ogygites* de Tromelin and Lebesconte, 1876, *Pseudobasilicus* Reed, 1931, *Birmanites* Sheng, 1934, *Opsimasaphus* Kielan, 1960 and *Nobiliasaphus* Přibyl and Vaněk, 1965 are closely similar and may prove to be synonymous. Recently, Rabano (1990) suggested that *Ogygites* should be used solely for the type species, *Ogygia desmaresti* Brongniart, 1822. *Pseudobasilicus* differs from *Birmanites* only in the shorter preglabellar field. A species recorded below shows a frontal area that occupies 36–39 per cent. of the cranidial length and is much longer than that of *Ptychopyge lawrowi* Schmidt, 1898 (p. 31, fig. 7), type species of *Pseudobasilicus*; for the time being we refer it to *Birmanites*.

Birmanites is a widely distributed Ordovician genus in Asia. In addition to the type species, the following are included, although some are based on inadequate material, or on pygidia only, and need to be further revised: *Ogygites yunnanensis* Reed, 1917, *Birmanites hupeiensis* Yi 1957, *Ogygites almatyensis* Chugaeva 1958, *Ogygites kolovae* Chugaeva 1958, *Birmanites dabashanensis* Lu, *in* Lu and Chang, 1974, *Birmanites yangtzeensis* Lu, 1975, *Birmanites politus* Lu, 1975, *Birmanites carinatus* Lu, *in* Lu *et al*., 1976, *Birmanites sichuanensis* Lee, 1978, *Birmanites sanduensis* Yin, *in* Yin and Lee, 1978, *Birmanites juxianensis* Ju, *in* Qiu *et al*., 1983; *Birmanites brevicus* Xiang and Zhou, 1987, *Birmanites elongatus* Xiang and Zhou, 1987 and *Birmanites yichangensis* Xiang and Zhou, 1987.

Birmanites brevicus Xiang and Zhou, 1987

Plate 1, figures 4–11

1983 *Birmanites brevicus* Xiang and Zhou, *in* Zeng *et al*., pl. 7, fig. 12 [*nomen nudum*].
1987 *Birmanites brevicus* Xiang and Zhou, p. 312.

Holotype. Exoskeleton (YI 70260), figured Xiang and Zhou, *in* Zeng *et al*. (1983, pl. 7, fig. 12), from the Kuniutan Formation (Llanvirn) at Huanghuachang, Yichang, western Hubei.

Figured specimens. Three exoskeletons (NI 80719–80720, 80722) and three cephala with attached thoracic segments (NI 80717–80718, 80721) from Bed 2.

Remarks. The present specimens agree well with the holotype of *B. brevicus*, described formally by Xiang and Zhou (1987). The frontal area is 36–39 per cent. of the cranidial length and 150 per cent. of the width between palpebral lobes, the pygidium is sub-trapezoidal in outline and, based on the new material, the pygidial doublure is narrower than in known forms, about half the pleural width along the anterior margin. The pygidium has five axial rings and furrowed pleural ribs on the

external surface, but up to ten are visible on the internal mould, as described by Xiang and Zhou (1987, p. 312).

B. brevicus is closely allied to *B. hupeiensis* Yi (1957, p. 552, pl. 3, fig. 1a–g), a Llandeilo–early Caradoc species described from the Miaopo Formation of western Hupei and the Shihtzupu Formation of northern Guizhou by Lu (1975, p. 319, pl. 7, figs 14–15; pl. 8, figs 1–7) and Zhou *et al.* (1984, p. 17, fig. 3c–f, i–j, m). Except for the much wider pygidial doublure, the latter species differs mainly in its longer frontal area (up to 50 per cent. the cranidial length). The pygidium of *B. hupeiensis* is mostly semi-elliptical, but a few specimens have a trapezoidal outline (see Lu 1975, pl. 8, fig. 5) like that in *B. brevicus*. In pygidia of the younger species the length varies from 60–75 per cent. of the width, and the length of the axis is 55–70 per cent. of the pygidium. Corresponding figures for a complete pygidium (Pl. 1, fig. 10) of *B. brevicus* are 62 per cent. and 73 per cent., and fall almost within the range of variation in *B. hupeiensis*.

Genus OGMASAPHUS Jaanusson, 1953

Type species. Asaphus praetextus Törnquist, 1884.

Ogmasaphus hannanicus (Lu, 1975)

Plate 2, figures 1–5

1975 *Pseudoasaphus* [*sic*] *hannanicus* Lu, p. 311, pl. 5, fig. 24.

Holotype. Incomplete cephalon with three attached thoracic segments (NI 16487), figured Lu (1975, pl. 5, fig. 24), from a horizon of Llanvirn age in the Siliangssu Formation, at Liangshan, Hanzhong, southern Shaanxi.

Figured specimens. One exoskeleton (NI 80725), one cephalon with five attached thoracic segments (NI 80724) and one pygidium with two attached thoracic segments (NI 80723) from Bed 2.

Description. Exoskeleton oval in outline with semicircular cephalon and pygidium of equal length; frontal area fairly narrow. Glabella convex, broadly rounded anteriorly, hourglass-shaped, constricted opposite palpebral lobes, from which it expands more gently forwards than backwards; no S0, but pair of indentations present close to axial furrows; median glabellar node posteriorly situated, about in line with posterior edge of palpebral lobes; median ridge faintly visible on exfoliated surface, extending forwards from median node; posterolateral furrow distinct, deeper than axial furrows, dies out adaxially. Low posterolateral glabellar lobe small, triangular. Anterior glabellar lobe shows four pairs of muscle scars on exfoliated surface: posterior scar is triangular, directed backwards, close to posterolateral glabellar furrow; remaining scars are oval, transverse, located on glabellar flank anterior to posterolateral furrow and adjacent to axial furrow. Palpebral lobe large, more than one-third cranidial length, crescentic in form, elevated above fixigena, well defined by broad palpebral furrow. Anterior sections of facial suture diverge forwards in broad curve, submarginal anteriorly; posterior sections extend outwards and slightly backwards in gently sigmoidal curve. Palpebral area of fixigena gently convex, as wide as long; posterior area short (exsag.), strip-like, with raised border which narrows adaxially, defined by shallow border furrow. Librigena without border but has raised edge; genal area transversely convex; eye socle vertical, narrow; eye large, length (exsag.) half that of cephalon (sag.); doublure wide, covered with dense terrace ridges, part of its inner margin close to eye socle.

Thoracic axis is bounded by distinct axial furrows that are gently curved adaxially, and occupies about 40 per cent. of overall width; rectangular axial ring moderately convex (tr.). Pleurae extend horizontally for short distance to the fulcrum, then curve gently down and slightly backwards. Pleural furrows distinct, but die out both abaxially and adaxially on external surface.

Pygidium broadly rounded posteriorly, 60–67 per cent. as long as wide. Axis convex, conical, occupies 37 per cent. of anterior width of pygidium and 87 per cent. of its sagittal length; it is well defined by broad axial furrows, including eight faintly defined rings and a small, rounded terminal piece in addition to a wide (sag.)

articulating half ring as shown in exfoliated specimens. Pleural region evenly convex, without defined border; inner part weakly displays four to five furrowed ribs on exfoliated surface; articulating half-rib ridge-like, faceted anterolaterally; first pleural furrow deeply incised. Doublure fairly broad, about half pleural width anteriorly; inner margins lightly convex adaxially except where indented around posterior part of axis (including seventh and eighth rings and terminal piece).

Remarks. Our specimens show a pair of shorter posterolateral glabellar furrows and an almost effaced occipital furrow, but otherwise agree well with the holotype, an internal mould. In our opinion these superficial differences are probably due to preservation. The species shares some features, such as the absence of a cephalic border and the more or less effaced S0, with both *Ogmasaphus* and *Asaphus* (*Neoasaphus*). Some Scandinavian species are intermediate between the two latter and, as Henningsmoen (1960, p. 236) believed, further work may prove *Ogmasaphus* to be no more than a subgenus of *Asaphus*. Reassignment of the present species to *Ogmasaphus* is suggested by the extremely narrow (sag.) frontal area of the cranidium and the fairly wide pygidial doublure, although the large eye and poorly defined pygidial border and pleural ribs are more similar to those of known species of *A.* (*Neoasaphus*).

Compared with *O. praetextus* (Törnquist) (see Jaanusson 1953, p. 427, pl. 5, figs 1–8) and *O. costatus* Jaanusson (1953, p. 433, pl. 6, figs 3–9; pl. 7, figs 1–4) from the middle Ordovician of Scandinavia, *O. hannanicus* has larger eyes, broader cephalic doublure and the anterior part of the glabella expands forwards more gently. The absence of a defined pygidial border, the weakly defined ribs, and the presence of librigenal spines (see Lu 1975, pl. 5, fig. 24) in *O. hannanicus* may also distinguish it from the Scandinavian species, although the features are shared by exceptional specimens of *O. costatus* (see Jaanusson 1953, pl. 6, figs 6, 9).

Several Chinese species strongly resemble *O. hannanicus*, especially in the extraordinarily large eyes (length half that of the cephalon), and may form a closely related species group. They include *Ogmasaphus* [*Asaphus*] *fenhsiangensis* (Yi 1957, p. 532, pl. 2, fig. 2a–b) (see Xiang and Zhou 1987, p. 309, pl. 35, fig. 11), *Ogmasaphus* [*Opsimasaphus*] *fusiformis* (Xia 1978, p. 161, pl. 29, fig. 10) [= *Opsimasaphus xilingxiaensis* Xia 1978, p. 161, pl. 29, figs 8–9 = *Pseudasaphus limbatus* Xia 1978, p. 162, pl. 30, fig. 4 only, *non* fig. 5; see Xiang and Zhou 1987, p. 310, pl. 33, fig. 5, pl. 35, fig. 8] and *Ogmasaphus triangularis* Xiang and Zhou 1987 (p. 311, pl. 35, fig. 7), all from the Miaopo Formation (Llandeilo–early Caradoc) of the Yichang area, western Hubei; and possibly also *Asaphus nebulosus* Gortani (1934, p. 76, pl. 18, fig. 1a–b) from the upper lower Ordovician of Karakorum. Among the listed species, only *Ogmasaphus fenhsiangensis* is well founded. The cranidium as described by Yi (1957) is almost indistinguishable from that of *P.*? *hannanicus*, but the thorax and pygidium recently illustrated by Xiang and Zhou (1987) differ considerably in the narrower thoracic axis (about as wide as the adjacent pleura), the even narrower pygidial axis (one-fifth to one-sixth the frontal breadth of the pygidium) with ten instead of eight defined axial rings, and the more distinct pleural furrows on the pygidium.

EXPLANATION OF PLATE 2

Figs 1–5. *Ogmasaphus hannanicus* (Lu, 1975); Bed 2. 1, NI 80723; pygidium with two attached thoracic segments; ×2·5. 2–3, NI 80724; cephalon with five attached thoracic segments, dorsal and lateral views; ×3. 4–5, NI 80725; incomplete exoskeleton, dorsal and lateral views; ×2.

Figs 6–12. *Zhenganites xinjiangensis* (Zhang, 1981). 6–7, NI 80726; Bed 2; enrolled exoskeleton, dorsal views; ×1·5. 8, NI 80727; Bed 3; hypostoma; ×2. 9, NI 80728; Bed 2; pygidium and five attached thoracic segments, showing pygidial doublure; ×1. 10–11, NI 80729; Bed 3; enrolled exoskeleton, dorsal and lateral views; ×2. 12, NI 80730; Bed 3; pygidium with attached thorax; ×1·5.

1

2

3

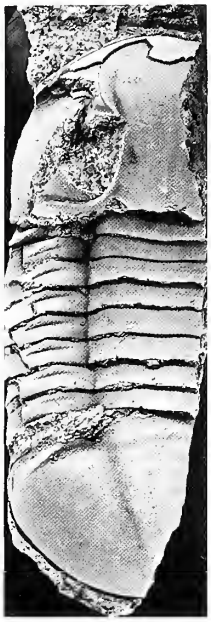

4

5

6

7

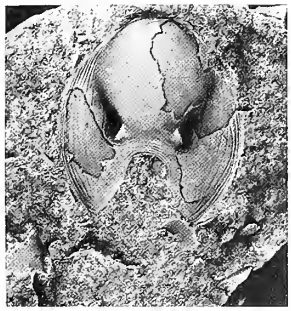

8

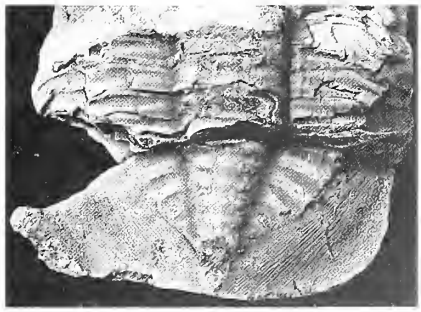

9

10

11

12

ZHOU *et al.*, *Ogmasaphus*, *Zhenganites*

Genus ZHENGANITES Yin, *in* Yin and Lee, 1978
(= *Eosoptychopyge* Zhang, 1981, p. 185)

Type species. Zhenganites guizhouensis Yin, *in* Yin and Lee 1978.

Diagnosis. Asaphine trilobites with narrow (tr.) glabella. Cephalon with flat border and librigenal spines; cranidium bluntly pointed frontally; frontal area moderately long; bacculae elongate, constricted; eyes very large, sited posteriorly; median glabellar node sited in front of line through posterior ends of palpebral lobes; cephalic doublure wide, part of its inner margin close to eye socle. Hypostoma deeply notched posteriorly. Pygidium broadly rounded posteriorly; axis markedly narrower posteriorly; pleural region with abaxially rounded ribs and distinct border; doublure fairly broad.

Remarks. Zhenganites guizhouensis Yin, *in* Yin and Lee, 1978 (p. 529, pl. 174, figs 3–5), from the Kuniutan Formation (Llanvirn) at Anchang, Zhengan, Guizhou, closely resembles *E. xinjiangensis* Zhang (1981, p. 185, pl. 68, figs 1–2), the type species of *Eosoptychopyge*. The cephala of the two are almost indistinguishable, although the preglabellar field is slightly wider (sag.) in *Z. guizhouensis*. The pygidium of *Z. guizhouensis* is incomplete but, from Yin's illustration and description, it differs from that of *E. xinjiangensis* mainly in the shallower pleural furrows. Differences between the two do not seem generically significant, and *Eosoptychopyge* is considered a junior subjective synonym of *Zhenganites*. The above diagnosis is based on the holotype of the type species and well preserved specimens of *Z. xinjiangensis* from our collection. Other species may include *Ptychopyge*? *hankiangensis* Lu, 1975 (p. 311, pl. 6, figs 7–9), from the *Ningkianolithus welleri* Zone (latest Arenig) in the Siliangssu Formation, Liangshan, Hanzhong, southern Shaanxi, and *Ptychopyge*? *changyangensis* Xiang and Zhou, 1987 (p. 314, pl. 36, fig. 12) from the Kuniutan Formation (Llanvirn), Yichang area, western Hubei. The pygidium is comparable in both these species and *Z. xinjiangensis*, and the three may be conspecific, but the cephala of *P. hankianensis* and *P.*? *changyangensis* is as yet unknown.

Zhenganites has an elongated cranidium and a narrow glabella; characteristic post-ocular nodes (or bacculae, see Fortey 1980*b*, p. 258) are absent but a pair of homologous elongated protuberances is well developed on the fixigena just behind the eye. The genus is closely related to *Ptychopyge* and allied genera (see Balashova 1964, 1976) such as *Pseudoptychopyge*, *Paraptychopyge* and *Metaptychopyge*. *Zhenganites* differs in the much larger eyes, more anteriorly placed median glabellar node, and the more broadly rounded concave posterior margin of the hypostoma. Some other characters considered generically important by Balashova (1964) are transitional between these Baltoscandian genera: the wide cephalic doublure recalls *Metaptychopyge* and *Ptychopyge*; the moderately long frontal area and fairly wide pygidial doublure are like those of *Paraptychopyge*; the bluntly pointed anterior margin of the cranidium is close to that of *Pseudoptychopyge*; and the more deeply notched hypostoma is generally similar to that of *Paraptychopyge* and *Metaptychopyge*.

Zhenganites xinjiangensis (Zhang, 1981)

Plate 2, figures 6–12; Plate 3, figures 1, 3

1981 *Eosoptychopyge xinjiangensis* Zhang, p. 185, pl. 68, figs 1–2.

Holotype. Enrolled exoskeleton (XTR 206), figured Zhang (1981, pl. 68, fig. 1a–b), from the topmost Upper Qiulitag Group [= Dawangou Formation] at Subaxi, Kalpin, north-western Tarim, Xinjiang.

Figured specimens. One enrolled exoskeleton (thorax incompletely exposed) (NI 80726) and one pygidium with five attached thoracic segments (NI 80728) from Bed 2; two cephala with thorax (NI 80729, 80731), one pygidium with thorax (NI 80730), one pygidium with two attached thoracic segments (NI 80732) and one hypostoma (NI 80727) from Bed 3.

Description. Cephalon about as wide and long as pygidium, gently convex, with librigenal spines; length 40–50 per cent. of width (longer in the small specimen); cephalic border low, flat, about 8–10 per cent. of cephalic length (sag.) and narrows moderately backwards. Glabella elongate, convex, broadly rounded frontally, slightly constricted opposite palpebral lobes, well defined by axial furrows, with prominent medial note sited in front of line through rear of palpebral lobes; distinct posterolateral furrows shallow towards median node; posterolateral lobes triangular, with two pairs weakly defined transverse depressions in exfoliated specimens; largely effaced S0 traceable near axial furrows on exfoliated surface opposite posterior ends of palpebral lobes. Baccula elongate, ridge-like, poorly defined abaxially, sited between posterior end of palpebral lobe and adaxial end of posterior border furrow. Large, semicircular palpebral lobe 45 per cent. the cranidial length, ill defined by obsolete palpebral furrow. Anterior sections of facial suture diverge gently until opposite anterolateral corners of glabella, where curve adaxially to meet in bluntly pointed ogive; each posterior section forms a sigmoidal curve. Frontal area usually 9–13 per cent. of cranidial length, being relatively shorter in larger specimens. Preglabellar field much narrower (sag.) than anterior border and declines gently to border furrow. Anterior area of fixigena slightly swollen, narrows backwards; palpebral area higher than adjacent part of glabella; posterior area narrow (exsag.), widens abaxially, and convex posterior border is well defined by deep border furrow. Librigena with convex (tr.) genal field and vertical eye socle; large crescentic eye up to 50 per cent. cranidial length; posterior border poorly defined; doublure wide, inner margin subparallel to lateral border furrow and, in part, close to eye socle. Hypostoma forked, longer than wide; sub-hexagonal middle body strongly convex, clearly delimited by deep, wide lateral border furrows and shallow posterior border furrow; posterolateral maculae distinct; lateral border widens posteriorly, with margin adaxially curved; posterior fork broadly based, bluntly pointed; broadly rounded median notch 30 per cent. overall length of hypostoma; borders covered with widely-spaced ridges subparallel to margin.

Thorax parallel-sided, with convex, uniformly wide axis about one-third overall width. Axial furrow deep, broad. Pleurae transverse as far as fulcra, where curve gently backwards and down, each narrowing to a pointed tip. Pleural furrow runs slightly backwards abaxially, shallowing adaxially on external surface.

Pygidium has length 50–53 per cent. width and is broadly rounded posteriorly. Convex axis has frontal width about 25 per cent. that of pygidium, tapering gently to the fourth ring furrow and then strongly to rounded tip, reaching inner margin of border; there are seven axial rings and terminal piece in addition to short (sag.) articulating half ring; ring furrows shallow on external surface, deep on exfoliated surface, and become fainter posteriorly. Axial furrow deep. Pleural field vaulted, with seven or eight ribs divided by deep, broad pleural furrows which end at inner margin of border; ribs convex, faintly furrowed, well rounded abaxially; articulating half-rib ridge-like, with broad (tr.) facet. Border slightly declined towards margins, occupies 17–20 per cent. pygidial length at sagittal line and widens gradually abaxially; no border furrow, but border well defined by change in convexity. Concave doublure 50–55 per cent. of frontal width of pleural region and is densely covered with terrace ridges subparallel to margins; inner margins of doublure diverge forwards from abaxial ends of sixth ring furrow, and extend backwards along the axial furrows to meet at tip of axis.

Genus MIOPTYCHOPYGE gen. nov.

Derivation of name. Mio (Greek, less) with *Ptychopyge*, a well known Baltoscandian asaphine genus.

Type species. Ptychopyge trinodosa Zhang, 1981.

Diagnosis. Cephalon semi-elliptical with broadly based librigenal spines; frontal area quite long (sag.); border flat, well defined; doublure wide (sag.). Cranidium bluntly pointed frontally; glabella relatively narrow; bacculae elongate, very narrow; preglabellar field shorter (sag.) than border; anterior sections of facial sutures diverge forwards slightly, intramarginal anteriorly; posterior sections sigmoidal. Eyes moderately large, located posteriorly. Hypostoma forked. Tips of thoracic pleurae extend into short, backwardly directed spines. Pygidium with uniformly tapered axis; inner part of pleural region with furrowed ribs; border slopes gently at periphery with no border furrow; doublure fairly broad, its inner margins diverging forwards from ends of sixth ring furrow.

Remarks. Some closely related Chinese species have in common a combination of characters transitional between *Ptychopyge* (*s.l.*) and *Pseudobasilicus* (*s.l.*). Baltoscandian species formerly included in these two groups were reassigned by Balashova (1964, 1971, 1976) to several genera and

subgenera, but relevant Chinese forms do not fit readily into any of them and the present group of species is sufficiently distinct to warrant allocation to a new genus. *Mioptychopyge* includes, in addition to the type species, the following Chinese taxa: *Asaphus suni* Endo, 1932 (p. 112, pl. 39, figs 11–17; 1935, p. 218; provisionally reassigned to *Ptychopyge* by Lu *et al.* 1965 and to *Ningkianites* by Chang and Jell 1983), *Basiliella zhenbaensis* Zhou, *in* Li *et al.*, 1975 (p. 150, pl. 18, figs 3–5) and *Pseudobasilicus taotsaotzensis* Lu, *in* Lu *et al.*, 1976 (p. 63, pl. 10, fig. 3). *Ptychopyge thebawi* Reed, 1915 (p. 32, pl. 6, figs 5–8) from the Hwe Mawng Beds (lower Ordovician), Northern Shan States, Burma, is also referable to the genus. Among the listed species, *Mioptychopyge zhenbaensis* and *M. suni* are both based on material from the same horizon (probably latest Arenig–Llanvirn) in the Siliangssu Formation of southern Shaanxi, and original specimens of *M. suni*, refigured by Chang and Jell (1983, fig. 4A–F) are virtually identical to those of *M. zhenbaensis*. The latter species differs only in having deeper pleural furrows on the pygidium, a character insufficient to justify specific separation.

Several late early Ordovician species from the Yangtze region, such as *Pseudobasilicus dawanicus* Lu, 1975 (p. 312, pl. 6, figs 1–3; pl. 7, figs 1–2), *Pseudobasilicus pseudodawanicus* Lu, 1975 (p. 314, pl. 5, fig. 25; pl. 6, figs 4–6), *Ptychopyge neichiensis* Kobayashi, 1951 (p. 30, pl. 2, figs 5–6), *Ptychopyge orientalis* Kobayashi, 1951 (p. 29, pl. 2, figs 3–4) and *Pseudobasilicus xiaotanensis* Zhang, *in* Qiu *et al.*, 1983 (p. 203, pl. 67, fig. 11) are believed to be allied, or even belong, to *Mioptychopyge*. However, they are founded either on juvenile specimens (*P. dawanicus*, *P. xiaotanensis*) or on inadequate or imperfectly preserved material (*P. orientalis*, *P. neichiensis*, *P. pseudodawanicus*). These forms are insufficiently well known for adequate revision.

Pseudobasilicus (*s.l.*) resembles *Mioptychopyge* especially in the presence of thoracic pleural spines, the fairly broad pygidial doublure (see, for example, Schmidt 1904, pl. 4, figs 3, 5, 7, for the type species of *Pseudobasilicus*, *P. lowrowi*) and the deeply and broadly indented posterior margin of the hypostoma. But it differs in the more divergent anterior sections and less sigmoidal posterior sections of the facial suture; the shorter frontal area; the absence of bacculae; the proportionally wider cephalon, librigena and pygidium; the narrower cephalic doublure; the stouter cranidium; the more posterior position of the eye (which almost reaches the posterior border furrow); the long (tr.), narrower (exsag.) posterior area of the fixigena, which narrows abaxially (cf. widens in *Mioptychopyge*); and the flatter pygidial border.

The relatively elongate cranidium, the strongly sigmoidal posterior sections and gently divergent anterior sections of the facial suture, and the postocular bacculae of the new genus are suggestive of *Ptychopyge* (*s.l.*); but in the latter there are no thoracic pleural spines, the posterior notch of the hypostoma is narrower (tr.) than that of *Mioptychopyge suni* (Endo) (see Zhou, *in* Li *et al.* 1975, p. 18, fig. 4), and the pygidial border is generally flat and well defined. Some other features of *Mioptychopyge* are shared with genera of the *Ptychopyge* group (*Ptychopyge s.s.*, *Pseudoptychopyge*, *Paraptychopyge*, *Metaptychopyge*) as follows: the broad cephalic doublure in *Mioptychopyge* is comparable to that of *Ptychopyge* (*s.s.*) and *Metaptychopyge*; the course of the anterior sections of the facial suture is similar to that in *Pseudoptychopyge*; the length of the frontal area and the position of the palpebral lobe compare to those of *Ptychopyge* (*s.s.*); and the broad pygidial doublure agrees with that of *Paraptychopyge*. The exoskeleton of *Mioptychopyge* is, in our opinion, closer to *Ptychopyge* (*s.l.*) than to *Pseudobasilicus*.

EXPLANATION OF PLATE 3

Figs 1, 3. *Zhenganites xinjiangensis* (Zhang, 1981); Bed 3. 1, NI 80731; cephalon with thorax; ×1·2. 3, NI 80732; pygidium, with two attached thoracic segments; ×1.

Figs 2, 4–10. *Mioptychopyge trinodosa* (Zhang, 1981). 2, NI 80733; Bed 3; pygidium; ×2. 4–5, 7. NI 80734; Bed 2; exoskeleton, dorsal and lateral views; ×2. 6, NI 80735; Bed 2; pygidium, showing doublure; ×1. 8, NI 80736; Bed 2; pygidium with thorax; ×2. 9, NI 80737; Bed 3; pygidium; ×1. 10, NI 80738; Bed 3; small pygidium; ×4.

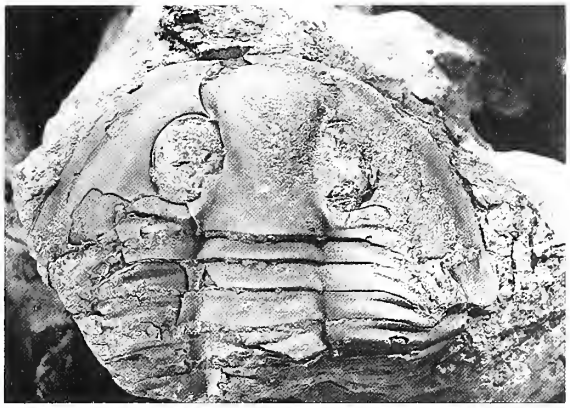

1

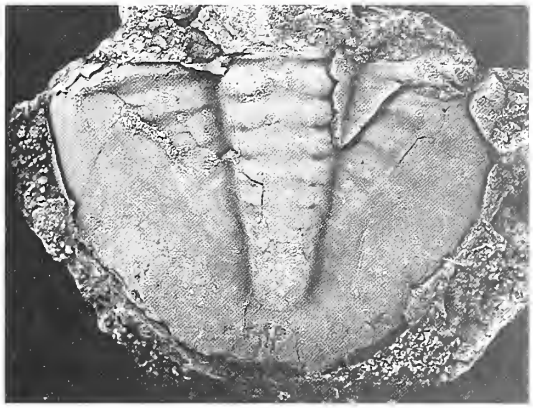

2

3

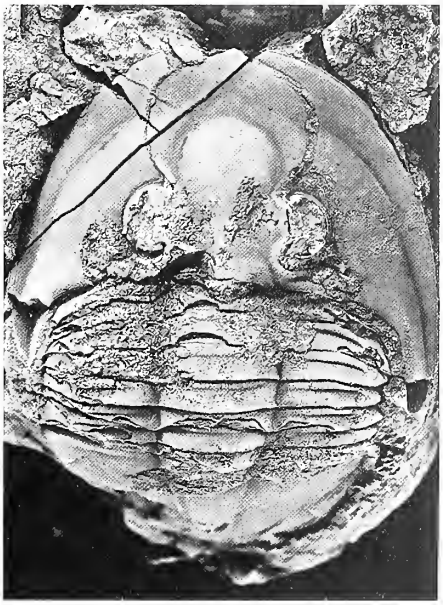

4

5

6

7

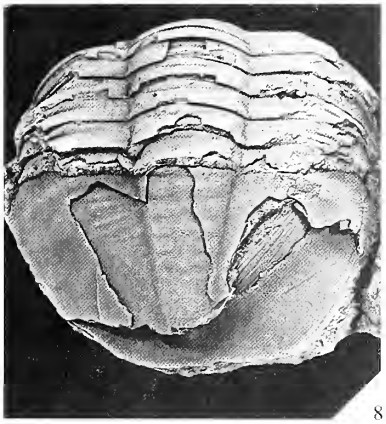

8

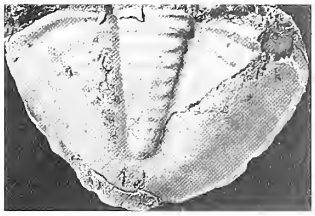

9

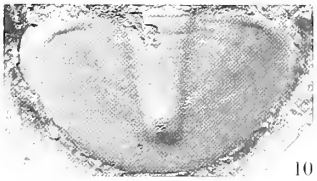

10

ZHOU *et al.*, *Zhenganites*, *Mioptychopyge*

Mioptychopyge trinodosa (Zhang, 1981)

Plate 3, figures 2, 4–10; Plate 4, figure 1

1981 *Ptychopyge trinodosa* Zhang, p. 185, pl. 65, fig. 10a–c

Holotype. Exoskeleton (XTR 202), figured Zhang (1981, pl. 65, fig. 10a–c), from the topmost Upper Qiulitag Group (= Dawangou Formation) at Kanlin, Kalpin, north-western Tarim, Xinjiang.

Figured specimens. One exoskeleton (NI 80734), one pygidium with thorax (NI 80736), one pygidium (NI 80735), and one cephalon with three attached thoracic segments (NI 80739) from Bed 2; three pygidia (NI 80733, 80737–80738) from Bed 3.

Description. Exoskeleton oval, gently convex. Semi-elliptical cephalon as long as pygidium, its length 55 per cent. the posterior width; cephalic border flat, one-fifth the cephalic length (sag.), narrows gradually abaxially and posteriorly, well defined by distinct, broad border furrow. Cranidium slightly wider than long, with width (tr.) of frontal area about two-thirds that along the posterior margin. Glabella convex, contracted opposite palpebral lobes, rounded frontally, two-thirds as wide as long, with prominent median node immediately in front of weak S0. Posterolateral furrows shallow, running backwards and abaxially from line through front end of palpebral lobe to meet at mid-point of S0; posterolateral lobe low, triangular. Three pairs of sub-triangular, smooth muscle-attachment areas on anterior part of preoccipital glabella are elongate and closely spaced; they extend adaxially forwards from axial furrows and become successively fainter and narrower (exsag.) anteriorly; second pair is opposite anterior end of palpebral lobe. Auxiliary impressions densely grouped in central part of frontal lobe demarcate an axially extended, spear-shaped ridge. Occipital ring uniformly wide (sag.), 14 per cent. of glabellar length. Distinct axial furrows shallower opposite palpebral lobe. Well preserved specimens show narrow (tr.), elongate baccula ill-defined abaxially, running between posterior end of palpebral lobe and proximal end of posterior border furrow. Palpebral lobe semicircular, 22 per cent. of cranidial length; distance between its posterior end and cranidial margin about one-eighth cranidial length. Anterior sections of facial suture run in broad curves on to border and then turn adaxially to meet medially at about 130° on margin; sigmoidal posterior sections cut posterior margin closer to axial furrow than to lateral margin. Frontal area 30 per cent. of cranidial length (sag.); preglabellar field shorter (sag.) than anterior border and slightly convex longitudinally. Palpebral area higher than posterolateral glabellar lobe; posterior area short (exsag.), narrows adaxially, and convex border well defined by deep border furrow. Librigena has wide, gently convex librigenal field; posterior border faintly defined; eye crescentic, 25 per cent. cranidial length; eye socle narrow, vertical; lateral and posterior borders and librigenal field narrow posteriorly, continuous with broadly based librigenal spine, sub-rhombic in cross section; doublure wide, its inner margin subparallel to lateral cephalic margin and, in part, close to eye socle.

Thoracic axis convex, slightly tapered, a little narrower (tr.) than adjacent pleura, delimited by broad, deep axial furrows. Axial rings uniformly wide (sag.); proximal part of each pleura parallel-sided, horizontal, but faceted distal part narrows abaxially to form moderately long spine; pleural furrow deep, subparallel to anterior margin of pleura, ends opposite midlength (tr.) of facet.

Pygidium semi-elliptical, moderately convex, without well defined border; width 60–82 per cent. the length (relatively longer in larger specimens). Convex, evenly tapered axis occupies 74–80 per cent. pygidial length, 24–32 per cent. anterior width, and is defined by deep axial furrows; there are six to ten axial rings and a rounded terminal piece, separated by shallow, broad ring furrows; segmentation more weakly developed on external surface than on exfoliated surface; each ring, when exfoliated, shows pair of oval muscle scars laterally; articulating half ring narrow (sag.), broadly rounded anteriorly. Pleural region moderately convex, declines laterally and posteriorly to pygidial margin; articulating half-rib ridge-like, widens to facet; incised first pleural furrow does not reach margin; five pairs of broad pleural furrows seen adaxially on exfoliated surface cross paradoublural line and die out; five pairs of ribs faintly furrowed. Doublure fairly broad; inner margins reach sixth ring furrow along axial furrows and then diverge forwards to attain frontal width 36–60 per cent. of pleural region; surface covered with terrace lines subparallel to margin. There are very fine transverse ridges on surface of axis and pleural region, and roughly transverse, fine anastomosing ridges on anterolateral angles.

Remarks. The present species most resembles *M. suni* (Endo, 1935), the type specimens of which have a pygidium with proportionally shorter (sag.) postaxial region, only 10–16 per cent. of pygidial length compared with 20–26 per cent. Cranidia in Endo's collection are too fragmentary to

interpret, but a sagittal muscle scar and auxiliary pit-like depressions seen on exfoliated surface of preoccipital part of the glabella are exactly comparable. An exfoliated cranidium of *M. suni* described by Zhou (*in* Li *et al.* 1975, p. 150, pl. 18, fig. 3) as *Basiliella zhenbaensis* (see above) compares closely to the present species except for the narrower (sag.) frontal area (21 per cent. length of cranidium) and deeper posterolateral glabellar and occipital furrows. However, the depth of furrows in trilobites, particularly asaphids, may vary with preservation.

The cranidium and pygidium of *M. trinodosa* recall *M. tatzaoensis* (Lu, *in* Lu *et al.* 1976), from the upper Ordovician of Ninglang, north-western Yunnan, and the Burmese species *M. thebawi* (Reed, 1915) (see above). But *M. thebawi* has a shorter (sag.) cephalic border and frontal area, *M. tatzaoensis* has a shorter (sag.) pygidial axis, and both have a longer glabella and deeper pleural furrows on the pygidium. *M. trinodosa* also resembles *Pseudobasilicus pseudodawanicus* Lu from the upper Dawan Formation (late Arenig) of western Hubei in many respects. The holotype (Lu 1975, pl. 5, fig. 25) of the latter has more divergent anterior sections of the facial suture, the front of the cranidium is more bluntly pointed, and the median node sited slightly more forwards, but some supposedly distinguishing characters are due to preservation. Specimens of the Hubei species are poorly preserved and further comparison is impossible. *P. pseudodawanicus* should be attributable to *Mioptychopyge* if its cephalic doublure and pygidium prove similar to those of *M. trinodosa.*

Subfamily ISOTELINAE Angelin, 1854

Genus LIOMEGALASPIDES Lu, 1975

Type species. Isotelus usuii Yabe, *in* Yabe and Hayasaka, 1920.

Liomegalaspides major (Zhang, 1981)

Plate 4, figures 2–7, 9

1981 *Ptychopyge major* Zhang, p. 185, pl. 65, figs 11–12.

Holotype. Pygidium (XTR 203), figured Zhang (1981, pl. 65, figs 11–12), from the topmost Upper Qiulitag Group (= Dawangou Formation) at Kanlin, Kalpin, north-western Tarim, Xinjiang.

Figured specimens. Three pygidia (NI 80742–80744) from Bed 2; one incomplete cranidium (NI 80741) and one pygidium (NI 80740) from Bed 3.

Description and remarks. The species was based by Zhang (1981) on two large pygidia. The holotype has a narrow doublure but no defined border, indicating that the species is referable to *Liomegalaspides* or *Megalaspides* rather than to *Ptychopyge.* Based on the new material we add the following description: (1) glabella is broadly rounded anteriorly, constricted between palpebral lobes and poorly defined on exfoliated surface; (2) frontal area is short (7 per cent. of cranidial length (sag.)) and flat; (3) palpebral lobe higher than glabella, its length about 20 per cent. that of cranidium and its anterior margin opposite centre of cranidium; (4) posterior area of fixigena short (exsag.), with no trace of posterior border furrow on external surface; (5) pygidial axis has short articulating half-ring, 11 rings and a small, posteriorly rounded terminal piece seen on exfoliated surface; (6) pleural regions gently convex with pair of articulating half-ribs defined by deep pleural furrows; (7) up to nine pairs of weakly furrowed ribs visible on internal mould; (8) pygidial doublure concave, narrow, uniformly wide, covered with fine terrace ridges, its inner margin subparallel to pygidial margin and just reaches end of axis; (9) length of pygidium 70–90 per cent. of width, and large specimens are more elongated. *L. major* differs from the type species of *Megalaspides, M. dalecarlicus* (Holm) from its named zone in the Arenig of Sweden (see Tjernvik 1956, p. 247, pl. 8, figs 4–13, text-figs 39C, 40A), in the longer sub-triangular pygidium, an hourglass-shaped rather than parallel-sided glabella, a shorter frontal area, and more divergent anterior sections of the facial suture. All these characters are diagnostic of *Liomegalaspides.*

The name *Liomegalaspides* as first proposed by Lu (*in* Lu and Chang 1974) was a *nomen nudum*, with no diagnosis or designation of type species. The genus was formally established by Lu (1975, p. 327) to include *L. hupeiensis* (Sun, 1931, p. 4, pl. 1, fig. 3a–h; Kobayashi 1951, p. 16, pl. 4, fig. 3 only; Lu, *in* Lu and Chang 1974, p. 126, pl. 49, figs 15–16; Lu 1975, p. 328, pl. 13, figs 8–10), from the *Azygograptus suecicus* Zone (mid Arenig) of Hubei and Sichuan, in addition to the type species *L. usuii* (Yabe, *in* Yabe and Hayasaka, 1920, p. 57, pl. 18, fig. 9; pl. 19, fig. 8; Kobayashi 1951, p. 27, pl. 2, figs 7–8; Lu, *in* Lu and Chang, 1974, p. 126, pl. 50, figs 1–2; Lu 1975, p. 328, pl. 13, figs 1–7), from the uppermost Dawan Formation (latest Arenig), western Hubei.

Other species from the upper lower Ordovician of the Yangtze Region possibly referable to the genus are: *Megistaspis* sp. of Li *et al.* (1975, p. 145, pl. 10, fig. 6), *Liomegalaspides huayingshanensis* Lee, 1978 (p. 239, pl. 102, figs 2–4), *L. banqiaoensis* Yin, *in* Yin and Lee, 1978 (p. 531, pl. 175, fig. 4), *Megalaspides zhenganensis* Yin, *in* Yin and Lee, 1978 (p. 530, pl. 174, figs 11–12), *M. xinhuangensis* Liu, 1982 (p. 327, pl. 223, fig. 9) and *M. yichangensis* Xiang and Zhou, 1987 (p. 315, pl. 36, fig. 14). Some of these are, however, based on poorly preserved specimens and require further revision.

Isoteloides liangshanensis Lu, 1957 (p. 279, pl. 152, figs 1–2; 1975, p. 322, pl. 9, figs 6–10, pl. 10, figs 1–11; Zhou *et al.* 1982, p. 263, pl. 65, fig. 16) from the *Ningkianolithus welleri* Zone (latest Arenig) in the Siliangssu Formation at Hanzhong, southern Shaanxi, is closely similar to the contemporaneous *L. usuii*, although the latter has less well defined furrows. Accurate comparison is difficult due to their different preservation, the former in shale and the latter in limestone. It is likely that *I. liangshanensis* is referable to *Liomegalaspides*, and the narrow cranidial border and more acute posterior area of the fixigena preclude its assignment to *Isoteloides*. Fortey (1979, p. 69) was inclined to reassign the species to *Stegnopsis* Whittington, 1965, but the type species, *S. solitarius* Whittington, 1965 (p. 344, pl. 20, figs 1–11; pl. 21, figs 1–4, 6; text-fig. 3) from the Table Head Formation of western Newfoundland, has a much wider cephalic border, more divergent anterior sections of the facial suture, a more posteriorly located palpebral lobe, and a much narrower (exsag.) postocular area of the fixigena.

Of the 12 asaphid species recorded by Weller (1907, 1913) from the upper lower Ordovician of northern Sichuan and southern Shaanxi, *Asaphus blackwelderi* Weller, 1913 (p. 286, pl. 26, figs 21–22; Chang and Jell 1983, fig. 3B, H) and *A. asiaticus* Weller, 1913 (p. 287, pl. 26, fig. 5; Chang and Jell 1983, fig. 3I) are indistinguishable from *L. liangshanensis* and we believe that all should be included in *L. blackwelderi*, the first described of the three.

L. major generally resembles the type species, *L. usuii*, but the latter has a proportionally shorter pygidium which is almost featureless except for a faint trace of axial furrows. *L. blackwelderi* compares closely with *L. major* in almost every respect, but has a shorter pygidium (length = 67–77 per cent. of width), a difference which may fall within the range of intraspecific variation, but this cannot yet be confirmed.

EXPLANATION OF PLATE 4

Figs 1. *Mioptychopyge trinodosa* (Zhang, 1981); Bed 2. NI 80739; incomplete cephalon with three attached thoracic segments; × 1·5.

Figs 2–7, 9. *Liomegalaspides major* (Zhang, 1981). 2–3, NI 80740; Bed 3; pygidium, dorsal and lateral views; × 2. 4, NI 80741; Bed 3; incomplete cranidium; × 2·5. 5, NI 80742; Bed 2; pygidium, showing part of doublure; × 1·5. 6, NI 80743; Bed 2; pygidium; × 0·66. 7, 9, NI 80744; Bed 2; pygidium, lateral and dorsal views; × 1.

Figs 8, 11–13. *Nileus walcotti* Endo, 1932. 8, NI 80746; Bed 3; cephalon of enrolled exoskeleton, × 1·5. 11–12, NI 80747; Bed 3; cephalon and thorax of enrolled exoskeleton, dorsal and lateral views; × 1·5. 13, NI 80748; Bed 2; cephalon with four attached thoracic segments; × 2.

Fig. 10. *Gog yangtzeensis* (Lu, 1975); NI 80745; Bed 3; incomplete pygidium; × 1.

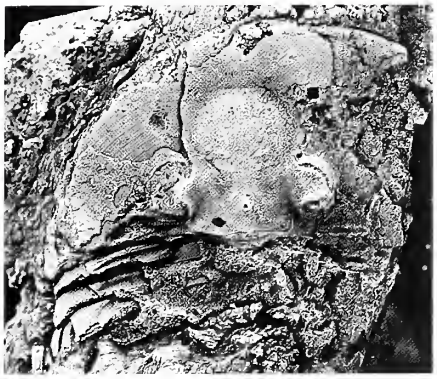

1

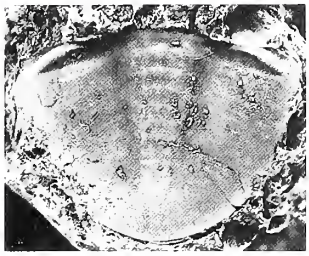

2

3

4

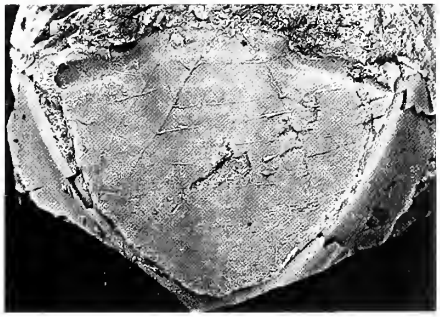

5

6

7

8

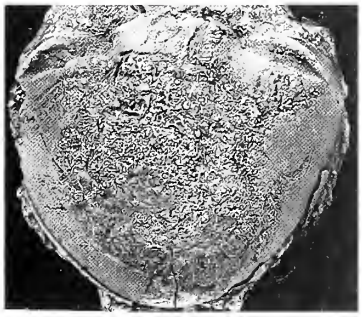

9

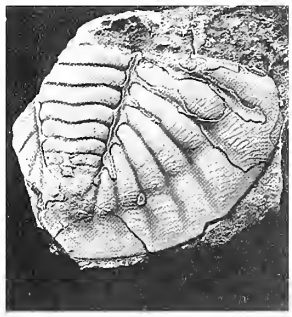

10

11

12

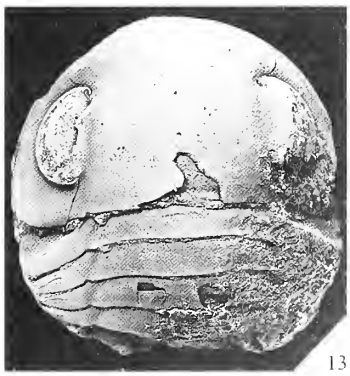

13

ZHOU *et al.*, Ordovician trilobites

Subfamily NIOBINAE Jaanusson, *in* Moore, 1959

Genus GOG Fortey, 1975*b*

Type species. Gog catillus Fortey, 1975*b*.

Gog yangtzeensis (Lu, 1975)

Plate 4, figure 10

1975 *Niobe yangtzeensis* Lu, p. 332, pl. 15, figs 4–5.
1977 *Niobe yangtzeensis* Lu; Zhou *et al.*, p. 214, pl. 63, fig. 13.
1984 *Niobe yangtzeensis* Lu; Sun, p. 379, pl. 147, figs 12–13.

Holotype. Pygidium (NI 16618), figured Lu (1975, pl. 15, fig. 4), from the upper Dawan Formation (late Arenig) at Tangya, Fenxiang, Yichang, western Hubei.

Figured specimen. Incomplete pygidium (NI 80745) from Bed 3.

Description. Semicircular pygidium has length 37 per cent. of width. Tapered convex axis is 77 per cent. of pygidial length and does not reach border furrow; seven well defined axial rings with ring furrows curved backwards medially; axial furrows deep; triangular terminal piece poorly delimited by weak axial furrows on exfoliated surface but merges with seventh pair of pleural ribs on external surface. Pleural region gently convex, with articulating half-rib and seven prominent, distally rounded ribs; deep, wide pleural furrows cross paradoublural line and border furrow almost to pygidial margin, and are successively more backwardly deflected. Articulating half-rib convex, widens (exs.) abaxially; facet low, short (exsag.), half pleural width; weak interpleural furrows seen on exfoliated surface. Border wide, flat; border furrow subparallel to margin, deep and wide from first pair of pleural furrows but shallows abruptly medially. Doublure reaches sixth ring furrow; inner margin slightly undulating, subparallel to border furrow. Surface of pleural region covered with dense anastomosing ridges, subparallel to margin, which become even finer and denser inside paradoublural line.

Remarks. Apart from its slightly greater width and broader border, the pygidium agrees well with that of *Gog explanatus* (Angelin, 1851, pl. 11, fig. 4; Fortey 1975*b*, pl. 4, fig. 2), from black limestone (probably late Arenig) at Skåne, Fågelsång, Sweden. It differs from that of *G. catillus* Fortey, 1975*b* (p. 26, pl. 1, fig. 1; pl. 2, fig. 1; pl. 3, figs 4–6), from the Olenidsletta Member (mid Arenig), Spitsbergen, and *G. pileiformis* Zhou, *in* Zhou *et al.*, 1982 (p. 264, pl. 66, figs 4–5), from the Miboshan Formation (Llanvirn), Tongxin, Ningxia, mainly in having a well defined border furrow and seven instead of eight or nine ribs. The less undulating margin of the doublure in *G. pileiformis* is, however, comparable.

The figured pygidium is identical with the holotype of *Niobe yangtzeensis*, described by Lu (1975, p. 332) as having six pairs of ribs, though a small seventh pair is present in the type material. The species recalls several Scandinavian early Ordovician forms of *Niobe*, such as the type species *N. frontalis* (Dalman, 1827) (Bohlin 1955, p. 143, pl. 6, figs 5–9), *N. insignis* Linnarsson, 1869 (Moberg and Segerberg 1906, p. 94, pl. 6, figs 6–9; Tjernvik 1956, p. 224, pl. 4, fig. 10, text-fig. 36A), *N. emarginula* Angelin, 1851 (Tjernvik 1956, p. 226, pl. 4, figs 14–17, text-fig. 36C) and *N. incerta* Tjernvik, 1956 (p. 225, pl. 4, figs 11–13, text-fig. 36B), in the broad pygidial doublure and well defined pygidial border but differs mainly in the pleural furrows, which almost reach the pygidial margin before dying out. In addition, the first three of these Scandinavian species have six rather than seven pairs of ribs and the last three have straight or medially straight ring furrows.

As *Niobe yangtzeensis* Lu was based on only two pygidia, and there is no associated cranidium in our collection, its generic position remains uncertain, but we reassign it to *Gog* because of its close resemblance to *G. explanatus*.

Family NILEIDAE Angelin, 1854

Genus NILEUS Dalman, 1827

Type species. Asaphus (*Nileus*) *armadillo* Dalman, 1827.

Nileus walcotti Endo, 1932

Plate 4, figures 8, 11–13; Plate 5, figures 1–11

1932 *Nileus walcotti* Endo, p. 113, pl. 39, fig. 10.
1934 *Nileus armadillo* Dalman; Gortani, p. 73, pl. 17, figs 2–3, *non* 4.
1934 *Nileus armadillo* var. *expansus* Gortani, p. 76, pl. 17, fig. 5a–c.
1975 *Nileus liangshanensis* Lu, p. 353, pl. 23, figs 7–11; pl. 24, figs 1–3.
1975 *Nileus liangshanensis* Lu; Li *et al.*, p. 147, pl. 13, fig. 7.
1981 *Nileus liangshanensis* Lu; Zhang, p. 189, pl. 71, figs 1–2.
1981 *Nileus armadilloformis* Lu; Zhang, p. 189, pl. 71, figs 4–6.
1983 *Nileus armadillo* Dalman; Chang and Jell, p. 206, fig. 6A–B.

Holotype. Incomplete cephalon with thorax (USNM 83770), figured Endo (1932, pl. 39, fig. 10) and Chang and Jell (1983, fig. 6A–B), from a Llanvirn horizon in the Siliangssu Formation, near Ningqiang, southern Shaanxi.

Figured specimens. One cephalon with four attached thoracic segments (NI 80748), one pygidium with thorax (NI 80753) and one hypostoma (NI 80752) from Bed 2; four enrolled exoskeletons (NI 80746–80747, 80749, 80755), two cephala (NI 80750–80751), one cranidium (NI 80754), and one pygidium with attached thorax (NI 80756) from Bed 3.

Description and remarks. Kobayashi (1951, p. 39) considered *Nileus walcotti* to be a synonym of *N. armadillo*, from the upper Arenig and lower Llanvirn of Sweden. However, the holotype of *N. walcotti*, recently refigured by Chang and Jell (1983), shows a smaller, more anteriorly sited palpebral lobe and a longer (exsag.) posterior area of the fixigena compared with the specimens of *N. armadillo* described by Schrank (1972, p. 365, pl. 6, figs 1, 3, 5–6). In addition, the type species has the median glabellar node situated farther back, the posterior sections of the facial suture are more divergent posteriorly, and the axial furrows more weakly defined. The two species are probably distinct. *N. liangshanensis* Lu, 1975, from the same horizon as *N. walcotti* in southern Shaanxi, matches that species closely and is considered a synonym.

N. walcotti was fully described (as *N. liangshanensis*) by Lu (1975), and we add the following on the basis of new material: (1) the median glabellar node seen on internal moulds is opposite the rear of the palpebral lobe, about 40 per cent. of glabellar length from posterior margin in palpebral view; (2) hypostoma is 64 per cent. as long as wide, broadly notched posteriorly; convex middle body occupies 40 per cent. of overall frontal width, is longer than wide, tapers backwards and is bluntly pointed posteriorly, defined by deep, wide lateral furrows, with pair of depressed, oval maculae sited on lateral margins opposite centre of hypostoma; anterior wing small, triangular; border gently convex, bounded by almost uniformly narrow rim; lateral border narrows posteriorly and has broadly rounded margin. Short (sag.) posterior border tripartite with triangular median projection; surface covered with coarse, transverse terrace ridges; (3) pygidium is 52–63 per cent. as long as wide. Large pygidia, except for axis, have surface covered by coarse, anastomosing terrace ridges which extend more or less transversely on the border but are slightly concave forwards on pleural region; in small pygidia, up to seven finer ridges seen behind articulating facet are subparallel to anterolateral margin (Pl. 5, fig. 6).

Juvenile specimens (Pl. 5, figs 3, 7, 10) resemble large individuals, but the glabella is wider, more strongly declined anteriorly; palpebral area of fixigena is longer (exsag.), only weakly defined by faint axial furrow; and anterior part of librigena is narrower (tr.). The first two of these also characterize *N. armadilloformis* Lu, 1975 (p. 351, pl. 21, figs 1–12; pl. 22, figs 1–7) from the upper part of the Dawan Formation, western Hubei, which may be closely related to the present species.

Zhang (1981) recorded *N. liangshanensis* and *N. armadilloformis* from the same horizon and locality as the new material but his account of the latter species was based largely on a juvenile exoskeleton (Zhang 1981, pl. 71, fig. 5a–c). On the basis of our material we believe that only a single species, *N. walcotti*, is present in Zhang's collection.

Specimens from the uppermost Arenig–lower Llanvirn of Karakorum, described by Gortani (1934) as *Nileus armadillo* Dalman and *N. armadillo* var. *expansus* Gortani, match those of *N. walcotti*, as noted by Kobayashi (1951). We agree with this conclusion except for one cephalon (Gortani 1934, pl. 17, fig. 4a–b) in which the glabella expands uniformly forwards, has the axial glabellar node situated further back, and is well defined by deep axial furrows; the specimen is probably referable to *Symphysurus*.

N. liangshanensis has also been reported from the lower middle Ordovician of western Hubei (Sun 1984, p. 384, pl. 155, fig. 4) and upper lower Ordovician of Hexian, Anhui (Qiu *et al.* 1983, p. 212, pl. 71, figs 1–2), but the cranidia from both localities are quite different from Lu's original material. *N. liangshanensis sensu* Qiu *et al.* has the median glabellar node and palpebral lobe sited further back, and the axial furrows are distally convex opposite the palpebral lobe; in *N. liangshanensis sensu* Sun the glabella is defined by deep axial furrows and is strongly constricted opposite the midpoint of the palpebral lobe, which is again more posteriorly placed. Both species should probably be excluded from the synonymy of *N. walcotti*, but the specimens are too poorly preserved for confident assignment.

N. walcotti is closely related to the Swedish Arenig species *N. exarmatus* Tjernvik, 1956 (p. 209, pl. 2, figs 16–21; Schrank 1972, p. 358, pl. 2, figs 1–10; pl. 3, figs 3–11, 14) and *N. orbiculatoides orbiculatoides* (Schrank, 1972, p. 361, pl. 4, figs 1–5; pl. 5, figs 1–2, as *N. exarmatus orbiculatoides*; see Fortey 1975*b*, p. 43) on the evidence of the hypostoma, librigena, cephalic doublure and the shape of the glabella and pygidium. But the Swedish forms differ in the intramarginal instead of marginal anterior sections of the facial suture, the subangular rather than rounded anterior cranidial margin, the larger palpebral lobe, the more posteriorly placed median glabellar node, and the shorter, more divergent posterior sections of the facial suture.

In shape of posterior area of fixigena, size and position of palpebral lobe, and location of median glabellar node, the Chinese form is also comparable to *N. porosus* Fortey, 1975*b* (p. 44, pl. 12, figs 1–14) from the higher part (latest Arenig–early Llanvirn) of the Profilbekken Member on Spitsbergen. Characteristic of the latter are: (1) fainter axial furrows parallel opposite eyes (cf. distinct and progressively divergent backwards in *N. walcotti*); (2) cephalic doublure wider (sag.); (3) librigena lacks lateral border; (4) smooth hypostoma has wider but more weakly defined middle body, and lateral margins are almost parallel as far as posterolateral angles (cf. evenly curved); (5) cranidial surface punctate; and (6) pygidial border rather poorly defined.

Family ILLAENIDAE Hawle and Corda, 1847

Genus ILLAENUS Dalman, 1827

Type species. Entomostracites crassicauda Wahlenberg, 1818.

EXPLANATION OF PLATE 5

Figs 1–11. *Nileus walcotti* Endo, 1932. 1–2, NI 80749; Bed 3; enrolled exoskeleton, dorsal views; × 1·5. 3, NI 80750; Bed 3; small cephalon, lateral view; × 6. 4, 9, NI 80751; Bed 3; cephalon, lateral and dorsal views; × 3. 5, NI 80752; Bed 2; hypostoma; × 3. 6, NI 80753; Bed 2; pygidium with thorax; × 3. 7, 10, NI 80754; Bed 3; small cranidium, lateral and dorsal views; × 6. 8, NI 80755; Bed 3; enrolled exoskeleton, showing cephalic doublure; × 1·5. 11, NI 80756; Bed 3; pygidium with thorax, showing pygidial doublure; × 1·5.

Figs 12–13. *Illaenus sinensis* Yabe, *in* Yabe and Hayasaka, 1920; NI 80757; Bed 2; exoskeleton, dorsal and lateral views; × 2.

1

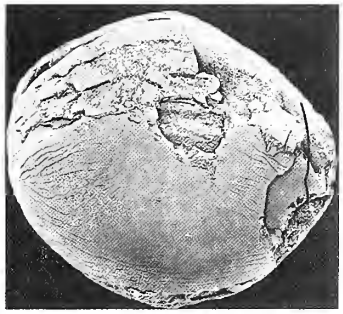

2

3

4

5

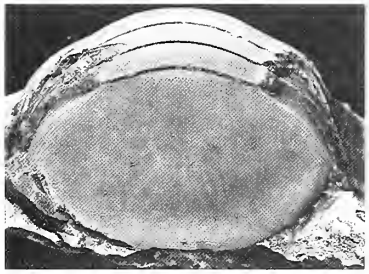

6

7

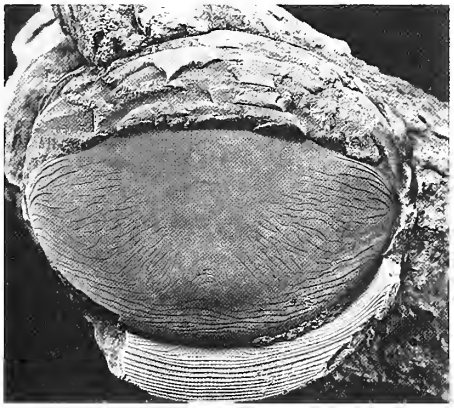

8

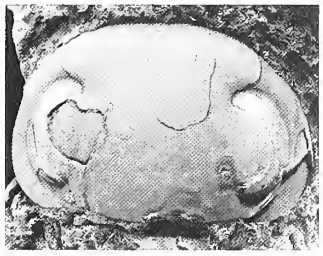

9

10

11

12

13

ZHOU *et al.*, *Nileus*, *Illaenus*

Illaenus sinensis Yabe, *in* Yabe and Hayasaka, 1920

Plate 5, figures 12–13; Plate 6, figures 1–4, 6, 9

1920 *Illaenus sinensis* Yabe, *in* Yabe and Hayasaka, p. 58, pl. 18, fig. 10.
1951 *Illaenus sinensis* Yabe; Kobayashi, p. 35, pl. 2, figs 1–2.
1957 *Illaenus sinensis* Yabe; Lu, p. 289, pl. 150, figs 1–4.
1965 *Illaenus sinensis* Yabe; Lu *et al.*, p. 561, pl. 118, figs 8–13.
1974 *Illaenus sinensis* Yabe; Lu and Chang, p. 128, pl. 51, figs 4–5.
1975 *Illaenus sinensis* Yabe; Lu, p. 380, pl. 31, figs 1–10; pl. 32, figs 1–5.
1977 *Illaenus sinensis* Yabe; Zhou *et al.*, p. 236, pl. 71, fig. 11a–c.
1978 *Illaenus sinensis* Yabe; Xia, p. 169, pl. 32, figs 7–9.
1981 *Illaenus sinensis* Yabe; Zhang, p. 194, pl. 72, fig. 9a–b.
1983 *Illaenus sinensis* Yabe; Qiu *et al.*, p. 220, pl. 74, fig. 7a–c.
1984 *Illaenus sinensis* Yabe; Sun, p. 390, pl. 150, figs 9–11.

Holotype. Cephalon and attached thorax, figured Yabe (*in* Yabe and Hayasaka 1920, pl. 18, fig. 10) and Kobayashi (1951, pl. 2, figs 1–2) from the uppermost Dawan Formation (latest Arenig), Yichang, western Hubei.

Figured specimens. One exoskeleton (NI 80757) from Bed 2; one exoskeleton (NI 80758), two pygidia (NI 80759, 80761) and one cephalon (NI 80760) from Bed 3.

Remarks. The species was redescribed by Lu (1975) using well-preserved specimens from the type area and horizon. Additional characters based on the new material are as follows: (1) pygidial doublure is about 60 per cent. length (sag.) of pygidium but narrows slightly abaxially; surface covered with widely spaced terrace lines subparallel to the margins but without medial groove; anterior margin broadly bicuspid; (2) pair of low, elliptical lunettes sited opposite eyes and abaxially adjacent to axial furrows, but less well defined on external surface than on internal mould; similar structures are also visible in well-preserved specimens from the Yangtze region figured by Lu (1975, pl. 31, fig. 3) and by Qiu *et al.* (1983, pl. 74, fig. 7a–c); (3) prosopon variable; in most specimens dorsal axis is traversed by distinct, anastomosing ridges, slightly curved, convex forwards, whilst similar, almost transverse ridges occur on genal region, subparallel to axial furrows on thoracic pleurae, and to pygidial margin on anterior part of pleural region; a small proportion of specimens have similar but much finer ridges on external surface of thorax, whilst cephalon and pygidium are almost smooth except for a few ridges along anterior flange of cephalon and pygidium; one exceptional but partly preserved cephalon (Pl. 6, fig. 6) is covered with coarse, anastomosing terrace ridges.

The bicuspid anterior margin of the pygidial doublure indicates that *I. sinensis* belongs to the *I. sarsi* species-group of Jaanusson (1957, p. 110). *I. sarsi* Jaanusson, 1954 (p. 575, pl. 2, figs 1–2; 1957, p. 114, pl. 4, figs 1–9), from the Llanvirn of Sweden, differs from the Chinese form in the shorter (sag.) pygidium and doublure, wider (tr.) fixigena, almost parallel posterior sections of facial suture, and less convex posterior part of glabella, but is otherwise similar. Two other members of the species group which closely resemble *I. sinensis* are: *I. hinomotoensis* Kobayashi, 1934 (p. 560, pl. 3, figs 22–29; Zhou and Fortey 1986, p. 193, pl. 10, figs 3–11, 13) [= *I. semioviformis* Kobayashi, 1934, p.

EXPLANATION OF PLATE 6

Figs 1–4, 6, 9. *Illaenus sinensis* Yabe, *in* Yabe and Hayasaka, 1920; Bed 3. 1–3, NI 80758; exoskeleton, dorsal and lateral views; × 1·5. 4, NI 80759; pygidium, showing doublure; × 1·5. 6, NI 80760; cephalon; × 2. 9, NI 80761; pygidium; × 2.

Figs 5, 7–8, 10–11. *Nanillaenus*? *primitivus* Zhang, 1981; Bed 3. 5, 7, NI 80762; pygidium of enrolled exoskeleton, dorsal and posterior views; × 3. 8, 11, NI 80763; cranidium, dorsal and lateral views; × 1. 10, NI 80764; right librigena; × 2.

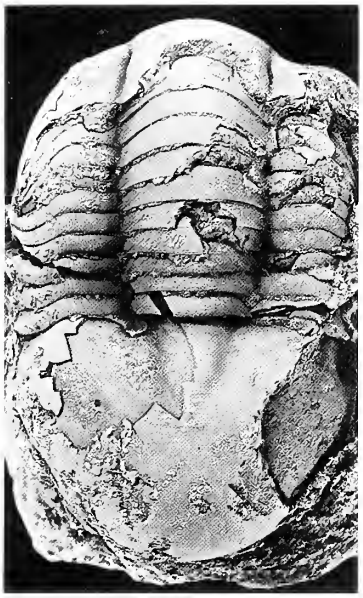

1

2

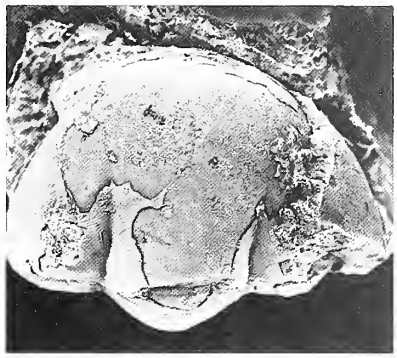

3

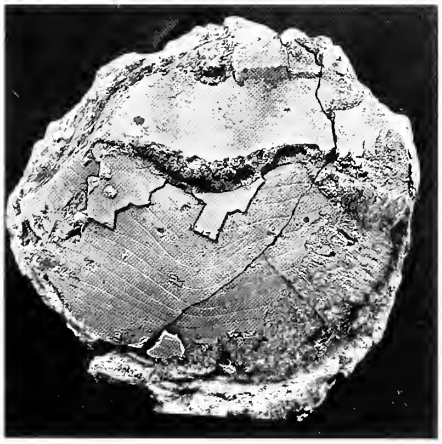

4

5

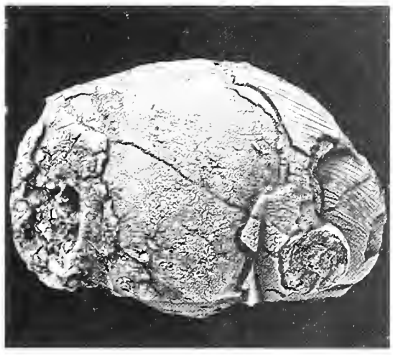

6

7

8

9

10

11

ZHOU *et al.*, *Illaenus*, *Nanillaenus*?

561, pl. 3, figs 30–31], the oldest species of *Illaenus* yet known, from the upper Tremadoc of South Korea and North China; and *I. tingi* Sun, 1931 (p. 10, pl. 2, fig. 3a–b; Zhou *et al.* 1984, pl. 20, fig. 4l–o) from the Llandeilo of Zunyi, Guizhou. The latter's cranidium agrees with that of *I. sinensis* but its pygidium is shorter (sag.), with broader axis, and the doublure occupies about 40 per cent. (cf. 60 per cent.) of pygidial length (sag.). The former species has a comparable pygidium but the doublure is shorter (sag.), crossed by a shallow median groove; the cranidium is longer, more gently declined; palpebral lobes are sited further forwards; and anterior sections of facial suture are subparallel instead of divergent forwards.

Illaenus sinensis is superficially similar, especially in its relatively long pygidium with narrow axis, to *I. spitiensis* Reed, 1912 (p. 95, pl. 14, figs 4–14; Gortani 1934, p. 88, pl. 19, fig. 3a–b) from the middle Ordovician of the central Himalayas and Karakorum, but in the latter the cranidium is more elongate, with completely defined glabella; the pygidium is less broadly rounded posteriorly with coarsely pitted external surface; the pygidial axis is much shorter (sag.), triangular, well defined posteriorly, and the pygidial doublure is much narrower (sag.), probably of *I. excellens* type (Jaanusson 1957, p. 111). A single cephalon referred by Gortani (1934, p. 83, pl. 43, fig. 7a–c) to *I. esmarki* (Schlotheim) [= *I. wahlenbergi* (Eichwald); see Jaanusson 1957, p. 139] from the upper lower Ordovician of Karakorum has a narrower glabella than *I. wahlenbergi* but is almost identical with that of *I. sinensis*. We omit it from our synonymy because the pygidium is unknown and, as Kobayashi (1951) noted, the posterior part of the glabella is less convex.

Genus NANILLAENUS Jaanusson, 1954

Type species. Illaenus conradi Billings, 1859.

Nanillaenus? primitivus Zhang, 1981

Plate 6, figures 5, 7–8, 10–11; Plate 7, figures 1–2, 6

1981 *Nanillaenus? primitivus* Zhang, p. 194, pl. 70, figs 5a–b, 6a–e.

Holotype. Incomplete exoskeleton (XTR 259), figured Zhang (1981, pl. 70, fig. 5a–b), from the topmost Upper Qiulitag Group (= Dawangou Formation), Kanling, Kalpin, north-western Tarim, southern Xinjiang.

Figured specimens. Two enrolled exoskeletons without librigenae (NI 80762, 80765), one cranidium (NI 80763) and one librigena (NI 80764) from Bed 3.

Description. Cranidium about 60 per cent. as long as wide, broadly rounded anteriorly, strongly curved down in front of line joining anterior ends of palpebral lobes. Axis convex (tr.) posteriorly, where it occupies 40 per cent. cranidial width; broad axial furrows converge and shallow forwards and die out frontally. Medium-sized palpebral lobe sited posteriorly; palpebral area protrudes strongly abaxially. Anterior sections of facial suture long, gently convergent forwards; posterior sections short, divergent. Librigena sub-triangular, steeply declined, with rounded genal angle; librigenal field slightly convex; eye semicircular and eye socle vertical; lateral border narrows posteriorly.

EXPLANATION OF PLATE 7

Figs 1–2, 6. *Nanillaenus? primitivus* Zhang, 1981; NI 80765; Bed 3; enrolled exoskeleton without librigenae, dorsal views; ×3.

Figs 3–4. *Carolinites ichangensis* Lu, 1975; Bed 2. 3, NI 80766; cranidium; ×5. 4, NI 80767; cranidium; ×6.

Figs 5, 7. *Ampyxina?* sp.; NI 80768; Bed 3; cranidium, dorsal and lateral views; ×4.

Figs 8–10. *Eccoptochile* sp.; NI 80769; Bed 2; exoskeleton. 8, 10, lateral and dorsal views of cephalon; ×3. 9, part of thorax and pygidium; ×4.

1

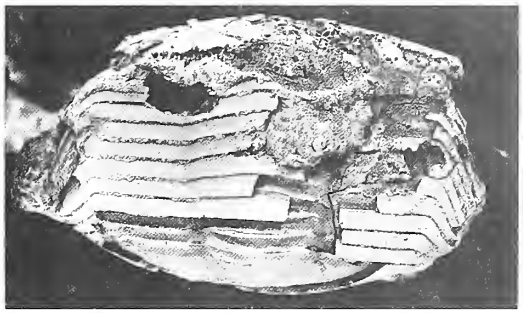

2

3

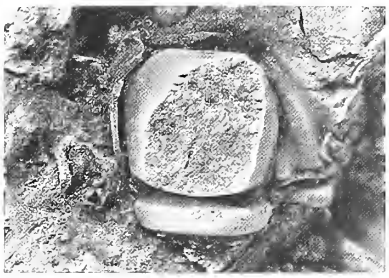

4

5

6

7

8

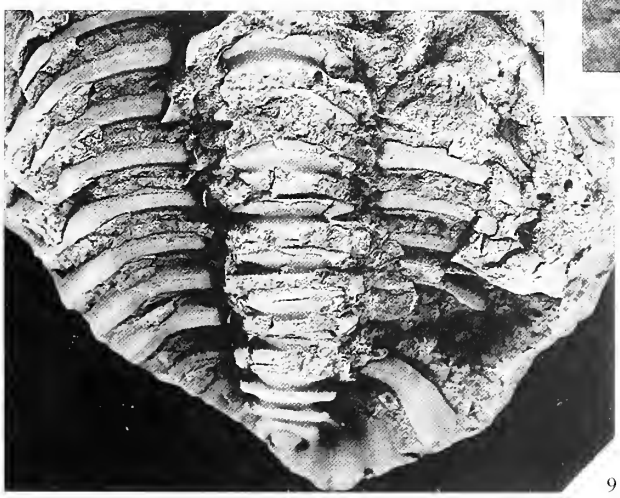

9

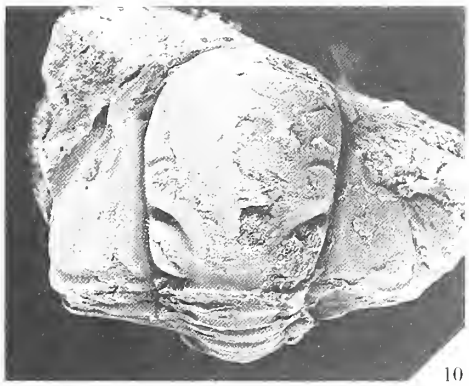

10

ZHOU *et al.*, Ordovician trilobites

Thorax of ten segments. Axis convex, about one-third overall width, slightly tapered backwards; axial furrows shallow. Pleural region featureless; inner part of each pleura horizontal, uniformly wide (exsag.); outer part (about one-fifth pleural width) faceted, bent down, and narrows to pointed tip.

Pygidium broadly rounded, 40–45 per cent. as long as wide, its width more than 70 per cent. that of cephalon; its anterior margin is straight as far as facet and then turns down sharply. Axis convex, tapered, occupies one-third frontal width of pygidium and merges posteriorly with pleural field; internal mould shows three poorly defined rings, narrow (sag.) articulating half ring delimited by shallow articulating furrow, and triangular terminal piece which is defined posterolaterally by pair of small oval muscle scars and is produced to form a postaxial ridge. Axial furrows broad. Pleural regions gently declined laterally and posteriorly; only broad first pleural furrow seen on internal mould. Doublure uniformly wide (tr.), equal to about one-quarter pygidial length (sag.); inner margin parallel to that of pygidium, just behind muscle scars medially.

External surface either smooth, or covered with anastomosing terrace ridges subparallel to margin on cephalon, and a few transverse ridges on pygidium. Doublure carries dense, fine terrace ridges, mostly subparallel to margin but flexing backwards slightly where they cross postaxial ridge.

Remarks. Apart from its smaller palpebral lobe and proportionally smaller pygidium with larger facets, the species could be referred to *Illaenus*. *I. angusticollis* Billings, 1859 (see Raymond and Narraway 1908, p. 245, pl. 61, figs 1–5), from the middle Ordovician of Quebec and Ottawa, Canada, closely resembles *N.*? *primitivus*, but differs in having a still smaller pygidium with posteriorly defined axis, eight or nine thoracic segments, and short librigenal spines. *I. angusticollis* was assigned by Jaanusson (1954) to *Nanillaenus*, in addition to the type species, *I. conradi* Billings (Raymond and Narraway 1908, p. 245, pl. 60, figs 9–10). Other species referred, some questionably, to *Nanillaenus* have been recorded from the middle Ordovician of North America (Shaw 1968, 1974; Chatterton and Ludvigsen 1976) and Scotland (Reed 1944; see also Tripp 1980, p. 132), and the Llanvirn of Argentina (Harrington and Leanza 1957). None is closely related to *N.*? *primitivus*, but *N.*? *punctatus* (Raymond 1905, p. 347, pl. 13, fig. 10; see Shaw 1968, p. 49, pl. 20, figs 17, 19, 21–28; 1974, p. 16, pl. 4, figs 3–4, 8, 10–18) resembles it in the fairly wide cranidium, the glabella well defined posteriorly by convergent axial furrows, the rounded genal angles, the ten thoracic segments, and the large pygidial facets; the Canadian species is distinguished by the better defined pygidial axis and anterior part of the glabella, the wider (sag.) pygidial doublure with bicuspid anterior margin and shallow median groove (instead of ridge), and the mostly pitted dorsal surface.

Shaw (1968, p. 49) considered *Nanillaenus* transitional between *Thaleops* and *Illaenus*, whilst Jaanusson (1954) regarded its eight-segmented thorax as distinctive of the genus; but according to Whittington (1963, p. 68) and Shaw (1968, p. 52) the number of thoracic segments is not a reliable generic criterion in illaenid classification. Chatterton and Ludvigsen (1976, p. 30) believed that *Nanillaenus* and *Thaleops* may prove synonymous with *Illaenus*. The present species exhibits characters intermediate between *Illaenus* and *Nanillaenus*, and we refer it questionably to the latter pending revision of the group.

Nanillaenus wuxiensis Lee, 1978 (p. 255, pl. 103, fig. 5) was based on a single pygidium from the uppermost Dawan Formation (latest Arenig), Wuxi, eastern Sichuan, and its generic position is uncertain in the absence of cephalon and thorax. The specimen differs from that of *N.*? *primitivus* in its broader, longer axis, well defined posteriorly, and in the faceted distal part of the anterior margin, which curves backwards only slightly.

Family TELEPHINIDAE Marek, 1952

Genus CAROLINITES Kobayashi, 1940

Type species. Carolinites bulbosus Kobayashi, 1940.

Carolinites ichangensis Lu, 1975

Plate 7, figures 3–4

1975 *Carolinites ichangensis* Lu, p. 288, pl. 2, figs 16–17.

1977 *Carolinites ichangensis* Lu; Zhou *et al.*, p. 187, pl. 55, figs 16–17.
1978 *Carolinites zunyiensis* Yin, *in* Yin and Lee, p. 507, pl. 169, fig. 13.
1983 *Carolinites ichangensis* Lu; Qiu *et al.*, p. 166, pl. 54, fig. 10.
1984 *Carolinites ichangensis* Lu; Sun, p. 367, pl. 146, fig. 11, *non* figs 12–14 [? = *C. bulbosus* Kobayashi, 1940].
1987 *Carolinites ichangensis* Lu; Xiang and Zhou, p. 306, pl. 34, figs 1–3.

Holotype. Cranidium (NI 16411), figured Lu (1975, pl. 2, fig. 16) from the uppermost Dawan Formation (latest Arenig), Tangya, Fenxian, Yichang, western Hubei.

Figured specimens. Two incomplete cranidia (NI 80766, 80767) from Bed 2.

Remarks. Specimens from Tarim match the holotype from the Yangtze region and show, in addition, that the surface of the cranidium is densely covered with fine granules. The species closely resembles *C. ekphymosus* Fortey, 1975*b* (p. 110, pl. 39, figs 1–13), from the upper Arenig of Spitsbergen, in the moderately large baccula, the finely granulate surface of the cranidium, the four-segmented pygidial axis, and the shape and proportions of the glabella. Further comparison is difficult owing to different size and preservation of figured specimens, but *C. ichangensis* has the fixigena apparently slightly wider than that of *C. ekphymosus*.

Carolinites [*Bathyurus*] *minor* (Sun, 1931, p. 19, pl. 3, fig. 1; see also Lu 1975, p. 290, pl. 2, fig. 20 and Sun 1984, p. 368, pl. 146, figs 9–10) and *C. subcircularis* Lu, 1975 (p. 289, pl. 2, figs 18–19) were both founded on small specimens from the middle–upper Dawan Formation (mid–late Arenig) of western Hubei, and differ from *C. ichangensis* in their broader fixigena and smaller baccula. These characters are in turn diagnostic of *C. transversus* Zhang, *in* Qiu *et al.*, 1983 (p. 167, pl. 54, figs 11–13) from the Shinianpan Formation (mid Arenig), Hexian, Anhui, and of the specimens from the corresponding horizon in western Hubei that Sun (1984, pl. 146, figs 12–14) referred to *C. ichangensis*. Evolutionary trends in *Carolinites* proposed by Fortey (1975*b*) suggest that the association of cranidial features seen in these Chinese forms is possessed only by *C genacinaca* Ross (*s.l.*), an early representative. The pygidium described for *C. subcircularis* and *C. transversus* has a three-segmented axis, and the librigena assigned to *C. transversus* has a very long, abaxially curved genal spine, suggesting that this group of closely related species belongs with *C. genacinaca genacinaca* Ross, 1951 (p. 84, pl. 18, figs 25–26, 28–36; Fortey 1975*b*, p. 112, pl. 37, figs 1–15, pl. 38, figs 1–3). Legg (1976, p. 5) and Henderson (1983, p. 146) recorded the type species *C. bulbosus* Kobayashi from the Arenig of, respectively, the Canning Basin and north-eastern Queensland, Australia, and suggested that *C. genacinaca* (*s.s.*) is a junior subjective synonym of the Australian species. We believe that *C. minor*, *C. subcircularis* and *C. transversus* may all prove to be junior synonyms of *C. bulbosus*, but further material from the Yangtze area is needed to clarify the nomenclature.

C. punctatus Zhang, *in* Qiu *et al.*, 1983 (p. 167, pl. 54, fig. 14), from the Xiaotan Formation (late Arenig–Llanvirn) strongly resembles *C. ichangensis* in the narrow fixigena and general form of the glabella, but is distinguished by the larger baccula and the dense, coarse granulation on the fixigena.

Family RAPHIOPHORIDAE Angelin, 1854
Subfamily RAPHIOPHORINAE Angelin, 1854

Genus AMPYXINA Ulrich, 1922

Type species. Endymionia bellatula Savage, 1917.

Ampyxina? sp.

Plate 7, figures 5, 7

Figured specimen. A cranidium (NI 80768) from Bed 3.

Description. Cranidium triangular, 54 per cent. as long as wide. Glabella extends for 37 per cent. of its length in front of fixigena, widest between front ends of fixigenae, where the width is 62 per cent. the sagittal length; occipital ring weakly convex, slightly arched backwards, defined by shallow S0; preoccipital portion of glabella strongly convex, broadly carinate, rounded and with tiny median tubercle anteriorly. Behind deeply incised, oval S1 the glabella is narrow (tr.) and expands over the short distance to S0; node-like L1 sited opposite adaxial end of posterior border. In front of S1, glabella is rhomboidal in outline, with four pairs of lateral muscle scars: two rearmost scars are large, sub-circular, depressed, close to each other; the anterior two are small, shallow, oval to triangular, closely spaced, with fourth scar just behind anterolateral angle of glabella. Baccula elongate, low, narrow (tr.), weakly defined abaxially and extends from end of S0 to point opposite anterior end of second muscle scar. Axial furrow deep, wide, shallower beside baccula. Fixigena triangular, moderately convex. Posterior border furrow deep, broad, transverse, ends at baccula opposite S1; almost parallel-sided posterior border is wide (exs.), convex. Facial suture gently curved, abaxially concave.

Remarks. According to Owen and Bruton (1980, p. 25) *Ampyxina* and *Raymondella* Reed, 1935 differ mainly in the thorax and pygidium. However, two cranidia in our collection have a rhomboidal rather than hemispherical glabella and elongate (exsag.) bacculae but lack anastomosing ridges on fixigena; for Whittington (1950, p. 559; 1959, pp. 487–488), these features are typical of *Ampyxina* rather than *Raymondella*, and we refer our specimens questionably to the former.

The Chinese form differs from other species of *Ampyxina* in its poorly defined, narrow (tr.), strip-like baccula, narrow (exsag.) fixigena, and the more forwardly protruding glabella. The anterior portion of the glabella in *Ampyxina lanceola* Whittington, 1959 (p. 486, pl. 34, figs 14–28; pl. 35, figs 26–35), from the Edinburg Formation (middle Ordovician) of Virginia, USA, is somewhat similar in outline but more rounded anteriorly, with a short frontal spine in the holotype instead of a tubercle, although the present specimen is larger. The latter may represent a new genus but is insufficient for formal definition.

Family CHEIRURIDAE Hawle and Corda, 1847
Subfamily ECCOPTOCHILINAE Lane, 1971

Genus ECCOPTOCHILE Hawle and Corda, 1847

Type species. Cheirurus claviger Beyrich, 1845.

Eccoptochile sp.

Plate 7, figures 8–10; Plate 8, figure 1; Text-figure 3

Figured specimen. Exoskeleton (NI 80769) from Bed 2.

Description. Exoskeleton elongate, oval in plan. Cephalon semi-elliptical, 32 per cent. overall length, 72 per cent. as long as wide, strongly convex. Highly convex glabella inflated, broadly rounded anteriorly, 70 per cent.

EXPLANATION OF PLATE 8

Fig. 1. *Eccoptochile* sp.; Bed 2; exoskeleton (see Pl. 7, figs 8–10), showing pygidium and thorax; ×3.

Figs 2–3, 6. *Sphaerocoryphe* (*Hemisphaerocoryphe*) *elliptica* (Lu, 1975); NI 80770; Bed 3; cephalon with thorax, dorsal and lateral views; ×5.

Figs 4–5. *Yanhaoia huayinshanensis* (Lu, 1975); NI 80774; Bed 3; cephalon with eight attached thoracic segments, dorsal and lateral views; ×3.

Figs 7–9. *Ovalocephalus primitivus extraneus* (Lu and Zhou, 1979); Bed 2. 7, NI 80771; cranidium. 8, NI 80772; pygidium. 9, NI 80773; pygidium with attached thoracic segments. All ×4.

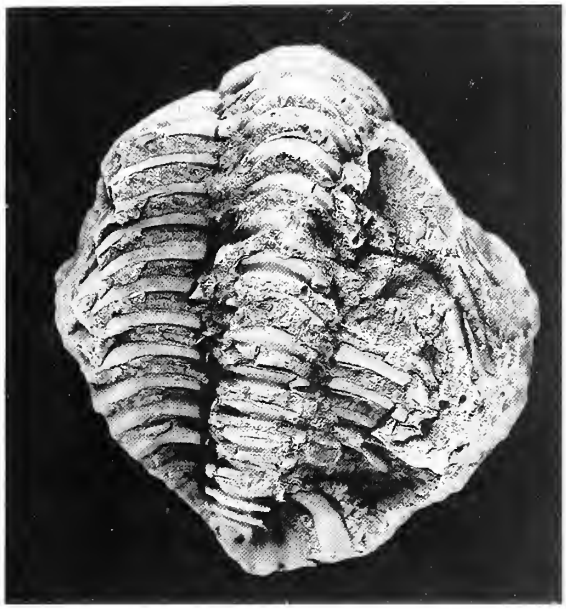

1

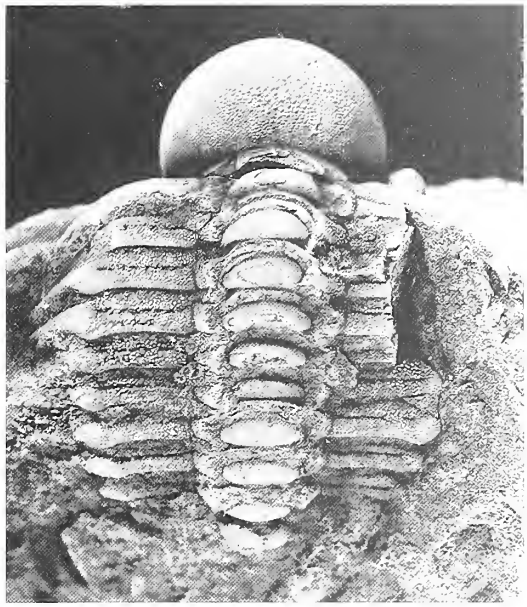

2

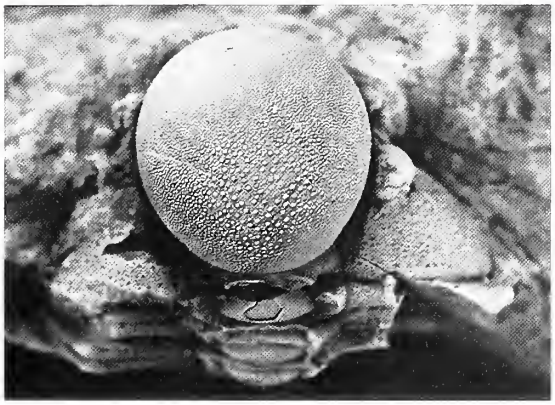

3

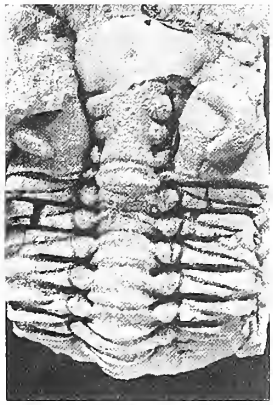

4

5

6

7

8

9

ZHOU *et al.*, Ordovician trilobites

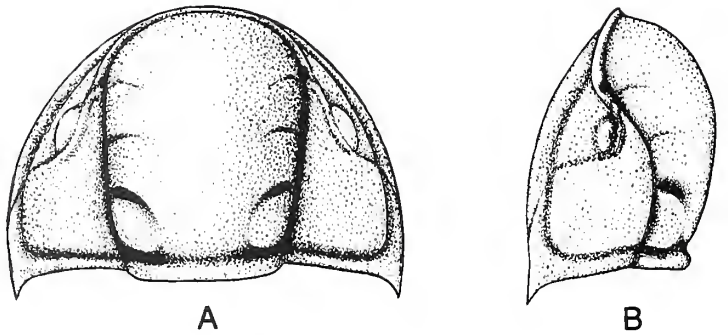

TEXT-FIG. 3. Reconstruction of cephalon of *Eccoptochile* sp., based on NI 80769. A, dorsal view; B, lateral view; ×3.

as wide as long, expands gently forwards to S3, where maximum width is 125 per cent. that of the base; occipital ring incompletely preserved; S0 broad, deep behind L1, shallow medially; frontal lobe overhangs deep preglabellar furrow; L1–L3 relatively narrow (tr.), subequal in length and width; L1 slightly bulbous, sub-triangular, 22 per cent. glabellar length and 25 per cent. basal glabellar width; S1 deep, wide, curved strongly backwards, shallowing markedly before reaching S0; S2 incised, arched forwards; S3 subparallel to S2 but shallower, with abaxial end behind fossula or anterolateral angle of glabella. Axial furrows wide, very deep. Palpebral lobe narrow, almost vertical, defined by distinct palpebral furrow that runs strongly backwards and slightly outwards, opposite frontal part of L2 and rear part of L3. Ocular ridge short, ends close to S3. Anterior sections of facial suture slightly convergent, meeting anterior cephalic margin in a broad curve; posterior sections run abaxially into lateral border, and curve through almost a right-angle to cut it obliquely. Anterior border narrow, upturned. Posterior area of fixigena rectangular, 30 per cent. of cephalic width, strongly declined abaxially; posterior border convex; posterior border furrow deep, wide, slightly narrower adaxially; lateral border furrow shallow. Palpebral and anterior areas sub-triangular, narrow (tr.). Librigena triangular, acutely angular to front and rear; doublure slightly concave.

Thorax of twelve segments, 57 per cent. length of exoskeleton. Axis strongly convex (tr.), narrows gently backwards, each ring about 30 per cent. width (tr.) of whole segment. Axial furrows deep, wide. Pleurae unfurrowed; proximal portion flat with median row of pits; distal portion curves backwards and down from fulcrum.

Pygidium short, broad, its length 11 per cent. that of carapace. Tapered, highly convex axis comprises articulating half ring, three axial rings and triangular terminal piece. Pleural region with two pairs of broad interpleural furrows and three pairs convex pleurae; each pleura widens backwards to short spine with probably blunt tip.

Remarks. The present species is probably new but we leave it in open nomenclature as only a single exoskeleton is available. Although it is well preserved, the pygidium is incomplete and the fixigenal spines are missing, but we believe the specimen can be assigned with confidence to *Eccoptochile*. Species of the genus were listed by Rabano (1990) from the upper Llanvirn–Ashgill of Europe and, probably, Morocco and Turkey. Of these, the present form most resembles the type species, *E. clavigera* (Beyrich) (see Hawle and Corda 1847, p. 130, pl. 6, fig. 69; Barrande 1852, p. 772, pl. 40, figs 1–9 only; Prantl and Přibyl 1948, pl. 6, figs 1–2; Horný and Bastl 1970, pl. 14, fig. 1) from the Letná Formation (Caradoc; see Štorch *et al.* 1993) of Bohemia, especially in the shape of the glabella, and size and location of the palpebral lobe; the cranidium figured by Horný and Bastl (1970) shows that S1 shallows abruptly rearwards but reaches S0 as in *E.* sp. However, in the present species S1 curves further backwards and L1–L3 are narrower, with L1 only one-quarter the basal glabellar width, compared with one-third in *E. clavigera*. Other features separating the Chinese form from the type species include: glabella more convex (sag., tr.); S2 more arched forwards and shorter; and frontal glabellar lobe shorter (sag.). These characters recall *E.*

ahmadenensis Romano, 1980 (p. 610, pl. 78, figs 8–9; pl. 79, figs 1–7; text-fig. 2a–c) [see also Hammann 1974, p. 105, pl. 11, figs 188–191; pl. 12, figs 192–198; text-fig. 39, as *E. mariana* (de Verneuil and Barrande, 1856); Henry 1980, p. 46, text-fig. 14, as *E.* cf. *mariana* (de Verneuil and Barrande); Rabano 1990, p. 158, pl. 28, figs 1–10] from the upper Llanvirn–Llandeilo (–?Caradoc) of Spain, Portugal, France and probably southern England; but apart from the wider (tr.) L1 and more or less sigmoidal S1, the eyes are sited further back (posterior ends level with S1) and the glabella of less deformed specimens is more narrowly rounded frontally in the European form. In addition, the holotype (Hammann 1974, pl. 12, fig. 192a–c) of *E. ahmadenensis*, a well-preserved cephalon, shows in dorsal view an angle between the anterior border of the cranidium and the lateral border of the librigena due to a sharp change in convexity (compare evenly rounded cephalic margin of *E. sinica*).

Subfamily DEIPHONINAE Raymond, 1913

Genus SPHAEROCORYPHE Angelin, 1854

Type species. Sphaerocoryphe dentata Angelin, 1854.

Subgenus HEMISPHAEROCORYPHE Reed, 1896
(= *Ellipsocoryphe* Lu, 1975, p. 428)

Type species. Sphaerexochus pseudohemicranium Nieszkowski, 1859.

Remarks. As noted by Přibyl *et al.* (1985), *Ellipsocoryphe* Lu, 1975 is indistinguishable from, and synonymous with *Hemisphaerocoryphe*, previously considered as a probable junior synonym of *Sphaerocoryphe* by Lane (1971) and by Holloway and Campbell (1974). Comparing *Hemisphaerocoryphe pseudohemicranium* (see Öpik 1937, p. 113, pl. 15, figs 1–2), from the middle Ordovician of Estonia, with *Sphaerocoryphe dentata* Angelin, 1854 (p. 66, pl. 34, figs 6, 6a; Kielan-Jaworowska *et al.* 1991, p. 234, figs 10–11), from the upper Ordovician (Ashgill) of Sweden, the most obvious difference is the development in the former species of a shorter (sag.) preoccipital depression, a term introduced by Holloway and Campbell (1974) to include S0 and part of the glabellar lobes. Silicified material of *Sphaerocoryphe hdvigseni* Chatterton (1980, p. 43, pl. 13, figs 1–30; text-fig. 9A–F) and *S. robusta* Walcott (Ludvigsen 1979, p. 44, pl. 18, figs 33–54) suggests that L1 and L2 (or most of it) are incorporated into the preoccipital depression; this may be an important character for all typical members of *Sphaerocoryphe* (Holloway and Campbell 1974). The specimen described below has a cranidium typical of *Hemisphaerocoryphe*; the swollen anterior part of the glabellar portion has traces of S1–S4 furrows or impressions. In most other typical members of the genus, including, in addition to the type species, *H. inflata* Nikolaisen, 1961 (p. 292, pl. 1, figs 11–12), *H. granulata* (Angelin, 1854, p. 76, pl. 39, figs 4, 4a; Warburg 1925, p. 388, pl. 10, figs 35–39; Männil 1958, p. 178, pl. 5, figs 4–7) and even *Sphaerocoryphe* sp. ind. of Reed (1906, p. 77, pl. 5, fig. 26) from the lower Ordovician of the Northern Shan States, Burma, S3 (level with palpebral lobe) and S4 are also visible, although S1 and S2 are usually indistinguishable owing to either poor preservation or effacement. Possibly only part of L1 is incorporated in the preoccipital depression of *Hemisphaerocoryphe*.

As the lateral glabellar furrows are visible with difficulty in most species of both *Sphaerocoryphe* and *Hemisphaerocoryphe*, it is more practical to consider the latter a subgenus of the former, as suggested by Přibyl *et al.* (1985). Additional differences between the subgenera include the more forwardly situated palpebral lobe and the anterior glabellar portion, which overhangs the preoccipital depression more strongly in *Sphaerocoryphe*, but neither is of generic importance. The only known pygidium of *Hemisphaerocoryphe* was described as *Sphaerocoryphe exserta* Webby,

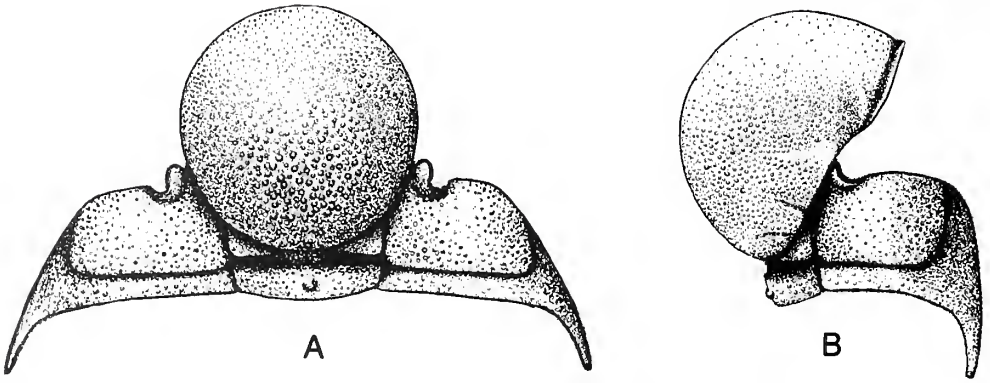

TEXT-FIG. 4. Reconstruction of cranidium of *Sphaerocoryphe* (*Hemisphaerocoryphe*) *elliptica* (Lu, 1975), based on NI 80770. A, dorsal view; B, lateral view; ×5.

1974 (p. 237, pl. 33, figs 1–9) from the Caradoc of New South Wales, Australia and closely resembles that of *Sphaerocoryphe*. Přibyl *et al.* (1985) considered the presence of a pair of free points between the largest spines to be distinctive, but as Tripp *et al.* (1997) pointed out, the points are only hyperextended ventral forks like those found in all species of *Sphaerocoryphe*.

Sphaerocoryphe (*Hemisphaerocoryphe*) *elliptica* (Lu, 1975)

Plate 8, figures 2–3, 6; Text-figure 4

1975 *Ellipsocoryphe elliptica* Lu, p. 429, pl. 43, figs 12, 14; text-fig. 46.
1978 *Ellipsocoryphe elliptica* Lu; Lee, p. 266, pl. 107, fig. 6a–b.

Holotype. Cranidium (NI 16932), figured Lu (1975, pl. 43, figs 12–14), from the upper Meitan Formation (late Arenig–earliest Llanvirn) of Huayingshan, north-east of Chongqing, Sichuan.

Figured specimen. Incomplete cephalon with nine attached thoracic segments (NI 80770) from Bed 3.

Description. Cranidium 60 per cent. as long as wide in plan, excluding fixigenal spines. Anterior portion of glabella spherical, slightly longer than wide, partly overhangs preoccipital depression and cheeks; it occupies 84 per cent. of glabellar length, 47 per cent. of cranidial width, excluding fixigenal spines, and is defined posteriorly by deep transverse furrow which may represent posterior branch of bifurcate S1. S1–S4 short, faint: S1 (probably its anterior branch) curves back slightly at posterolateral corner of the isolated anterior glabellar portion and merges abaxially with transverse furrow; S2 adaxially directed, opposite anterior end of preoccipital depression; S3 and S4 appear as smooth areas sited, respectively, level with palpebral lobe and at anterolateral corner of glabella. Preoccipital depression almost joins occipital furrow medially, with abaxial pair of flat, triangular preoccipital lobes which are weakly inflated adjacent to axial furrows to form small, rounded nodes covered with dense, fine granules. Occipital ring convex, 70 per cent. width of anterior glabellar portion and defined by deep S0; small median node visible on holotype is not seen on exfoliated surface of the present specimen. Axial furrows deep, wide. Fixigena sub-rectangular, abaxially declined; palpebral lobe L-shaped, vertical, its front end in-line with mid-point of anterior glabellar portion and close to axial furrow. Posterior and lateral borders broad, widening towards genal angle where they meet at base of fixigenal spine. Border furrow distinct. Anterior section of facial suture runs forwards and down; posterior section transverse, cuts lateral border at point opposite S3. Librigena triangular; eye socle vertical; eye spherical in lateral view, reniform in plan, its length 16 per cent. that of anterior glabellar portion.

Thorax of nine segments. Axis almost parallel-sided, occupies 44 per cent. width of thorax and is transversely convex, bounded by distinct axial furrows. Proximal part of pleura flat, rectangular, 74 per cent. of overall

width (tr.) and with incised, intermittent, transverse median pleural furrow; distal part forms broad-based tubular spine which narrows backwards and slightly down.

Surface densely and finely granulose, with scattered, coarser granules medially on posterior half of anterior glabellar portion; finer granules on cheeks, with sparsely distributed pits on intervening areas.

Remarks. The holotype is a tiny, slightly deformed cranidium, from which the new specimen differs in the wider anterior portion of the glabella, but this may result from changes during ontogeny. An occipital node seen on the holotype which cannot be verified as the occipital ring is exfoliated in the present specimen. Compared with the type species and other typical members of *Hemisphaerocoryphe*, *S.* (*H.*) *elliptica* is characterized mainly by the more flattened preoccipital segment with a pair of rather poorly demarcated lateral nodes. The species is probably the oldest known representative of the Deiphoninae, a subfamily interpreted as being derived from the cheirurid lineage *Laneites–Ceraurinella* (Přibyl *et al.* 1985) or from early cheirurids such as *Krattaspis* Öpik, 1937 (Chatterton 1980), although Lane (1971) considered that both Cheirurinae and Deiphoninae may have come from a common stock. The morphology of *S.* (*H.*) *elliptica* is highly specialized, and without evidence of its ontogeny the species cannot be used to support either of the above hypotheses.

Family HAMMATOCNEMIDAE Kielan, 1960

Genus OVALOCEPHALUS Koroleva, 1959

(= *Hammatocnemis* Kielan, 1960, p. 141)

Type species. *Ovalocephalus kelleri* Koroleva, 1959.

Remarks. Zhou and Dean (1986) pointed out that differences between *Ovalocephalus* and *Hammatocnemis* Kielan, 1960 fall within the range of intrageneric variation, and more recently the two were considered synonymous by Dean and Zhou (1988), Tripp *et al.* (1989) and Hammann (1992).

Ovalocephalus primitivus extraneus (Lu and Zhou, 1979)

Plate 8, figures 7–9

1979 *Hammatocnemis primitivus extraneus* Lu and Zhou, p. 426, pl. 1, figs 1–13; pl. 2, figs 1–8; text-fig. 5a–c.

1981 *Hammatocnemis primitivus* Lu; Zhang, p. 209, pl. 77, figs 3–4.

Holotype. Cephalon (NI 56541), figured Lu and Zhou (1979, pl. 1, figs 1–9), from the uppermost Zotzeshan Formation (latest Arenig) at Laoshidan, Haibowan, Nei Mongol.

Figured specimens. One cranidium (NI 80771), one pygidium with attached thoracic segments (NI 80773), and one pygidium (NI 80772) from Bed 2.

Description. Glabella convex, two-thirds as wide as long, anterior portion gently expanded and broadly rounded frontally; lenticular occipital ring twice as wide as long, 20 per cent. length of glabella, and wider than preoccipital ring, well defined by deep S0; preoccipital ring low, ridge-like, arched forwards medially and widens (tr.) abaxially to form pair of convex elliptical lobes; preoccipital furrow transverse, deep abaxially; anterior glabellar portion carries four pairs lateral furrows; S1–S3 short, equally spaced, successively shallower; S1 runs slightly back adaxially, S2 directed adaxially, S3 extends slightly forwards and located opposite front end of palpebral lobe; S4 in front of anterolateral glabellar angle and directed backwards. Axial furrow deep, wide. Palpebral lobe high, narrow, carries distinct palpebral furrow, its posterior end level with L1. Palpebral area triangular; posterior area sub-rectangular, distal part declined abaxially.

Pygidium about twice as wide as long; gently tapered low axis has four rings, broadly rounded terminal piece, and ring furrows that are successively shallower; axial furrows distinct frontally but shallow around tip

of axis. Pleural region declined abaxially, comprising four pleurae separated by deep interpleural furrows; first three pleurae extend slightly backwards beyond margin and end in free points (see Zhang 1981, pl. 77, fig. 4b). Surface of glabella and pygidium densely granulose.

Remarks. The new material is identical with specimens from the same horizon and area, described as *Hammatocnemis primitivus extraneus* by Lu and Zhou (1979, pl. 2, figs 5–8) but as *H. primitivus* by Zhang (1981). We refer them here to *O. primitivus extraneus* as the occipital ring is much longer (sag.) than that of *O. primitivus primitivus* (Lu, 1975, p. 441, pl. 45, figs 4–14). *O. primitivus extraneus* has been regarded as the ancestral form of Species group 2 of *Ovalocephalus* (Zhou and Dean 1986), characterized by having the entire median preoccipital ring between the preoccipital lobes. Diagnostic of the subspecies are: shorter (exsag.) posterior area of fixigena; palpebral lobe longer, sited further back; glabella less constricted at L1; S4 present; first three pygidial pleurae extend beyond posterior margin as short free points. These are considered as primitive characters in the *O. primitivus extraneus–O. tetrasulcatus* evolutionary lineage (Lu and Zhou 1979) and have proved useful in distinguishing older forms from related younger species such as *O. intermedius* (Lu and Zhou, 1979), *O. obsoletus* (Zhou and Dean, 1986), *O. kanlingensis* (Zhang, 1981), *O. tetrasulcatus* (Kielan, 1960), *O. kelleri* Koroleva, 1959 and *O. globosus* Abdullaev, 1972.

Family PTERYGOMETOPIDAE Reed, 1905
Subfamily PTERYGOMETOPINAE Reed, 1905

Genus YANHAOIA gen. nov.

Derivation of name. After Professor Lu Yanhao, author of the type species, which is the only known pterygometopine in China.

Type species. Pterygometopus huayinshanensis Lu, 1975.

Diagnosis. Cephalon with short fixigenal spines and large eyes. Glabella has three pairs of deep glabellar furrows; S1 bifurcate, S2 and S3 parallel, anteriorly directed adaxially; L1–3 of subequal length. Frontal glabellar lobe with shallow medial depression. Anterior section of facial suture runs along preglabellar furrow.

Remarks. Pterygometopus huayinshanensis Lu, 1975 (p. 462, pl. 50, figs 6–10; Zhou *et al.* 1982, p. 292, pl. 72, fig. 4), from the upper lower Ordovician of Sichuan and southern Shaanxi, displays some typical pterygometopine characters, such as: frontal glabellar lobe strongly expanded laterally; L1 and L2 of almost equal length; palpebral lobe stands very high above glabella; and frontal margin of large eye reaches anterior part of axial furrow (see Ludvigsen and Chatterton 1982; Jaanusson and Ramsköld 1993). The pygidium is not yet known, but the straight S3, directed slightly backwards abaxially, and short (exsag.) L3 suggest that this is an aberrant form whose affinities with other pterygometopine species are uncertain (cf. Zhou and Dean 1989, p. 137), and we follow Jaanusson and Ramsköld (1993, p. 745) in considering it to represent a new, as yet monotypic genus.

Pterygometopus Schmidt, 1881 differs from *Yanhaoia* in the following characters: wider cephalon and frontal glabellar lobe; posterior part of glabella more strongly tapered; preglabellar furrow more distinct; genal angles rounded; curved S3 runs slightly backwards adaxially; longer L3; eyes smaller; anterior section of facial suture runs in front of, instead of inside, preglabellar furrow; and posterior section runs along a sulcus described by Whittington (1950, p. 539) as 'the continuation of the palpebral furrow out to the lateral border'. *Yanhaoia* resembles *Ingriops* Jaanusson and Ramsköld, 1993, from the Llanvirn of northern Estonia and Östergötland, Sweden, in several respects, especially the glabellar outline, bifurcate S1, large eyes, presence of genal spines, and the siting of the anterior section of the facial suture in the preglabellar furrow. The Baltoscandian genus

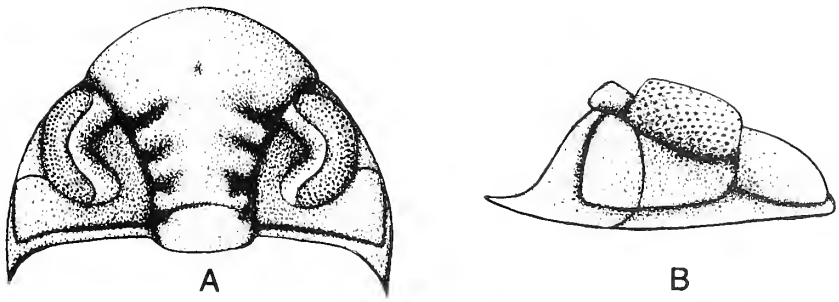

TEXT-FIG. 5. Reconstruction of cephalon of *Yanhaoia huayinshanensis* (Lu, 1975), based mainly on holotype, NI 16991 (Lu 1975, pl. 50, figs 6, 9). A, dorsal view; B, lateral view; ×4.

is distinguished by the more pointed front of cephalon and glabella; adaxial extension of S3; longer L3; and triangular, rather than trapezoidal, frontal glabellar lobe, which lacks a median depression.

Yanhaoia huayinshanensis (Lu, 1975)

Plate 8, figures 4–5; Text-figure 5

1975 *Pterygometopus huayinshanensis* Lu, p. 462, pl. 50, figs 6–10.
1978 *Pterygometopus huayinshanensis* Lu; Lee, p. 280, pl. 107, fig. 14.
1982 *Pterygometopus huayinshanensis* Lu; Zhou *et al.*, p. 292, pl. 72, fig. 4.

Holotype. Cephalon (NI 16991), figured Lu (1975, pl. 50, figs 6–10), from the lower part of the Neichiashan Series (probably Llanvirn) at Huayingshan, north-east of Chongqing, Sichuan.

Figured specimen. Incomplete cephalon with eight attached thoracic segments (NI 80774) from Bed 3.

Description. Cephalon semi-elliptical, about three-quarters as long as wide, declined anteriorly and laterally, with short genal spines. Convex glabella broadly rounded frontally, narrows forwards to S1 and then expands strongly so that anterior width is twice that across L1; occipital ring lenticular with pair of rounded lateral lobes; distinct S0 deepens abaxially; S1–S3 deeply incised; S1 bifurcate, S2 and S3 parallel, straight, directed adaxially forwards; L1–L3 of almost equal length (exsag.); L1 rounded, L2 and L3 directed abaxially backwards, and L3 slightly wider (tr.) than L2; frontal lobe trapezoidal, expanded forwards, with small median depression; axial furrow deep, broad. Palpebral lobe high, with distinct palpebral furrow, its length (sag.) about half that of glabella; front end of lobe reaches axial furrow immediately in front of S3, and posterior end opposite L1. Palpebral area of fixigena declines adaxially and anteriorly. Posterior section of facial suture sigmoidal. Eye large, crescentic, with vertical eye socle.

Thorax subparallel-sided, strongly convex transversely. Axis about two-fifths the thoracic width, well defined by distinct axial furrows. Axial ring rectangular, with pair of rounded axial nodes visible on internal mould. Inner part of pleura horizontal, with deep, wide, diagonal pleural furrow; outer part declines steeply to pointed tip.

Remarks. Only two specimens of the species were previously known, the holotype and a well-preserved cephalon with five attached thoracic segments, from the middle part (Llanvirn) of the Siliangssu Formation at Nanzheng, southern Shaanxi (Zhou *et al.* 1982). The new specimen, although incomplete, compares closely with both; the tiny fixigenal spine on the right side of the cephalon can also be distinguished on the holotype.

Acknowledgements. Research was supported by the 'Special Funds for Palaeontology and Palaeoanthropology' (No. 8901) from the Academia Sinica. Work was completed in the Department of Earth Sciences, University of Wales Cardiff, and the Department of Geology, National Museum and Gallery of Wales, Cardiff, during

a visit by Zhou Zhiyi sponsored by the Royal Society, London. We thank R. M. Owens for helpful discussion, and Hu Shangqing and Ren Yugao for technical assistance.

REFERENCES

ABDULLAEV, R. N. 1972. [Trilobites of the Upper Ordovician of Bukantan.] 103–126. *In* MASYMOV, A. S. and ABDULLAEV, R. N. (eds). [*New data on the fauna of the Palaeozoic and Mesozoic of Uzbekistan.*] Akademiya Nauk Uzbekskoy SSR Instituta Geologii i Geofiziki, FAN, Tashkent. [In Russian].

AN TAIXIANG 1987. [*The Lower Palaeozoic conodonts of South China.*] Beijing University Press, 238 pp. [In Chinese].

ANGELIN, N. P. 1851. *Palaeontologia Suecica I. Iconographia Crustaceorum formationis transitionis, Fasc. 1.* Samson and Wallin, Lund, 1–24.

—— 1854. *Palaeontologia Scandinavica 1: Crustacea formationis transitionis. Fasc 2.* Samson and Wallin, Lund, 21–92.

BALASHOVA, E. A. 1964. [Morphology, phylogeny and stratigraphic occurrence of the Early Ordovician subfamily Ptychopyginae in the Baltic region.] *Voprosy Paleontologii*, **4**, 3–56. [In Russian].

—— 1971. [Trilobites of the new subfamily Pseudobasilicinae.] *Voprosy Paleontologii*, **6**, 52–60. [In Russian].

—— 1976. [*Systematics of the trilobites of Asaphina and their representatives in the USSR.*] Nedra, Leningrad, 215 pp. [In Russian].

BARRANDE, J. 1852. *Système silurien du centre de la Bohême. 1ère partie. Recherches paléontologiques. Vol. 1. Crustacés, Trilobites.* Prague and Paris, xxx + 935 pp.

BEYRICH, E. 1845. *Ueber einige böhmische Trilobiten.* G. Reimer, Berlin, 47 pp.

BILLINGS, E. 1859. Description of some new species of trilobites from the Lower and Middle Silurian rocks of Canada. *Canadian Naturalist and Geologist*, **4**, 367–383.

BOHLIN, B. 1955. The Lower Ordovician Limestones between the Ceratopyge Shale and the Platyurus Limestone of Böda Hamn. *Bulletin of the Geological Institute of Uppsala*, **35**, 111–173.

BRADLEY, J. H. 1925. Trilobites of the Beekmantown in the Philipsburg region of Quebec. *The Canadian Field Naturalist*, **39** (1), 5–9.

BRONGNIART, A. 1822. *Histoire naturelle des Crustacés fossiles, sous les rapports zoologiques et géologiques. Savoir: les Trilobites.* F.-G. Levrault, Paris, 65 pp.

BURMEISTER, H. 1843. *Die Organisation der Trilobiten aus ihren lebenden Verwandten entwickelt; nebst einer systematischen Uebersicht aller zeither beschriebenen Arten.* Berlin, xii + 147 pp.

CHANG WENTANG and JELL, P. A. 1983. Chinese Ordovician trilobites housed in the Smithsonian Institute. *Memoir of the Association of Australasian Palaeontologists*, **1**, 195–208.

CHATTERTON, B. D. E. 1980. Ontogenic studies of Middle Ordovician Trilobites from the Esbataottine Formation, Mackenzie Mountains, Canada. *Palaeontographica, Abteilung A*, **171**, 1–74.

—— and LUDVIGSEN, R. 1976. Silicified Middle Ordovician Trilobites from the South Nahanni River Area, District of Mackenzie, Canada. *Palaeontographica, Abteilung A*, **154**, 1–106.

CHEN XU and BERGSTRÖM, S. M. (eds). 1995. The base of the *austrodentatus* Zone as a level for global subdivision of the Ordovician System. *Palaeoworld*, **5**, 1–117.

CHUGAEVA, M. N. 1958. [The Ordovician trilobites of the Chu-Ili Mountains.] *Trudy Geologicheskogo Instituta Akademiya Nauk SSSR*, **9**, 5–136. [In Russian].

COCKS, L. R. M. and FORTEY, R. A. 1990. Biogeography of Ordovician and Silurian faunas. 94–104. *In* MCKERROW, W. S. and SCOTESE, C. R. (eds). Palaeozoic palaeogeography and biogeography. *Memoir of the Geological Society, London*, **12**, 1–433.

DALMAN, J. W. 1827. Om Palaeaderna eller de så kallade Trilobiterna. *Kungliga Svenska Vetenskapsakademiens (Stockholm), Handlingar*, **1**, 266–294.

DEAN, W. T. 1985. Relationships of Cambrian–Ordovician faunas in the Caledonide–Appalachian Region, with particular reference to trilobites. 17–47. *In* GAYER, R. A. (ed.). *The tectonic evolution of the Caledonide–Appalachian Orogen.* Vieweg, Wiesbaden, 165 pp.

—— and ZHOU ZHIYI 1988. Upper Ordovician trilobites from the Zap Valley, southeast Turkey. *Palaeontology*, **31**, 621–649.

ENDO, R. 1932. The Canadian and Ordovician formations and fossils of South Manchuria. *Bulletin of United States National Museum*, **164**, 1–152.

—— 1935. Additional fossils from the Canadian and Ordovician rocks of the Southeast Manchouguo. *Science Reports of the Tohoku Imperial University, (2, Geology)*, **16** (4), 191–223.

FORTEY, R. A. 1975*a*. Early Ordovician trilobite communities. *Fossils and Strata*, **4**, 339–360.

—— 1975*b*. The Ordovician Trilobites of Spitsbergen. II. Asaphidae, Nileidae, Raphiophoridae and Telephinidae of the Valhallfonna Formation. *Norsk Polarinstitutt Skrifter*, **162**, 1–207.
—— 1979. Early Ordovician trilobites from the Catoche Formation (St George Group), Western Newfoundland. *Bulletin of the Geological Survey of Canada*, **321**, 61–114.
—— 1980*a*. Generic longevity in Lower Ordovician trilobites: relation to environment. *Paleobiology*, **6**, 24–31.
—— 1980*b*. *Basilicus tyrannus* (Murchison) and the glabellar structure of asaphid trilobites. *Bulletin of the British Museum (Natural History), Geology*, **34** (4), 255–264.
—— 1984. Global earlier Ordovician transgressions and regressions and their biological implications. 37–50. *In* BRUTON, D. L. (ed.). Aspects of the Ordovician System. *Palaeontological Contributions from the University of Oslo*, **295**, 1–228.
—— 1985. Pelagic trilobites as an example of deducing the life habits of extinct arthropods. *Transactions of the Royal Society of Edinburgh: Earth Sciences*, **76**, 219–230.
—— HARPER, D. A. T., INGHAM, J. K., OWEN, A. W. and RUSHTON, A. W. A. 1995. A revision of Ordovician series and stages from the historical type area. *Geological Magazine*, **132**, 15–30.
—— and SHERGOLD, J. H. 1984. Early Ordovician platformal trilobites, Nora Formation, central Australia. *Palaeontology*, **27**, 315–366.
GORTANI, M. 1934. Fossili Ordoviciani del Caracorùm. *Spedizione Italiana del Filippi nell' Himàlaia, Caracorùm e Turechestàn Cinne (1913–14). Series 2*, **5**, 1–97.
HAMMANN, W. 1974. Phacopina und Cheirurina (Trilobita) aus dem Ordovizium von Spanien. *Senckenbergiana lethaea*, **55**, 1–151.
—— 1992. The Ordovician trilobites from the Iberian Chains in the province of Aragon, NE-Spain. 1. The trilobites of the Cystoid Limestone (Ashgill Series). *Beringeria*, **6**, 1–219.
HARRINGTON, H. J. and LEANZA, A. F. 1957. Ordovician trilobites of Argentina. *Special Publications of the Department of Geology, University of Kansas*, **1**, 1–276.
HAWLE, I. and CORDA, A. J. C. 1847. *Prodrom einer monographie der böhmischer Trilobiten*. J. G. Calve'sche Buchhandlung, Prague, 176 pp.
HENDERSON, R. A. 1983. Early Ordovician faunas from the Mount Windsor Subprovince, northeastern Queensland. *Memoir of the Association of Australasian Palaeontologists*, **1**, 145–175.
HENNINGSMOEN, G. 1960. The Middle Ordovician of the Oslo Region, Norway. 13. Trilobites of the family Asaphidae. *Norsk Geologisk Tidsskrift*, **40**, 203–257.
HENRY, J.-L. 1980. Trilobites ordoviciens du Massif Armoricain. *Mémoires de la Société géologique et minéralogique de Bretagne*, **22**, 1–250.
HOLLOWAY, D. J. and CAMPBELL, K. S. W. 1974. The Silurian trilobite *Onycopyge* Woodward. *Palaeontology*, **17**, 409–421.
HORNÝ, R. and BASTL, F. 1970. *Type specimens of fossils in the National Museum Prague. Vol. 1, Trilobita*. Museum of Natural History, Prague, 11–354.
JAANUSSON, V. 1953. Untersuchungen über baltoskandische Asaphiden I. Revision der mittelordovizischen Asaphiden des Siljan-Gebietes in Dalarna. *Arkiv för Mineralogi och Geologi*, **1** (14), 377–464.
—— 1954. Zur Morphologie und Taxonomie der Illaeniden. *Arkiv for Mineralogi och Geologi*, **1** (20), 545–583.
—— 1957. Unterordovizische Illaeniden aus Skandinavien. *Bulletin of the Geological Institutions of the University of Uppsala*, **37**, 79–165.
—— and RAMSKÖLD, L. 1993. Pterygometopine trilobites from the Ordovician of Baltoscandia. *Palaeontology*, **36**, 743–769.
KIELAN, Z. 1960. Upper Ordovician trilobites from Poland and some related forms from Bohemia and Scandinavia. *Palaeontologia Polonica*, **11**, 1–198.
KIELAN-JAWOROWSKA, Z., BERGSTRÖM, J. and AHLBERG, P. 1991. Cheirurina (Trilobita) from the Upper Ordovician of Västergötland and other regions of Sweden. *Geologiska Föreningens i Stockholm Förhandlingar*, **113**, 219–244.
KOBAYASHI, T. 1934. The Cambro-Ordovician Formations and Faunas of South Chosen. Palaeontology. Part 2. Lower Ordovician Faunas. *Journal of the Faculty of Science, Imperial University of Tokyo, Section 2*, **3** (9), 521–585.
—— 1940. Lower Ordovician Fossils from Caroline Creek, near Latrobe, Mersey River District, Tasmania. *Papers of the Proceedings of the Royal Society of Tasmania for 1939*, 67–76.
—— 1951. On the Ordovician Trilobites in Central China. *Journal of the Faculty of Science, Imperial University of Tokyo, Section 2*, **8** (1–3), 1–87.
KOROLEVA, M. N. 1959. [New genera of trilobites from the Middle and Upper Ordovician of northern Kazakhstan.] *Doklady Akademii Nauk SSSR*, **124**, 1313–1316. [In Russian].

LANE, P. D. 1971. British Cheiruridae (Trilobita). *Monograph of the Palaeontographical Society*, **125** (530), 1–95, pls 1–16.

LEE SHANJI 1978. Trilobita. 179–284. *In* [*Palaeontological atlas of Southwest China, Sichuan (1)*.] Geological Publishing House, Beijing. [In Chinese].

LEGG, D. P. 1976. Ordovician trilobites and graptolites from the Canning Basin, Western Australia. *Geologica et Palaeontologica*, **10**, 1–58.

LI YAOXI, SONG LISHENG, ZHOU ZHIQIANG and YANG JINGYAO 1975. [*Stratigraphical gazetteer of Lower Palaeozoic, western Dabashan*.] Geological Publishing House, Beijing, 372 pp. [In Chinese].

LINNARSSON, J. G. O. 1869. Om Vestergötlands Cambriska och Siluriska Aflagringar. *Kungliga Svenska Vetenskapsakademiens (Stockholm) Handlingar*, **8** (2), 1–89.

LIU YIREN 1982. Trilobita. 290–347. *In* [Palaeontological atlas of Hunan.] *Geological Memoirs of China Ministry of Geology and Mineral Resources*, **2** (4), 290–347. [In Chinese].

LU YANHAO 1957. Trilobita. 249–294. *In* [*Index fossils of China. Invertebrates (3)*.] Science Press, Beijing. [In Chinese].

—— 1975. Ordovician trilobite faunas of central and southwestern China. *Palaeontologia Sinica, New Series B*, **11**, 1–484. [In Chinese and English].

—— and CHANG WENTANG 1974. [Ordovician trilobites.] 124–136. *In* [*A Handbook of stratigraphy and palaeontology in Southwest China*.] Science Press, Beijing, 454 pp. [In Chinese].

—— —— CHU CHAOLING, CHIEN YIYUAN and HSIANG LEEWEN 1965. [*Trilobites of China*.] Science Press, Beijing, 766 pp. [In Chinese].

—— and ZHOU ZHIYI 1979. Systematic position and phylogeny of *Hanmatocnemis* (Trilobita). *Acta Palaeontologica Sinica*, **18**, 415–434. [In Chinese with English abstract].

—— ZHU ZHAOLING, QIAN YIYUAN, ZHOU ZHIYI, CHEN JUNYUAN, LIU GENGWU, YU WEN, CHEN XU and XU HANKUI 1976. [Ordovician biostratigraphy and palaeozoogeography of China.] *Memoirs of the Nanjing Institute of Geology and Palaeontology, Academia Sinica*, **7**, 1–83. [In Chinese].

LUDVIGSEN, R. 1979. A trilobite zonation of Middle Ordovician rocks, southwestern district of Mackenzie. *Bulletin of the Geological Survey of Canada*, **312**, 1–98.

—— and CHATTERTON, B. D. E. 1982. Ordovician Pterygometopidae (Trilobita) of North America. *Canadian Journal of Earth Sciences*, **19**, 2179–2206.

MÄNNIL, R. 1958. Trilobites of the Families Cheiruridae and Encrinuridae from Estonia. *Trudy Instituta Geologii Akademii Nauk Estonskoi SSR*, **3**, 165–212. [In Russian with Estonian and English summaries].

MAREK, L. 1952. Contribution to the stratigraphy and fauna of the uppermost part of the Králův Dvůr Shales (Ashgillian). *Sborník Ústředního Ústavu Geologického (Paleont.)*, **19**, 429–455. [In Czech, with English summary].

MIKULIC, D. G. 1980. Trilobites in Paleozoic carbonate buildups. *Lethaia*, **14**, 45–56.

MOBERG, J. C. and SEGERBERG, C. O. 1906. Bidrag till kannedomen om Ceratopyge-regionen med Sarskild hansyn till dess utrecking i Fögelsångstrakten. *Meddelanden från Lunds Universitets Årsskrifter Geologiska Faltklubb, Series B*, **2**, 1–113.

MOORE, R. C. (ed.) 1959. *Treatise on invertebrate paleontology. Part O. Arthropoda 1*. The Geological Society of America and the University of Kansas Press, Lawrence and Meriden, xix + 560 pp.

NIESZKOWSKI, J. 1859. Zusätze zur Monographie der Trilobiten der Ostsee-provinzen, nebst der Beschreibung einiger neuen obersilurischen Crustaceen. *Archiv für die Naturkunde Liv-, Ehst- und Kurlands. Dorpat, Series 1*, Bd **2**.

NIKOLAISEN, F. 1961. The Middle Ordovician of the Oslo Region, Norway. 7. Trilobites of the suborder Cheirurina. *Norsk Geologisk Tidsskrift*, **41**, 279–310.

ÖPIK, A. 1937. Trilobiten aus Estland. *Acta et Commentationes Universitatis Tartuensis (Dorpatensis), A*, **32** (3), 1–163.

OWEN, A. and BRUTON, D. L. 1980. Late Caradoc–early Ashgill trilobites from central Oslo Region, Norway. *Paleontological Contributions from the University of Oslo*, **245**, 1–63.

PILLET, J. 1973. Sur quelques Trilobites Ordoviciens d'Iran oriental. *Annales de la Société Géologique du Nord*, **93**, 33–38.

—— 1976. *Pseudocalymene* Pillet 1973 et *Eucalymene* Lu 1975 (Calymenina, Trilobites). *Compte Rendu Sommaire des Séances de la Société Géologique de France*, **3**, 96.

PRANTL, F. and PŘIBYL, A. 1948. Classification of some Bohemian Cheiruridae (Trilobitae). *Sborník Národního Musea v Praze*, **3B** (1), 1–44.

PŘIBYL, A. and VANĚK, J. 1965. Neue Trilobiten des böhmischen Ordoviziums. *Vestnik Ústředního Ústavu Geologického*, **40**, 277–282.

—— —— and PEK, I. 1986. Phylogeny and taxonomy of Family Cheiruridae (Trilobita). *Acta Universitatis Palackianae Olomucensis: Facultas Rerum Naturalium*, **83** *(Geographica–Geologica 24)*, 107–193.

QIU HONGAN, LU YANHAO, ZHU ZHAOLIN, BI DECHANG, LIN TIANRUI, ZHOU ZHIYI, ZHANG QUANZONG, QIAN YIYUAN, JU TIANYIN, HAN NAIREN and WEI XIUZHE 1983. Trilobita. 28–254. *In* [*Palaeontological atlas of East China.*] Geological Publishing House, Beijing. [In Chinese].

RABANO, I. 1990. *Trilobites del Ordovícico Medio del sector meridional de la zona Centroiberica española.* Boletin Geológico y Minero, Publicaciones Especiales, Madrid, 233 pp.

RAYMOND, P. E. 1905. Trilobites of the Chazy limestone. *Annals of the Carnegie Museum*, **3**, 328–386.

—— 1913. Subclass Trilobita. *In* EASTMAN, C. R. (ed.). *Text-book of Paleontology*. 2nd edition. Vol. 1. London, 839 pp.

—— and NARRAWAY, J. E. 1908. Notes on Ordovician trilobites: Illaenidae from the Black River Limestone, near Ottawa, Canada. *Annals of the Carnegie Museum*, **4**, 242–255.

REED, F. R. C. 1896. Woodwardian Museum notes. Notes on the evolution of the genus *Cheirurus*. *Geological Magazine, Decade 4*, **3**, 117–123, 161–167.

—— 1905. The classification of the Phacopidae. *Geological Magazine, Decade 5*, **2**, 172–178, 224–228.

—— 1906. The Lower Palaeozoic fossils of the Northern Shan States, Burma. *Memoirs of the Geological Survey of India, Palaeontologia Indica, New Series*, **2** (3), 1–154.

—— 1912. Ordovician and Silurian fossils from the Central Himalayas. *Memoirs of the Geological Survey of India, Palaeontologia Indica, New Series*, **7** (2), 1–168.

—— 1915. Supplementary Memoir on new Ordovician and Silurian Fossils from the Northern Shan States. *Memoirs of the Geological Survey of India, Palaeontologia Indica, New Series*, **6** (1), 1–98.

—— 1917. Ordovician and Silurian fossils from Yun-Nan. *Memoirs of the Geological Survey of India, Palaeontologia Indica, New Series*, **6** (3), 1–86.

—— 1931. A review of the British species of the Asaphidae. *Annals and Magazine of Natural History, Series 10*, **7**, 441–472.

—— 1935. The Lower Palaeozoic trilobites of Girvan. Supplement No. 3. *Monograph of the Palaeontographical Society*, **88** (400), 1–64, pls 1–4.

—— 1944. Five new Ordovician trilobites. *Geological Magazine*, **81**, 58–64.

ROMANO, M. 1980. The trilobite *Eccoptochile* from the Ordovician of Northern Portugal. *Palaeontology*, **23**, 605–616.

ROSS, R. J. Jr 1951. Stratigraphy of the Garden City Formation in northeastern Utah, and its trilobite faunas. *Bulletin of the Peabody Museum of Natural History, Yale University*, **6**, i–vi, 1–161.

SAVAGE, T. E. 1917. The Thebes Sandstone and Orchard Creek Shale and their faunas in Illinois. *Transactions of the Illinois State Academy of Science*, **10**, 261–275.

SCHMIDT, F. 1881. Revision der ostbaltischen silurischen Trilobiten nebst geognostischer Übersicht des ostbaltischen Silurgebiets, Abtheilung 1, Phacopiden, Cheiruriden und Encrinuriden. *Mémoires de l'Académie Impériale des Sciences de St.-Pétersbourg, Série 7*, **30** (1), 1–237.

—— 1898. Revision der Ostbaltischen Silurischen Trilobiten. Abtheilung 5, Asaphiden. Lieferung 1. *Mémoires de l'Académie Impériale des Sciences de St.-Pétersbourg, Série 8*, **6** (11), 1–46.

—— 1904. Revision der Östbaltischen Silurischen Trilobiten. Abtheilung 5, Asaphiden. Lieferung 4. *Mémoires de l'Académie Impériale des Sciences de St.-Pétersbourg, Série 8*, **14** (10), 1–62.

SCHRANK, E. 1972. *Nileus*-Arten (Trilobita) aus Geschieben des Tremadoc bis tieferen Caradoc. *Berichte der deutschen Gesellschaft geologische Wissenschaften, A, Geologie und Paläontologie*, **17** (3), 351–375.

SHAW, F. C. 1968. Early Middle Ordovician Chazy Trilobites of New York. *Memoir of the New York State Museum and Science Service*, **17**, 1–163.

—— 1974. Simpson Group (Middle Ordovician) trilobites of Oklahoma. *Memoir of the Paleontological Society*, **6**, 1–54.

SHENG, S. F. 1934. Lower Ordovician trilobite fauna of Chikiang. *Palaeontologia Sinica, Series B*, **3**, 1–19.

ŠTORCH, P., FATKA, O. and KRAFT, P. 1993. Lower Palaeozoic of the Barrandian area (Czech Republic) – a review. *Coloquios de Paleontologia*, **45**, 165–191.

SUN, Y. C. 1931. Ordovician trilobites of Central and Southern China. *Palaeontologia Sinica, Series B*, **7**, 1–47.

SUN ZHENHUA 1984. Trilobita. 328–422. *In* [*Palaeontological atlas of Hubei Province.*] Hubei Science and Technology Press, Wuhan. [In Chinese].

TJERNVIK, T. E. 1956. On the Early Ordovician of Sweden. Stratigraphy and Fauna. *Bulletin of the Geological Institutions of the University of Uppsala*, **36** (2–3), 107–284.

TÖRNQUIST, S. L. 1884. Undersökningar öfver Siljansområdets trilobitfauna. *Sveriges Geologiska Undersökning, Afhandlingar*, C**66**, 1–101.

TRIPP, R. P. 1980. Trilobites from the Ordovician Balclatchie and lower Ardwell groups of the Girvan district, Scotland. *Transactions of the Royal Society of Edinburgh: Earth Sciences*, **71**, 123–145.

—— RUDKIN, D. M. and EVITT, W. R. 1997. Silicified trilobites of the genus *Sphaerocoryphe* from the Middle Ordovician of Virginia. *Canadian Journal of Earth Sciences*, **34**, 770–788.

—— ZHOU ZHIYI and PAN ZHENQIN 1989. Trilobites from the Upper Ordovician Tangtou Formation, Jiangsu Province, China. *Transactions of the Royal Society of Edinburgh: Earth Sciences*, **80**, 25–68.

TROMELIN, G. de and LEBESCONTE, P. 1876. Présentation de fossiles paléozoïques du département d'Ille-et-Vilaine et note additionnelle sur la faune silurienne de l'Ouest de la France. *Compte rendu de la 4ème session de l'Association française pour l'Avancement des Sciences*. Nantes, 683–687.

ULRICH, E. O. 1922. Ordovician hypoparian genera of Trilobites. *Bulletin of the Geological Society of America*, **33**, 205–206.

VERNEUIL, E. de and BARRANDE, J. 1856. Description des fossiles trouvés dans les terrains siluriens et dévoniens d'Almaden, d'une partie de la Sierra Morena et des montagnes de Tolède. *Bulletin de la Société Géologique de France*, **12**, 964–1025.

WAHLENBERG, G. 1818. Petrificata telluris Svecanae. *Nova Acta Regiae Societatis Scientiarum Upsaliensis*, **8**, 1–116.

WARBURG, E. 1925. The trilobites of the Leptaena Limestone in Dalarne. *Bulletin of the Geological Institutions of the University of Uppsala*, **17**, 1–450.

WEBBY, B. D. 1974. Upper Ordovician trilobites from central New South Wales. *Palaeontology*, **17**, 203–252.

WELLER, S. 1907. Description of new species of Ordovician fossils from China. *Proceedings of the United States National Museum*, **32**, 557–563.

—— 1913. A report on Ordovician fossils collected in eastern Asia in 1903–04. *Publications of the Carnegie Institution of Washington*, **54** (3), 279–294.

WHITTINGTON, H. B. 1950. Sixteen Ordovician genotype trilobites. *Journal of Paleontology*, **24**, 531–565.

—— 1959. Silicified Middle Ordovician trilobites: Remopleuridiidae, Trinucleidae, Raphiophoridae, Endymioniidae. *Bulletin of the Museum of Comparative Zoology, Harvard College*, **121** (8), 371–496.

—— 1963. Middle Ordovician trilobites from Lower Head, western Newfoundland. *Bulletin of the Museum of Comparative Zoology, Harvard University*, **129**, 1–118.

—— 1965. Trilobites of the Ordovician Table Head Formation, western Newfoundland. *Bulletin of the Museum of Comparative Zoology, Harvard University*, **132**, 277–441.

—— and KELLY, S. R. A. 1997. Morphological terms applied to Trilobita. 313–319. *In* KAESLER, R. L. (ed.). *Treatise on invertebrate paleontology. Part O. Arthropoda 1. Trilobita, revised.* Volume 1. The Geological Society of America, Inc. and the University of Kansas, Boulder, Colorado and Lawrence, Kansas, xxiv + 530 pp.

XIA SHUFANG 1978. Ordovician trilobites. 157–185. *In* [*Sinian to Permian stratigraphy and paleontology of East Yangtze Gorge area.*] Geological Publishing House, Beijing. [In Chinese].

XIANG LIWEN and ZHOU TIANMEI 1987. Trilobita. 294–335. *In* WANG XIAOFENG, XIANG LIWEN, NI SHIZHAO, ZENG QINGLUAN, XU GUANGHONG, ZHOU TIANMEI, LAI CAIGEN and LI ZHIHONG, *Biostratigraphy of the Yangtze Gorges Area (2). Early Palaeozoic Era.* Geological Publishing House, Beijing. [In Chinese with English abstract].

YABE, H. and HAYASAKA, I. 1920. *Palaeontology of South China. Geographical research in China, 1911–16. Report 3.* Tokyo Geographical Society, 221 pp.

YI YONGEN 1957. The Caradocian trilobite fauna from the Yangtze-Gorges. *Acta Palaeontologica Sinica*, **5**, 527–560. [In Chinese with English summary].

YIN GONGZHENG and LEE SHANJI 1978. Trilobita. 385–595. *In* [*Palaeontological atlas of Southwest China. Guizhou (1).*] Geological Publishing House, Beijing. [In Chinese].

ZENG QINLUAN, NI SHIZHAO, XU GUANGHONG, ZHOU TIANMEI, WANG XIAOFENG, LI ZHIHONG, LAI CAIGEN and XIANG LIWEN 1983. Subdivision and correlation on the Ordovician in the Eastern Yangtze Gorges, China. *Bulletin of the Yichang Institute of Geology and Mineral Resources, Chinese Academy of Geological Sciences*, **6**, 1–56.

ZHANG TAIRONG 1981. Trilobita. 134–213. *In* [*Palaeontological atlas of Northwest China. Xinjiang (1).*] Geological Publishing House, Beijing. [In Chinese].

ZHOU DIKANG, ZHOU TIANRONG and WANG PU 1991. Division of geological ages of Qiuritag Group in northeastern Tarim. 37–43. *In* JIA RUNXU (ed.). *Research of petroleum geology of northern Tarim Basin in China.* China University of Geoscience Press. [In Chinese with English abstract].

ZHOU QINGJIE and ZHENG JIANJING (eds) 1990. [*Structural analysis of Tarim.*] Science Press, Beijing, 144 pp. [In Chinese].

ZHOU TIANMEI, LIU YIREN, MENG XIANSONG and SUN ZHENHUA 1977. Trilobita. 140–266. *In* [*Palaeontological atlas of Central and South China (1)*.] Geological Publishing House, Beijing. [In Chinese].

ZHOU ZHIQIANG, LI JINGSEN and QU XINGUO 1982. Trilobita. 215–460. *In* [*Palaeontological atlas of Northwest China: Shaanxi, Gansu and Ningxia Volume, Part 1, Pre-Cambrian to Early Palaeozoic*.] Geological Publishing House, Beijing. [In Chinese].

ZHOU ZHIYI and CHEN PEIJI 1990. [Preface.] iii–v. *In* ZHOU ZHIYI and CHEN PEIJI (eds). [*Biostratigraphy and geological evolution of Tarim*.] Science Press, Beijing. [In Chinese].

—— and —— 1992. Preface. i–iii. *In* ZHOU ZHIYI and CHEN PEIJI (eds). *Biostratigraphy and geological evolution of Tarim*. Science Press, Beijing.

—— CHEN XU, WANG ZHIHAO, WANG ZONGZHE, LI JUN, GENG LIANGYU, FANG ZONGJIE, QIAO XINGDONG and ZHANG TAIRONG 1990. [Ordovician of Tarim.] 56–130. *In* ZHOU ZHIYI and CHEN PEIJI (eds). [*Biostratigraphy and geological evolution of Tarim*.] Science Press, Beijing, 366 pp. [In Chinese].

—— —— —— —— —— —— —— —— —— 1992. Ordovician of Tarim. 62–139. *In* ZHOU ZHIYI and CHEN PEIJI (eds). *Biostratigraphy and geological evolution of Tarim*. Science Press, Beijing, 399 pp.

—— and DEAN, W. T. 1986. Ordovician trilobites from Chedao, Gansu Province, north-west China. *Palaeontology*, **29**, 743–786.

—— —— 1989. TRILOBITE EVIDENCE FOR GONDWANALAND IN EAST ASIA DURING THE ORDOVICIAN. *Journal of Southeast Asian Earth Sciences*, **3** (1–4), 131–140.

—— and FORTEY, R. A. 1986. Ordovician trilobites from North and Northeast China. *Palaeontographica, Abteilung A*, **192**, 157–210.

—— LIN HUANLING and NI YUNAN 1996. Early Palaeozoic plate tectonics and geological evolution. 3–21. *In* ZHOU ZHIYI and DEAN, W. T. (eds). *Phanerozoic geology of Northwest China*. Science Press, Beijing, 316 pp.

—— YIN GONGZHENG and TRIPP. R. P. 1984. Trilobites from the Ordovician Shihtzupu Formation, Zunyi, Guizhou Province, China. *Transactions of the Royal Society of Edinburgh: Earth Sciences*, **75**, 13–36.

—— ZHOU ZHIQIANG and ZHANG JINLIN 1989. Ordovician trilobite biofacies of North China Platform and its western marginal area. *Acta Palaeontologica Sinica*, **28**, 296–313. [In Chinese with English summary].

ZHOU ZHIYI

YUAN WENWEI

Nanjing Institute of Geology and Palaeontology
Academia Sinica, Chi-Ming-Ssu
Nanjing, China

W. T. DEAN

Department of Earth Sciences
PO Box 914, University of Wales
Cardiff CF1 3YE, UK
and Department of Geology
National Museum of Wales
Cardiff CF1 3NP, UK

ZHOU TIANRONG

05 Project Administration
Bureau of Petroleum Geology of Southwest China
Guiyang, China

Typescript received 31 October 1996
Revised typescript received 29 April 1997

FLUID DYNAMICS OF THE GRAPTOLITE RHABDOSOME RECORDED BY LASER DOPPLER ANEMOMETRY

by BARRIE RICKARDS, SUSAN RIGBY, JERRY RICKARDS *and* CHRIS SWALES

ABSTRACT. A precise laser based technique has been used to measure changes in fluid velocity over a range of graptolite models mounted in a wind tunnel. Results from this laser Doppler anemometer (LDA) show the flow to be altered significantly by spines on the sicula and by the morphology of the thecae. A single virgellar spine retards flow along the 'naked' (ventral) side of the sicula and directs it instead over the thecae. More complicated sicular spine arrays in Ordovician biserial graptolites produce trailing vortices and turbulence. These results are important for three reasons. First, they demonstrate that this tool offers a means of quantitatively and non-intrusively assessing the hydrodynamic function of aspects of graptolite morphology and has the potential to enable us to understand the specific oceanic conditions for which graptolites evolved. Second, they show that, with flow controlled by sicular and thecal morphology, the zooids were unlikely to have fed within the stagnant zones of the thecal apertures; it is more likely that they fed at some distance from these apertures, either with lophophores extended into the sea or having themselves crawled along spines. The stagnant or quiet zones provided a resting position. However, it remains to be tested if food particles have a tendency to accumulate in these stagnant zones. Third, as graptolite models are stable in fluids only when flow is from sicula to nema, it seems likely that graptolites with relatively simple metathecae arrayed themselves in this fashion relative to motion in the oceans.

FOR most of this century graptolite research has focused on the objective of understanding the rhabdosomal and thecal morphology of specimens which have usually suffered varied diagenetic and tectonic alteration. An important spin-off from this work has been an appreciation of evolutionary lineages and hence the determination of a precise biostratigraphy. But, until recent decades, attempts at an understanding of the functional morphology of the class Graptolithina, or of the hydrodynamics of the planktic order Graptoloidea, have been limited.

Some suggestions have been rather bizarre, such as that of Nimmo (1847) who considered that graptolite stipes were merely the serrated tail spines of *Raja pastinaca*, the sting ray. Of the serious hypotheses, that of Lapworth (1897) that the planktic forms were actually epiplanktic, enjoyed popularity in the first half of this century, but was eventually abandoned in view of the lack of evidence for any form of attachment: indeed synrhabdosomes could not be epiplanktic in any circumstances. Bulman (1955, 1964, 1970) and Kozłowski (1966, 1970) surveyed the body of evidence supporting the idea that the graptoloids were holoplanktic and acted in passive response to the vagaries of ocean currents. This was essentially the approach adopted by Rickards (1975), who tended to support Bulman's concept of vacuolated tissue rather than Kozłowski's (1970) concept of large gas-filled, bulbous membranes. The weakness of several of these arguments supporting passive response, especially of Bulman's (1964) model which argues against diurnal migration of the colonies, was highlighted in Kirk's (1969, 1972) papers, which pointed out that graptolites would have starved if they had not moved position relative to the enclosing water mass. Hence Kirk adopted an automobile model in which concerted zooidal activity moved the colonies by spiralling them up and down. Bulman (1964) was not opposed to spiral movements, comparing

[Palaeontology, Vol. 41, Part 4, 1998, pp. 737–752, 1 pl.]

the probable movement of *Cyrtograptus* to that of the living umbrella sponge *Axoniderma*, which spirals upwards in response to the slightest ocean turbulence, and then reverses the process as turbulence wanes. The arguments against the automobility hypothesis were discussed by Rickards (1975) and will not be repeated here. When Bulman was researching his 1964 paper, both researchers had extensive discussions with marine biologists working on planktic communities. Whilst these workers were wholly opposed to automobility and in favour of passive response and vacuolated tissue, they insisted that the colonies would have to move through the water in some fashion. It is important not to conflate the two arguments. Movement of graptoloids relative to water was clearly vital, but the method of movement remains in dispute.

An important effect of all these studies was to focus attention for the first time not merely upon the mode of life of graptolites but upon their possible hydrodynamic function. This was investigated further by Rigby (Rigby and Rickards 1989; Rigby 1991, 1992) who suggested, from testing graptolite models, that the rhabdosomal morphology itself caused spiral motion: thus multi-branched dichograptids as well as sparsely branched diplograptids and monograptids would have been capable of spiralling through sea water. More recently, Rickards (1996) outlined arguments for the nema and virgula being rotational agents. The work of Jenkins (in press) on turbulence in the ocean has demonstrated that finer scale features of the rhabdosome were important to graptolite hydrodynamics. The effect of these structures can only be assessed using physical models. The modelling by Rigby (*in* Rigby and Rickards 1989) and by Melchin and Doucet (1996) have provided useful insights into graptolite hydrodynamics but have failed to quantify accurately flow over a rhabdosome. We present such quantitative results here.

Experiments using accurate models of graptoloids in controlled conditions of fluid flow offer the possibility of assessing the effect of spines and thecal morphology on the movement of fluid over a rhabdosome. Such movement would have occurred regardless of whether the rhabdosome was still, with water passing over it, or in motion through still water. The effects would have had importance for the colony as a whole, in terms of the drag produced by the rhabdosome, and for the individual zooids which must have fed from water moving past the thecal apertures. In the present study, the impact of variations in thecal morphology and the effect of spines at the proximal end of graptolite colonies are assessed with respect to their effect on fluid dynamics.

PREVIOUS USE OF HYDRODYNAMIC ANALYSES

Relatively few studies have been undertaken in which models of fossils were tested for their hydrodynamic properties. Those which have been conducted have investigated two properties of fossil organisms; rates of feeding and rates, or means, of movement.

Feeding experiments were initiated by Rudwick and Cowen (1968), who analysed the likely feeding patterns of aberrant strophomenides through the construction of anatomical models. Later work, such as that of Melchin and Doucet (1996) on graptolites, has emphasized the potential of these methods. Melchin and Doucet reported that currents reaching a conical colony entered the cone via the sides, between the stipes, but left by the aperture of the cone (i.e. upwards).

The first and seminal work using models to assess the hydrodynamics of movement in fossils was that of Jefferies and Minton (1965), who tested aluminium models of the bivalve *Bositra* to estimate sinking rates of this form. In these experiments, fluids of different viscosities and models of fixed size were used to estimate sinking velocities of bivalves with different sizes and densities. Based on their results, Jefferies and Minton were able to suggest that the presence of tentacles might have enabled *Bositra* to sink slowly at all growth stages. This was considered positive evidence for an epiplanktic mode of life when considered with other lines of argument. Later work on trilobites (Fortey 1985) has used models of species with different body shapes to assess the likelihood of a nektic mode of life from the frictional drag created by each shape. Real size models of the trilobites were suspended in water, moving at varying speeds. Displacement of the model was used to calculate drag and dye streams were used to visualize the wakes created by the models.

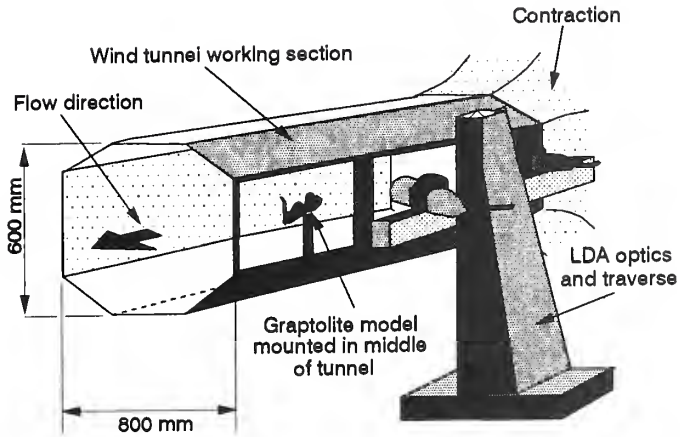

TEXT-FIG. 1. Bristol University wind tunnel, showing the configuration of the model in an air stream, within the working section of the array.

Simple modelling of graptoloids (Rigby and Rickards 1989) demonstrated that a variety of shapes of rhabdosome created a spiralling motion which would have been advantageous to a living graptoloid colony. Models of real size and likely density were allowed to fall through fresh water and sea water (see Rickards and Rigby in press) and their rates of fall and orientations during movement recorded visually and with video cameras.

Each of these studies has demonstrated the value of physical modelling in assessing the likely hydrodynamic properties of fossil organisms. However, in a sense, all have been qualitative guides rather than quantitative assessments of the flow. The problem has been resolved in the present study by the use of laser Doppler anemometry, a technique which offers the potential to collect large amounts of accurate velocity data from the flow around models of fossils.

EXPERIMENTAL TECHNIQUE

The above discussion has highlighted the need for a better understanding of the nature of fluid flow around graptolites. In order to simplify the acquisition of flow velocity measurements in the region of the thecae and around the sicular aperture, larger scale models of graptolites were used for this work. In order to avoid the difficulties of taking measurements on an object as it moves through a fluid (Bradshaw 1970) the experiments were performed in a wind tunnel. A wind tunnel provides a uniform stream of air over a fixed model placed in the working section, hence giving equivalent conditions to the model moving through a stationary fluid. Text-figure 1 shows the principal components of the low speed wind tunnel employed for these tests (Department of Aerospace Engineering, University of Bristol). Simple numerical conversions render measurements in air comparable to those in water.

Measurement of fluid flow

Numerous techniques are available for the investigation of airflows. Most methods are qualitative in nature, providing only a visual indication of the flow behaviour, and consequently are limited in their value. However, they are easy to employ and cheap, and are thus still widely used. Examples include the injection of dyes/pigments or smoke into the flow to indicate its overall direction, and the use of tufts attached to surfaces which move to align themselves with the flow.

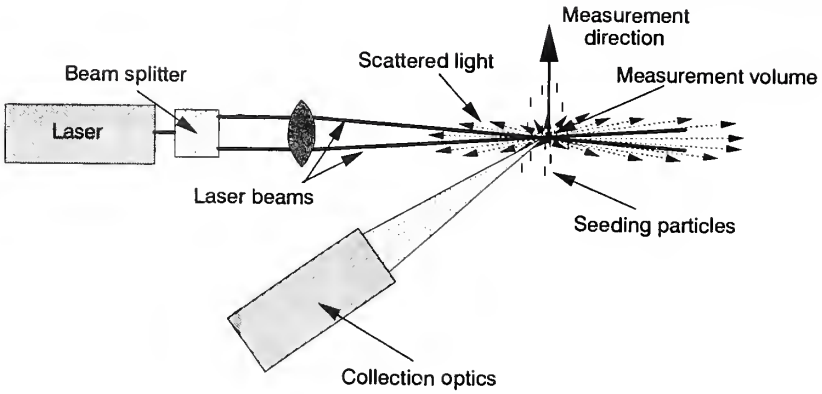

TEXT-FIG. 2. Introduction to LDA theory. Seeding particles are counted and their velocity and direction measured by their scattering effect on light collected from three mutually orthogonal laser pairs.

In addition, there are several quantitative techniques which are available for flow measurement. The two most commonly used quantitative techniques are pitot-static probes, relying on measurement of dynamic air pressure which is proportional to the square of the velocity, and hot-wire anemometers. A hot-wire anemometer consists of a very fine wire, typically 5 μm in diameter, which is heated by an electric current and mounted on the prongs of a small 'fork' positioned in the airflow. As the air flows over the wire it tends to cool it down, thus reducing its electrical resistance. Consequently the wire can be calibrated to indicate velocity in terms of the additional current required to maintain the wire at a constant temperature.

Optical methods of flow measurement have been in use for around 30 years but it is only recently that reliable commercial systems have become available. Laser Doppler anemometry (LDA) is probably the most commonly used of these due to its excellent reliability and accuracy. Most current LDAs operate by the Differential Doppler technique (Drain 1980). In this method two laser beams overlap to form a small region known as the *measurement volume*. When small seeding particles (typically around 1 μm diameter), which are injected into the flow, pass through the measurement volume they scatter two distinct frequencies of light. This Doppler effect is due to the difference in relative velocity between the seeding particle and the point of origin of each of the two laser beams. When the scattered light is collected by a photodetector the two light signals interfere with each another, producing a 'burst', the frequency of which is directly proportional to the velocity of the particle and hence the airflow. The measured velocity vector is in the plane of the two intersecting laser beams and perpendicular to their bisector (Text-fig. 2).

The three component Dantec LDA system used for these tests has three such pairs of beams, each pair of different wavelength, and therefore three velocity components can be acquired simultaneously from which the magnitude of the flow in any direction can then be determined. The three pairs of beams are emitted from two optic heads mounted on a triaxial traverse mechanism and are focused to a single common measurement volume which is approximately spherical and less than 0·1 mm in diameter. The traverse mechanism can position the measurement volume at any point in space within a 0·6 m × 0·6 m × 0·6 m virtual cube, to a resolution better than 0·01 mm. Each optic head is able to receive scattered light as well as to transmit the laser beams. This collected light is passed via fibre-optic cables to three photomultipliers, which convert the scattered light into electrical signals. These signals are processed to obtain the Doppler frequency and hence the flow velocity by three Burst Spectrum Analysers, one for each wavelength.

The LDA has several advantages over pitot-static probes and hot-wires. The technique is non-invasive; in other words, it does not affect the flow it is trying to measure. In addition, it is able to

measure both the direction and magnitude of the velocity vector, which is essential in regions where reversed flow is expected, such as around thecae. Furthermore, the 3 component LDA system used in this work is able to measure three velocity components simultaneously and at the same point in space. Other techniques cannot offer true spatial coincidence and thus cannot match the spatial resolution of the LDA.

Experimental set-up and the graptolite models

Scale models of graptolites were tested within Bristol University's low speed, low turbulence wind tunnel as is generally the case in wind tunnel testing. Vogel (1981) stated that 'it is possible to compare flow over bodies of different sizes, and between air and water, as long as there is a similarity of Reynolds number between the two situations'. The Reynolds number is a dimensionless index which helps to describe the interaction between solids and fluids. It can be defined as:

$$Re = lU/u$$

where l = characteristic length of the model (or the real specimen) in the direction of flow, U = velocity and u = kinematic viscosity of the fluid. The kinematic viscosity of sea water at 20 °C is $1{\cdot}047 \times 10^{-6}$ m^2 s^{-1}, while for air at the same temperature it is $1{\cdot}5 \times 10^{-5}$ m^2 s^{-1}.

Essentially, the principle of dynamic similarity has been used in these experiments to ensure that comparison is valid between the models and reality. However, the velocity of a graptolite in seawater is an unknown in this equation, and would clearly have varied with oceanographic conditions. It is necessary to estimate likely speeds, and to establish extremes beyond which a graptolite would have been unlikely to go during normal conditions. The simplest method of estimating likely graptolite velocities is by analogy with modern plankton. Diel migration is almost ubiquitous in this group and most movement is of the order of 50–400 m in 12 hours (Raymont 1983). As they move both up and down in this time, these figures are effectively doubled and give velocities of $2{\cdot}3 \times 10^{-3}$ ms^{-1} to 2×10^{-2} ms^{-1}) (Raymont 1983). In reality, this is probably the lower end of the velocity spectrum which graptolites experienced, as turbulence in the sea water surrounding them would have subjected them to velocities which were orders of magnitude greater than this. Although the overall movement might have been relatively small, an object suspended in sea water would be extensively buffeted in most conditions so that the total movement would be much larger than the apparent distance covered.

The wind tunnel used in this series of experiments runs at a minimum velocity of 0·1 ms^{-1}. For the model of *Amplexograptus maxwelli*, this gives a Reynolds number for the model of 1733, which is dynamically similar to a real specimen moving at a velocity of 0·28 ms^{-1}. This is higher than the minimum values predicted from considerations of the modern system, but well within the range of velocities encountered by plankton in modern oceans (Raymont 1983). Although not ideal, this is considered a good first approximation. The same reasoning also applies to the other two models.

Three models were used. All were made by Cynthia Clarkson in the 1950s, from a waxy resin, and are housed in the Sedgwick Museum, Cambridge. All are morphologically accurate and are copied from isolated graptolite material held by the Museum:

1. An early growth stage of *Saetograptus chimaera* (Barrande) with the sicula and an incomplete th1, 75 times larger than the real specimen.
2. A model of *Saetograptus chimaera* with three thecae, each bearing a pair of spines, 75 times larger than actual size.
3. A model of *Amplexograptus maxwelli* with six thecae, of which $th2^3$ is incomplete, 40 times larger than actual size.

The model graptolites were mounted on a slim strut in the centre of the wind tunnel working section (Text-fig. 1), with optical access for the laser beams provided through a glass window. The

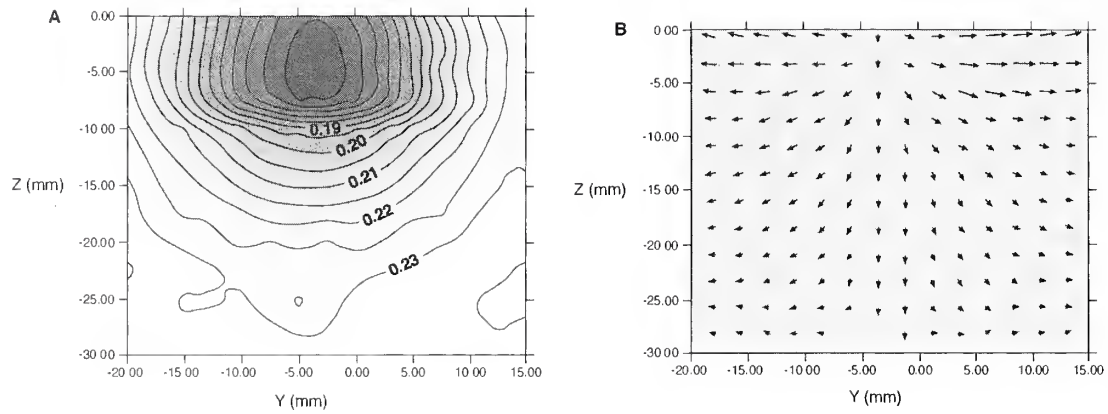

TEXT-FIG. 3. A, contour plot of U velocity for model A at X = 16·5 mm, just proximal to the sicular aperture. In all of these figures, the X axis runs parallel to the long axis of the colony, beginning at the tip of the virgular spine and ending at the tip of the sicula. Y and Z axes are mutually orthogonal to this, the Z axis being vertical. B, vector plot in YZ plane for model A at X = 16·5 mm.

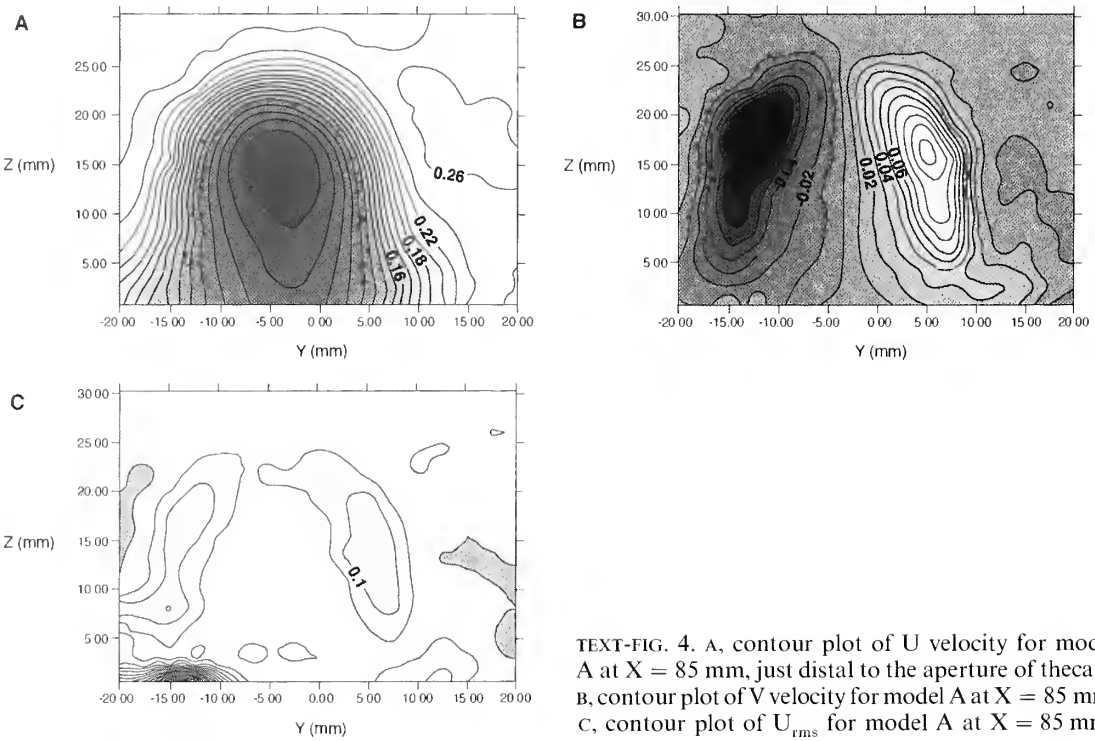

TEXT-FIG. 4. A, contour plot of U velocity for model A at X = 85 mm, just distal to the aperture of theca 1. B, contour plot of V velocity for model A at X = 85 mm. C, contour plot of U_{rms} for model A at X = 85 mm.

models were positioned in the wind tunnel so that fluid flow was from the sicula to the nema as this is believed to be the only hydrodynamically stable position for a body of this shape. The axis system was such that the X direction was horizontal, the Y and Z axes formed an orthogonal grid at right

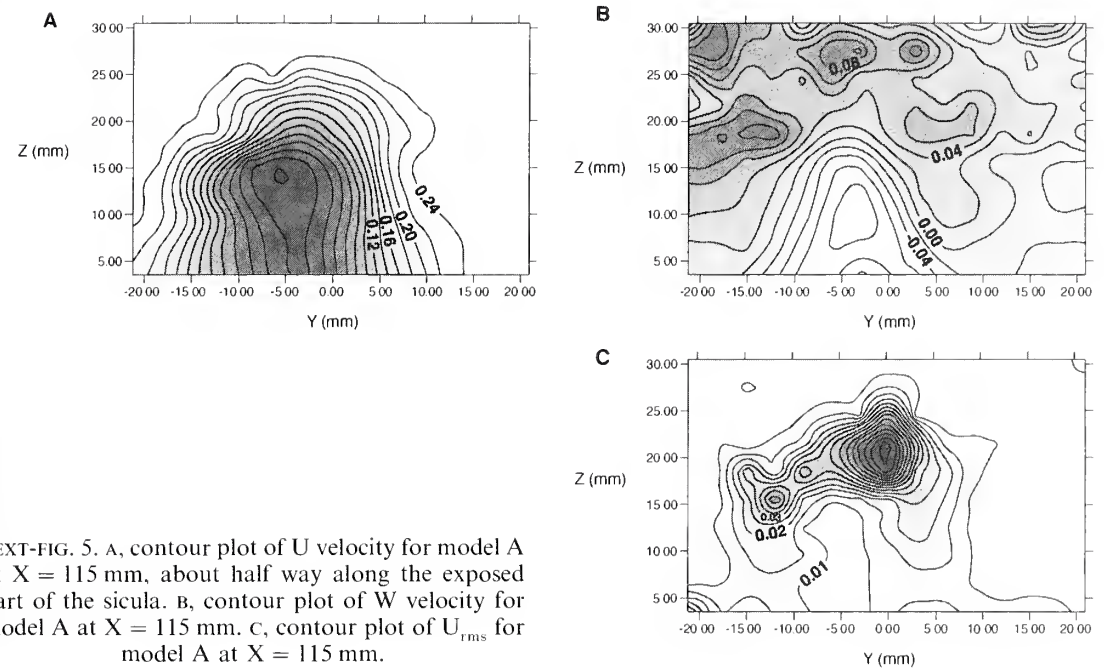

TEXT-FIG. 5. A, contour plot of U velocity for model A at X = 115 mm, about half way along the exposed part of the sicula. B, contour plot of W velocity for model A at X = 115 mm. C, contour plot of U_{rms} for model A at X = 115 mm.

angles to this. Conventions of sign in Bristol are positive in the upflow direction for X, positive towards the LDA traverse for Y and positive in a vertical downward direction for Z. However, these have been reversed in subsequent figures in this paper for clarity (i.e. so that the direction of flow generated within the main body of the tunnel is positive).

Data were acquired for each model at various stations from the tip of the sicula to the tip of the nema. Particular attention was paid to the regions of greatest anticipated interest such as around the thecae and the sicular aperture. Each two dimensional traverse was aligned in the YZ plane, in other words at a fixed distance downstream of the sicula, and consisted of measurements taken at several hundred discrete stations. At each traverse position the mean velocity and the degree of variation in velocity were measured in each component of flow direction (X, Y and Z). The traverse grid spacing was generally 2 mm, although the spacing varied according to the extent of the region of interest and the required resolution. Once a suitable traverse had been programmed, data acquisition started at the first traverse position and stopped when a sufficient number of seeding particles had passed through the measurement volume for accurate mean and turbulence information to be calculated, typically around 3000 samples. This process was then repeated at each subsequent measurement position. The time required for data acquisition was about one hour for each traverse program, that is at each X-position: the total data acquisition time was around 20 hours.

Plotting of results

Results were plotted as contour graphs for U, V and W velocities (in the X, Y and Z directions respectively) and for U_{rms}, the root mean square of U velocity which indicates the level of turbulence. Contours were generated using the software package, Surfer for Windows (Copyright Golden Software, Inc. 1994), and the data points were manipulated into contour form by kriging with a linear variogram. Vector plots were also produced for V and W velocities. These have been synthesized into diagrams which show flow patterns over the whole rhabdosome for each model.

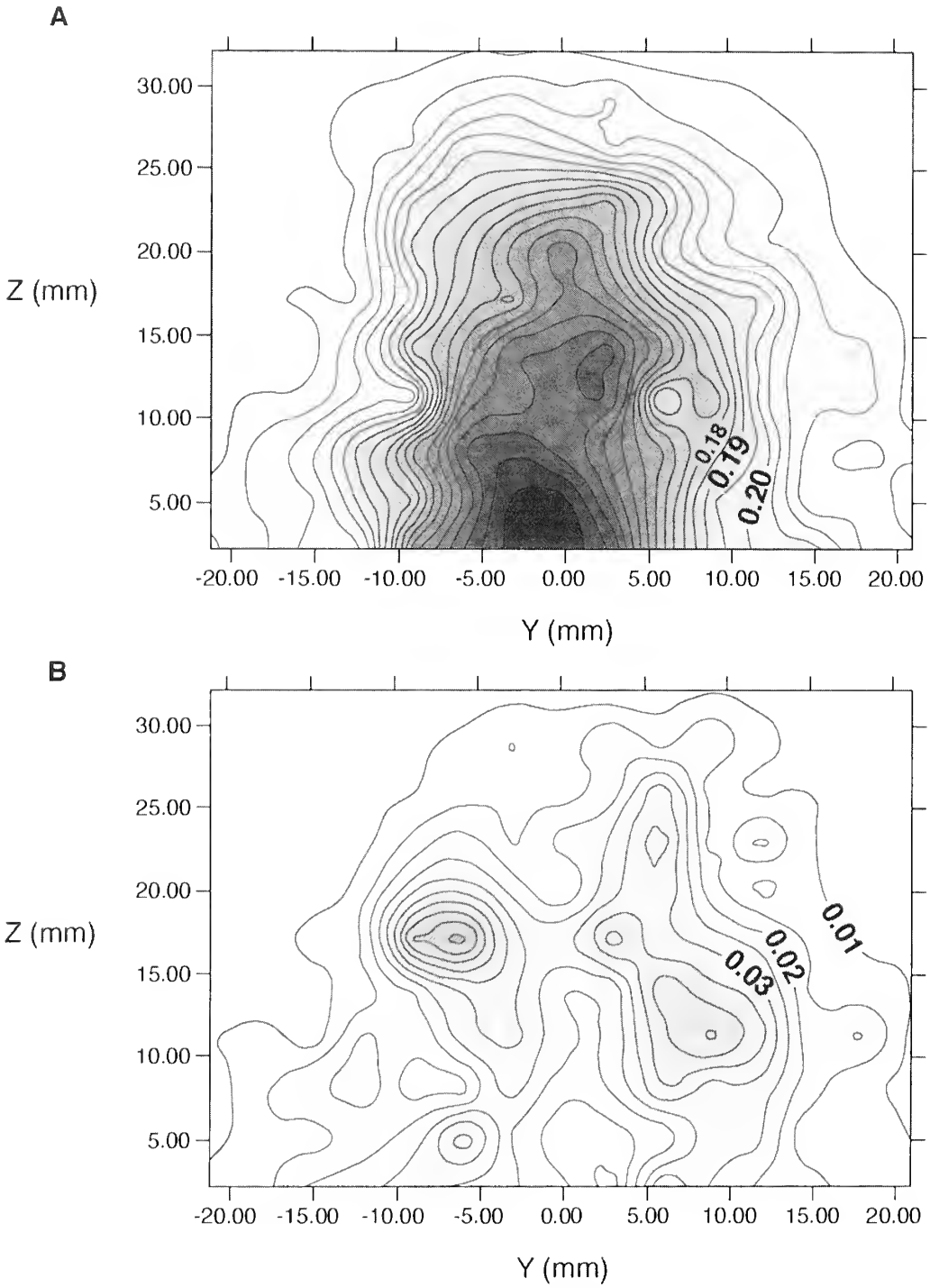

TEXT-FIG. 6. A, contour plot of U velocity for model A at X = 147 mm, towards the closed tip of the sicula. B, contour plot of U_{rms} for model A at X = 147 mm.

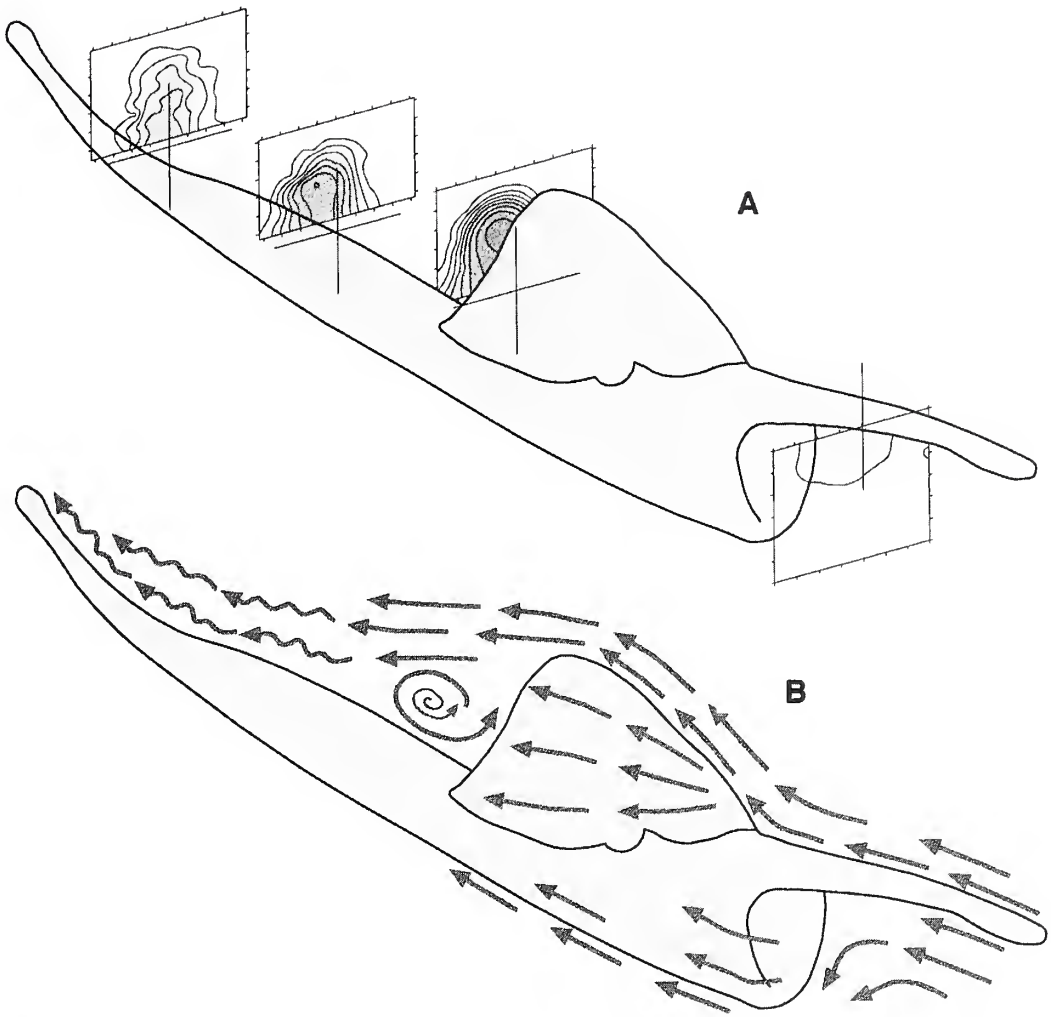

TEXT-FIG. 7. Graptolite model A, with U velocity contour plots, and a sketch showing flow over the model.

RESULTS

Saetograptus chimaera (*Barrande*), *model A*

Four traverses were made of this model, one close to the sicular opening, one just distally of the thecal aperture and two along the length of the nema. The most proximal traverse shows that fluid is deflected around the sicular aperture, partly by the action of the virgella, with flow stagnating within the aperture itself. Flow is directed around the rhabdosome, to the sides and over the theca. Flow along the sicula is retarded by the virgella (Text-fig. 3).

The second traverse, made immediately distally of the aperture of th1 shows that as fluid encounters the thecal aperture, velocity decreases in a zone immediately downstream or distal of it. This is caused by recirculation of fluid in this region and it is therefore a relatively quiet, low velocity region. Fluid also contracts into this region from the sides. Turbulence increases distally of the thecal rim (Text-fig. 4).

At traverse three, the recirculating pocket of fluid generated by the theca is still visible. Flow is

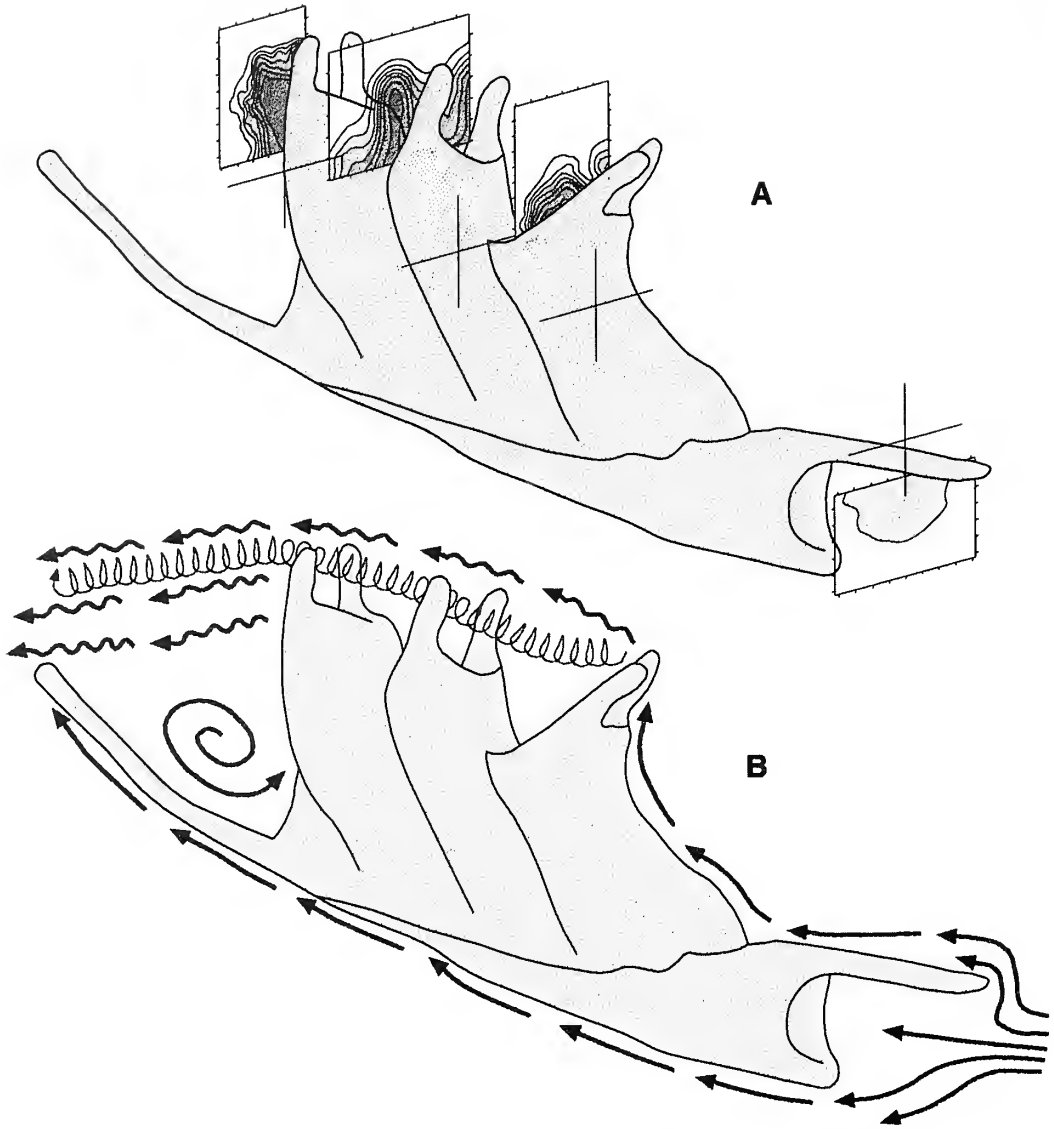

TEXT-FIG. 8. Graptolite model B, with U contour plots, and a sketch showing flow over the model.

directed along the nema and turbulence has increased here to about four times the level in the freestream (Text-fig. 5). This pattern is maintained to traverse four, at which point turbulence has increased to between eight and ten times the undisturbed level and the 'shadow' of the theca as recorded by U velocity is beginning to decay (Text-fig. 6).

These observations are summarized in Text-figure 7, and summaries alone are provided for subsequent models.

Saetograptus chimaera (*Barrande*), *model B*

Four traverses were made along the length of this graptolite, as shown in Text-figure 8. A broadly similar pattern of flow was measured over this model as was found for model A. Distinct differences

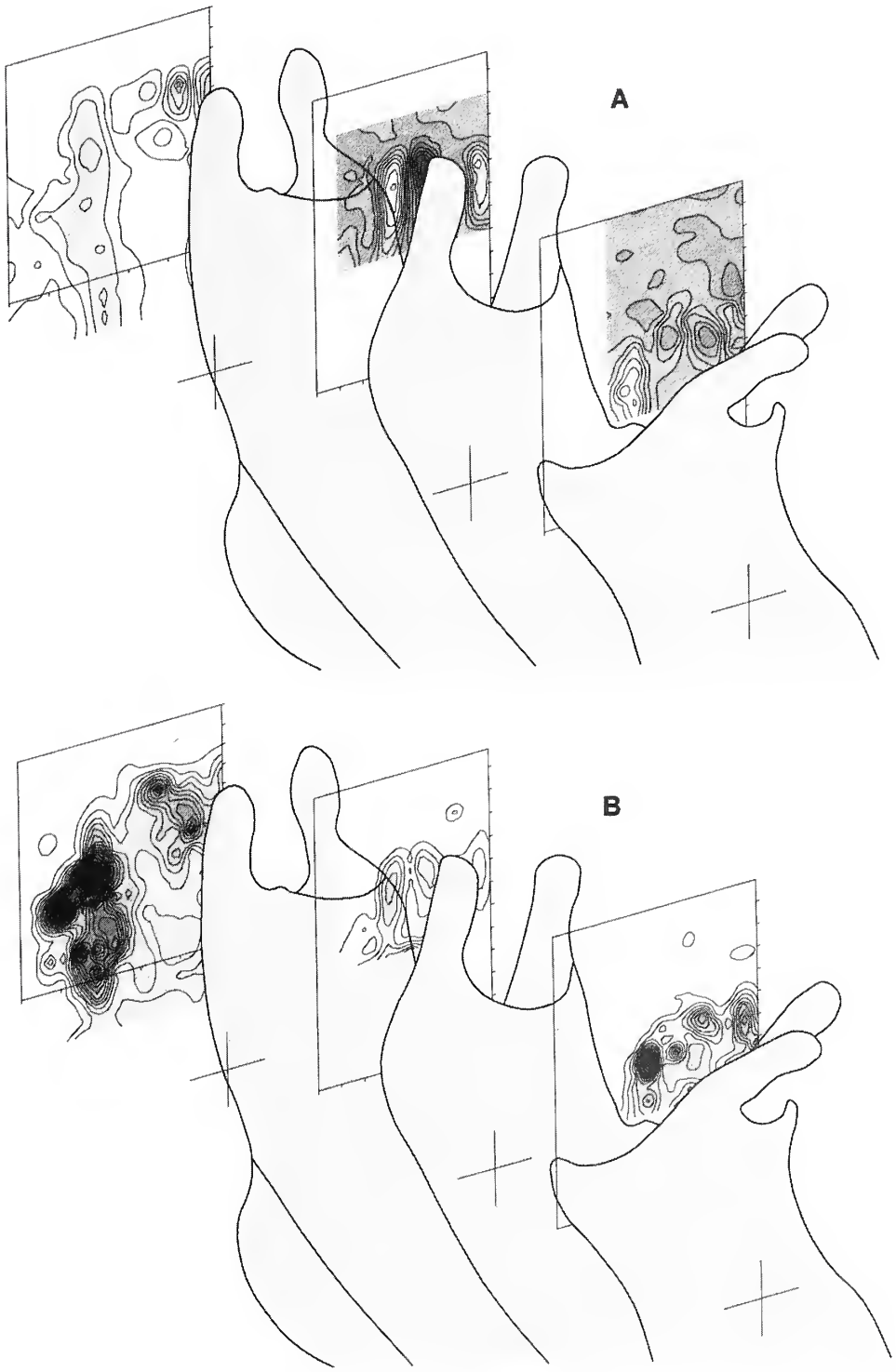

TEXT-FIG. 9. Contours plots of A, V velocity, and B, U_{rms} for model B, showing the effect of paired thecal spines.

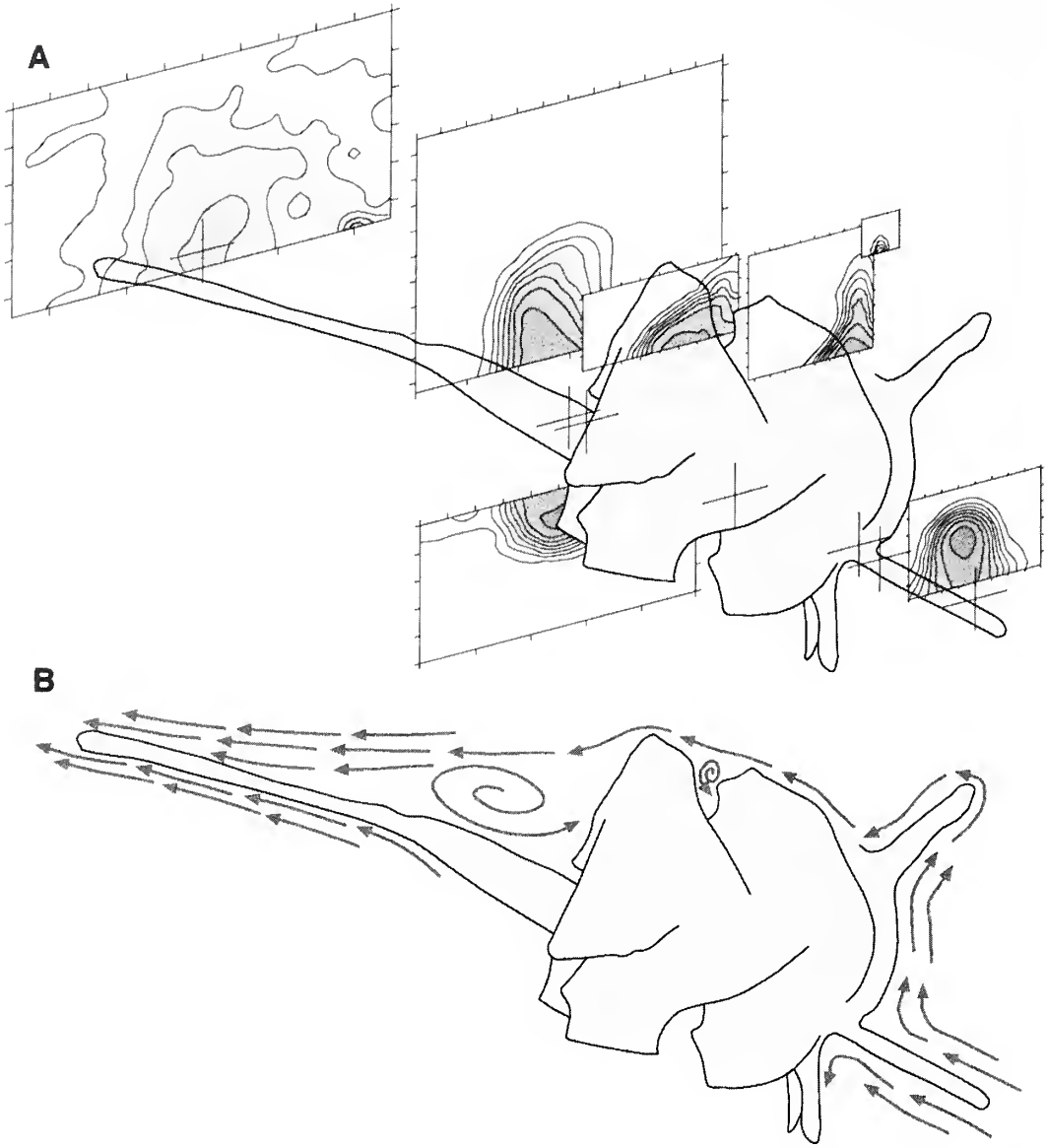

TEXT-FIG. 10. Graptolite model C, with U velocity contour plots and a sketch showing flow over the model.

were caused by the greater number of thecae and by the presence of spines on the thecal apertures. The overall pattern of flow is shown in Text-figure 8 and new features of interest are described below.

Traverse two was taken between the first and second thecal apertures and shows the effect of the two spines which characterize the thecal apertures of this species. Two vortices are created by these spines and shed downstream. The third and fourth traverses, taken distally of the second and third thecae, show that these vortices interfere with those created by subsequent spines so that a wide turbulent zone is created (Text-fig. 9).

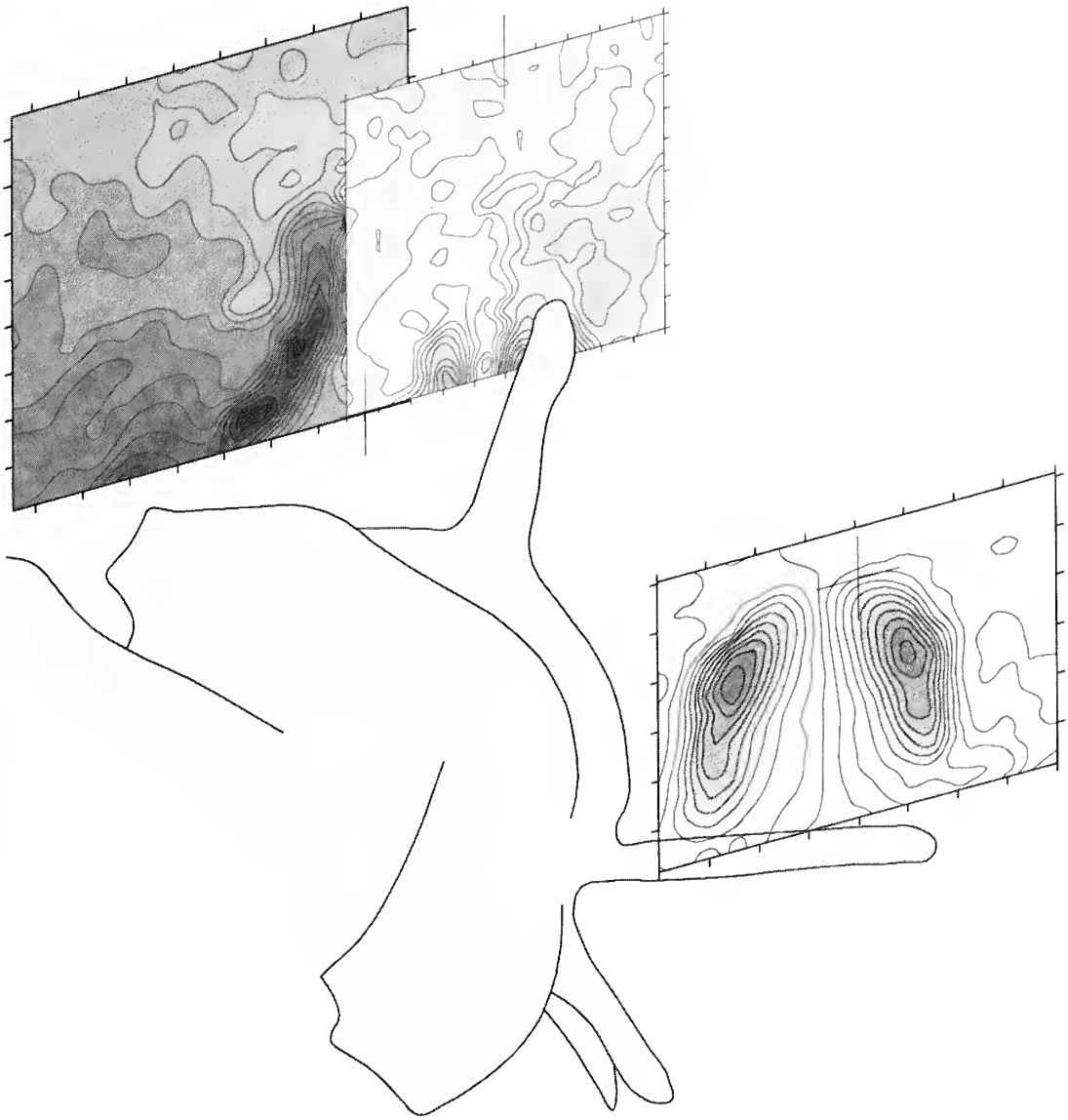

TEXT-FIG. 11. V velocity contour plots over the proximal region of model C.

Amplexograptus maxwelli *Decker, model C*

Eight traverses were made around this model, most of which had their shape defined by the complicated morphology of the graptolite which limited the areas where the lasers could penetrate. The positions of these traverses are shown in Text-figure 10.

Flow encounters both the sicular aperture and the smooth bend of th1[1]. Flow is smooth over this theca to begin with, but it forms vortices as it encounters the thecal spine. The vortices are still effective as they encounter traverse three, which is distal to the aperture of th1[1] (Text-fig. 11).

Further along the model, flow resembles that observed for model 1, but with increasing turbulence with distance along the rhabdosome (Text-fig. 10).

CONCLUSIONS

These results are the first to show details of fluid flow over a graptolite rhabdosome. The most important observation is the general one that many aspects of rhabdosome morphology have a measurable hydrodynamic function which has not previously been recognized. The generation, by spines, of vortices and of increasing turbulence along the rhabdosome is one such observation. The generation of recirculation cells distal to thecal apertures is another. This implies that hydrodynamic effects were a major control on the evolution of different morphologies of graptolites.

The importance of hydrodynamic effects to a graptolite colony would have been two-fold and can be divided into effects on the functioning of the entire colony in the water and on the effects on a single zooid which needed to feed from surrounding sea water. Turbulent wakes would have had the result of increasing drag on the colony and might have slowed it down. However, an assessment of the overall effects of rhabdosome morphology on colony function requires more experimentation.

For a zooid, the pattern of flow around a thecal aperture would have been vital. This study highlights the importance of examining modifications to the thecal apertures of graptolites in more detail. For simple apertures, the observation that flow rate in the aperture itself is low, and that fluid recirculates into the thecal apertures of the models suggests that feeding did not occur within the thecae. Instead, it seems probable that the zooids extended into the surrounding water, or climbed spines where these were present near to the thecal apertures, in order to feed. Modern pterobranchs feed in this manner in order to avoid the low-flow region close to the sea bed (Rigby 1993). Feeding would probably not have occurred in the stagnant area created at the sicular aperture of *S. chimaera*, implying either great mobility of this zooid, its mortality as the colony grew or its lack of feeding function. A second possible function of the virgellar spine might have been to allow this zooid to feed upstream of the stagnant region, although a prime function must have been to deflect flow away from the sicular aperture and along the metatheca of th1.

REFERENCES

BRADSHAW, P. 1970. *Experimental fluid mechanics*. Pergamon Press, Oxford, 413 pp.

BULMAN, O. M. B. 1955. Graptolithina with sections on Enteropneusta and Pterobranchia. *In* MOORE, R. C. (ed.). *Treatise on invertebrate paleontology. Part V*. Lawrence, Kansas, xvii+101 pp.

—— 1964. Lower Palaeozoic plankton. *Quarterly Journal of the Geological Society, London*, **120**, 455–476.

—— 1970. Graptolithina. *In* TEICHERT, C. (ed.). *Treatise on invertebrate paleontology. Part V*. 2nd edition. Geological Society of America and University of Kansas Press, Lawrence, Kansas, xxxii+163 pp.

DRAIN, L. E. 1980. *The laser Doppler technique*. Wiley and Sons, London and New York, 214 pp.

FORTEY, R. A. 1985. Pelagic trilobites as an example of deducing the life habits of extinct arthropods. *Transactions of the Royal Society of Edinburgh: Earth Sciences*, **76**, 219–230.

JEFFERIES, R. P. S. and MINTON, P. 1965. The mode of life of two Jurassic species of *Posidonia* (Bivalvia). *Palaeontology*, **8**, 156–185.

JENKINS, C. in press. Graptolites in a realistic ocean: hydrodynamics, turbulence and encounter. *Alcheringa*.

EXPLANATION OF PLATE 1

Fig. 1. Model of *Amplexograptus maxwelli*.

Figs 2–3. Models of *Saetograptus chimaera*. 3, early growth stage. Scale bars represent 10 mm. Growth lines are slightly schematic, drawn on to the models.

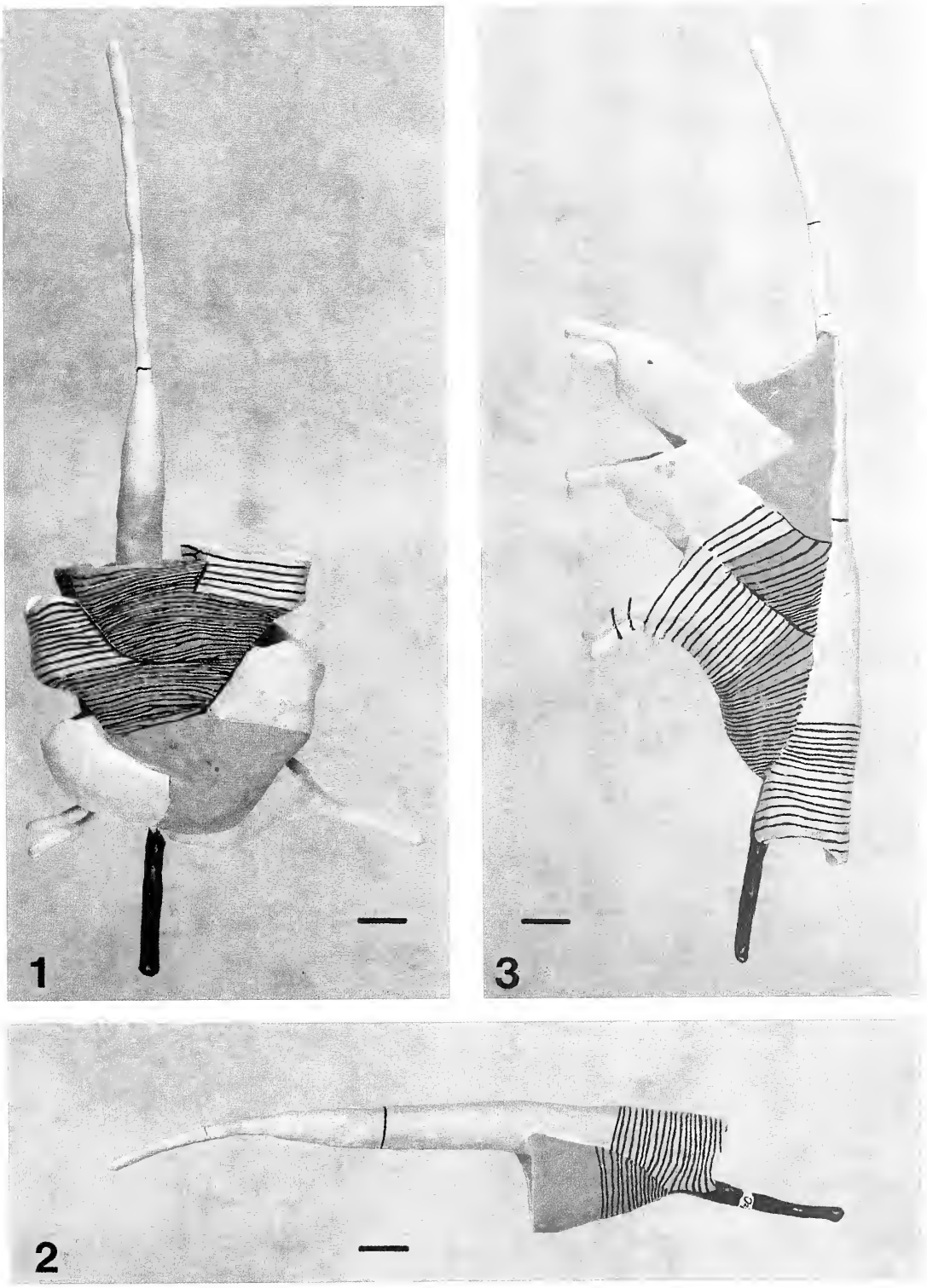

RICKARDS *et al.*, graptolite models

KIRK, N. H. 1969. Some thoughts on the ecology, mode of life and evolution of the Graptolithina. *Proceedings of the Geological Society, London*, **1659**, 273–292.
—— 1972. More thoughts on the automobility of graptolites. *Journal of the Geological Society, London*, **128**, 127–133.
KOZLOWSKI, R. 1966. On the structure and relationships of graptolites. *Journal of Paleontology*, **40**, 489–501.
—— 1970. Nouvelles observations sur les rhabdolpleurides (Pterobranches) Ordovicien. *Acta Palaeontologica Polonica*, **15**, 3–17.
LAPWORTH, C. 1897. Die lebensweise der Graptolithen. 238–258. *In* WALTER, J. (ed.). Lebensweise fossilen meeresthiers. *Zeitschrift der Deutsches Geologisches Gesellschaft*, **49**, 1–453.
MELCHIN, M. and DOUCET, K. M. 1996. Modelling flow patterns in conical dendroid graptolites. *Lethaia*, **29**, 39–46.
NIMMO, M. 1847. Letter to the editor. *Calcutta Journal of Natural History*, **7**, 358–359.
RAYMONT, J. E. G. 1983. *Plankton and productivity in the oceans*. Volume 2: *Zooplankton*. Second edition. Pergamon Press, Oxford, 325 pp.
RICKARDS, R. B. 1975. Palaeoecology of the Graptolithina, an extinct class of phylum Hemichordata. *Biological Reviews of the Cambridge Philosophical Society*, **50**, 397–436.
—— 1996. The graptolite nema: problem to all our solutions. *Geological Magazine*, **133**, 343–340.
—— and RIGBY, S. in press. The functional morphology of graptolites. *In* SAVAZZI, E. *The functional morphology of invertebrate fossils*. John Wiley and Sons, London and New York, 317 pp.
RIGBY, S. 1991. Feeding strategies in graptoloids. *Palaeontology*, **34**, 797–813.
—— 1992. Graptoloid feeding efficiency, rotation and astogeny. *Lethaia*, **25**, 51–68.
—— 1993. Graptolites come to life. *Nature*, **362**, 209–210.
—— and RICKARDS, R. B. 1989. New evidence for the life habit of graptoloids from physical modelling. *Paleobiology*, **15**, 402–413.
RUDWICK, M. J. S. and COWEN, R. 1968. The functional morphology of some aberrant strophomenide brachiopods from the Permian of Sicily. *Bolletin Societa Paleontologia Italica*, **6**, 113–176.
VOGEL, S. 1981. *Life in moving fluids: the physical biology of flow*. Willard Grant Press, Boston, Mass., 298 pp.

BARRIE RICKARDS
Department of Earth Sciences
University of Cambridge
Downing Street
Cambridge CB2 3EQ, UK

SUSAN RIGBY
Department of Geology and Geophysics
Grant Institute
University of Edinburgh
West Mains Road
Edinburgh EH9 3JW, UK

JERRY RICKARDS
TWR Group plc.
Leafield Technical Centre
Leafield, Witney
Oxon. OX8 5PF, UK

CHRIS SWALES
Department of Aerospace Engineering
Queen's Building
University Walk
Bristol BS8 1TR, UK

Typescript received 14 February 1997
Revised typescript received 17 November 1997

PROBLEMS FOR TAXONOMIC ANALYSIS USING INTRACRYSTALLINE AMINO ACIDS: AN EXAMPLE USING BRACHIOPODS

by DEREK WALTON

ABSTRACT. Multivariate statistical analysis of the absolute abundance of amino acids extracted from the intracrystalline sites of brachiopods has the potential for constructing a molecular phylogeny. In all cases, separation of the brachiopods was possible to subordinal level and in some cases to subfamilial level. Older samples showed a merging of closely related genera, indicating the loss of specificity caused by the degradation of amino acids. Amino acid data alone are therefore not sufficient for molecular taxonomy in fossils; the degradative pathways should be sought to allow reconstruction of the original amino acid content.

THE use of proteins and amino acids to differentiate between Recent taxa is an established technique in taxonomic analysis (e.g. Dussart 1983). Mutations in the DNA may result in changes in the primary sequence of a protein and this is reflected in the relative abundance of the amino acids. Speciation is marked by a deviation of the amino acid composition. One of the stated long-term aims of molecular palaeontology is the establishment of a molecular phylogeny through the direct sequencing of fossil peptides and comparison with the sequence in Recent organisms (Curry 1988). Although this approach may have a great deal of value (Cohen 1994), the reality is, however, not straightforward. There have been very few reports of the sequencing of proteins from the shells of organisms (Sucov *et al.* 1987; Robbins and Donachy 1991; Cusack *et al.* 1992) and this paucity of sequence information for shell proteins makes comparisons with information from the fossil record difficult.

Consequently, the use of proteins from the fossil record as a taxonomic tool is restricted, even though their remains occur in the shells and bones of a wide range of organisms and their persistence is well documented (e.g. Abelson 1954; Jope 1967; Wyckoff 1972; Weiner *et al.* 1976; Collins *et al.* 1991; Kaufman *et al.* 1992). It has long been recognized that the original proteins are degraded over time through peptide bond degradation to form mixtures of smaller peptides which are so complex as to defy further purification in most circumstances (Abelson 1954, 1955; Akiyama 1971; Hare and Hoering 1977; Armstrong *et al.* 1983; Qian *et al.* 1995; Walton 1996, in press; cf. Robbins and Brew 1990). Unless a mosaic of overlapping fossil peptides could be used to reconstruct a fossil protein, the rates of amino acid substitution in proteins could not be measured and thus the molecular phylogeny could not be completed. As amino acid substitutions only affect relatively few sites in proteins (Cusack *et al.* 1992), it is likely that these changes would not be observed in fossil peptides.

Decomposition of proteins releases amino acids, and a number of studies have demonstrated that phylogenetic information is recoverable through statistical analysis of the amino acid composition of Recent (e.g. Degens *et al.* 1967; Cornish-Bowden 1979, 1983; MacFie *et al.* 1988; Robbins and Healy-Williams 1991; Walton *et al.* 1993) and fossil (King and Hare 1972; Haugen *et al.* 1989; Robbins and Brew 1990; Kaufman *et al.* 1992; Walton 1996) samples. However, the analysis of fossil proteinaceous remains is hindered as the amino acids undergo severe degradation with the loss of information from the shell, and a subsequent decrease in specificity in the analysis (e.g. Hare and Mitterer 1969; Hare 1974; Robbins and Donachy 1991; Kaufman *et al.* 1992; Walton in press).

Although intracrystalline proteins (*sensu* Sykes *et al.* 1995), are protected by the inorganic phase

[Palaeontology, Vol. 41, Part 4, 1998, pp. 753–770]

(Towe 1980; Collins *et al.* 1988) they are also highly degraded (Collins *et al.* 1991; Walton 1996), thus ensuring that it is unlikely that meaningful sequence data can be resolved from fossil organisms. However, intracrystalline amino acids retain phylogenetic information, as the carbonate of the shell approximates to a closed system (Collins *et al.* 1988; Albeck *et al.* 1993; Walton *et al.* 1993) and thus leaching should not occur. This is in contrast to the more open intercrystalline sites that are prone to leaching of material from the shell (Sykes *et al.* 1995). The residual amino acids and peptides recovered from intracrystalline sites are remnants of the original protein and may be examined in the same way as those extracted from Recent samples (Walton 1996). For amino acids to be of value in the taxonomy of fossils, it is essential that degradative patterns are recognized and that amino acids are extracted from the most protected sites.

The aim of this study was threefold: (1), to undertake multivariate statistical analysis of the amino acid composition of intracrystalline molecules extracted from fossil brachiopods; (2), to demonstrate that taxonomically relevant information can be retrieved despite the degradation of the proteins and amino acids; (3), to highlight potential problems in taxonomic analysis using amino acids and to suggest ways in which such analyses might be refined. The amino acid compositions of these brachiopods and their degradative pathways will be discussed elsewhere (Walton in press) and are not considered in great detail here. This study is concerned with the application of the data to palaeontological analysis.

MATERIALS AND METHODS

Sample collection

Samples of brachiopods (*Neothyris lenticularis*, *Calloria inconspicua*, *Terebratella sanguinea* and *Notosaria nigricans*) and molluscs (turratellids and pectenids) were collected from the rich and diverse fauna of the South Wanganui Basin, North Island, New Zealand (Text-fig. 1; Table 1). These samples contain intracrystalline proteins and amino acids which have been partially characterized (Cusack *et al.* 1992; Walton *et al.* 1993; Walton and Curry 1994; Walton 1996, in press), and have proved to be near-ideal for the investigation of fossil macromolecules as their shells are composed of diagenetically stable low-Mg calcite. Molluscs were collected from the shell beds to act as outgroups in the analysis and to ensure that similarities in the data were due to taxonomic similarities, rather than the homogenization of the amino acid content through the shell bed.

The tectonic setting of the South Wanganui Basin (a back-arc basin) has allowed rapid subsidence and the accumulation of up to 4 km of sediments, most deposited in shallow marine conditions (Anderton 1981), although estuarine and terrestrial facies are recorded (Fleming 1953). Interspersed throughout the sedimentary sequence are a number of richly fossiliferous shell beds containing abundant macrofossils, ranging in age from 120 Ka to *c.* 2·6 Ma.

Sample preparation

Samples were prepared according to the methods of Walton and Curry (1994), in which shells that were excessively bored or fractured were excluded from further study. Adhering sediment was scrubbed from the sample and encrusting epifauna removed by scraping. Articulated shells were disarticulated and body tissue (only present in Recent samples) removed before being incubated in an aqueous solution of bleach (10 per cent. v/v) for 2 hours at room temperature, washed extensively with Milli RO™ water (Millipore) and air dried. Samples were ground using a ceramic pestle and mortar, and the powder incubated in an aqueous solution of bleach (10 per cent. v/v) under constant motion for 24 hours at room temperature, then washed by repeated agitation with MilliQ™ water (Millipore) and centrifugation (typically ten washes) and lyophilized.

An aqueous solution of HCl (2M) at a ratio of 11 μl/mg was used to dissolve the shell powder and release the incarcerated biomolecules. Once demineralization was complete, insoluble particles were removed by centrifugation (20 g.h.). All samples were hydrolysed by vapour-phase HCl (6N) automated hydrolysis (Applied Biosystems 420A; Dupont *et al.* 1989). Standard proteins and peptides were used during every analysis to ensure that hydrolysis proceeded to completion. Blank

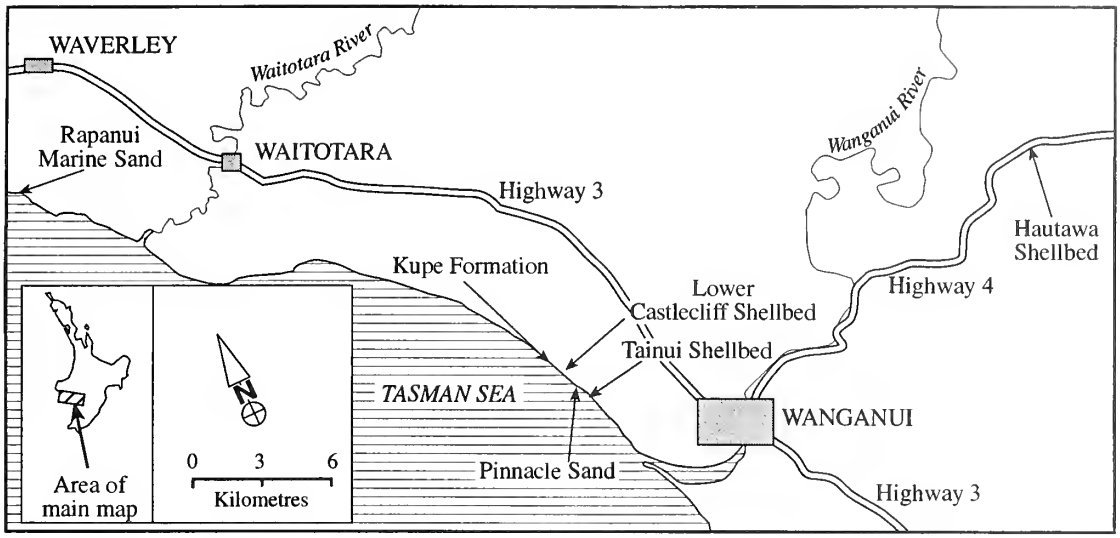

TEXT-FIG. 1. Locations of the horizons from which samples were collected (adapted from Fleming 1953).

TABLE 1. Locations of samples utilized in this study. Grid references correspond to the maps accompanying Fleming (1953).

Horizon	Location	Grid reference
Rapanui Marine Sand	Waipipi Beach	N137/168 993
Tainui Shellbed	Castlecliff Beach	N137/485 888
Pinnacle Sand	Castlecliff Beach	N137/479 895
Lower Castlecliff Shellbed	Castlecliff Beach	N137/470 902
Kupe Formation	Castlecliff Beach	N137/459 908
Hautawa Shellbed	Parapara Road	N138/803 029

analyses were included to check for background levels of contamination. Individual amino acids were derivatized using phenylisothiocyanate (Heinrikson and Meredith 1984), and transferred to a dedicated narrowbore hplc system for separation and quantification. Analyses were repeated at least three times. The data were subjected to principal components analysis (PCA; Davis 1986) using the statistical analysis program DATADESK™.

It is usual 'to extract only enough eigenvectors to remove the majority, say 75 per cent., of the total variance of the data matrix' Sneath and Sokal (1973, p. 246). From computer calculations, it can be seen that the majority of the variance within the samples can be defined by the first three eigenvectors. This representation of the amino acids in PCA form in three dimensional space is a useful method of comparing multivariate distributions of a larger sample size.

RESULTS

The state of molecular preservation of the intracrystalline proteins and amino acids in these fossils is reported elsewhere (Walton 1996, in press). Proteins are almost completely hydrolysed by 120 Ka and the amino acids have degraded relatively rapidly (although at different rates and by different pathways) over the 2·2 Ma of the study. This degradation of amino acids will lead to changing concentrations of the molecules, therefore changing the data for the PCA (Walton in press). As a consequence, the resolution of the PCA should decrease as samples of increasing age are analysed.

Interpretation was made in two ways, within and between individual horizons, in order to

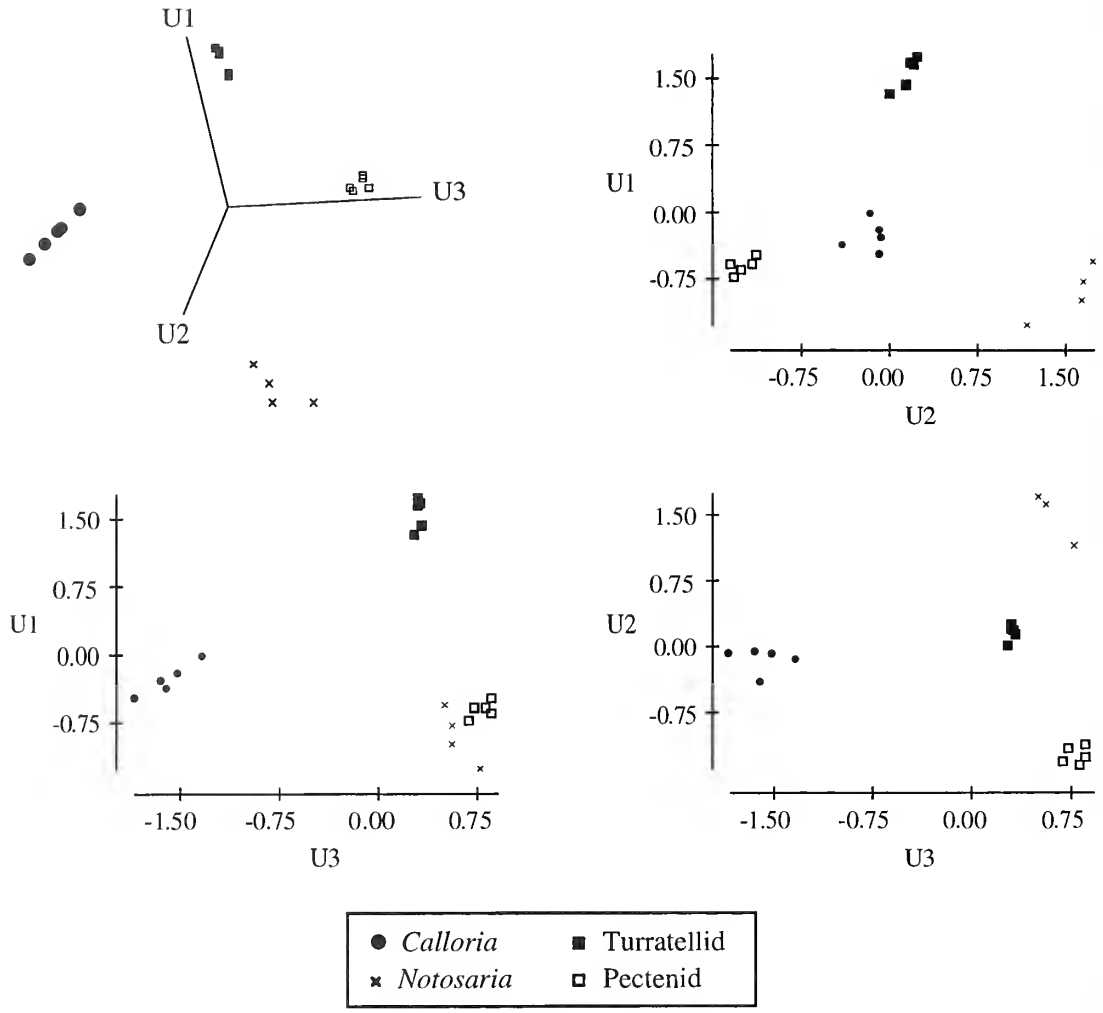

TEXT-FIG. 2. Plots of the first three principal components for the concentration of amino acids from samples collected from the Rapanui Marine Sand. Scatterplots are shown in this and subsequent figures to allow better interpretation of the 3D plot to the left, in which the axes are at 90°. Note the good separation of all data points.

determine how time will affect the separation of groupings identified in Walton *et al.* (1993). As the PCA is derived from a specific dataset (i.e. the amino acid content of fossils from a horizon), graphical representations from each horizon cannot be compared directly (as the information in each diagram is sourced from different data). To compare data from different horizons it is therefore necessary to complete a new PCA including all of the data simultaneously rather than individually.

Samples collected from the same horizon should be of approximately the same age, and will have been subjected to approximately the same geological processes during their history. The effect of this is to render the horizon as a time plane (similar to that of the Recent, a 'snapshot' of geological time, although see Norris and Grant-Taylor (1989) and Wehmiller *et al.* (1995) for discussion of homogeneity in shell beds). Changes in the amino acid content due to diagenetic alteration will be of approximately the same order in all samples, and hence differences between the amino acid compositions will be due to the initial biochemical composition of the species alone. This is obviously an oversimplification of possible relationships, and the amino acid composition of the

TABLE 2. Principal component analysis calculated from the absolute abundance of amino acids in the sample. Only the first three eigenvectors and eigenvalues are given in each case. NI = data not included for PCA.

	Sample location																	
	Rapanui Marine Sand			Tainui Shellbed			Pinnacle Sand			Lower Castlecliff Shellbed			Kupe Formation			Hautawa Shellbed		
Eigenvalue	**e1**	**e2**	**e3**	**e1**	**e2**	**e3**	**e1**	**e2**	**e3**	**e1**	**e2**	**e1**	**e1**	**e2**	**e3**	**e1**	**e2**	**e3**
Values	7·908	3·824	1·355	6·588	3·931	2·158	6·841	3·515	1·902	8·437	2·901	1·501	10·047	2·894	0·601	5·992	3·423	1·954
Variance	56·5	27·3	9·7	47·1	28·1	15·4	48·9	25·1	133·6	60·3	20·7	10·7	71·8	20·7	4·3	46·1	26·3	15
Proportion																		
Total variance		93·5			90·6			87·6			91·7			96·8			87·4	
Eigenvectors	**V1**	**V2**	**V3**	**V1**	**V2**	**V3**	**V1**	**V2**	**V3**	**V1**	**V2**	**V3**	**V1**	**V2**	**V3**	**V1**	**V2**	**V3**
D	−0·248	0·260	0·407	−0·272	0·209	0·381	−0·327	0·162	0·269	−0·321	−0·106	−0·208	−0·304	0·119	−0·071	−0·329	0·249	0·166
E	**−0·334**	−0·099	0·069	−0·352	−0·172	−0·018	−0·341	−0·143	−0·020	**−0·329**	0·001	0·135	**−0·311**	−0·030	0·129	−0·125	**−0·453**	0·200
S	−0·241	−0·346	0·233	−0·236	−0·374	0·070	−0·333	−0·191	−0·054	−0·313	−0·137	−0·231	−0·233	0·254	0·124	−0·218	−0·205	0·137
G	−0·294	0·241	−0·238	−0·251	0·327	−0·241	−0·071	0·387	−0·406	0·030	**0·549**	−0·196	−0·275	0·258	−0·250	−0·328	−0·144	−0·376
R	−0·271	0·229	0·080	**−0·362**	0·067	−0·115	**−0·363**	−0·085	−0·040	−0·296	0·015	−0·208	−0·299	−0·005	0·236	NI	NI	NI
T	−0·295	−0·041	0·056	−0·167	0·350	0·356	−0·144	**0·427**	0·318	−0·314	−0·008	−0·231	−0·002	**−0·517**	**−0·579**	**−0·356**	0·248	0·090
A	**−0·342**	−0·082	−0·005	**−0·363**	0·121	0·122	**−0·361**	0·164	0·018	−0·326	0·073	−0·185	**−0·309**	0·091	−0·109	**−0·390**	0·089	−0·126
P	−0·251	0·176	**−0·530**	−0·213	0·032	**−0·473**	−0·039	0·046	**−0·444**	−0·139	0·356	**0·493**	−0·301	−0·101	−0·315	0·084	**−0·511**	−0·125
Y	−0·187	**0·404**	0·229	−0·198	**0·417**	0·076	−0·143	**0·488**	0·019	−0·051	**0·518**	−0·167	−0·293	0·182	0·190	−0·329	0·267	0·105
V	−0·300	−0·012	**−0·444**	−0·277	0·110	−0·440	−0·177	0·170	**−0·594**	−0·138	0·489	0·069	−0·305	0·119	−0·077	−0·212	−0·209	**−0·459**
I	−0·228	−0·345	−0·181	−0·298	−0·275	−0·141	−0·335	−0·211	−0·079	−0·321	0·008	−0·001	−0·300	0·029	**−0·386**	−0·218	−0·331	−0·068
L	−0·171	**−0·409**	0·287	−0·142	**−0·433**	0·150	−0·254	−0·303	0·144	−0·305	−0·146	0·293	−0·168	**−0·489**	0·198	0·134	−0·215	**0·594**
F	−0·249	0·317	0·253	−0·183	−0·028	**0·388**	−0·141	0·342	0·282	−0·227	−0·023	**0·595**	−0·212	−0·427	0·181	−0·313	−0·055	0·322
K	−0·273	−0·320	0·022	−0·299	−0·295	0·140	−0·358	−0·168	−0·007	**−0·329**	−0·084	−0·030	−0·250	−0·314	0·368	−0·344	−0·211	0·222

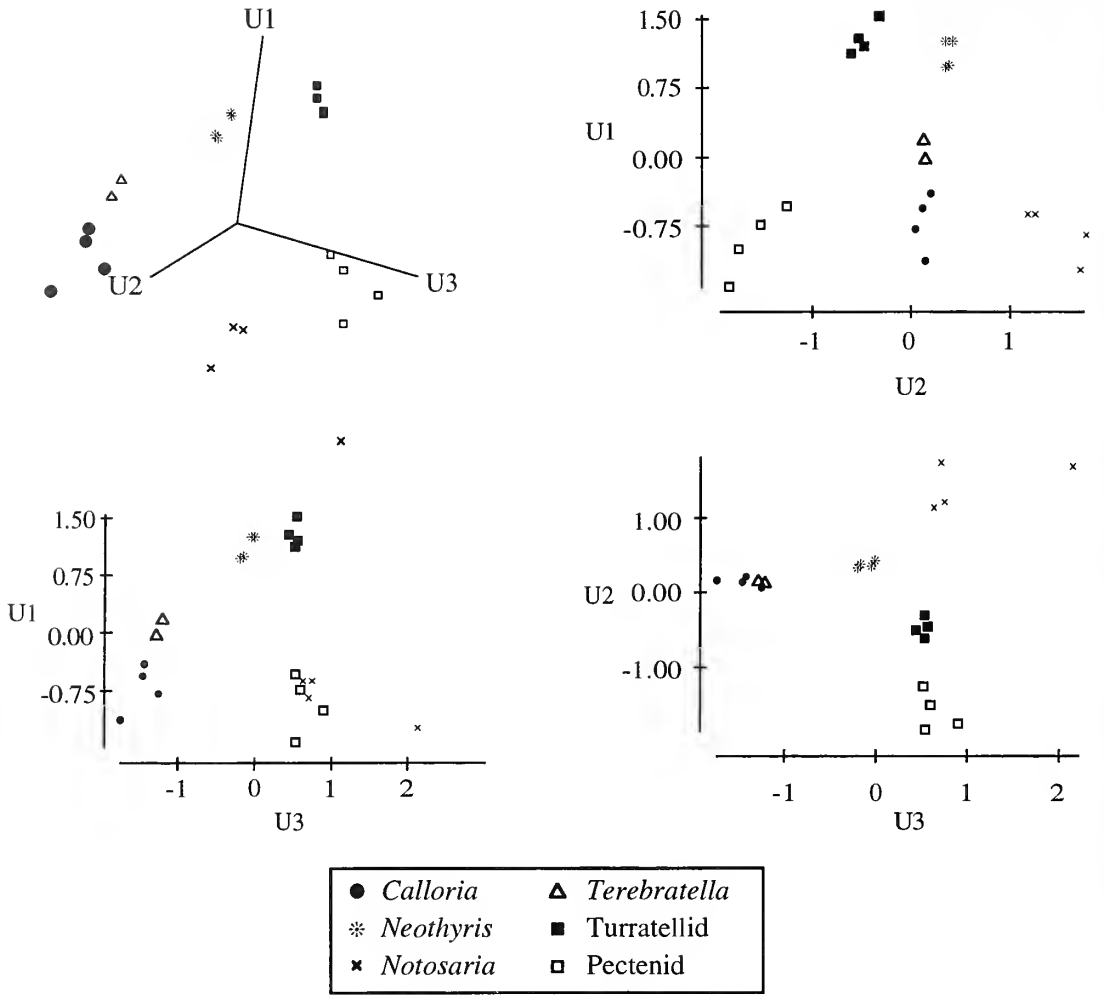

TEXT-FIG. 3. Plots of the first three principal components for the concentration of amino acids from samples collected from the Tainui Shellbed. All samples are well separated, with classification of the Terebratulida to the subordinal level (see text).

fossils will be distorted over time by, for example, the rate and degree of diagenetic production of some amino acids, which will in turn depend on the initial concentration, the effect of carbohydrates and of different mixtures of amino acids in the sample (Walton in press). However, as the amino acids are contained within a single time plane, and provided that there has been no homogenization of the amino acid composition of the samples in the horizon through time, similar methods of taxonomic discrimination can be used as for the Recent samples (Walton *et al.* 1993). Amino acids are referred to by their standard three letter codes (Appendix 1).

Within horizons

The Rapanui Marine Sand (*c.* 0·12 Ma) is the youngest of the horizons considered in the present study. The first three principal components (Table 2) contain 93·5 per cent. of the total variation of the dataset, mainly due to Glutamic acid (Glu) and Alanine (Ala) for the first, Tyrosine (Tyr) and Leucine (Leu) for the second, and Aspartic acid (Asp), Proline (Pro) and Valine (Val) for the third.

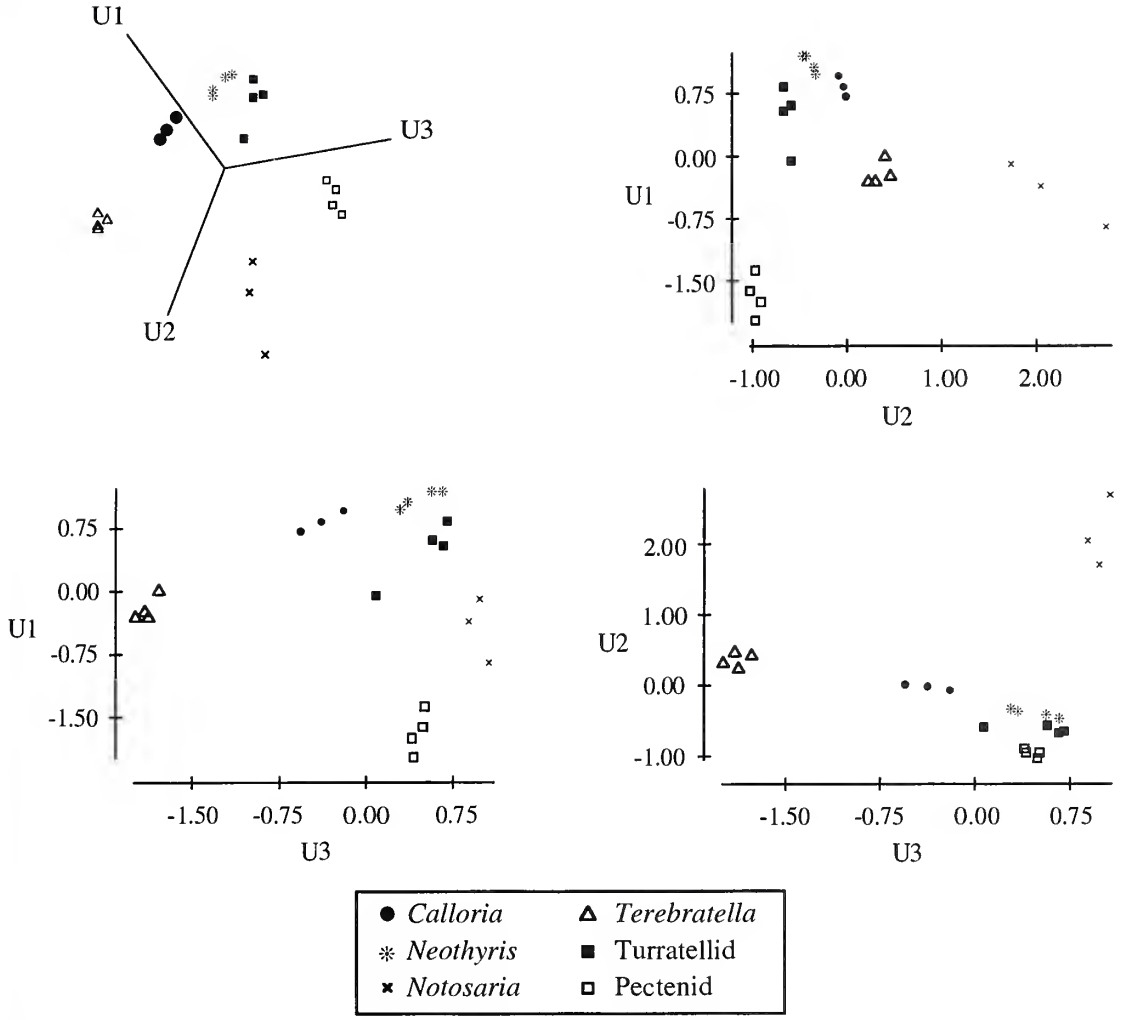

TEXT-FIG. 4. Plots of the first three principal components for the concentration of amino acids from samples collected from the Pinnacle Sand. All samples are well separated to the subordinal level (see text).

Graphical representation of the first three principal components (Text-fig. 2) shows that separation of samples by this method is good to at least the subordinal level. Specimens of *Neothyris lenticularis* present in the sample collected are derived (Walton 1992) and are not included in this analysis.

For the Tainui Shellbed (*c.* 0·40 Ma), PCA recalculates 90·6 per cent. of the variance within the first three eigenvalues (Table 2). The variability of the first principal component is caused mainly by Arginine (Arg) and Ala (Table 2), the second by Tyr and Leu, and the third by Pro and Val. A plot of the samples on the first three eigenvectors shows that there is good separation of the genera in space (Text-fig. 3). There has been no homogenization of the amino acid composition in samples through the horizon. The brachiopod samples are well separated at the ordinal level, with *Notosaria nigricans* (Rhynchonellida) plotting well away from the three species assigned to the Terebratulida. The three species in the Terebratulida may also be separated.

The first three principal components for the samples from the Pinnacle Sand (*c.* 0·42 Ma) contain 87·6 per cent. of the variation of the samples (Table 2). The first principal component has variation mainly due to the concentration of Arg and Lysine (Lys), the second due to Threonine (Thr) and

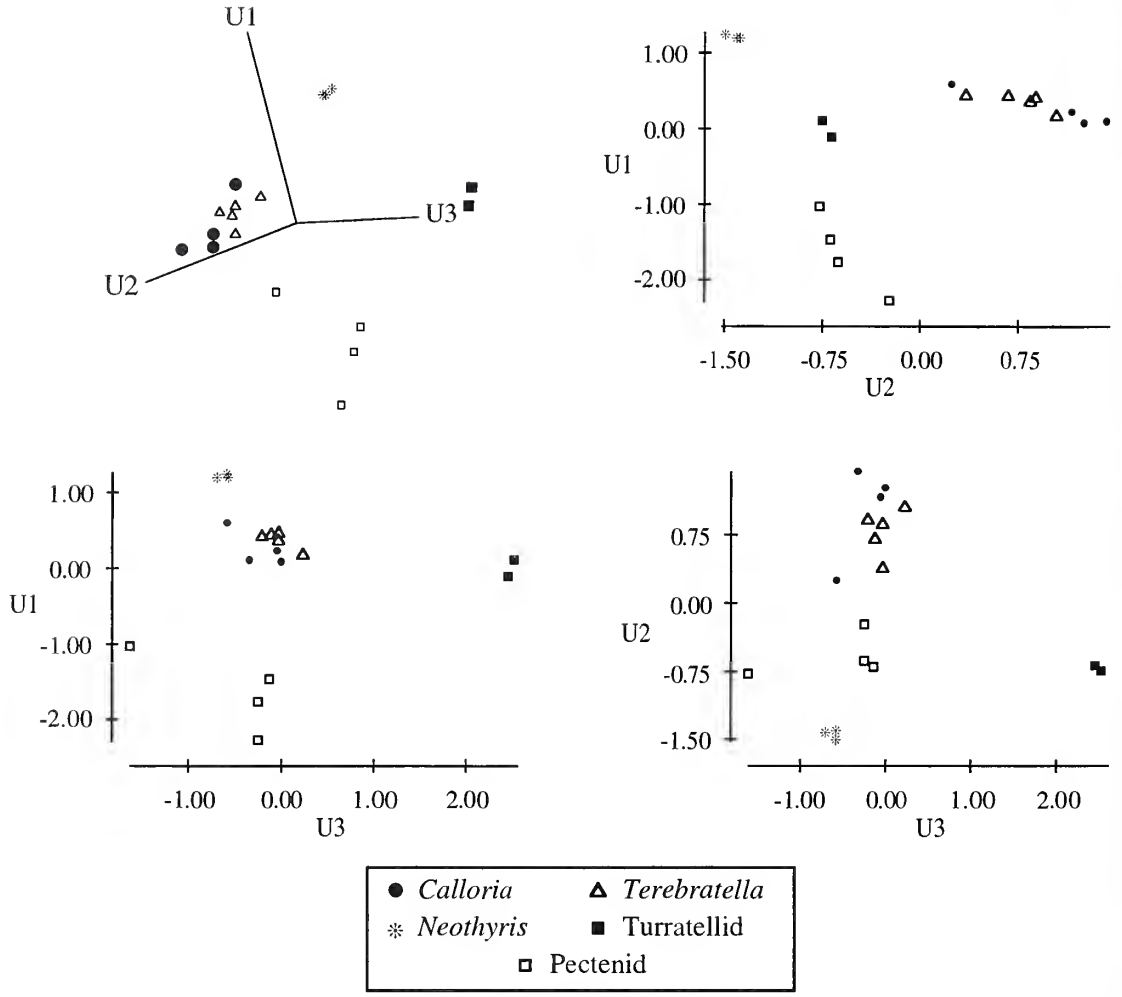

TEXT-FIG. 5. Plots of the first three principal components for the concentration of amino acids from samples collected from the Lower Castlecliff Shellbed. Note the merging of data points for the Terebratulida caused by the reduction of information available due to the degradation of amino acids in the sample (see text).

Tyr, and the third to Glycine (Gly), Pro and Val. Once again, there is good separation for all samples at the ordinal level (Text-fig. 4).

Samples from the Lower Castlecliff Shellbed (*c.* 0·44 Ma) are beginning to show the influence of time. The first three principal components contain 91·7 per cent. of the dataset variation (Table 2), which is due to Glu and Lys in the first principal component, the second by Gly, Tyr and Val, and the third has variation mainly due to Pro and Phenylalanine (Phe). Although the outgroups are well separated from the brachiopods (Text-fig. 5), and *Neothyris lenticularis* is separated, the brachiopod samples assigned to the subfamily Terebratellinae are plotting closer together and the data for the samples are beginning to merge, lowering the level of taxonomic information available.

Samples from the Kupe Formation (*c.* 0·5 Ma) did not include either *Notosaria nigricans* or a pectenid. The first three principal components contain 96·8 per cent. of the variation of the dataset (Table 2), due mainly to the variation of Glu and Ala for the first principal component, Thr and Leu for the second, and Thr for the third. All samples are well separated (Text-fig. 6).

The data for the Hautawa Shellbed (*c.* 2·20 Ma) show that 87·4 per cent. of the variation of the

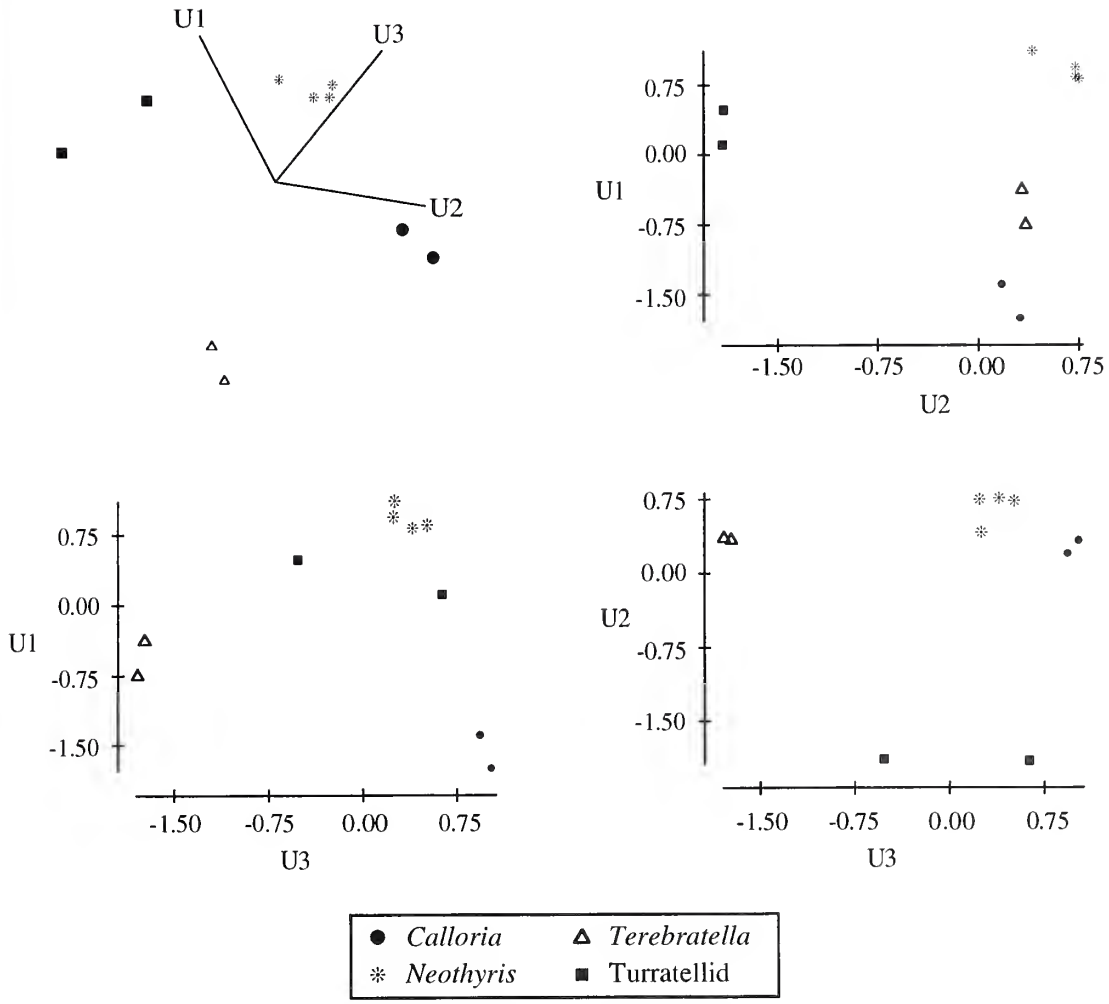

TEXT-FIG. 6. Plots of the first three principal components for the concentration of amino acids from samples collected from the Kupe Formation. Although separation is possible to below the subfamily level, there are fewer data points available and these tend to be more widely separated within a grouping (see text).

dataset is contained within the first three principal components (Table 2). This is due mainly to Thr and Ala for the first principal component, Glu and Pro for the second and Val and Leu for the third. No Arg remained in any sample and thus was omitted from the PCA. The samples are well separated by the amino acid data (Text-fig. 7), with both outgroups and *Notosaria nigricans* plotting away from the Terebratulida. Within this latter group, *Calloria inconspicua* and *Neothyris lenticularis* are also well separated, although the data points are more widely spaced for each taxon.

Between horizons

All samples analysed in this study were incorporated into the same dataset and a new PCA completed, in order to ascertain whether a taxonomic signal was preserved through geological time at a high enough level to allow similar samples to plot close together. The abundances of Serine (Ser), Arg and Thr were omitted from this calculation, as in some of the older samples they are completely decomposed.

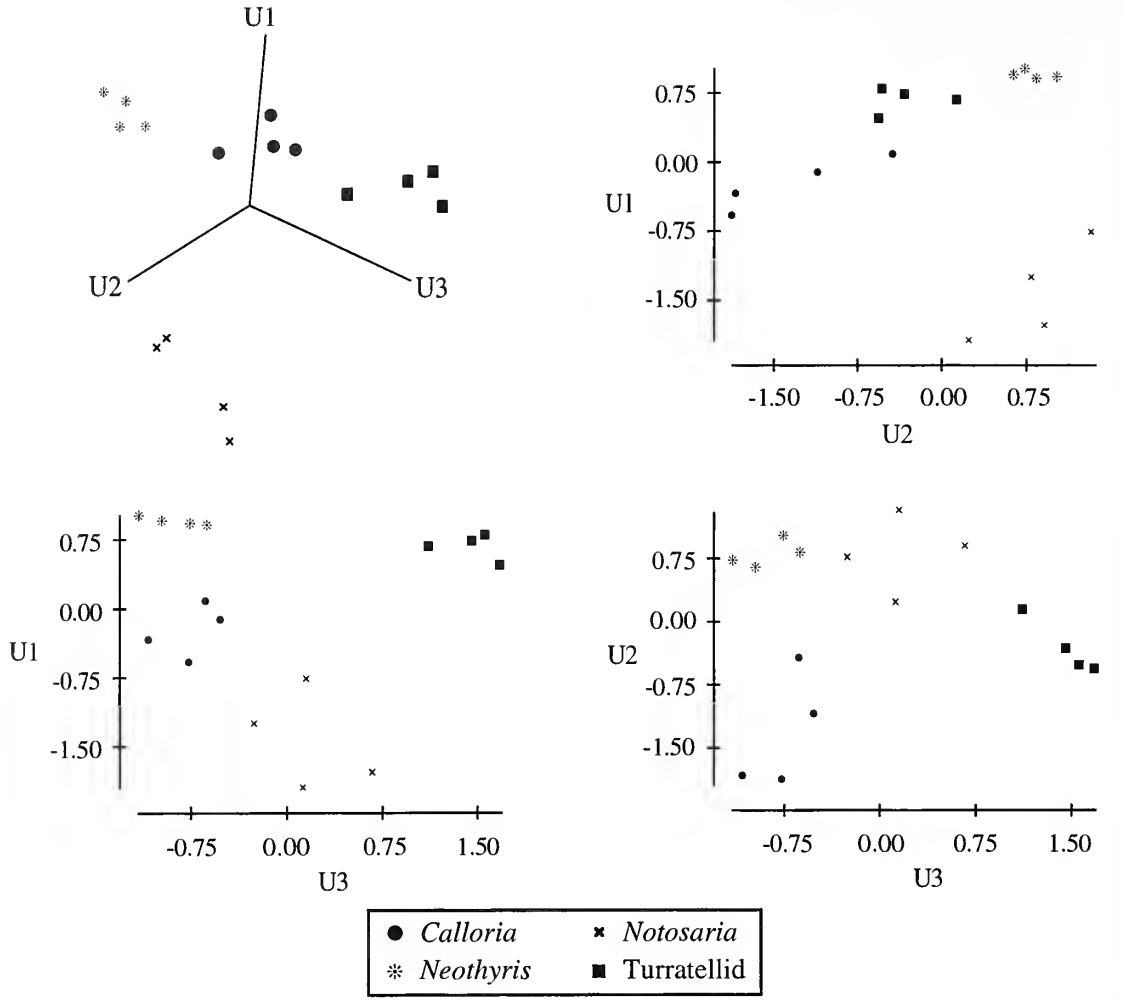

TEXT-FIG. 7. Plots of the first three principal components for the concentration of amino acids from samples collected from the Hautawa Shellbed. Note the spreading of the data within the groupings caused by the loss of specificity due to amino acid degradation (see text).

For comparison between horizons the data was examined in two ways. Text-figure 8A shows the plot of the first three principal components derived from the absolute concentration of amino acids in the samples. The first three principal components contain 89·4 per cent. of the total variation present in the dataset, although the data points do not appear to contain any significant order and there is a great deal of overlap between the taxa. Text-figure 8B was constructed using the relative abundance of the amino acids, with 82·4 per cent. of the variation in the dataset being contained within the first three principal components. In this case the taxa may be split into four main groupings: Terebratulida, Rhynchonellida, pectenids and turratellids. There is clearly a major difference between the two datasets, although the groupings show that some degree of taxonomic separation is possible from a dataset that includes both Recent and fossil material, back to 2·2 Ma.

The two outgroups, pectenids and turratellids, form distinct groupings, as would be expected from members of different phyla. The brachiopods form two groups, with Rhynchonellida grouping away from Terebratulida. Within Terebratulida, no differentiation can be made, as the variation in

the data causes a spread that encompasses the data from the entire order. Several of the samples plot away from their respective groupings, and there is considerable spread within groups, caused by the differing ages and therefore differing amounts of decomposition of the amino acids.

DISCUSSION

The amino acid compositions extracted from intracrystalline sites and presented here are complex datasets containing up to 14 variables. Information contained within datasets of this size are difficult to assimilate, and it is difficult to observe the relationships between amino acids as these are between every member of the dataset rather than between one or two variables. PCA has the advantage of summarizing this large amount of information into fewer, derived variables which may then be used to differentiate the samples. Such a method has been used in the classification of Recent and fossil Foraminifera (King and Hare 1972; Haugen *et al.* 1989) and Recent molluscs (Degens *et al.* 1967). In studies that included both fossil and Recent data in the same calculations there is a large spread of data within the analyses, similar to that observed in this study.

The format of the data to be processed by multivariate analysis is of importance, as this may affect the behaviour of the data. Kaufman *et al.* (1992) identified three ways in which amino acid data could be expressed for utilization in amino acid taxonomy, none of which is without problems:

1. The absolute concentration of the amino acids in the sample. Although this is a true reflection of the abundance, it is prone to errors in the measurement of sample size and from the behaviour of the molecules in response to different buffer conditions across several analyses. When samples of differing age are compared, there may be problems with much of the difference between samples being taken up in the variation due to the spread of concentration in a particular taxon (caused by the differential degradation of the molecules over time), rather than in the actual differences between the samples.
2. The use of relative concentration of amino acids in the sample (proportions of the total composition) suffers from closed array interdependency, whereby an error in the measurement of one component is reflected in the abundance of the others. The degradation of unstable amino acids and the production of others will also affect the relative abundance the original molecules. However, such an analysis will preserve the relative abundance of each amino acid and is useful when samples of different age are studied (see above).
3. Ratios of the absolute abundance of amino acids, usually in pairs. The main drawback of this approach is the number of possible pairs of amino acids considered for analysis. As a result, it is usually a subset of the possible pairs which are examined. For example, Andrews *et al.* (1985) and Haugen *et al.* (1989) considered eight amino acid ratios, whilst Kaufman *et al.* (1992) examined a subset of five, consisting of the most stable molecules. This approach results in the loss of information from the other amino acids not included in the samples.

Ratios between the amino acids have been the most common of the data formats thus far utilized for amino acid taxonomy of fossils (e.g. Jope 1967; Haugen *et al.* 1989; Kaufman *et al.* 1992). However, from the data presented in this study the ratios between the pairs of amino acids range over a wide scale, and there is an overlap between the ratios. Walton and Curry (1994) suggested utilizing relative abundances in PCA, although the level of information retrieved by this is less than when the absolute abundances are used (Text-fig. 9; cf. Text-fig. 5). For these reasons, and recognizing the problems outlined above, it is considered that the highest levels of taxonomic information in this case are revealed through the use of absolute abundances of amino acids.

For each horizon in this study, every grouping of samples has a characteristic amino acid signature that is sufficiently different to allow separation of different taxa and convergence of similar taxa. Each major grouping is discrete, indicating that there has been no homogenization of the amino acids in the horizon. Samples that have a similar amino acid composition will plot closer together than those which have a different composition. Samples which are morphologically distinct (e.g. members of different phyla or classes) have amino acid compositions that are very different. Hence the brachiopods are well separated from the outgroups (molluscs) in all cases. Within a class,

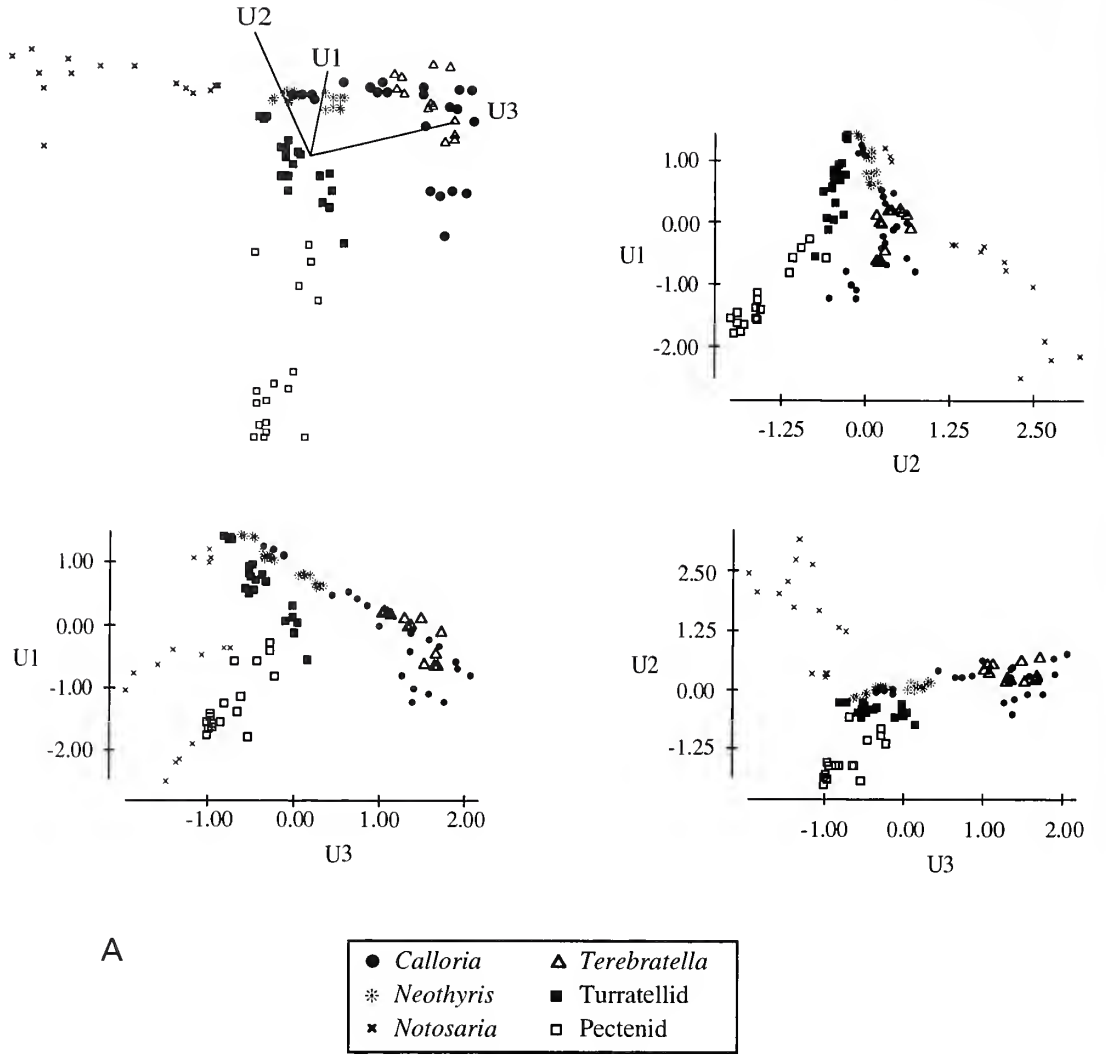

TEXT-FIG. 8. For legend see opposite.

separations are also very distinct at the ordinal level (e.g. between Rhynchonellida and Terebratulida). These amino acid signatures must reflect original genetic differences between the samples.

In fossil samples, as might be expected, the best separation of the taxa is gained when utilizing the youngest samples. As samples from successively older horizons are considered, the level of taxonomic information present within the shell generally decreases. This is due to the older samples containing macromolecules which have been degraded to a higher degree than have those of younger samples. This degradation is recognized by the merging of the formerly discrete groupings, representing the loss of differences between the amino acid compositions of the taxa. As degradation proceeds, differences between the relative amino acid composition will be reduced (by the loss of the less stable molecules and the gain, both relative and absolute, of others). The merging of datapoints represents the decay of unstable amino acid molecules and the diagenetic production of others which are important in differentiating between species. This process has an endpoint of the amino

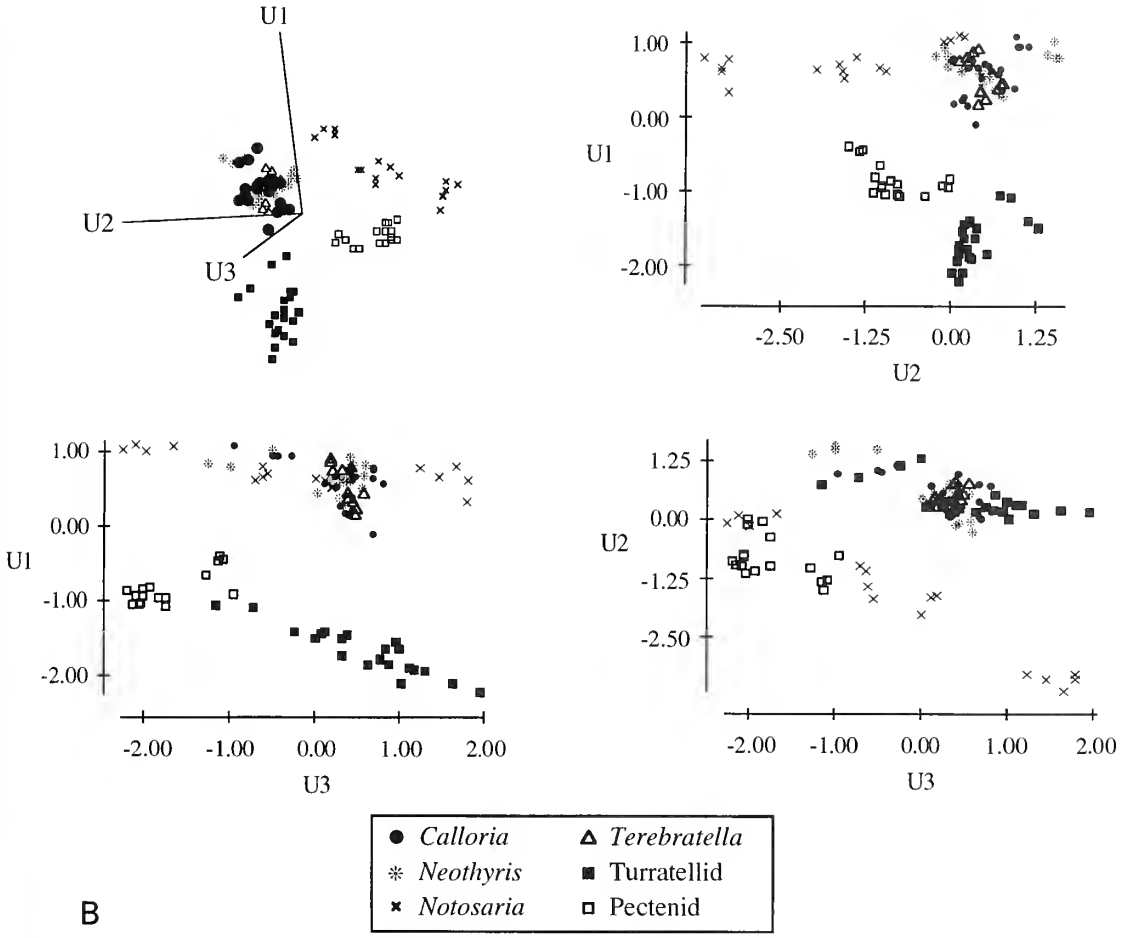

TEXT-FIG. 8. Plots of the first three principal components for the concentration (A) and relative abundance (B) of amino acids in all samples combined together to examine the preservation of taxonomic signal in samples of differing ages. In A, it is not possible to recognize definite groupings. This is caused by much of the variation being taken up by the difference in abundance of the individual amino acids in the sample, rather than the difference in composition between the samples. However, in B, four groupings may easily be identified. In this case, the variation due to concentration in the sample size is removed by using the relative proportions of the amino acids which are preserved regardless of the concentration (see text).

acid content being similar (although not identical) in all samples. Merging of samples demonstrates the importance of retaining as much original information as possible; selecting groups of amino acids as the starting point for taxonomic analysis may reduce the level of taxonomic significance observed.

When samples of different ages are analysed together, a 'typical' amino acid composition is recognized which enables groupings of similar organisms to be made. The degradation of amino acids does not distort the amino acid signature of the sample to a level where it is similar to others from a different order. The degradation of unstable amino acids over time follows a pattern that is similar for all brachiopod species analysed (Walton 1996, in press). It is likely that the same will hold true for other samples. Once free from their proteins, the amino acids will behave as individual molecules and their degradation will no longer be influenced by the primary or higher order structure of the protein. No contaminating extraneous molecules will be included in the analysis,

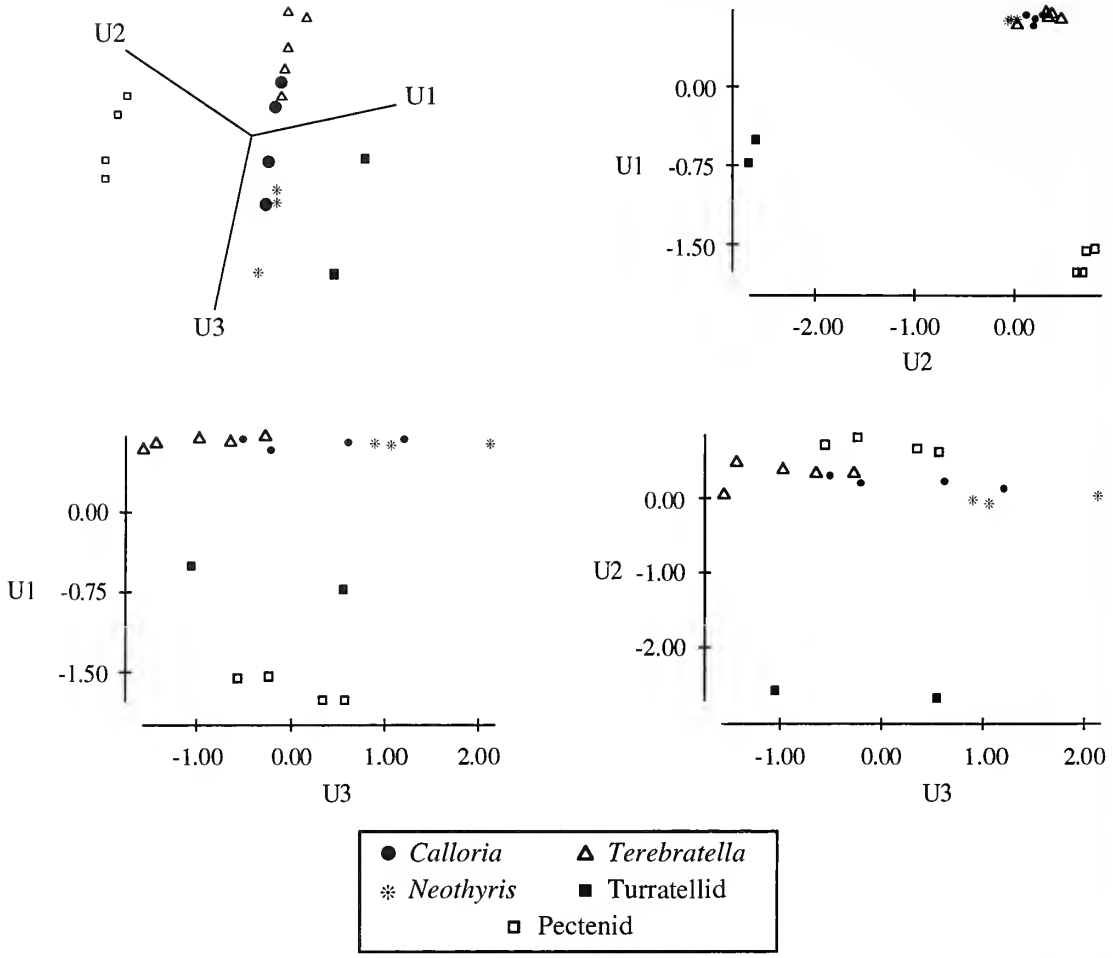

TEXT-FIG. 9. Plots of the first three principal components for the relative proportions of amino acids from samples collected from the Lower Castlecliff Shellbed. Note the loss of detail in the analysis, resulting from lower amounts of information preserved by the relative proportions of amino acids (see text).

provided that the molecules remain within the shell and are not released by shell recrystallization, etc. Degradation of the amino acids occurs, but the relationships between these amino acids must not change significantly over time, thus allowing similar samples to be grouped together. There is some change due to the effect of time on the samples, indicated by the spread of the samples within the groupings, which represents this decay and diagenetic production of amino acids.

Using standard amino acid analysers, the level of information described here may possibly be the highest to be gained routinely from fossil samples. This is not as high as was initially hoped for amino acids recovered from intracrystalline sites, as these were thought to be better protected (Curry 1988). In Recent samples, this method can distinguish between genera in all cases, and possibly also species (investigated with *Neothyris*; Walton *et al.* 1993). The degradation of the molecules has led to a decrease in the amount of information retained which may be recorded by the instrumentation used. It is likely that further analyses using other techniques, such as GC-MS, may refine this information level by quantifying the degradative remains of amino acids. In addition to the amino acids there is a range of other molecules present within the shell that may provide

further phylogenetic information, or may mask a true relationship. In particular, taxonomically important molecules will be formed from the original amino acids through a range of degradative reactions (Walton in press) and the products may not be amino acids and hence will not be recorded. Indeed, there will be a range of intermediates, but degradation will ultimately lead to the formation of short-chain hydrocarbons (Thompson and Creath 1966).

If the degradative pathways are known, then the reaction products can be assayed and the original amino acid composition restored to extract the taxonomic information. This is similar to the suggestion of Kaufman *et al.* (1992) who attempted to reconstruct the amino acid composition by calculating the rate of degradation based on the rate of amino acid racemization. These compositions were related to Recent counterparts for identification. However, the method of Kaufman *et al.* (1992) relies upon there being a recognized Recent representative of taxa used in comparison studies and the absence of significant evolution of the protein over geological time. Clearly, if amino acid taxonomy is to be of general use in palaeontology, both of these problems must be overcome. Reconstruction of the original amino acid composition of the fossil through analysis of the degradation products will enable taxa with no living representatives to undergo this type of analysis.

Even though it is more than 40 years since the first amino acids were recovered from the shells of fossils (Abelson 1954), we still know very little regarding many of the rates and pathways of protein and amino acid degradation. Some reactions are known, however: for example, one of the degradation products of Arg is ornithine. The concentration of ornithine in shells varies inversely to the concentration of Arg (Walton in press). This is the only pathway by which ornithine can be formed in the shell and therefore represents an unambiguous link with the parent molecule. Recognition of such linkages should be possible for many of the original molecules and therefore the original composition may be reconstructed. However, not all molecules will have such an unambiguous pathway. Ser degrades (through a number of intermediates) to form Ala (Bada *et al.* 1978), resulting in the increased level of Ala seen in brachiopods (Walton 1996), in Foraminifera (Haugen *et al.* 1989) and molluscs (Kaufman *et al.* 1992). This Ala will be indistinguishable from the original Ala in the sample and will therefore distort the analysis. However, the degradative pathways of other amino acids (e.g. Val, Leu) are unknown or poorly understood and must be recognized prior to any attempted reconstruction of the amino acids for use in taxonomy.

CONCLUSIONS

The results of this study show that, despite high levels of amino acid degradation, taxonomic information is preserved in intracrystalline molecules. This information may be observed by using graphical presentation of multivariate statistical analysis of the relative proportions of amino acids. In all samples, separation is possible to at least subordinal level and in some cases to subfamilial level on the basis of amino acid composition alone. The diagrams may be considered as analogous to geochemical discrimination diagrams, as the majority of the groupings described above would be recognized, even if morphologically derived groupings were not known.

The degree of taxonomic discrimination is less than was hoped at the start of this study, but still represents the preservation of characteristic amino acid signatures. This may be refined by examination of the degradative remains of fossils. A full understanding of degradative pathways, to allow the reconstruction of the parent molecules from the degradation products, is a prerequisite to allow detailed taxonomic information to be retrieved from the organic component of shells. Amino acid data alone may not be sufficient in the fossil record to fulfil the aims of a molecular taxonomy.

Acknowledgements. This work was undertaken during the tenure of a UK NERC studentship (GT4/89/GS/42) at the University of Glasgow, and was written during a University of Derby sabbatical, both of which are gratefully acknowledged. This manuscript benefited from the critical reading of Maggie Cusack, Matthew

Collins and an anonymous referee. Helen Wilkins and Ann Agarogda (Derby) and Sandra McCormack (Glasgow) are thanked for technical assistance.

REFERENCES

ABELSON, P. H. 1954. Organic constituents of fossils. *Yearbook of the Carnegie Institute of Washington*, **53**, 97–101.

—— 1955. Organic constituents of fossils. *Yearbook of the Carnegie Institute of Washington*, **54**, 107–109.

AKIYAMA, M. 1971. The amino acid composition of fossil scallop shell proteins and non-proteins. *Biomineralisation*, **3**, 65–70.

ALBECK, S., AIZENBERG, L., ADDADI, L. and WEINER, S. 1993. Interactions of various skeletal intracrystalline components with calcite crystals. *Journal of the American Chemical Society*, **115**, 11691–11697.

ANDERTON, P. W. 1981. Structure and evolution of the South Wanganui Basin, New Zealand. *New Zealand Journal of Geology and Geophysics*, **24**, 39–83.

ANDREWS, J. T., MILLER, G. H., DAVIES, D. C. and DAVIES, K. H. 1985. Generic identification of fragmentary Quaternary molluscs by amino acid chromatography – a tool for Quaternary and palaeontological research. *Geological Journal*, **20**, 1–20.

ARMSTRONG, W. G., HALSTEAD, L. B., REED, F. B. and WOOD, L. 1983. Fossil proteins in vertebrate calcified tissues. *Philosophical Transactions of the Royal Society of London, Series B*, **301**, 301–343.

BADA, J. L., SHOU MING-YUNG, MAN, E. H. and SCHROEDER, R. A. 1978. Decomposition of hydroxy amino acids in foraminifera tests; kinetics, mechanism and geochronological implications. *Earth and Planetary Science Letters*, **41**, 67–76.

COHEN, B. L. 1994. Immuno-taxonomy and the reconstruction of brachiopod phylogeny. *Palaeontology*, **37**, 907–911.

COLLINS, M. J., CURRY, G. B., QUINN, R., MUYZER, G., ZOMERDIJK, T. and WESTBROEK, P. 1988. Sero-taxonomy of skeletal macromolecules in living terebratulid brachiopods. *Historical Biology*, **1**, 207–224.

—— MUYZER, G., CURRY, G. B., SANDBERG, P. and WESTBROEK, P. 1991. Macromolecules in brachiopod shells: characterization and diagenesis. *Lethaia*, **24**, 387–397.

CORNISH-BOWDEN, A. 1979. How reliably do amino acid composition comparisons predict sequence similarities between proteins? *The Journal of Theoretical Biology*, **76**, 369–386.

—— 1983. Relating proteins by amino acid composition. *Methods in Enzymology*, **91**, 60–75.

CURRY, G. B. 1988. Amino acids and proteins from fossils. 20–33. *In* RUNNEGAR, B. and SCHOPF, J. W. (eds). *Molecular evolution and the fossil record*. Short Courses in Paleontology, 1. Paleontological Society, Knoxville, 167 pp.

CUSACK, M., CURRY, G. B., CLEGG, H. and ABBOTT, G. 1992. An intracrystalline chromoprotein from red brachiopod shells: implications for the process of biomineralisation. *Comparative Biochemistry and Physiology, Series B*, **102**, 93–95.

DAVIS, J. C. 1986. *Statistics and data analysis in geology*. John Wiley & Sons, New York, 646 pp.

DEGENS, E. T., SPENCER, D. W. and PARKER, R. H. 1967. Paleobiochemistry of molluscan shell proteins. *Comparative Biochemistry and Physiology*, **20**, 553–579.

DUPONT, D. R., KEIM, P. S., CHUI, A., BELLO, R., BOZZINI, M. and WILSON, K. J. 1989. A comprehensive approach to amino acid analysis. 284–294. *In* HUGLI T. E. (ed.). *Techniques in protein chemistry*. Academic Press, New York, 612 pp.

DUSSART, G. B. J. 1983. The amino acid composition of fresh-water mollusc shells in relation to phylogeny and environment. *Journal of Molluscan Studies*, **49**, 213–223.

FLEMING, C. A. 1953. *The geology of the Wanganui Subdivision*. Department of Scientific and Industrial Research, Wellington, 362 pp.

HARE, P. E. 1974. Amino acid dating of bone – the influence of water. *Yearbook of the Carnegie Institute of Washington*, **73**, 576–581.

—— and HOERING, T. C. 1977. The organic constituents of fossil mollusc shells. *Yearbook of the Carnegie Institute of Washington*, **76**, 625–631.

—— and MITTERER, R. M. 1969. Laboratory simulation of amino acid diagenesis in fossils. *Yearbook of the Carnegie Institute of Washington*, **67**, 205–208.

HAUGEN, J.-E., SEJRUP, H.-P. and VOGT, N. B. 1989. Chemotaxonomy of Quaternary benthic foraminifera using amino acids. *Journal of Foraminiferal Research*, **19**, 38–51.

HEINRIKSON, R. L. and MEREDITH, S. C. 1984. Amino acid analysis by reverse-phase high-performance liquid chromatography: precolumn derivatization with phenylisothiocyanate. *Analytical Biochemistry*, **136**, 65–74.

JOPE, M. 1967. The protein of brachiopod shell – II. Shell protein from fossil articulates: amino acid composition. *Comparative Biochemistry and Physiology*, **20**, 601–605.

KAUFMAN, D. S., MILLER, G. H. and ANDREWS, J. T. 1992. Amino acid composition as a taxonomic tool for molluscan fossils: an example from Pliocene–Pleistocene Arctic marine deposits. *Geochimica et Cosmochimica Acta*, **56**, 2445–2453.

KING, K., Jr and HARE, P. E. 1972. Amino acid composition of the test as a taxonomic character for living and fossil planktonic foraminifera. *Micropaleontology*, **18**, 285–293.

MacFIE, H. J. H., LIGHT, N. D. and BAILEY, A. J. 1988. Natural taxonomy of collagen based on amino acid composition. *The Journal of Theoretical Biology*, **131**, 401–418.

NORRIS, R. M. and GRANT-TAYLOR, T. L. 1989. Late Quaternary shellbeds, Western Shelf, New Zealand. *New Zealand Journal of Geology and Geophysics*, **32**, 343–356.

QIAN YAORONG, ENGEL, M. H., GOODFRIEND, G. A. and MACKO, S. A. 1995. Abundance and stable carbon isotope composition of amino acids in molecular weight fractions of fossil and artificially aged mollusk shells. *Geochimica et Cosmochimica Acta*, **59**, 1113–1124.

ROBBINS, L. L. and BREW, K. 1990. Proteins from the organic matrix of core top and fossil planktonic foraminifers. *Geochimica et Cosmochimica Acta*, **54**, 2285–2292.

—— and DONACHY, J. E. 1991. Mineral regulating proteins from fossil planktonic foraminifera. 139–148. *In* SIKES, C. S. and WHEELER, A. P. (eds). *Surface reactive peptides and proteins*. American Chemical Society, Washington DC, 416 pp.

—— and HEALY-WILLIAMS, N. 1991. Towards a classification of planktonic foraminifera based on biochemical, geochemical and morphological criteria. *Journal of Foraminiferal Research*, **21**, 159–167.

SNEATH, P. H. A. and SOKAL, R. R. 1973. *Numerical taxonomy*. W. H. Freeman and Company, San Francisco, 573 pp.

SUCOV, H. M., BENSON, S., ROBINSON, J. R., BRITTEN, R. Y., WILT, F. and DAVIDSON, E. H. 1987. A lineage-specific gene encoding a major matrix protein of the sea urchin embryo spicule. II. Structure of the gene and derived sequence of the protein. *Developmental Biology*, **120**, 507–519.

SYKES, G. A., COLLINS, M. J. and WALTON, D. I. 1995. The significance of a geochemically isolated intracrystalline organic fraction within biominerals. *Organic Geochemistry*, **23**, 1059–1065.

THOMPSON, R. R. and CREATH, W. B. 1966. Low molecular weight hydrocarbons in Recent and fossil shells. *Geochimica et Cosmochimica Acta*, **30**, 1137–1152.

TOWE, K. M. 1980. Preserved organic ultrastructure: an unreliable indicator for Paleozoic amino acid biogeochemistry. 65–74. *In* HARE, P. E., HOERING, T. C. and KING, K. J. (eds). *Biogeochemistry of amino acids*. John Wiley & Sons, New York, 558 pp.

WALTON, D. I. 1992. Biogeochemistry of brachiopod intracrystalline proteins and amino acids. Unpublished Ph.D. thesis, University of Glasgow.

—— 1996. Degraded intracrystalline proteins and amino acids from fossil brachiopods and considerations for amino acid taxonomy. 289–297. *In* COPPER, P. and JIN, JUISO (eds). *Brachiopods*. Balkema Press, Rotterdam, 373 pp.

—— in press. Degradation of intracrystalline proteins and amino acids in fossil brachiopods. *Organic Geochemistry*.

—— and CURRY, G. B. 1994. Extraction, analysis and interpretation of intracrystalline amino acids from fossils. *Lethaia*, **27**, 179–184.

—— CUSACK, M. and CURRY, G. B. 1993. Implications of the amino acid composition of Recent New Zealand brachiopods. *Palaeontology*, **36**, 883–896.

WEHMILLER, J. F., YORK, L. L. and BART, M. L. 1995. Amino acid racemization geochronology of reworked Quaternary mollusks on US Atlantic coast beaches: implications for chronostratigraphy, taphonomy, and coastal sediment transport. *Marine Geology*, **124**, 303–337.

WEINER, S., LOWENSTAM, H. A. and HOOD, L. 1976. Characterization of 80 million year old mollusk shell proteins. *Proceedings of the National Academy of Science, USA*, **73**, 2541–2545.

WYCKOFF, R. W. G. 1972. *The biochemistry of animal fossils*. Scientechnica, Bristol, 151 pp.

DEREK WALTON
Division of Earth Sciences
University of Derby
Kedleston Road
Derby DE22 1GB, UK

Typescript received 9 December 1996
Revised typescript received 27 August 1997

APPENDIX

The one letter and three letter codes for the amino acids used in this study.

Amino acid	Three letter code	One letter code	Amino acid	Three letter code	One letter code
Alanine	Ala	A	Lysine	Lys	K
Arginine	Arg	R	Phenylalanine	Phe	F
Aspartic acid	Asp	D	Proline	Pro	P
Glutamic acid	Glu	E	Serine	Ser	S
Glycine	Gly	G	Threonine	Thr	T
Isoleucine	Ile	I	Tyrosine	Tyr	Y
Leucine	Leu	L	Valine	Val	V

A REDESCRIPTION OF THE ANOMALOCYSTITID MITRATE *RHENOCYSTIS LATIPEDUNCULATA* FROM THE LOWER DEVONIAN OF GERMANY

by M. RUTA *and* C. BARTELS

ABSTRACT. The anomalocystitid mitrate *Rhenocystis latipedunculata*, from the Lower Devonian Hunsrückschiefer of Rhineland, Germany, is reconstructed and redescribed. *Rhenocystis* is characterized by transverse, terrace-like ridges on two antero-posteriorly elongate, postero-lateral areas of the dorsal head skeleton and on the posterior third of the ventral head skeleton; the relatively small size of the ventral plates of the second transverse row; a suture between the mid-ventral plates of the first and third row; the relatively large size of the placocystid plate; the presence of rocking articulations between dorsal and ventral fore tail plates; a transversely expanded and recumbent anterior styloid blade; a robust, spike-like posterior blade; and four morphologically distinct regions in the hind tail. *Rhenocystis* closely resembles *Placocystites forbesianus* from the middle Silurian of England and *Victoriacystis wilkinsi* from the upper Silurian of Australia, with which if forms a clade within the anomalocystitids of boreal type.

IN this paper, we reconstruct and redescribe the Lower Devonian anomalocystitid mitrate *Rhenocystis latipedunculata* Dehm, 1932 from the Hunsrückschiefer of the Rhineland, Germany, and discuss its affinities. *Rhenocystis* is one of the most abundant boreal anomalocystitids known to date. Intense collecting activity during the last 20 years has yielded several new specimens which provide additional morphological information. The recently collected material comes from the Eschenbach-Bocksberg roof-slate quarry near the village of Bundenbach, Germany (Text-fig. 1A). As with other Hunsrückschiefer fossils, it is difficult to establish the precise levels in which the specimens were found, as these were collected from 'hills' of waste slabs (Bartels and Brassel 1990). A privately owned specimen found near Gemünden (Dehm 1934) represents the only record of *Rhenocystis* outside the Bundenbach area. In the present work, the plate nomenclature is based on a revised terminology of the anomalocystitid skeleton which will be discussed by one of us (MR) elsewhere. This paper is dedicated to Professor Richard Dehm for his contribution to the knowledge of the anomalocystitid mitrates.

Repositories. BMNH, The Natural History Museum, London, UK; BSPHG, Bayerische Staatssammlung für Paläontologie und Historische Geologie, Munich, Germany; DBM-HS, Deutsches Bergbau-Museum, Bochum, Germany.

GEOLOGICAL SETTING

Lithology, palaeoenvironment and age. A recent, comprehensive summary of the geology and stratigraphy of the Hunsrückschiefer (or Hunsrück Slate) is found in Bartels and Brassel (1990). The fossils are preserved in dark grey slates of mid Early Emsian age (Krebs 1979; Briggs *et al.* 1996). The presence of euhedral crystals of chlorite and muscovite formed *in situ* indicates that the sediment was subject to metamorphism at relatively low temperature and high pressure (anchizone; see Briggs *et al.* 1996). Cleavage lies at various angles with respect to the bedding planes, and is commonly visible on the surface of the fossils.

There is no general consensus as to the depth of water at which the sediment was deposited;

[Palaeontology, Vol. 41, Part 4, 1998, pp. 771–806, 10 pls]

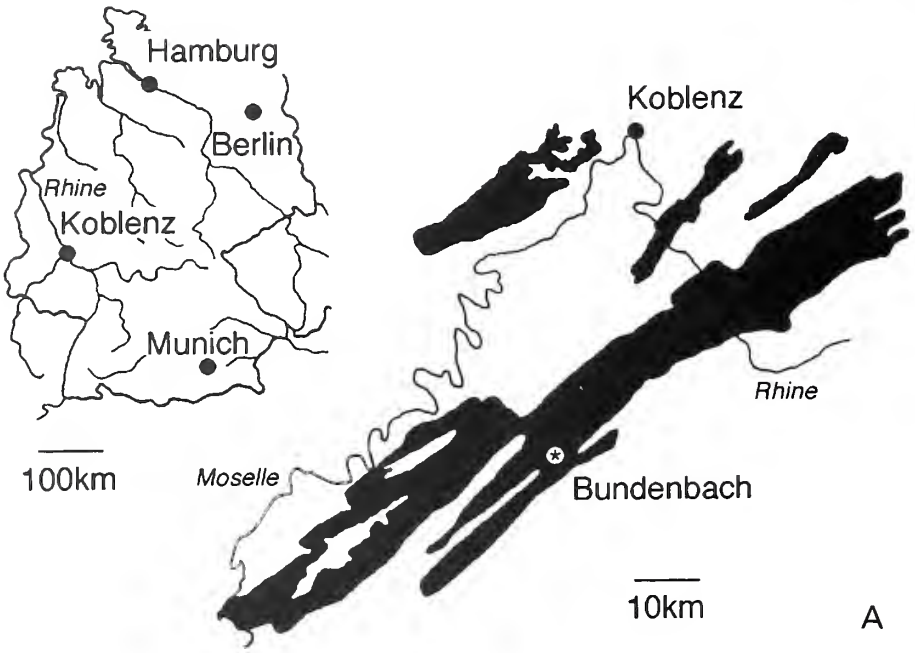

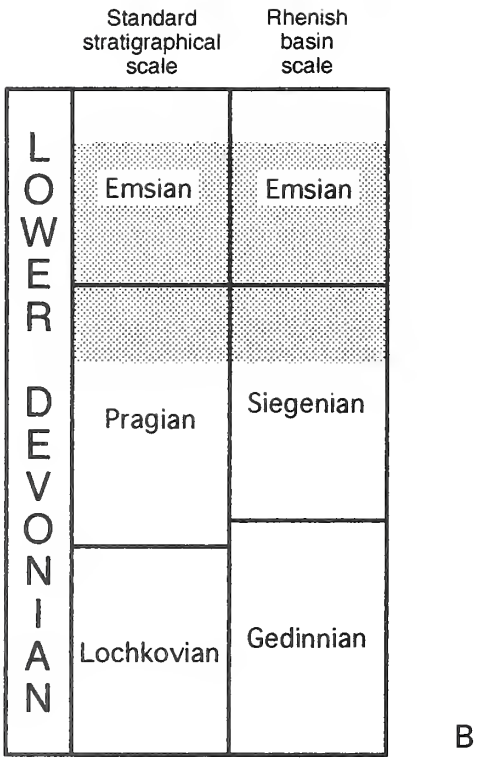

TEXT-FIG. 1. A, distribution of the Hunsrückschiefer outcrops; B, approximate stratigraphical position of the Hunsrückschiefer in the Lower Devonian (stippled area).

although variable in different parts of the basin, the maximum depth was probably not much greater than 200 m (Briggs *et al.* 1996; see also Stürmer and Bergström 1973; Krebs 1979, and references therein). The basin became shallower both in a north-westerly and in a south-easterly direction. The Hunsrück Slate deposits represent an intra-shelf basin within the Rhenohercynian basinal province. The nature of the lithofacies, the presence of distal turbidites (which explains in part the sandy intercalations) often preserving assumed allochthonous fossils, the fact that most of the autochthonous echinoderms possess thin skeletons (presumably suggesting a relatively deep water environment), the presence of few solitary corals, the absence of stromatoporoids, and the preponderance of nektic and planktic organisms among the non-echinoderm taxa show that the Hunsrück Slate facies can be assigned to the Hercynian magnafacies. According to Krebs (1979), such a facies possibly reflects an open marine environment.

According to more recent interpretations (O. Sutcliffe, pers. comm. to MR 1997), the palaeoenvironment of the typical Hunsrück Slate fossils probably corresponds to the interchannel areas of a submarine fan. A muddy substrate benthic community lived in oxygenated waters above the level of the storm wave base and was occasionally buried by sediment transported by density currents caused by sudden influxes of mud (Stürmer and Bergström 1973; Bartels and Brassel 1990; Briggs *et al.* 1996).

In the Rhenish basin stratigraphical scale of Germany (Text-fig. 1B), the lithologies of the Hunsrück Slate are assigned either to the lowermost Emsian (or Ulmen substage) (Hunsrück Slate *sensu stricto*) or to the interval between the uppermost Siegenian (Heredorf substage) and the middle Lower Emsian (Singhofen substage) (Hunsrück Slate *sensu lato*). The Bundenbach rocks are generally attributed to the uppermost Ulmen substage; as such, they are part of the Hunsrück Slate *sensu stricto*. However, recent study of the lithology of the Hunsrück Slate (O. Sutcliffe, pers. comm. to MR 1997) reveals that the Bundenbach rocks should be assigned to the Singhofen substage, based on the presence of volcanic tuffs. Therefore, the Bundenbach slates should be regarded as middle Lower Emsian following the Rhenish stratigraphical subdivisions.

A more precise correlation with other Early Devonian rocks is possible on the basis of Hercynian faunal elements. The presence of dacryoconarids (Alberti 1982) and of representatives of the *Anetoceras* goniatite fauna (Chlupač 1976) indicates that the Bundenbach rocks are probably mid Zlichonian in age (*praecursor* dacryoconarid Zone), and hence well above the uppermost Pragian.

Taphonomy and diagenesis. The presence of well preserved articulated fossils in the Hunsrückschiefer indicates that the organisms were buried rapidly and that transport was either absent or occurred over short distances. Fossils belonging to different phyla are often closely associated on the same slab or even overlap each other. These associations are sometimes regarded as accumulations of dead organisms in shallow areas of the sea floor, which were relatively protected from the action of bottom currents; interruption of transport caused by obstacles is also often invoked to explain such accumulations. There are indications that some heterogeneous associations reflect, in part, life associations, and that organisms lying close to each other were probably engaged in a particular biological activity (e.g. exploitation of the same localized food source) before being killed by burial. Many of the crinoids are found rooted in place and merely smothered by turbidity currents. Several vagile organisms left tracks before dying (e.g. Richter 1941; Seilacher and Hemleben 1966; Bartels and Brassel 1990). The analysis of trace fossils (O. Sutcliffe, pers. comm. to MR 1997) indicates that many organisms were alive before, during and after the mud influx episodes.

The vast majority of specimens of *Rhenocystis* are virtually complete. Disruption of the skeletal plates is rare and affects mainly the head. The flexibly articulated upper lip plates, for example, are often found displaced, and the same is true for the lateral elements of the anteriormost transverse row of ventral plates. Conversely, the mid-ventral placocystid plate (Caster 1952), or plate V17 (see below), is often articulated with the rest of the skeleton; this condition occurs rarely in other anomalocystitid mitrates (Derstler and Price 1975; Jefferies and Lewis 1978; Ubaghs 1979; Craske and Jefferies 1989; Parsley 1991; Ruta 1997). The spines are usually in place, or only slightly displaced. The tail is often complete.

Exceptional preservation of soft tissues in Hunsrückschiefer fossils, with authigenic pyrite replacing organic matter, has been documented in some echinoderms and arthropods (Stürmer *et al.* 1980; Bartels and Brassel 1990), and has been studied in detail by Briggs *et al.* (1996). Unfortunately, soft tissue preservation has not been documented in *Rhenocystis*, owing to extensive pyritization. In many specimens, mass concentration of small to medium-sized euhedral crystals of pyrite, with large euhedral crystals often interspersed throughout, line the edges of the articulated spines, the sutures between adjacent skeletal head plates as well as the lumens of broken tails. Concentrations of large crystals are probably the effect of localized phenomena of supersaturation (Murowchick and Barnes 1987; Briggs *et al.* 1996). Aggregations of subhedral to large euhedral crystals, the latter sometimes found isolated and formed presumably during later stages of diagenesis (Briggs *et al.* 1996), are visible on the external surface of the articulations between dorsal and ventral fore tail plates, on the styloid blades, across the sutures between adjacent hind tail segments, and along the external margins of the hind tail ossicles and plates. Such aggregations form irregular patches or lumps of different shapes and sizes. Often, the pyrite replacing the calcitic skeleton has a fine texture.

METHODS

The vast majority of the specimens was prepared using an air-abrasive machine and fine iron powder as an abrasive. This technique leads to spectacular results (see Bartels and Brassel 1990), leaving the fossils virtually untouched and fully exposed. The specimens were wetted with water or, in the case of extensive pyritization, sprayed with ammonium chloride before being photographed. The best photographic results were obtained using a low angle of illumination, which allows plate sutures to be distinguished from penetrative cleavage (see also Dehm 1932, 1934).

Most Hunsrückschiefer fossils are deformed to various degrees by tectonic strain. Ramsay and Huber (1983) provided a detailed account of tectonic strain analysis. The application, advantages and limitations of such analysis to deformed fossils have been discussed by Wellman (1962), Cooper (1990), Fortey and Owens (1992), Hughes and Jell (1992) and Rushton and Smith (1993) among others. Almost undeformed, dorso-ventrally compressed individuals of *Rhenocystis* indicate that, like the vast majority of the anomalocystitids, this mitrate was externally bilaterally symmetrical in life. It is, therefore, possible to identify, with some approximation, the positions of the longitudinal and a transverse axis. These would be orthogonal in undeformed specimens. The restoration involves the construction of a strain ellipse starting from deformed right angles, under the assumptions that the deformation occurred homogeneously in the planes of bedding, that the specimens lay flat on or within such planes, and that their dorso-ventral flattening, due to compaction and loss of water, did not modify their original shape and size (Cooper 1990; Rushton and Smith 1993).

The available methods of fossil retrodeformation using deformed right angles require either two specimens or one specimen and the direction of mineral elongation (Cooper 1990). Stürmer *et al.* (1980) and Jefferies (1984) published X-ray photographs of a slab with *c.* 17 individuals of *Rhenocystis* lying close to each other and at different depths with respect to the two main surfaces of the slab. A cast of the slab was made available for study. Of the *c.* 17 individuals of *Rhenocystis*, eight are exposed in dorsal view. Specimens BMNH EE 5886/1–2 and 5 were chosen for the strain analysis and photographed. For each specimen, the positions of the longitudinal and a transverse axis were estimated. The axes are indicated by black bars drawn directly on the photograph (Text-fig. 2A–B). The determination of the position of the two axes, like all the subsequent steps of the retrodeformation process, is subject to error. The most obvious source of error occurs because individuals show a certain amount of disruption, albeit small. Each of the above-mentioned assumptions underlying the application of strain analysis constitutes an additional source of error.

Of the various techniques available to correct for tectonic distortion of fossils (see review in Cooper 1990), we chose Breddin curves, a graphical method used to calculate the strain ratio from the values of angular shear strain (deviation from the right angle) and angular orientation of the

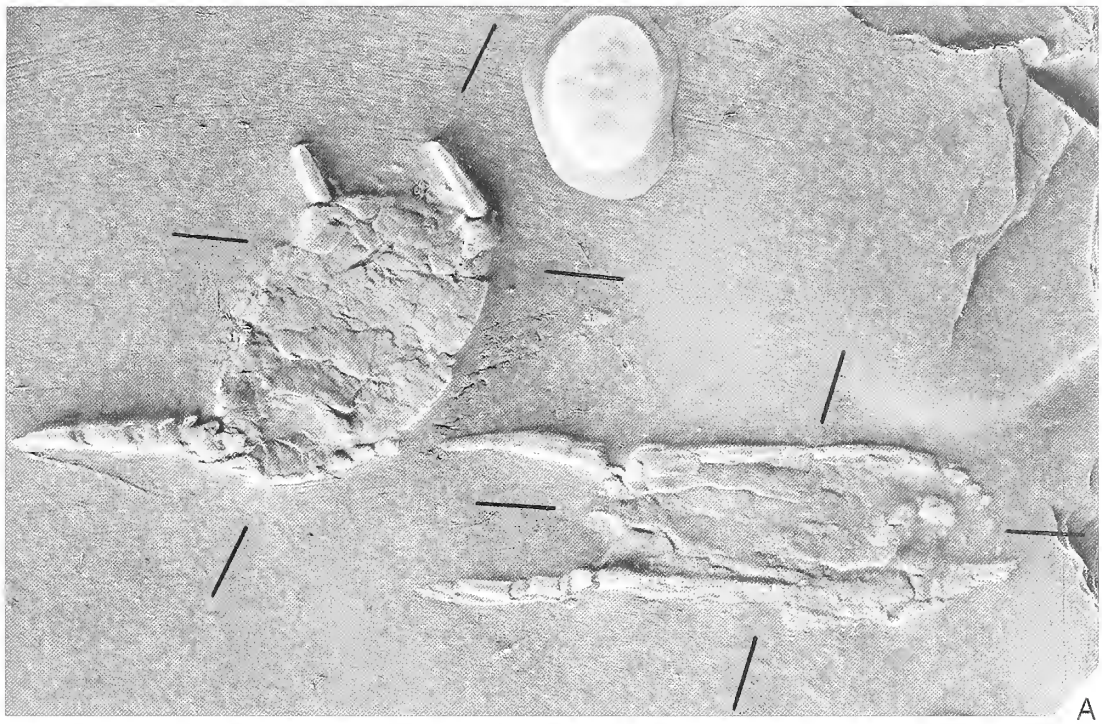

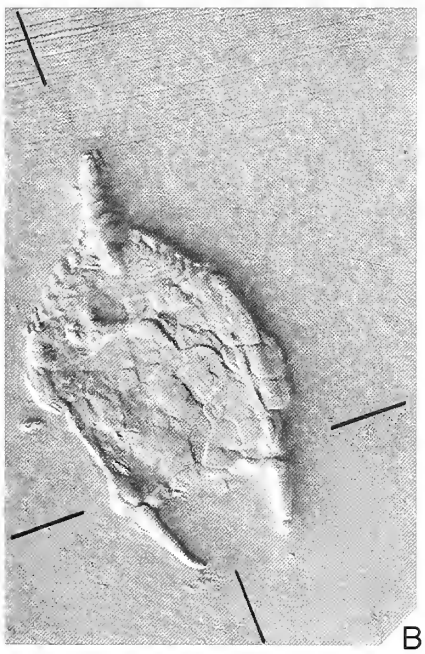

TEXT-FIG. 2. Application of the strain analysis to three specimens of *Rhenocystis latipedunculata*. A, BMNH EE 5886/1-2; B, BMNH EE 5886/5; C, greatest principal extension direction. The original photograph was cut so as to reduce the real distances between the three specimens without changing their mutual orientations; the solid lines represent the estimated positions of the longitudinal and of a transverse axis in each specimen. Both figures × 2.

fossils with respect to the axes of the strain ellipse (Ramsay and Huber 1983). A set of curves allows the strain ratio and the direction of the axes of the strain ellipse to be determined approximately.

The Breddin curves method gave a strain ratio value of *c.* 1·37. On the basis of this value, it was

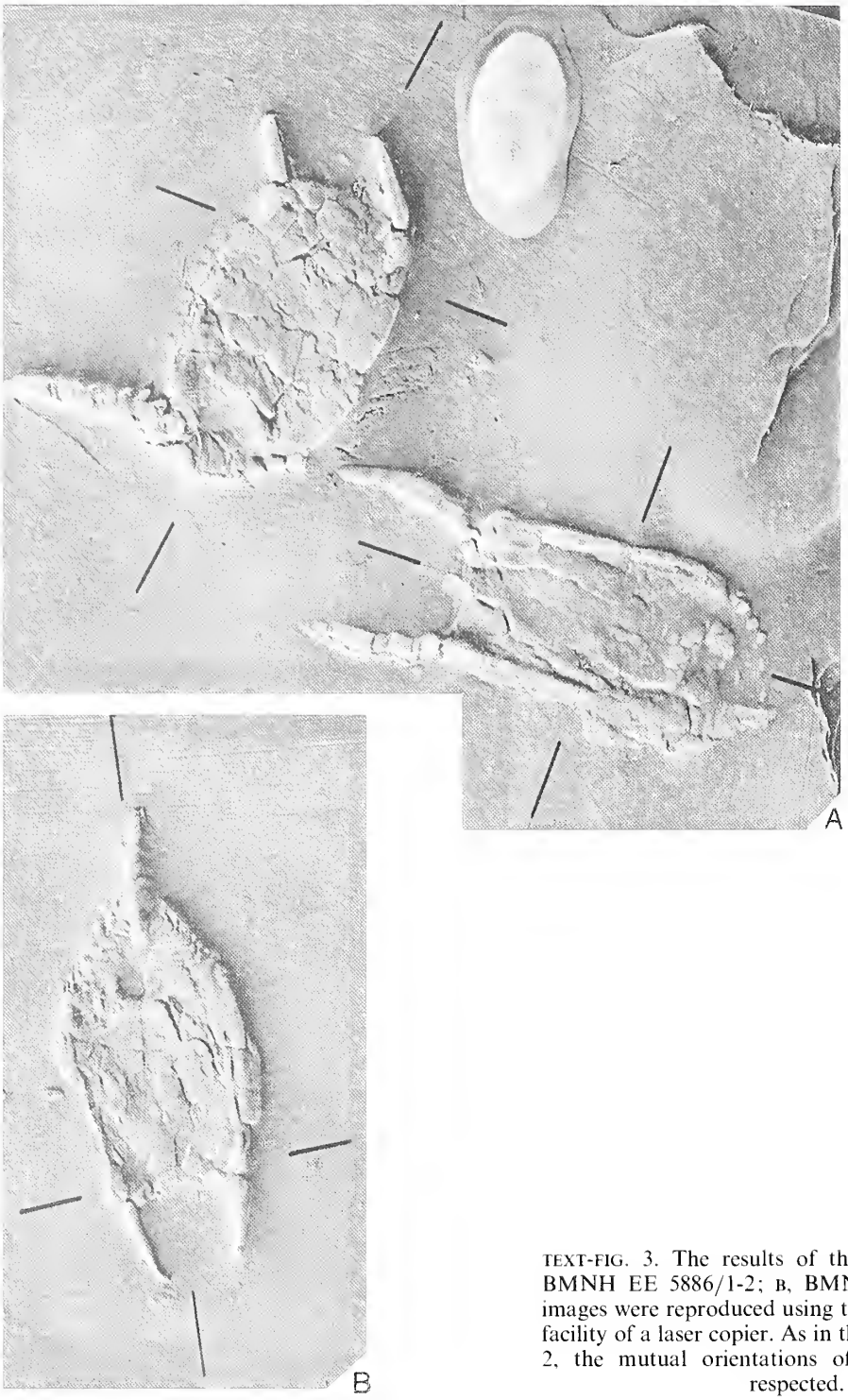

TEXT-FIG. 3. The results of the strain analysis; A, BMNH EE 5886/1-2; B, BMNH EE 5886/5. The images were reproduced using the anamorphic zoom facility of a laser copier. As in the case of Text-figure 2, the mutual orientations of the specimens are respected.

possible to retrodeform the three specimens of *Rhenocystis* using the simple technique outlined by Rushton and Smith (1993). The directions of the two axes of the strain ellipse were drawn on the original photograph before the latter was cut into two parts for publication (Text-fig. 2A–B). The original photograph was photocopied (Text-fig. 3) applying the 'anamorphic zoom' facility of a laser copier, which enables the operator to change the relative lengths of two orthogonal axes once the greatest principal extension direction (long axis of the strain ellipse; Text-fig. 2C) is known.

The laser copy image shows that the relative proportions of BMNH EE 5886/1–2 and 5 are approximately the same, although in none of the three corrected specimens is the longitudinal axis accurately perpendicular to the transverse axis, by reason of the amount of error introduced during the retrodeformation process. The approximate values of the angles between these axes (clockwise measurements are positive) are 87° in BMNH EE 5886/1 (Text-fig. 3A), 93° in BMNH EE 5886/2 (Text-fig. 3A), and 86° in BMNH EE 5886/5 (Text-fig. 3B). The results of the retrodeformation process are to be considered only as a crude estimate of the original external morphology of the fossils.

SYSTEMATIC PALAEONTOLOGY

Superphylum DEUTEROSTOMIA Grobben, 1908
(Stem group of the Craniata?)

Genus RHENOCYSTIS Dehm, 1932

Type species. Rhenocystis latipedunculata Dehm, 1932 by monotypy.

Rhenocystis latipedunculata Dehm, 1932

Plates 1–10; Text-figures 2–6

1932 *Rhenocystis latipedunculata* Dehm, p. 66, figs 1–6; pl. 2, figs 1–4.
1934 *Rhenocystis latipedunculata* Dehm; Dehm, p. 24, fig. 2a–e; pl. 1, figs 4–9; pl. 2, figs 1–2.
1952 *Rhenocystis* Dehm 1933 [*sic*]; Caster, p. 19, fig. 2i–j.
1960 *Rhenocystis* Dehm 1933 [*sic*]; Gill and Caster, p. 45.
1961 *Rhenocystis latipedunculata* Dehm; Kuhn, p. 12, figs 13, 1–4, 14.
1968 *Rhenocystis latipedunculata* Dehm; Ubaghs, p. 560, figs 332, *6*, 359, *1a–b*.
1970 *Rhenocystis latipedunculata* Dehm; Kutscher, p. 96.
1975 *Rhenocystis latipedunculata* Dehm; Kutscher, p. 48, fig. 5a–e.
1987 *Rhenocystis* Dehm; Regnault and Chauvel, p. 672.
1989 *Rhenocystis* Dehm 1933 [*sic*]; Craske and Jefferies, p. 95.
1990 *Rhenocystis latipedunculata* Dehm; Bartels and Brassel, p. 175, fig. 161.
1990 *Rhenocystis latepedunculata* [*sic*]; Cripps, p. 59.
1991 *Rhenocystis* Dehm; Parsley, p. 13.
1991 *Rhenocystis latipedunculata*; Südkamp, p. 239.

Holotype. BSPHG 1928 VII 2.

Type locality, type horizon and age. Bundenbach, Rhenish Massif, Germany; *praecursor* dacryoconarid Zone; 'Hans' sequence; Upper Pragian to Lower Emsian.

Additional material. BMNH E 23605, 23660, 29315–29316, EE 5647, 5886 (P31), 5887 (Brassel SNG 108), 5888 (Brassel SNG 110), 5889 (Brassel SNG 111), 5890 (Brassel SNG 112), 5891 (Brassel SNG 114), 5892 (Brassel SNG 116), 5893 (Brassel SNG 117), 5894 (XXI 22a), 5895 (XXI 22b), 5898 (BSPHG 1928 VII 1), 5899 (BSPHG 1928 VII 2), 5900 (BSPHG 1930 III 17), 5901 (BSPHG 1931 I 48), 5902 (BSPHG 1931 I 49); DBM-HS 295–302, 347, 472, 524, 564, 566–567, 570, 727, 743–745, 750. WB 514.

WB 514 is a provisional registration number for a specimen in the Deutsches Bergbau-Museum, Bochum. Labels in parentheses for BMNH EE 5886–5895 refer to originals in the Senckenberg Museum, Frankfurt, whereas those for BMNH EE 5898–5902 refer to originals in the Staatssammlung, Munich.

The Bergbau-Museum material comes from the Eschenbach-Bocksberg quarry near Bundenbach (approximate coordinates: 07°27′ E; 49°51′ N), but precise data concerning the localities where the other specimens were found are not known.

Diagnosis. Anomalocysitid mitrate with five transverse rows of ventral plates; in antero-posterior succession, such rows consist of five, four, three, five and three elements respectively; V1 and V5 comparatively small with respect to the other elements of the first row; V6–V9 subequal in size and much smaller than V2–V4; V3 and V12 in contact with each other, thus interrupting the second transverse row; V17 rounded and comparable in size to V16 and V18; sutures between V15 and V16, and between V18 and V19, medially convex; V21 shield-shaped and deeply inserted between V20 and V22, but not separating these two plates completely; posterior part of the lateral margins of V20 and V22 slightly turned laterally; presence of two centro-dorsal plates A and C; flexible articulation formed by plates MOP and right and left LOP against plates DLM, A and C; spines slightly convex externally in dorsal aspect and with a blunt median and a sharp lateral edge; ventral sculpture consisting of robust, transversely elongate, terrace-like ridges mainly confined to plates V20–V22; posterior ventral ridges more irregular than anterior ventral ridges; dorsal sculpture consisting of ridges mainly confined to plates PLM; lateral head walls well-developed and sloping slightly ventralward and lateralward; fore tail much wider anteriorly than posteriorly, and with dorsal plates smaller than the ventral plates; rocking articulations between dorsal and ventral fore tail plates; styloid with dorsal keel, a transversely expanded, recumbent anterior blade, and a robust, spike-like posterior blade; the latter is triangular in cross section and bears a flat, transverse posterior surface; first hind tail ossicle robust and comparable in size and shape to the posterior styloid blade; successive proximal ossicles decreasing rapidly in size; ossicle shape changing remarkably throughout the length of the tail; most ventral hind tail plates with a lateral knob; proximal hind tail plates with a longitudinal keel near their dorsal margin.

DESCRIPTION AND FUNCTIONAL MORPHOLOGY

Variation: how many species of Rhenocystis?

The application of strain analysis (see above) demonstrates that estimates of body proportions in deformed fossils by visual inspection are highly misleading (Cooper 1990; Rushton and Smith 1993). Several examples from the Hunsrück Slate show that the shapes of individuals of the same species occurring on the same slab or found at a considerable distance from one another can be dramatically affected by distortion. Individual, ontogenetic, sexual or specific variations in *Rhenocystis* cannot be discerned on the basis of the available evidence. As Dehm (1934) pointed out, part of the observed variation in *Rhenocystis*, such as the number of segments in the terminal region of the hind tail, may be an artefact of preservation. The spines seem to represent an exception in this respect, as discussed below.

It can be shown that, at least in some cases, pyritization is partly responsible for the supposed observed differences in the morphology of spines, tail segments, and head plates, whereby aggregations of pyrite crystals or pyrite infillings causes variations in the width, section or outline of these structures. On the basis of the morphological data available, and of a comparison of the

---

EXPLANATION OF PLATE 1

Figs 1–6. *Rhenocystis latipedunculata* Dehm, 1932; Bundenbach; Upper Pragian to Lower Emsian, *praecursor* dacryoconarid Zone; Hunsrückschiefer of Rhineland, Germany. 1, WB 514; juvenile specimen in dorsal aspect with complete tail. 2, BMNH EE 5886/5; complete dorsal head skeleton and partial tail. 3, DBM-HS 567; partially disrupted ventral head skeleton. 4, BMNH EE 5900; complete ventral head skeleton and partial tail. 5, BMNH EE 5901; complete ventral head skeleton and tail. 6, BMNH EE 5899 (cast of St 1928 VII 2, holotype); complete ventral head skeleton. All × 3.

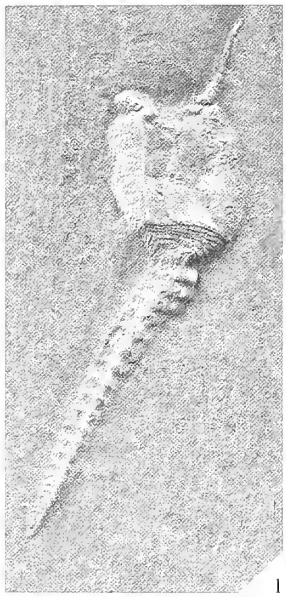
1

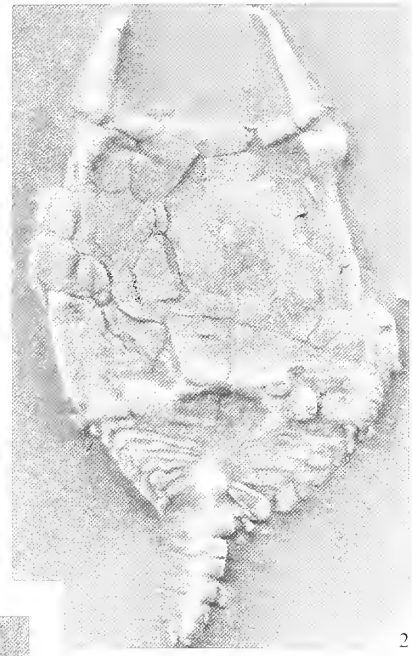
2


3

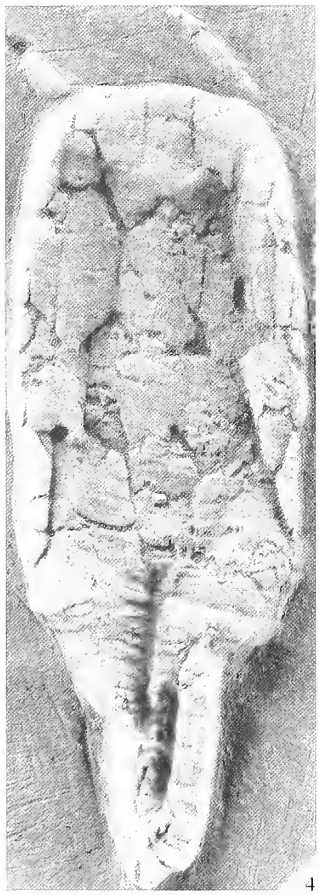
4


5

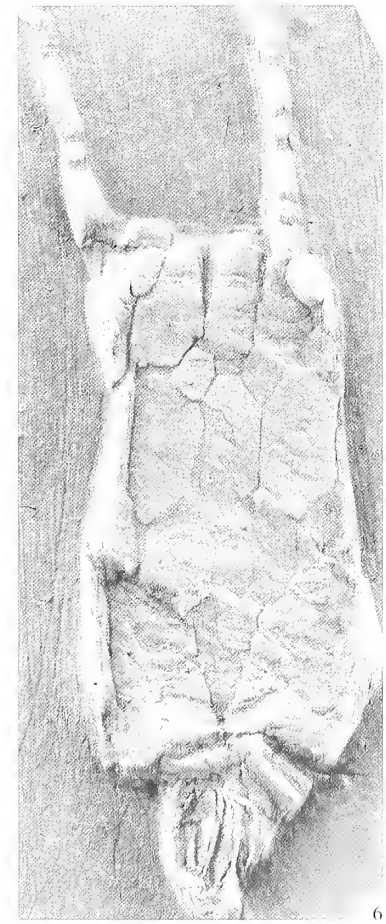
6

RUTA and BARTELS, *Rhenocystis*

new material of *Rhenocystis* with that figured by Dehm (1932, 1934), it is reasonable to assume that all the individuals of this mitrate belong to a single species.

A very small specimen in the collections of the Deutsches Bergbau-Museum, Bochum, provisionally labelled as WB 514 (Pl. 1, fig. 1), is likely to represent a juvenile of *Rhenocystis latipedunculata*, as revealed by its dorsal plating pattern (especially by the shape of the lateral margins of plates PM) and by the morphology of the hind tail. In comparison with adults of *Rhenocystis*, WB 514 possesses a less elongate head, larger lateral head walls, longer and more slender spines, and a longer and stouter hind tail. The hind tail has a smaller number of segments (about 26) in comparison with that of adult individuals (about 60); the ossicles of the first two segments, however, are much larger than those belonging to successive segments and comparable in size to the posterior styloid blade. The remaining hind tail segments change in size gradually along most of the length of the tail, whereas their shape is almost constant. In the distal quarter of the appendage, the ossicles are approximately as long as high and are hemicylindrical in shape. WB 514 is the only specimen whose hind tail is almost straight as preserved.

The head

The head of adult individuals of *Rhenocystis* is slightly longer than wide and box-shaped. It has a flat dorsal surface, a gently convex ventral surface, and two almost vertical, lateral walls which become progressively deeper antero-posteriorly (Text-figs 4–5). Several morphological details of the ventral head skeleton indicate that *Rhenocystis* has affinities with *Placocystites forbesianus* de Koninck, 1869 and *Victoriacystis wilkinsi* Gill and Caster, 1960 (see also Jefferies and Lewis 1978; Ruta 1997). *Mongolocarpos minzhini* Rozhnow, 1990 may also be closely related to *Placocystites*, *Rhenocystis* and *Victoriacystis* (see below).

In its general proportions, the head of *Rhenocystis* closely resembles that of *Victoriacystis*. Interestingly, in the smallest known specimen, WB 514 (Pl. 1, fig. 1), the head is about as long as wide. The same condition is also observed in juveniles and adults of *Placocystites*, as documented by Jefferies (1984).

Dorsal head skeleton (Text-figs 4B, 5A; Pl. 1, figs 1–2; Pl. 2, fig. 4; Pl. 3, fig. 3; Pl. 4, fig. 4; Pl. 5, figs 4–5; Pl. 6, fig. 1; Pl. 7, figs 1, 3; Pl. 8, fig. 1; Pl. 9, fig. 3). The dorsal head skeleton is composed of 11 marginal and two centro-dorsal plates. The marginal plates are divided into a group of six lateral elements arranged in pairs, an anterior transverse row composed of three elements framing the mouth opening dorsally, and a posterior group of two elements in contact with each other mid-dorsally.

The six lateral marginal plates comprise an anterior or distal pair (DLM) which gives insertion to the oral spines (see below); an intermediate pair (ILM) which occupies most of the length of the left and right lateral head margins; and a posterior or proximal pair (PLM) which contributes to the posterior head excavation (Text-figs 4B, 5A). Each of the lateral marginal plates is divided morphologically into a dorsal, horizontal part and a lateral, almost vertical part, meeting at an angle of about 90°. Restoration of deformed specimens and accurate delimitation of plate boundaries in several distorted individuals show that *Rhenocystis* does not possess sharp lateral head margins, as hypothesized by Dehm (1932) on the basis of a comparison with *Placocystites*. In dorso-ventrally compressed specimens, the lateral head walls lie flush with either the ventral or the dorsal head skeleton, and can be mistaken for folded parts of the ventral surface (e.g. Pl. 1, figs 1–6; Pl. 4, figs 4–6; Pl. 5, fig. 4; Pl. 7, figs 2–3; Pl. 8, fig. 4).

The anterior, transverse row of dorsal marginal plates (MOP and left and right LOP) is flexibly articulated with the centro-dorsal elements A and C, and with the left and right DLM (Pl. 1, fig. 2; Pl. 4, fig. 4; Pl. 7,

---

EXPLANATION OF PLATE 2

Figs 1–4. *Rhenocystis latipedunculata* Dehm, 1932; Bundenbach; Upper Pragian to Lower Emsian, *praecursor* dacryoconarid Zone; Hunsrückschiefer of Rhineland, Germany. 1, DBM-HS 567; anterior half of ventral head skeleton and spines. 2, DBM-HS 566; spine morphology. 3, DBM-HS 564; complete, but heavily deformed ventral head skeleton, complete spines and ventral sculpture. 4, DBM-HS 750; anterior half of slightly disrupted dorsal head skeleton, with possible articulation tubercle for the left oral spine on the left DLM; note the finely tapering spines and the shape of the left ILM. All × 5.

1

2

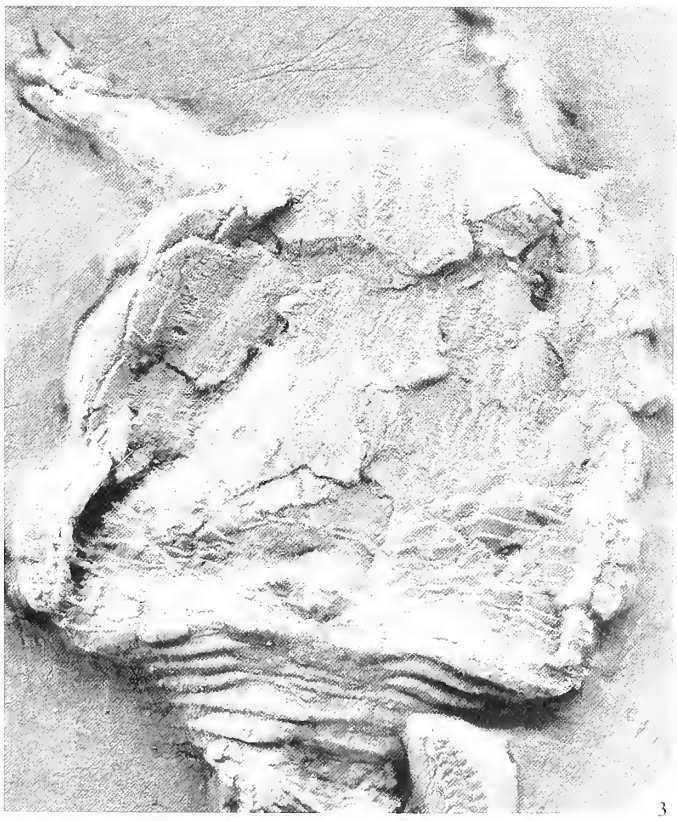

3

4

RUTA and BARTELS, *Rhenocystis*

figs 1, 3). Such flexible articulation is also present in *Victoriacystis* (Gill and Caster 1960; Ruta 1997) and in the austral Allanicytidiidae (Caster 1954, 1983; Caster and Gill 1968; Philip 1981; Haude 1995; Ruta and Theron 1997). Preliminary results of a cladistic analysis by the senior author show that a flexible upper lip evolved in parallel in the clade (*Rhenocystis latipedunculata* + *Victoriacystis wilkinsi*) and in Allanicytidiidae (*contra* Ruta and Theron 1997). In *Victoriacystis*, MOP and LOP possess a slightly pronounced ridge along their posterior margins, which fits into a shallow groove on the anterior margins of A, C, and of the left and right DLM. Some specimens of *Rhenocystis* show a similar, although less evident articulation between plates MOP and LOP and the plates lying immediately posterior to them. The relative flexibility of the anterior dorsal region of the head may explain why the latter is often found disrupted to a larger extent than the rest of the skeleton. The left and right LOP are sub-triangular in outline, and show a gently curved anterior margin; MOP is sub-rectangular with an almost straight anterior margin. Unlike *Victoriacystis*, *Rhenocystis* does not have a knobbly ornament on MOP.

The left and right PM are much longer than wide. The proximal quarter of their lateral margins turns abruptly medianward. Their posterior margins are almost straight and are longer than their anterior margins. These are slightly convex towards C, and join the latter forming three angles of 120°. Plates PM contribute to the tail insertion together with the left and right PLM, V20 and V22 (Text-figs 4B, 5A; Pl. 1, fig. 2; Pl. 4, fig. 3; Pl. 7, fig. 3; Pl. 8, fig. 1), and resemble their homologues in *Victoriacystis* in their general proportions.

Plate A, or anomalocystid plate (Caster 1952), is wider anteriorly than posteriorly. As in most anomalocystidids (and in some mitrocystitids), A lies close to the left anterior angle of the dorsal skeleton, surrounded by the left LOP, DLM and ILM, and by C (Text-figs 4B, 5A; Pl. 1, fig. 2; Pl. 4, fig. 3; Pl. 7, figs 1, 3). The suture between A and C is gently convex postero-medially, more so than in *Victoriacystis*, but less so than in *Placocystites*. C reaches its maximum width at the level of its anterior third, where it contacts A and the right DLM.

The sculpture of the dorsal head skeleton consists of transversely elongate, widely spaced, robust ridges which, as usual in mitrates, show a steeper anterior slope and a gentler posterior slope (cuesta-shaped ribs of Jefferies 1986) (Text-fig. 4B; Pl. 1, fig. 2; Pl. 3, fig. 3; Pl. 5, figs 4–5; Pl. 6, fig. 1; Pl. 7, figs 1, 3; Pl. 8, fig. 1; Pl. 9, fig. 3). The ridges occupy the dorsal surface of the left and right PLM and those parts of the lateral head surfaces formed by the vertical extensions of plates PLM and, sometimes, ILM. Eight to 12 ridges are visible on both the left and the right PLM. The four or five most posterior ridges are more closely spaced than the remaining ridges and are orientated at an angle with respect to the longitudinal axis of the head. A few short ridges are visible near the posterior half of the lateral margins of plates PM in some specimens. The ridges on the vertical parts of plates PLM seem to correspond in number and position with those on their dorsal surfaces (see also Jefferies and Lewis 1978; Ruta 1997). The dorsal and lateral ridges occasionally show a sinuous course. When this condition occurs, they tend to break up irregularly (e.g. Pl. 6, fig. 1). Three or four ribs are sometimes visible on the posterior third of the vertical parts of plates ILM and, more rarely, on their dorsal parts.

Ventral head skeleton (Text-figs 4C, 5B; Pl. 1, figs 3–6; Pl. 2, figs 1, 3; Pl. 3, figs 1, 4–5; Pl. 4, figs 2–3, 5–6; Pl. 5, figs 1–3; Pl. 6, figs 3–4; Pl. 7, fig. 2; Pl. 8, figs 3–4; Pl. 9, figs 1, 4). The ventral head skeleton consists of 20 plates arranged in five transverse rows (Dehm 1932). These are numbered antero-posteriorly using Roman numerals (see also Ruta 1997; Ruta and Theron 1997).

Row I is five-plated (Pl. 1, figs 4–6; Pl. 4, figs 3, 6; Pl. 5, figs 1–2). For Dehm (1932, 1934), three plates (labelled as plates 5) were present in life, but his interpretation was certainly a result of different modes of preservation in different specimens, as well as disruption of row I. The two lateral plates, V1 and V5, are small, sub-trapezoidal elements, not always clearly visible in the available specimens. Sometimes, they are found superimposed on the admedian plates V2 and V4 (Pl. 2, fig. 3; Pl. 7, fig. 2; Pl. 9, fig. 1). Often, they are displaced

---

EXPLANATION OF PLATE 3

Figs 1–5. *Rhenocystis latipedunculata* Dehm, 1932; Bundenbach; Upper Pragian to Lower Emsian, *praecursor* dacryoconarid Zone; Hunsrückschiefer of Rhineland, Germany. 1, DBM-HS 567; posterior half of disrupted ventral head skeleton. 2, BMNH EE 5886/3; spine morphology. 3, BMNH EE 5886/8; partially disrupted specimen in dorsal aspect with partial tail. 4, DBM-HS 524; partially preserved ventral head skeleton and complete hind tail. 5, DBM-HS 299; almost complete ventral head skeleton, complete spines, partially exposed fore tail and disrupted proximal region of the hind tail. Figs 1–2, ×5; figs 3–5, ×3.


1

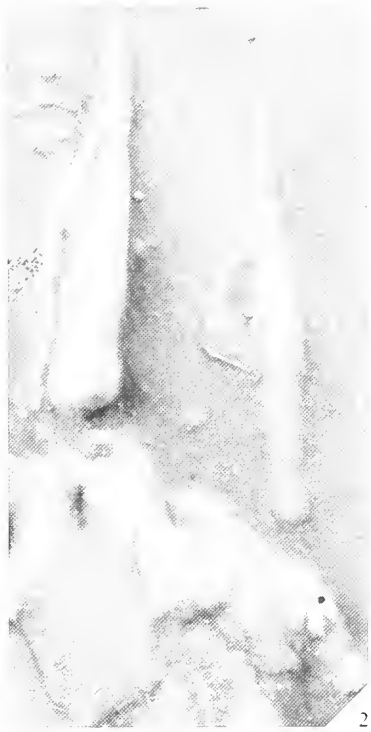
2


3

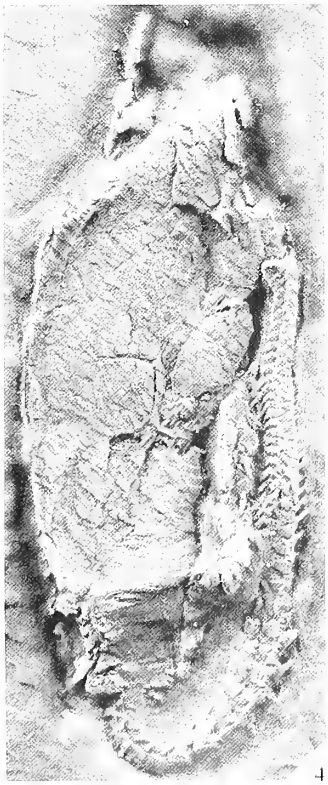
4


5

RUTA and BARTELS, *Rhenocystis*

or partly covered by the surrounding elements (Pl. 1, fig. 3; Pl. 2, fig. 1; Pl. 4, fig. 5; Pl. 5, fig. 3; Pl. 9, fig. 4). The admedian plates, V2 and V4, are sub-pentagonal in outline and three to four times as large as V1 and V5. The mid-ventral plate, V3, is sub-trapezoidal. Its postero-lateral angles are truncated and form two short sutures with the admedian plates of row II. Its lateral margins are sometimes straight or, more often, gently concave outward, and converge slightly anteriorly. Its posterior margin is sutured with V12, and is one-third to one-half the maximum width of V3.

Row II consists of four plates, labelled as V6–V9 (plates 4 of Dehm 1932), approximately as large as or only slightly larger than V1 and V5, and sub-pentagonal in outline (Text-figs 4C, 5B; Pl. 1, figs 4–6; Pl. 4, figs 3, 6; Pl. 5, figs 1–2; Pl. 7, fig. 2; Pl. 9, fig. 1). V7 and V8 are much wider than long, whereas V6 and V9 are approximately as long as wide. Plates V6–V9 constitute the most distinctive feature of the ventral head skeleton of *Rhenocystis*, as they partially separate row I from row III. In such forms as *Bokkeveldia oosthuizeni* Ruta and Theron, 1997 and *Victoriacystis* (see Ruta 1997), row II is completely inserted between rows I and III. The new material of *Rhenocystis* confirms most of Dehm's (1932, 1934) observations on the shape and relative position of V6–V9. However, we could find no evidence of complete separation between V6 and V7 or between V8 and V9, except perhaps in the holotype, although the disrupted ventral skeleton of this specimen makes it difficult to delimit the plate boundaries accurately (Pl. 1, fig. 6). The V6/V7 and V8/V9 sutures are orientated obliquely with respect to the longitudinal axis of the head.

The three plates of row III, V10, V12 and V14 (plates 3 of Dehm 1932), are the largest elements of the anterior half of the ventral skeleton (Text-figs 4C, 5B; Pl. 1, figs 3–6; Pl. 2, figs 1, 3; Pl. 3, figs 1, 4–5; Pl. 4, figs 2–3, 5–6; Pl. 5, figs 1–2; Pl. 6, figs 3–4; Pl. 7, fig. 2; Pl. 9, figs 1, 4). V12 is octagonal and slightly longer than wide. Its posterior angle is truncated by V17 (see below). V12 and V14 are seven-sided plates with an irregular outline. The presence of a transverse row of three large polygonal elements just anterior to the centre of the ventral head skeleton also characterizes *Mongolocarpos*, *Placocystites* and *Victoriacystis* (Jefferies and Lewis 1978; Rozhnov 1990; Ruta 1997).

Row IV consists of five plates, V15–V19 (plates 2 of Dehm). As in *Placocystites forbesianus* and *Victoriacystis*, the sutures between V15 and V16 and between V18 and V19 are slightly convex medianward (Jefferies and Lewis 1978; Ruta 1997) (Text-figs 4C, 5B; Pl. 1, figs 5–6; Pl. 4, fig. 6; Pl. 5, fig. 2; Pl. 7, fig. 2). The central element, V17 or placocystid plate (Caster 1952), is unusually large in comparison with its homologue in such anomalocystitids as *Placocystites* and *Victoriacystis*, its size being comparable to or greater than that of V16 and V18 (Pl. 1, figs 4–6; Pl. 2, fig. 3; Pl. 3, fig. 4; Pl. 4, figs 2, 6; Pl. 5, fig. 2; Pl. 6, fig. 3; Pl. 8, fig. 3). In other anomalocystitids, V17 varies in shape, size and relative position with respect to the surrounding plates (Ubaghs 1979; Kolata and Jollie 1982; Jefferies 1984; Craske and Jefferies 1989; Parsley 1991; Ruta 1997). V12, V16, V18 and V21 are truncated where they abut against V17.

Row V consists of three plates, V20–V22. V20 and V22 (plates b of Dehm) are in contact with each other along a short suture lying immediately posterior to V21, and are the largest elements of the posterior half of the ventral skeleton (Text-figs 4C, 5B; Pl. 1, figs 3–6; Pl. 2, fig. 3; Pl. 3, figs 1, 4–5; Pl. 4, figs 2–3, 5–6; Pl. 5, figs 2–3; Pl. 6, fig. 3; Pl. 7, fig. 2; Pl. 8, figs 3–4). Posteriorly, they contribute to the head excavation for the tail insertion. Their lateral margins are gently sinuous, and turn abruptly away from the longitudinal axis of the head at the level of their posterior third, when observed in ventral view. V20 and V22 are similar in general proportions and relative size to the corresponding plates in *Victoriacystis*, but are more elongate than their homologues in *Placocystites*. V21 (plate v of Dehm) is a shield-shaped element, only slightly longer than wide and rhomboidal in outline. Its postero-lateral margins are not uniformly convex outward, but show a sudden change in curvature in the distal part of their posterior third. The antero-lateral margins are much shorter than the postero-lateral margins, and gently convex anteriorly, as in *Placocystites*.

EXPLANATION OF PLATE 4

Figs 1–6. *Rhenocystis latipedunculata* Dehm, 1932; Bundenbach; Upper Pragian to Lower Emsian, *praecursor* dacryoconarid Zone; Hunsrückschiefer of Rhineland, Germany. 1, BMNH E 23660; anterior, intermediate and part of the posterior regions of the hind tail in left lateral aspect. 2, DBM-HS 564; general aspect of the ventral head skeleton, distribution of the ventral sculpture and well-preserved hind tail. 3, DBM-HS 301; partially preserved plate arrangement in the anterior half of the ventral head skeleton, complete spines and extensive overlap of some fore tail rings. 4, BMNH EE 5886/2; partially preserved dorsal head skeleton and complete spines. 5, DBM-HS 297; complete, but heavily disrupted ventral skeleton and complete tail. 6, DBM-HS 300; complete ventral head skeleton and partially exposed hind tail. Fig. 1, ×5; figs 2–6, ×3.

1

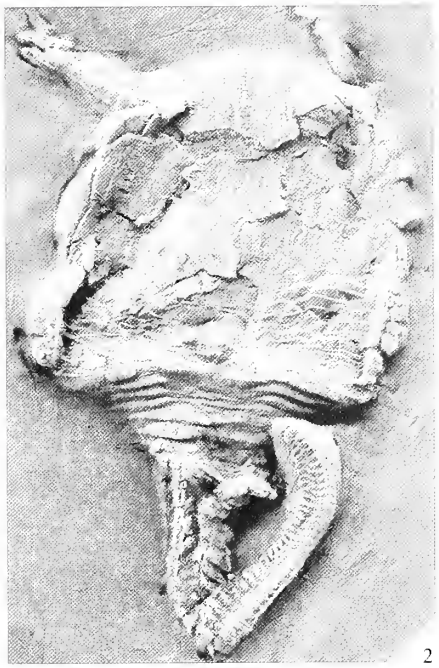

2

3

4

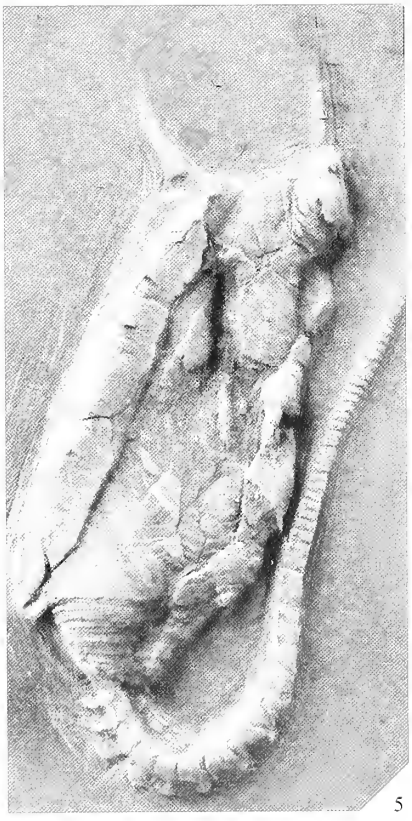

5

6

RUTA and BARTELS, *Rhenocystis*

The sculpture of the ventral head skeleton is usually confined to row V, although some specimens show short ridges near the posterior-lateral angles of V15 and V19 and/or near the postero-median angles of V16 and V18 (Text-fig. 4A, C, E; Pl. 1, figs 3–6; Pl. 2, fig. 3; Pl. 3, figs 1, 4–5; Pl. 4, figs 2, 5–6; Pl. 5, figs 2–3; Pl. 6, fig. 3; Pl. 7, fig. 2; Pl. 8, figs 3–4; Pl. 9, fig. 4). As in the case of the dorsal head skeleton, the ridges are comparatively more robust than in other anomalocystitids, and less numerous. Although the morphology of the posterior half of its ventral head skeleton recalls that of *Victoriacystis* (see Gill and Caster 1960; Ruta 1977), *Rhenocystis* differs from the latter in that its ventral ridges (especially those on V20 and V22) are more irregular posteriorly, where they delimit two transversely elongate, smooth areas near to the posterior margins of V20 and V22. These areas, also visible in *Placocystites* and *Victoriacystis*, delimit a change in the curvature of V20 and V22 (Jefferies and Lewis 1978; Jefferies 1984; Parsley 1991; Ruta 1997).

The spines (Text-fig. 4A–C; Pl. 1, figs 1–6; Pl. 2 figs 1–4; Pl. 3, figs 2–5; Pl. 4, figs 2–6; Pl. 5, figs 1–5; Pl. 6, fig. 4; Pl. 7, figs 1–3; Pl. 8, fig. 4; Pl. 9, figs 1, 4). As noted by Dehm (1932, 1934), the spines of *Rhenocystis* (called horns by Dehm) vary considerably in shape and relative size. In most specimens, they are approximately as long as the anterior head margin, and show a slightly convex, sharp, lateral edge and a concave, blunt, median edge. This morphology is also found in *Placocystites* (Jefferies and Lewis 1978; Jefferies 1984). In cross section, the spines are roughly elliptical, the greater axis of the cross section being horizonal.

In some specimens, however, the spines are almost straight, cigar-like, and slightly shorter than the anterior head margin. In some cases, this shape results from the fact that the spines are not fully exposed. The finely drawn-out and slender spine shape observed by Dehm (1934) in a few specimens is almost certainly due to deformation without breakage. In addition, the extensive degree of pyritization often cancels any sign of breakage, resulting in uniformly tapering spine stumps.

The spines are slightly expanded proximally. A comparison with other anomalocystitids suggests that a socket was present on their proximal surface (Pl. 1, figs 2–3, 5; Pl. 2, fig. 1; Pl. 3, fig. 2; Pl. 7, fig. 3). The latter accommodated a toroidal process visible in some specimens on the anterior surface of the left and right DLM (Text-figs 4D, 5B; Pl. 1, figs 2, 5; Pl. 3, fig. 5; Pl. 4, fig. 4; Pl. 7, figs 1, 3). The presence of a space between the spine insertion and the lateral margin of each of the two plates LOP, as well as between the spine insertion and the antero-lateral angles of the left and right DLM, suggests that, as in *Placocystites*, a fold of integument was probably wrapped around the base of each spine (see Jefferies and Lewis 1978 for a functional interpretation of this integument). However, no direct evidence of such a fold can be observed in *Rhenocystis*.

The spines may have acted as a supporting and steering device in life. Their sharp, lateral edge probably cut a way open through the sediment during the lateral stroke. A similar function was hypothesized by Jefferies and Lewis (1978) and Jefferies (1984) for *Placocystites*, whose spine morphology recalls that of *Rhenocystis*.

The tail

As in all mitrates, the tail of adult individuals of *Rhenocystis* is divided into fore (proximal), mid (intermediate) and hind (distal) tail in order of increasing distance from the posterior head excavation. Articulated specimens in different orientations with respect to the bedding planes allow an accurate reconstruction of the external aspect of the tail. Its internal features, however, are not known, as isolated tail segments have not been found and the lumen of broken tails is usually filled with pyrite crystals or framboids which obliterate its fine morphological details.

In the smallest known specimen, WB 514 (Pl. 1, fig. 1), the anteriormost hind tail segments show well-differentiated dorsa ossicular processes which are larger than those belonging to more posterior segments (see

---

EXPLANATION OF PLATE 5

Figs 1–5. *Rhenocystis latipedunculata* Dehm, 1932; Bundenbach; Upper Pragian to Lower Emsian, *praecursor* dacryoconarid Zone; Hunsrückschiefer of Rhineland, Germany. 1, DBM-HS 301; slightly deformed anterior third of the ventral head skeleton with complete spines. 2, BMNH E 29316; complete, articulated ventral head skeleton and partially exposed fore and hind tail. 3, DBM-HS 296; disrupted ventral head skeleton and tail. 4, DBM-HS 750; showing a fully exposed and exceptionally well preserved tail; the right half of the dorsal head skeleton is folded and crushed. 5, BMNH EE 5898; showing almost complete, but partly disrupted dorsal head skeleton, a broken left spine and a complete tail. Fig. 1, ×6; figs 2–5, ×3.

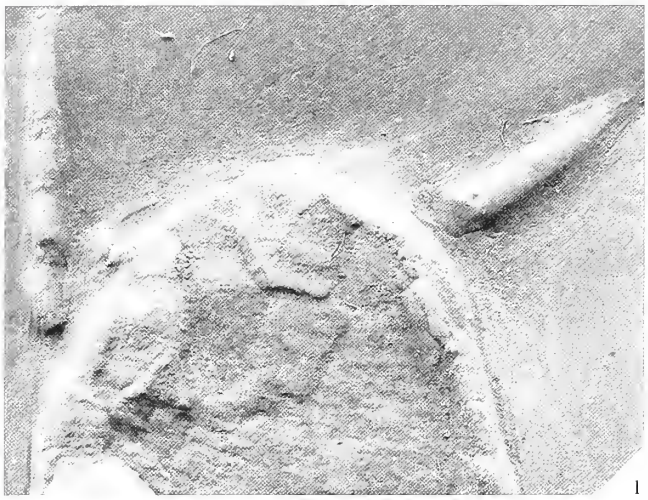
1


2


3


4


5

RUTA and BARTELS, *Rhenocystis*

above). Conversely, the posteriormost segments are much simpler in shape. These features suggest that during growth, new segments were probably added at the distal tip of the hind tail.

The fore tail: morphology (Text-figs 4A–C, 6; Pl. 1, figs 1–2, 4–6; Pl. 2, fig. 3; Pl. 3, figs 3, 5; Pl. 4, figs 2–3, 5; Pl. 5, figs 2, 4–5; Pl. 6, fig. 1; Pl. 7, fig. 3; Pl. 8, figs 1, 3). The fore tail skeleton is composed of tetramerous rings. A maximum of eight rings can be observed in the best preserved specimens, although, as in the case of several other anomalocystitids, their precise number is uncertain. The width of the rings, but not their height, decreases rapidly antero-posteriorly; as a result, the fore tail is about three times as wide near the junction with the head as near the insertion of the mid tail (Text-fig. 4B–C, E; Pl. 1, figs 2, 4–5; Pl. 2, fig. 3; Pl. 3, fig. 3; Pl. 4, figs 2, 5; Pl. 5, figs 2, 4–5; Pl. 7, fig. 3; Pl. 8, figs 1, 3). The cross section of the fore tail is difficult to reconstruct due to compaction and distortion.

A comparison with *Victoriacystis* (Gill and Caster 1960; Ruta 1997) suggests that in *Rhenocystis*, the most anterior rings are sub-elliptical and strongly compressed dorso-ventrally, whereas the most posterior rings are sub-circular. Each ring overlaps its posterior neighbour. The degree of overlap is greater in the anterior half of the fore tail than in the posterior half.

In some specimens, a fold of polyplated, presumably flexible integument is partly visible between each ring (Pl. 2, fig. 3; Pl. 4, figs 2, 5; Pl. 5, fig. 4; Pl. 6, figs 1–2; Pl. 8, figs 1, 3). The plates of the integument are small and transversely elongate. The distal margin of each fold occupies a narrow gap present between each of the four ring plates and the corresponding plates of the next posterior ring (Text-figs 4A, 6A). This gap results from a proximo-distal shortening of the median half of each plate. An irregular thickening runs along the distal margins of the ring plates.

Anteriorly in the fore tail, the two dorsal plates of each ring are smaller than the two ventral plates, but such difference in size is not significant in the two most posterior rings. The degree of curvature of the ventral plates is greater than that of the dorsal plates throughout the fore tail length; as a result, the external surface of the ventral plates contributes to about two-thirds of the lateral aspect of the fore tail. In each ring, the two dorsal plates are in contact with each other mid-dorsally along a vertical and presumably flat surface; likewise, the two ventral plates are rigidly sutured mid-ventrally. Each dorsal plate forms a rocking articulation with the ventral plate of the same side. In those specimens in which the fore tail is dorso-ventrally compressed, flexed laterally or disrupted as a result of compaction, the dorsal and ventral fore tail plates are sometimes found separated, allowing some morphological details of their articulation surfaces to be observed (Pl. 1, fig. 2; Pl. 3, fig. 3; Pl. 5, figs 4–5; Pl. 7, fig. 3; Pl. 8, fig. 1).

The dorso-lateral end of each ventral plate is slightly expanded antero-posteriorly and thickened with respect to the rest of the plate. Its articulation surface slopes downward in a latero-median and in an antero-posterior direction. The articulation surface is elliptical to rounded in outline in dorsal aspect, and carries a transversely elongate, shallow pit which occupies its posterior half (Text-fig. 6B). None of the specimens examined shows the articulation surface of the dorsal plates. However, in those specimens in which the fore tail is strongly flexed lateralward, a small, rounded knob is visible near the posterior half of the ventro-lateral end of each dorsal plate; this knob fits into the shallow pit of the articulation surface of the ventral plate of the corresponding side (Pl. 1, fig. 2; Pl. 3, fig. 3; Pl. 7, fig. 3; Pl. 8, fig. 1).

The fore tail: function. Rhenocystis could presumably flex its fore tail to a considerable extent, both in the horizontal and in the vertical plane, as indicated by several details of the constructional morphology of the fore tail rings and by the modes of preservation of many specimens. The degree of overlap, as well as the large size of the proximal fore tail rings and the presence of rocking articulations between dorsal and ventral fore tail plates, are also observed in *Victoriacystis* (Gill and

---

EXPLANATION OF PLATE 6

Figs 1–4. *Rhenocystis latipedunculata* Dehm, 1932; Bundenbach; Upper Pragian to Lower Emsian, *praecursor* dacryoconarid Zone; Hunsrückschiefer of Rhineland, Germany. 1, DBM-HS 570; showing complete hind tail with coiled distal end; ×4. 2, DBM-HS 750; close-up of the mid and hind tail, mainly in right lateral aspect; ×5. 3, DBM-HS 524; close-up of hind tail and posterior sculpture of the ventral head skeleton; ×5. 4, BMNH EE 5902; partially preserved ventral skeleton and complete hind tail; ×3.

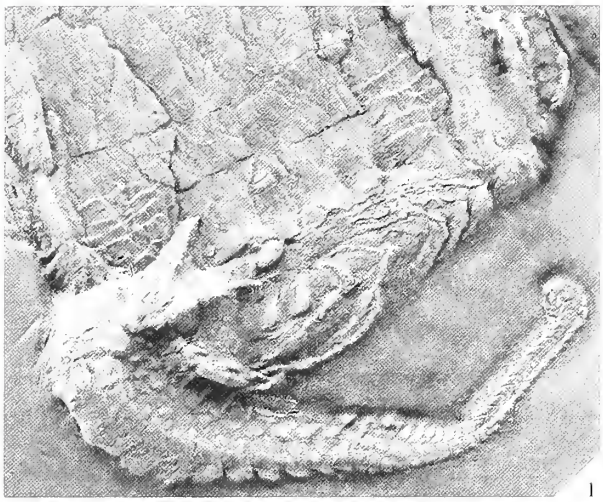

1

2

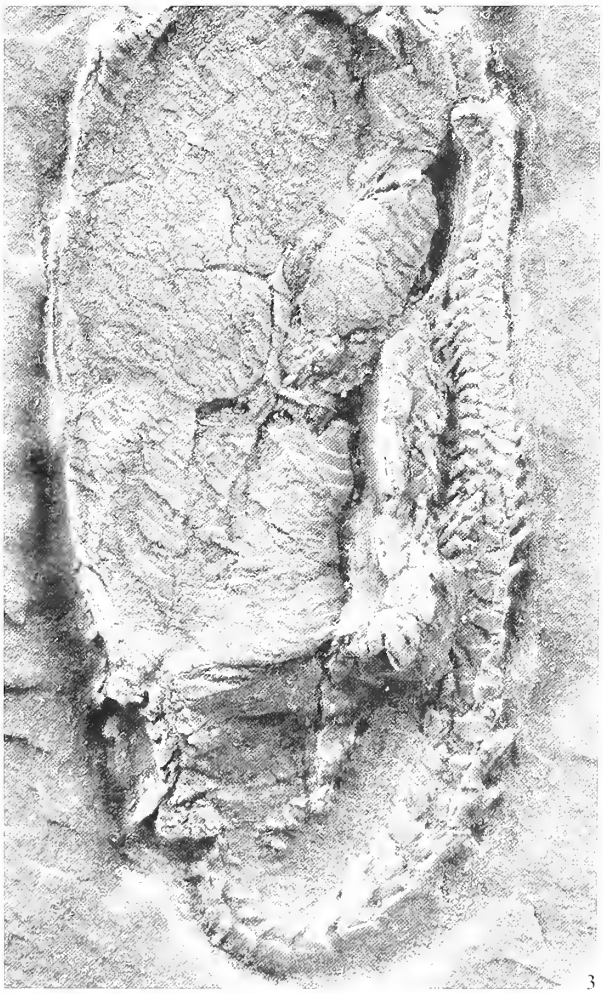

3

4

RUTA and BARTELS, *Rhenocystis*

Caster 1960; Ruta 1997). Folds of flexible, polyplated integument between each fore tail ring were described by Jefferies and Lewis (1978) in *Placocystites*, and by Kolata and Guensburg (1979) in *Diamphidiocystis drepanon*. They are probably present also in *Enoploura popei* Caster, 1952 (Parsley 1991) and *Placocystella africana* (Reed, 1925) (Ruta and Theron 1997). Fore tail integument folds were not observed by Ruta (1997) in *Victoriacystis*, although this may be due to preservation.

The folds of polyplated integument are comparatively less expanded antero-posteriorly in *Rhenocystis* than in *Placocystites*, and there is no evidence that they were strongly recumbent posteriorly in the former. The dorsal and ventral integument folds of *Rhenocystis* do not differ appreciably in size; this indicates that the fore tail was perhaps equally flexible both dorsalward and ventralward. Conversely, the integument folds of *Placocystites* are particularly well developed on the dorsal surface of the fore tail, and may have enabled the latter to flex mainly towards the ventral head surface (Jefferies and Lewis 1978; Savazzi *et al.* 1982; Jefferies 1984; Savazzi 1994).

As in *Victoriacystis*, the lateral rocking articulations probably allowed the dorsal and ventral fore tail plates of *Rhenocystis* to rotate about a transverse axis relative to each other (Ruta 1997). Lateral movements of the dorsal and ventral plates were probably hindered by the oblique orientation of their articulation surfaces. Such orientation may also have prevented dorso-ventral deformation of the fore tail rings. Additional strength may have been provided by the mid-dorsal and mid-ventral sutures. The fore tail rings were likely to act both as rigid and as flexible units, enabling the tail to perform a wide variety of movements.

The mid tail: morphology (Text-fig. 4A–B; Pl. 1, figs 1–2; Pl. 3, fig. 3; Pl. 5, fig. 4; Pl. 6, figs 1–2, 4; Pl. 7, fig. 3; Pl. 8, fig. 1; Pl. 9, fig. 2). The skeleton of the mid tail consists of a massive element, the styloid, and its associated paired plates. As in other mitrates, the number of plates is difficult to determine (Kolata and Jollie 1982; Parsley 1991; Beisswenger 1994; Ruta 1997; Ruta and Theron 1997). The styloid is generally poorly preserved. A small process, partly visible in some disrupted specimens (e.g. Pl. 1, fig. 2; Pl. 7, fig. 3), projects from the styloid antero-ventrally. The process probably occupied the posterior part of the fore tail lumen, where it probably gave insertion to muscles in life. The dorsal and lateral surfaces of the styloid are observed only in few individuals.

The styloid is slightly longer than wide and bears two dorsal blades which differ in shape and size, and are separated by the broad, saddle-like dorsal styloid surface (Text-fig. 4A–B; Pl. 1, figs 1–2; Pl. 3, fig. 3; Pl. 5, fig. 4; Pl. 6, fig. 2). The maximum width of the styloid is at the level of its anterior blade. The anterior blade is broadly semicircular in outline in dorsal aspect, anteriorly recumbent in position, and carries a sharp, mid-dorsal keel. The keel fades gradually in a proximal direction and disappears before reaching the free margin of the anterior blade. Distally, it merges into the posterior blade. The posterior blade is much higher and stouter than the anterior blade, and broadly rectangular in lateral aspect. Its anterior margin is sigmoidal in lateral view, and does not seem to have been sharp. In none of the specimens examined is the posterior blade completely visible. Dorsally, the posterior blade shows a blunt apex. From the dorsal apex, the posterior surface of the blade widens progressively ventralward, but its articulation surface is not visible. The lateral surfaces of the blade are slightly depressed in their dorsal third, and become gently convex outward before merging into the lateral walls of the styloid.

The mid tail: function. The styloid of *Rhenocystis* closely resembles that of *Victoriacystis* in its general proportions and in the shape and relative size of its two blades (Gill and Caster 1960; Ruta

---

EXPLANATION OF PLATE 7

Figs 1–5. *Rhenocystis latipedunculata* Dehm, 1932; Bundenbach; Upper Pragian to Lower Emsian, *praecursor* dacryoconarid Zone; Hunsrückschiefer of Rhineland, Germany. 1, DBM-HS 570; complete, but highly deformed dorsal head skeleton; ×4. 2, BMNH E 23660; general aspect of the ventral head skeleton; ×3. 3, BMNH EE 5886/1; complete but heavily damaged dorsal head skeleton and partial tail; ×3. 4, BMNH EE 5886/3; showing variation in the morphology of the hind tail segments; ×3. 5, DBM-HS 524; close-up of the distal part of the intermediate region of the hind tail; ×20.

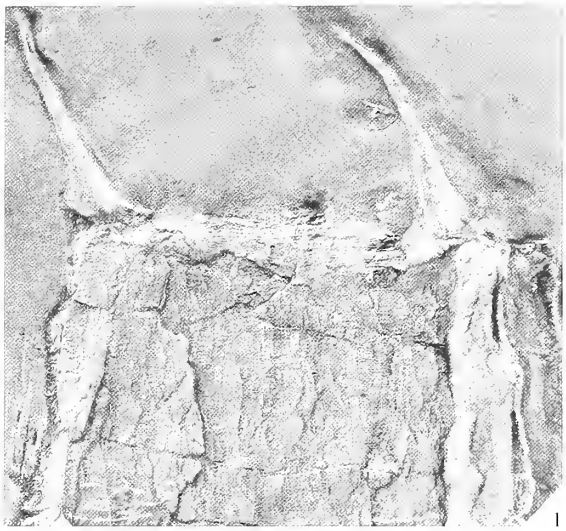
1


2

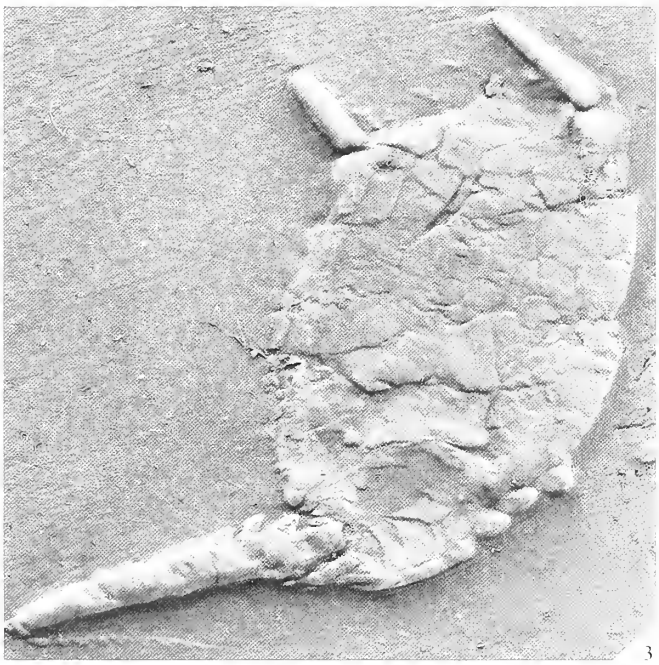
3


5

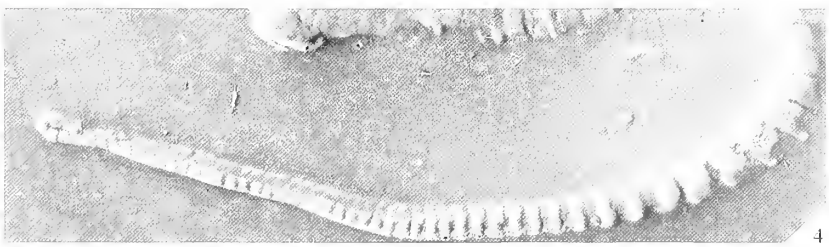
4

RUTA and BARTELS, *Rhenocystis*

1997). The styloid may have enhanced leverage of the tail in life, separating two regions, the fore and the hind tail, with different mechanical properties (Parsley 1991; Ruta 1997). The recumbent anterior blade and the dorsal keel were probably scarcely effective in life as anchoring devices. However, the massive posterior blade and the proximal hind tail ossicles were probably suitable for this function (see also discussion below).

The hind tail: morphology (Text-fig. 4A–C; Pl. 1, figs 1–2, 4–5; Pl. 3, figs 3–5; Pl. 4, figs 1–3, 5–6; Pl. 5, figs 2–5; Pl. 6, figs 1–4; Pl. 7, figs 3–5; Pl. 8, figs 1–4; Pl. 9, figs 2–4; Pl. 10, figs 1–5). The hind tail skeleton is composed of segments, each consisting of a dorsal ossicle and a pair of ventral plates articulated with it, and shows significant morphological variation throughout its length. Proximo-distally, the hind tail can be divided into an anterior, an intermediate, a posterior and a terminal region.

The anterior region of the hind tail consists of five or six segments characterized by the remarkable development of the dorsal ossicles (Text-fig. 4A; Pl. 5, fig. 4; Pl. 6, figs 2, 4; Pl. 8, fig. 1; Pl. 9, fig. 2). The ossicles decrease in size from the first to the fifth or sixth segment, but this decrease is not gradual. The height of the first three ossicles diminishes only to a small extent in passing from the first to the second and from the second to the third segment. The height of the fourth ossicle is about two-thirds that of the third ossicle. The fifth ossicle is only slightly smaller than the fourth. Finally, the sixth ossicle is about one-third the height of the first and is comparable in size and shape to the anterior ossicles of the intermediate region.

The ossicles of the anterior region are approximately equal in length. The first ossicle closely resembles the posterior styloid blade. Each of the first five or six ossicles can be divided morphologically into a ventral part, bearing an anterior and a posterior articulation surface, and a dorsal process. As isolated ossicles have not been found, the articulation surfaces cannot be reconstructed. The ventral parts of the four most anterior ossicles are connected to each other through a peg-and-socket mechanism, clearly visible in lateral view: in each ossicle, the lower half of the anterior margin of the ventral part shows a protruding knob, which fits into a shallow excavation of the posterior margin of the next anterior ossicle.

A similar articulation mechanism was described by Ruta (1997) in *Victoriacystis wilkinsi*, and by Ruta and Theron (1997) in *Placocystella africana*. In the ossicles of the intermediate region of the hind tail, the peg-and-socket articulation is less pronounced. In the posterior and terminal regions, the anterior and posterior ossicular margins are slightly sinuous to straight.

In cross section, the ossicles of the anterior region are gently convex externally in their lower third. The lateral surfaces of their ventral parts merge gradually into those of their dorsal processes; at this level, the lateral ossicular surfaces are slightly concave outward, but become almost vertical in the upper third of the processes. The dorsal margins of the processes do not seem to have been sharp. Their lateral surfaces merge anteriorly into a blunt, vertical margin. The dorsalmost part of their posterior surfaces is flat and roughly triangular. The ventral ossicular margins are vaguely chevron-shaped in lateral view. In the first three or four ossicles, the anterior arm of the chevron is much shorter than the posterior arm. In successive ossicles of the anterior region, as well as in the ossicles of the intermediate and of most of the posterior region of the hind tail, the ventral ossicular margins are likewise chevron-shaped, but the two arms of the chevron are subequal in length. The ventral ossicular margins of the distalmost ossicles are slightly convex ventralward to straight in lateral aspect.

The intermediate region of the hind tail consists of six or seven segments of approximately equal length. These differ from the segments of the anterior region in that the dorsal ossicular processes are comparatively much smaller and confined to the posterior third of the dorsal ossicular surface. From the apex of each process, the dorsal ossicular margin slopes anteriorly and slightly ventralward following a gently sinuous course. In the two or three posteriormost segments of the intermediate region, the dorsal ossicular processes are slightly inclined backward, so that the apex of each process slightly overhangs the posterior articulation surface of the

---

EXPLANATION OF PLATE 8

Figs 1–4. *Rhenocystis latipedunculata* Dehm, 1932; Bundenbach; Upper Pragian to Lower Emsian, *praecursor* dacryoconarid Zone; Hunsrückschiefer of Rhineland, Germany. 1, DBM-HS 744; close-up of hind tail in left lateral aspect; ×5. 2, DBM-HS 566; anterior region of the hind tail in left lateral aspect; ×6. 3, DBM-HS 564; morphology of the tail and posterior sculpture of the ventral head skeleton; ×5. 4, BMNH EE 5890; incomplete ventral head skeleton and well-preserved hind tail; ×3.

1

2

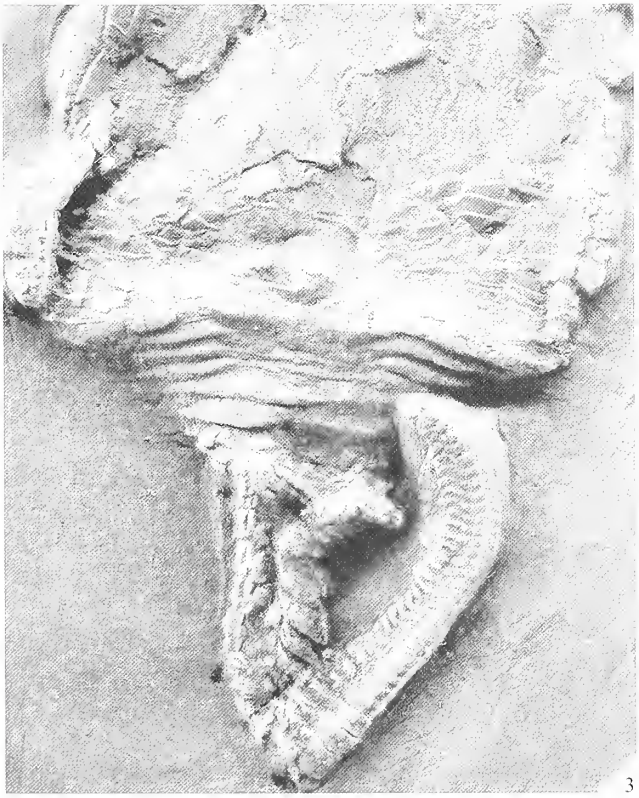

3

4

RUTA and BARTELS, *Rhenocystis*

corresponding ossicle (Text-fig. 4A; Pl. 1, fig. 5; Pl. 3, figs 2, 5; Pl. 5, figs 4–5; Pl. 6, figs 1–4; Pl. 7, fig. 4; Pl. 8, figs 1–4; Pl. 9, figs 2–4).

The posterior region of the hind tail is composed of five or six segments. The ossicles are approximately hemicylindrical and decrease uniformly in size in an antero-posterior direction. Their length is slightly greater than their width and the length/width ratio remains approximately constant. The ossicles bear a slightly pronounced, knob-like, postero-dorsal apex (Text-fig. 4A; Pl. 1, fig. 5; Pl. 3, fig. 4; Pl. 4, figs 1–2, 5; Pl. 5, figs 4–5; Pl. 6, figs 1–4; Pl. 7, fig. 4; Pl. 8, figs 1, 3–4; Pl. 9, figs 3–4).

In those adult specimens in which complete tails are preserved, the terminal region of the hind tail has a minimum of about 30 and a maximum of about 45 recorded segments. The ossicles of this region are approximately as long as wide and become progressively smaller antero-posteriorly. The postero-dorsal apex is either strongly reduced or absent. In lateral view, the anterior and posterior ossicular margins are almost straight, especially at the level of the last ten or 15 segments.

The modes of preservation of various specimens suggest that the terminal part of the hind tail was probably more flexible than the rest of the appendage. In some specimens, the terminal region is straight; in others, it is slightly bent dorsally; more commonly, it curves ventrally along a tight curve; in two individuals, its distalmost end is coiled (Text-fig 4A; Pl. 1, fig. 5; Pl. 3, fig. 4; Pl. 4, figs 2, 5; Pl. 5, figs 4–5; Pl. 6, figs 1–4; Pl. 7, figs 4–5; Pl. 8, figs 1, 3–4; Pl. 9, figs 2–4; Pl. 10, figs 1–5).

The paired ventral hind tail plates change gradually in shape and size from the anterior to the terminal region of the hind tail, and overlap each other antero-posteriorly. The degree of overlap increases from the anterior to the terminal region of the hind tail. In some specimens in which the hind tail is partly disrupted, the dorsal ossicles are visible in ventro-lateral aspect (Pl. 3, fig. 4; Pl. 4, fig. 2; Pl. 6, fig. 3; Pl. 8, fig. 3). A longitudinal, shallow groove runs on the ventro-lateral projections of the dorsal ossicles. This groove accommodates the dorsal margins of the ventral plates. When ossicles and plates are articulated with each other and are observed in lateral aspect, the grooves are not visible, since the lowermost part of the external surfaces of the ventro-lateral projections of each ossicle abuts against the upper part of the inside of the plates.

The ventral plates of the anterior, intermediate and part of the posterior regions of the hind tail are slightly longer than wide, and strongly arcuate in cross section (Text-fig. 4A, C). Their posterior margins are sinuous and slope ventralward and posteriorly in lateral aspect. The left and right plates meet along the mid-ventral line forming a gently rounded ventral surface. The plates of the distal part of the posterior region and those of the terminal region of the hind tail are roughly semicircular, almost as long as wide, and only slightly arcuate in cross section. Their posterior margins are convex.

In these two regions, the left and right plates meet at an obtuse angle mid-ventrally. Some specimens show that the distal ventral plates were arranged along two alternating rows, the right plates being slightly displaced anteriorly with respect to the corresponding elements of the left side (e.g. Pl. 6, fig. 2; Pl. 10, fig. 3). A knob is present near the dorsal margin of all ventral plates except those of the most anterior region of the hind tail. In the intermediate region, the knob is approximately equidistant from the anterior and the posterior margin of each plate (Pl. 6, fig. 2; Pl. 8, fig. 3; Pl. 10, figs 3–5). In the posterior and terminal regions, the knob is displaced slightly posteriorly. The plates of the anterior region show a dorsal, horizontal thickening (Pl. 8, fig. 1).

The hind tail: function. The large degree of overlap of the paired ventral plates in an antero-posterior direction and the preservation of several specimens suggest that the hind tail could be bent towards the ventral side of the head along a tight curve. Dorsal flexion was likely to occur in life, but probably to a lesser extent. The ossicles abut against each other when the tail is reconstructed in various degrees of dorsal flexion. The mechanical constraints imposed by the ossicles are especially evident in those mitrates in which the anterior and posterior ossicular surfaces as well as the

---

EXPLANATION OF PLATE 9

Figs 1–4. *Rhenocystis latipedunculata* Dehm, 1932; Bundenbach; Upper Pragian to Lower Emsian, *praecursor* dacryoconarid Zone; Hunsrückschiefer of Rhineland, Germany. 1, BMNH E 23660; close-up of the anterior half of the ventral head skeleton and of the spines; ×6. 2, DBM-HS 298; hind tail morphology; ×4. 3, BMNH EE 5887; hind tail with characteristically bent distal quarter; ×5. 4, BMNH EE 5895; ventral head skeleton and articulated tail; ×3.

1

2

3

4

RUTA and BARTELS, *Rhenocystis*

articulations between dorsal ossicles and ventral plates are known in detail (e.g. Jefferies 1967, 1968, 1973, 1986; Jefferies and Lewis 1978; Kolata and Jollie 1982; Ruta and Theron 1997), but are inferred to have existed also in *Rhenocystis*.

Mechanical constraints preventing the hind tail of *Rhenocystis* from achieving a high degree of dorsal flexion are more evident at the level of its anterior region, where the ossicles show remarkably well developed dorsal processes, and leave a narrow space between adjacent segments even when the hind tail is straight. More posteriorly, the degree of dorsal flexion was perhaps higher, as the processes are either poorly developed or absent.

In most mitrates the tail is often found flexed towards the ventral side of the head (Hall 1858; Caster 1954; Caster and Gill 1968; Kolata *et al.* 1991; Parsley 1991; Ruta 1997; Ruta and Theron 1997), but rare occurrences of dorsally bent hind tails are known (e.g. Kolata and Jollie 1982; Parsley 1991). If, as suggested by Jefferies (1986), most of the lumen of the hind tail housed muscles in life, these were presumably located mainly between the ventral plates and the ventro-lateral extensions of the dorsal ossicles. Post-mortem contraction of these muscles is expected to cause ventralward bending of the hind tail.

Although there is no direct evidence of the modalities of insertion of such muscles, it is reasonable to assume that each was connected to different segments in order to ensure mobility (Jefferies 1967, 1986; Kolata and Jollie 1982). Dorsal muscles and or ligaments are likely to have been present between the articulation surfaces of adjacent ossicles to counteract the action of the ventral muscles. Reconstructed cross sections of the hind tail segments in several mitrates (e.g. Jefferies 1967, 1968, 1986; Kolata and Jollie 1982; Ruta and Theron 1997) show that the estimated volume of the ventral muscles largely exceeded that of the dorsal muscles.

Elsewhere (Ruta 1997), it has been pointed out that the hypothesized functions of the various regions of the mitrate appendage differ to a considerable extent depending upon the affinities and life-style proposed for these animals (Ubaghs 1968; Philip 1981; Kolata and Jollie 1982; Jefferies 1984, 1986; Parsley 1991), but most arguments put forward to explain their life mode await corroboration. The morphology of the hind tail of *Rhenocystis* deserves further comments.

Almost certainly, the hind tail played an important rôle in the locomotion of the animal (Jefferies 1984). Its terminal and part of its posterior regions were certainly extremely flexible. The width of the tail was small compared with that of the head and, therefore, unlikely to have supplied a powerful thrusting action enabling the animal to drag itself along. The total surface area of the ventral plates seems to have been too small to provide an effective bearing surface, as in the model proposed by Jefferies (1984). If movement occurred at all, it was probably very disadvantageous energetically.

It is here proposed that, although rearward locomotion was plausible, as suggested by the kind and distribution of the head sculpture (Jefferies 1984, 1986), lateral rather than dorso-ventral thrusting actions of the tail were probably involved in the locomotory cycle. The lateral surfaces of the plates and ossicles of the anterior and intermediate regions of the hind tail may have provided the required bearing surface whereas the posterior and terminal regions were likely to act as a probing tool.

EXPLANATION OF PLATE 10

Figs 1–5. *Rhenocystis latipedunculata* Dehm, 1932; Bundenbach; Upper Pragian to Lower Emsian, *praecursor* dacryoconarid Zone; Hunsrückschiefer of Rhineland, Germany. 1, DBM-HS 750; distal end of the hind tail, showing overlapping plates. 2, DBM-HS 566; distal end of the hind tail, with overlapping plates and terminal segment. 3, DBM-HS 570; terminal hind tail region; note the shape and extensive overlap of the plates, the presence of a knob in a subcentral position near their dorsal margins, and the distal, coiled end. 4, DBM-HS 524; terminal hind tail region; note the arrangement of plates and ossicles and the distal end bending slightly ventralward and showing the terminal segment. 5, DBM-HS 564; terminal hind tail region and morphology of the distalmost ossicles. All × 20.

1

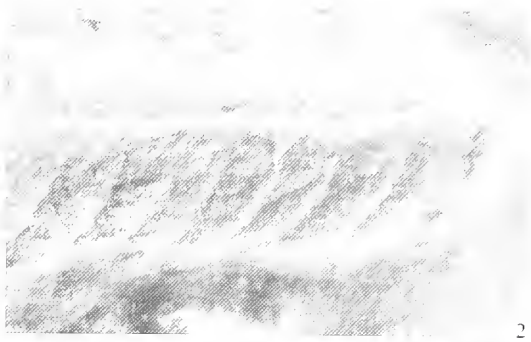

2

3

4

5

RUTA and BARTELS, *Rhenocystis*

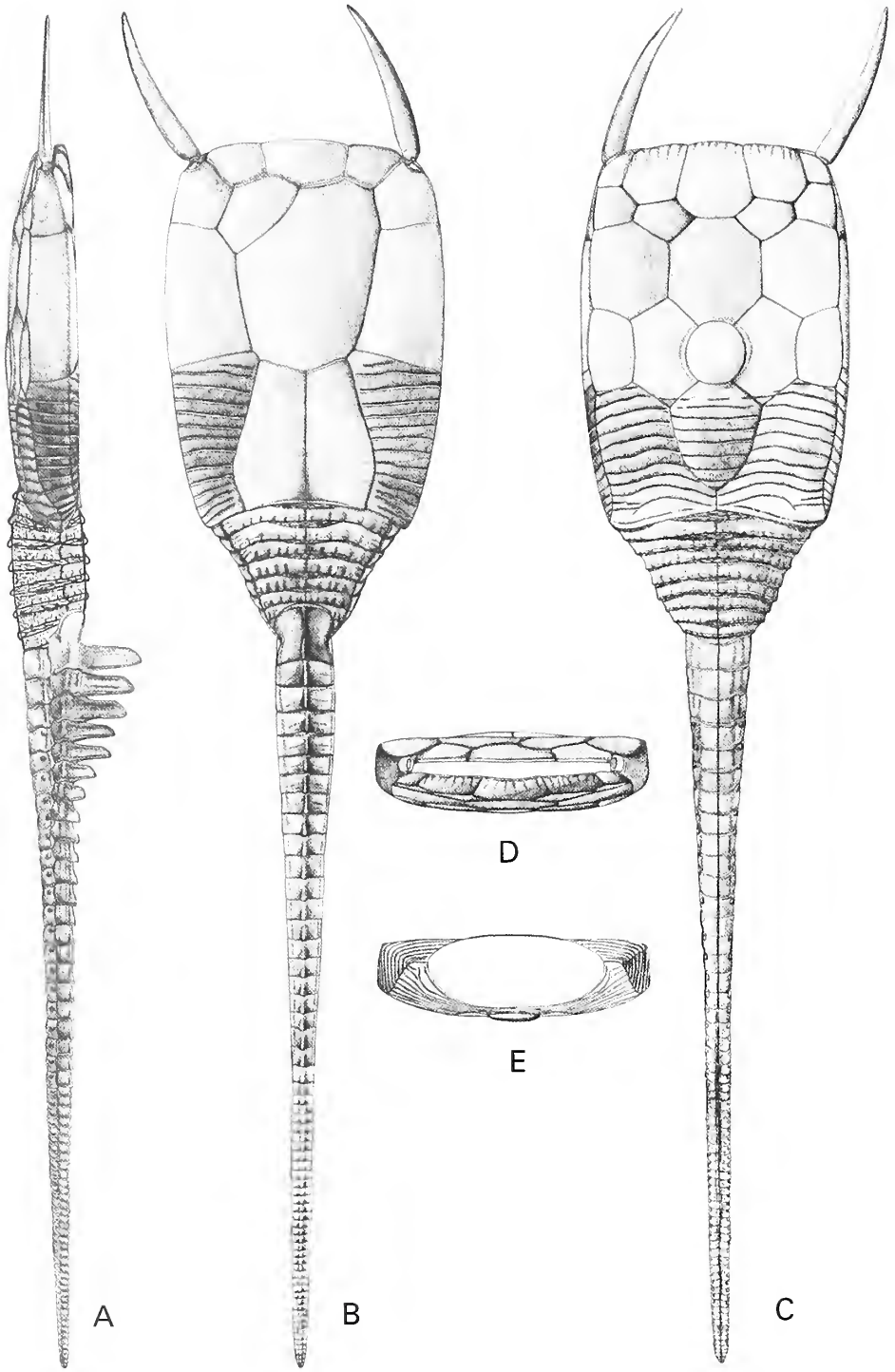

TEXT-FIG. 4. *Rhenocystis latipedunculata* Dehm, 1932. Reconstruction of the external skeletal morphology. A, left lateral view; B, dorsal view; C, ventral view; D, anterior view; E, posterior view.

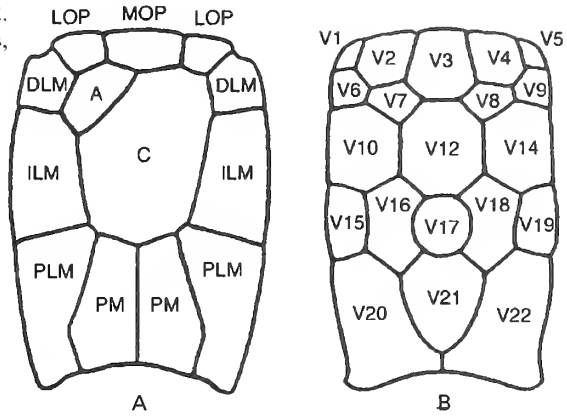

TEXT-FIG. 5. *Rhenocystis latipedunculata* Dehm, 1932. Plate nomenclature. A, dorsal head skeleton; B, ventral head skeleton.

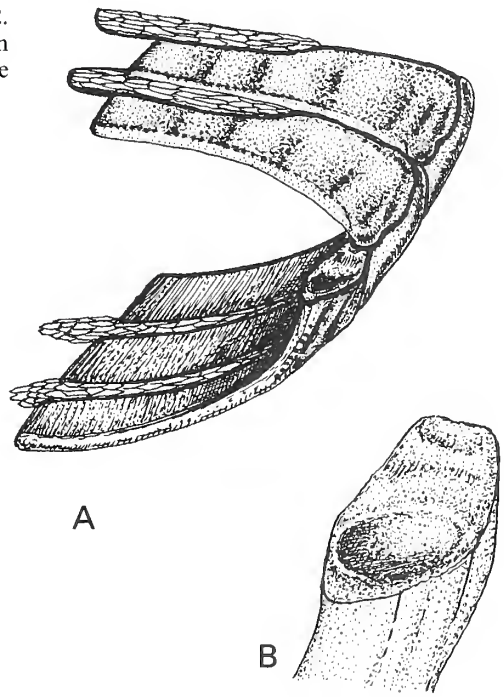

TEXT-FIG. 6. *Rhenocystis latipedunculata* Dehm, 1932. A, reconstruction of the rocking articulation between dorsal and ventral fore tail plates; B, sketch of the articulation surface of a ventral fore tail plate.

As regards life-style orientation, the ossicles of the anterior and part of the intermediate regions of the hind tail probably exerted the strongest bearing action when thrust down into the sediment and pushed against it laterally. *Rhenocystis* may have lived convex-side upward, probably just below the surface of the sea floor. The fore tail may have acted as the main motor during the locomotion, pushing alternatively leftward and rightward. Between each lateral thrust, the tail would be lifted up, partially freed from sediment, rotated in a direction opposite to that of the preceding lateral thrust and lowered down before performing the following lateral thrust.

The presence of well-developed lateral walls and the fact that the head was longer than wide suggest that yawing movements were probably limited during locomotion (see also Jefferies 1984). The general shape of the head and the distribution of the sculpture in mitrates were probably related to each other. In all of the anomalocystitids in which the length of the head is greater than its width,

the sculpture (terrace-like ridges, pustules, riblets, etc.) occupies the proximal half or third of both the dorsal and the ventral surface of the head skeleton, or is strongly reduced (or even absent) on one or both of the two surfaces (e.g. *Enoploura*, *Rhenocystis* and *Victoriacystis*). Conversely, in those anomalocystitids in which the head is approximately as long as wide, the distribution of the sculpture is often more extensive (e.g. *Allanicytidium*, *Notocarpos* and *Placocystites*).

As suggested by Jefferies (1984), the gripping action of the most posterior ridges of both the dorsal and the ventral surface of *Rhenocystis* was perhaps mostly important in the initial phases of the locomotory cycle, and may have counteracted pitching movements of the head resulting from the downward thrust of the tail into the sediment.

AFFINITIES

Most of the works discussing mitrate classification and relationships predate the 'cladistic revolution' (Caster 1952; Gill and Caster 1960; Ubaghs 1968); they attempted to detect evolutionary trends in the absence of a comprehensive pattern of character distribution (Derstler 1979; Jefferies 1986, 1991; Craske and Jefferies 1989; Parsley 1991) or focused on only a small number of taxa (Philip 1981; Caster 1983; Ruta and Theron 1997).

Since the publication of the carpoid volume of the *Treatise on invertebrate paleontology* (Ubaghs 1968), several new mitrate species have been described. Most of these belong to the Anomalocystitida as defined by Caster (1952) (Ubaghs 1968; Kolata and Guensburg 1979; Philip 1981; Kolata and Jollie 1982; Caster 1983; Regnault and Chauvel 1987; Rozhnov 1990; Parsley 1991; Haude 1995; Ruta and Theron 1997). Despite a few recent attempts to investigate the evolutionary history of this group (Parsley 1991; Ruta and Theron 1997), we are still far from reaching a consensus on its phylogeny. The monophyletic status of Anomalocystitida is likewise debated (e.g. Ubaghs 1979; Craske and Jefferies 1989; Parsley 1991; Beisswenger 1994; Ruta and Theron 1997).

Dehm (1932) assigned *Rhenocystis latipedunculata* to the family Anomalocystitidae (*nomen correctum* Bassler, 1938, *pro* Anomalocystidae Meek, 1872), together with the genera *Anomalocystites* Hall, 1858, *Enoploura* Wetherby, 1879, *Iowacystis* Thomas and Ladd, 1926 (transferred to the solutes by Bather in 1928; see Caster 1968) and *Placocystites* de Koninck, 1869. According to Dehm (1932), *Rhenocystis* and *Placocystites* constitute a well-characterized group within the Anomalocystitidae, due to their similar ventral plating patterns.

Caster (1952) placed *Placocystites* and *Rhenocystis* in the subfamily Placocystinae, which, together with Basslerocystinae and Enoplourinae, formed part of the family Placocystidae. Placocystidae was included by Caster (1952) in the suborder Placocystida, which comprised the vast majority of the anomalocystitid genera known at that time. The suborder Anomalocystida was erected by Caster (1952) to include the family Anomalocystitidae containing the single genus *Anomalocystites*. According to Caster (1952), *Rhenocystis* and *Placocystites* share the presence of two plastron somatic plates, A and Cs (plates A and C herein) and a placocystid plate (plate V17 herein).

In assigning *Victoriacystis* to the Placocystitidae (amended from Placocystidae Caster, 1952), Gill and Caster (1960) postulated that *Placocystites*, *Rhenocystis* and *Victoriacystis* could be arranged in an evolutionary sequence, characterized by an increase in the number of transverse rows of ventral plates. However, examination of better preserved, recently collected material of *Victoriacystis* (Ruta 1997) shows that this genus possesses five rows of ventral plates, and not six as proposed by Gill and Caster (1960).

Ubaghs (1968, p. S555) grouped Anomalocystida and Placocystida into a single suborder Anomalocystitida, because the distinction made by Caster (1952) between these suborders was based on '... the erroneous assumption that the Anomalocystitida [*sic*] are provided with segmented brachia and the Placocystida with unsegmented rodlike processes. In fact, as demonstrated by Caster..., the Anomalocystitida [*sic*] have no jointed brachia... Therefore they do not differ in any essential way from the placocystid genera' [the segmented brachia and the rodlike processes correspond to the

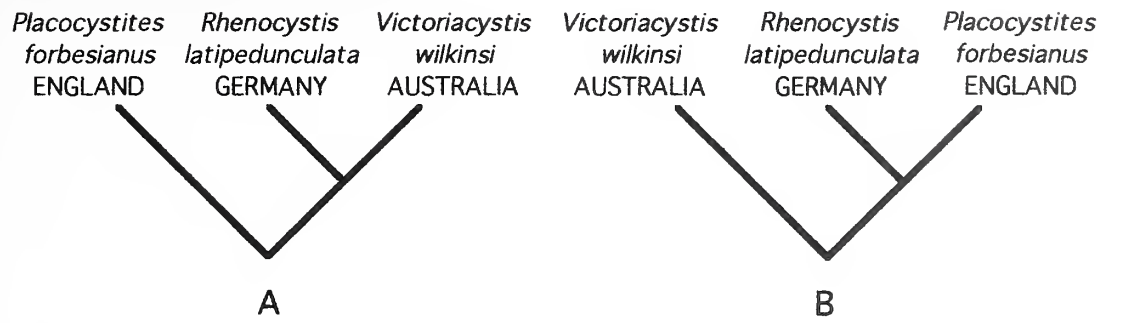

TEXT-FIG. 7. Alternative three-taxon/three-area arrangements for the anomalocystitid mitrates *Placocystites forbesianus*, *Rhenocystis latipedunculata* and *Victoriacystis wilkinsi*. A, the results of a parsimony analysis indicate that *Placocystites forbesianus* is the sister group to *Rhenocystis latipedunculata* + *Victoriacystis wilkinsi*; B, a compatibility analysis places *Victoriacystis wilkinsi* as the sister group to the clade (*Placocystites forbesianus* + *Rhenocystis latipedunculata*).

articulated spines in the terminology adopted here]. Ubaghs (1968) placed *Placocystites* and *Rhenocystis* in the family Anomalocystitidae together with *Anomalocystites*, *Ateleocystites* Billings, 1858, *Basslerocystis* Caster, 1952, *Enoploura* and *Victoriacystis* (according to Parsley 1991, *Basslerocystis* is a junior synonym of *Anomalocystites*). Other anomalocystitid genera were assigned to the families Australocystidae Caster, 1954 and Allanicytidiidae Caster and Gill, 1968.

A sister group relationship between *Rhenocystis* and *Victoriacystis* was first proposed by Parsley (1991) in his reconstructed phylogeny of the anomalocystitids, in which the families Anomalocystitidae and Placocystitidae were kept separate. One of us (MR) is currently working on a comprehensive cladistic analysis of the anomalocystitids using the program PAUP version 3.1.1 (Swofford 1993). The analysis, which will form the subject of another paper, yields three equally parsimonious trees in all of which *Placocystites forbesianus* is placed as the sister group of (*Rhenocystis latipedunculata* + *Victoriacystis wilkinsi*). The characters are optimized using the accelerated transformation (ACCTRAN) option of PAUP, whereby homoplasies are accounted for in terms of distal reversals by placing character changes as close to the tree root as possible (Kitching 1992). For the purposes of the present paper, we shall focus on the character distribution in *Placocystites forbesianus*, *Rhenocystis latipedunculata* and *Victoriacystis wilkinsi*.

The clade (*Placocystites forbesianus* + (*Rhenocystis latipedunculata* + *Victoriacystis wilkinsi*)) (Text-fig. 7A) is supported by three characters. The first character, uniquely shared by these three taxa, pertains to the shape of the lateral margins of the left and right dorsal plates PM, which are strongly convex lateralward throughout most of their length. The second character shows one reversal, and refers to the presence of a suture between plates V3 and V12 (observed in *Placocystites* and *Rhenocystis*, but not in *Victoriacystis*). The third character relates to the presence of two short, straight margins which truncate the left and right postero-lateral angles of plate V3 (observed in *Placocystites* and *Rhenocystis* and reversed once in *Victoriacystis*).

The sister group relationship between *Rhenocystis* and *Victoriacystis* is supported by five synapomorphies: dorsal terrace-like ridges confined to the left and right plates PM and PLM only; posterior quarter of the lateral margins of the left and right plates PM turned medianward and intersecting the posterior dorsal margin of the head; anterior styloid blade recumbent; fore tail three times as wide anteriorly as posteriorly and occupying most of the posterior head surface; dorsal fore tail plates much smaller than the ventral fore tail plates.

The following eight characters, not uniquely derived, also support the clade (*Rhenocystis latipedunculata* + *Victoriacystis wilkinsi*): ventro-lateral extensions (lateral head walls) of the dorsal lateral marginal plates about as large as their dorso-median extensions; lateral head walls sloping slightly ventro-laterally; flexible upper lip; centro-dorsal plate C much narrower posteriorly than

anteriorly; terrace-like ridges confined to the posterior third of the ventral skeleton only; anterior styloid blade expanded transversely; presence of a sharp, mid-dorsal styloid keel; styloid keel projecting on the dorsal surface of the anterior styloid blade.

DISCUSSION

Rhenocystis differs from *Placocystites* in having five rather than four transverse rows of ventral plates (Dehm 1932, 1934; Caster 1952; Ubaghs 1968), and from *Victoriacystis* in that the ventral plates of the second row are relatively small in comparison with those of the first and third rows (Ruta 1997). In *Placocystites*, the two anteriormost transverse rows of the ventral skeleton correspond to the first and the third row of *Rhenocystis* and *Victoriacystis*. On the basis of its ventral plating pattern, *Placocystites* may be regarded as the end member of an evolutionary lineage in which the second row of central plates (which completely separates the first from the third row in *Victoriacystis*) became progressively reduced in size (as in *Rhenocystis*), and eventually disappeared (the condition observed in *Placocystites*).

The most parsimonious distribution of character changes, however, shows that the reduction of the second row in *Rhenocystis* and its loss in *Placocystites* do not represent successive stages of a transformation series. Interestingly, Gill and Caster (1960) hypothesized that an increase rather than a reduction in the number of ventral plates characterized the anomalocystitids of boreal type. Part of their argument, however, was based on an incorrect reconstruction of the plating pattern of *Victoriacystis*, as explained above (Ruta 1997).

The sister group relationship between *Placocystites* and the two sister taxa *Rhenocystis* and *Victoriacystis* maximizes character congruence, and should be preferred to alternative arrangements emphasizing conjectures of morphological transformation. However, it is interesting to compare the results of the parsimony analysis with those of a compatibility analysis (MR, unpublished data) in which *Victoriacystis wilkinsi* is placed as the sister group of (*Rhenocystis latipedunculata* + *Placocystites forbesianus*) (Text-fig. 7B). Depending upon which of the three equally parsimonious trees obtained with PAUP is considered, the arrangement (*Victoriacystis wilkinsi* + (*Rhenocystis latipedunculata* + *Placocystites forbesianus*)) found in the compatibility run requires eight or nine additional steps in the parsimony analysis.

The sister group relationship between *Rhenocystis* and *Victoriacystis* has interesting implications for the phylogeny and the palaeobiogeography of the anomalocystitids. It has long been assumed that the boreal and the austral taxa formed two distinct groups, but very few studies have attempted to test this hypothesis against a phylogenetic framework (see Derstler 1979). New anatomical information on *Victoriacystis* (Ruta 1997) shows that this mitrate has boreal affinities and it is not closely related to other anomalocystitids from the southern hemisphere, contrary to previous suggestions (e.g. Parsley 1991; Ruta and Theron 1997).

Almost certainly, an active interchange of anomalocystitid faunas between the northern and the southern palaeocontinents must have taken place in the late early or early mid Palaeozoic (Derstler 1979). That an interchange occurred is also confirmed by the recent description of the early Devonian South African mitrate *Bokkeveldia oosthuizeni* (Ruta and Theron 1997), the ventral plating pattern of which closely resembles that of several boreal taxa such as *Anomalocystites* (see Parsley 1991). For Caster (1954) and Derstler (1979), the Siluro-Devonian austral mitrates clearly derived from boreal forms.

A cladistic analysis (MR, unpublished data) shows that the vast majority of austral anomalocystitids, represented by the family Allanicytidiidae (Caster and Gill 1968; Philip 1981; Caster 1983; Haude 1995; Ruta and Theron 1997), is closely related to the mid to late Ordovician North American genus *Enoploura*. *Rhenocystis* and *Victoriacystis*, on the other hand, constitute the most derived taxa within a clade consisting mainly of boreal forms. The history of this clade is still poorly understood.

Unpublished data (MR) on ancestral area reconstructions applied to the Anomalocystitida as defined by Ubaghs (1968), as well as to several subgroups within this clade, indicate that North

America is the most likely to be part of the geographical area in which the anomalocystitids of boreal type (including *Rhenocystis*) originated. The ancestral area data were obtained using the approach devised by Bremer (1992, 1995; see also Ronquist 1994, 1995 for a discussion). Briefly, the Bremer method assesses the probability that the geographical area in which a taxon is found is also part of the ancestral distribution of the group to which that taxon belongs. Each area character is optimized according to two complementary approaches. First, the assumption is made that area absences represent the derived state. Second, it is assumed that area presences are the derived condition.

It is possible to hypothesize that the Anomalocystitida migrated several times from the boreal to the austral continents between the late Ordovician and the Early Devonian, and that North America represented the centre of origin of the group (see also Derstler 1979). Allanicytidiidae (Caster and Gill 1968) perhaps constitutes the only anomalocystitid clade whose origin and evolutionary history were entirely confined to the southern hemisphere.

However, such model is highly speculative and relies on contingent evidence from the poor fossil record of the group; the possibility that the anomalocystitids had a wider geographical distribution and that their centre of origin lay outside North America cannot be ruled out.

CONCLUSIONS

The number of anomalocystitids described during the last 30 years equals that known at the time of publication of the *Treatise on invertebrate paleontology* (Ubaghs 1968). It took more than a century to recognize these fossils as a distinctive group after the first published account of a representative of them (Billings 1858). Several recent studies have provided insights into their detailed morphology and character distribution (e.g. Jefferies and Lewis 1978; Kolata and Guensburg 1979; Parsley 1991; Haude 1995; Ruta 1997), and new material awaits proper description (Derstler 1979).

In this paper, *Rhenocystis latipedunculata* Dehm, 1932 from the German Lower Devonian is redescribed and its relationships are discussed. The general morphology and plate arrangement of *Rhenocystis* fit into the anatomical pattern of the boreal taxa from which, however, *Rhenocystis* differs in several respects. *Rhenocystis* most closely resembles *Victoriacystis* and *Placocystites*, and represents an important link between austral and boreal Siluro-Devonian mitrates.

Acknowledgements. Two anonymous referees and Dr A. R. Milner (Department of Biology, Birkbeck College, London) offered suggestions to improve the manuscript. A European Community grant (Training and Mobility of Researchers Programme) enabled MR to visit Germany in April, 1996. We thank the workers of the Eschenbach-Bocksberg roof-slate mine for allowing us to visit the Bundenbach quarry; Drs G. Brassel (Senckenbergmuseum, Frankfurt) and V. Will (Rockenhausen) for making several specimens available for study; Dr O. Sutcliffe (Department of Geology, University of Bristol) for clarifying aspects of the geology and stratigraphy of the Bundenbach area; Dr G. Plodowski (Senckenbergmuseum, Frankfurt), Prof. D. Herm (Staatssammlung, Munich) and Mr J. Bodtländer (Bundenbach) for donating casts and specimens to The Natural History Museum; Dr R. P. S. Jefferies (Palaeontology Department, The Natural History Museum) for help with the references; Dr J. W. Cosgrove (Royal School of Mines, Imperial College, London) for advice on the strain analysis; Mr P. Crabb (Photographic Unit, The Natural History Museum) for the photographs. This work forms part of a Ph.D. project carried out by MR at the University of London (Birkbeck College).

REFERENCES

ALBERTI, G. K. B. 1982. Nowakiidae (Dacryoconarida) aus dem Hunsrückschiefer von Bundenbach (Rheinisches Schiefergebirge). *Senckenbergiana Lethaea*, **36**, 451–463.

BARTELS, C. and BRASSEL, G. 1990. *Fossilien im Hunsrückschiefer-Dokumente des Meereslebens im Devon*. Georg-Weierbach, Idar-Oberstein, 232 pp.

BATHER, F. A. 1928. *Dendrocystis* in North America. *Bulletin of the Canada Department of Mines*, **49**, 5–8.

BASSLER, R. S. 1938. *Fossilium Catalogus, I: Animalia, pars 83. Pelmatozoa Palaeozoica*. Verlag für Naturwissenschaft, Grevenhage, 194 pp.

BEISSWENGER, M. 1994. A calcichordate interpretation of the new mitrate *Eumitrocystella savilli* from the Ordovician of Morocco. *Paläontologische Zeitschrift*, **68**, 443–462.

BILLINGS, E. 1858. On the Cystideae of the Lower Silurian rocks of Canada. *Figures and Descriptions of Canadian Organic Remains*, **3**, 9–74.

BREMER, K. 1992. Ancestral areas: a cladistic reinterpretation of the center of origin concept. *Systematic Biology*, **41**, 436–445.

—— 1995. Ancestral areas: optimization and probability. *Systematic Biology*, **44**, 255–259.

BRIGGS, D. E. G., RAISWELL, R., BOTTRELL, S. H., HATFIELD, D. and BARTELS, C. 1996. Controls on the pyritization of exceptionally preserved fossils: an analysis of the Lower Devonian Hunsrück Slate of Germany. *American Journal of Science*, **296**, 633–663.

CASTER, K. E. 1952. Concerning *Enoploura* of the Upper Ordovician and its relation to other carpoid Echinodermata. *Bulletins of American Paleontology*, **34**, 1–47.

—— 1954. A Devonian placocystoid echinoderm from Paraná, Brazil. *Paleontologia do Paraná* (Centennial Volume), 137–148.

—— 1983. A new Silurian carpoid echinoderm from Tasmania and a revision of the Allanicytidiidae. *Alcheringa*, **7**, 321–335.

—— and GILL, E. D. 1968. Family Allanicytidiidae, new family. S561–S564. *In* MOORE, R. C. (ed.). *Treatise on invertebrate paleontology. Part S. Echinodermata 1*, (*2*). Geological Society of America and University of Kansas Press, Boulder, Colorado and Lawrence, Kansas, 650 pp.

CHLUPAČ, I. 1976. The oldest goniatite faunas and their stratigraphical significance. *Lethaia*, **9**, 303–315.

COOPER, R. A. 1990. Interpretation of tectonically deformed fossils. *New Zealand Journal of Geology and Geophysics*, **33**, 321–332.

CRASKE, A. J. and JEFFERIES, R. P. S. 1989. A new mitrate from the Upper Ordovician of Norway, and a new approach to subdividing a plesion. *Palaeontology*, **32**, 69–99.

CRIPPS, A. P. 1990. A new stem craniate from the Ordovician of Morocco and the search for the sister group of the craniata. *Zoological Journal of the Linnean Society*, **100**, 27–71.

DEHM, R. 1932. Cystoideen aus dem rheinischen Unterdevons. *Neues Jahrbuch für Mineralogie, Geologie und Paläontologie, Beilige-Band, Abteilung A*, **69**, 63–93.

—— 1934. Untersuchungen an Cystoideen des rheinischen Unterdevons. *Sitzungsberichte der mathematisch-naturwissenschaftlichen Abteilung der Bayerischen Akademie der Wissenschaften zu München für 1934*, 19–43.

DERSTLER, K. L. 1979. Biogeography of the stylophoran carpoids (Echinodermata). 91–104. *In* GRAY, J. and BOUCOT, A. J. (eds). *Historical biogeography, plate tectonics and the changing environment*. Oregon State University Press, Corvallis, 500 pp.

—— and PRICE, J. W. 1975. The Lower Devonian echinoderm *Anomalocystites* in Pennsylvania. *Pennsylvania Geology*, **6**, 7–9.

FORTEY, R. A. and OWENS, R. M. 1992. The trilobite *Angelina* unstretched. *Geology Today*, **8**, 219–221.

GILL, E. D. and CASTER, K. E. 1960. Carpoid echinoderms from the Silurian and Devonian of Australia. *Bulletins of American Paleontology*, **41**, 5–71.

GROBBEN, K. 1908. Die systematische Einteilung des Tierreiches. *Verhandlungen der Zoologisch-Botanischen Gesellschaft in Wien*, **58**, 491–511.

HALL, J. 1858. Scientific intelligence, II, geology, 4. Crinoids of New York. *American Journal of Science and Arts*, **25**, 277–279.

HAUDE, R. 1995. Echinodermen aus dem Unter-Devon der argentinischen Präkordillere. *Neues Jahrbuch für Geologie und Paläontologie, Abhandlungen*, **197**, 37–86.

HUGHES, N. C. and JELL, P. A. 1992. A statistical/computer-graphic technique for assessing variation in tectonically deformed fossils and its application to Cambrian trilobites from Kashmir. *Lethaia*, **25**, 317–330.

JEFFERIES, R. P. S. 1967. Some fossil chordates with echinoderm affinities. 163–208. *In* MILLOT, N. (ed.). *Echinoderm biology*. Academic Press, London, 240 pp.

—— 1968. The subphylum Calcichordata (Jefferies 1967) – primitive fossil chordates with echinoderm affinities. *Bulletin of the British Museum (Natural History), Geology Series*, **16**, 243–339.

—— 1973. The Ordovician fossil *Lagynocystis pyramidalis* (Barrande) and the ancestry of amphioxus. *Philosophical Transactions of the Royal Society of London, Series B*, **265**, 409–469.

—— 1984. Locomotion, shape, ornament and external ontogeny in some mitrate calcichordates. *Journal of Vertebrate Paleontology*, **4**, 292–319.

—— 1986. *The ancestry of the vertebrates*. British Museum (Natural History), 376 pp.

—— and LEWIS, D. N. 1978. The English Silurian fossil *Placocystites forbesianus* and the ancestry of the vertebrates. *Philosophical Transactions of the Royal Society of London, Series B*, **282**, 205–323.

KITCHING, I. J. 1992. The determination of character polarity. 22–43. *In* FOREY, P. L., HUMPHRIES, C. J., KITCHING, I. J., SCOTLAND, R. W., SIEBERT, D. J. and WILLIAMS, D. M. (eds). *Cladistics*. Oxford University Press, Oxford, 191 pp.

KOLATA, D. R., FREST, T. J. and MAPES, R. H. 1991. The youngest carpoid: occurrence, affinities and life mode of a Pennsylvanian (Morrowan) mitrate from Oklahoma. *Journal of Paleontology*, **65**, 844–855.

—— and GUENSBURG, T. E. 1979. *Dianphidiocystis*, a new mitrate carpoid from the Cincinnatian (Upper Ordovician) Maquoketa Group in southern Illinois. *Journal of Paleontology*, **53**, 1121–1135.

—— and JOLLIE, M. 1982. Anomalocystitid mitrates (Stylophora, Echinodermata) from the Champlainian (Middle Ordovician) Guttenberg Formation of the Upper Mississippi Valley Region. *Journal of Paleontology*, **56**, 531–565.

KONINCK, M. L. de 1869. Sur quelques échinodermes remarquables des terrains paléozoiques. *Bulletin de l'Académie Royale des Sciences Belgique*, **28**, 544–552.

KREBS, W. 1979. Devonian basinal facies. 125–139. *In* HOUSE, M. R., SCRUTTON, C. T. and BASSETT, M. G. (eds). The Devonian System. *Special Papers in Palaeontology*, **23**, 1–353.

KUHN, O. 1961. Die Tierwelt der Bundenbacher Schiefer. *Neue Brehm-Bucherei*, **274**, 48.

KUTSCHER, F. 1970. Die Versteinerungen des Hunsrückschiefers. *Aufschluss*, **19**, 87–100.

—— 1975. Beitrage zur Sedimentation und Fossilfuhrung des Hunsrückschiefers. 41. Cystoideen-Arten im Hunsrückschiefer. *Notizblatt des hessischen Landesamtes für Bodenforschung zu Wiesbaden*, **103**, 43–52.

MEEK, F. B. 1872. Descriptions of new species of fossils from the Cincinnati group of Ohio. *American Journal of Science*, **3**, 423–428.

MUROWCHICK, J. B. and BARNES, H. L. 1987. Effects of temperature and degree of supersaturation on pyrite morphology. *American Mineralogist*, **72**, 1241–1250.

PARSLEY, R. L. 1991. Review of selected North American mitrate stylophorans (Homalozoa: Echinodermata). *Bulletins of American Paleontology*, **100**, 5–57.

PHILIP, G. M. 1981. *Notocarpos garratti*, gen. et sp. nov., a new Silurian mitrate carpoid from Victoria. *Alcheringa*, **5**, 29–38.

RAMSAY, J. G. and HUBER, M. I. 1983. *The techniques of modern structural geology. Volume 1: strain analysis*. Academic Press, London, 307 pp.

REED, F. R. C. 1925. Revision of the fauna of the Bokkeveld beds. *Annals of the South African Museum*, **22**, 27–226.

REGNAULT, S. and CHAUVEL, J. 1987. Découverte d'un échinoderme carpoïde (Stylophora–Mitrata) dans le Devonien inférieur du Maroc. *Geobios*, **20**, 669–674.

RICHTER, R. 1941. Marken und Spuren im Hunsrückschiefer 3. Fahrten als Zeugnisse des Lebens auf dem Meeresgrunde. *Senckenbergiana*, **23**, 218–260.

RONQUIST, F. 1994. Ancestral areas and parsimony. *Systematic Biology*, **43**, 267–274.

—— 1995. Ancestral areas revisited. *Systematic Biology*, **44**, 572–575.

ROZHNOV, S. V. 1990. New representatives of the class Stylophora (Echinodermata). *Paleontological Journal*, **24**, 34–45.

RUSHTON, A. W. A. and SMITH, M. 1993. Retrodeformation of fossils – a simple technique. *Palaeontology*, **36**, 927–930.

RUTA, M. 1997. A redescription of the Australian mitrate *Victoriacystis* with comments on its functional morphology. *Alcheringa*, **21**, 81–101.

—— and THERON, J. N. 1997. Two Devonian mitrates from South Africa. *Palaeontology*, **40**, 201–243.

SAVAZZI, E. 1994. Functional morphology of boring and burrowing invertebrates. 43–82. *In* DONOVAN, S. K. (ed.). *The palaeobiology of trace fossils*. Wiley, Chichester, 308 pp.

—— JEFFERIES, R. P. S. and SIGNOR, P. W. III 1982. Modification of the paradigm for burrowing ribs in various gastropods, crustaceans and calcichordates. *Neues Jahrbuch für Geologie und Paläontologie, Abhandlungen*, **164**, 206–217.

SEILACHER, A. and HEMLEBEN, C. 1966. Spurenfauna und Bildungstiefe des Hunsrückschiefers. *Notizblatt des hessischen Landesamtes für Bodenforschung zu Wiesbaden*, **94**, 40–53.

STÜRMER, W. and BERGSTRÖM, J. 1973. New discoveries on trilobites by X-rays. *Paläontologische Zeitschrift*, **47**, 104–141.

—— SCHAARSCHMIDT, F. and MITTMEYER, H.-G. 1980. Versteinertes Leben im Röntgenlicht. *Kleine Senckenberg-Reihe*, **11**, 1–80.

SÜDKAMP, W. 1991. Der Hunsrückschiefer Fundstellen–Fossilien–Präparation. *Fossilien*, **8**, 237–247.

SWOFFORD, D. L. 1993. *PAUP: Phylogenetic Analysis Using Parsimony, Version 3.1.1*. Illinois Natural History Survey, Champaign, Illinois, 257 pp.

THOMAS, A. O. and LADD, H. S. 1926. Additional cystoids and crinoids from the Maquoketa Shale of Iowa. *University of Iowa Studies in Natural History*, **11** (8), 5–18.

UBAGHS, G. 1968. Stylophora. S496–S565. *In* MOORE, R. C. (ed.). *Treatise on invertebrate paleontology. Part S. Echinodermata 1*, (*2*). Geological Society of America and University of Kansas Press, Boulder, Colorado and Lawrence, Kansas, 650 pp.

—— 1979. Trois Mitrata (Echinodermata: Stylophora) nouveaux de l'Ordovicien de Tchécoslovaquie. *Paläontologische Zeitschrift*, **53**, 98–119.

WELLMAN, H. W. 1962. A graphical method for analysing fossil distortion caused by tectonic deformation. *Geological Magazine*, **99**, 348–353.

WETHERBY, A. G. 1879. Description of a new family and genus of lower Silurian Crustacea. *Journal of the Cincinnati Society of Natural History*, **1**, 162–166.

M. RUTA
Department of Biology
Birkbeck College
Malet Street
London WC1E 7HX
and
Department of Palaeontology
The Natural History Museum
Cromwell Road
London SW7 5BD, UK

C. BARTELS
Deutsches Bergbau-Museum
Am Bergbaumuseum 28
D-44791 Bochum, Germany

Typescript received 2 December 1996
Revised typescript received 15 September 1997

NOTES FOR AUTHORS

The journal *Palaeontology* is devoted to the publication of papers on *all aspects* of palaeontology. Review articles are particularly welcome, and short papers can often be published rapidly. A high standard of illustration is a feature of the journal. Four parts are published each year and are sent free to all members of the Association. *Typescripts* should conform in style to those already published in this journal, and should be sent (with a disk, if possible) to the Secretary of the Publications Committee, **Dr R. Wood, Department of Earth Sciences, University of Cambridge, Downing Street, Cambridge CB2 3EQ,** who will supply detailed instructions for authors on request (these are published in *Palaeontology* 1996, **39**, 1065–1075).

Special Papers in Palaeontology is a series of substantial separate works conforming to the style of *Palaeontology*.

SPECIAL PAPERS IN PALAEONTOLOGY

In addition to publishing *Palaeontology* the Association also publishes *Special Papers in Palaeontology*. **Members** may subscribe to this by writing to the Membership Treasurer: the subscription rate for 1998 is £55·00 (U.S. $120) for Institutional Members, and £20·00 (U.S. $36) for Ordinary and Student Members. A single copy of each *Special Paper* is available on a non-subscription basis to Ordinary and Student Members *only*, for their personal use, at a discount of 25 per cent. below the listed prices: contact the Marketing Manager. **Non-members** may obtain Nos 39–58 (excluding 44) at cover price from Blackwell Publishers Journals, P.O. Box 805, 108 Cowley Road, Oxford OX4 1FH, UK, and older issues from the Marketing Manager. For all orders of *Special Papers* through the Marketing Manager, please add £1·50 (U.S. $3) per item for postage and packing.

PALAEONTOLOGICAL ASSOCIATION PUBLICATIONS

Special Papers in Palaeontology

For full catalogue and price list, send a self-addressed, stamped A4 envelope to the Marketing Manager. Numbers 2–48, excluding 44, are still in print and are available together with those listed below:

49. (for 1993): Studies in palaeobotany and palynology in honour of Professor W. G. Chaloner, F.R.S. Edited by M. E. COLLINSON *and* A. C. SCOTT. 187 *pp.*, 38 *text-figs*, 27 *plates*. Price £50 (U.S. $100).
50. (for 1993): Turonian ammonite faunas from central Tunisia, *by* G. R. CHANCELLOR, W. J. KENNEDY *and* J. M. HANCOCK. 118 *pp.*, 19 *text-figs*, 37 *plates*. Price £40 (U.S. $80).
51. (for 1994): *Belemnitella* from the Upper Campanian and Lower Maastrichtian Chalk of Norfolk, England, *by* W. K. CHRISTENSEN. 84 *pp.*, 22 *text-figs*, 9 *plates*. Price £35 (U.S. $70).
52. (for 1994): Studies on Carboniferous and Permian vertebrates. Edited by A. R. MILNER. 148 *pp.*, 51 *text-figs*, 9 *plates*. Price £45 (U.S. $90).
53. (for 1995): Mid-Dinantian ammonoids from the Craven Basin, north-west England, *by* N. J. RILEY. 87 *pp.*, 51 *text-figs*, 8 *plates*. Price £40 (U.S. $80).
54. (for 1995): Taxonomy and evolution of Llandovery biserial graptoloids from the southern Urals, western Kazakhstan, *by* T. N. KOREN' *and* R. B. RICKARDS. 103 *pp.*, 23 *text-figs*, 14 *plates*. Price £40 (U.S. $80).
55. (for 1996): Studies on early land plant spores from Britain. Edited by C. J. CLEAL. 145 *pp.*, 23 *text-figs*, 28 *plates*. Price £45 (U.S. $90).
56. (for 1996): Fossil and Recent eggshell in amniotic vertebrates: fine structure, comparative morphology and classification, *by* K. E. MIKHAILOV. 80 *pp.*, 21 *text-figs*, 15 *plates*. Price £35 (U.S. $70).
57. (for 1997): Cambrian bradoriid and phosphatocopid arthropods of North America, *by* DAVID J. SIVETER *and* M. WILLIAMS. 69 *pp.*, 8 *text-figs*, 9 *plates*. Price £30 (U.S. $60).
58. (for 1997): Himalayan Cambrian trilobites, *by* P. A. JELL *and* N. C. HUGHES. 113 *pp.*, 10 *text-figs*, 32 *plates*. Price £40 (U.S. $80).
59. (for 1998): Late Ordovician brachiopods from the South China Plate and their palaeogeographical significance, *by* ZHAN REN-BIN *and* L. R. M. COCKS. 70 *pp.*, 15 *text-figs*, 9 *plates*. Price £30 (U.S. $60).

Field Guides to Fossils

These are available only from the Marketing Manager. Please add £1·00 (U.S. $2) per book for postage and packing *plus* £1·50 (U.S. $3) for airmail. Payments should be in Sterling or in U.S. dollars, with all exchange charges prepaid. Cheques should be made payable to the Palaeontological Association.

1. (1983): Fossil Plants of the London Clay, *by* M. E. COLLINSON. 121 *pp.*, 242 *text-figs*. Price £7·95 (U.S. $16) (Members £6 or U.S. $12).
2. (1987): Fossils of the Chalk, *compiled by* E. OWEN; *edited by* A. B. SMITH. 306 *pp.*, 59 *plates*. Price £11·50 (U.S. $23) (Members £9·90 or U.S. $20).
3. (1988): Zechstein Reef fossils and their palaeoecology, *by* N. HOLLINGWORTH *and* T. PETTIGREW. iv+75 *pp.* Price £4·95 (U.S. $10) (Members £3·75 or U.S. $7·50).
4. (1991): Fossils of the Oxford Clay, *edited by* D. M. MARTILL *and* J. D. HUDSON. 286 *pp.*, 44 *plates*. Price £15 (U.S. $30) (Members £12 or U.S. $24).
5. (1993): Fossils of the Santana and Crato Formations, Brazil, *by* D. M. MARTILL. 159 *pp.*, 24 *plates*. Price £10 (U.S. $20) (Members £7.50 or U.S. $15).
6. (1994): Plant fossils of the British Coal Measures, *by* C. J. CLEAL *and* B. A. THOMAS. 222 *pp.*, 29 *plates*. Price £12 (U.S. $24) (Members £9 or U.S. $18).
7. (1996): Fossils of the upper Ordovician, *edited by* D. A. T. HARPER *and* A. W. OWEN. 312 *pp.*, 52 *plates*. Price £16 (U.S. $32) (Members £12 or U.S. $24).

Palaeontology

VOLUME 41 · PART 4

CONTENTS

Printed in Great Britain at the University Press, Cambridge ISSN 0031–0239